



Proceedings of the 14th International Congress of the International Radiation Protection Association

Cape Town, South Africa
9 – 13 May 2016

Volume 3 of 5

5- Optimisation and Design of New Facilities

6- Radiation Detection and Dosimetry

Organised in collaboration with:



International Labour Office



INTERNATIONAL SOCIETY OF
RADIOGRAPHERS &
RADIOLOGICAL
TECHNOLOGISTS



The Proceedings of the 14th International Congress of the International Radiation Protection Association are divided into 5 volumes, as follows:

Volume 1 of 5

Area 1: Fundamental Science
Area 2: Policy, Standards and Culture

Volume 2 of 5

Area 3: Medical
Area 4: General Ionising Radiation Protection

Volume 3 of 5

Area 5: Optimisation and Design of New Facilities
Area 6: Radiation Detection and Dosimetry

Volume 4 of 5

Area 7: Environment and Natural Background
Area 8: Transport / Sealed Source Management
Area 9: Non-ionising Radiation

Volume 5 of 5

Area 10: Emergency Preparedness and Management
Area 11: Decommissioning, Waste Management and Remediation
Area 12: Societies

Proceedings of the 14th International Congress of the International Radiation Protection Association

EDITORIAL TEAM

Christopher Clement, Jack Valentin,
Haruyuki Ogino, Devon Foote, Julie Reyjal,
Laila Omar-Nazir

Published by
The International Radiation Protection Association



www.irpa.net

© 2017 International Radiation Protection Association

ISBN 978-0-9989666-3-2

Table of Contents

VOLUME 1

IRPA14 Membership List

Editorial

Preface

How to Protect the Public When You Can't Measure the Risk -- The Role of Radiation Epidemiology Author: John D. Boice, Jr.....	1
What Can We Learn from Studies of Nuclear Workers? Author: Ethel Gilbert.....	2
Area 1: Fundamental Science	3
Attenuation Coefficients of Some Species of Wood Authors: Chioma Nwankwo, Olatunde Oni, Folorunso Ogundare.....	4
Scoping Study of Possible Chronic Health Effects for Workers at the Rössing Uranium Mine Authors: Douglas Chambers, Gunhild von Oertzen, Paul J. Villeneuve, Ron Stager, Sylvain Saint Pierre	11
Pregnancy Outcomes in Women Exposed Along the Techa River Authors: Elena Pastukhova, Sergey Shalaginov, Alexander Akleyev.....	18
Amelioration of radiation-induced DNA damage in human and animal cells mediated by natural compounds of plant and animal origin Authors: Goran Gajski, Marko Gerić, Branka Mihaljević, Saveta Miljanić, Vera Garaj-Vrhovac	26
Ionizing Radiation and Metastasis: The Dark Side of a Keystone Treatment in Cancer Authors: Guadalupe Vedoya, Nora Mohamad, Mónica Táquez Delgado, Tamara Galarza, Rosa Bergoc, Ernesto Crescenti, Graciela Cricco, Gabriela Martín	31
Concentrations of Radiocesium and ⁹⁰Sr in Agricultural Plants Collected from Local Markets and Experimental Fields before Resuming Agriculture in Fukushima Prefecture Authors: Hirofumi Tsukada, Tomoyuki Takahashi, Satoshi Fukutani, Makoto Akashi	37
The Detriment in Radiation Protection Authors: Jonas Buermeyer, Samaneh Emami, Kaija Spruck, Joachim Breckow.....	43
Establishment of Concentration Ratios Riparian and Shrub Steppe Areas of the Eastern Washington Columbia Basin Authors: Jonathan Napier, Elizabeth Reudig, Leah Minc, David Bytwerk, Kathryn Higley	48
Development of a Standard Procedure for the Irradiation of Biomolecules Authors: Marc Benjamin Hahn, Tihomir Solomun, Susan Meyer, Hans-Jörg Kunte, Maria-Astrid Schröter, Heinz Sturm.....	56
Modelling the decrease in ambient dose rate from the Chernobyl fallout using data from the Swedish municipality measurement system Authors: Mattias Jönsson, Martin Tondel, Mats Isaksson, Robert Finck, Robert Wälinder, Afrah Mamour, Christopher Rääf	60
Reconstruction of the Montenegro territory contamination with ²³⁸Pu using ²³⁸Pu/²³⁹⁺²⁴⁰Pu activity ratio Authors: Nevenka M. Antović, Perko Vukotić, Nikola Svrkota	66
A probabilistic/stochastic model for contamination levels of Cs-137 in wild boars Authors: Philipp Hartmann, Laura Urso, Ulrich Fielitz, Martin Steiner	74
Results of proficiency test using radioactive brown rice sample contaminated by the accident at Fukushima Daiichi Nuclear Power Plant Authors: Rio Furukawa, Yasuhiro Unno, Akira Yunoki, Shioka Hamamatsu, Mayumi Hachinohe, Tsutomu Miura, Masayuki Mizui, Hidesuke Itadzu	81
The non-linear effects of low dose ionizing radiation on the eye lens and the tools needed to determine Authors: Roy A. Quinlan; Alexia Kalligeraki, Miguel Jarrin, Robert Pal.....	89
Shielding design for reducing secondary neutron doses to paediatric patients during intracranial proton therapy: Monte Carlo simulation of the neutron energy spectrum and its organ doses Authors: Shinnosuke Matsumoto, Koba Yusuke, Kohno Ryosuke, Choonsik Lee, Wesley E. Bolch, Michiaki Kai.....	96
A Study on UF₆ Transportation Accident Scenarios and Diffusion Model Authors: Shutang Sun, Guoqiang Li, Hongchao Sun, Feng Yan, Jiangang Zhang.....	102

Optimization of Sr/Y-90 measurement instrument for contaminated mixture sample without chemical separation	
<i>Authors: Yasuhiro Unno, Toshiya Sanami, Shinichi Sasaki, Masayuki Hagiwara, Akira Yunoki</i>	108
Development of Integrated Nuclear Emergency Command and Decision Support System for Nuclear Power Plant	
<i>Authors: Yang Yapeng, Zhang Jiangang, Feng Zongyang, Tang Rongyao, Jia Linsheng, Xu Xiaoxiao</i>	114
Cognitive and Cerebrovascular Effects Induced by Low Dose Ionizing Radiation 'CEREBRAD' (Grant agreement: 295552)	
<i>Author: Abderrafi Benotmane</i>	121
Evaluation of the Effect of Low and Intermediate Frequency Electromagnetic Waves on Radiosensitivity	
<i>Authors: Angela Chinhengo, Antonio Serafin, Bianca Hamman, John Akudugu</i>	122
Educational and Occupational Outcomes of Childhood Cancer Survivors 30 Years after Irradiation	
<i>Authors: Agnes Dumas, Claire Berger, Pascal Auquier, Gérard Michel, Brice Fresneau, Rodrigue Allodji, Nadia Haddy, Carole Rubino, Gilles Vassal, Dominique Valteau- Couanet, Sandrine Thouvenin-Doulet, Leonie Casagrande, H�el�ene Pacquement, Chiraz El-Fayech, Odile Oberlin, Catherine Guibout, Florent De Vathaire</i>	123
Radiation Survival Curve for Paediatrics Rhabdomyosarcoma Cells	
<i>Authors: Alexander F. Ibrahim, Siddig T. Kafi, Omer F. Idris</i>	124
How Nuclear Issues are Imagined: Social Perception in Relation to Radiation Protection	
<i>Author: Alejandro Igor Margetic</i>	125
Chromosomal Aberrations and Telomere Dysfunction Induced by Low Dose- irradiation Measured by Telomere and Centromere Staining	
<i>Authors: Akram Kaddour, Bruno Colicchio, Luc Morat, Corina Cuceu, Elie El Malouf, Monika Frenzel, Leonhard Heidingsfelder, Eric Laplagne, William Hempel, Mich�ele Elmay, Laure Sabatier, Radhia M'kacher</i>	126
Transmission of Induced Chromosomal Aberrations and Telomere Dysfunction through Successive Mitotic Divisions in Human Lymphocytes after In Vitro Exposure Measured by Telomere and Centromere Staining	
<i>Authors: Akram Kaddour, Bruno Colicchio, Diane Baron, Corina Cuceu, Monika Frenzel, Luc Morat, Eric Laplane, William Hempel, Laure Sabatier, Radhia M'kacher</i>	127
EPI-CT - European Cohort Study of Paediatric CT Risks: Challenges, Achievements and Perspectives	
<i>Authors: Ausrele Kesminiene, Sarah Baatout, Elisabeth Cardis, Michael Hauptmann, Andreas Jahnen, Magnus Kaijser, Carlo Maccia, Mark Pearce, Isabelle Thierry-Chef</i>	128
DNA Double Strand Break Formation and Repair in Human Fibroblasts Continuously Exposed to X-ray Radiation	
<i>Authors: Andreyan Osipov, Anna Grekhova, Margarita Pustovalova, Ivan Ozerov, Petr Eremin, Natalia Vorobyeva, Dmitry Klovov</i>	129
DNA Double-strand Break Repair in Mammalian Cells Exposed to Low-LET Radiation at Low Doses: The Controversy Continues	
<i>Authors: Andreyan Osipov, Aleksandr Samoylov, Andrey Bushmanov, Dmitry Klovov</i>	130
The ANDANTE Project: A Multidisciplinary Evaluation of the Risk from Neutrons Relative to Photons	
<i>Authors: Andrea Ottolenghi, Giorgio Baiocco, Vere Smyth, Klaus Trott</i>	131
Morphological and Molecular Analysis of Radiation-Induced Posterior Capsule Opacification (PCO) of the Lens	
<i>Authors: Andr�es Rossini, Severino Michelin, Marta Bouchez, Ana Julia Molinari, Diana Dubner, Marina DiGiorgio</i>	132
Muscular Pathology due to High Dose Irradiation in Human Muscle	
<i>Authors: Alhondra Solares-P�erez, Val�erie Allamand, Ga�etan Gruel, Fran�ois Trompier, Gillian Butler-Browne, Vincent Mouly, Marc Benderitter, Eric Bey, St�ephane Flamant, Radia Tamarat</i>	133
Alveolar Macrophages as a Key Target for Decorporating Agents Following Pulmonary Contamination with Moderately Soluble Actinides	
<i>Authors: Anne Van der Meeren, Olivier Gr�emy, Agn�es Moureau, David Laurent, Nina Griffiths, Pierre Laroche, Jaime F. Angulo-Mora</i>	134

Refinement of In Vitro Approaches for Radiotoxicological Studies to Predict Actinide Bioavailability In Vivo <i>Authors: Anne Van der Meeren, Olivier Grémy, Pierre Laroche, Jaime Angulo, Nina Griffiths</i>	135
Effect of Natural Chronic Low Dose Radiation on Human Population Residing in High Background Radiation Areas of Kerala Coast, in Southwest India <i>Author: Birajlaxmi Das</i>	136
Radiomodifying Effects of Medicinal Plants <i>Centella asiatica</i> and <i>Withania somnifera</i> <i>Authors: Bianca Hamman, Antonio Serafin, Angela Chinhengo, Vikash Sewram, John Akudugu</i>	137
R Highlights of the Russian Health Studies Program and Updated Research Findings <i>Author: Barrett N. Fountos</i>	138
Modifying the Cytokinesis-Block Micronucleus Assay for Triage Biodosimetry <i>Authors: Christina Beinke, Matthias Port, Armin Riecke, Christian Ruf, Michael Abend, Harry Scherthan</i>	139
Ionising Radiation Biological Markers for Health Risk Prediction <i>Author: Coretchi Liuba</i>	140
Sustainable Development and Nuclear Law in Argentina <i>Authors: Cecilia Tula, Mariana Arias</i>	141
Design, Development and Application of a Desk-Top Laser Produced Plasma X-Ray Source for Radiobiology Studies <i>Authors: Daniel Adjei, Anna Wiechec, Przemyslaw Wachulak, Mesfin Getachew Ayele, Janusz Lekki Wojciech M. Kwiatek, Marie Davidková, Andrzej Bartnik, Henryk Fiedorowicz, Ladislav Pina, Jakub Svobod</i>	142
Low Dose Effect Research at the Electric Power Research Institute <i>Author: Donald Cool</i>	143
Role of Radiation Dose in Cardiac and Cerebrovascular Disease Risk following Childhood Cancer: Results from CEREBRAD and PROCARDIO FP7-European Projects <i>Authors: Florent de Vathaire, Rodrigue Allodji, Giao Vu-Bezin, Florent Dayet, Damien Llanas, Cristina Veres, Mohamedamine Benadjaoud, Rafi Benotmane, Mike Atkinson, Mike Hawkins, Leontien Kremer, Elisabeth Cardis, David Winter, Lieke Feijen, Elisa Pasqual, Nadia Haddy, Ibrahima Diallo</i>	144
Dose-related Effects of Long-term Radiation Exposure on Aquatic Biota within the Chernobyl Exclusion Zone: 30 years after accident <i>Authors: Dmitri Gudkov, Natalia Shevtsova, Natalia Pomortseva, Elena Dzyubenko, Alexander Kaglyan, Alexander Nazarov</i>	145
R The International Nuclear Workers Study (INWORKS): a collaborative epidemiological study to improve knowledge about health effects of protracted low dose exposure <i>Authors: Dominique Laurier, David B Richardson, Elisabeth Cardis, Robert D Daniels, Michael Gillies, Jackie O'Hagan, Ghassan B Hamra, Richard Haylock, Klervi Leuraud, Monika Moissonnier, Mary K Schubauer-Berigan, Isabelle Thierry-Chef, Ausrele Kesminiene</i>	146
R Estimates of Radiation Effects on Cancer Risks in The Mayak Worker, Techa River and Atomic Bomb Survivor Studies <i>Authors: Dale L. Preston, Mikhail E. Sokolnikov, Lyudmila Yu. Krestinina, Daniel O. Stram</i>	147
Study on Cytotoxic Effects of the Auger Electron Emitter Technetium-99m in Functional Rat Thyroid Cells <i>Authors: Dominik Oskamp, Marcus Unverricht-Yeboah, Anugrah Gawai, Roshni Murali, Ekkehard Pomplun, Ralf Kriehuber</i>	148
R The Growth of Biostatistics and Estimation of Cancer Risk Estimates: Past, Current, and Future Challenges <i>Authors: Daniel O. Stram, Dale Preston</i>	149
External Irradiation of the Thyroid Results in Non-Targeted Transcriptional Response in the Kidneys and Liver <i>Authors: Eva Forssell-Aronsson, Britta Langen, Nils Rudqvist, Johan Spetz, Johan Swanpalmer, Khalil Helou</i>	150

Genome-wide Transcriptional Response in Normal Tissues are Influenced by Time of Day of I.V. Injection of ¹³¹I in Mice <i>Authors: Eva Forssell-Aronsson, Britta Langen, Nils Rudqvist, Toshima Z Parris, Khalil Helou</i>	151
R The potential impact of circadian rhythms on paediatric medical imaging and radiotherapy <i>Authors: Eva Forssell-Aronsson, Roy A Quinlan</i>	152
DS02R1: Improvements to Atomic Bomb Survivors' Input Data and Implementation of Dosimetry System 2002 (DS02) and Resulting Changes in Estimated Doses <i>Authors: Eric Grant, Kotaro Ozasa, Harry Cullings</i>	153
Solid cancer incidence among the Life Span Study of atomic bomb survivors: 1958-2009 <i>Authors: Eric J. Grant, Kotaro Ozasa</i>	154
Protein Status in Atomic Workers in Distant Period after Long-term Occupational Combined Low-dose Exposure <i>Authors: Evgeniia Kirillova, Maria Zakharova, Taisa Uryadnitskaya, Christopher Loffredo</i>	155
Cancer Incidence among Mayak Workers <i>Authors: Elena Labutina, Nezahat Hunter, Irina Kuznetsova</i>	156
Comparison of Total Antioxidant Capacity level between radiation workers in diagnostic radiology and other staffs of hospital in Zahedan <i>Authors: Fatemeh Ramrodi, Farnaz Farifteh, Amir Hossein Zarghami, AliReza Nakhaee, Dariush Askari, Jalal Ordoni, Yazdan Salimi, Mohammad Hossein Jamshidi, Hamed Dehghani</i>	157
Effects of Radon Inhalation on Biophysical Properties of Blood in Rats <i>Authors: Fayez Shahin, Omar Abdel-Salam</i>	158
Assessment of Respiratory Toxicity of ITER-like Tungsten Metal Nanoparticles using an in vitro 3D Human Airway Epithelium Model <i>Authors: George Isabelle, Hagege Agnès, Herlin Nathalie, Vrel Dominique, Rose Jérôme, Sanles Marcos, Orsiere Thierry, Uboldi Chiara, Grisolia Christian, Rousseau Bernard, Malard Véronique</i>	159
Beyond Paternalism and Strategy: Understanding Radiological Risks as a Mutual Learning Experience <i>Authors: Gaston Meskens, Tanja Perko</i>	160
Survey of the Effect of Ionizing Radiation Energy on the Blood Indices of Occupationally Exposed Staff (radiologic technologists and radiologists) <i>Authors: Hamid Behrozi, Mohammad Hossein Jamshidi, Kimia Benabbas, Marziyeh Daemolzeqr, Yazdan Salimi, Dariush Askari, Jalal Ordoni, Hamed Dehghani</i>	161
Development of Radiological Protection Powder <i>Authors: Hiroki Ohtani, Yuya Ishita</i>	162
Risk of Thyroid Cancer Incidence due to Living Close to Atomic Facility in Childhood <i>Authors: Irina Martinenko, Mikhail Sokolnikov</i>	163
Retrospective Estimation of Organ Doses for an Epidemiology Study of CT Scanning in Paediatric Patients (EPI-CT) <i>Authors: Isabelle Thierry-Chef, Jérémie Dabin, Joahannes Hermen, Tore S. Istad, Andreas Jahnen, Lucian Krille, Choonsik Lee, Carlo Maccia, Arvid Nordenskjöld, Hilde Olerud, Steven L Simon, Lara Struelens, Ausrele Kesminiene</i>	164
Biological Dosimetry after Total Body Irradiation (TBI) for Hematologic Malignancy Patients using Premature Chromosomal Condensation in Combination with Fluorescence in Situ Hybridization <i>Authors: Julien Dossou, Dominique Violot, Theodore Girinsky, Patrice Carde, Jean-Henri Bourhis, Claude Parmentier, Radhia M'kacher</i>	165
Doses and risks from radon and other internal emitters and their control <i>Author: John Harrison</i>	166

Synthesis of Novel Psammaplin A-based Radiosensitizers <i>Authors: Jin Ho Kim, Chan Woo Wee, Hak Jae Kim, Soo Youn Suh, Eun Sook Ma, Boom Soo Shin, Il Han Kim</i>	167
Responses to Radiation and Fate of Cells <i>Authors: Jin Kyu Kim, Mi Young Kang, Remigius A. Kawala, Tae Ho Ryu, Jin-Hong Kim</i>	168
Radiation-Induced p53 Level Determines Radiosensitivity of Cells <i>Authors: Jin Kyu Kim, Min Young Kang, Yun-Jong Lee, Jin-Hong Kim, Jacobus P. Slabbert</i>	169
Development and Validation of a Multivariate Calibration Strategy for Direct Analysis of Trace Elements in Soft Tissue Utilizing Chemometric Energy Dispersive X-Ray Fluorescence and Scattering (EDXRFS) Spectroscopy <i>Authors: Justus Okonda, Angeyo Kalambuka, Seth Kisia, Michael Mangala</i>	170
Radiation Shielding perfection at Design and construction Stages <i>Author: Joseph Rugut</i>	171
Application of the Spencer-Attix Cavity Theory for Determination of Conversion Coefficient for Ambient Equivalent Dose with TLD-100 Dosimeters Calibrated in Air Kerma <i>Authors: Jose T Alvarez Romero, Fernando Gonzalez Jimenez</i>	172
Evaluation of Fission Energy Deposition in the SAFARI-I Nuclear Reactor <i>Authors: Linina Jurbandam, Oscar Zamonsky</i>	173
Lung Cancer Risk from Radon and Smoking – Additive or Multiplicative Effect <i>Author: Ladislav Tomasek</i>	174
Risk of Leukemia in Uranium Miners <i>Author: Ladislav Tomasek</i>	175
Chronic Bronchitis Incidence in the Cohort of Mayak Production Association Workers Occupationally Exposed to Radiation <i>Authors: Tamara Azizova, Galina Zhuntova, Richard Haylock, Maria Moseeva, Evgenia Grigorieva, Maria Bannikova, Zinaida Belyaeva, Evgeniy Bragin</i>	176
Microdosimetric Measurements for Electron Irradiation of DNA under Physiological Conditions: Low Energy Electrons vs. Radicals <i>Authors: Marc Benjamin Hahn, Tihomir Solomun, Susan Meyer, Hans-Joerg Kunte, Heinz Sturm</i>	177
Markers of Neural Degeneration and Regeneration in Blood of Cardiac Catheterization Personals <i>Authors: Mohamed ElKhafif, Soheir Korraa, Nevine Noussier, Walid Elhammady, Eman El Gazzar, Hanan Diab</i>	178
Regulatory Culture and its Role in Radiation Protection <i>Authors: Marcela Ermacora, Chris Englefield</i>	179
The Hybrid Analytical – Voxel Head Phantom for Activity Measurement of ²⁴¹Am in Cranial Bone <i>Author: Marko Fulop</i>	180
Occupational and Medical Exposure: The Contribution to Carcinogenic Risk In Mayak Worker Cohort <i>Authors: Mikhail Osipov, Mikhail Sokolnikov</i>	181
Baseline Lifetime Mortality Risk from Circulatory Disease in Japan <i>Authors: Michiya Sasaki, Haruyuki Ogino, Takatoshi Hattori</i>	182
DNA Repair Genes XRCC1 and XRCC3 Polymorphisms and the Level of Micronuclei in Industrial Radiographers <i>Authors: Mahsa Shakeri, Farideh Zakeri, Vahid Changizi, Mohammad Reza Farshidpour, Mohammad Reza Rajabpour</i>	183
Mayak Worker Cancer Mortality <i>Authors: Mikhail Sokolnikov, Dale Preston, Dan Stram</i>	184

Repair of Ionizing Radiation-Induced DNA Damage and Risk of Second Cancer in Childhood Cancer Survivors <i>Authors: Nadia Haddy, Laurence Tartier, Serge Koscielny, Elisabeth Adjadj, Carole Rubino, Laurence Brugières, Hélène Pacquement, Ibrahima Diallo, Florent de Vathaire, Dietrich Averbeck, Janet Hall, Simone Benhamou...</i>	
The Role of the Scientific Review Group in the Russian Health Studies Programs: Key Contributions and Influence and Impact on Radiation Protection <i>Author: Nolan Hertel</i>	186
A Comprehensive Study on Tritium Release from Nuclear Accidents and Impact of Tritiated Water on Postnatal Development of Mouse Cerebellum <i>Authors: Narendra Jain, A. L. Bhati</i>	187
Current State of Pharmacologic Radioprotection for Clinical Exposure to Ionizing Radiation <i>Authors: Nivethan Vela, Joe Barfett, Kieran Murphy, David Mikulis</i>	188
Ameliorating Effects of Bone Marrow Transplantation and Zinc Supplementation on Physiological and Immunological Changes in γ-Irradiated Rats <i>Authors: Omaima Ashry, Maha Soliman, Mervat Ahmed, Yasmin Abd El Naby</i>	189
Occupational Exposure to ^7Be – A Case Study <i>Authors: Ofer Aviv, Hanan Datz, Shlomi Halfon, Zohar Yungrais, Erez Daniely</i>	190
Early and Late Alterations of Neurochemical, Behavioral, and Somatic Criteria in Rats Exposed to ^{12}C ions and γ-rays <i>Authors: Oleg Belov, Ksenia Belokopytova, Ara Bazyan, Vladimir Kudrin, Viktor Narkevich, Aleksandr Ivanov, Gennady Timoshenko, Eugene Krasavin</i>	191
Integrating Dosimetry, Radiobiology and Epidemiology to study the Effects of Occupational Exposure to Uranium in Europe: the CURE Project <i>Authors: Olivier Laurent, Maria Gomolka, Richard Haylock, Eric Blanchardon, Augusto Giussani, Will Atkinson, Derek Bingham, Sarah Baatout, Ladislav Tomasek, Elisabeth Cardis, Janet Hall, Dominique Laurier</i>	192
Investigations of radiation exposures in the aftermath of the Chernobyl accident <i>Author: Rolf Michel</i>	193
A New Tool for Genotoxic Risk Assessment: Re-evaluation of Cytokinesis-Block Micronucleus Assay using Semi-Automated Scoring following Telomere and Centromere Staining <i>Authors: Radhia M'kacher, Narjes Zaguia, Francis Finot, Luc Morat, André Essahli, Corina Cuceu, Bruno Colicchio, Leonhard Heidingsfelder, Eric Laplagne, William Hempel, Laure Sabatier</i>	194
Change in Peripheral Blood Lymphocyte Telomere Length and the Occurrence of Secondary Cancers in Hodgkin Lymphoma Patients <i>Authors: Radhia M'kacher, Theodore Girinsky, Bruno Colicchio, Michelle Ricoul, Corina Cuceu, Luc Morat, Monika Frenzel, Aude Lenain, Leonhard Heidingsfelder, William Hempel, Alain Dieterlen, Laure Sabatier, Patrice Carde</i>	195
Radiation Dose to the Eyes in the Risk of Cataract after Non-Retinoblastoma Solid Childhood Cancers <i>Authors: Rodrigue Sètchéou Allodji, Chiraz El-Fayech, Amar Kahlouche, Boris Schwartz, Odile Oberlin, Mohamed Benadjaoud, Julien Bullet, Ibrahima Diallo, Carole Rubino, Nadia Haddy, Florent de Vathaire</i>	196
Risk of Subsequent Leukaemia after a Solid Tumour in Childhood: Radiotherapy and Chemotherapy Side Effects <i>Authors: Rodrigue Sètchéou Allodji, Boris Schwartz, Cristina Veres, Nadia Haddy, Carole Rubino, Marie-Cécile Le Deley, Jérémie Vu Bezin, Jean Chavaudra, Dimitri Lefkopoulos, Eric Deutsch, Odile Oberlin, Ibrahima Diallo, Florent de Vathaire</i>	197
Simulation-extrapolation Method to Address Errors in Atomic Bomb Survivor Dosimetry on Solid Cancer and Leukaemia Mortality Risk Estimates, 1950-2003 <i>Authors: Rodrigue Sètchéou Allodji, Boris Schwartz, Ibrahima Diallo, Dominique Laurier, Florent de Vathaire</i>	198
Chernobyl, 30 Years on – Health Effects <i>Author: Richard Wakeford</i>	199
Immunological Monitoring of the Personnel at Radiation Hazardous Facilities <i>Authors: S.M. Kiselev, M.E. Sokolnikov, L.V. Lyss, N. I. Ilyina</i>	200


Raman Spectroscopy as an Analytical Tool for Ionizing Effect Studies in Pig Lens “Ex Vivo” and “In Vitro” <i>Authors: Severino Michelin, Andres Rossini, Emilia Halac, Diana Dubner, Ana Molinari</i>	201
Current Status of the Biological Study on Low-Dose Ionizing Radiation Effects in KHNP-RHI, Korea <i>Authors: Seon Young Nam, Kwang Hee Yang</i>	202
Role of AKT and ERK Pathway in Controlling Radio-Sensitivity and Adaptive Response by Low-Dose Radiation in Human Immune Cells <i>Authors: Seon Young Nam, Hyung Sun Park, Ga Eun You, Kwang Hee Yang, Ji Young Kim</i>	203
Non-cancer Effects in the Cohort of Mayak PA Workers Occupationally Exposed to Radiation <i>Authors: Tamara Azizova, Evgeniya Grigorieva, Maria Bannikova, Richard Haylock, Nazahat Hunter</i>	204
Micro- and Mesocosms for Assessing Ecosystem Effects of Radiation – A Review <i>Authors: Tanya Hevroy, Clare Bradshaw, Hallvard Haanes, Elisabeth Hansen, Runhild Gjelsvik, Alicja Jaworska, Louise Jensen, Emmanuel Lapied, Deborah Oughton</i>	205
An Update on a Rapid Method of Biological Dosimetry to Assist in the Event of a Nuclear Emergency <i>Authors: Timothy Sebeela, JP Slabbert, V.V. Vandersickel, D. Serfontein</i>	206
Radioiodine Transfer from Seaweed to Abalone <i>Authors: Toshihiro Shibata, Yoshio Ishikawa, Yuichi Takaku, Shun-ichi Hisamatsu</i>	207
Clinical Features of Subacute Radiation Syndrome <i>Authors: Valeriy Krasnyuk, Anastasia Ustyugova</i>	208
The Frequency of Chromosome Aberrations in Peripheral Blood Lymphocyte Cultures and Risk of Disease Development after Radiation Exposure <i>Authors: Vladimir Nugis, Maria Kozlova</i>	209
Airborne I-131 detection on Internal Surface of Buildings using Common Household Products <i>Authors: Yung-Chang Lai, Ying-Fong Huang, Yu-Wen Chen, Mei-Ling Chung</i>	210
History of Ultra-Sonography Examination for Thyroid in the Residents Near Nuclear Power Plants <i>Authors: Young-Khi Lim, Kwang-Pil Ko, Keun-Young Yoo, Sue K. Park, Aesun Shin, Keon Wook Kang</i>	211
Pu isotopes in Surface Soils in China: Its Concentration and Isotopic Ratio <i>Authors: Youyi Ni, Wenting Bu, Wei Dong, Qiuju Guo</i>	212
Development and Application of High Intensity D-T Fusion Neutron Generator (HINEG) <i>Authors: Yican Wu, Song Gang, Yongfeng Wang, Taosheng Li, Xiang Ji, Chao Liu, Jieqiong Jiang</i>	213
ESR Dosimetry with Ceramic and Glass Materials from Electronic Components for Dose Assessment in Radiation Accident <i>Authors: Zhe Liu, Zhiping Luo, Jinfeng Huang, Guowen Zheng</i>	214
  Results of RELID Study 2014 - Buenos Aires, Argentina Retrospective Evaluation of Lens Injuries and Dose <i>Authors: Papp, C., Romano-Miller, M.; Descalzo, A., Michelin, S., Molinari, A., Rossini, A., Plotkin, C.; Bodino, G., Esperanza, G., Di Giorgio, M., Touzet, R.</i>	215
Area 2: Policy, Standards and Culture	216
Integration of radiation safety in management systems in Swedish health care – success or distress <i>Author: Anja Almén</i>	217
Some Suggestions to Adequate the IAEA Safety Standards Series No. 49 According to the General Safety Requirements Part 3 from IAEA <i>Authors: Adelia Sahyun, Carlos N. Ghobril, Clarice F. Perez, Gian Maria Sordi</i>	224
Restoring the “R” in ALARA <i>Author: Brant A. Ulsh</i>	228
De minimis non curat lex or endless optimization? <i>Author: Bernd Lorenz</i>	236

Ethics and radiation protection in biomedical research in the post-Fukushima era: <i>up to date</i> <i>Author: Chieko Kurihara</i>	244
e-Learning – Radiation Safety Training Course <i>Author: Carolyn Mac Kenzie</i>	253
The Romanian Society for Radiological Protection – 25 years as Associate Society to IRPA <i>Authors: Constantin Milu, Ion Chiosila, Nicolae-Mihail Mocanu</i>	256
Radiation Safety Climate in a University Setting <i>Authors: Caitlin Root, Robert Sinclair, Konstantin Povod, Nicole Martinez</i>	259
Young Scientists and Professionals (YSP) – Austria’s Young Generation as best practice example <i>Authors: Ch. Stettner, F. Kabrt, E. Langegger, N. Baumgartner</i>	267
Carbon Molecular Sieves used in the Sampling and Monitoring Technology of Krypton in the Atmosphere <i>Authors: Deng Achang, Ma Xiongnan, Zhu Jun, Xiao Xiangzhong, Zhang Aiming</i>	270
Public Acceptance of Nuclear Technology: education and communication to transform old prejudices and inspire new thoughts <i>Author: Denise S. Levy</i>	277
Enhancing communication on Radiological Protection throughout Brazil <i>Authors: Denise S. Levy, Gian M. A. A. Sordi, Demerval L. Rodrigues, Janete C. G. Carneiro</i>	284
Radiation Protection Culture in Waste Management <i>Authors: G. Hampel, J. Feinhals, H. Völkle</i>	291
Comments on the General IAEA Safety Requirements – Part 3 – and Suggestions for the Next Publications <i>Author: Gian Maria Sordi</i>	298
5th European IRPA Congress (4-8 June 2018): <i>Encouraging Sustainability in Radiation Protection</i> <i>Authors: Hielke Freerk Boersma, Bert Gerritsen, Gert Jonkers, Jan Kops, Lars Roobol, Carel Thijssen</i>	304
L Band EPR Tooth Dosimetry for neutron <i>Authors: Ichiro Yamaguchi, Hitoshi Sato, Hiraku Kawamura, Tuyoshi Hamano, Hiroshi Yoshii, Mituru Suda, Minoru Miyake, Naoki Kunugita</i>	309
Promoting Radiation Safety Culture in the UK: General Users Sector <i>Authors: J. R. Croft, A. MacDonald, R. Fannin, R. Hill, P. Boulton, D. Orr, A. Bannon</i>	316
Promoting Radiation Safety Culture in the UK <i>Authors: J. R. Croft, R. Coates, C. Edwards, C.-L. Chapple, K. Davies, A. MacDonald</i>	324
Radiation Protection Quantities for the Assessment of Stochastic Effects: <i>Should we be more Papal than the Pope?</i> <i>Authors: Jozef Sabol, Jana Hudzietzová, Bedřich Šesták</i>	331
"A North-American first: a state-of-the-art fully functional Linac for teaching to the next generations of therapists and physicists in a college" <i>Authors: Mathieu Bergeron, Louis Archambault, Luc Beaulieu</i>	336
2015 IRPA survey of professionals on the new dose limit to the lens of the eye, and wider issues associated with tissue reactions <i>Authors: Marie Claire Cantone, Merce Ginjaume, Saveta Miljanić, Colin J. Martin, Keiichi Akahane, Louisa Mpete, Severino C. Michelin, Cinthia M. Flannery, Lawrence T. Dauer, Stephen Balter</i>	342
Introducing on-line modules in the Swedish Master’s Degree Programme for Applied Radiation Protection 14 <i>Authors: Mattias Jönsson, Mats Isaksson, Robert Finck, Christopher Rääf</i>	349
Management of Radioactive Waste: Public Perceptions Versus Scientific Views <i>Author: Mogwera Khoathane</i>	355

New EU-Regulations for Radon at Workplaces and their Consequences on the Regulatory Radiation Protection in Bavaria <i>Authors: Markus Trautmannsheimer, Simone Körner</i>	364
Contributions from Women to the Radiation Sciences <i>Authors: Nicole Martinez, Elizabeth Gillenwalters</i>	370
Argentine Plan for strengthening occupational radiation protection infrastructure framed in the RLA 9075 IAEA Project <i>Authors: Nancy Puerta Yepes, Ana Rojo, Adrián Discacciatti, Marina Di Giorgio, Laura Castro, Fabio López, Analía Canoba</i>	379
Activities of EUTERP, the European Training and Education in Radiation Protection Foundation <i>Authors: Richard Paynter, Folkert Draaisma, Penelope Allisy, Michèle Coeck, Friedrich Hoyler, Marcel Schouwenburg, Joanne Stewart</i>	387
A model for determining risk constraints for potential exposures of the public and limitations of the activity of radionuclides released by accidents in nuclear facilities <i>Author: Robert R. Finck</i>	391
The Advantages of Creating a Positive Radiation Protection Safety Culture in the Higher Education and Research Sectors <i>A report from the Working Group on Culture in Research and Teaching</i> <i>Authors: T. Coldwell, P. Coleb, C. Edwards, J. Makepeace, C. Murdock, H. Odams, R. Whitcher, S. Willis, L. Yates</i>	399
Education and Training of Workers for Development of a Safety Culture in a Radioactive Facility <i>Authors: Zayda Haydeé Amador Balbona, Miguel Antonio Soria Guevara</i>	409
Assessment of radiation science studies in 4 successive years <i>Authors: Banafsheh Zeinali-Rafsanjani, Mahdi Haghghatafshar, Mahdi Saeedi-Moghadam, Mohammad-Amin Mosleh-Shirazi</i>	415
Y Gender demographics in radiation protection <i>Authors: Elizabeth Gillenwalters, Nicole Martinez</i>	419
The FORO Project on Safety Culture in Organizations, Facilities, and Activities with Sources of Ionizing Radiation <i>Authors: Rubén Ferro Fernández, Jorge Arciniegas Torres, Ana Blanes Tabernero, Ana M. Bomben, Rodolfo Cruz Suárez, Claudia Da Silva Silveira, E. Ordoñez Gutiérrez, Jorge F. Perera Meas, Renán Ramírez Quijada, Ricardo Videla Valdebenito</i>	427
The Intersection of Public Health and Radiation Protection in Radiation Emergencies <i>Author: Armin Ansari</i>	435
Assessment of the Safety Culture at Facilities Involved in Management of the Spent Nuclear Fuel and Radioactive Waste <i>Authors: Alexander Bobrov, Sergey Kiselev, Malgorzata Sneve, Victor Scheblanov</i>	436
The Decision Threshold and Other Characteristic Limits: An Approach to Re- evaluating the Current Computational Paradigm <i>Authors: Alexander Brandl, Jenelle Mann</i>	437
Lessons learned from 4th African Regional Congress of the International Radiation Protection Association (AFRIRPA04) held in Morocco <i>Authors: Abdelmajid Choukri, Oum Keltoum Hakam</i>	438
Safety Culture Issues in Nuclear Fusion Activities <i>Author: Altair de Assis</i>	439
Communication in an Organization within a Framework of Social Responsibility <i>Authors: Andrea Docters, Maria B. Lucuix</i>	440
Interdisciplinary Approach to Radiation and Nuclear Safety Education <i>Author: Andrejs Dreimanis</i>	441

Education and Training in Radiopharmacy: The INSTN Approach <i>Author: Akli Hammadi</i>	442
Experience of Belarus to the Introduction of International Radiation Safety Standards to the National System <i>Authors: Alena Nikalayenka, Sergey Sychik, Viktoia Kliaus</i>	443
R The Evaluation of the Real Alpha Value in Brazil and Its Projection until the Year 2050 <i>Authors: Adelia Sahyun, Carlos N. Ghobril, Clarice F. Perez, Gian Maria Sordi</i>	444
Radiation Protection in Medical Field in Cameroon <i>Authors: Augustin Simo, Maurice Ndontchueng Moyo, Yolande Huguette Ebele Yigbedeck, Richard Samba Ndi</i>	445
EURADOS IDEAS Guidelines Spanish Translation: A New Tool for Training Activities from the Collaboration between SEPR-SAR Radiation Protection Societies <i>Authors: Borja Bravo, Eduardo Sollet, Ana Maria Rojo, Inés Gomez</i>	446
Engaging Communities to Discuss Nuclear Power Options for the Future <i>Author: Barbara L. Hamrick</i>	447
An IRPA, WHO, IOMP Initiative on Radiation Protection Culture in Medicine <i>Authors: Bernard Le Guen, María Del Rosario Perez, Madan M. Rehani</i>	448
Regulating the Security of Radioactive Sources in South Africa and Institutionalising Nuclear Security Culture and Effective Physical Protection <i>Author: Boikanyo Ntuane</i>	449
Fraudulent Exams in the Training of Reactor Supervisors at the Laguna Verde Nuclear Power <i>Author: Bernardo Salas</i>	450
R Plenary Panel International Standards – RP in Medicine <i>Author: Claire Cousins</i>	451
R Radiation Safety Culture in the UK Medical Sector: A top to bottom strategy <i>Authors: Claire-Louise Chapple, Andy Bradley, Maria Murray, Phil Orr, Jill Reay, Peter Riley, Andy Rogers, Navneet Sandhu, Jim Thurston</i>	452
Implementation in the Republic of Moldova the Requirements of Directive 2013/59 / Euratom on Indoor Radon Concentrations <i>Authors: Coretchi Liuba, Bahnarel Ion</i>	453
Workshop on Radiopathology and Radiation Protection at the Annual Rotating Internship, School of Medicine at the University of Buenos Aires <i>Authors: Cinthia Papp, Mónica Gardey, Gerardo Rank, Roberto Agüero, Mara Scarabino, Adriana Cascón</i>	454
Implications of ICRP 103, the International and the European Basic Safety Standards on the use of Dose Constraints in the Management and Disposal of Radioactive Waste, Including Waste Containing Elevated Levels of Naturally Occurring Radionuclides in France <i>Authors: Marie-Odile Gallerand, Christophe Serres, Didier Gay, François Besnus, Jérôme Guillevic</i>	455
Dose Limits in Radioactive Waste Management: Interdisciplinary Perspectives from the German ENTRIA Project <i>Authors: Clemens Walther, Achim Brunnengräber, Peter Hocke, Karena Kalmbach, Claudia König, Sophie Kuppler, Klaus-Jürgen Röhlig, Ulrich Smeddinck</i>	456
The ICRP System of Protection for Existing Exposure Situations: The Work of Committee 4 to Elaborate the Framework for Protection <i>Author: Donald Cool</i>	457
Policy Standards and Culture <i>Author: David Crawford</i>	458
The UK Ministry of Defence Radon Safety Programme <i>Authors: Dee Emerson, Dean Williams</i>	459

R Certified Training for Nuclear and Radioactive Source Security <i>Authors: Daniel Johnson, Brunelle Battistella, Pierre Legoux</i>	460
Radiation Safety Culture at United States Nuclear Power Plants <i>Author: Ellen Anderson</i>	461
43 Years of Experience in Training in Radiation Protection <i>Author: Eduardo Medina-Gironzini</i>	462
Experience in the Use of Social Networks in Radiation Protection <i>Author: Eduardo Medina-Gironzini</i>	463
Nuclear regulators need to adopt international standards applicable to radiation measuring instruments into their national legislation <i>Author: Emma Snyman</i>	464
ICNIRP: Preliminary Thoughts on Protection Principles for Non-Ionizing Radiation <i>Author: Eric van Rongen</i>	465
Ethical Considerations on the Empowerment of People Living in Contaminated Areas after a Nuclear Accident <i>Authors: François Rollinger, Jacques Lochard, Thierry Schneider</i>	466
The Inter-Agency Committee on Radiation Safety – 25 years of Cooperation Efforts to Harmonize International Radiation Protection and Safety <i>Authors: Ferid Shannoun, Miroslav Pinak, Ted Lazo, Carl Blackburn, Stephan Mundigl, Malcolm Crick, Shengli Niu, Pablo Jimenez, María Pérez, Hans Menzel, Christopher Clement, Miroslav Voytchev, Renate Czarwinski, Alain Rannou</i>	467
Lessons Learned from the Fukushima Event: The Radiation Protection Emergency Preparedness <i>Authors: Giorgio Cucchi, Lorenzo Isolan, Federico Rocchi, Marco Sumini</i>	468
Interplay of Nuclear Power on Earth and in Space: Nuclear Energy as Sustainable Energy <i>Author: Gordana Lastovicka-Medin</i>	469
Scientific Issues, Emerging Challenges and Emerging Digital Social Innovations for Radiation and Radiological Protection <i>Author: Gordana Lastovicka-Medin</i>	470
Workers' Knowledge on Radiation Protection. A Survey at Mongi Slim Hospital <i>Author: Hager Kamoun</i>	471
R Importance to Engage in Dialogue with the Affected Population after the Acute Phase of an Accident <i>Author: Hans Vanmarcke</i>	472
Establishing Radiation Protection Culture for Local Residents Left in the outside Boundary of Fukushima and Challenges facing Mothers and Children <i>Author: Hiroko Yoshida</i>	473
Scientific, Societal, Implementation and Regulatory Challenges of Radiological Protection <i>Authors: Ingemar Lund, Ted Lazo</i>	474
Radiation Protection in a Mixed Contaminant Context, Risk Assessment Methodologies <i>Authors: Ivica Prlic, Hrvoje Mesic, Mladen Hajdinjak, Jerko Sisko, Domagoj Kosmina, Tomislav Bituh</i>	475
OPERRA-HARMONE: Harmonising Modelling Strategies of European Decision Support Systems for Nuclear Emergencies <i>Authors: Jan Christian Kaiser, Shan Bai, Johan Camps, Thomas Charnock, Damien Didier, Fabricio Fiengo, Laurent Garcia-Sanchez, Jérôme Groell, Christophe Gueibe, Kerstin Hürkamp, Olivier Isnard, Anne Nisbet, Wolfgang Raskob, Marie Simon Cornu, Christian Staudt, Lieve Sweeck, Jochen Tschiersch, Jordi Vives i Batlle, Samantha Watson, Mark Zheleznyak</i>	476
How to Develop and Maintain an Effective Training Program in Radiation Protection <i>Authors: Joe Cortese, Liz Krivososov</i>	477

Delineation of Radon Prone Areas for Mandatory Radon Measurement in Workplaces in the Czech Republic <i>Authors: Jana Davidková, Karla Petrová</i>	478
Nuclear Security Consideration for Radiation Protection Professionals <i>Authors: Jason Harris, Edward Waller</i>	479
Communicating Risk to the Public: An Important Element in Mitigating the Impact of a Radiological Terrorist Attack <i>Authors: Jozef Sabol, Bedrich Sestak, Ivo Petr</i>	480
Improvement in Radioactive Waste Management over the Past 40 Years in the U.S <i>Author: J. Scott Kirk</i>	481
Current Discussions in Japan Health Physics Society regarding Radiation Protection of the Lens of the Eye <i>Authors: Keiichi Akahane, Takeshi Iimoto, Takeshi Ichiji, Satoshi Iwai, Hiroyuki Ohguchi, Kazuko Ohno, Tadahiro Kurosawa, Chiyo Yamauchi-Kawaura, Hideo Tatsuzaki, Norio Tsujimura, Nobuyuki Hamada, Toshiyuki Hayashida, Yutaka Hotta, Tadashi Yamasaki, Sumi Yokoyama</i>	482
 The Ethical Foundations of the Radiological Protection System <i>Author: Kunwoo Cho</i>	483
Assessing and Promoting Radiation Safety Culture in the UK Nuclear Sector <i>Authors: Karl Davies, John Croft, Ellie Krukowski, John Bradshaw</i>	484
Managing Suitably Qualified and Experienced Persons (SQEP) Requirements to Meet Business Need <i>Authors: Kenneth Gibbs, Robin Wells</i>	485
The Selected Issues Related to the Development of National Legislation Based on ICRP103, IAEA BSS and EU BSS <i>Authors: Karla Petrová, Jana Davidková</i>	486
Updating the Radiation Protection Guidance for the United States <i>Authors: Kenneth Kase, Michael Boyd, John Boice, Armin Ansari</i>	487
Unification of Legal and Procedural Documentation for Emergency Response in the FMBA of Russia <i>Authors: Liudmila Bogdanova, Yuriy Salenko</i>	488
Development of Nuclear Security infrastructure in Nigeria: Achievements Challenges and prospects <i>Author: Mbet Akpanowo</i>	489
Practical Aspects of Applying Ethics to Occupational Exposures within the Nuclear Sector <i>Author: Marie Barnes</i>	490
Stakeholder Dialogue Webinar: Experience and Lessons for Young and Old Experts and Researchers <i>Authors: Mike Boyda, Ted Lazob</i>	491
Goals and Intermediate Results of the 7FP ENETRAP III Project <i>Authors: Michèle Coeck, Joanne Stewart, Annemarie Schmitt-Hannig, Paul Livolsid, Sascha Trumm, Marisa Marco</i>	492
Problems Associated with Radiation Protection Training Programs <i>Author: Mohamed Goma</i>	493
The INEX 5 Exercise: Notification, Communication and Interfaces for Catastrophic Radiological Events <i>Authors: Mike Griffiths, Olvido Guzman</i>	494
Mini UAS based Gamma Spectrometry Measurements in case of Emergency <i>Author: Markku Kettunen</i>	495
Radon occupancy factor for the public areas, needs for revision <i>Authors: Mohsen Shafiee, Sajad Borzoueisileh, Razieh Rashidfar</i>	496
An Insight into the Nuclear Security Science and Policy Institute at Texas A&M University <i>Author: Mani D. Shah</i>	497

Education Standards and Standards Education (ESSE) Process in Radiation Protection in a National Education Cycle <i>Author: Mehdi Sohrabi</i>	498
The URPS Hypothesis for Universal Radiation Protection Standardization <i>Author: Mehdi Sohrabi</i>	499
Lessons from Fukushima Daiichi Nuclear Accident and Efforts of Nuclear Regulation Authority <i>Author: Nobuhiko Ban</i>	500
Balancing Theory and Practicality: Engaging Non-Philosophers in Ethical Decision Making <i>Authors: Nicole Martinez, Daniel Wueste</i>	501
The 4th Workshop on Science and Values in Radiological Protection Decision Making <i>Authors: Nataliya Shandala, Aleksandr Rakhuba, Ted Lazo</i>	502
Cs-137 Contamination Incident at Scrap Yard in South Africa <i>Author: Nico van der Merwe</i>	503
Evaluation of the National Legislative & the Regulatory Framework of Security of Sealed Radioactive Sources in interim Storage <i>Authors: Oumkeltoum Hakam, Mohamed Maital, Assia Lasfar</i>	504
South African Perspective for Radon in Dwellings and the Anticipated Regulatory Control Measures <i>Author: Obusitse John Pule</i>	505
Contribution of a Master Program in Radiation Protection to Building Competencies in Morocco and Regionally <i>Authors: Oum Keltoum Hakam, Abdelmajid Choukri</i>	506
Promoting Nuclear Security Culture through the International Nuclear Security Education Network (INSEN) <i>Authors: Oum Keltoum Hakam, Guido Gluschke, Dmitriy Nikonov</i>	507
 Nuclear New Build – Integrating Cultural Differences in Radiation Protection <i>Authors: Peter A Bryant, Valentin Haemmerli, Peter Cole</i>	508
What to Say to the General Public: CT Doses are Safe or Causing Cancer? <i>Author: Pradip Deb</i>	509
The IAEA Safety Standards – Current and Future Perspectives <i>Author: Peter Johnston</i>	510
1,200 High School Students Involved in Radiation Protection Actions: Eight Years of Experience Feedback in Dissemination of Radiation Protection Culture. <i>Authors: Paul Livolsi, Thierry Schneider, Lucie D'Ascenzo, Sylvie Charron, Emmanuel Bouchot, Pascal Remond</i>	511
 Prudence in Radiation Protection - How Much? A Case Study <i>Author: Roger Coates</i>	512
Ethical Basis of Radiation Protection <i>Author: Richard Toohey</i>	513
The 1980 Sievert Lecturer: Lauriston S. Taylor <i>Author: Richard Toohey</i>	514
Management of Contaminated Goods in Post Accidental Situation: Synthesis of European Stakeholders' Panels <i>Authors: Sylvie Charron, Sandra Lafage, Jean-François Lecomte, Thierry Schneider, Pascal Crouail, Christophe Murith, Bruno Cessac, Vanessa Parache</i>	515
Establishment of a New Nuclear Regulatory Authority in Ghana <i>Authors: Stephen Inkoom, Geoffrey Emi-Reynolds, Emmanuel O. Darko, Abdel Razak Awudu, Joseph K. Amoako, Augustine Faanu, Margaret Ahiadeke, Ebenezer O. Appiah, Ann Mensah, Daniel N. Adjei, Adriana Nkansah</i>	516

Lessons learned from the Fukushima Dai-ichi accident and safety enhancements for the restart of nuclear power plants in Japan <i>Author: Shinichi Kawamura</i>	517
Accreditation Model of Courses in Radiation Protection in Medicine: One proposal to Latin America countries <i>Authors: Simone Kodlulovich Renha, Lidia Vasconcellos de Sá</i>	518
Development of Practical Guidance's for Workplace Monitoring in Nuclear and Radiation Facilities - an IAEA TECDOC Project <i>Authors: Suriya Murthy Nagamani, Jizeng Ma, Miraslov Pinak</i>	519
Management of Malaysian Nuclear Agency's License: Experiences and Challenges <i>Authors: Suzilawati Muhd Sarowi, Azimawati Ahmad, Mohd Fazlie Abdul Rashid, Noor Fadilla Ismail, Hairul Nizam Idris</i>	520
Microdistribution of Plutonium in Human Skeleton. Should we Change the ICRP Model? <i>Authors: Sergey Romanov, Ekaterina Lyovkina, Elena Labutina</i>	521
A Tool for Implementing the UNSCEAR Methodology for Estimating Human Exposures from Radioactive Discharges <i>Authors: Tracey Anderson, Kelly Jones, Helen Grogan, Ed Waller, Lynn Hubbard, Jane Simmonds</i>	522
International Standards for Managing Radionuclides in Food and Drinking Water <i>Authors: Tony Colgan, Carl Michael Blackburn, Maria Perez del Rosario, Igor Gusev</i>	523
Transition of Public Awareness and Its Factor Analysis Concerning Nuclear Energy and Radiation Application Based on Japanese Nationwide Fixed-Points Poll <i>Authors: Takeshi Iimoto, Kazuhisa Kawakami, Hiroshi Kimura, Masayuki Tomiyama, Makoto Funakoshi, Noriaki Sakai, Itaru Takahashi, Yumiko Kawasaki</i>	524
Communicating Radiological Concepts in Plain Language: The Value of International Consistency <i>Authors: Ted Lazo, Maria Perez, Shengli Niu, Miroslav Pinak, Carl Blackburn, Pablo Jimenez, Stephan Mundigl, Malcolm Crick, Chris Clement, Renate Czarwinski</i>	525
ICRP Stakeholder Dialogues: Lessons for the International Community <i>Author: Ted Lazo</i>	526
Management of Protection through Prevailing Circumstances: Interpretation of the ICRP System of Radiological Protection <i>Author: Ted Lazo</i>	527
Plain Language We Can All Understand <i>Author: Ted Lazo</i>	528
Developing Radiation Protection Culture at School: The Experience of the 2015 France-Japan High School Students Radiation Protection Workshop in Fukushima <i>Authors: Thierry Schneider, Daniel Ayrault, Sylvie Charron, Takashi Hara, Ryugo Hayano, Claire Schneider, Hiroyuki Takano</i>	529
Measurement and Data Analysis Concepts Combined with Data Assimilation Techniques for Source Term Reconstruction and Dose Assessment <i>Authors: Ulrich Stoehlker, Martin Bleher, Florian Gering</i>	530
Optimizing a Commercial Radiation Portal Monitor for Spot Traffic Controls <i>Authors: Udo Strauch, Reto Linder, Eike Hohmann, Rouven Philipp, Sabine Mayer</i>	531
Training as Awareness Factor and Dissemination of the Brazilian Nuclear Area <i>Authors: Valéria Pastura, Antonio Carlos Mol, Ana Paula Legey, Eugenio Marins</i>	532
INSTN: The Most Complete Training Centre for First Time Nuclear Plant Workers <i>Author: Vial Thierry</i>	533
Comparison between Brazilian Radiation Protection Norm and the Basic Safety Standards Published in 2014 <i>Authors: Wagner De Souza Pereira, Alphonse Kelecom, Ademir Xavier Da Silva</i>	534

Licensing of Nuclear Facilities in Brazil: Radiological Aspects <i>Authors: Wagner de Souza Pereira^{a,b}, Ana Cristina Lorençob, Alphonse Kelecom, Ademir Xavier da Silva</i>	535
The Principle of Low Risk and Optimization and the Connection with the ALARA concept. Exemption, Exclusion and Clearance <i>Authors: Wagner De Souza Pereira, Alphonse Kelecom, Ademir Xavier Da Silva</i>	536
The State of the Art about the Radiation Protection System in the World <i>Authors: Wagner de Souza Pereira, Alphonse Kelecom, Ademir Xavier da Silva</i>	537
The Importance of Including the Human Error Factor and Decision Making in Training and Education Programs to Avoid Radiological Incidents of Accidents <i>Author: Walter Truppa</i>	538
Individual Monitoring for External Exposure of Users at Synchrotron Radiation Facilities and New Solutions <i>Authors: Xiaobin Xia, Guanghong Wang, Jianzhong Zhou, Pingan Fei, Sixin Liu</i>	539
VOLUME 2	
Area 3: Medical	540
Pediatric Head CT examination doses in two university teaching Hospitals in Tunisia <i>Authors: Bouaoun Abir, Latifa Ben Omrane, Azza Hammou</i>	541
Spanish Radiation Protection Association (SEPR) Working Groups in Radiation Protection in Medicine <i>Authors: Gil-Agudo, Antonio; Ruiz-Cruces, Rafael; Almansa-López, Julio; Torres-Cabrera, Ricardo; Martí-Climent, Josep María; Sanjuanbenito-Ruiz de Alda, Waldo; Prieto-Martín, Carlos; Macías-Dominguez, Maria Teresa</i>	545
Regulatory T cells (Tregs) as a possible prognostic marker in radiation skin injury <i>Authors: Ana Julia Molinari, Mercedes Portas, Andrés Rossini, Severino Michelin, Diana Dubnera</i>	549
Head and Neck Immobilization Masks: Increase in Dose Surface evaluated by EBT3, TLD-100 and PBC Method <i>Authors: Arnie Verde Nolasco, Luiz Oliveira Faria</i>	555
MCNPX versus DOSXYZnrc in patient specific voxel-based phantom calculations <i>Authors: Banafsheh Zeinali-Rafsanjani, Kamal Hadad, Mahdi Saeedi-Moghadam, Reza Jalli</i>	563
Justification of CT examinations National surveys in Sweden <i>Authors: Carl Bladh, Torsten Cederlund, Sven Richter</i>	566
The transposition and the practical implementation of the Council Directive 2013/59/Euratom in the medical field in Romania <i>Author: Constantin Milu</i>	569
Level 2 justification is now part of the national system for introduction of new health technologies within the specialist health service in Norway <i>Authors: Eva G. Friberg, Reidun Silkosef, Ingrid E. Heikkilä, Jan F. Unhjem</i>	576
Proposed diagnostic reference levels for coronary angiography, left ventriculography and pacemaker placement in South Africa: 3-year improvement from 2012-2015 <i>Authors: Hendrik Johannes de Vos, Christoph Jan Trauernicht</i>	583
Procedure for measurement of Intrinsic Efficiency of a High Energy Collimator Gamma camera <i>Authors: Hugo Pérez-García, Raquel Barquero, Monica Gómez-Incio</i>	592
Simulation of a High Energy Collimator Gamma camera with MCNPX <i>Authors: Hugo Pérez-García, Raquel Barquero, Monica Gómez-Incio</i>	597
Local Computed Tomography Dose Index and Dose Length Product Values Agree with Published European DRLs <i>Authors: I. Garba, A. M. Tabari, A. Dare, M. Yahuza, M. Barde, M. Abba</i>	602
A Review of Occupational Radiation Exposure among Medical Professionals in Canada (1985-2006) <i>Author: Jing Chen</i>	607

The use of the Monte Carlo simulation method for assessing the radiation burden of the hands of workers during some risky manipulations with radiopharmaceuticals <i>Authors: Jana Hudzietzová, Marko Fülöp, Pavol Ragan, Jozef Sabol, P. Povinec,</i>	613
Y Radiation dose optimization in paediatric conventional imaging using automatic dose data management software <i>Authors: Luis Alejo, Eva Corredoira, Zulima Aza, Rodrigo Plaza-Núñez, Antonio Serrada</i>	618
Practical Lessons for a Dosimetry Program <i>Authors: Michelle Baca, Chad Hopponen</i>	627
Large scale multi-national studies on radiation protection of children in CT <i>Author: Madan M. Rehani</i>	635
Extension of the IAEA-International Nuclear and Radiological Event Scale (INES) for Medical Events <i>Authors: Marc Valero, Maria Luisa Ramirez Vera, Nera Belamaric</i>	640
Control of Radiation Exposure to Pediatric Patients at Conventional Radiology and Cardiac Centers at Dubai Hospital <i>Authors: Najlaa K. Almazrouei, Jamila S. Alsuwaidi, Adel H. Hashish</i>	649
Radioprotection in Radiosynovectomy Concerning Accompanying Persons and the Public <i>Authors: Susie Medeiros Oliveira Ramos, Sylvia Thomas, Mônica Araújo Pinheiro, Mirta Bárbara Torres Berdeguez, Lidia Vasconcellos de Sá, Sergio Augusto Lopes de Souza</i>	657
Physicians' Knowledge about patient Radiation Exposure from CT Examinations: Case of Hassan II Hospital Agadir-Morocco <i>Authors: Slimane Semghouli, Bouchra Amaoui, Abdelmajid Choukri, Oum Keltoum Hakam</i>	663
Changes in patients' radiation doses during CT exams in Japan (1997-2014) <i>Authors: Shoichi Suzuki, Yuuta Matsunaga, Ai Kawaguchi, Kazuyuki Minami, Masanao Kobayashi, Yasutaka Takei, Yasuki Asada</i>	669
Estimation of response characteristics for radiophotoluminescent glass dosimeters in X-ray diagnosis by using Monte Carlo simulation method <i>Authors: Toshioh Fujibuchi, Emi Ishibashi</i>	674
Small size OSL dosimeter to measure patient exposure dose in X-ray diagnosis - Evaluation of invisibility <i>Authors: Tohru Okazaki, Hiroaki Hayashi, Kazuki Takegami, Yoshiki Mihara, Natsumi Kimoto, Yuki Kanazawa, Takuya Hashizume, Ikuo Kobayashi</i>	678
Analysis of reasons for the multiple scans of paediatric CT examinations: Finding whether there is possible confounding by indication. <i>Authors: Takayasu Yoshitake, Koji Ono, Tsuneo Ishiguchi, Michiaki Kai</i>	684
A Multi-Center Study on Eye Lens Radiation Doses for Medical Staff Performing Non-Vascular Interventional Procedures in Japan <i>Authors: Kosuke Matsubara, Yasutaka Takei, Ikuo Kobayashi, Hiroshige Mori, Kimiya Noto, Shoichi Suzuki, Takayuki Igarashi, Keiichi Akahane</i>	686
FTS (Fused Toes Homolog) can be a Target to Modulate Radiosensitivity in Uterine Cervix Cancer Cells and Normal Cells <i>Authors: Arunkumar Anandharaj, Senthilkumar Cinghu, Won-Dong Kim, Jae-Ran Yu, Woo-Yoon Park</i>	687
Standardized and Automated Risk Assessment Forms for a Dutch Radiation Organization <i>Authors: Arjanka Bandstra, Marcel Wiegman</i>	688
Bonn Conference 2012 - Implementation of Results <i>Author: Axel Böttger</i>	689
Radiological Zoning and Radiation Exposure Assessment of External Staff in the CHU-Ibn Rochd-Casablanca Nuclear Medicine Service <i>Authors: Abdelmajid Choukri, Said Ouzouh, Oum Keltoum Hakam, Rachida El Gamoussi, Amal Guensi</i>	690
Multistep Optimization Approach in Medical Radiology - The Patient Imperative <i>Author: Andrejs Dreimanis</i>	691


R Y Advanced aspects of radiation protection in the use of particle accelerators in the medical field <i>Authors: Angelo Infantino, Gianfranco Cicoria, Giulia Lucconi, Davide Pancaldi, Sara Vichi, Federico Zagni, Domiziano Mostacci, Mario Marengo</i>	692
French Recommendations on the Conditions of Implementation of “New Techniques and Practices” in Radiotherapy <i>Authors: Aurelie Isambert, Eric Lartigau, Albert Lisbona, Philippe Cadot, Sylvie Derreumaux, Olivier Dupuis, Jean-Pierre Gérard, Dominique Ledu, Marc-André Mahé, Vincent Marchesi, Jocelyne Mazurier, Aurelien De Oliveira, Olivier Pharé, Marc Valero, Bernard Aubert</i>	693
A Cross-sectional Study of Nuclear Cardiology Practices and Radiation Exposure in Africa: Results from the IAEA Nuclear Cardiology Protocols study (INCAPS) <i>Authors: Andrew J. Einstein, Salah Bouyoucef, Thomas Pascual, Mathew Mercuri, Mboyo D.T.W. Vangu, Adel Allam, Madan Rehani, Ravi Kashyap, Maurizio Dondi, Diana Paez</i>	694
Quality Control of Radiography X-ray Generators in Kerman Province, South-Eastern Iran <i>Authors: Ali Jomehzadeh, Zahra Jomehzadeh, Mohammadbagher Tavakoli</i>	695
Occupational Dose Profiles of Radiation Workers in Oman Hospitals: A 5-year Dose Analysis <i>Authors: Arun Kumar L. S., Jamal Al-Shanfari, Saeed Al-Kalbani</i>	696
Investigation of Potential Use of ¹²⁴Xe-incorporated Amorphous Si Films in Brachytherapy <i>Authors: Alexandre Leal, Telma Fonseca, Lucas Reis</i>	697
Evaluation of Patient Dose in Interventional Cardiology <i>Authors: Ayoub Momivand, Reza Zohdiaghdam, Zhaleh Behrouzki, Ebrahim Khayati Shal</i>	698
Review of Radiation Safety in Medical Diagnosis in Kenya <i>Author: Arthur Omondi Koteng</i>	699
Study on Incidence of Radiation Induced Cataract among Radiographers in Interventional Fluoroscopy <i>Authors: Aruna Pallewatte, Suvini Karunaratne, MPN Piyasena</i>	700
The Impact of Fluoroscopic Technique on Incidence of Radiation Injuries in Neurointervention <i>Author: Aruna Pallewatte</i>	701
Tandem KAP Meters Calibration Parameters by Monte Carlo Simulation using Reference RQR Radiation Qualities <i>Authors: Ademar Potiens Jr., Nathalia Costa, Eduardo Correa, Lucas Santos, Vitor Vivolo, Marie Da Penha Potiens</i>	702
The IAEA Latin American Working Group on Internal Dosimetry of Radionuclides in Human Body <i>Authors: Ana Rojo, Nancy Puerta, Bernardo Dantas, Arlene Reis, Mariella Teran, Rodolfo Cruz Suarez</i>	703
The Effect of Single Catheter on Patient and Operator Radiation Dose during Trans-radial Coronary Angiography <i>Authors: Ali Tarighatnia, Amirhossein Mohammadalian, Alireza Farajollahi, Morteza Ghojzade</i>	704
The Impact of Both Radial & Pelvic Lead Shields on Operator Radiation Exposure during Trans-radial Coronary Procedures <i>Authors: Ali Tarighatnia, Aida Khaleghifard, Amirhossein Mohammadalian, Alireza Farajollahi, Morteza Ghojzade</i>	705
R Establishing Diagnostic Reference Levels for Conventional X-ray Procedures in the Russian Federation <i>Author: Aleksandr Vodovatov</i>	706
Computing Calibration Factor with Visual Monte Carlo – VMC simulations of an Accident Contamination with ^{99m}Tc <i>Authors: Bruno Mendes, Fernanda Paiva, Marco Aurelio Lacerda, John Hunt, Telma Fonseca</i>	707
Establishing the Quality Management Baseline in the use of Computed Tomography Machines in Kenya <i>Authors: Bernard Ochieng, Geoffrey Korir, Jeska Wambani</i>	708
Radiation Exposure in Interventional Procedures <i>Authors: Bernard Ochieng, Geoffrey Korir, Jeska Wambani</i>	709

Study on the Effects of Gorkha Earthquake in Radiological Facilities (Nepal) <i>Authors: Buddha Ram Shah, Shanta Lal Shrestha, Kanchan Prasad Adhikary</i>	710
Evaluation of Important Physical Parameters in Micro Beam Radiotherapy of Lung Tumors <i>Authors: Banafsheh Zeinali-Rafsanjani, Mohammad-Amin Mosleh-Shirazi, Mahdi Haghatafshar, Mahdi Saeedi-Moghadam</i>	711
Dicentric Assay in DTC Patients with High Dose Radioiodine Therapy <i>Authors: Chung Mei-Ling, Huang Ying-Fong, Chen Yu-Wen, Jong Shiang-Bin, Lai Yung-Chang</i>	712
Animal Sporting Events and Radioprotection Management <i>Authors: Roy Catherine, Audigie Fabrice, Coudry Virginie, Malet Christophe, Sgro Geraldine</i>	713
Occupational Exposure Observations at Groote Schuur Hospital <i>Authors: Christoph Trauernicht, Tobie Kotzé</i>	714
R Comparison of Primary Doses Obtained in Three 6 MV Photon Beams Using a Small Attenuator <i>Author: C Trauernicht</i>	715
Detector Dependence of the Measured Spectra of the OncoSeed IMC6711 Iodine-125 Seed <i>Authors: Christoph Trauernicht, Paul Papka, Peane Maleka, Egbert Hering, Freek Du Plessis</i>	716
Measured Anisotropy of the OncoSeed IMC 6711 Iodine-125 Seed <i>Authors: Christoph Trauernicht, Paul Papka, Egbert Hering, Freek Du Plessis</i>	717
The Monte Carlo Simulation Study of Secondary Neutron Dose for Proton Therapy at Samsung Medical Center using FLUKA <i>Authors: Chae Young Lee, Jin Sung Kim, Yong Hyun Chung, Sungkoo Cho, Dae-Hyun Kim, Youngyih Han, Jongho Kim, Yunho Kim, Sangmin Lee, Chan Woo Park</i>	718
Biological Effects of Radioactive Hot Particles on the Human Lung. Assessment of the Cancer Risk <i>Authors: Diana Apostolova, Zdravko Paskalev</i>	719
Mathematical Modeling of Dose Profile of a Dental Facilities <i>Authors: Deise Diana Lava, Diogo da Silva Borges, Maria de Lourdes Moreira, Antonio Cesar Ferreira Guimarães</i>	720
In Young Women: Justification of Breast Ultrasound Rather than Combined Breast Ultrasound and Mammography. Radiation Protection Perspective <i>Authors: Dina Salama, Hanan Gewfel</i>	721
Cone Beam CT Patient Dose in Paediatric Cardiac Catheterization Procedures <i>Authors: Eva Corredoira Silva, Luis Alejo Luque, Eliseo Vañó Carruana, Cristina Koren, Rodrigo Plaza, Antonio Serrada, Carlos Huerga Cabrerizo</i>	722
Proposal of a spreadsheet to monitor units verification for intracranial radiosurgery treatments <i>Authors: Erick Hernandez, Ricardo Contreras, Miguel Ortega</i>	723
Establishment of National Dose Reference Levels (DRLs) for Digital Mammography Practices at the UAE <i>Authors: Fatima Al Kaabi, Najla Al Mazrouei, Jamila AlSuwaidi, Jacek Janaczek, Alfani Al Ameri, Sara Booz, Wadha AlShamsi</i>	724
Risk of a Second Kidney Carcinoma Following Childhood Cancer: Role of Chemotherapy and Radiation Dose to Kidneys <i>Authors: Florent de Vathaire, Boris Schwartz, Chiraz El-Fayech, Rodrigue Allodji, Bernard Escudier, Mike Hawkins, Ibrahima Diallo, Nadia Haddy</i>	725
Developing Light Nano-Composites with Improved Mechanical Properties for Neutron Shielding <i>Authors: Fatemeh Jamali, SMJ Mortazavi, MR Kardan, Sedigheh Sina, MA Mosleh-Shirazi, Jila Rahpeyma</i>	726
Evaluation of the Scattered Radiation Field in an Interventional Radiology Room <i>Authors: Francesca Mariotti, Paolo Ferrari, Lorenzo Campani, Elena Fantuzzi, Luisa Pierotti, Pier Luca Rossi</i> ..	727
In Vivo Dosimetry for the Measurement of Doses to Breast Cancer Patients During External Beam Radiotherapy Treatment, using the Optically Stimulated Luminescence (OSL) Dosimeters at the Douala General Hospital, Cameroon <i>Authors: Fokou Mvoufo, Samba Richard</i>	728

UNSCEAR's Assessment of Medical Exposure <i>Author: Ferid Shannoun</i>	729
Radiation Dose in Childhood Cancer Management: Challenges and Recommendations for Dose Reduction <i>Author: Hamid Abdollahi</i>	730
Review and Evaluation of Imaging Methods and Analysis of Images Obtained by Magnetic Resonance Imaging to Determine the Absorbed Dose in the Phantom by Polymer Gel Dosimetry <i>Authors: Hamed Dehghani, Amin Farzadnia, Saeed Shanehsazzadeh, Yazdan Salimi, Jalal Ordoni, Dariush Askari, Mohammad Hossein Jamshidi</i>	731
Standard Calibration of Ionization Chambers Used in Radiation Therapy Dosimetry and Evaluation of Uncertainties <i>Authors: HyoJin Kim, Sung Jin Noh, Hyun Kim, Sang koo Kang, Manwoo Lee, Dong Hyeok Jeong, Kwangmo Yang, Yeong-Rok Kang</i>	732
Radiological Risk Assessment in Tunisian University Hospital <i>Authors: Hager Kamoun, Samar Kallela, Mohamed Faouzi Ben Slimane</i>	733
An Automated Mechanical Quality Assurance System for Medical Accelerators using a Smartphone <i>Authors: Hwiyoung Kim, Il Han Kim, Hyunseok Lee, Sangmin Lee, Sung-Joon Ye</i>	734
Patient Doses in a Hybrid Operating Room <i>Authors: Hugo Perez-Garcia, Carlos Andrés Rodríguez, Manuel Agulla Otero, Ricardo Torres Cabrera, Raquel Barquero Sanz</i>	735
Comparison of Patients CTDI from Two Different "Make" 16-SLICE CT Scanners in Maiduguri North Eastern Nigeria <i>Authors: Idris Garba, Aisha Abba Kato, Auwal Abubakar, Chogozie Nwobi, Mansur Yahuza, Nasiru Isha Fagge</i>	736
Hearing Radiation and its Application to in Vivo Radiation Dosimetry during Radiation Treatment <i>Authors: I.J. Kima, J.H. Kim, C.Y. Yi, C.H. Kim, J.S. Kim, E.Y. Park, Y.H. Jung</i>	737
Effectiveness of Dose Modulation Technique of CT scan on Organ Dose <i>Authors: Il Park, Seung Cheol Oh, Kwang Pyo Kim</i>	738
Application of Prospective Approaches in Preventing Accidental Exposure in Radiotherapy: A Review of Italian Experiences <i>Authors: Ivan Veronese, Marie Claire Cantone, Luisa Begnozzi</i>	739
Survey of Radiation Protection in Patients Undergoing X-ray Medical Examination <i>Authors: Justina Achuka, Mojisola Usikalu</i>	740
Long Half-Life Isotopes Europium-152 and Europium-154 Found in Hospital Waste <i>Authors: Janneke Ansems, Bunna Damink, Jelle van Riet, Corinne Valk, Ruud Hack</i>	741
Prospective Risk Assessment of the Use of Radioactive Iodine-125 Seeds for the Localisation of Impalpable Breast Lesions <i>Authors: Janneke Ansems, Bunna Damink, Jelle van Riet, Pieter Buijs, Els Vanaert</i>	742
Global Developments in DRLs and Assessment of Medical Exposures <i>Author: John Damilakis</i>	743
Persistence of Dicentric Chromosomes associated with Telomere Dysfunction: A Biomarker of Prognosis in Patients Undergoing Total Body Irradiation <i>Authors: Julien Dossou, Theodore Girinsky, Dominique Violot, Jean-Henri Bourhis, Eric Lartigaux, Luc Morat, Claude Parmentier, Radhia M'kacher</i>	744
Dosimetric Analysis with the Specifically Selected Low-Dose Threshold on Gamma Evaluation for VMAT QA <i>Authors: Ji-Hye Song, Min-Joo Kim, So-Hyun Park, Seu-Ran Lee, Min-Young Lee, Dong Soo Lee, Tae Suk Suh</i>	745

Y The Influence of the Dose Calculation Resolution of VMAT Plans on the Calculated Dose for Eye Lens and Optic Apparatus <i>Authors: Jong Min Park, So-Yeon Park, Jung-in Kim, Hong-Gyun Wu, Jin Ho Kim</i>	746
R Monte Carlo Estimation of Effective Dose to Patients Undergoing Contrast Based X-Ray Fluoroscopy Procedures <i>Authors: J. E Ngaile, P. Msaki, R. Kazema</i>	747
An Assessment of Radiographers' Technical and Protective Performance in Hospitals Affiliated to Birjand University of Medical Sciences in 2012 <i>Authors: Jalal Ordoni, Saeid Ghasemi, Dariush Askari, Yazdan Salimi, Fatemeh Ramrodi, Mohammad Hossein Jamshidi, Hamed Dehghani</i>	748
Patient Radiation Safety Control in Nuclear Medicine Practices in View of the New Basic Safety Standards (BSS) <i>Authors: Jamila S AlSuwaidi, Priyank Gupta, Shabna Miyath</i>	749
New X-ray Technology Results in 70% Dose Reduction in Pacemaker and Implantable Cardioverter Defibrillator (ICD) Implantations <i>Authors: Joris van Dijk, Jan Paul Ottervanger, Peter Paul Delnoy, Martine Lagerweij, Siert Knollema, Cornelis Slump, Piet Jager</i>	750
The Study on the Interspace Materials of Radiographic Anti-Scattering Grid with Monte Carlo Calculation <i>Authors: Jun Woo Bae, Hee Reyoung Kim</i>	751
¹³¹I Activity in the Thyroid in Members of the Nuclear Medicine Medical Personnel <i>Authors: Kamil Brudecki, Aldona Kowalska, Pawel Zagrodzki, Artur Szczodry, Tomasz Mroz, Pawel Janowski, Jerzy Wojciech Mietelski</i>	752
Impact of Earthquake on Radiological Facilities in Kathmandu Valley <i>Authors: Kanchan P. Adhikari, Yaduram Panthi, Deepak Subedi</i>	753
Radiation Dose from Whole Body F-18 FDG PET/CT: Nationwide Survey in Korea <i>Authors: Keon Wook Kang, Hyun Woo Kwon, Jong Phil Kim, Jin Chul Paeng, Hong Jae Lee, Jae Sung Lee, Gi Jeong Cheon, Dong Soo Lee, June-Key Chung</i>	754
Using I-125 Seeds for Localisation; a Retrospective Overview of Radiation Safety Issues <i>Author: Linda Janssen-Pinkse</i>	755
Activimeter Response Behaviour Analysis Related to Well Depth <i>Authors: Lilian Kuahara, Eduardo Corrêa, Maria da Penha Potiens</i>	756
Digital Breast Tomosynthesis: Preliminary Results of Patient Radiation Dose Survey in a Brazilian Facility <i>Authors: Larissa Oliveira, Fernando Mecca, Simone Renha</i>	757
Measurement of Entrance Skin Dose for Pediatric Patients during Cardiac IVR <i>Authors: Lue Sun, Yusuke Mizuno, Takashi Moritake</i>	758
New Concept: Reduction of Dose of the Lens <i>Authors: Lue Sun, Yuji Matsumaru, Takashi Moritake</i>	759
Development of a Specialization Program in Radiation Protection: Proposal to CPLP <i>Authors: Lidia V. Sá, Simone K. Renha</i>	760
Diagnostic Reference Levels in CT: First Experience in one Major Hospital in Algeria <i>Authors: Merad Ahmed, Khelassi-Toutaoui Nadia, Mansouri Boudjema</i>	761
Occupational Radiation Exposure in Nuclear Medicine <i>Authors: Mashari Alnaaimi, Mohammed Alkhoryaf, Fareda Alkandri, Mousa Aldouij, Mohamed Omer, Nawaf Abughath, Talal Salhudeen</i>	762
High Voltage Consideration to Determine the Dose Received by Patient in Conventional Radiology <i>Authors: Mbolatiana Anjarasoa Luc Ralaivelo, Andriambololona Raelina, Edmond Randrianarivony, Solofonirina Ravelomanantsoa, Hery Fanja Randriantseheno, Ralainirina Dina Randriantsizafy, Tiana Harimalala Randriamora, Veroniaina Raharimboangy, Tahiry Razakarimanana, Hary Andrianarimanana Razafindramiandra</i>	763

Diagnostic Reference Levels for Fluoroscopically Guided Interventions at a Major Australian Hospital <i>Authors: Mohamed Badawy, Tegan Clark</i>	764
Image Quality and Patient Dose Assessment in Simple Radiographic Examinations in Ghana <i>Authors: Mary Boadu, Stephen Inkoom, Cyril Schandorf, Geoffrey Emi-Reynold, Emmanuel Akrobortu</i>	765
Determination of attenuation properties of lead glasses used in the catheterization laboratory <i>Authors: Marcin Brodecki, Marek Zmyslony</i>	766
Dose Reassessment Applied in Routine TL Dosimetry by using the PTTL method in LADIS Laboratory <i>Authors: Maciej Budzanowski, Renata Kopec, Anna Bieniarz-Sas</i>	767
Occupational Doses of Medical Staff in Interventional Cardiology Procedures and Correlations with Patient Dose Levels <i>Authors: Maciej Budzanowski, Agnieszka Szumska, Renata Kopec</i>	768
Out-of-field Dose and Risk of Radiogenic Second Cancer for children Treated with Craniospinal 3D-Conformal RadioTherapy or TomoTherapy <i>Authors: Marijke De Saint-Hubert, Željka Knežević, Natalia Adamek, Marija Majer, Liliana Stolarczyk, Remy Savelli, Vedran Rajevac, Saveta Miljanić, Pawel Olko, Roger M. Harrison, Filip Vanhavere, Dirk Verellen, Lara Struelens</i>	769
Evaluation of Thyroid Function after Radiotherapy for Patients with Breast Cancer <i>Authors: Masomeh Dorri Gav, Seyed Mahmood Reza Aghamiri, Mohammd Hossien Bahreini Toosi</i>	770
Preliminary Diagnostic References Levels of Audit CT at Aristide LeDantec National Hospital <i>Authors: Magatte Diagne, Fama Gning, Mamadou Moustapha Dieng, Latifatou Gueye</i>	771
Frequency of Overscan in Standard CT Protocols <i>Authors: Michael Galea, Mohamed Badawy</i>	772
Overview of the Activities on Eye Lens Dosimetry within EURADOS WG 12 (Dosimetry in medical imaging) <i>Authors: Merce Ginjaume, Isabelle Clairand, Eleftheria Carinou, Olivera Ciraj Bjelac, Paolo Ferrari, Marta Sans-Merce, Jad Farah, Frank Becker, Vadim Chumak, Josiane Daures, Joanna Domienik, Zoran Jovanovic, Renata Kopec, Dragana Krstic, Agnieszka Szumska, Denisa Nikodemova, Pedro Teles, Sara Principi, Filip Vanhavere, Željka Knežević</i>	773
Imaging for Saving Kids - Improving Radiation Safety in Paediatric Radiology <i>Authors: Donald Frush, Lawrence Lau, Maria del Rosario Perez, Michael G Kawooya</i>	774
Evaluation of Survived Neuronal Tissue Area around Brain Tumor Lesions Post Radiation Therapy by Diffusion-weighted Imaging (DWI) <i>Authors: Mohammad Hossein Jamshidi, Alireza Eftekhari Moqadam, Jafar Fatahi, Hamid Behrozi, Yavar Shahvali, Jalal Ordoni, Yazdan Salimi, Dariush Askari, Hamed Dehghani</i>	775
Surveying the Relationship between Brain CT Scan Findings in Children with a Clinical Signs and Determining the Appropriate Indications for Requesting CT Scan <i>Authors: Mohammad Hossein Jamshidi, Hamid Behrozi, Dariush Askari, Jalal Ordoni, Yazdan Salimi, Hamed Dehghani</i>	776
Radiation Emergency Medicine Preparedness: Web-Based Reporting of News and Events from SREMC to Target Expert Groups <i>Authors: Marita Lagergren Lindberg, Karin Lindberg, Rolf Lewensohn, Giuseppe V., Masucci, Jack Valentin, Leif Stenke</i>	777
Evaluation of Organ Doses and Cancer Risk from Paediatric Head CT Examination – Phantom Study <i>Authors: Marija Majer, Željka Knezevic, Saveta Miljanic, Liu Haikuan, Weihai Zhuo</i>	778
Radiation Protection Optimization in I-131 Therapy of Thyroid Cancer to Ablate Postthyroidectomy Remnants or Destroy Residual or Recurrent Tumour <i>Author: Mario Medvedec</i>	779
Operational Radiation Safety with Y-90 Microspheres <i>Authors: Mark Miller, Charles Martin III</i>	780

In-Vivo Tooth Dosimetry Using L Band EPR. The Research Involving Human Subjects Related to Fukushima Nuclear Power Plant Accident <i>Authors: Minoru Miyake, Ichiro Yamaguchi, Yasuhiro Nakai, Hiroshi Hirata, Naoki Kunugita, Harold Swartz</i>	781
Establishment of Local DRLs on Standard Radiographic Examinations and Estimation of Cancer Risk for Paediatric and Adult Patients at Two Tunisian Hospitals <i>Authors: Mohamed Mogaadi, Latifa Ben Omrane, Azza Hammou</i>	782
Audit of Clinical Image Quality in Chest Radiography using Visual Grading Analysis <i>Authors: Michael Sandborg, Jonas Nilsson Althen, Erik Tesselaar</i>	783
Radiation Protection in Medical Imaging and Radiation Oncology: A Cooperative Effort between IOMP and IRPA <i>Authors: Magdalena Stoeva, Richard Vetter, K.Y. Cheung, Renate Czarwinski, Francesca McGowan</i>	784
Monte Carlo Calculation of Neutron Doses to Organs of a Female Undergoing A Pelvic 18 MV Irradiation <i>Authors: Mansour Zabihzadeh, Seyyed Rabi Mahdavi, Mohammad Reza Ay, Zahra Shakarami</i>	785
Study of the Radiation Effect on the Biological Cellule DNA by Determination Bragg Peak Position of the Proton Beams <i>Authors: Noura Harakat, Jamal Inchaouh, Abdenbi Khouaja, Mohammed Benjelloun, Hamid Chakir, Said Boudhaim, Zouhair Housni, Mohamed Lhadi Bouhssa, Abdellatif Kartouni, Mohamed Reda Mesradi, Sara Stimade, Meriem Fiak, Mustapha Krim</i>	786
 Internal dose assessment of new ¹⁷⁷Lu-radiopharmaceuticals and its role in radiation protection of patients <i>Authors: Nancy Puerta Yepes, Ana Rojo, Sebastián Gossio, José Luis Crudo</i>	787
Design Shielding Assessment for a Nuclear Medicine Service <i>Authors: Osvaldo Brígido-Flores, José Hernández-García, Orlando Fabelo-Bonet, Adelmo Montalván-Estrada</i> 788	
Performance Study of Hybride Imaging SPECT/CT: Case of Nuclear Medicine Service - Ibn Sina Hospital in Rabat-Morocco <i>Authors: Oum Keltoum Hakam, Abdelmajid Choukri, Rajaa Sebihi, Youness Esserhir El Fassi</i>	789
Comprehensive quality audits in radiation oncology, diagnostic and interventional radiology <i>Authors: Ahmed Meghzifene, Ola Holmberg</i>	790
International Response to the Bonn Call for Action – from the Viewpoint of the Organizers of the Bonn Conference: the IAEA <i>Author: Ola Holmberg</i>	791
Assessment of the Practice of Optimizing Paediatric Doses in Conventional Radiography in Cameroon <i>Authors: Odette Ngano Samba, Jean Bernard Kamgang, Ariane Lynda Kengne Fonkam, Emmanuel Chi, Lukong Cornelius Fai, Jean Yomi</i>	792
Can Standard CT be replaced by Contrast Enhanced Ultra-low-dose CT with Iterative Reconstruction for the Screening of Patients Admitted with Acute Abdominal Pain? A Comparative Study <i>Authors: Pierre-Alexandre Poletti, Minerva Becker, Thomas Perneger, Christoph D Becker, Alexandra Platon</i>	793
Radiological and Dosimetrical Aspects of CO₂ Peripheral DSA: Optimization of X-ray Spectrum <i>Authors: Pier Luca Rossi, David Bianchini, Alessandro Lombi, Giacomo Feliciani, Manami Zanzi, Romano Zannoli, Ivan Corazza</i>	794
Establishment of National Diagnostic Reference Levels for Nuclear Medicine in Australia <i>Authors: Paul Marks, Toby Beveridge, Peter Thomas, Anna Hayton, Anthony Wallace</i>	795
Survey of Knowledge about Radiation Dose in Radiological Investigation in Kermanshah Hospitals, Iran <i>Authors: Rasool Azmoonfar, Hosein Faghirnavaz, Edalat Morovati, Hosein Younesi</i>	796
Measurement of ¹³¹I activity with a High Energy Gamma Camera <i>Authors: Raquel Barquero, Hugo Perez-Garcia, Monica Gomez-Incio</i>	797
Situation of Radiation Therapy, Cancer Diagnosis and Radiation Protection of Patients in Cameroon <i>Authors: Richard Ndi Samba, Augustin Simo, Ernest C. Nwabueze Okonkwo</i>	798

R Promoting Fluoroscopic Personal Radiation Protection Equipment: Unfamiliarity, Facts, and Fears <i>Author: Stephen Balter</i>	799
Traceability of the KAP-Meters Used for Patient Dosimetry in Radiodiagnostic <i>Authors: Sorin Bercea, Constantin Cenusă, Ioan Cenusă, Aurelia Celarel, Elena Iliescu</i>	800
Radiation Dose Assessment for Abdominal Computed Tomography <i>Authors: Seung Cheol Oh, Il Park, Kwang Pyo Kim</i>	801
Implementation on Methodology for the Calibration of well type chambers used in ¹⁹²Ir-Brachytherapy Sources <i>Authors: Stefan Gutierrez Lores, Gonzalo Walwyn Salas, Jorge Luis Morales</i>	802
Study of the ¹³¹I Thyroid Monitoring Measurements Using MCNP Simulations <i>Authors: Sebastián Gossio, Nancy Puerta, Ana Rojo</i>	803
Dosimetric Studies of Radionuclide Therapy of Neuroendocrine Tumors with ¹⁷⁷Lu-Dotatate <i>Authors: Santosh Kumar Gupta, Suhas Singla, Chandrasekhar Bal</i>	804
Managing the Gaseous Waste in Nuclear Medicine: A Novel Approach <i>Authors: Shahed Khan, Eleonora Santos</i>	805
Monitoring and Evaluating the Air Concentration of Radionuclides in the Vicinity of a Nuclear Medicine Facility <i>Authors: Shahed Khan, Eleanora Santos</i>	806
Neutron Measurement for Proton Therapy Facility at Samsung Medical Center with Wobbling and Line Scanning Mode using WENDI-2 <i>Authors: Sangmin Lee, Jin Sung Kim, Sungkoo Cho, Dae-Hyun Kim, Jungho Kim, Yunho Kim, Youngyih Han, Sung-Joon Ye, Chae Young Lee, Yong Hyun Chang</i>	807
Utilizing 3D Scanner/Printer for a Dummy Shield: Monte Carlo Dose Calculations on Artefact-free CT Images of a Metallic Shield for Electron Radiation Therapy <i>Authors: Jong In Park, Il Han Kim, Jaegi Lee, Hyeonseok Lee, Sung-Joon Ye, Sangmin Lee</i>	808
Comparison of Cadmium Zinc Telluride (CZT) with Photomultiplier Tube (PMT) Detectors in SPECT and Bismuth Germanate (BGO) in PET <i>Authors: Seyed Mohsen Zahraei-Moghadam, Mehdi Saeedi –Moghadam, Banafsheh Zenali –Rafsenjani, Masoumeh Dorri-Gev, Fatemeh Shekoochi –Shooli</i>	809
Nurses Knowledge of Ionizing Radiation and Radiation Protection during Mobile Radiodiagnostic Examinations <i>Author: Samuel Opoku</i>	810
Personal Radiation Monitoring of Occupationally Exposed Radiographers in the Biggest Tertiary Referral Hospital in Ghana <i>Author: Samuel Opoku</i>	811
Health Physicist Monitors Own Medical Dose from Radioiodine Thyroid Ablation Procedure <i>Authors: Sander Perle, Kip Bennett, Chad Hopponen, Michael Lantz</i>	812
R Evaluation of Eye Lens Doses of Interventional Cardiologists <i>Authors: Sumi Yokoyama, Shoichi Suzuki, Hiroshi Toyama, Shinji Arakawa, Satoshi Inoue, Yutaka Kinomura, Ikuo Kobayashi</i>	813
Development of Thermoplastic Mask set up Monitoring System using Force Sensing Resistor (FSR) Sensor <i>Authors: Tae Ho Kim, Siyong Kim, Min-Seok Cho, Seong-Hee Kang, Dong-Su Kim, Kyeong-Hyun Kim, Dong-Seok Shin, Tae-Suk Suh</i>	814
Measurements of Photon Spectra around IVR for the Evaluation of Eye-lens Dose <i>Authors: Tadahiro Kurosawa, Masahiro Kato, Sumi Yokoyama</i>	815
RADIREC: System for Mapping and Collecting Entrance Skin Dose during Neurointerventional Radiology <i>Authors: Takashi Moritake, Lue Sun, Koichiro Futatsuya, Satoru Kawauchi, Yasuhiro Koguchi, Mikito Hayakawa, Yuji Matsumaru</i>	816

Diagnostic Reference Levels (DRLs) for CT Examinations in Adults in Cameroon <i>Authors: Thierry Ndzana Ndah, Boniface Moifo, Mathurin Neossi Nguena</i>	817
The Dose Kernels for Pencil Beam and Differential Pencil Beam of Photons with Spectrum of Treatment Machine with ⁶⁰Co Source and their Analytical Approximations <i>Authors: Vladimir Klimanov, Alexey Moiseev, Maria Kolyvanova</i>	818
Radiation Protection of the Public and of the Immediate Family of a Patient Following the Therapy with Iodine-131 <i>Author: Youssef Ech Chaykhy</i>	819
A Study Evaluating the Dependence of the Patient Dose on the CT Dose Change in a SPECT/CT Scan <i>Authors: Young-Hwan Ryu, Ho-Sung Kim, Kyung-Rae Dong, Chang-Bok Kim, Yun-Jong Lee</i>	820
A Study on Quantitative Analysis of Exposure Dose Caused by Patient Depending on Time and Distance in Nuclear Medicine Examination <i>Authors: Young-Hwan Ryu, Ho-Sung Kim, Yun-Jong Lee, Kyung-Rae Dong, Jin-Kyu Kim, Chang- Bok Kim</i>	821
Medical Personnel Radiation Safety in Autopsies for Radiation Accidents <i>Author: Yulia Kvacheva</i>	822
Evaluating Patient Dose in Conventional Radiology for Ten Routine Projections in Tehran, Iran: Recommendation for Local Diagnostic Reference Levels <i>Authors: Yazdan Salimi, Mohammad Reza Deevband, Dariush Askari, Jalal Ordoni, Mohammad Hossein Jamshidi, Isaac Shiri, Hamed Dehghani, Hamid Behrozi</i>	823
Eye Lens Dosimetry: Measurement in Hospitals <i>Authors: Zina Cemusova, Daniela Ekendahl, Lucie Sukupova, Michael Zelizko, Martin Mates, Kamil Sedlacek, Jiri Novotny, Iva Krulova</i>	824
A National Audit Programme for Radiotherapy Centres <i>Author: Zakithi Msimang</i>	825
Calculation of Organs Doses and Secondary Cancer Risk during Mantle Field Radiotherapy for Hodgkin's Lymphoma <i>Authors: Zahra Shakarami, Mansour Zabihzadeh, Mohammad Javad Tahmasebi Birgani, MohammadAli Behrooz, Hojatollah Shahbazian</i>	826
Organ doses and associated cancer risks for CT examinations of thorax <i>Authors: Marija Majer, Željka Knežević, Jelena Popić Ramač, Hrvoje Hršak, Saveta Miljanić</i>	827
Optimization of image quality and patient dose in radiographs of paediatric extremities using direct digital radiography <i>Authors: Jones A., Ansell C., Jerrom C., Honey Id</i>	828
Area 4: General Ionising Radiation Protection	829
Side by Side Monitoring Test for Radon Emissions from an Underground Uranium Mine <i>Authors: Douglas Chambers, David Frydenlund, Jaime Massey, Ron Stager, Kathy Weinel</i>	830
From Radiation Solutions for Engineering Problems to Engineering Solutions for Radiation Problems: the uses of industrial radiation <i>Author: Edward Waller</i>	838
Patrimonial management of source term in French nuclear power plants <i>Authors: François Drouet, Serge Blond, Alain Rocher, Charlotte Dabat-Blondeau, François Renard, Samir Ider</i>	847
Public Dose Assessments for Atmospheric Pathways at Rössing Uranium Mine, Utilising Direct Monitoring Data <i>Author: Gunhild von Oertzen</i>	853
Health impact assessment of recovery/disposal options of sewage sludge: methodology and critical parameters <i>Authors: Hélène Caplin, Alain Thomassin</i>	862
Criticality Safety and Control System for Nuclear Fuel Fabrication Plant <i>Authors: H. A. Elsayed, M. K. Shaat, M. E. Nagy, S. A. Agamy</i>	869

Study on the transfer of Polonium-210 from soil and sediment to cattle in a catchment area influenced by gold mining <i>Author: Immanda Louw</i>	876
Release Fractions from Airborne Fluid and Slurry Spills <i>Authors: Judith Ann Bamberger, John A. Glissmeyer</i>	884
Basic Characterization of a Radioactive Facility and Evaluation of Risk Agents <i>Authors: Carneiro, J. C. G. G., Alves, A. S., Sanches, M. P., Rodrigues D. L., Levy, D. S, Sordi, G. M. A. A</i>	892
Supervision of German miners at small underground construction sites of old mining to prevent high radon exposures <i>Author: Jörg Dehnert</i>	900
Analysis of Gamma-Ray Skyshine Contribution to Dose Rates Exterior to an Above-Ground Waste Storage Facility Using Radiation Transport Models <i>Authors: Jenelle Mann, Norbert Zoeger, Roman Koppitsch, Alexander Brandl</i>	905
Use of Real-Time Radon Progeny Monitors in Uranium Mines <i>Authors: John Takala, Andre Boucher, Mikhail Ioffe, Kari Toews</i>	912
Verification of main shielding bodies at Atucha-2 during full power operation <i>Authors: Martin Brizuela, Felipe Albornoz, Elianna Cuello</i>	917
Newcomers, new build – the industry view <i>Author: Marcel Lips</i>	921
Lanthanides Patterns as a Nuclear Forensic Signature from a Uranium Mine in South Africa <i>Authors: Manny Mathuthu, Ntokozo Khumalo, Malayita M. Baloyi, Refilwe N. Maretela</i>	925
A Review of Gamma Cell 220 Research Irradiator External Dose Rates <i>Authors: Michael Shannon, Ryan Howell, Spencer Mickum, Robert Rushton</i>	931
Interpretation of Data Collected During Individual Monitoring of Uranium Dioxide Exposure: Collective Dose Assessment <i>Authors: N. Blanchin, E. Davesne, E. Blanchardon, E. Chojnacki, D. Franck, M. Ruffin</i>	936
Monte Carlo analyses for BNCT using near-threshold $^7\text{Li}(p,n)$ neutrons <i>Radiation source, shielding, activation, and external exposure</i> <i>Authors: Noriaki Nakao, Kazuaki Kosako, Noriyosu Hayashizaki, Tatsuya Katabuchi, Tooru Kobayashi</i>	943
Nuclear New Build – Disseminating Radiation Safety Culture in the Supply Chain <i>Authors: Peter A. Bryant, Peter Cole</i>	952
On the ingestion of Cs-137 at Volincy municipality in Belarus about 30 years after the Chernobyl accident <i>Authors: Peter Hill, Petro Zoriy, Herbert Dederichs, Burkhard Heuel-Fabianek, Jürgen Pillath</i>	960
In preparation for future reduction of the dose limit for the lens of the eye – an assessment at Swedish nuclear facilities <i>Author: V. Nilsson</i>	968
Findings of radiological events in the Centre of Isotopes in Cuba <i>Author: Zayda Haydeé Amador Balbona</i>	974
Occupational Exposure in Production of Radiopharmaceuticals and Labeled Compounds in Cuba <i>Authors: Zayda Haydeé Amador Balbona, Miguel Antonio Soria Guevara</i>	984
Estimation of air born radioactivity induced by 8GeV class electron LINAC accelerator <i>Author: Yoshihiro Asano</i>	993
Principles of Formation of Risk Groups for Occupational Diseases for Workers of Facilities Using Nuclear Energy during Obligatory Medical Examinations in the Russian Federation <i>Authors: Andrey Kretov, Andrey Bushmanov, Alexander Samoilov</i>	1002

PREDO – A Strengthened Dose Assessment for Routine Discharges by Swedish Nuclear Installations <i>Authors: Anna Maria Blixt Buhr, Helene Alpfjord, Rodolfo Avila, Roman Bezhenar, Robert Broed, Anna Fermvik, Eva Grusell, Kenneth Häggkvist, Vladimir Maderich, Veronika Rensfeldt, Synnöve Sundell-Bergman, Cor W.M Timmermans, Stefan Willemsen, Govert deWith</i>	1003
Improvement of the Dose Estimation in Case of an Occupational ²⁴¹Am Incorporation Event <i>Authors: Anna Pántya, Andor András, Tamás Pázmándi, Péter Zagyvai</i>	1004
Argentinian Intercomparison on Interpretation of Data from Internal Exposure Sceneries for Dose Assessment <i>Authors: Ana Rojo, Nancy Puerta, Sebastian Gossio, Inés Gomez Parada</i>	1005
Economic Losses of the Nuclear Industry Related to Loss of Workers Occupational Disability for Medical Reasons <i>Authors: Alexander Samoilov, Andrey Bushmanov, Andrey Kretov</i>	1006
3A vii Safety and Risk Assessment Safety Assessment for Non-Reactor Facilities <i>Author: Bethany Louise Cawood</i>	1007
RadProtect® Increases Survival Rate in Novel Murine Slow and Low (S&L) Irradiation Model <i>Authors: Chia-Hung Chen, Jen-Ling Wang, Wei-Chuan Liao, Chau-Hui Wang, Tzu-ying Hung, Alan Liss</i>	1008
Development of Mesh-Type ICRP Reference Phantoms and its Implications <i>Author: Chan Hyeong Kim</i>	1009
Devaluation of Rhinoceros Horn through Nuclear Techniques <i>Authors: Charles Kros, Jan Rijn Zeevaart, Arnaud Faanhof, Frikkie de Beer, Deon Kotze, Dave Hudson-Lamb, Frederik Botha, Gawie Nothnagel</i>	1010
The Radiological and Health Impacts to the Residents of the Tudor Shaft Informal Settlement <i>Authors: Dawid de Villiers, Gert Liebenberg, Rean Swart, Rietha Oosthuizen, Juanette John, Hanlie Liebenberg-Enslin, Didintle Modisamongwe, Grant Walters</i>	1011
Mathematical Modeling of the Aging Process of the Containment Spray Injection System using the Fault Tree Method <i>Authors: Diogo da Silva Borges, Deise Diana Lava, Maria de Lourdes Moreira, Antonio Cesar Ferreira Guimarães</i>	1012
Determination of the Detection Efficiency of ¹³¹I in Thiroid using Monte Carlo Method <i>Authors: Dayana Ramos Machado, Yoan Yera Simanca, Gladys M. López Bejerano, Nancy Acosta Rodriguez</i>	1013
Uranium Aerosols in Nuclear Fuel Manufacturing <i>Authors: Edvin Hansson, Håkan Pettersson, Christine Fortin, Mats Eriksson</i>	1014
The Future Free Electron Laser Facility SwissFEL from a Radiation Protection Point of View <i>Authors: Eike Hohmann, Roland Luescher, Elisa Musto, Albert Fuchs, Sabine Mayer</i>	1015
Assessment of Beam Dump Activation for RAON Heavy Ion Accelerator in Korea <i>Authors: Eunjoong Lee, Cheolwoo Lee, Sungchul Yang, Young-Ouk Lee, Kyeongjin Park, Gyuseong Cho</i>	1016
Area Monitoring on Nuclear Fuel Cycle Facilities <i>Authors: Elizabeth Renteria, Paula Nuñez, Analia Saavedra, Nestor Fruttero, Allan Segato</i>	1017
How Spanish Nuclear Power Plant have Implemented Lessons Learned from the Fukushima Accident in the Radiation Protection Field <i>Author: Eduardo Sollet</i>	1018
Setting up an Occupational Radiation Protection Program in NORM Industry: A Case Study in Mining Industry in the Democratic Republic of the Congo <i>Authors: Francois Kazadi Kabuya, Vincent Lukanda Mwamba, Leonard Woto Makontsh, Robert Lwamba Ilonda</i>	1019

Monitoring and Mapping of Radon Concentration within Ghana Atomic Energy Commission <i>Authors: Francis Otoo, Emmanuel Ofori Darko, Massimo Garavaglia, Concettina Giovani, Silvia Pividore, Bentil Aba Andam, Geoffrey Emi-Reynolds, Lucas Piccini</i>	1020
GIS Mapping and Background Ionizing Radiation (BIR) Assessment of Solid Mineral Mining Sites in Enugu State, Nigeria <i>Authors: Avwiri Gregory, Agbalagba Ezekiel, Osimobi Jude, Ononugbo Patience</i>	1021
Using a Portable Neutron Generator in an Open Field: The Radiation Protection Assessment <i>Authors: Gian Marco Contessa, Nadia Cherubini, Alessandro Dodaro, Luigi Lepore, Giuseppe Augusto Marzo, Sandro Sandri</i>	1022
Testing of Burn-up Calculation Method based on Chebyshev Rational Approximation with IAEA-ADS Benchmark <i>Authors: Guangyao Sun, Wending Fan, Lijuan Hao, Binhang Zhang, Jing Song, Pengcheng Long, Liqin Hu</i> ..	1023
Assessment of Occupational Exposure of ‘Conflict Mineral’ Artisanal Mine Workers via Radiogenic and Dosimetric Characterization of High Background Radiation Area (HBRA) Columbite-Tantalite (Coltan) <i>Authors: Hudson Angeyo Kalambuka, Leon Ntihakose, Jayanti Patel, David Maina</i>	1024
 Towards a Novel Modular Architecture for CERN Radiation Monitoring <i>Authors: Hamza Boukabache, Michel Pangallo, Nicola Cardines, Gael Ducos, Antonio Bellotta, Ciarán Toner, Daniel Perrin, Doris Forkel-Wirth</i>	1025
Assessment of Internal Dose due to Intake of Food for Determination of Representative Person in Normal Operation of Nuclear Power Plant <i>Authors: Hyungjoon Yu, Insu Chang, Jungil Lee, Jang-Lyul Kim, Bonghwan Kim</i>	1026
Practical use of Graph Theory to Reduce the Individual Doses of the Employees Working in Areas with High Background Radiation <i>Authors: Iliia Kudrin, Ivan Mazur, Konstantin Chizhov, Victor Kryuchkov</i>	1027
Development and Implementation Experience of Information-Analytical System of Radiation Safety of Workers <i>Authors: Ivan Mazur, Iliia Kudrin, Chizhov Konstantin, Kryuchkov Viktor</i>	1028
Recent Developments in Occupational Exposure Reduction in Nuclear Power Plants <i>Authors: Jason Harris, David Miller</i>	1029
Practical Impacts of NORM Standards on Mining and Minerals Processing <i>Author: Jim Hondros</i>	1030
Radiation Protection in the South African Mining and Minerals Extraction Industries <i>Author: James Larkin</i>	1031
Improved Approach to Estimate Fission Product Inventory using TRITON in SCALE 6.1 for a Nuclear Reactor with Gadolinium Burnable Poison <i>Authors: Jaehoon Song, Kyoyoun Kim</i>	1032
The Field Characterization Around the High Energy X-ray Cargo Screenings <i>Authors: Kamil Szewczak, Katarzyna Woloszczuk</i>	1033
Occupational Exposure during Fusion Research on PF-1000 Unit <i>Authors: Kamil Szewczak, Slawomir Jednorog</i>	1034
Room Submersion Calculations of Noble Gas Dose Rate Coefficients <i>Authors: Ken Veinot, Shaheen Dewji, Michael Bellamy, Keith Eckerman, Nolan Hertel, Mauritius Hiller</i>	1035
Residual Activity in Lead and Bismuth Materials induced by 100-40 MeV Protons <i>Authors: Leila Mokhtari Oranj, Nam-Suk Jung, Joo-Hee Oh, Hee-Seock Lee</i>	1036
Security of Radioactive Materials in Oil & Gas Industry (Compliance & Challenges) <i>Author: Mohammad Aref</i>	1037
Egypt Experience with Research Reactors Operation, Nuclear and Radiological Activities Law as a Step for Building Nuclear Power Reactors <i>Author: Mohamed Goma</i>	1038

Direct Measurement of Radium Levels in Waste Water Samples using Portable Medium Resolution Gamma Spectrometers <i>Authors: Michael Iwatschenko-Borho, Scott Masiella, Richard Oxford, James Williams</i>	1039
Practical Application Illustrating Excellence in Radiological Protection at the Koeberg Nuclear Power Station <i>Author: Marc Maree</i>	1040
Improvement of Underground Radon Concentrations at a South African Gold Mine <i>Author: Marc Vermeijs</i>	1041
Building Nuclear Security Culture in Morocco <i>Authors: Oumkeltoum Hakam, Abdelmajid Choukri, Taha Laghouazi</i>	1042
The Role of Radiation Protection in Nuclear Forensics: From the Crime Scene to the Laboratory <i>Authors: Philemon Magampa, Gedion Nkosi</i>	1043
EcoMine – A Software Package based on Ecolego to Assess the Radiological Impact of Mining Sites and Activities <i>Authors: Rodolfo Avila, Erik Johansson, Japie van Blerk</i>	1044
U and Th Source Term Characterisation in Selected Gold Tailings of the Witwatersrand (South Africa): A Geochemical Modelling and Reaction Network Approach <i>Authors: Robert Hansen, Japie Van Blerk</i>	1045
Radiation Protection Research <i>Author: Rebecca Tadesse</i>	1046
Radiation Protection Aspects of Uranium In Situ Recovery / In Situ Leach Facilities <i>Author: Steven Brown</i>	1047
Worker Protection Implications of the Solubility and Human Metabolism of Modern Uranium Mill Products <i>Authors: Steve Brown, Douglas Chambers</i>	1048
Dust Management on Tailings Storage Facilities at a South African Gold Mine <i>Authors: SJ van Wyk, CF Human</i>	1049
Risk of Radon Induced Health Effect: Evaluation Methods and Practical Application <i>Authors: Sergey Kiselev, Vladimir Demin</i>	1050
Comparison of the Efficacy of Neutron Shielding of Aluminum and Polyethylene Composites Containing Micro and Nano-Sized B₄C and Carbon Nanotubes <i>Authors: SMJ Mortazavi, Fatemeh Jamali, MR Kardan, Sedigheh Sina, MA Mosleh-Shirazi, Jila Rahpeyma</i>	1051
Assessment on Occupational Exposure in Malaysia: Practices and Trends <i>Authors: Suzilawati Muhd Sarowi, John Konsoh, Ahmad Bazlie Abdul Kadir</i>	1052
Advance Determination of Respiratory Protection Needs when Performing Destructive Work on Structural Materials <i>Author: Scott Schwahn</i>	1053
Reduction in Doses and Lung Cancer Risks among Canadian Uranium Miners between 1930s and 2013 <i>Authors: Tristan Barr, Pascale Reinhardt, Patsy Thompson, Douglas Chambers, Ron Stager, Occupational Cancer Research Center</i>	1054
Operational Health Physics Development Activities Related to Fast Reactor Fuel Fabrication and Pyro-Reprocessing <i>Authors: Ravi T, Akhila R, Krishnakumar D N, Rajagopal V, Jose M T, Venkatraman B, Satyamurthy S A V</i>	1055
The Information System on Occupational Exposure (ISOE): Trends and Lessons <i>Authors: Tae-Won Hwang, Olvido Guzman</i>	1056
Protecting Humans and the Environment the Next Hundred Thousands of Years <i>Authors: Ulrik Kautsky, Eva Andersson, Tobias Lindborg, Anders Löfgren, Sara Nordén, Peter Saetre</i>	1057

Assessment of Belarusian NPP for Protection of the Public <i>Author: Viktoryia Kliaus</i>	1058
Development of a Dose Assessment Code for the Radiation Protection of Representative Person in Korea <i>Authors: Won Tae Hwang, Eun Han Kim, Moon Hee Han, Hae Sun Jeong</i>	1059
Effect of Particle Size and Percentages of Boron Carbide on the Thermal Neutron Radiation Shielding Properties of HDPE/B4C Composite: Experimental and Simulation Studies <i>Authors: Zahra Soltani, Farhood Ziaie</i>	1060

VOLUME 3

Area 5: Optimisation and Design of New Facilities	1061
Monte Carlo Modeling and Verification of the Shielding for an Ionizing Radiation Test Laboratory <i>Authors: C. Stettner, N. Baumgartner, M. Blaickner, C. Hranitzky</i>	1062
Preconcentration of cobalt metal ions onto imprinted polymer hydrogels <i>Authors: Ghada A. Mahmoud, Hegazy E. A, S. M. Elbakery</i>	1065
Dose Constraint – a Mysterious Concept of Radiation Protection <i>Author: Helena Janžekovič</i>	1072
Establishment of a Laboratory for Gamma-ray Spectrometry of Environmental Samples Collected in Fukushima <i>Authors: Jun Saegusa, Tomoyuki Yoda, Satoshi Maeda, Tsutomu Okazaki, Shuichi Otani, Toshio Yamaguchi, Yoshiyuki Kurita, Atsushi Hasumi, Chushiro Yonezawa, Minoru Takeishi</i>	1078
New Remote Controlled Experiments in Nuclear Chemistry <i>Authors: Jan-Willem Vahlbruch, Wolfgang Schulz, Claudia Fournier, Paul Hanemann, Sebastian Büchner, Clemens Walther</i>	1086
Introduction and assessment of new heavy weight concrete shields using Monte Carlo simulation <i>Authors: Mahdi Saeedi-Moghadam, Mahdi Kazempour, Sedigheh Sina, Reza Jalli, Banafsheh Zeinali-Rafsanjani</i>	1094
Exposure Rate Assessment From Selected Cathode Ray Tube Devices <i>Authors: Ife-Adediran O. O., Arogunjo A. M.</i>	1100
 Case Study: Radiation Protection measures when designing an extension of a Nuclear Medicine Department <i>Authors: Youness Esserhir El Fassi, Jean-Élie Fontaine, Mathieu Valla, Siham El Moghni, Youness Haddoudi, Paul Livolsi, Abdelmajid Choukri, Oum Keltoum Hakam</i>	1108
Optimization of occupational exposure during first operations with ¹⁸F in Cuba <i>Author: Zayda Haydeé Amador Balbona</i>	1117
The Role of the Radiological Protection Team as a Stakeholder in the Design Phase of a Nuclear Facility: the Case of Brazilian Conversion Plant <i>Authors: Ana Cristina Lourenço, Wagner de Souza Pereira</i>	1126
Design Study of ELI-NP Beam Dumps: Radioprotection Issues and Monte-Carlo Simulations <i>Authors: Adolfo Esposito, Oscar Frasciello, Maurizio Pelliccioni</i>	1127
Preliminary Thermo-mechanical Design of the Main Dump for the High Energy Electron Beam Lines in ELI-NP <i>Authors: Adolfo Esposito, Lina Quintieri</i>	1128
Radioprotection Issues for the STAR Project <i>Authors: Adolfo Esposito, Oscar Frasciello, Fiorello Martire, Maurizio Pelliccioni</i>	1129
Cyclotron Production of Sc and V Radionuclides from Natural Titanium for Medical Applications <i>Authors: Ahmed Rufai Usman, Mayeen Uddin Khandaker, Hiromitsu Haba, Naohiko Otuka</i>	1130
Design Approval and Registration for Radiation Devices <i>Authors: BokHyoung Lee, SangEun Han, KiWon Jang, JongRae Kim, WooRan Kim, KyungWha Kim, Younjin Park</i>	1131

Preliminary Analysis of Radiation Characteristic for 250 MeV Proton Accelerator Driven Sub-critical System	
<i>Authors: Bin Li, Qi Yang, Bo Chang, Chao Liu, Liqin Hu</i>	1132
New CZT (H3D) Technology Employed at Cook Nuclear Plant Achieves Immediate Individual Isotopic Identification and Verifies Adequacy of Temporary Shielding	
<i>Author: David Miller</i>	1133
Radiation Protection for NORM Industries – Results of the European Joint Research Project ‘Metrology for Processing Materials with High Natural Radioactivity (MetroNORM)	
<i>Authors: Franz Josef Maringer, Sylvie Pierre, Teresa Crespo Vazquez, Monika Mazanova, Pierino De Felice, Branko Vodenik, Mario Reis, Mikael Hult, Laszlo Szücs, Simon Jerome, Alexander Muring, Roy Pöllänen, Andreas Baumgartner, Boris Bulanek, Boguslaw Michalik, Nathalie Michielsen, Julian Dean, Philippe Cassette, Franz Kabrt, Hannah Moser</i>	1134
Effectiveness of the Shielding Mechanism in Rooms Housing X-ray Diagnostic Equipment - A Case Study of Mulago Hospital	
<i>Authors: Festo Kiragga, Rebecca Nakatudde, Akisophel Kisolo</i>	1135
KIRDI’S Role in the Project “Promoting Safety, Self-reliance and Sustainability of Non-Destructive (NDT) Testing Facilities”	
<i>Author: Humphrey Lumadede</i>	1136
Requirements for Specific Safety Issues - Fire, Earthquake, and Flooding – at Large Particle Accelerator Facilities	
<i>Authors: Hee-Seock Lee, Arim Lee, Nam-suk Jung, Joohee Oh, Leila Mokhtari Oranj</i>	1137
Modernisation of the Radiation Monitoring Systems at Research and Training Reactors in Hungary	
<i>Authors: János Petrányi, Dénes Elter, Imre Szalóki, Máté Solymosi, László Manga</i>	1138
Environmental Radiation and Meteorological Monitoring Systems of a Greenfield Nuclear Power Plant	
<i>Authors: Juho Rissanen, Jussi Huutilainen</i>	1139
Evaluation of Carbon -14 Released from Small Power Reactor	
<i>Authors: Kyo-Youn Kim, Ha-Young Kim, Jae Hoon Song</i>	1140
Development of a Methodology to Correlate Safety Classification of Components to the Maintenance Programme of a Facility	
<i>Author: Muhammad Akbar</i>	1141
Applicability of Lessons Learned from the Fukushima Accident to Radioactive Material Users	
<i>Authors: Shawn Smith, Catherine Haney</i>	1142
Local Shield Model around Beam Target Stations using Radiation Transport Code MCNPX	
<i>Authors: Tebogo Kupi, Johann van Rooyen, Raymond Njinga</i>	1143
Validation of Experimental Measurements of Activity for Radioisotopes in SAFARI-1 Reactor	
<i>Author: Tholakele Ngeleka</i>	1144
Robotic HPGe Spectrometer for Radionuclide Analysis	
<i>Authors: Vladimir Gostilo, Alexander Sokolov</i>	1145
Area 6: Radiation Detection and Dosimetry	1146
A New Approach to Worker Internal Dosimetry and its Impact on Radiation Protection	
<i>Authors: Alan Birchall, Vadim Vostrotin, Matthew Puncher, Alexander Efimov, Bruce Napier</i>	1147
Approach to uncertainties in exposure, dose and risk estimates for uranium workers within the CURE project	
<i>Authors: Augusto Giussani, Sophie Ancelet, Derek Bingham, Eric Blanchardon, Richard Bull, Estelle Davesne, James Grellier, Olivier Laurent, Dominique Laurier, Matthew Puncher, Tony Riddell</i>	1155
Joint Coordinating Committee on Radiation Effects Research Project 1.1: Techa River Population Dosimetry	
<i>Authors: Bruce A Napier, Marina O Degteva, Evgenia I Tolstykh, Natalia B Shagina, Elena A Shishkina, Marina I Vorobiova, Nickolay G Bougrov, Lynn R Anspaugh</i>	1162

Joint Coordinating Committee on Radiation Effects Research Project 2.4: Mayak Worker Dosimetry <i>Authors: Bruce Napier, Alexander Efimov, Alan Birchall, Vadim Vostrotin, Matthew Puncher, Alexandra Sokolova, Klara Suslova, Scott Miller, Alexay Zhdanov, Evgeney Vasilenko</i>	1168
Waterfowl-specific Computational Models for use in Internal Dosimetry <i>Authors: Dawn Montgomery, Jennifer Paloni, Nicole Martinez</i>	1174
Project 1.2b: Techa River Population Cancer Morbidity and Mortality <i>Authors: Daniel O. Stram, Lyudmila Krestinina, Dale Preston, Alexander Akleyev</i>	1182
Assessment of equivalent dose of the lens of the eyes and the extremities to workers under nonhomogeneous exposure situation in nuclear and accelerator facilities by means of measurements using a phantom coupled with Monte Carlo simulation <i>Authors: Hiroshi Yoshitomi, Masayuki Hagiwara, Munehiko Kowatari, Sho Nishino, Toshiya Sanami, Hiroshi Iwase</i>	1188
Implementation of Co-worker Models for the Reconstruction of Dose under an Occupational Radiation Exposure Compensation Program <i>Author: James W. Neton</i>	1196
Experience with Wound Dosimetry in Uranium Mining and Processing <i>Authors: John Takala, Kari Toews</i>	1204
Response of $^{10}\text{B}+\text{ZnS}(\text{Ag})$ as neutron detector in Radiation Portal Monitors <i>Authors: Karen A. Guzmán-García, H.R. Vega-Carrillo, Eduardo Gallego, Alfredo Lorente, Juan A. González</i>	1213
Wrist, finger, and crystalline dosimetry study with radiopharmacists and nursing technicians for various applications and tests, using various radiopharmaceuticals, for adjustment of a percentage factor between difference values obtained at the extremities to optimize the dosimetry in nuclear medicine services. <i>Authors: Maria Inês Calil Cury Guimarães, Sato, Karen A. K., Leandro F. Souza, Leia R. Santo, Elaine C. Santo, Ivani B. Melo, Heber S. Videira, Julia A. Gonzalez, Carlos A. Buchpiguel, Josefina da Silva Santos, Adélia Sahyun</i>	1221
Direct Surface Contamination Measurement of Low Energy Beta and Electron Capture Isotopes <i>Authors: Michael Iwatschenko-Borho, Reinhard Loew</i>	1224
The Facility of Radiation Standards in Japan Atomic Energy Agency, present status and its research works on dosimetry <i>Authors: Munehiko Kowatari, Hiroshi Yoshitomi, Sho Nishino, Yoshihiko Tanimura, Tetsuya Ohishi, Michio Yoshizawa</i>	1230
Evaluation of radiation detectors for a possible integration into the automated survey system TIM in the Large Hadron Collider (LHC) <i>Authors: Markus Widorski, Frédéric Aberle, Cristina Adoriso, Daniel Perrin</i>	1239
Investigations into Radiation Dose Distribution in a Computed Tomography Fluoroscopy Room: Monte Carlo Studies <i>Authors: Prince Kwabena Gyekye, Frank Becker, Geoffrey Emi-Reynolds</i>	1245
PIMAL: A GUI-Driven Software Package To Conduct Radiation Dose Assessments Using Realistic Phantom Postures <i>Authors: Shaheen Dewji, Mauritius Hiller, Nolan Hertel, Sami Sherbini, Mohammad Saba</i>	1251
Comprehensive Study on the Response of Neutron Dosimeters in Various Simulated Workplace Neutron Calibration Fields <i>Authors: Sho Nishino, Katsuya Hoshi, Norio Tsujimura, Munehiko Kowatari, Tadayoshi Yoshida</i>	1258
Estimation of basic characteristics about scintillation type survey meter using multi pixel photon counter <i>Author: Toshioh Fujibuchi</i>	1264
Comparison of dose rate measurements of commercially available hand- held gamma detectors with radiation protection dose meter <i>Authors: Theo Köble, Hermann Friedrich</i>	1268
Estimation of detective efficiency of CdZnTe semiconductor detector and NaI(Tl) scintillation detector <i>Authors: Takatoshi Toyoda, Toshioh Fujibuchi</i>	1273

A study of Energy-Compensating Metal Filter of Semiconductor Detector for Personal Dosimetry in X-ray Diagnosis <i>Authors: Kento Terasaki, Toshioh Fujibuchi, Hiroo Murazakic, Taku Kuramoto, Yoshiyuki Umezu, Yang Ishigaki, Yoshinori Matsumoto</i>	1279
Determination of fission radionuclides activities in a real fission gamma-ray field <i>Authors: Žlebčík P. , Malá H., Huml O.</i>	1285
Radiation-induced Color Bleaching of Methyl Red in Polyvinyl Alcohol (PVA) Film Dosimeter <i>Authors: Awad Alzahrany, Ahmed Basfar, Khalid Rabaeh</i>	1293
Characterization of HPGe Detectors using Computed Tomography <i>Authors: Angelica Hedman, Jalil Bahar Gogani, Micael Granström, Lennart Johansson, Jonas Andersson, Henrik Ramebäck</i>	1294
Optimized Detector for in Situ Low Energy Gamma Spectrometry in Close Geometries <i>Authors: Angelica Hedman, Göran Ågren, Lennart Johansson, Jalil Bahar Gogani, Henrik Ramebäck</i>	1295
Delineation of Radiation Dose Pattern in Radiation Workers and Dose Optimization Using Dose Reduction Methodologies <i>Authors: Ajai Kumar Shukla, Dhiraj Kumar Tewari</i>	1296
Establishment of a National Dose Register in South Africa <i>Authors: Alan Muller, Nthabiseng Mohlala</i>	1297
Public In Vivo Thyroid Monitoring for Dose Estimation after Accidental Intake of I-131. Experiences from Scandinavia <i>Authors: Asser Nyander Poulsen, Henrik Roed, Lilián del Risco Norrlid, Mats Isaksson, Bjorn Lind, Óskar Halldórson Holm, Jussi Huikari</i>	1298
Comparison of Radiation Dose Assessment Methodology used for the Public Living in the Area Contaminated with Radioactive Materials <i>Authors: A Ra Go, Min Jun Kim, Kwang Pyo Kim</i>	1299
Argentinian Intercomparison Exercise on Internal Dosimetry: ¹³¹I Thyroid Monitoring <i>Authors: Ana Rojo, Nancy Puerta, Sebastian Gossio, Ines Gomez Parada</i>	1300
Performance Comparison of OSLD (Al₂O₃:C) and TLD (LiF:Mg,Cu,P) in Accreditation Proficiency Testing <i>Authors: Alexander Romanyukha, Mathew Grypp, Anthony Williams</i>	1301
Test of Ring, Eye Lens and Whole Body Dosemeters for the Dose Quantity Hp(3) to be used in Interventional Radiology <i>Authors: Agnieszka Szumska, Renata Kopeć, Maciej Budzanowski</i>	1302
From Filter Swipe Test to Bioavailability: A Rapid Experimental Approach to Assess Actinide Behaviour Following Internal Contamination <i>Authors: Anne Van der Meeren, Agnès Moureau, Sylvie Coudert, Pierre Laroche, Jaime Angulo, Nina Griffiths</i>	1303
Microphotonics Approaches to Nuclear Forensics Analysis <i>Authors: Bobby Bhatt, Hudson Angeyo, Alix Dehayem-Massop</i>	1304
Determination of Scattering Factors Associated to the In Vivo Monitoring of Iodine-131 in the Thyroid <i>Authors: Bernardo Dantas, Fabiana Lima, Ana Leticia Dantas, Eder Lucena, Rodrigo Gontijo, Carlaine Carvalho, Clovis Hazin</i>	1305
μ-TPC: A New Recoil Nuclei Telescope for Low Energy Neutron Fields characterization <i>Authors: Benjamin Tampon, Daniel Santos, Olivier Guillaudin, Jean-François Muraz, Lena Lebreton, Thibaut Vinchon, Nadine Sauzet</i>	1306
A Passive Neutron Dosimeter for Measurement in Mixed Neutron-Photon Fields <i>Authors: Sören Mattsson, Maria Christiansson, Christian Bernhardsson</i>	1307
 The Russian Human Radiobiological Tissue Repository: A Unique Resource for Studies of Plutonium-Exposed Workers <i>Authors: Christopher Loffredo, David Goerlitz, Svetlana Sokolova, Leonidas Leondaridis, Mariya Zakharova, Valentina Revina, Evgeniya Kirillova</i>	1308

Characterization and Measurement of Dosimetry X-ray Bean on Kenya <i>Authors: Collins Omondi, David Otwoma</i>	1309
® International Standards on Radioactivity Measurement for Radiological Protection: Status and Perspectives <i>Authors: Dominique Calmet, Roselyne Ameen, Aude Bombard, Stephane Brun, Francois Byrde, Jing Chen, Jean-Marie Duda, Maurizio Forte, Marc Fournier, Ales Fronka, Thomas Haug, Margarita Herranz, Amir Husain, Simon Jerome, Martin Jiranek, Steven Judge, Sang Bog Kim, Pieter Kwakman, Jeanne Luyen, Montse LLaurado, Rolf Michel, David Porterfield, Andry Ratsirahonana, Anthony Richards, Katerina Rovenska, Tetsuya Sanada, Christoph Schuler, Laurence Thomas, Shinji Tokonami, Andrey Tsapalov, Takahiro Yamada</i>	1310
A Method for Response Time Measurement of Ionization Chamber Type Survey Meter <i>Authors: Dehong Li, Bin Guo, Jianwei Wang, Di Wu, Xingdong Li</i>	1312
The Primary Standard for Air Kerma at the NIM for the Gamma Radiation of 137Cs <i>Authors: Dehong Li, Peiwai Wang, Jianwei Huang, Bin Guo, Di Wu</i>	1313
Dosimetry for Radiological Protection at the New Research Facility, ELI-NP <i>Authors: Elena Iliescu, Sorin Bercea, Iani Mitu, Aurelia Celarel, Constantin Cenusu</i>	1314
Determination of a Urine Reference Level for an Individual Monitoring Programme for Uranium <i>Author: Frik Beeslaar</i>	1315
Data Recording Regarding the Dose Assessment due to X-ray Generator Sources and the ²⁴¹Am Calibration Curve Usefulness <i>Authors: Felicia Mihai, Ana Stochioiu, Catalina Tuca</i>	1316
® Integrated Operational Dosimetry System at CERN <i>Authors: Gérald Dumont, Fernando Baltasar Dos Santos Pedrosa, Pierre Carbonez, Doris Forkel- Wirth, Pierre Ninin, Eloy Reguero Fuentes, Stefan Roesler, Joachim Vollaire</i>	1317
Biodosimetry of in Vitro Human Lymphocytes exposed to ⁶⁰Co γ-rays and DNA Incorporated ¹²³I <i>Authors: Hein Fourie, Jacobus Slabbert, Richard Newman, Philip Beukes, Neil Rossouw</i>	1318
Development of Radiation Portal Monitoring System based on Energy Weighted Algorithm for Gamma Spectroscopy <i>Authors: Hyuncheol Lee, Wook-Geun Shin, Han Rim Lee, Chang-Il Choi, Chang-Su Park, Hong- Suk Kim, Chul Hee Min</i>	1319
Results of the EURADOS Intercomparisons IC2014 on Whole Body Dosimeters for Photons <i>Authors: Hannes Stadtmann, Tom Grimbergen, Andrew McWhan, Ana Maria Romero, Markus Figel, Christian Gärtner</i>	1320
Improving Potential in a Retrospective Dosimetry using Common Plastics by Extracting Inorganic Materials <i>Authors: Insu Chang, Jang-Lyul Kim, Jungil Lee, Tae-Hyoung Kim, Seung-Kyu Lee, Bong-Hwan Kim</i>	1321
Performance of Eye Lens Dosimeters in use in Europe <i>Authors: Isabelle Clairand, Merce Ginjaume, Filip Vanhavere, Eleftheria Carinou, Josiane Dures, Marc Denoziere, Edilaine Honorio da Silva, Maria Roig, Sara Principi, Laurent Van Rychehem</i>	1322
Contemporary Radiation Protection Trends – Do we need a New Yype of Digital Personal Dosimeters to be used in Medicine, Homeland Security, Environmental Protection and Emergencies? <i>Authors: Ivica Prlic, Marija Suric Mihic, Mladen Hajdinjak, Tomislav Mestrovic, Zdravko Cerovac</i>	1323
Rare-earth Doped Silica Fibres for Dosimetry Applications in Medicine <i>Authors: Ivan Veronese, Mauro Fasoli, Norberto Chiodini, Eleonora Mones, Cristina De Mattia, Eduardo D'Ippolito, Marie Claire Cantone, Anna Vedda</i>	1324
DosiKit, Innovative Solution for On-site External Radiation Biodosimetry <i>Authors : Julie Bensimon, Caroline Bettencourt, Sandrine Altmeyer, Arnaud Tupinier, Nicolas Ugolin, Sylvie Chevillard</i>	1325
Analysis of Photon Energy Distribution at the Working Places in Nuclear Power Plants Using In-situ CZT Detectors <i>Authors: Jeongin Kim, Seokon Kang, Meeseon Jeong</i>	1326

Monte Carlo Approach to Accidental Dose Reconstruction Based on the EPR Measurements of Absorbed Dose to Human Teeth <i>Authors: Jeongin Kim, Hoon Choi, Byoungil Lee</i>	1327
 Development of two new single-exposure, multi-detector neutron spectrometers for radiation protection applications in workplace monitoring <i>Authors: J.M. Gómez-Ros, R. Bedogni, D. Bortot, C. Domingo, A. Esposito, M.V. Introini, M. Lorenzoli, G. Mazzitelli, M. Moraleda, A. Pola, D. Sacco</i>	1328
The Influence of the Dose Calculation Resolution of VMAT Plans on the Calculated Dose for Eye Lens and Optic Apparatus <i>Authors: Jong Min Park, So-Yeon Park, Jung-in Kim, Hong-Gyun Wu, Jin Ho Kim</i>	1329
Dosimetry Aspects for the Development of an Irradiator for Cross-linking of Cables using ⁶⁰Co Gamma Rays <i>Authors: Jain Reji George, B K Pathak</i>	1330
Development and Applications of Super Monte Carlo Simulation Program for Advanced Nuclear Energy Systems <i>Authors: Jing Song, Liqin Hu, Pengcheng Long, Tao He, Lijuan Hao, Mengyun Cheng, Huaqing Zheng, Shengpeng Yu, Guangyao Sun, Tongqiang Dang, Qi Yang, Bin Wu, Chaobin Chen, Ling Fang, Yican Wu, FDS Team</i>	1331
Study of Eye Lens Dose at the Nuclear Industries in Sweden <i>Authors: Lisa Bäckström, Karin Andgren</i>	1332
Direct Ion Storage Dosimetry Roadmap <i>Authors: Kip Bennett, Michael Lantz, Matti Vuotilla, Jani Rakkola</i>	1333
Implementation of a New BeOSL Dosimetry Platform Utilizing Lean Manufacturing Tools <i>Authors: Kip Bennett, Mike Lantz, Joel White, Gordon Sturm, Reiner Esser, Timo Wiedenmann, Jay Thomas</i>	1334
  Monte Carlo calibration of the whole body counting detection system for <i>In Vivo</i> measurement of people internally contaminated with ⁹⁰Sr <i>Authors: Karin Fantinová, Pavel Fojtík, Irena Malátová</i>	1335
Backscatter Response of Different Personal Dosimeter Detectors for Water Slab and Cylindrical Calibration Phantoms <i>Authors: Kristine Marie Romallosa, Hiroshi Yoshitomi</i>	1336
Dosimetric Uncertainty Analysis of the Optically Stimulated Luminescence Dosimeter System in the Philippines <i>Authors: Kristine Marie Romallosa, Marianna Lourdes Grande, Estrella Caseria</i>	1337
Development of the Electronic Personal Dosimeter Based on Scintillator for a Mobile Phone Application <i>Authors: Kyeongjin Park, Daehee Lee, Hyunjun Yoo, Eunjoong Lee, Hyunduk Kim, Hojong Chang, Gyuseong Cho, Alexander Solodov</i>	1338
Salty Nuts and Snacks for Retrospective Dosimetry <i>Authors: Maria Christiansson, Christian Bernhardsson, Therese Geber-Bergstrand, Sören Mattsson, Christopher Rääf</i>	1339
Dosimetric Evaluation of a Radiological Accident involving a Gammagraphy Industrial Source of ¹⁹²Ir (44 Ci)-Multidisciplinary Approach <i>Authors: Marina Di Giorgio, Analía Radl, Adrian Discacciatti, Diana Dubner, Sebastian Gossio, Francois Trompier, Ezequiel Soppe, Adriana Coppola, Mayra Deminge, Julieta Rearte, Ana Molinari, Ignacio Menchaca, Fabio Lopez, Gaston Castro, Mariana Egan, Mercedes Portas</i>	1340
In Light Optically Stimulated Luminescence Dosimetry for Occupational Workers in the Philippines <i>Authors: Marianna Grande, Kristine Romallosa, Estrella Caseria, Ahmad Bazlie</i>	1341
Particle Size Distributions of Radioactive Aerosols in the Atmosphere <i>Authors: Miroslav Hýža, Petr Rulík, Helena Malá, Vera Beckova</i>	1342
Optical Stimulated luminescence from Citrine for High-Doses Dosimetry <i>Authors: Maria Ines Teixeira, Linda V.E. Caldas</i>	1343

Performance Data of a new Active Personal Dosimeter in Respect to Gamma, Beta and Pulsed X-ray Radiation	
<i>Authors: Michael Iwatschenko-Borho, Alan Laing, Ling Luo, Cassidy McKee, Greg Nelson, Ralf Pijahn, Norbert Trost</i>	1344
Calibration of Conventional Survey Meters for Soft X-ray Below 5 keV	
<i>Authors: Masahiro Kato, Tadahiro Kurosawa, Toshihiko Hino, Yoshinori Inagaki</i>	1345
Retrospective Review of Dosimeter Film Processing	
<i>Authors: Mirela Kirr, Christopher Passmore</i>	1346
Design of Long Counter Having Flat Response from Few keV up to 150 MeV	
<i>Authors: Mohamed Mazunga, Taosheng Li, Yanan Li, Jieqiong Jiang, Yican Wu</i>	1347
Measurement of Occupational Doses of Ionising Radiation to the Whole body of Diagnosis Radiologists	
<i>Author: Maryam Pourkaveh</i>	1348
Calculation of 2D Dose Distribution in an Inhomogeneous Phantom using Artificial Neural Network with Best Training Method	
<i>Authors: Mahdi Saeedi-Moghadam, Banafsheh Zeinali-Rafsanjani, Kamal Hadad, Sepideh Sefidbakht</i>	1349
Photoneutron Secondary Cancer Risk Estimation by a Novel Position-Sensitive Detection Method	
<i>Authors: Mehdi Sohrabi, Amir Hakimi</i>	1350
A New Method for Effective Dose Calculation based on the Ambient Dose Height Distribution	
<i>Authors: Niroojiny Sangarapillai, Mario Liebmann, Bjoern Poppe, Heiner von Boetticher</i>	1351
Development of a New Optical Reading Technique for Dosimetric Gels based on the Analysis of the Scattering Light	
<i>Authors: Olivier Bleuse, Régine Gschwind, Yannick Bailly</i>	1352
Performance Assessment of the Criticality Dosimetry System at The Belgian Nuclear Research Centre SCK•CEN	
<i>Authors: Olivier Van Hoey, Filip Vanhavere, Marcel Reginatto</i>	1353
PROCORAD's International Proficiency Testing for Radio-Bioassays	
<i>Authors: Robert Fottorino, Bernadette Peleau, Christian Hurtgen</i>	1354
 Assessment of Dose Calibrators Performance in Nuclear Medicine Department in Sudan	
<i>Author: Suhaib Alameen</i>	1355
A Simple, Reliable and Inexpensive Microscopy-Based Method for Radiation Biodosimetry	
<i>Authors: Sudhir Chandna, Shwetanjali Nimker, Kanupriya Sharma, Vijaypal Singh</i>	1356
Secondary Neutron Dose Assessment from Proton Therapy Using Passive Scattering at The National Cancer Centre (NCC)	
<i>Authors: Sang Eun Han, Se Byeong Lee, Gyuseong Cho, Kyeongjin Park</i>	1357
Traceable Measurements for Radiation Protection Industry in South Africa	
<i>Author: Sibusiso Jozela</i>	1358
Development of the Performance Testing Procedure for the New Proposed Portable Gamma Irradiation System	
<i>Authors: Seung Kyu Lee, Hyungjoon Yu, Insu Chang, Hyoungtaek Kim, Jungil Lee, Jang-Lyul Kim, Bong-Hwan Kim</i>	1359
Development of the Probabilistic Internal Dosimetry Code	
<i>Authors: Siwan Noh, Jai-Ki Lee, Jong-Il Lee, Jang-Lyul Kim</i>	1360
Effect of Radon Progeny on Real Time Alpha-CAM Monitoring in Uranium Facility	
<i>Authors: TaeHyoungh Kim, JunBok Lee, Jong Il Lee, Bong Hwan Kim</i>	1361
PoCAMon – All in one Personal Online Continuous Air Monitor, Gamma Dose Meter and Gas warner	
<i>Author: Thomas Strel</i>	1362

R Implementation of ICRP 116 Dose Conversion Coefficients for Reconstructing Organ Dose in a Radiation Compensation Program Authors: Timothy Taulbee, Keith McCartney, Richard Traub, Matthew Smith, James Neton	1363
Tracking System for Radiation Works Using Passive RFID Technology to Enhance Radiation Protection Authors: Yunjong Lee, Jin Kyu Kim, Jinwoo Lee, Young-Hwan Ryu, Ho-Sung Kim, Kyung-Rae Dong, Eun-Jin Choi	1364
Capability Study of Multi-function Dose Rate Meter Based on Hemisphere CdZnTe Detector Authors: Ying Wang, Wenjun Xiong, Zhiping Luo, Jizeng Ma, Ling Chen	1365
Combination of Automated Chromatographic Separation and Off-line Cherenkov Counting in Determination of Low Level Activity of Sr-90 Authors: Željko Grahek, Ivana Coha	1366

JC@ A9`**Area 7: Environment and Natural Background** 1367

Health Detriment Associated with Exposure to Natural Radioactivity from the Soil of Ondo and Ekiti States South Western, Nigeria. Authors: A.E. Ayodele, A. M. Arongunjo, J. I. Ajisafe, O.T. Arije	1368
---	------

Radioactivity Level of Drilled Well Water across Selected Cities in Ondo and Ekiti States, Southwestern Nigeria and its Radiological Implications Authors: A. E. Ayodele, A. M. Arongunjo, J. I. Ajisafe, O. T. Arije	1376
---	------

Y Dating of a sediment core from Lake Biel (Switzerland) and source characterization of fallout Pu Author: Anja Pregler	1382
---	------

Preliminary survey of radon population exposure in east Romanian region Authors: Andreea Teodor, Irina Anca Popescu, Constantin Milu	1390
--	------

Excess Lifetime Cancer Risk of Cosmetic Powders Authors: Chioma Nwankwo, Damilola Folley, Olawunmi Gbolagade	1397
--	------

Monitoring of ambient dose equivalent at the boundary of nuclear sites to verify compliance with the regulations Authors: Cristina P. Tanzi, M. Farahmand, P. Kwakman, R.B. Tax, A.P.P.A. van Lunenburg, G.J.E Slagt, L.P. Roobol	1404
---	------

Determination of the activity concentrations of natural occurring radionuclides in foodstuffs for public dose assessments Authors: Deon Kotze, Immanda Louw, Charles Krös	1409
---	------

Monitoring the environmental radiation by using a new gas-filled proportional counter probe as a quasi-spectroscopic system Authors: Dirk Peter Schmalfuß, Uwe Hoffmann, Julia Glück, Andreas Meister	1416
---	------

Radiological assessment of natural radioactivity in groundwater from Greater Accra Region of Ghana: Gross alpha and gross beta measurements and annual committed effective dose evaluation. Authors: E.J.M. Nguelem, M. Ndontchueng, E.O. Darko	1422
---	------

Y Correlations of Radon Measurements in Soil Gas and Indoor for Improving the Prediction of an Area's Radon Potential Authors: Franz Kabrt, Andreas Baumgartner, Harry Friedmann, Valeria Gruber, Wolfgang Ringer, Franz Josef Maringer	1429
---	------

Radiation Measurement Systems and Experiences in Japan after the Fukushima Accident Author: Frazier L. Bronson	1437
--	------

Y Environmental radiation monitoring in the gold mining region East Cameroon Authors: Dallou G. B., Ngoa Engola L., Ndjana Nkoulou II, J. Emmanuel, Saïdou, Kwato Njock M. G.	1446
--	------

Environmental Dosimetry of Mining Areas: Case of Abandoned Uranium Site, Vinaninkarena- Antsirabe, Madagascar	
<i>Authors: Hary A. Razafindramiandra, Tiana h. Randriamora , Elijaona H. Rakotomalala Anja, Raelina Andriambololona, R. Dina Randriantsizafy, Mbolatiana A. L. Ralaivelo , Edmond Randrianarivony, Solofonirina D. Ravelomanantsoa, Joseph L. R. Zafimanjato, H. Fanja Randriantseheno</i>	1454
The European Radioecology Alliance: Encouraging the Coordination and Integration of Research Activities in Radioecology	
<i>Authors: Hildegard Vandenhove, Jacqueline Garnier-Laplace, Almudena Real, Maarit Muikku, Catherine Lecomte-Pradines, Åste Søvik, Brenda J. Howard, Pere Masque, Rafael Tenorio</i>	1461
A cancer risk due to natural radiation on the Coast of Montenegro	
<i>Authors: Ivanka Antović, Nikola Svrkota, Danko Živković, Nevenka M. Antović</i>	1470
A Survey of Indoor Gamma Dose Rates in Selected Dwellings and Offices in Abeokuta, South Western Nigeria	
<i>Authors: Okeyode, I.C., Oladotun, I.C., Mustapha, A.O., Alatise, O.O., Bada, B.S., Makinde V., Akinboro, F.G., Al-Azmi, D.</i>	1478
Natural radioactivity of samples from the building industry in South Africa	
<i>Authors: I. Ramathhape, D. Kotze, I. Louw</i>	1486
The ICRP Publication 126 on Radiological Protection against Radon Exposure	
<i>Authors: Jean-François Lecomte, Stephen Solomon, John Takala, Thomas Jung, Per Strand, Christophe Murith, Sergey Kiselev, Weihai Zhuo, Ferrid Shannoun, Augustin Janssens</i>	1492
Curies Contaminated Notebook	
<i>An analysis of a notebook and papers, originally belonging to Marie Curie, which are now retained by the Wellcome Collection, London</i>	
<i>Authors: Lindsey Simcox, Jon Taylor</i>	1497
Comparison of Federal Guidance Reports 12 and 15: External Exposure to Radionuclides in Soil, Air, and Water	
<i>Authors: M.B. Bellamy, K.G. Veinot, M.M. Hiller, S.A. Dewji, K.F. Eckerman, C.E. Easterly, N.E. Hertel, R.W. Leggett</i>	1504
Thoron Exhalation Rate and ²³²Th Content in Traditional Building Materials Used in the Coastal Region of Kenya	
<i>Authors: Margaret Chege, Nadir Hashim, Abdallah Merenga, Oliver Meisenberg, Jochen Tschiersch</i>	1511
A comparison of a commercial and specifically developed (CTBTO-VGSL) software packages used in high-resolution gamma-spectrometry on their applicability and accuracy in NORM analysis of environmental samples, which includes optimization of spectrum analysis parameter settings and sum-coincidence and self-absorption corrections	
<i>Authors: Monnicca M. Rapetsoa, Arnaud Faanhofa, Deon Kotze, Robert Lindsay</i>	1515
K-40 levels in the South Adriatic Sea environment (Montenegro)	
<i>Authors: N. M. Antović, I. Antović, N. Svrkota</i>	1520
Would Radiation Deter Space Exploration	
<i>Author: Nicholas Sion</i>	1528
Development of absolute measurement instrument for radioactivity of Radon gas	
<i>Authors: Rio Furukawa, Yasuhiro Unno, Akira Yunoki, Yasushi Sato</i>	1538
Determination of radon emission rate regarding to constructional energy- saving-measures	
<i>Authors: Thomas Neugebauer, Hans Hingmann, Jonas Buermeyer, Anna-Lisa Grund, Volker Grimm†, Joachim Breckow</i>	1543
Selection of Potassium Fertilizer Application Method to Reduce Uptake of Cs-137 in Brown Rice	
<i>Authors: Takashi Saito, Kazuhira Takahashi, Takeshi Ota, Tomoyuki Makino</i>	1550
Findings of the control and monitoring of liquid releases from the Centre of Isotopes of Cuba	
<i>Authors: Zayda Haydeé Amador Balbona, Pilar Oropesa Verdecia</i>	1557
Findings of the control and monitoring of airborne releases from the Centre of Isotopes of Cuba	
<i>Authors: Zayda Haydeé Amador Balbona*, Miguel Antonio Soria Guevara</i>	1564

Radiation Ecology and Human Health. Regional and Global Problems <i>Authors: Z.Paskalev, G.Vassilev, V.Baduline, D.Apostolova</i>	1570
Potassium-40 determination in NPK fertilizer by CZT-500s gamma spectrometry in the LPNPE Lab <i>Authors: A. Justinien Franck Ratovonjanahary, Hery Tiana Rakotondramanana, Haritiana L. Ralalarisoa, H. Léonce Randria-Mampianina, Solofonirina D. Ravelomanantsoa</i>	1572
Characterization of Airborne Particulates Containing Naturally Occurring Radioactive Materials in Investment Casting Facilities <i>Authors: Yong Gun Kim, Cheol Kyu Choi, Boncheol Goo, Kwang Pyo Kim</i>	1578
Spatial Distribution of Naturally Occurring Radioactive Materials (²³⁵U, ²³⁸U, ²²⁸Th, ²³⁰Th, ²³²Th, ²²⁶Ra, ²²⁸Ra and ⁴⁰K) in the Marine Sediment Samples Along the Red Sea Coast of Saudi Arabia <i>Authors: A. A. Alzahrany, M. A. Farouk, E. I. Shabana, A. A. Al-Yousef, K. N. Alnajem, F. I. Al-Masoud</i>	1584
Radon Mass Exhalation Rates of Selected Building Materials in Tanzania <i>Authors: Aloyce Amasi, Kelvin Mark Mtei, Pawel Jodlowski, Chau Nguyen Dinh</i>	1585
Assessment of Natural Radionuclide Content of Some Public Well Water within Ondo and Ekiti States, South-western Nigeria <i>Authors: Adeolu Ayodele, Adeseye Arogunjo, Olubodun Arije</i>	1586
Study of Particular Problems Appearing in NORM Samples and Recommendations for Best Practice Gamma-ray Spectrometry <i>Authors: Andreas Baumgartner, Michael Stietka, Franz Kabrt, Hannah Moser, Franz Josef Maringer</i>	1587
Public Exposure due to Radon and External Radiation from Ornamental Rock Indoors <i>Authors: André Luiz do Carmo Leal, Dejanira da Costa Lauria</i>	1588
Outdoor Thoron and Thoron Progeny in a Thorium-rich Area in Norway <i>Authors: Anne Liv Rudjord, Hallvard Haanes, Trine Kolstad, Alexander Mauring, Ingvild Finne, Sven Dahlgren</i>	1589
Advanced Approach to Assessment of Potential Radon Hazard of Building Sites in Russia <i>Authors: Albert Marennyy, Peter Miklyaev, Andrey Tsapalov, Tatyana Petrovac, Sergey Kiselev</i>	1590
Complex Monitoring Study of Radon Field Generation in Soils under Various Geological and Climatic Conditions in Russia (2011 – 2015) <i>Authors: Albert Marennyy, Peter Miklyaev, Andrey Tsapalov, Andrey Penezhev, Sergey Kiselev</i>	1591
Ⓡ Area Monitoring of Ambient Dose rates in some parts of South Western Nigeria using a GPS integrated Dosimetric System <i>Authors: A.O. Mustapha, O.O. Alatise, I.C. Okeyode, V. Makinde, F.G. Akinboro, D. Al-Azmi</i>	1592
Dose Assessment from Groundwater Water Consumption in Central Portugal <i>Authors: Alcides Pereira, Luis Neves</i>	1593
Experimental and Numerical Studies for Understanding of Radon Emanation in Environmental Materials <i>Authors: Akihiro Sakoda, Yuu Ishimori</i>	1594
The Principle of Uncertainty Assessment of the Average Annual Radon Indoor based on Measurement Results of Different Duration <i>Authors: Andrey Tsapalov, Albert Marennyy, Peter Miklyaev, Sergey Kiselev</i>	1595
The Effect of Relative Humidity and Temperature Variability on Continuous Environmental Radon Monitoring <i>Author: Bashir Muhammad</i>	1596
Forecast and Analysis of Atmospheric Effluent Deposition Influenced by Buildings of Nuclear Power Plant under Normal Operation <i>Authors: Bo Wang, Qiong Zhang, Ruiping Guo</i>	1597
Radon and Energy Efficient Buildings <i>Authors: Constantin Cosma, Alexandra Cucos, Tiberius Dicu</i>	1598
Assessment of Radiological Hazards from Gold Mine Tailings in Gauteng Province, South Africa <i>Authors: Caspah Kamunda, Manny Mathuthu, Morgan Morgan</i>	1599

Sensitivity Study of Inhalation Dose by Airborne Particulate Properties <i>Authors: Cheol Kyu Choi, Yong Gun Kim, Jaekook Lee, Kwang Pyo Kim</i>	1600
The ICRP System for Radiation Protection of the Environment <i>Authors: Carl-Magnus Larsson, Kathryn Higley, Almudena Real, David Copplestone, Jacqueline Garnier-Laplace, Jianguo Li, Kazuo Sakai, Per Strand, Alexander Ulanovsky, Jordi Vives i Batlle</i>	1601
Spatial Distribution of Background Radiation in Kuwait Using Different Car Borne Gamma Probes <i>Author: Darwish Al-Azmi</i>	1602
Verification of Skin-Point-Source Method to Assess Annual Effective Dose by Usage of TENORM Added Consumer Products <i>Authors: Do Hyeon Yoo, Wook-Geun Shin, Jae Kook Lee, Yeon Soo Yeom, Chan Hyeong Kim, Chul Hee Min</i>	1603
A Dynamic Model to Assess Radiation Dose Rate of Biota in Freshwater Lake <i>Authors: Dong-Kwon Keum, In Jun, Kwang-Muk Lim, Byeong-Ho Kim, Yong-Ho Choi</i>	1604
Radioecological Assessments of Natural Occurring Radioactive Materials and Dose Estimation of The Public Residing Around Mt. Homa, Homabay County, Kenya <i>Authors: David Otwoma, Simon Bartilol, Jayant Patel</i>	1605
Novel Method to make a Calibrated Thoron Source <i>Authors: Elmughera Elhag, Robert Lindsay, Joash Ongori</i>	1606
Radon Gas and Other NORM Testing of Building Materials in Israel for Public Health and Safety (Category 3F) <i>Author: Ehud Ne'eman</i>	1607
Cost-Benefit Analysis Approach to Risk Assessment of Natural Radioactivity in Powdered and Liquid Milk Products Consumed in Nigeria <i>Authors: Ezekiel O. Agbalagba, Gregory O. Avwiri</i>	1608
Comparison of Efficiency of Techniques Radon Measurement (^{222}Rn) in Air and Water with Active Detectors and Passive Detectors <i>Authors: Evaldo Paulo de Oliveira, Paulo Roberto Rocha Ferreira, Mariza Ramalho Franklin</i>	1609
Organization, Some Results and Perspectives of Protection from Radon in Italy in the European Context <i>Authors: Francesco Bochicchio, Sara Antignani, Carmela Carpentieri, Gennaro Venoso</i>	1610
 The IUR FORUM : Worldwide harmonization of networks to support integration of scientific knowledge and consensus development in radioecology <i>Authors: François Bréchnignac, Rudolf Alexakhin, Andréas Bollhöfer, Kristin E. Frogg, Frank Hardeman, Kathy Higley, Thomas G. Hinton, Lawrence A. Kapustka, Wendy Kuhne, Kins Leonard, Olivier Masson, Kenji Nanba, Graham Smith, Karen Smith, Per Strand, Hildegard Vandenhove, Tamara Yankovich, Satoshi Yoshida</i>	1611
Thoron: Radon's Lesser-Known Sister – Results from a National Survey in the Netherlands <i>Authors: Fieke Dekkers, Roelf Blaauboer, Martijn vd Schaaf, Harry Slaper, Ronald Smetsers</i>	1613
^{40}K, ^{226}Ra And ^{228}Ra in Soils of Rio de Janeiro State, Brazil: A Preliminary Study <i>Authors: Fernando Ribeiro, Dejanira Lauria, Jose Ivan Silva, Fernanda Cunha</i>	1614
Gamma in Situ Survey in an Experimental Research Area <i>Authors: Fernando Ribeiro, Rocio Reis, Monique Gabriel</i>	1615
Measurement of ^{137}Cs and ^{40}K in Wild Mushrooms and their Transfer Factors <i>Authors: Fei Tuo, Qiang Zhou, Jing Zhang, Wenhong Li, Qing Zhang</i>	1616
Assessment of Natural Radioactivity and its Radiological Impact in Ortum Region in Kenya <i>Author: Felix Wanjala</i>	1617
Radiation from Building Materials in South Africa including Granite Samples with High Concentrations of Radium <i>Authors: Farrel Wentzel, Robert Lindsay</i>	1618
Ionising Radiation from the Zanzibar Coastline: Exposure to Residents and Tourists Visiting Zanzibar <i>Authors: Gharib Mohamed, Robert Lindsay, Peane Maleka, Joash Ongori</i>	1619

Results from Interlaboratory Comparison on Gross Alpha/Beta Activity Measurement in Waters <i>Authors: Gordana Pantelic, Marija Jankovic, Natasa Sarap, Dragana Todorovic</i>	1620
Source Identification of Iodine-131 in Environmental Samples around the HANARO <i>Authors: Geun-Sik Choi, Jong-Myoung Lim, Young-Gun Ko, Mee Jang, Won-Young Kim, Wannoo Lee, Young-Yong Ji, Hyuncheol Kim, Chang-Jong Kim, Young-Hyun Cho, Chung-Sup Lim, Kun-Ho Chung</i>	1621
Natural Radioactivity Systematics in a Complex Hydrothermic Environment <i>Authors: Hudson Angeyo Kalambuka, Paul Tambo, Jayanti Patel, Michael Mangala</i>	1622
Measurements of Radon Concentrations in Drinking Water in Cities, China <i>Authors: Hongxing Cui, Yunyun Wu, Bing Shang, Jianxiang Liu</i>	1623
¹⁴C Activity in Atmospheric CO₂ and Biological Samples Around the Nuclear Power Plant Krško, Slovenia <i>Authors: Ines Krajcar Bronić, Bogomil Obelić, Jadranka Barešić, Nada Horvatinčić, Borut Breznik, Aleš Volčanšek, Andreja Sironić, Damir Borković</i>	1624
Control of Emissions from a Gold and Uranium-mining Polluted Catchment in a Semi-arid Region of South Africa: The Varkenslaagte Stream <i>Authors: Isabel Weiersbye, Peter Dye, Hlanganani Tutu, Ewa Cukrowska, Christopher Curtis, Julien Lusilao, Elisee Bakatula, Bruce McLeroth, Jozua Ellis, Etienne Grond, Maxine Joubert, Salome Mthombeni, Ike Rampedi, Christopher Davies, Patricia Omo-Okoro, Henk Nel, Joel Malan, Herman Coetzee</i>	1625
The Potential for Phytoremediation of Uranium Contaminated Substrata on the Witwatersrand Basin of South Africa: Extraction and Harvesting Versus in Situ Sequestration <i>Authors: Isabel Weiersbye, Ewa Cukrowska, Jozua Ellis, Peter Dye, Bruce McLeroth, Hlanganani Tutu, Luke Chimuka, Nosipho Mntungwa, Maxine Joubert, Shakera Arendse</i>	1626
Uranium in Phosphate mining <i>Author: Jacques Bezuidenhout</i>	1627
Uranium in Wild and Cultivated Leafy Vegetables and Consumption Patterns: A Risk Assessment <i>Authors: Jenny Botha, Isabel Weiersbye, Jozua Ellis, Hlanganani Tutu</i>	1628
Ⓡ Calculation of Lifetime Lung Cancer Risks Associated with Indoor Radon Exposure Based on Various Radon Risk Models <i>Author: Jing Chen</i>	1629
Measurement Results of Background Radiation Levels in Seals <i>Authors: Jing Chen, Weihua Zhang, Baki Sadi, Xiaowa Wang, Derek Muir</i>	1630
The Current Status and Plans for Safety Management of NORMs in South Korea <i>Authors: Jaekook Lee, Jaewoo Park, Zu Hee Woo, Boncheol Koo, Ki Hoon Yoon, Chang-Su Park, Byung-Uck Chang</i>	1631
Pre-assessment of Dose Rates for Marine Biota from Discharge of Nuclear Power Plants <i>Authors: Jingjing Li, Senlin Liu, Yongxing Zhang, Ling Chen, Yuan Yan, Weiya Cheng, Hailin Lou, Yongbao Zhang</i>	1632
Radon Profiles in Soil on Mine Dump <i>Authors: Joash Ongori, Robert Lindsay</i>	1633
Internal Radiation Exposure Dose From Some Commonly Consumed Food Stuff in Lagos A Commercial City in Nigeria <i>Authors: Kayode I. Ogungbemi, Moses A. Aweda, Olusola O. Oyebola, Margarent A. Adedokun, Chima E. Ireogbu</i>	1634
Seasonal and Diurnal Variation of Outdoor Radon Concentrations in Urban and Rural Area of Morocco <i>Authors: Lhoucine Oufni, Rabi Rabi</i>	1635
Ⓡ Study on a step-advanced filter monitor for continuous radon progeny measurement <i>Authors: Lei Zhang, Jinming Yang, Qiuju Guo</i>	1636
Survey of the Radon Environment within Lagos State Nigeria: A Preliminary Report <i>Authors: Margret Akinloye, Oluwasayo Abodunrin</i>	1637

The Importance of Understanding Basic Concepts in Radiological Environmental Impact Assessment <i>Authors: Moon Hee Han, Hae Sun Jeong, Hyo Joon Jeong, A Reum Kil, Eun Han Kim, Won Tae Hwang</i>	1638
High Precision Gamma Dose Rate Measurements using a Spectroscopic Pager <i>Authors: Michael Iwatschenko-Borho, Erich Leder, Ralf Pijahn, Norbert Trost</i>	1639
Tritium Content in the Velika Morava River Basin: Evaluation Effective Ecological Half-Life <i>Authors: Marija Jankovic, Natasa Sarap, Gordana Pantelic, Dragana Todorovic</i>	1640
Assessing the Northern Benguela Upwelling System for Radioactivity Levels: A Baseline Study <i>Authors: Martina Rozmaric, Deon Charles Louw, Isabelle Levy, Oxana Blinova, Mai Khanh Pham, Jean Bartocci, Iolanda Osvath, David Osborn, Samorna Brian Mudumbi, Tuuovauri Kauroua Sharon Kahunda, Elena Chamizo, Ljudmila Benedik</i>	1641
Comprehensive radionuclide analysis and dose assessment of thermal and mineral waters in Croatia <i>Authors: Krmpotić Matea, Rožmarić Martina, Petrincec Branko, Bituh Tomislav, Benedik Ljudmila, Fiket Željka</i>	1642
Radioactivity values for soil replaced at some building at Tikrit University <i>Author: Mohanad Salih</i>	1643
Development of a Measurement Procedure for Radon in Waterworks <i>Author: Michael Stietka, Andreas Baumgartner, Franz Kabrt, Franz Josef Maringer</i>	1644
Natural Radionuclides in River Sediments of Poços de Caldas Plateau - Brazil: Geogenic or Anthropogenic Contribution? <i>Authors: Nivaldo Da Silva, Heber Alberti, Marcos Roberto Nascimento, Rodrigo Bonifácio, Heliana Azevedo, Raul Villegas</i>	1645
Pubic Exposure due to Indoor Radon in Three Municipalities of Poços de Caldas Plateau - Brazil <i>Authors: Nivaldo Da Silva, Berenice Navarro, Ubirani Otero, Tarcisio Cunha</i>	1646
Estimation of Terrestrial Air-Absorbed Dose Rate from the Data of Regional Geochemistry Database <i>Authors: Nan Gan, Kuang Cen, Rong Ye</i>	1647
The Study of Environmental Contamination and Public Health in the Vicinity of the Uranium Legacy Sites in the Tajik Republic <i>Authors: Natalya Shandala, Vladimir Seregin, Aleksandr Tukov, Sergey Kiselev, Vladimir Shlygin, Aleksandr Pozhidaev, Mirzoshokir Hojion</i>	1648
The Study of Environmental Contamination and the Public Health in the Vicinity of Uranium Legacy Sites in the Kyrgyz Republic <i>Authors: Natalia Shandala, Vladimir Seregin, Aleksandr Tukov, Sergey Kiselev, Aleksey Titov, Sergey Akhromeev, Aleksandr Pozhidaev, Gulnura Abasova, Aleksander Samoylov</i>	1649
Estimation of Natural Ionizing Radiation Levels Based on the Data of Gamma- Ray Spectrometry and Regional Geochemical Data in Zhuhai City Urban, China <i>Authors: Nanping Wang, Ling Zheng, Xingming Chu, Ting Li, Hongtao Liu, Xiaohong Meng</i>	1650
Evaluation of Radioactivity Concentrations in Some Bottled Drinking Water Produced in Nigeria and Associated Radiological Risk to Consumers <i>Authors: Oladele Ajayi, Ademola Abokede</i>	1651
Radiological Hazard Assessment of Natural Radionuclides in Soils of Some Oil-Producing Areas in Imo State, Nigeria <i>Authors: Oladele Ajayi, Chidiebere Dike</i>	1652
Radionuclide Concentrations in Edible Mushrooms Consumed in South- Western Nigeria and Radiation Dose Due to their Consumption <i>Authors: Oladele Ajayi, Olusola Omotoso</i>	1653
Vertical Migration of Some Natural Radionuclides in Soils of Some Oil- Producing Areas in Imo State, Nigeria <i>Authors: Oladele Ajayi, Chidiebere Dike</i>	1654
Assessment of Radionuclide Concentrations in Some Cereals and Tea Products Available in Nigeria <i>Authors: Olufunmilayo Alatise, Irete Okeyode, Christianah Adebessin</i>	1655

Radioactivity Levels in Samples of Detergent Powder available in Local Markets of South-western Nigeria <i>Authors: Olufunmilayo Alatise, Thomas Olaniyan</i>	1656
Polonium-210 Concentration in Cuban Tobacco Products and their Contribution to the Annual Effective Dose by Inhalation of Cigarette Smoke <i>Authors: Osvaldo Brígido-Flores, Orlando Fabelo-Bonet, Adelmo Montalván-Estrada</i>	1657
Cancer Risk from Radon in Drinking Water in South-western Nigeria <i>Authors: Olatunde Michael Oni, Adetola Olive-Adelodun, Emmanuel Abiodun Oni</i>	1658
Radiological Impact Assessment within the Context of the Environmental Impact Assessment Process Associated with the Proposed South African Nuclear Power Programme; Challenges Associated with a Multiagency and Regulatory Overlap Environment <i>Authors: Paul Fitzsimons, Elisabeth Nortje</i>	1659
Integrating the Radiation Protection System for Human and Non-Human Biota: How to do it in Practice <i>Authors: Diego Telleria, Peter Johnston</i>	1660
A Map of Moscow Geogenic Radon Potential <i>Authors: Peter Miklyaev, Tatyana Petrova, Albert Marennyy, Andrey Tsapalov, Sergey Kiselev</i>	1661
Outdoor Radon Levels in China <i>Authors: Qifan WU, Ziqiang Pan, Senlin Liu</i>	1662
A Platform for Assessment of Doses to the Public from Routine Discharges of Radionuclides to the Environment from Nuclear Installations <i>Authors: Rodolfo Avila, Robert Broed, Erik Johansson, Vladimir Maderich, Roman Bezhenar</i>	1663
Radon In-Air Assessments within Selected Wine Cellars in the Western Cape (South Africa) and its Associated Effective Radiation Exposure Dose <i>Authors: Ryno Botha, Robert Lindsay, Richard Newman, Peane Maleka</i>	1664
Environmental Thoron: Monitoring, Techniques and Dose Conversion <i>Author: Rakesh Chand Ramola</i>	1665
Influence of Release Height on Radioactive Gas Effluent in Short-term for Nuclear Power Plant in China <i>Authors: Ruiping Guo, Chunlin Yang, Chunming Zhang</i>	1666
Synergistic Effect of Caffeine and Melatonin against Radiation Induced Damage in C57BL/6 Mice at Sub Lethal Radiation Dose <i>Authors: Ritu Kushwaha, Dhruv K Nishad, Aseem Bhatnagar</i>	1667
Radiation Protection Calculations for both ingestion of ²²⁶Ra and ²²⁸Ra in Reservoir and Spring Water from Central Region of Cameroon <i>Authors: Rose Lydie Marie, Oum Keltoum Hakam, Abdel Majid Choukri</i>	1668
Gamma-emitting Radionuclides Analysis in Water Samples from Two Mines in South Africa <i>Author: Raymond Njinga</i>	1669
Setting Up a Continuous Monitor for Controls the Temporal Variability of ²²²Rn in the Atmosphere and Groundwater of the Tadla Basin, Morocco <i>Authors: Radouan Saadi, Hamid Marah, Oum Keltoum Hakam</i>	1670
Radon-thoron Discriminative Measurements and Corresponding Dosimetry in the Thorium Bearing Region of Lolodorf, Cameroon <i>Authors: Saidou, Shinji Tokonami, Miroslaw Janik</i>	1671
A New Facility for Assuring the Measurements Traceability in the Environment Dosimetry <i>Authors: Sorin Bercea, Aurelia Celarel, Constantin Cenusă, Elena Iliescu, Ioan Cenusă</i>	1672
Bioaccumulation Factor of the Heavy Metal in Marine Organism from the Korean Coast <i>Authors: Seokwon Choi, Heungjun Cho, Daeji Kim, Jungseok Chae</i>	1673
In-situ Measurements of Radon Levels in Water, Soil and Exhalation Rate using Continuous Active Radon Detector <i>Author: Sanjeev Kumar</i>	1674

Exposure to External Gamma Radiation Emitted from Soil of the High Background Radiation Areas of Ramsar Reduces Bacterial Susceptibility to Antibiotics <i>Authors: SMJ Mortazavi, Samira Zerei, Mohammad Taheri, Saeed Tajbakhsh, S Ranjbar, F Momeni, Samaneh Masoumi, Leila Ansari, SAR Mortazavi, Masoud Haghani, S Taeb</i>	1675
Discharge of Gaseous Radioactive Waste in FDG Synthesis: Clearance Levels and Licensing in Italy <i>Authors: Sandro Sandri, Maurizio Guarracino, Ruggero Cifani</i>	1676
External Evaluation of the Amounts of Exposures and Intern to the Telluric Radiations Gamma, in the South-East of Gabon <i>Authors: Sylvere Yannick Loemba Mouandza, Alain-Brice Moubissi, Germain Hubert Ben-Bolie, Patrice Ele Abiama, Bouchra Ramzi, Mohammed Zaryah</i>	1677
Challenges in Managing Exposures due to Natural Radiation Sources <i>Authors: Tony Colgan, Trevor Boal</i>	1678
Radioactivity in Some Leafy Vegetables in Roodepoort South Africa <i>Authors: Thulani Dlamini, Victor Tshivhase, Manny Mathuthu</i>	1679
Determination of Natural Radioactivity in the North East Beach Sands of Madagascar <i>Author: Tiana Harimalala Randriamora</i>	1680
Availability and Reliability of Meteorological Data for Atmospheric Dispersion Models <i>Authors: Tamas Pázmándi, Sándor Deme, Lilla Hoffmann, Péter Szántó</i>	1681
A Study on Adsorption of the Radioactive Noble Gases in the Atmosphere by a Portable Sampling System <i>Authors: Wannoo Lee, Young-Yong Ji, Young-Hyun Cho, Sando Choi, Jiyoung Park, Geen-sik Choi, Hyuncheol Kim, Jong-Myong Lim</i>	1682
Animal-to-water Concentration Ratios of Various Elements in Marine Ecosystems around two Korean Nuclear Sites <i>Authors: Yong-Ho Choi, Kwang-Muk Lim, In Jun, Byung-Ho Kim, Dong-Kwon Keum</i>	1683
Review of Approaches based on ²¹⁰Po and other Daughters of ²²²Rn for Retrospective Estimate of Radon Concentration <i>Authors: Yazdan Salimi, Mohammad Reza Kardan, Mohammad Reza Deevband, Dariush Askari, Jalal Ordoni, Mohammad Hossein Jamshidi, Hamed Dehghani, Fatemeh Ramrodi, Hamid Behrozi</i>	1684
A Simple Method for Measurement of Radon in Groundwater <i>Authors: Yunyun Wu, Hongxing Cui, Bing Shang, Jianxiang Liu</i>	1685
Application of Non-equilibrium Adsorption Model in the Migration of Radionuclides <i>Author: Zhu Jun</i>	1686
Environmental Impact Assessment of the NPP Krško for Period of 5 years <i>Authors: Zeljka Knezevic, Zeljko Grahek, Borut Breznik</i>	1687
Area 8: Transport / Sealed Source Management	1688
Validation Testing of Canberra-Obayashi Mobile type TruckScan Pre- production Unit <i>Authors: Atsuo Suzuki, Frazier L. Bronson, Masaru Noda, Naoya Takada, Keizo Yamasaki</i>	1689
Regulatory actions in the case of a radioactive source stuck in an oil well <i>Authors: Marcela G. Ermacora, Claudia Chiliutti, Valeria Amado, Horacio Lee Gonzáles, Hugo Vicens</i>	1700
Safety and security of sealed sources during transportation to remote area in Egypt <i>Author: M A M Gomaa</i>	1707
Orphan sources search and secure in Republic of Serbia – planning, implementation and current status <i>Authors: Milan Vujovic, Maja Eremic-Savkovic, Ivana Avramovic, Vedrana Vuletic, Slađan Velinov</i>	1710
The worldwide problem of Disused Sealed Radioactive Sources (DSRS) and what should be done to alleviate the situation. <i>Author: Robin George Heard</i>	1718

Assessment of the radiological consequences of accidents in vehicle transportation of radioactive material in the area of Bologna <i>Authors: Sara Vichi, Sara Baldazzi, Angelo Infantino, Gianfranco Cicoria, Giulia Lucconi, Domiziano Mostacci, Mario Marengo</i>	1725
Actions for Spent Radioactive Sources Removal <i>Authors: Teresa Ortiz, Elena Alcaide</i>	1732
Y Leak Radiation Assessment of Scanner HCV-Mobile, THSCAN Scanner And Scanner HCP-Portal <i>Authors: Tahiry Razakarimanana, H.A. Razafindramandra, Raelina Andriambololona, J.L.R. Zafimanjato, R.D. Randriantsizafy</i>	1738
Occupational exposure in the transport of radioactive materials in Cuba <i>Authors: Zayda Haydeé Amador Balbona, Miguel Antonio Soria Guevara</i>	1743
Safety Assessment for Incident-Free Pilot Transportation of Decontamination Radioactive Waste Resulting from the Fukushima Nuclear Power Plant Accident <i>Authors: Min Jun Kim, A Ra Go, Kwang Pyo Kim</i>	1750
Operation of Radiation Source Location Tracking System <i>Authors: BokHyoung Lee, CheolHong Um, KiWon Jang, DaeHyung Cho</i>	1758
Designing a Physical Protection System for the 444 TBq Co-60 Irradiation Facility at the Centre for Applied Radiation Science and Technology, Mafikeng, South Africa <i>Authors: Cyrus Cyril Arwui, Victor Tshivhase</i>	1759
IAEA Approach to Cradle to Grave Control and Management of Disused Sealed Radioactive Sources <i>Authors: Monika Kinker, Gerard Bruno, Hilaré Mansoux</i>	1760
Safety Case of The Libyan Central Radioactive Waste Storage Facility <i>Authors: Husam Shames, Usama Elghawi</i>	1761
Safety and Radiation Protection Requirements for Cargo and Containers Inspection Services in Brazil <i>Authors: Josilto Aquino, Alfredo Ferreira Filho, Marcello Nicola</i>	1762
Radiation Protection in Radioactive Material Transport <i>Authors: Li Guoqiang, Zhuang Dajie, Wang Xuexin, Sun Hongchao, Wang Renze, Zhang Jianguang</i>	1763
Practical Application Illustrating Excellence in the Safety and Security of Industrial Radiography Sources Employed at the Eskom, Generation Power Stations <i>Author: Marc Maree</i>	1764
Safe Transport of Radioactive Material in Argentina <i>Authors: María Soledad Rodríguez Roldán, Alejandro Fernández, Emiliano Juanena, Christian Elechosa</i>	1765
Spent fuel elements transfer between the Units I and II of the Atucha Nuclear Power Plant in Argentina <i>Authors: María Soledad Rodríguez Roldán, Alejandro Fernández, Emiliano Juanena, Christian Elechosa</i>	1766
Challenges in Managing Radiation Safety Program at a Biotech Facility <i>Author: Rao Goriparthi</i>	1767
Intermediate Nuclear Waste Return December 2015 <i>Author: Steven Dimitrovski</i>	1768
Strategies to Improve the Safety Culture in the Field of Industrial Radiography in Peru <i>Author: Susana Gonzales</i>	1769
Detection of Orphan Industrial Neutron and Americium Sources in Metal Scrap Cargo <i>Author: Michael Iwatschenko-Borho</i>	1770
Area 9: Non-Ionising Radiation	1771
Evaluation of bone density importance in pediatric MR only treatment planning <i>Authors: Banafsheh Zeinali-Rafsanjani, Reza Faghihi, Mahdi Saeedi-Moghadam, Reza Jalli</i>	1772

Simulation of heat distribution in a phantom for a Philips Sonalleve MRgHIFU unit <i>Authors: Barbara Caccia, Silvia Pozzi, David Bianchini, Francesco Marcocci, Enrico Menghi, Marcello Benassi</i>	1776
R Extrapolation techniques for evaluation of 24 hours average electromagnetic field emitted by Radio Base Station installations: spectrum analyzer measurements of LTE and UMTS signals <i>Authors: Elisa Nava, Stefano Mossetti, Daniela de Bartolo, Ivan Veronese, Marie Claire Cantone, Cristina Cosenza</i>	1777
Managing Non-Ionizing Radiation through International Basic Safety Standards <i>Authors: Jacques Abramowicz, Efthymios Karabetos, Sigurdur Magnusson, Rudiger Matthes, Mirjana Moser, Shengli Niu, John O'hagan, Rick Tinker, Emilie Van Deventer</i>	1778
Designing a Laser Lab, Errors and Solutions <i>Author: Ken Barat</i>	1779
Threshold Dose Estimation for Short Delay Onset of Cataract after In Vivo exposure to Ultraviolet Radiation, a General Strategy for Threshold Estimation for Continuous Dose Response Functions <i>Authors: Per Söderberg, Konstantin Galichanin, Nooshin Talebizadeh, Zhaohua Yu</i>	1780
Effects of Early Life Exposure to RF Fields <i>Authors: Kerry Broom, Jutta Jarvinen, Darren Addison, Zenon Sienkiewicz</i>	1781
JC@ A9)	
Area 10: Emergency Preparedness and Management	1782
Study on the Protection Planning Actions and Response to Nuclear or Radiological Emergency <i>Authors: Perez, Clarice F.A., Sahyun, Adelia, Freitas, Kenia A.M.</i>	1783
The reality of the low radiation dose on population in Fukushima Daiichi 20km zone <i>Author: Jun Takada</i>	1788
Y Application of virtual reality technology to minimize the dose to the example of staff emergency training at the center for radioactive waste management <i>Authors: K. Chizhov, I. Kudrin, I Mazur, A. Tsovyanov, L. Bogdanova, M. Grachev, I. Tesnov, N.-K. Mark, I. Szöke, V. Kryuchkov</i>	1796
Emergency Preparedness – a continuously improving Process <i>Author: Marcel Lips</i>	1804
Medium and Long-Term Inhalation Dose Following a Major Radioactive Deposition Event <i>Author: Mauro Magnoni</i>	1812
Development and Current Status of a Carbone gamma-ray Survey System, KURAMA-II <i>Authors: Minoru Tanigaki, Ryo Okumura, Koichi Takamiya, Nobuhiro Sato, Yasuhiro Kobayashi, Hirofumi Yoshino, Hisao Yoshinaga, Akihiro Uehara</i>	1818
Socially - psychophysiological Adaptation of the Patient, who has Suffered at Failure the Chernobyl Nuclear Power Station, transferred Acute Radiation Sickness of IV Heaviest Degree and Local Radiation Injuries I-IV of Severity Level. <i>Author: N.A. Metlyaeva</i>	1826
Early measurements of members of the public after the Fukushima Daiichi NPP accident: Data made available to the EURADOS WG7 Survey <i>Authors: P. Fojtík, M.A. Lopez, D. Franck, J. Oško, U. Gerstmann, C. Scholl, A.L. Lebacqz, B. Breustedt, L. del Risco Norrild</i>	1836
Large scale monitoring of radioiodine in thyroid: equipment and preparedness in the Czech Republic <i>Authors: P. Fojtík, S. Kavan, L. Novotná, T. Svobodová, E. Čermáková, J. Baloun, J. Helebrant</i>	1845
Investigation of the radiological performances of commercial Active Personal Dosimeters for the use of the PSI fire brigade radiation protection squad <i>Authors: R. Philipp, B. Hofstetter-Boillat, E. Hohmann, S. Mayer</i>	1848
The Analytical Platform of the PREPARE project <i>Authors: W. Raskob, S. Möhrle, S. Bai, T. Müller</i>	1851

Determination of Radionuclides Surface Concentration and Radiation Level In Fukushima Prefecture, Japan: November 2014 <i>Authors: Godwin Ekong, Isa Sambo, Saiyadi Sulaiman</i>	1857
Selective Bone Marrow Shielding as an Approach to Protecting Emergency Personnel <i>Authors: Oren Milstein, Gideon Waterman, Kenneth Kase, Itzhak Orion</i>	1864
RENEB – The European Network for Emergency Preparedness and Scientific Research <i>Authors: Ulrike Kulka, Elisabeth Ainsbury, Leonard Barrios, Octavia Gil, Eric Gregoire, Alicja Jaworska, Simone Mörtl, Ursula Oestreicher, Gabriel Pantelias, Laurence Roy, Laure Sabatier, Sylwester Sommer, Georgia Terzoudi, Francois Trompier, Pedro Vaz, Anne Vral, Clemens Woda, Andrzej Wojcik</i>	1872
Absorbed Dose Measurements using Ordinary Salt on Anthropomorphic Phantoms – Novel Conversion Coefficients to Effective Dose for Various Exposure Geometries <i>Authors: Christian Bernhardsson, Therese Geber-Bergstrand, Jonas Jarneborn, Maria Christiansson</i>	1873
Monitoring and Dose Assessment for Children for Internal Radiation Contamination Following a Radiological or Nuclear Emergency <i>Authors: Chunsheng Li, Florence Ménétrier, Armin Ansari, George Etherington, Wi-Ho Ha, Jean- Rene Jourdain, Boris Kukhta, Osamu Kurihara, Maria Lopez, Arlene Alves dos Reis, Ana Rojo, Stephen Solomon, Jianfeng Zhang, Zhanat Carr</i>	1874
The Radiation Situation in the Area of Radioactive Trace Resulted From the Accident in a Nuclear Submarine at the Chazhma Bay <i>Authors: Dmitry Isaev, Alexey Titov, Sergey Kiselev, Vladimir Shlygin, Natalia Novikova, Renata Starinskaya</i>	1875
 Mass media communication of emergency issues and countermeasures in a nuclear accident. Fukushima reporting in European newspapers <i>Authors: Eduardo Gallego, Marie Claire Cantone, Deborah. H. Oughton, Tanja Perko, Iztok Prezelj, Yevgeniya Tomkiv</i>	1876
The Development of Concept of “Virtual Cytogenetic Biodosimetry Laboratory” for Radiation Emergencies in Occupational Field <i>Authors: Franz Fehring, N. Maznyk, Chr. Johannes, T. Sipko, N. Pshenichna</i>	1877
Radiological Situation at the Chernobyl Shelter Site Thirty Years after the Accident <i>Authors: Gunter Pretzsch, Viktor Krasnov</i>	1878
Assessment of Measurement Capabilities in Nuclear Accident <i>Author: Helena Janzekovic</i>	1879
Study on the Derived Response Level in Case of a Radiological Accident <i>Authors: Hyeong-Ki Shin, Juyoul Park</i>	1880
Training of RPEs for Emergency Response <i>Authors: Heleen van Elsäcker-Degenaar, Folkert Draaisma</i>	1881
Research Priorities in Emergency and Recovery Preparedness and Response: the NERIS Strategic Research Agenda <i>Authors: Johan Camps, Thierry Schneider, Wolfgang Raskob</i>	1882
Mapping of Radiation Fields in Areas with Complex 3D Source Geometries Using a Shielded Two-Detector Configuration and Data Processing <i>Authors: Jonas Jarneborn, Marcus Persson, Christopher Rääf, Robert Finck</i>	1883
Dose Re-estimation Method in Emergency Radiation Exposure Situation <i>Authors: Jungil Lee, Insu Chang, Jang Lyul Kim, Kisoo Chung</i>	1884
Introduction of Uncertainty of Atmospheric Dispersion Calculation and Improvements of Urban Countermeasure Modelling in an Operational Decision Support System <i>Authors: Steen Hoe, Kasper Andersson, Jens Havskov Sørensen, Carsten Israelson</i>	1885
Protection Actions Decision Making Support during Nuclear Emergency in China <i>Authors: Jiangang Zhang, Yapeng Yang, Zongyang Feng, Linsheng Jia, Shutang Sun</i>	1886

Capabilities of the New Mobile Laboratory of the Nuclear Forensic Laboratory <i>Author: Károly Bodor</i>	1887
Ongoing Work to Enhance Post-accident Radiation Protection at Swedish Nuclear Power Plants <i>Authors: Karin Fritioff, Staffan Hennigor, Marie Carlsson, Michael Pettersson, Ingela Svensson</i>	1888
A Spectrometry Acquisition System for UAS based on Raspberry Pi <i>Authors: Magnus Gårdestig, August Ernstsson, Håkan Pettersson</i>	1889
Comprehensive Approach to Assess Radiation Induced Individual Health Injuries and Prognostic Clinical Evaluation using Integrative "Dosimetry" Strategies <i>Authors: Matthias Port, Christina Beinke, Michael Abend</i>	1890
NEA Framework for the Post-Accident Management of Contaminated Food <i>Authors: Michael Siemann, Matt Cooper, Ted Lazo</i>	1891
Industrial Radiography Accident at the Rio Turbio Power Plant: Causes of the Event <i>Authors: Maria Teresa Alonso Jimenez, Irene Raquel Pagni, Eleazar Martin Ameal</i>	1892
 Off-site Emergency Planning at UK Nuclear Licensed Sites <i>Authors: Paul Leonard, Gareth Thomas</i>	1893
Preliminarily Integrated Simulation for Severe Accident of CLEAR-I based on Virtual Reactor Virtual4DS <i>Authors: Tao He, Jinbo Zhao, Zihui Yang, Pengcheng Long, Liqin Hu, Team FDS</i>	1894
Review on Spraying Water Soluble Resin to fix the Radioactive Material after Fukushima Accident <i>Authors: Qiong Zhang, Bo Wang, Ruiping Guo</i>	1895
Training Emergency Plan in a Nuclear Installation <i>Authors: Ruy Ferraz, Ricardo Bitelli</i>	1896
 Suitability of portable radionuclide identifiers for emergency incorporation monitoring <i>Authors: Roman Galeev, Gernot Butterweck, Markus Boschung, Bénédicte Hofstetter-Boillat, Eike Hohmann, Sabine Mayer</i>	1897
Nuclear and radiological emergencies - making early health protection decisions under uncertainty <i>Authors: Stephanie Haywood, Simon French, Matthew Hort</i>	1898
Development of Prediction Models for Ambient Dose Equivalent Rates in Inhabited Areas after the Fukushima Daiichi Nuclear Power Plant Accident <i>Authors: Sakae Kinase, Tomoyuki Takahashi, Hideaki Yamamoto, Kimiaki Saito</i>	1899
²¹⁰Po Version of the Yasser Arafat's Death. Results of the Russian investigations: Part 2. Medical research <i>Authors: Yulia Kvacheva, Vladimir Uiba, Leonid Ilyin, Alexandr Samoilov, Yuriy Abramov, Irina Galstyan, Boris Kukhta, Natalia Nadezhina, Vladimir Stebelkov, Alexandr Tsovyanov, Sergey Shinkarev, Vladimir Yatsenko</i>	1900
²¹⁰Po Version of the Yasser Arafat's death. Results of the Russian Investigations: Part 1. Physical Research <i>Authors: Sergey Shinkarev, Vladimir Uyba, Alexander Samoylov, Leonid Ilyin, Yulia Kvacheva, Yury Abramov, Irina Galstyan, Angelina Guskova, Boris Kukhta, Natalia Nadezhina, Vladimir Stebelkov, Alexander Tsovyanov, Vladimir Iatsenko</i>	1901
Health Risk Assessment of Emergency Personnel Regarding Radiation Exposures during the Aftermath of the Crash of Malaysia Airlines flight MH-17 <i>Author: Tjerk Kuipers</i>	1902
Surveillance of Radioactivity in the Atmosphere by the Deutscher Wetterdienst (DWD) – Monitoring and Prognosis <i>Authors: Thomas Steinkopff, Joachim Barth, Axel Dalheimer, Jochen Förstner, Hubert Glaab, Michael Mirsch</i>	1903
 'SUDOQU': A New Methodology for Deriving Criteria for Radiological Surface Contamination <i>Author: Teun van Dillen</i>	1904
Post-Fukushima Dai-ichi Review of Radioactive Materials Users and Panoramic Irradiators <i>Author: Vincent Holahan, William Lee, Gordon Bjorkman</i>	1905


Possible Mechanism of Realization of High Doses from Beta-Particles Exposures to the Atomic-Bomb Survivors in the Area of Wet Fallout <i>Author: Victor Kryuchkov, Sergey Shinkarev, Boris Kukhta, Evgeniya Granovskaya, Konstantin Chizhov, Masaharu Hoshi</i>	1906
Regulatory Emergency Control Centre Improvement Initiatives <i>Author: Vanessa Maree</i>	1907
Application of Backpack Radiation Detection Systems for Evaluation of External Exposure after the Chernobyl Accident <i>Authors: Valery Ramzaev, Anatoly Barkovsky, Ivan Romanovich, Jonas Jarneborn, Sören Mattsson, Christian Bernhardsson</i>	1908
R Nuclear and radiological preparedness: The achievements of the European Research Project PREPARE <i>Authors: Wolfgang Raskob, Thierry Schneider, Florian Gering, Sylvie Charron, Mark Zhelezniak, Spyros Andronopoulos, Gilles Heriard-Dubreuil, Johan Camps</i>	1909
UAV Carried Emergency Radiation Detection System for Severe Nuclear Accident <i>Authors: Yang Liu, Zhiping Luo, Luzhen Guo, Guowen Zheng, Hongchao Pang, Qin Chen</i>	1910
Area 11: Decommissioning, Waste Management and Remediation	1911
Y Analysis of radioactive inventory for radionuclide contained in liquid effluents, resulting from the decommissioning of a nuclear research reactor <i>Authors: Carmen Tuca, Ana Stochioiu, Mitica Dragusin, Daniela Gurau and Felicia Mihai</i>	1912
Discussion on practical application of radiation protection system for radioactive waste management in existing exposure situations <i>Authors: Daisuke Sugiyama, Takatoshi Hattori</i>	1918
The Role of Radiation Protection Considerations in Decommissioning A brief look at safety culture in Iraq and Ukraine <i>Authors: Eric K. Howell, Rodolfo Avila, John Rowat, David Kenagy, Ronald Chesser</i>	1924
Calculation of Dose Rates at the Surface of Storage Containers for High- Level Radioactive Waste <i>Authors: Erik Poenitz, Clemens Walther, Thomas Hassel</i>	1932
Radiological Assessment Approach for Decisions on Mining-Related Remediation Projects <i>Author: Gert de Beer</i>	1939
Application of an Artificial Neural Network for Evaluation of Activity Concentration Exemption Limits in NORM Industry by Gamma-ray Spectrometry <i>Authors: Hannah Wiedner, Virginia Peyrés, Teresa Crespo, Marcos Mejuto, Eduardo García-Toraño, Franz Josef Maringer</i>	1948
No Nuclear Power - No Disposal Facility? <i>Author: J. Feinhals</i>	1957
Radiation Protection In The Dismantling Of Nuclear Power Plants <i>Authors: Oscar González, José Campos, Teresa Ortiz</i>	1964
German Guidelines put into Practise: Inhalation or Ingestion? A study of a specific case of incorporation in an incident at a facility for dismantling nuclear installations <i>Authors: Peter Hill, Martina Froning, Burkhard Heuel-Fabianek</i>	1972
Investigation into the Pu uptake pathway in Corn (Zea mays) <i>Authors: Stephanie Hoelbling, Fred Molz, Brian Powell, Nishanth Tharayil, Nicole Martinez</i>	1978
Application of USNRC Regulatory Guide 4.21 for Decommissioning Feasibility and Life-Cycle Planning KHNP APR1400 Design Certification Project <i>Authors: Seunggi Lee, Sangho Kang, Irving Tsang, Sara Amitrani</i>	1986
The Post Fukushima Events Development and Severe Accidents Overview: Activities to Enhance Safety and Radiation Protection Regarding Academy Perspective <i>Author: Tadashi Narabayashi</i>	1994

Radioactive waste management in case of incidental melting of a Co-60 source <i>Authors: Teresa Ortiz Ramis, Elena Alcaide Trenas, Pablo Belinchon</i>	2004
Comparative Study of Radioactive Waste Management Standards in Brazil <i>Authors: Ana Cristina Lourenço, Wagner de Souza Pereira</i>	2011
Radioecological Monitoring at the Areas of the Former Military Technical Bases at the Russian Far East <i>Authors: Akhromeev Sergey, Kiselev Sergey, Titov Alexey, Isaev Dmitry, Seregin Vladimir, Gimadova Tamara</i>	2012
The Radiological Risk Assessment for Workers Involved in Liquid Waste Transfer Operations <i>Authors: Ana Stochioiu, Carmen Tuca, Mitica Dragusin, Daniela Gurau, Felicia Mihai</i>	2013
R Slaying the Dragon – The story of one FPSO, twenty odd Vietnamese and 3 concrete mixers. Decontamination and disposal of NORM <i>Authors: Annelize van Rooyen, Anthony O'Brien</i>	2014
Issues Related to Regulation, Control, and Waste Management of Natural Radioactive Scales with Low Specific Activity in Oil Producing Establishments in Libya <i>Author: Bulgasem El-Fawaris</i>	2015
R A comparison of remediation after the Chernobyl and Fukushima Daiichi accidents <i>Authors: Brenda J Howard, Sergey Fesenko, Mikhail Balonov, Gerhard Pröhl, Shinichi Nakayama</i>	2016
Radioactive Waste Management without Adherence to Standards at the Laguna Verde Nuclear Power Plant, Mexico <i>Author: Bernardo Salas</i>	2017
Statistical Learning Approaches Applied to the Calculation of Scaling Factors for Radioactive Waste Characterization <i>Authors: Biagio Zaffora, Matteo Magistris, Francesco Paolo La Torre, Gilbert Saporta, Catherine Luccioni, Jean-Pierre Chevalier</i>	2018
R The Swiss approach to deal with radium legacies from the watch industry The Radium action plan (2016-2019) <i>Authors: Christophe Murith, Sybille Estier, Martha Palacios, Sebastien Baechler</i>	2019
Post closure safety of the SFR repository for short-lived low- and intermediate level waste <i>Authors: Eva Andersson, Fredrik Vahlund, Klas Källström, Ulrik Kautsky</i>	2020
Development of a Standardised Screening Procedure for the Evaluation of Sites Potentially Contaminated with NORM in Austria <i>Authors: Eva Maria Lindner, Claudia Landstetter, Michael Tatzber, Fabian Rechberger, Michael Dauke, Christian Katzlberger</i>	2021
Critical Factors for Radiological Closure Criteria for Uranium Mine Remediation <i>Author: Frank Harris</i>	2022
The International Standards for the Safety of Radioactive Waste Management <i>Author: Gerard Bruno</i>	2023
Talking to the Future: Sustainable Solutions for Radioactive Waste <i>Author: Gordana Lastovicka-Medin</i>	2024
The Dose Calculation on Graphite Waste Samples of the Decommissioned KRR-2 <i>Authors: Heereyoung Kim, Deokjung Lee</i>	2025
Characterization of Concrete Structures to Determine the Strategy for the Decommissioning of the 250 MeV CGR Cyclotron of the Ghent University in Belgium <i>Authors: Isabelle Meirlaen, Myriam Monsieurs, Hubert Thierens, Luc Ooms, Sven Boden, Luc Noynaert</i>	2026
Waste Management at the Decommissioning of the Ghent University Research Reactor Thetis in Belgium <i>Authors: Isabelle Meirlaen, Myriam Monsieurs, Hubert Thierens, Patrick Maris, Luc Noynaert, Luc Ooms</i>	2027

R Decontamination and Recovery of a Nuclear Facility to allow Continued Operation	
<i>Author: Josh Cavaghan</i>	2028
General Principles for the Short and Long Term Management of Former Uranium Mining Sites in France	
<i>Authors: Jérôme Guillevic, Marie Odile Gallerand, Gwenaëlle Lorient, Christophe Serres</i>	2029
Safety Standards for the Management and Disposal of Radioactive Waste from Uranium Mining in France	
<i>Authors: Jérôme Guillevic, Marie-Odile Gallerand, Gwenaëlle Lorient, Christophe Serres</i>	2030
Enhancing Regulatory Oversight of Radioactive Sources through International Cooperation	
<i>Author: Jack Ramsey</i>	2031
New Measurement Systems for Clearance of Radioactive Materials from Nuclear Facilities Decommissioning	
<i>Authors: Jiri Suran, Jana Smoldasova, Petr Kovar, Lukas Skala, Bent Pedersen, Dirk Arnold, Daniel Zapata, Pierino de Felice, Doru Stanga, Simon Jerome</i>	2032
Development of Postulated Initiating Event's Scenarios for the Decommissioning of Korean 1400 MWe PWR	
<i>Authors: Kyomin Lee, Sangho Kang, Keunsung Lee</i>	2033
Impact Assessment on Rn-222 in a Radioactive Waste Disposal Facility	
<i>Authors: Luis Fuentes, José-Luis Pinilla, Teresa Ortiz</i>	2034
The Process of Industrialization of the Management of Radioactive Waste: The Example of High Energy Accelerators Waste at CERN	
<i>Authors: Luisa Ulrici, Yvon Algoet, Luca Bruno, Doris Forkel-Wirth, Francesco Paolo La Torre, Matteo Magistris, Christian Theis, Ralf Trant, Helmut Vincke, Nick Walter</i>	2035
NORM Waste in Oil & Gas Industry (Challenges & Solutions)	
<i>Author: Mohammad Aref</i>	2036
Disposal of Norm Waste from Oil and Gas Industry by Underground Injection (Case Study)	
<i>Authors: Michael Cowie, Roman Bilak, Steve Wasson, Kelly Hatch</i>	2037
Waste Management Protocols for Iridium-192 Sources Production Laboratory Used in Cancer Treatment	
<i>Authors: Maria Elisa C. M. Rostelato, Carla Daruich de Souza, Daiane C. Barbosa de Souza, Carlos A. Zeituni, Rodrigo Tiezzi, Osvaldo L. da Costa, Bruna Teiga Rodrigues, João A. Moura, Anselmo Feher, Anderson Sorgatti, Eduardo Santana de Moura, José Ronaldo de Oliveira Marques, Rafael Melo dos Santos, Dib Karam Jr.</i>	2038
Clearance and Declassification of Research Reactor Thetis at Ghent University, a Prime for Belgium	
<i>Authors: Myriam Monsieus, Isabelle Meirlaen, Hubert Thierens, Karel Strijckmans, Geert Cortenbosch, Luc Noynaert, Luc Ooms, Sven Boden</i>	2039
Methods used for Clearance of the Rooms of Former Research Reactor Thetis at Ghent University, Belgium	
<i>Authors: Myriam Monsieus, Isabelle Meirlaen, Hubert Thierens, Geert Cortenbosch, Luc Ooms, Sven Boden</i>	2040
Removal of Radiocesium Aqueous Solution using Activated Carbon Modified with Anionic Surfactant	
<i>Authors: Michael Olatunji, Mayeen Khandaker, Yusoff Amin, Ekramul Mahmud</i>	2041
R Norwegian-Russian Cooperation in Nuclear Legacy Regulation: Continuing Experience and Lessons	
<i>Authors: Malgorzata K. Sneve, Natalya Shandala, Alexey Titov, Vladimir Seregin, Sergey Kiselev</i>	2042
Rationale for a Comprehensive Assessment of Radio-Ecological Safety of Near Surface Radioactive Waste Storage Facilities	
<i>Authors: Alexander Samoylov, Nataliya Shandala, Igor Korenkov, Tatyana Lashchenova, Vladimir Romanov</i>	2043
Assessing the Environmental Impact of Man-made Radioactive Contamination at the Andreeva Bay Site for Temporary Storage of Spent Nuclear Fuel and Radioactive Waste	
<i>Authors: Natalia Shandala, Vladimir Seregin, Anna Filonova, Aleksey Titov, Vladimir Shlygin, Malgozhata Sneve, Graham Smyth</i>	2044

Radiation Situation around the Shipyards Involved in Decommissioning/Dismantlement of Nuclear Submarines	
<i>Authors: Nataliya Shandala, Alexey Titov, Maria Semenova, Vladimir Seregin, Anna Filonova</i>	2045
The study of the Ground Water Contamination. The Study of the Environmental Conditions of the Region during Remediation of the Andreeva Bay STS	
<i>Authors: Natalya Shandala, Vladimir Seregin, Sergey Kiselev, Stanislav Geras`kin, Malgorzhata Sneve, Graham Smith</i>	2046
The Status of Occupational Exposure Source Term Measurement with In-situ Gamma-ray Spectrometry for NPPs in China	
<i>Authors: Qinjian Cao, Xueqi Chang, Liye Liu, Wanchun Xiong, Yunshi Xiao, Sanqiang Xia</i>	2047
Study on spraying water soluble resin for Fukushima Dai-ichi nuclear power plant accident	
<i>Authors: Qiong Zhang, Ruiping Guo, Bo Wang, Liang Wang, Fudong Liu, Xiaoqiu Chen</i>	2048
Achievements by the NORM and Legacy Sites Working Group of the IAEA MODARIA Project	
<i>Author: Rodolfo Avila</i>	2049
NORMALYSA – A Tool for Risk Assessment to Support Remediation of Legacy Sites Contaminated with NORM and Artificial Radionuclides	
<i>Author: Rodolfo Avila</i>	2050
 Information Management System Supporting a Multiple Property Survey Program with Legacy Radioactive Contamination	
<i>Authors: Ron Stager, Douglas Chambers, Gerd Wiatzka, Monica Dupre, Micah Callough, John Benson, Erwin Santiago, Walter van Veen</i>	2051
Uranyl Ions Adsorption to Na-GMZ and Interactions with FA Adsorption: experiments and modelling	
<i>Authors: Yuanlv Ye, Liang Wang, Fudong Liu, Yahua Qiao</i>	2052
Occupational Dose Evaluation during Decommissioning of a Radiological Facility	
<i>Authors: Zamazizi Dlamini, Frik Beeslaar</i>	2053
Area 12: Societies	2054
Argentine Radiation Protection Society (SAR): 50 years Straightening Radiation Protection	
<i>Author: Ana María Bomben</i>	2055
The History of the South African Radiation Protection Society	
<i>Author: Christoph Trauernicht</i>	2056
Belgian Society for Radiation Protection	
<i>Authors: Tom Clarijs, Patrick Smeesters, Claire Stievenart, Andrzej Polak, Pascal Froment</i>	2057

Note:

Submissions marked with  represent entries published in a Special IRPA 14 issue of *Radiation Protection Dosimetry*.

Submissions marked with  represent entries by contestants for the Young Scientists and Professionals Award.

**The Proceedings of the 14th International Congress of the International Radiation
Protection Association
Volume 3 of 5**

Area 5: Optimisation and Design of New Facilities

Monte Carlo Modeling and Verification of the Shielding for an Ionizing Radiation Test Laboratory

C. Stettner^{a*}, N. Baumgartner^a, M. Blaickner^b, C. Hranitzky^a

^aSeibersdorf Labor GmbH, Seibersdorf, Austria.

^bAustrian Institute of Technology, Vienna, Austria.

Abstract. NDT (nondestructive testing) bunkers require – like radiological treatment rooms used for medical therapy – the use of sufficient shielding to protect the outside world from the radiation used inside the room. The necessary thickness of the shielding needs to be known before the start of the construction work and thus has to be determined already during the planning phase. Most facility designs allow for a simplified calculation based on the designated radio nuclide to be used, its activity and its dose rate constant. Using attenuation factors, which are published in technical literature or in engineering standards, act as a baseline to estimate the required thickness of the shielding for a given material. In case of a more complex geometry of the exposure room (e.g. a maze entrance), an unusual collimation of the beam or the exposure of a considerable amount of mass that introduces a significant additional contribution to the backscattering (e.g. during material testing), the use of engineering standards might not be applicable any more to get reliable results for the calculated shielding thicknesses. In this case the use of Monte Carlo based simulations techniques can help to develop shielding designs that are efficient in terms of radiation protection and costs. Possible candidates for such Monte Carlo tools are codes such as e.g. MCNPX, FLUKA or Geant 4. These tools can be used to develop a numerical model of the exposure facility that shall represent the real facility to a reasonable detailed degree. Typical aspects considered in such numerical models include the ground plan of the facility, wall thicknesses and materials, the position of the source and details of the source container. During the planning phase of our new laboratory we developed Monte Carlo models using MCNP and FLUKA. Both classical calculations based on engineering standards and numerical calculations have been performed and the obtained results have been compared to assess the required thicknesses and geometry of the shielding design. After the construction was finalized measurements have been performed using passive and active dosimeters. The measured results are compared to the numerical ones. From this comparison we can judge the reliability of the performed calculations and can use the gathered experience for future developments of shielding designs.

1 INTRODUCTION

Facilities for nondestructive testing with ionizing radiation require specially designed enclosed rooms, so-called bunkers, with adequate shielding to protect the environment from radiation exposure. Therefore, in planning new installations it is necessary to know the radiation field around the source to be able to assess the shielding requirements. Guidelines for the construction of such bunker shielding can be found in technical literature or engineering standards. However, these are usually based on analytical calculations for idealized geometry set-ups. Thus, for more complex facility designs like using an entrance maze, these simplified calculations might not be applicable to obtain reliable data on the necessary shielding.

For such installations a detailed shielding analysis can be conducted using Monte Carlo based simulation tools, as e.g. FLUKA, MCNP/X or Geant 4. Such simulation techniques enable the development of a very realistic numeric model of the gamma irradiation facility by considering the ground plan, the source position and the source container as well as wall thicknesses and materials.

2 BUNKER DESIGN AND SIMULATION

Seibersdorf Laboratories designed a radiation bunker for long-time exposure using a sealed Co-60 source with a nominal activity of 74TBq. With regard to the safety requirements, especially the planned entrance maze and different cable-feedthroughs had to be considered.

Subsequently a Monte Carlo based code was used to simulate the shielded room. To determine the appropriate parameters for the simulation code some measurements on backscattering and attenuation of photons were performed already in the planning stage with dose rate meters (Automess, Seibersdorf, Graetz).

Furthermore, during the construction works samples of the used concrete were tested for their density and composition (simulation was fed by the manufacturing data) as well as the attenuation determined and compared to the simulation.

Figure 1: TEC-Laboratory: Ionizing radiation test laboratory on the campus Seibersdorf



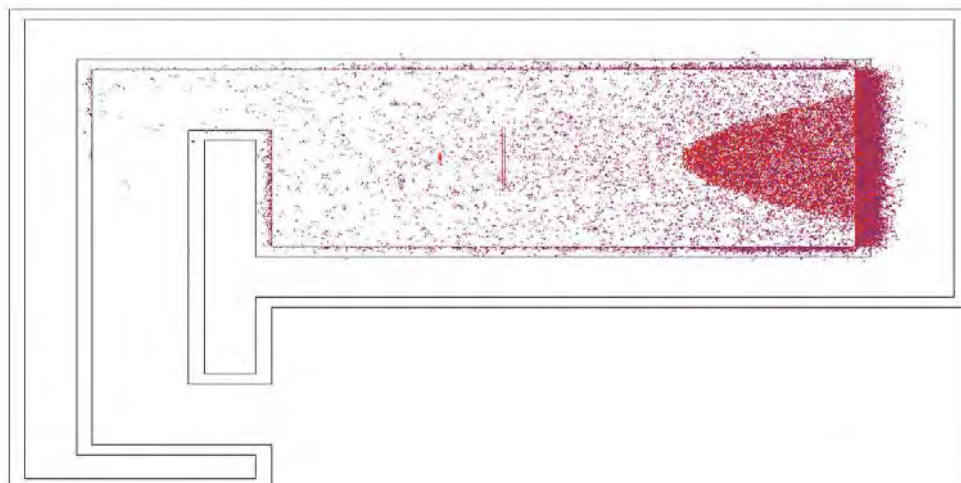
3 VERIFICATION OF THE SIMULATION RESULTS

Directly after completion of the bunker scattering and attenuation effects of the model were validated against experimental measurements at defined positions within the bunker with an Ir-192 source (nominal activity 3TBq).

The deviations between the values found from the simulation and the experimental measurements were in the range of 2% to 28%. These deviations could be traced back on uncertainty of measurements, statistical effects and simplifications of the developed simulation-codes.

Subsequently the finally used Co-60 source was installed and the simulation results were also validated against dose rate measurements. The deviation of all of the measurements compared to the simulation was less than 20%.

Figure 2: Ground plan of TEC-Laboratory with simulated photon interaction events in the concrete ground and walls of the irradiation room.



4 CONCLUSIONS

Monte Carlo based simulations are an important tool to improve radiation protection applications. Together with the continuously increasing computing power this method offers the potential to evaluate complex shielding requirements and attenuation factors very cost and time efficient.

Nevertheless involved experts should always verify the used simulation code and design criteria. Furthermore, it has to be ensured, that made assumptions are based on justifiable estimates. The disregard of different factors, like secondary electrons or radiation scattered by additional inventory not simulated in a bunker as well as setting an energy cut-off might improve the simulation time but can cause critical effects. In addition, preliminary tests of individual parts of the planned exposure room (e.g. source, material, geometry) for the validation of the simulation code will improve its reliability.

Anyway, a reasonable safety factor for the shielding requirements should always be considered. Thus, even for the upper limits of the deviations from the expected results, the protection of the environment from radiation exposure has to be ensured.

5 ACKNOWLEDGEMENTS

Special thanks to Austria's radiation protection association, that supports the participation of IRPA14. Many thanks to my employer Seibersdorf Laboratories for promoting my technical and vocational skills.

Preconcentration of cobalt metal ions onto imprinted polymer hydrogels

Ghada A. Mahmoud*, Hegazy E. A, S. M. Elbakery

National Center for Radiation Research and Technology , Atomic Energy Authority, P.O. Box 29, Nasr City, Cairo, Egypt.

Abstract. Acrylamide/N-vinyl-2-pyrrolidone-starch (AAM/NVP)-starch imprinted hydrogel was prepared for selective removal of cobalt ions. The hydrogels were prepared by free radical polymerization using gamma irradiation technique in the presence of Co ions as a template and N,N-methylenebisacrylamide (MBA) as a crosslinker. The imprinted hydrogel was applied for a selective removal of Co ions from wastewater. It was found that the optimum pH of adsorption was found to be 5 at equilibrium time 8h. The pseudo-second-order kinetic model and the Langmuir adsorption model described well the adsorption data. It was also found that the imprinted (AAM/NVP)-starch hydrogel exhibited an affinity towards Co ions from a solution mixture of Pb^{2+} , Ni^{2+} , and Co^{2+} .

KEYWORDS: *Gamma radiation; imprinted polymer; Cobalt ions; hydrogels.*

1 INTRODUCTION

Various toxic heavy metal ions discharged into the environment through different industrial activities constitute one of the major causes of environmental pollution [1]. Heavy metals are natural components of the earth's crust and cannot be degraded or destroyed. To a small extent they enter in our bodies via food, drinking water, and air. It accumulates mainly in bones, heart, skin and various glands that are a considerable health problem [2, 3]. The removal of toxic and polluting metal ions from industrial effluents is an important challenge to avoid the major causes of water and soil pollution. Various methods have been proposed to remove heavy metal ions from waste waters using ion exchange resins, some of which includes adsorption, electrolytic or liquid extraction, electron dialysis, chemical precipitation, membrane filtration, biosorption and chelating resins [4]. Molecular imprinting has been reported widely for synthesizing selective sorbents for various molecules and metal ions [5]. These are macro porous materials with highly selective binding cavities for recognizing a specific molecule or structurally related compounds, they can lead to highly selective separations [6]. Many synthetic low molecular weight organic receptors capable of encapsulating reagents have been designed by incorporating certain binding groups such as hydrogen bonding, electrostatic, hydrophobic, .. etc into the cavity in a host that are complementary to the template molecules, which can show high affinity and good selectivity towards their template molecules over the close structural analogues [7]. A better selectivity is achieved when polymerization is carried out with complexes of metal ions with ligands. The choice of perfect complexing ligand is important as it directly influences the selectivity of the sorbent. Coordination geometry coordination number of the metal ion and the charge and size of the ion also influence the selectivity [8, 9].

In the previous study, we prepared (Acrylamide/2-vinylpyrrolidone) imprinted hydrogel [10]. In this study, 2-vinylpyridone (NVP) and acrylamide (AAM) were used as complexing monomers with starch to form a biodegradable imprinted gel by irradiation technique. The imprinted hydrogel was used for the selective removal of Co ions from the aqueous environment. For this purpose, the factors affecting the uptake were studied such as pH, time and the metal ion feed concentration.

*Ghada A. Mahmoud, ghadancrrt@yahoo.com

2 MATERIALS AND METHODS

2.1 Materials

NVP and AAm were purchased from (Merck, Germany). Water soluble starch was supplied from Nasr Company for Medical Supplies, Egypt, and was used as received. All other chemicals are reagent grade and used without further purification.

2.2 Preparation the imprinted hydrogel

A solution of 10 % starch was prepared by dissolving 10 g of starch powder in 100 ml distilled water, heated and stirred at 110°C for 45 min then cooled to room temperature. An aqueous solution of 20% AAm/NVP was prepared by dissolving a proper weight of each monomer in an equal ratio in 100 ml distilled water. The (AAm/NVP)-starch by mixing the two prepared solutions where the polymer comonomer composition 2:1. Then 0.01 g of metals salts were added in the presence of 5 % of N, N dimethylbisacrylamide (MBA) as a cross-linker. The homogenous solution was transferred into glass tubes to be irradiated by ⁶⁰Co gamma source at a radiation dose of 20kGy at the National Center for Radiation Research and Technology, Cairo, Egypt. After copolymerization, the vials were broken the formed polymeric cylinders were removed and cut into discs of 2 mm thickness and 5 mm diameter. All samples were washed in mineral acid (2M of HCl) to remove the metal ions and were washed in excess distilled water to remove excess of mineral acid, then air dried at room temperature. The above steps were repeated without addition of metal ions for preparation a reference hydrogel.

2.1 Adsorption studies

A stock standard of Co(II) solution of 1000 mg/ L was prepared by dissolving an appropriate amount of analytical grade CoCl₂ in distilled water. The working solutions containing different concentrations of metal ions were prepared by stepwise dilution of the stock solution. The pH values were adjusted by addition of 0.1 mol/L NaOH or HCl solution. A 20 ml of various metal ions solutions were incubated with a known weight of the dried samples and allowed to equilibrate for different conditions. The residual concentrations of the metal ions were investigated by atomic absorption spectrophotometer (Perkin Elmer model 2380). The amount of metal ions adsorbed per unit mass was calculated by using the following equation:

$$q_e \text{ (m mol/L)} = \frac{(C_0 - C_e) \times V}{w} \quad (1)$$

where, q_e is the adsorption capacity of the imprinted hydrogels (m mol/l); C_0 and C_e are the concentrations of the initial and equilibrium metal ions solution (mg/L), respectively, V is the volume of the aqueous solution and w is the mass of dry hydrogels (g)[11].

3 RESULTS AND DISCUSSIONS

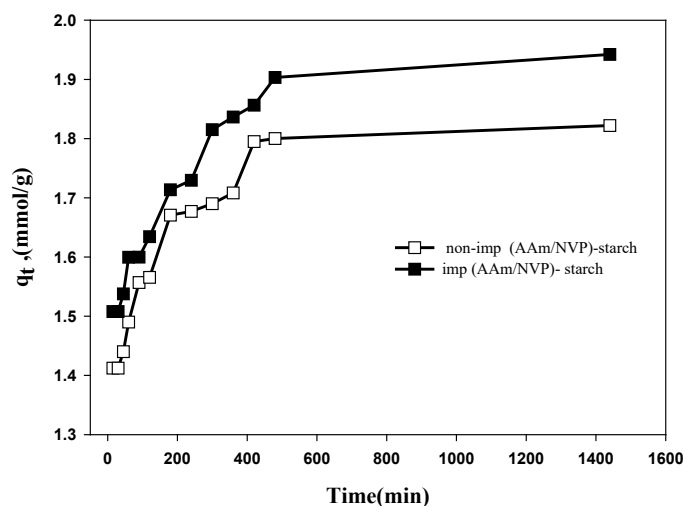
3.1 Adsorption Studies

Hydrogels possess a remarkably high swelling capacity in water due to the hydrophilic nature of its network that is sufficiently expanded to allow a fast diffusion process of the adsorbates [12]. The imprinted polymer has been recommended as a selective sorbents carrier for the template ions over other coexisting ions by memory effect [13]. In this part factors affect the adsorption; such as pH, contact time and initial metals concentration are evaluated.

3. 1. 1 Effect of time

Figure 1 shows the adsorption capacity as a function of contact time of non-imprinted and imprinted (AAm/NVP)-starch hydrogels towards Co^{2+} . It is clear that the adsorbed amount of Co^{2+} increased with increasing time until the equilibrium reached within 8 h. It can be noted that non-imprinted and imprinted (AAm/NVP)-starch hydrogel seems a good ability for adsorption of Co^{2+} ions. This may be due to starch polymer with their anhydroglucose repeated units along their backbones are considered to be ideal for heavy metals removal because these anhydroglucose units contain large number of active functional groups capable of complexation with the metal ions. In these complexes, the linkage between the metal ion and the functional group of the carbohydrate polymer is mainly of the coordination type [14]. It can be also noted that the imprinted (AAm/NVP)-starch hydrogel has adsorption capacity than the non-imprinted one under the same conditions. These results confirmed the formation of the imprinted hydrogel.

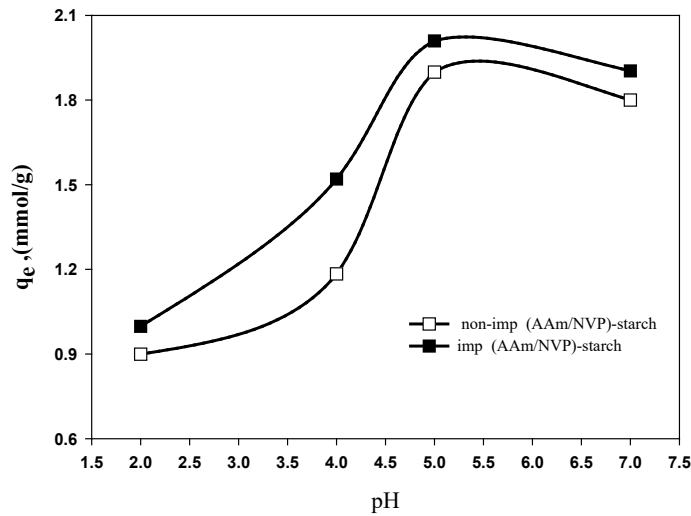
Figure 1: Effect of contact time on the adsorption of Co^{2+} onto (AAm/NVP)-starch at pH; 7 and initial metal ion concentration 500 mg/L.



3. 1. 2 Effect of pH

The effect of pH on the adsorption of Co^{2+} ions with non-imprinted and imprinted (AAm/NVP)-starch hydrogels was investigated and shown in Fig. (2). The adsorption capacity increased with increasing pH up to pH 5, which is the perfect pH, a little decrease was observed above this value may due to precipitation of ions as a hydroxide. As the pH increased the concentration of H^+ decreased thus the active groups are deprotonated so the Co^{2+} ions can easily chelate with polymeric legends. An additional possible explanation of increasing sorption with increasing pH is that hydrolyzed species have a lower degree of hydration, i.e. less energy is necessary for removal or reorientation of the hydrated water molecules upon binding [15].

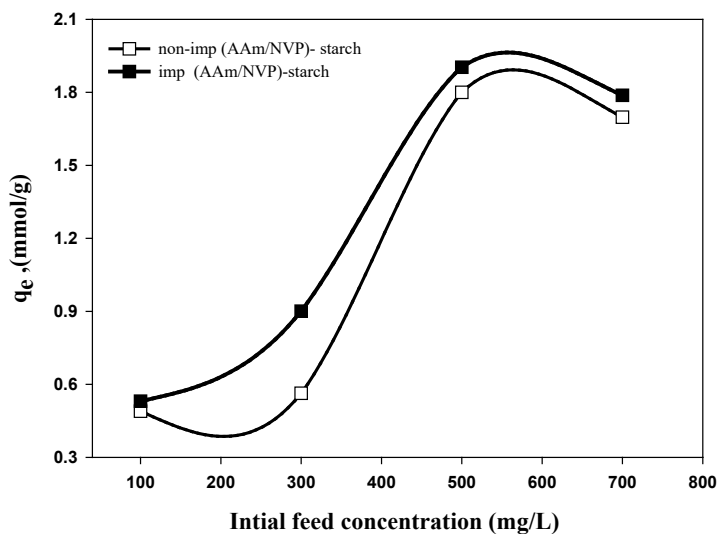
Figure 2: Effect of pH on the adsorption of Co^{2+} onto (AAm/NVP)-starch at ambient temperature, contact time 8h and initial feed concentration 500 mg/L.



3.1.3 Effect of initial concentration

Figure 3 shows the effect of initial Co^{2+} concentration on the adsorption capacity of non-imprinted and imprinted (AAm/NVP)-starch hydrogels. As seen in Fig.3 the adsorption capacity of the hydrogels increases with increasing in the initial feed concentration up to 500 mg/L and tends to decrease above this value. The increase of adsorption at low concentrations due to increase the driving force to overcome all mass transfer resistances between the solid and the aqueous phase and resulting in higher metal ion adsorption [16]. At low concentration the adsorption sites on the hydrogel are vacant and sufficient to combine with the metal ions. When the concentration of metal ions increases the remaining surface sites are difficult to be occupied and the metal ions combining with the active groups gradually decreases [17].

Figure 3: Effect of initial feed concentration on the adsorption of Co^{2+} onto (AAm/NVP)-starch at ambient temperature, pH; 5 and contact time 8h.



3.2 Kinetics and Isotherm studies

Lagergren's pseudo-first-order (eq 2) and the pseudo-second-order models [18] were applied to study the kinetics of the prepared hydrogel and the obtained data were summarized in Table 1.

$$\log(q_e - q_t) = \log q_e - \frac{k_1}{2.303} t \quad (2)$$

$$\frac{t}{q_t} = \frac{1}{k_2 q_e^2} + \frac{1}{q_e} t \quad (3)$$

where q_e (mg/g) is the adsorption capacity at any time t (min), q_e is the equilibrium adsorption capacity (mg/g), k_1 is the pseudo-first-order rate constant (min^{-1}) and k_2 ($\text{g mg}^{-1} \text{min}^{-1}$) is the pseudo-second-order rate constant. It can be noted from Table 1 that the pseudo-second-order kinetic model was described well the experimental data ($R^2 > 0.99$). Therefore, the adsorption may be a chemical process through sharing electrons between the hydrogel and the Co^{2+} .

The Langmuir (eq 4) and the Freundlich (eq 5) isotherm models [19] were applied to fit the experimental data as shown in Table 1.

$$\frac{C_e}{q_e} = \frac{C_e}{q_{\max}} + \frac{1}{n \cdot q_{\max}} \quad (4)$$

$$\log q_e = \log k_f + \frac{1}{n} \log C_e \quad (5)$$

where q_{\max} represents the maximum amount of adsorbed metal ions on the gel (mg/g), and b is the the Langmuir model constant of (L/mg), k_f is the Freundlich isotherm constant and $1/n$ (dimensionless) is the heterogeneity factor. The experimental data fitted well the Langmuir model ($R^2 \geq 0.99$) that also confirmed the chemical reaction may occur between the hydrogel and the Co^{2+} .

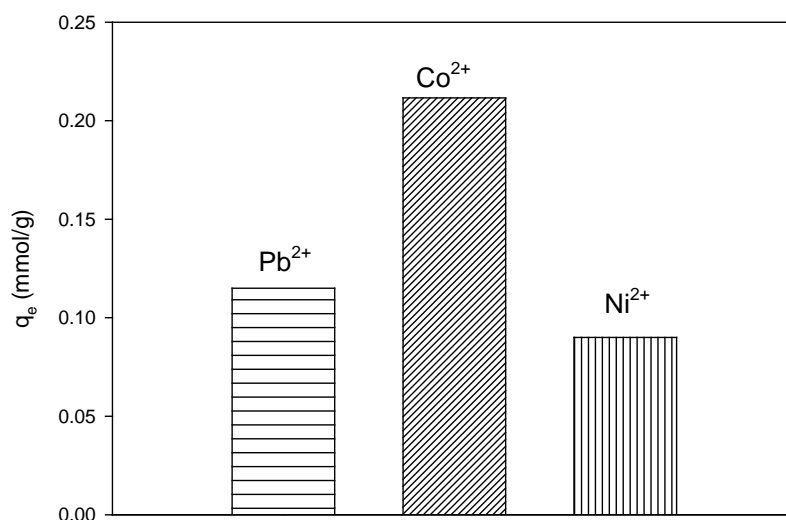
Table 1: Parameters of kinetic and isotherm models for adsorption of Co^{2+} onto the imprinted and non imprinted (AAm/NVP)-starch hydrogel.

Model	parameters	Non-imprinted	<i>Imprinted</i>
		q_e , exp (mmol/L)	0.941
Pseudo-first order	k_1 (min^{-1})	1.15	1.80
	q_e (mmol/g)	0.570	0.524
	R^2	0.96	0.92
Pseudo-second-order	k_2 (g/m mol min)	0.128	0.129
	q_e (m mol/g)	1.29	1.35
	R^2	0.99	0.99
Langmuir	q_m (mmol/g)	0.242	0.315
	n	0.014	0.015
	R^2	0.99	0.99
Freundlich	K_f (m mol/g(L/g) $^{1/n}$)	0.062	0.069
	$1/n$	0.835	0.84
	R^2	0.97	0.98

3.3 Selectivity of (AAm/NVP)-starch hydrogels towards Co ions

The effect of the imprinted molecule (Co^{2+}) on the selectivity of (AAm/NVP)-starch hydrogel was investigated. For this purpose, a solution contains Co^{2+} , Ni^{2+} and Pb^{2+} ions of total solution concentration 500 mg/L was used. Figure 4 shows the selectivity of the imprinted (AAm/NVP)-starch hydrogel towards Co^{2+} ions by immersing 1g of the dry hydrogel in a mixture of the three metal ions in the feed solution. It can be observed that there is a selectivity of the imprinted hydrogel towards Co^{2+} ions that the hydrogel has specific recognize to it. It should know that the affinity of (AAm/NVP)-starch hydrogel towards the individual solution of these metal ions were found to be in the order of; $\text{Pb}^{2+} > \text{Ni}^{2+} > \text{Co}^{2+}$ but not included in this study. It can be concluded that the (AAm/NVP)-starch hydrogel has a memory towards Co^{2+} ions has an imprint to it.

Figure 4: Schematic diagram of the Selectivity of (AAm/NVP)-starch imprinted hydrogel towards different metal ions in the same feed solution, total feed solution, 500 mg/L, contact time; 8 h and pH; 5.



4 CONCLUSIONS

A biodegradable imprinted hydrogel of acrylamide/N-vinyl-2-pyrrolidone-starch was successfully prepared by gamma irradiation for removal of cobalt ions. A brief study of factors affecting the adsorption capacity was done and compared data with that obtained by the non-imprinted hydrogel. The optimum adsorption pH was found to be 5 at equilibrium time 8h. The pseudo-second-order kinetic model and the Langmuir adsorption model described well the adsorption data. The selective study was done using a solution mixture of cobalt, nickel, and lead ions. The results confirmed the successfully preparation of the imprinted (AAm/NVP)-starch hydrogel with a selectivity of cobalt ions.

5 REFERENCES

- [1] Kandile, N. G., Nasr, A. S., 2014. New hydrogels based on modified chitosan as metal biosorbent agents. *International Journal of Biological Macromolecules* 64, 328–333.
- [2] Repo, E., Warchol, J. K. Kurniawan, T.A., et al., 2010. Adsorption of Co(II) and Ni(II) by EDTA- and/or DTPA-modified chitosan: Kinetic and equilibrium modeling. *Chemical Engineering Journal* 161, 73–82.
- [3] Singh, D.K., Mishra, S., 2010. Synthesis, characterization and analytical applications of Ni(II)-ion imprinted polymer. *Applied Surface Science* 256, 24(1) 7632-7637.
- [4] Vinodh, R., Padmavathi, R., Sangeeth, D., 2011. Separation of heavy metals from water samples using anion exchange polymers by adsorption process. *Desalination* 267, 267–276.
- [5] P. Abdul Nishad, A. Bhaskarapillai, S. Velmurugan, et al., 2012. Cobalt (II) imprinted chitosan for selective removal of cobalt during nuclear reactor decontamination. *Carbohydrate Polymers* 87, 2690–2696.
- [6] Hu, J-H., Feng, T., Li, W-L., et al., 2014. Surface molecularly imprinted polymers with synthetic dummytemplate for simultaneously selective recognition of ninephthalate esters. *Journal of Chromatography A* 1330, 6–13.
- [7] Zhang, H., 2014. Water-compatible molecularly imprinted polymers: Promising synthetic substitutes for biological receptors. *Polymer* 55, 699-714.
- [8] Yılmaz, V., Hazer, O., Kartal, Ş., 2013. Synthesis, characterization and application of a novel ion-imprinted polymer for selective solid phase extraction of copper (II) ions from high salt matrices prior to its determination by FAAS. *Talanta* 116, 322–329.
- [9] Guo, B., Deng, F., Zhao, Y., et al., 2014. Chaktong Au Magnetic ion-imprinted and –SH functionalized polymer for selective removal of Pb(II) from aqueous samples. *Applied Surface Science* 292, 438–446.
- [10] Mahmoud, G. A., Hegazy, E.A., Badway, N.A., et al., 2016. Radiation synthesis of imprinted hydrogels for selective metal ions adsorption. *Desalination and Water Treatment* 57(35) 16540-16551.
- [11] Liu, Y., Cao, Q., Luo, F., Chen, J., 2009. Biosorption of Cd²⁺, Cu²⁺, Ni²⁺ and Zn²⁺ ions from aqueous solutions by pretreated biomass of brown algae. *Journal of Hazardous Materials* 163 (2009) 931–938.
- [12] Renault, F., Morin-Crini, N., Gimbert, F., 2008. Cationized starch-based material as a new ion-exchanger adsorbent for the removal of C.I. Acid Blue 25 from aqueous solutions. *Bioresource Technology* 99, 7573–7586.
- [13] Singh, D.K., Mishra, S., 2010. Synthesis, characterization and analytical applications of Ni(II)-ion imprinted polymer. *Applied Surface Science* 256, 7632–7637.
- [14] Abdel-Halim, E.S., Al-Deyab, S.S., 2014. Preparation of poly(acrylic acid)/starch hydrogel and its application for cadmium ion removal from aqueous solutions. *Reactive and Functional Polymers* 75, 1–8.
- [15] Hawari, A.H., Mulligan, C.N., 2006. Biosorption of lead (II), cadmium (II), copper(II) and nickel(II) by anaerobic granular biomass. *Bioresource Technology* 97, 692–700.
- [16] Montazer-Rahmati, M.M., Rabbani, P., Abdolali, A., et al., 2011. Kinetics and equilibrium studies on biosorption of cadmium, lead, and nickel ions from aqueous solutions by intact and chemically modified brown algae. *Journal of Hazardous Materials* 185, 401–407.
- [17] Huang, Z., Wu, Q., Liu, S., et al., 2013. A novel biodegradable -cyclodextrin-based hydrogel for the removal of heavy metal ions. *Carbohydrate Polymers* 97, 496–501.
- [18] Mahmoud, G.A., Mohamed, S. F., Hassan, H. M., 2014. Removal of methylene blue dye using biodegradable hydrogel and reusing in a secondary adsorption process. *Desalination and Water Treatment* 54(10) 2765-2776.
- [19] Mahmoud, G.A., Mohamed, S. F., 2012. Removal Of Lead Ions From Aqueous Solution Using (Sodium Alginate / Itaconic Acid) Hydrogel Prepared By Gamma Radiation. *Australian Journal of Basic and Applied Sciences*, 6(6): 262-273.

Dose Constraint – a Mysterious Concept of Radiation Protection

Helena Janžekovič^{a*}

^aSlovenian Nuclear Safety Administration, Litostrojska 54, 1000 Ljubljana, Slovenia

Abstract. The concept of dose constraints (DCs) introduced by the ICRP in the ICRP 60 decades ago occupies operators and regulators even today. As pointed out in 1996 by the Joined Expert Group from the OECD and the EC the concept was not new even then. Despite the fact that a concept seems very logical even a very brief look to a use of DCs in different practices reveals that designers and operators as well as others involved in radiation protection did not achieve harmonisation when and how to use DCs. It was recognised as a challenging issue which required further development. The concept of DCs is sometimes hidden behind other physical parameters which are derived from DCs using specific models. The new IAEA BSS (2014) and the EU BSS (2013) emphasise a use of DCs. In optimisation of protection of the members of the public DCs set by the regulatory body or in legislation have actually also a role of a dose limits which shall not be exceeded. DCs for occupational exposures are particularly carefully studied when practices are associated with higher risks, e.g. industrial radiography and decommissioning. Implementation of generalised DCs in the legislation for specific practices using graded approach could be beneficial for specific regulatory regimes. However, the main focus of operators and regulatory bodies shall be not on the levels of DCs but on the implementation of the optimisation process conducted by the operator bellow the DCs.

KEYWORDS: *dose constraints; optimisation; radiation protection; member of the public; occupational exposure.*

1 INTRODUCTION

Dose constraints (DC) have been introduced in the recommendations of the ICRP about 25 years ago in order to handle inequity, i.e. the possibility that some individuals may be subject to much more exposure than the average. Namely, the ICRP introduced a concept of DCs in the ICRP Publication 60 (ICRP 60) [1]. Despite the fact that evolution of radiation protection concepts, standards, recommendations and guidelines took place it seems that the concept is not very well understood by licensees and registrants (operators) and also not by regulators. As a consequence, the implementation of DCs is a subject of different views and perspective. In addition, in all these years, strong international networks were established or have been reinforced either among national regulators, qualified experts and operators. But this did not lead to better understanding or harmonised approach to implementation of DCs.

On a contrary, dose limits are well understood concept where regulators, qualified experts, operators and other stakeholders, such as designers of sources and equipment, did not find any specific points of disagreement. However, it can be discussed that actually a dose of the members of the public cannot be actually controlled on an individual level as individual dose to the member of the public is not a subject of measurements of a dose of that individual. The actually dose of the member of the public is based on assumptions related to sources as well as the time of exposures. In reality, a regulator body does not know all individual sources which can cause exposure of an individual member of the public. So the assumptions used by the regulatory body must be based on a conservative approach.

The concept of DCs requires even more analyses as the dose limit concept. DCs shall be implemented in the system of radiation protection in harmonised way not to hinder global regime of radiation protection. In the last decades this regime developed through applying the same concepts, standards and guides all over the world while allowing needed flexibility to states in order to take into account specific issues. It can be noted that while the concept of DCs is actually quite old some reluctance to use DCs in the regulatory framework can be observed. In particular, the control of a regulatory body focused on the use of DCs is still an open issue.

* Presenting author, e-mail: helena.janzekovic@gov.si

2 A CONCEPT OF DOSE CONSTRAINTS

DCs are used in relation to one of three main principles of radiation protection, i.e. optimisation. Optimisation is “the likelihood of incurring exposure, the number of people exposed, and the magnitude of their individual doses should all be kept as low as reasonably achievable, taking into account economic and societal factors” as stated in ICRP Publication 103 (ICRP 103) [2]. In this principle three parameters are included and one of them is individual dose.

The concept of DCs is introduced as an instrument to be used in order to optimise radiation protection in planned exposure situations. Namely, as stated in [2] a DC is “prospective and source-related restriction on the individual dose from a source, which provides a basic level of protection for the most highly exposed individuals from a source, and serves as an upper bound on the dose in optimisation of protection for that source.” The source can be physical source, facility, task or program, i.e. removal of old sources in an irradiator and loading new ones. A DC is related to individual doses and not to the likelihood of incurring exposure or the number of people exposed.

The concept of DCs shall be used in the process of optimisation of protection to assist in ensuring that all exposures are kept as low as reasonably achievable, societal and economic factors being taken into account. In everyday life the process of optimisation can be a complex issue for an operator as well as for a regulatory body. In relation to any particular source within a practice optimisation of protection shall be in place based on restriction on two groups of parameters:

- individual doses, i.e. by restricting one particular element of optimisation,
- risks to individuals in case of potential exposure i.e. by using risk constraints as given in [2].

DCs are not linked to so-called potential exposures which are a part of the planned exposure situations.

The ICRP introduced for existing and emergency exposure situations reference levels to be used in optimisation of radiation protection. Table 1 gives the overview of instruments to be used in planned, existing and emergency exposure situations.

Table 1: Basic instruments to be used in exposure situations.

Planned Exposure Situation	Instruments	
	Existing Exposure Situation	Emergency Exposure Situation
Dose constraints	Reference levels	Reference levels
Risk constraints		

The concept of DCs is one of two cornerstones of optimisation of protection in planned exposure situations. DCs apply for individual doses, i.e. effective and organ doses.

3 DOSE CONSTRAINTS AND EXPOSURES

The ICRP 103 gives additional recommendation how to use DCs. DCs are related to:

- occupational exposures,
- exposures for the members of the public,
- medical exposures where DCs are applied only for doses of carers and comforters and for doses in medical research.

In general, DCs are not recommended to be used in medical exposures except for both situations mentioned above. Establishment of DCs for medical exposures in these cases require requiring specific approach, e.g. involvement of ethical committees. On the international level some guidance or discussions have been published for such particular situations as for example document from HERCA [3]. As medical exposures are somehow very specific further analysis of a use of DCs does not include DCs in medical exposure situations.

For occupational and public exposures, the ICRP 103 elaborates additional recommendations. In occupational exposures “a DC is a value used to limit the range of options considered in the process of optimisation”, while for public exposure “a DC is an upper bound on the annual doses that members of the public should receive from the planned operation of any controlled source”. It must be noted that these two recommendations already instruct a user of DCs how to apply DCs in occupational and public exposure situations stressing somehow also differences in these two approaches. The ICRP 103 also proposes bands of DCs to be used.

4 DOSE CONSTRAINTS IN THE EVERYDAY LIFE

4.1 Analysis of a Use of Dose Constraints

The ICRP 60 recommendations triggered a need for further analysis and guidelines on a use of DCs. Documents specifically oriented on a use of dose constraints are relatively rare. The list of documents includes publications of OECD/NEA from 1997 and 2011 [4, 5], IAEA [6] from 2002 and ALARA Newsletter from 2012 [7].

The current IAEA international basic safety standards (IAEA BSS) given in [8] as well as the European Union basic safety standards (EU BSS) [9] emphasise a use of DC. However, it must be noted that foreseen use of DCs based on both documents might result in some differences as the difference in definition of optimisation in both documents already exists. While in the IAEA document factors to be taken into account in the optimisation process include „environmental factors“, the EU document states that optimisation of radiation protection shall take into account „current state of technical knowledge“.

Although the DC concept is used at the planning stage of the exposures it is also used in retrospective dose assessment. Both documents related to basis safety standards are specific about the timeframe. The ICRP 103 is focusing on effective dose and „in retrospective dose assessment for demonstrating compliance with dose limits, or for comparing with dose constraints or reference levels“. On the other the IAEA document states: “After exposures have occurred, the dose constraint may be used as a benchmark for assessing the suitability of the optimized strategy for protection and safety (referred to as the protection strategy) that has been implemented and for making adjustments as necessary.” Despite the fact that dose constrains are to be used in planning phase of exposure, the users of DCs shall take lessons to be learned from each planned exposure situations and in this respect analysing of a use of DCs in optimisation process which took place seem to be inevitable.

As a rule, DCs are just one of many levels to be used in everyday control of occupational or public exposure in planned exposure situations. A list of names of such levels include among others action level, dose level, investigation level, collective dose constraint, target level, threshold on optimisation and operational level. Reaching or exceeding such levels results in the actions of operators and regulatory body as required. As a rule, operators are carefully following such levels which are functioning as so-called “hold points” triggering additional precautions. One of the purpose of such levels is to notify operators and regulators in a due time that prescribed levels given in the legislation or authorisation could be exceeded in near future if no changes in operational procedures are going to take place. This approach is putting a focus of an operator to those individuals where the highest individual doses can be expected. Such levels are also used to simplify comparison among operators and to identify so-called “good practice”.

4.2 Protection of the Members of the Public

Optimisation of protection of the members of the public is based on the assessment of the dose to the members of the public related to specific source. Besides DCs related to a specific source so-called derived physical quantities derived are established, such as activity of specific radioisotope release from a nuclear facility in a specific period of time. Such quantities are derived from pre-established DCs using a specific model or a combination of models. For example, when planning a new facility

with industrial irradiator or industrial radiography equipment the regulatory body can set the DC of 0.3 mSv/y for a dose to the members of a public or it can set specific limit on dose rates at pre-defined locations, e.g. outside the shielding and at the entrance. When derived quantities are used DCs are somehow hidden behind the model used and deep understanding of the model applied shall be present at operator's and regulatory body's site. The regulatory body might set DCs or derived physical quantities for each facility at the site where many facilities exist or set DCs or derived physical quantities for a site as a whole.

As a rule, DCs or derived physical quantities to be used in optimisation of protection to the members of the public are given in:

- legislation related to a particular source, e.g. dose rates outside a shielding of irradiation rooms used for industrial radiography or
- the authorisation of a practice related a particular source, e.g. liquid and gaseous releases from a particular nuclear power plant as well as dose rate at its fence and clearance levels for solid materials.

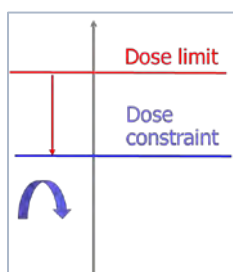
DCs are used in initial authorisation process, i.e. all options where levels above DCs would be involved are rejected. In addition, they are used also later in other phases of physical source, facility or a program, e.g. when modifications or decommissioning are taking place. According to the EU BSS, best available techniques, i.e. current state of technical knowledge is one of the component to be used by operators and regulatory bodies in the optimisation process. As the result all obsolete techniques leading to doses above prescribed DC shall be rejected.

In everyday life a regulatory body is analysing:

- levels of doses or derived quantities in appropriate interval, e.g. 100 μ Sv/4 months, so that the annual dose used as a DC is not exceeded,
- optimisation process conducted by the licensee.

The focus of the regulator shall not be only on levels mentioned above but on the optimisation process taking place below DCs as show on figure 1.

Figure 1: Optimisation process shall take place also below dose constraint value.



As a rule, DCs for the member of the public are established in close collaboration with qualified experts, professional organisations and study of state-of-the-art control, i.e. use of standards. Even more, designers and producers of new sources or equipment are focused on DCs as their products can be rejected if a dose to a member of the public seems to be too high. For example, producers of non-medical exposure X-ray devices using transmission techniques try to decrease a dose to the members of the public to about few μ Sv/scan in order to limit the exposure of passengers at airports and other places where such equipment is supposed to be used.

4.3 Dose Constraints and Occupational Exposure

Implementation of DCs for occupational exposure is a complex task where many possibilities for optimisation exist. Constraints on occupational doses were introduced even before the introduction by the ICRP. In order to respect dose limit operators needed to follow individual doses of those workers whose doses might reach dose limit, i.e. the focus of operators was on the most exposed individuals. Operators used and are using also today internal levels, i.e. „hold points”. Tasks related to the highest

doses, i.e. doses close to such “hold points” are carefully managed and lessons learned are included, e.g. a use of mock up models and robots is in place. Such approach is largely used in nuclear facilities and managing other sources related to high risks, for example sources of Category 1 and 2 defined in [10].

According to the IAEA BSS and EU BSS DCs for occupational exposure are set by an operator. The role of the regulatory body in establishment of DCs is not defined. Regarding reported practices of different countries given in [5] there is a considerable concern that involvement of a regulatory body in setting DCs could result in establishment of „new dose limits“, i.e. such DCs might be related to actions of a regulator. However, taking into account the analysis of the authorisation process even today it can be discussed that the regulatory authority is deeply involved in setting DCs for occupational exposure. This can be demonstrated using basic documentation used for authorisation procedures.

- An operator shall prepare updated safety assessment where also all doses in normal operation shall be assessed as well as probability and magnitudes of doses related to anticipated events, e.g. fires and earthquakes.
- Radiation Protection Program of the operator shall contain optimisation, e.g. addressing among other issues optimisation related to itinerant workers and establishment ALARA committee as appropriate.
- An operator shall present to a regulatory body appropriate use of standards related to sources and equipment, e.g. leakage radiation of X-ray tube, dose rate on the surface of a container and shielding calculations for a blood irradiator.
- A regulator shall demonstrate a use of operational experiences from other operators as well as information from the producer of a source and equipment in order to conduct optimisation in line with the latest technical knowledge.

In all these documents DCs are already present although they can be somehow hidden. In everyday life DCs or derived quantities from above mentioned documentation are used as a benchmark in line with the IAEA retrospective use of DCs. For example, the occupational dose of 2 mSv/y of a staff member in a control room of a reactor whose dose in normal operation shall be below 0.3 mSv/y is going to trigger investigation conducted at least by the radiation protection officer of the facility.

However, in some countries a discussion to implement so-called „authorised general DCs“ for specific practices given in legislation is going on. As reported in [5] some countries have already implemented such approach. In particular, such approach seems to be appropriate to industrial radiography where sources of Category 2 from [2] are used, e.g. TBq sources of ^{60}Co and ^{192}Ir . Industrial radiography requires constant attention of a regulatory body due to the fact that:

- occupational doses are relatively high comparing to other practices, i.e. as a rule foreseen doses in normal operation conditions are above 6 mSv/year and
- risks associated are high, e.g. the list of IAEA publication on accidents is quite long and includes documents such as given in [11, 12].

For such particular practices the implementation of “authorised general DCs”, e.g. the DC of 10 mSv/y, in the legislation might:

- help the operator to manage exposures and
- enhance the awareness of the workers.

When implementing “authorised general DCs” for specific practices graded approach shall be fully implemented, i.e. focus of the regulator shall be on the practices posing the highest risks. In addition, it might be more appropriate to use authorised DCs on a case by case basis during authorisation processes. In both cases all pro and cons shall be carefully studied by regulatory body, operators, experts and other stakeholders taking into account that not every approach is suitable for every country.

5 CONCLUSIONS

The optimisation process based on DCs is an integral part of radiation protection and safety in planned exposure situations. However, it must be noted that DCs are sometimes hidden behind other concepts. As a rule, they are widely used in a design of sources and equipment. In optimisation of protection of the members of the public a DC set by the regulatory body or in legislation have actually also a role of a dose limit which shall not be exceeded. DCs for occupational exposures are particularly carefully studied when practices are associated with higher risks, e.g. industrial radiography and decommissioning. Implementation of generalised DCs in the legislation for specific practices using graded approach could be beneficial for specific regulatory regimes. However, the main focus of operators and regulatory bodies shall be not on the levels of DCs but on the implementation of the optimisation process conducted by the operator below the DCs.

6 REFERENCES

- [1] ICRP, 1991. 1990 Recommendations of the International Commission on Radiological Protection. ICRP Publication 60. Ann. ICRP 21(1–3).
- [2] ICRP, 2007. The 2007 Recommendations of the International Commission on Radiological Protection. ICRP Publication 103. Ann. ICRP 37(2–4).
- [3] HERCA, 2010. ¹³¹I therapy: Patient release criteria. Heads of Radiation Protection Authorities. Retrieved on 2016-05-12 http://www.herca.org/docstats/Annexe%20I_HERCA-OH_2011_0005_HERCA_Release%20criteria%2030062010.pdf.
- [4] OECD/NEA and EC, 1997. Consideration on the Concept of Dose Constraint. NEA.
- [5] OECD/NEA, 2011. Dose Constraints in the Optimisation of Occupational Protection. OECD/NEA/CRPPH/R(2011). NEA.
- [6] IAEA, 2002. Optimisation of Radiation Protection in the Control of Occupational Exposure. IAEA Safety Reports Series No. 21. International Atomic Energy Agency, Vienna.
- [7] Fennel, S. (2012) A Survey of the Use of Dose Constraints Across Europe. European ALARA Newsletter, Issue 30 - February 2012. European ALARA Network. Retrieved on 2016-05-12 from <http://www.eu-alara.net/index.php/newsletters-mainmenu-37.html>.
- [8] IAEA, FAO, ILO, et al., 2014. Radiation Protection and Safety of Radiation Sources: International Basic Safety Standards. IAEA Safety Standards Series No. GSR Part 3. International Atomic Energy Agency, Vienna.
- [9] EU 2014, Council Directive 2013/59/EURATOM of 5 December 2013 Laying Down Basic Safety Standards for Protection Against the Dangers Arising from Exposure to Ionising Radiation, and Repealing Directives 89/618/Euratom, 90/641/Euratom, 96/29/Euratom, 97/43/Euratom and 2003/122/Euratom. Official Journal of the European Union. L 13/1-73.
- [10] IAEA, 2005. Categorisation of Radioactive Sources. IAEA Safety Standards, Safety Guide No. RS-G-1.9. International Atomic Energy Agency, Vienna.
- [11] IAEA, 1998. Lessons Learned from Accidents in Industrial Radiography. IAEA Safety Reports Series No. 7. International Atomic Energy Agency, Vienna.
- [12] IAEA 2009. The Radiological Accident in Nueva Aldea. International Atomic Energy Agency, Vienna.

Establishment of a Laboratory for Gamma-ray Spectrometry of Environmental Samples Collected in Fukushima

Jun Saegusa, Tomoyuki Yoda, Satoshi Maeda, Tsutomu Okazaki, Shuichi Otani, Toshio Yamaguchi, Yoshiyuki Kurita, Atsushi Hasumi, Chushiro Yonezawa, Minoru Takeishi

Sector of Fukushima Research and Development, Japan Atomic Energy Agency, 7th Floor, NBF-Unix Building, 6-6 Sakae-machi, Fukushima 960-8031, Japan.

Abstract. After the nuclear accident at the Fukushima Daiichi Nuclear Power Plant in March 2011, the Japan Atomic Energy Agency has newly set up a laboratory for radioactivity analysis in Fukushima. At the laboratory, radioactivity concentrations of environmental samples such as soil, water, dust filter, plant, etc., approximately 1,000 samples in a month, are measured with high-resolution gamma-ray spectrometry systems. The systems employ n-type HPGe detectors from Ortec. Since September 2012, characterization and upgrade of the systems have been performed aimed at enhancing reliability of analysis and convenience of customers. Resolving both systematic and technical issues, the laboratory has been accredited the ISO/IEC 17025 standard as a testing laboratory for radioactivity analysis.

KEYWORDS: *Fukushima Daiichi Nuclear Power Plant accident; radioactivity analysis; environmental radioactivity; gamma-ray spectrometry; HPGe detector; ISO/IEC 17025.*

1 INTRODUCTION

The nuclear accident at the Fukushima Daiichi Nuclear Power Plants (NPPs) in March 2011 resulted in the release of a significant amount of fission and activation products, particularly volatile iodine and cesium, into the environment around the Tohoku region of Japan. As of November 2013, ambient dose-equivalent rates in the outdoor environments of Fukushima Prefecture vary from the background level to as much as 40 μSv per hour [1]. Radiation monitoring and clean-up activities have been conducted widely and continuously across the region to address the environmental situation [2, 3].

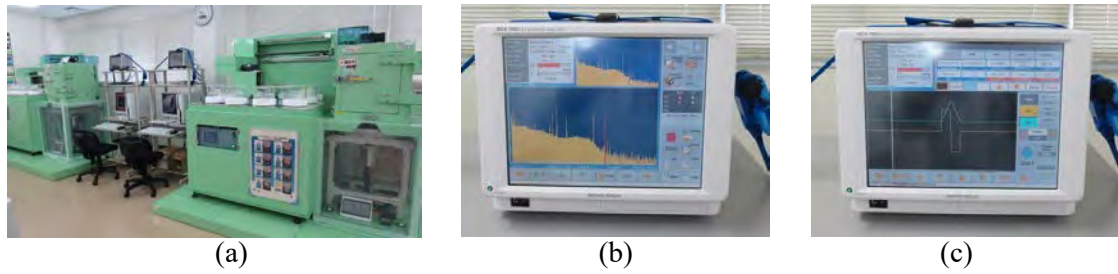
For such activities, radioactivity analysis for a variety of environmental samples is primarily of importance. At present, major radionuclides detected in the Fukushima environment are ^{134}Cs ($t_{1/2}$: 2.1 y) and ^{137}Cs ($t_{1/2}$: 30 y) (hereinafter collectively referred to as radiocesium), for which the gamma-ray spectrometry is applicable [4, 5].

To cope with these needs, in September 2012, the Japan Atomic Energy Agency (JAEA) has newly set up a laboratory (Sasakino Analytical Laboratory) for radioactivity analysis in the Sasakino district of Fukushima-city, approximately 65 km northwest of the damaged NPPs. Based on high-resolution gamma-ray spectrometry with HPGe detectors, the laboratory has measured approximately 24,000 samples collected in Fukushima (off-site the NPPs) until its closure (relocation) at the end of March 2016.

The laboratory has then moved to the Fukushima Prefecture Center for Environmental Creation in Miharu-town, approximately 45 km west of the NPPs, which was established as a central facility for studies related to the environmental restoration of Fukushima. The gamma-ray spectrometry measurements are currently carried out by approximately five staff members.

This paper overviews the laboratory and related R&Ds for enhancing reliability of the gamma-ray spectrometry carried out in the laboratory.

Figure 1: (a) Germanium detectors installed in the Sasakino Analytical Laboratory. (b) MCA-7600 commercially available from Seiko EG&G, with a pulse-height spectrum, and (c) with a digital signal after the trapezoidal filtering in the screen.



2 OVERVIEW OF GAMMA-RAY SPECTROMETRY

2.1 Germanium Detectors and Associated Electronics

The laboratory equips with five HPGe detectors (GMX40P4-76 by Ortec), two of which have an automatic sample changer, each installed in a 100 mm thick lead shielding box. The detectors are n-type coaxial closed-end type, with 40-44% relative efficiency, resolutions 1.9-2.0 keV in FWHM for 1,333 keV peak and peak-to-Compton ratios of 59-64:1. Each detector is mechanically cooled by X-Cooler II (CFG-X-Cool-II-115 by Ortec).

Electric signals from the detector are fed into a charge-sensitive preamplifier A257N by Ortec. Thereafter, signal amplification and pulse-height analysis are processed based on digital signal processing with a multi-channel analyser (MCA), either MCA7 or MCA-7600, in combination with the control software Gamma-studio [6], all from Seiko EG&G Co. Ltd., Japan. Both MCAs consist of 14-bit fast ADC, digital PHA based on the trapezoidal filtering [7] and HV supply. Photographs of these systems are shown in Fig. 1.

2.2 Samples and Reference Radiation Sources

The laboratory has been measuring radioactivity concentrations of versatile environmental samples using the systems. Most of these samples are taken by research teams of JAEA for the investigation projects intended to elucidate the behaviour and characteristics of radiocesium in the environment [8, 9]. Measurements are also made for samples routinely collected for the environmental radiation monitoring performed by the central government of Japan. Measurement results for the monitoring are immediately opened to the public via the government's website [10].

Figure 2: (a) Measured samples collected in Fukushima (see Table 1 for the definition of “U8” and “V1”). (b) Number of measured samples and its breakdown since the establishment of the laboratory.

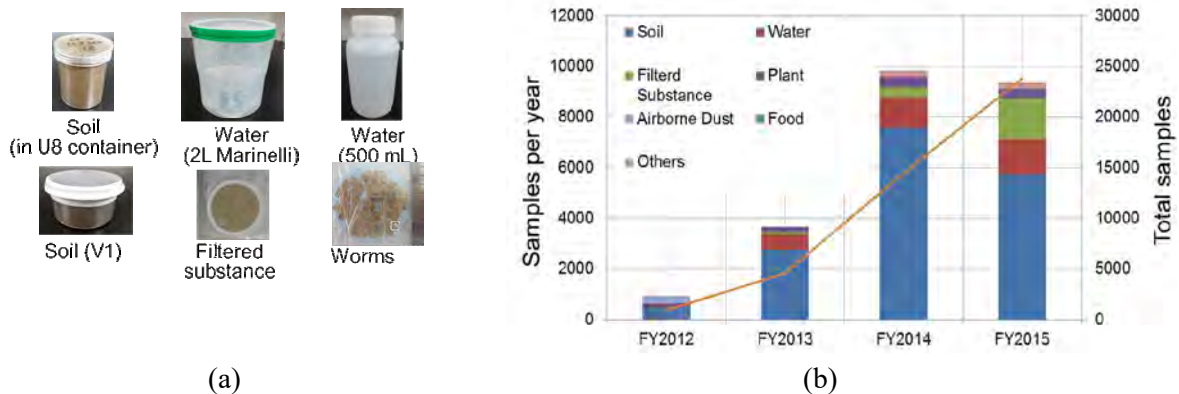


Figure 3: Reference volume sources used for efficiency calibration of the systems. Radionuclides were homogeneously distributed in epoxy resin with a density of 1 g cm^{-3} .



As shown in Fig. 2 (a, b), these samples includes soil, water, plant, food, dust in the atmosphere, filtered substance, etc. Measured sample, except for the dust and filtered substance, is packed in a plastic container with predetermined shape.

Performance check of the systems is carried out with reference radiation sources provided by the Japan Radioisotope Association [11]. In addition, multiple gamma-emitting standard volume sources (including 11 nuclides (^{241}Am , ^{109}Cd , ^{57}Co , ^{139}Ce , ^{203}Hg , ^{113}Sn , ^{85}Sr , ^{134}Cs , ^{137}Cs , ^{88}Y and ^{60}Co)) sources purchased from Eckert & Ziegler Isotope Products [12] (Fig. 3), are used for the efficiency calibrations and quality control (QC) of the systems. A list of available sample shapes and the corresponding Minimum Detectable Concentrations (MDCs; confidence level: 99.5%) based on the Cooper's definition [13] are summarized in Table 1.

Table 1: Sample containers for gamma-ray spectrometry at the laboratory, accompanied with corresponding detection efficiencies and MDCs for ^{137}Cs in the case sample material filled in each container with 1 g cm^{-3} density is set onto the detector endcap through 1 mm-thick polymethylmethacrylate protection cover.

Container ID	U8	V1	V3	V11	Bottle	Marinelli beaker
Dimension in cm ^(a) (volume in cm^3)	$4.7^\Phi \times 5.7$ (100)	$5.8^\Phi \times 2.4$ (63)	$9.2^\Phi \times 4.7$ (310)	$13^\Phi \times 6.7$ (850)	$7.7^\Phi \times 11$ (500)	$14^\Phi \times 14$ (2,000)
Detection efficiency ^(b)	1.8×10^{-2}	2.6×10^{-2}	1.5×10^{-2}	1.0×10^{-2}	9.5×10^{-3}	1.4×10^{-2}
Total detection efficiency ^(c)	1.8	1.6	4.7	8.5	4.8	28
MDC (Bq kg^{-1}) with respect to measurement time ^(d)						
5 minutes	36	36	13	7.6	15	2.0
10 minutes	21	21	7.6	4.4	8.6	1.1
30 minutes	9.3	9.4	3.4	2.0	3.9	0.51
1 hours	5.9	6.0	2.2	1.2	2.5	0.32
2 hours	3.9	3.9	1.4	0.82	1.6	0.21
5 hours	2.3	2.3	0.84	0.48	0.96	0.12
10 hours	1.6	1.6	0.57	0.33	0.65	0.09
15 hours	1.2	1.3	0.46	0.26	0.52	0.07
63 hours	0.59	0.60	0.22	0.12	0.25	0.03

^(a) $1^\Phi \times 2$ indicates 1 cm in inner diameter of the container and 2 cm in sample height (thickness).

^(b) per radiation, ^(c) per sample, ^(d) live time.

2.3 Spectrum Analysis and Calculation of Radioactivity

A series of spectrum analysis needed for calibrations and sample measurements is basically carried out by the commercial software Gamma-studio (Seiko EG&G Co. Ltd) [6], an interactive analysis software dedicated for controlling germanium detectors and their electronics, peak search, computation of peak area by the Covell and/or peak fitting methods, nuclide identification, calculations of radioactivity, various types of corrections, as well as output of analysis results report. In Japan, there has been a de facto standard for the analysis of radioactivity in samples, especially those for environmental radiation monitoring and radiation control purposes [14]. Gamma-studio is one of such software developed so as to comply with this standard, and the radioactivity concentration, a , of each radionuclide in the sample with a mass of m is obtained from the net count, $n_{N,E}$, of the peak using:

$$a = \frac{n_{N,E}/t_g}{P_E \cdot \varepsilon_E \cdot m \cdot f_E}, \quad (1)$$

where t_g is the sample spectrum counting time, P_E is the gamma-ray emission probability with energy E , ε_E is the detection efficiency, and f_E is the correction factor considering all necessary corrections [15].

The correction factor f_E includes several factors such as the decay corrections for a reference date, the self-absorption corrections between samples and a standard source, the corrections for counting losses due to true coincidence-summing and random summing, and the corrections for different measurement geometry which results from different sample positioning and filling conditions with those of the standard source measured at the time of calibrations.

Among the correction factors, the decay corrections, self-absorption corrections, true coincidence-summing corrections (based on the peak-to-total ratio method [14, 16, 17]) can be made with the Gamma-studio software. For the geometry differences, corrections are made with the correction factors experimentally obtained by the laboratory. The experiments bring a single or multiple radiation source(s) with different setting positions and/or filling heights. It also involves extensive range of Monte Carlo simulations with radiation transport codes like MCNP and CREPT-MCNP [18, 19]. Figure 4 (a) is an example of geometry set-up for the calculation of geometry correction factors, and the resultant factors for geometry differences for 662 keV photon (Fig. 4 (b)), although the correction factors are less dependent on photon energy in the range over 100 keV.

Figure 4: (a) Modelling of a germanium detector and a sample in the V1 container (blue: germanium crystal, purple: aluminium endcap, mount-cup and contact pin, yellow: beryllium window, green: polymethylmethacrylate cover and supporting jigs, brown: V1 container, pink: sample, light blue: air). (b) Comparison of correction factors obtained by the experiments and simulations for a soil sample having different filling heights with the standard volume source filled in the V1 container.

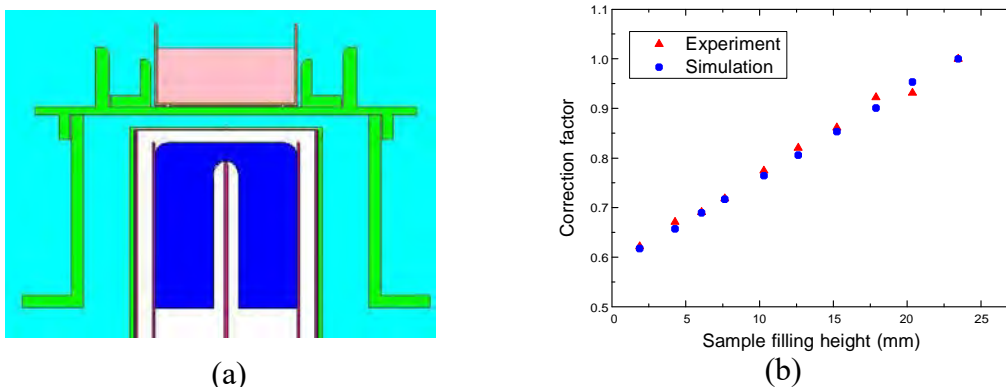
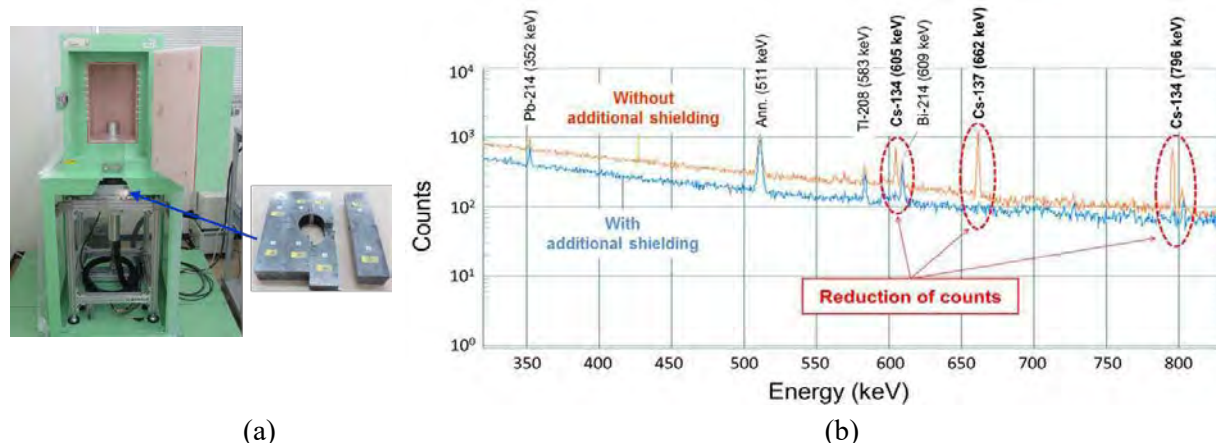


Figure 5: (a) Main shielding box (left) and additional shielding (right, dimension: 350×350×50 mm). (b) Background spectra measured before and after placing the additional shielding. Measurement time: 2,000,000 second each.



3 CHARACTERIZATION OF THE SYSTEMS AND RELATED R&DS FOR THE IMPROVEMENT OF ANALYSIS QUALITY

Since October 2012, characterization of the systems and related R&Ds have been performed aimed at enhancing the reliability of analysis results and convenience of customers. These approaches include theoretical and experimental investigations on the efficiency transfer method for samples having different filling height with the standard sources, reduction of background count rates due to the natural and accident-oriented radiations, determination of the true coincidence-summing correction factors, interpretation of gain-shift magnitude with the ambient temperature variation, counting-loss correction methods for high activity samples, etc.

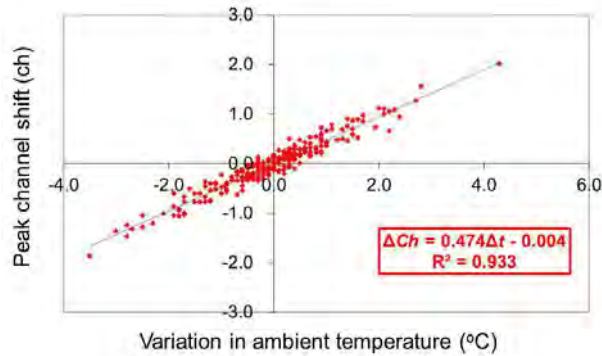
3.1 Background Reduction and Minimum Detectable Concentrations

At the time of system installation, ¹³⁷Cs peak was found in the background spectrum. Because the detectors were set on the second floor, streaming radiations from the ground outside of the building, not decontaminated, was considered to be the main reason for this. An additional lead shielding was placed for preventing the streaming at the position shown in Fig. 5 (a).

By placing the additional shielding, the interference peak was successfully removed (Fig. 5 (b)). This brought benefits that a required MDC of ¹³⁷Cs can be achieved in a shorter measurement time than before. For example, as listed in Table 2, the time needed for attaining the 1.5 Bq kg⁻¹ of MDC was halved by the addition.

Table 2: Relation between measurement time and MDCs for ¹³⁷Cs, for a soil sample packed in the V1 container.

MDC (Bq kg ⁻¹) (99.5% confidence level)	Required measurement time (live time in sec.)		Reduction rate of measurement time
	Without additional shielding	With additional shielding	
10	2,200	1,450	34%
7.6	3,600	2,300	36%
1.5	100,000	44,000	56%

Figure 6: Relationship between temperature variation and peak channel shift.

3.2 Temperature Dependency of Detector Response

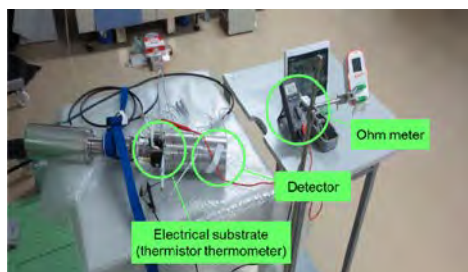
As part of QC, daily check of detectors and their electronics are carried out using standard point sources including ^{137}Cs and ^{60}Co . By comparing peak centroids, FWHMs and peak areas with ambient temperature variation, clear correlation was found between the temperature variation and energy shift of a peak.

As shown in Fig. 6, the position of 1333 keV peak (centroid channel) shifted upwards approximately 0.3 ch (0.15 keV) per 1 °C increase of ambient temperature. By continuously comparing ambient temperature and that of/around the crystal, linear relationship between them was found to be approximately 0.34 °C increase in cooling temperature of the crystal as the ambient temperature rose 1 °C (Fig. 7 (a, b)). Using the relationship, the peak shift can mostly be explained by the temperature dependency of the electron-hole-pair production energy for germanium (0.03% decrease per 1 K [20]), which results in the increase of the number of created electron-hole-pairs and thus the pulse-height of a signal.

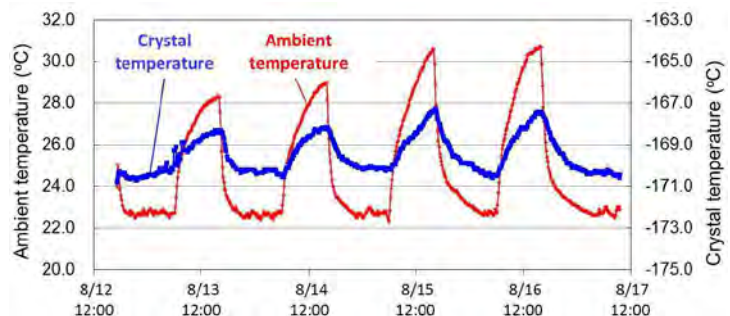
3.3 Counting-loss at High Counting-rates

In general, pulse processing electronics and analysis software normally apply a correction for the dead time of ADC. However, at high counting-rate, pile-up of signals still occurs and is unavoidable. Therefore, estimation of the correction factor for the effect was carried out with the two-source method for a 662 keV peak [17]. A single ^{137}Cs point source was positioned at a fixed distance (approximately 15 cm) from the detector endcap. By adding another point source (^{57}Co) at different distances, the dead time of the system was changed.

Figure 7: (a) Measurement of crystal temperature of germanium detector. (b) Variation of ambient temperature and crystal temperature of a germanium detector. The ambient temperature was forcibly changed with an air-conditioning equipment in the room for this experiment.



(a)



(b)

Figure 8: Counting-loss as a function of dead time of a HPGe detector system, (a) by conventional analogue signal processing, and (b) by DSP with MCA-7600.

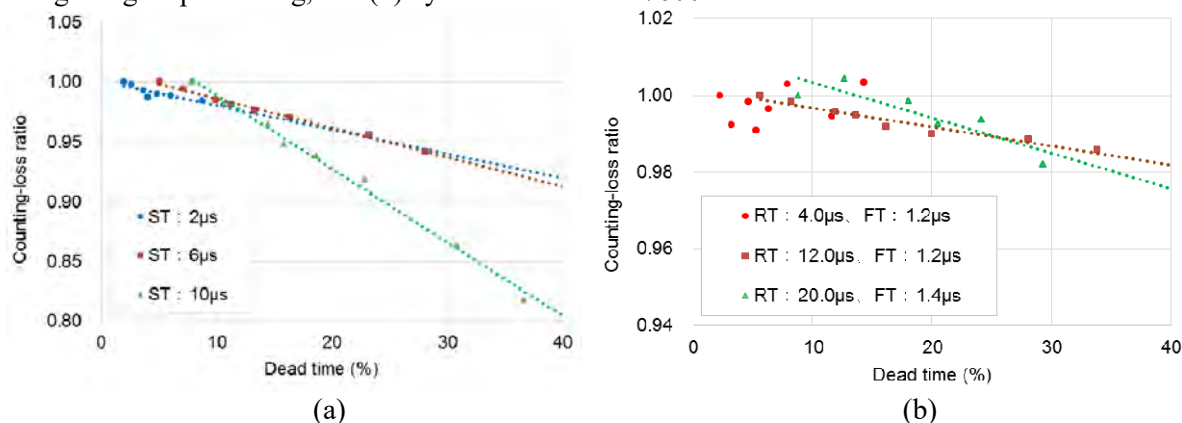


Figure 8 (a) shows relations between the dead time and the loss of peak counts for 662 keV when the output signals were processed through an analogue spectroscopy amplifier (Ortec 662) and the PHA board (7600-500 on the MCA-7600). When the shaping time (ST) of the amplifier was set at 10 μs, the peak counts for 662 keV was underestimated approximately 13% in the case the dead time was 30%, compared with the case the ^{57}Co source was not added. With the shorter STs of 2 μs and 6 μs, the counting-losses were smaller but still around 6%. Instead, in the case a digital system (digital PHA board 7600-200 on the MCA-7600) was used, the counting-losses were significantly reduced (less than 2% at dead time 30%) even if the equivalent ST (6 μs for the rise time (RT) of 12 μs and flat-top time of 1.2 μs) was selected (Fig. 8 (b)). Because the dead time is usually around 5% when the standard sources are measured, the correction of the counting-loss can be minimized using the DSP system.

3.4 Quality Assurance

In addition to the daily check of the systems, the laboratory, as a means to external quality assurance, regularly participated in the proficiency test exercises and interlaboratory comparisons of radioactivity analysis for samples containing radiocesium.

The laboratory so far participated in three proficiency test exercises based on ISO/IEC 17043 [21]. The exercises were performed with certified reference materials of brown rice and dried beef, provided by key laboratories in Japan. In each exercise, the laboratory achieved the *satisfactory* results on the assessment of ^{134}Cs and ^{137}Cs radioactivity concentrations.

With the continuing challenges, in October 2015, the laboratory has been accredited the ISO/IEC 17025 standard [22] by the Japan Accreditation Board (JAB), as a testing laboratory for radioactivity analysis based on gamma-ray spectrometry with germanium detectors.

4 SUMMARY AND CONCLUSION

JAEA has newly set up a laboratory for radioactivity analysis in Fukushima after the nuclear accident in March 2011. At the laboratory, radioactivity concentrations of environmental samples are determined based on high-resolution gamma-ray spectrometry. Although the laboratory has a short history, R&Ds required for demonstrating quality of analysis have been started, and will be carried on.

Taking advantage of the established laboratory and developed techniques, prompt and accurate analysis on radioactivity quantification for various environmental samples is achieved. Provision of reliable information on these activities also promotes the reassurances of the people in Fukushima. JAEA will keep contribute to secure and early restoration of the Fukushima environment.

5 REFERENCES

- [1] Japan Atomic Energy Agency, 2016. Database for Radioactive Substance Monitoring Data. Retrieved 2016-04-21 from: <http://emdb.jaea.go.jp/emdb/portals/b136/>.
- [2] IAEA, 2011. Summary Report of the Preliminary Findings of the IAEA Mission on Remediation of Large Contaminated Areas Off-site the Fukushima Dai-ichi NPP, NE/NEFW/2011. Retrieved 2016-02-23 from: <http://www.iaea.org/sites/default/files/preliminaryfindings2011.pdf>.
- [3] Baba, M., 2013. Fukushima accident: What happened?, *Radiation Measurements*, 55, 17–21.
- [4] Chino, M., Nakayama, H., Nagai, H., et al., 2011. Preliminary estimation of release amounts of ¹³¹I and ¹³⁷Cs accidentally discharged from the Fukushima Daiichi Nuclear Power Plant into the atmosphere, *Journal of Nuclear Science and Technology*, 48(7), 1129–1134.
- [5] Povinec, P.P., Hirose, K. and Aoyama, M., 2013. Fukushima Accident: Radioactivity Impact on the Environment, 1st ed., Elsevier, pp.116–128.
- [6] Seiko EG&G, 2010. Spectrum Analysis by Gamma Studio, DS-P600—Operation Manual, Rev. 2.0.0.0, Seiko EG&G Co. Ltd., Chiba, Japan (in Japanese).
- [7] Jordanov, V.T., Knoll, G.F., Huber, A.C., et al., 1994. Digital techniques for real-time pulse shaping in radiation measurements, *Nuclear Instruments and Methods in Physics Research A*, 353, 261–264.
- [8] Sasaki, Y., Abe, H., Mitachi, K., et al., 2015. The transfer of radiocesium from the bark to the stemflow of chestnut trees (*Castanea crenata*) contaminated by radionuclides from the Fukushima Dai-ichi nuclear power plant accident, *Journal of Environmental Radioactivity*, <http://dx.doi.org/10.1016/j.jenvrad.2015.12.001>.
- [9] JAEA, 2012. Efforts to Establish Modelling Techniques for Forecasting the Distribution of Radioactive Materials, Topics Fukushima, No. 7, Japan Atomic Energy Agency, Fukushima, Japan, pp.1–2.
- [10] Nuclear Regulation Authority of Japan, 2016. Monitoring Information of Environmental Radioactivity Level. Retrieved 2016-04-22 from: <http://radioactivity.nsr.go.jp/en/>.
- [11] Japan Radioisotope Association, 2016. Supply—Radionuclides/Labeled Compounds. Retrieved 2016-04-22 from: <http://www.jrias.or.jp/e/cat02/index.html>.
- [12] Eckert & Ziegler Isotope Products, 2012. Eckert & Ziegler Reference & Calibration Sources—Product Information catalogue, R&C 2007 v1.0, Homepage: <http://www.ezag.com>.
- [13] Cooper, J.A., 1970. Factors determining the ultimate detection sensitivity of Ge(Li) gamma-ray spectrometers, *Nuclear Instruments and Methods*, 82, 273–277.
- [14] Ministry of Education, Culture, Sports, 1992. Science and Technology of Japan (MEXT), Gamma-ray Spectrometry by Germanium Semiconductor Detectors. In: *Radioactivity Measurement Series*, vol. 7, Japan Chemical Analysis Center, Chiba, Japan (in Japanese).
- [15] ISO, 2015. Measurement of Radioactivity in the Environment—Soil—Part 3: Test Method of Gamma-emitting Radionuclides Using Gamma-ray Spectrometry. ISO 18589-3, International Standardization Organization, Geneva, Switzerland.
- [16] Gilmore, G.R., 2007, *Practical Gamma-ray Spectrometry*, 2nd Ed., John Wiley & Sons, England.
- [17] American National Standards Institute, 1999, American National Standard for Calibration and Use of Germanium Spectrometers for the Measurement of Gamma-Ray Emission Rates of Radionuclides. ANSI N42.14-1999, The Institute of Electrical and Electronics Engineers, Inc., New York.
- [18] X-5 Monte Carlo Team, RSICC, 2005. MCNP—Monte Carlo N-particle Transport Code, version 5, LANL Manual LA-UR-03-1987, Oak Ridge National Laboratory, Los Alamos.
- [19] Saegusa, J., 2008. CREPT-MCNP 1.1 (Calibration Code for the Representative Point Method with MCNP), JAEA-Data/Code 2008-017, Japan Atomic Energy Agency, Ibaraki, Japan.
- [20] Pehl, R.H., Goulding, F.S., Landis, D.A., et al., 1968. Accurate determination of the ionization energy in semiconductor detector, *Nuclear Instruments and Methods*, 59, 45–55.
- [21] ISO, IEC, 2010. Conformity Assessment—General Requirements for Proficiency Testing. ISO/IEC 17043:2010, International Standardization Organization, Geneva, Switzerland.
- [22] ISO, IEC, 2005. General Requirements for the Competence of Testing and Calibration Laboratories. ISO/IEC 17025:2005, International Standardization Organization, Geneva, Switzerland.

New Remote Controlled Experiments in Nuclear Chemistry

Jan-Willem Vahlbruch, Wolfgang Schulz, Claudia Fournier, Paul Hanemann, Sebastian Büchner, Clemens Walther

Institute for Radioecology and Radiation Protection (IRS), Leibniz University of Hanover, Germany

Abstract. As part of the CINCH II project (Cooperation in Education and Training in Nuclear Chemistry) remote controlled experiments have been developed to support education and training in nuclear chemistry. Even though such remote controlled experiments will never substitute real hands-on training, they can be a useful addition to traditional training with a particular value to institutions without laboratories for radioactive work, or laboratories with very limited equipment and radioactive sources. Also the teaching material will help to enable institutions to offer nuclear chemistry courses even for small numbers of learners. This will help to broaden the nuclear chemistry education and to contribute to the preservation of competence. Three remote controlled experiments have been designed: one experiment to analyse different environmental samples by using a HP-GE-detector for gamma-spectrometry, a second one to demonstrate the potential of electrochemical deposition techniques for the measurement of radionuclides and a third one to show and explain the basis of ion-chromatography. In this contribution the purpose and the setup of these three experiments are described and different opportunities to use and analyze the measured data in consideration of the previous knowledge of students are explained.

KEYWORDS: *education and training in radiochemistry; remote controlled experiments.*

1 INTRODUCTION

In its 2000 report “Nuclear energy, a cause for concern?” [1] the Nuclear Energy Agency testified a lack of training and education in the field of nuclear chemistry in the European countries. The demand for these skills would not decrease even if Europe decides to phase out its nuclear energy, as they are needed even more for the decommissioning of nuclear plants as well as for radiological applications outside of the energy sector. In order to mitigate the effects of the decline of number of staff qualified in nuclear chemistry, the CINCH-II project is aiming at the European co-ordination of education in nuclear chemistry [2].

Objectives of the CINCH-II project include:

- To further develop and implement the plan for the European master's degree in nuclear chemistry
- To develop a Training Passport in Nuclear Chemistry and prepare the grounds for the European Credit system for Vocational Education and Training (ECVET)
- To lay the foundations of a Nuclear Chemistry Education and Training Platform
- To develop methods of raising awareness of the possible options for nuclear chemistry in potential students, academia and industry
- To develop a sustainable system for mobility securing mechanisms for an efficient mobility program of trainers and trainees within the Nuclear Chemistry Network

The Institute for Radioecology and Radiation protection (IRS) of the Leibniz University of Hanover, Germany, contributes to this project by developing three fully remote-controlled experiments spotlighting on different aspects of nuclear chemistry. These automated labs allow a user to operate complete radiochemical experiments through the internet from anywhere in the world. Although hands-on-experiments will always be the first choice for teaching basic radiochemical knowledge and skills, remote controlled experiments are much closer to real work in a laboratory than e.g. computer simulations and can be seen as a true enhancement of modern learning concepts [3]. Different level of difficulties concerning the analysis of the experiment can be implemented and minor errors (as they might happen during real work in a laboratory also) can be made by operating the system via the

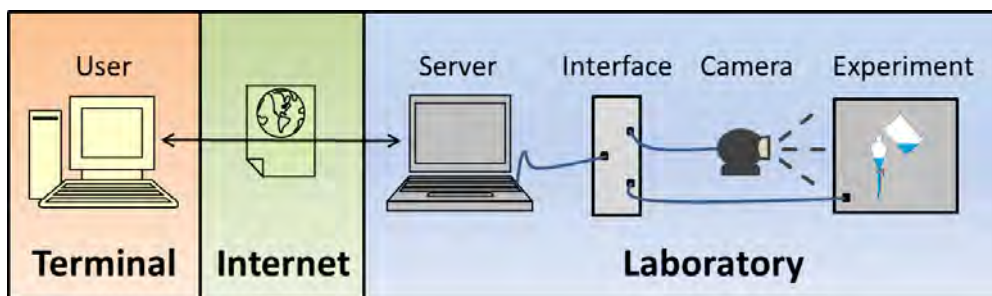
Internet. That enhances the learning effect compared with computer simulations significantly and can therefore contribute to the Education and Training of students in radiochemistry.

The handling of radioactive material in a chemical laboratory is a high cost factor with respect to the man-power, the lab space and material. It can be observed that the number of universities who are willing to conduct these time-consuming and work-intensive experiments is decreasing constantly. For these universities remote-controlled experiments can be seen as an important alternative as a teaching tool with the aim to offer a practical education and training in nuclear chemistry.

2 REMOTE CONTROLLED EXPERIMENTS

The basic concept of remote controlled experiments is in general quite simple and shown in figure 1.

Figure 1: General set-up of remote controlled experiments [4]



The host of the experiment has to define a registration-procedure to avoid an overlap of logins at the same time. After the user has received its registration-code he can login to a server via internet by using its own terminal. While a camera provides a live video-feed the student can perform the experiment, control different parameters and collect the data. After the experiment has been finished, the data will be sent via e-mail to the user who can start to analyze the collected data.

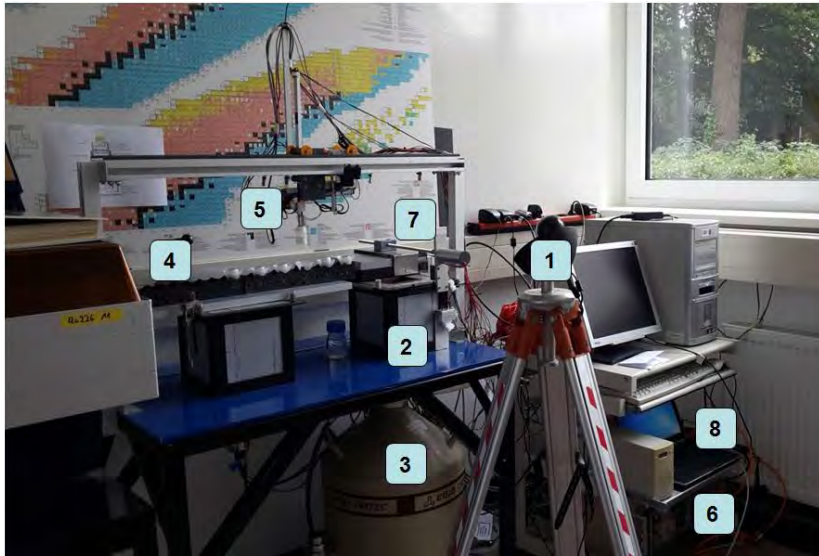
All three remote-controlled experiments described in this article have been developed by using LabView™.

2.1 GammaLab

The GammaLab remote controlled experiment is focused on teaching gamma spectrometry by using environmental samples, and on showing the importance of characteristic limits in the evaluation of a gamma spectrum. The setup is shown in figure 2.

The experimental setup is developed using Lego Mindstorm NXT motors, which makes it possible to position by remote control different samples in a freely selectable sequence on a germanium detector. The user controls the setup through an interface (figure 3) that allows him to move the samples, to start the measurements, to watch the spectrum during the measurement (figure 4) and to retrieve the measured data in detail (via e-mail after the measurement). He also has the possibility to close a shielding which is located over the germanium detector, in order to decrease the background (necessary when measuring samples with low radioactivity).

Figure 2: GammaLab setup



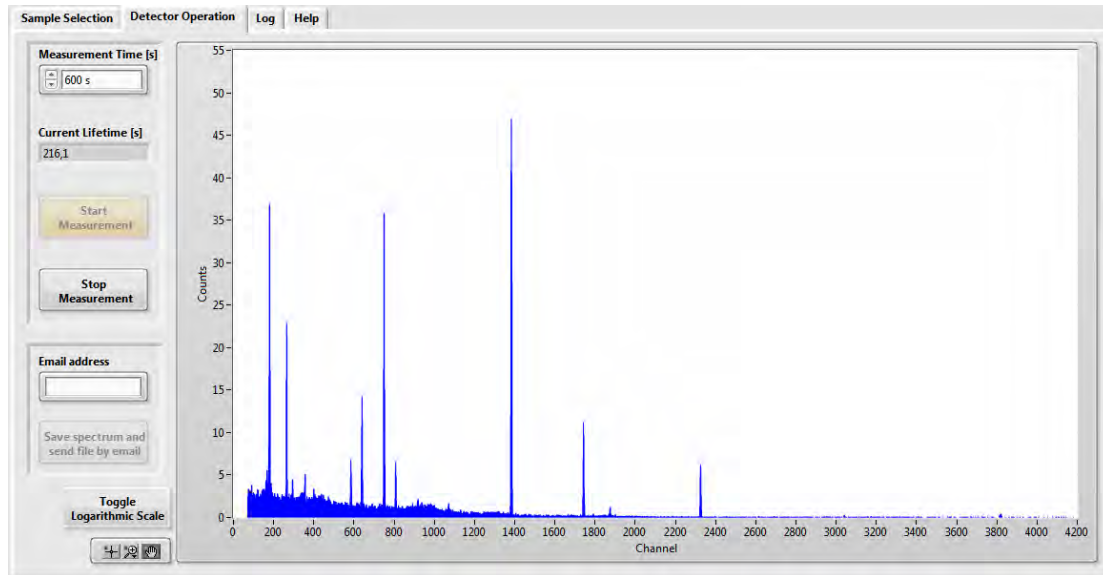
1. webcam for video-feed
2. germanium detector
3. liquid nitrogen coolant
4. rack with radioactive samples containing different activities
5. remote controlled sample changer
6. data acquisition system
7. lead shielding of the detector
8. computer for data transfer

This GammaLab experiment can be used for several teaching goals:

- Demonstration on gamma spectroscopy.
- A list of unattributed samples is given with the task to identify the samples by analysing the measured gamma-spectra
- Understanding when and why the knowledge of the characteristic limits is important and how corresponding calculations have to be performed.

Figure 3: Panel to operate GammaLab



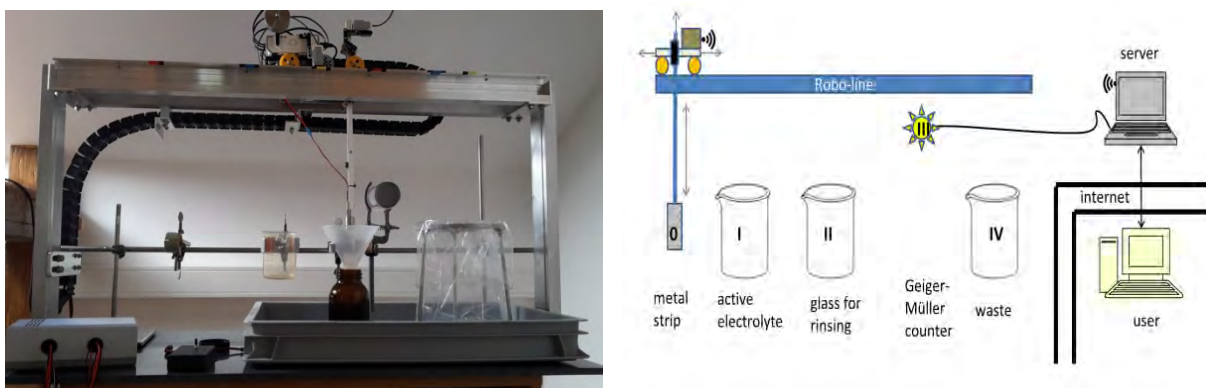
Figure 4: Spectrum measured by GammaLab

Depending on the teaching goal of the experiment, a more or less detailed explanation of the physical process behind gamma spectrometry is provided. There are several available samples which can be measured:

- a depleted U-fuel pellet which contains nuclides of the U-238 and U-235 decay chains,
- uranium glass beads,
- monazite sand, which contains mostly the radionuclides of the Th-232 decay chain,
- contaminated soil from an IAEA collaborative study (Ra-226 contamination),
- phosphogypsum from an IAEA collaborative study, which has an increased content of natural radionuclides,
- two U-232 solutions of different filling height,
- two pitchblende solutions of different filling heights, with radionuclides of the U-238 and U-235 decay series,
- a sample taken from the gate of the Fukushima Daiichi nuclear reactor after the accident and
- an environmental water sample.

2.2 PAULA (Programmable AUtodepositionLAB)

With this experiment the user is able to control via internet an autodeposition experiment. The teaching goal of the experiment is the demonstration of electrochemical deposition techniques for the measurement of radionuclides. In figure 5 the real experiment is presented, side by side with a diagram.

Figure 5: Setup of PAULA

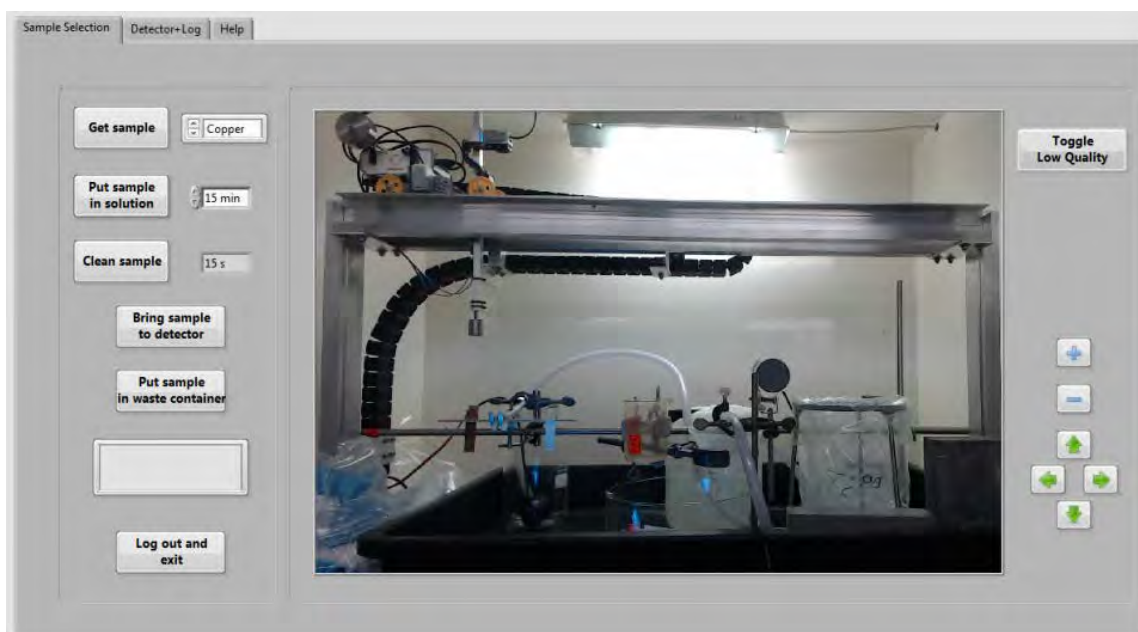
The setup is similar to the one of GammaLab, the robotic arm being built with Lego Mindstorm EV3. The remote controlled arm makes it possible to move a metallic strip to different stations:

- a sample selection station, where the user can select the desired metallic strip (0)
- a glass which contains an active electrolyte (I), e.g. 20 kBq Tc-99
- a glass for rinsing (II)
- a Geiger-Müller counter (III)
- a waste bag (IV)

After performing a blank measurement with a Geiger-Müller counter of a metal strip, the user has to immerse the strip in an Ammonium-pertechnetate ($\text{NH}_4^{99}\text{TcO}_4$) solution in water. Depending on the electrochemical potential of the metal, the reduction of the pertechnetate ions in solution will lead to a deposition of TcO_2 on the metal surface. After immersion the strip has to be cleaned by rinsing it with water (to ensure that the solution is not sticking to it anymore). A new measurement of the strip will show that radioactive material has deposited on it. The strip can be immersed several times in the solution to show the increase of deposited radioactivity on the strip until a saturation level is reached. After finishing the experiment, the strip can be disposed of in the waste container. The previous steps can be repeated using a more noble metal (for example copper instead of steel) with the result that no measurable radioactivity will be deposited.

The experiment can be used to teach and demonstrate fundamentals in electrochemistry and the use of deposition techniques for the measurement of radioactivity. As the radioactive technetium deposited on the metal strips can be measured with very high efficiency by the Geiger - Müller counter (which is one important outcome of the experiment), the experiment works with very low total activities (approx. one five-hundredth of the exemption limit according to the German Radiation Protection Ordinance [5]). In figure 6 the front-panel of PAULA is shown.

Figure 6: Front-panel to operate PAULA



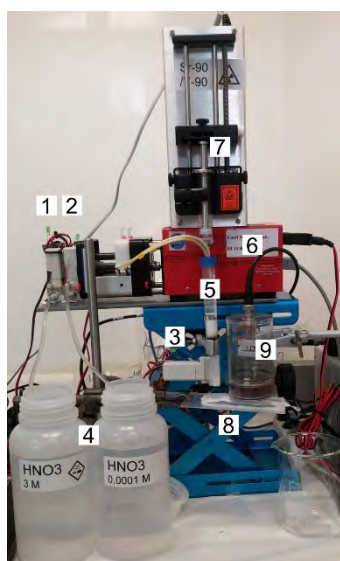
2.3 IONLab

IONLab is a basic remote-controlled ion-chromatography setup. It allows the user to apply a mixture of radionuclides onto a column and then use a selection of solvents for the elution [4]. The separation is followed by a Geiger-detection that yields a simple chromatogram of the activity. In order to enhance out-of solution-detection a small slide takes up the drop-shaped liquid coming from the column and transforms it into a thin-layered laminar flow. The experiment can be used to learn the fundamentals in theoretical, as well as practical chromatography and demonstrates the potential of chromatographical methods for the separation of radionuclides. At the moment it is set-up to perform an Y-90/Sr-90-separation using Sr-Resin as a solid extraction phase and different nitric acid concentrations for the separate elution. The setup (see figure 7) consists out of

- a syringe pump, which injects activity onto a column,
- a peristaltic pump, which helps to bring two different eluents to the column,
- two containers, one with 3M HNO₃ and one with 0.0001M HNO₃,
- a Geiger-Müller counter,
- a slide, which slows down the liquid drop, so it stays longer under the detector and the measurement lasts longer and
- a waste container.

The first action is to condition the column for approximately five minutes. The counting rate can be set in the tab 'measurement' by entering the desired time interval in the field 'measurement time' (the optimal choice for the measurement interval is 20s). Also the overall measurement time can be chosen there (default time is 30 minutes). After the column is sufficiently conditioned, the actual separation experiment can begin: the radioactive solution can be injected using the syringe pump by pressing 'Inject activity' in the field 'Injection'. The animated experimental scheme in the lower right corner, as well as the camera window of the injection process, can be used to follow the status of the experiment. After completed injection the user should wait a few seconds for the applied volume to distribute uniformly at the upper end of the separation column. In the field 'solvent pump' the desired elution rate for the experiment can be chosen and the elution can start. At this moment also the Geiger-Muller-counter measurement should start. After several minutes, a clear signal will be drawn in the chromatogram. After this signal drops significantly the user has to change the eluent and a second peak will be measured in the chromatogram. After this second peak fades the experiment has finished and the measured data can be sent via e-mail to the user. A screenshot of the front-panel can be seen in figure 8.

Figure 7: Setup of IONLab [4]

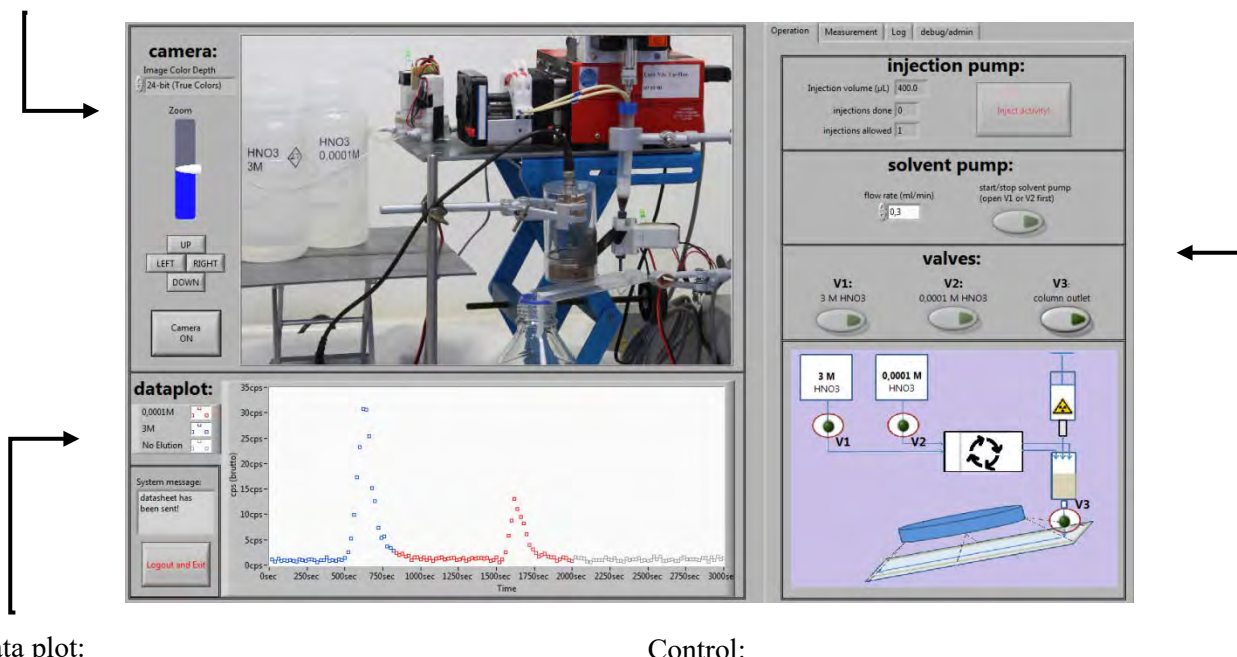


Components:

- 1, 2 – valves for solvent selection
- 3 – valve for column-control
- 4 – eluent reservoirs
- 5 – separation column filled with solid phase
- 6 – peristaltic pump for solvent pumping
- 7 – syringe pump for injection of the radionuclide-mix
- 8 – detection-slide to take up and spread the solution
- 9 – Geiger counter for online-detection

Figure 8: IONLab-surface [4]Video Feed:

A camera capturing the whole experiment streams a live-feed to the user.

Data plot:

- A chromatogram of the activity is building up throughout the experiment.
- Based on the data the user has to decide when to do crucial tasks like changing solvents.
- All data generated is logged and may be copied or sent via e-mail to the user's address.

Control:

- The components involved (valves, pumps, detector) are handled directly by the user.
- The experiment is not "self-running"! Bad decisions in the operation will yield bad results.

3 CONCLUSION

Educational experiments have always been an indispensable tool for generations of students and teachers in natural sciences [6]. Concerning radiochemical education experimental setups using radioactive material are a high cost factor in terms of man-power, lab-space and material. To support teachers and students in the field of radiochemical education all together six remote-controlled experiments have been set up in the CINCH II project, three of them (GammaLab, PAULA and IONLab) at the Institute for Radioecology and Radiation Protection (IRS), Leibniz University of Hanover, Germany. Although simulations can never replace hands-on experiments, educational concepts might be supported by the use of remote-controlled experiments. By performing the remote-controlled experiments build at IRS, students all over the world can improve their knowledge about fundamental radiochemical basics and measurement-techniques. Depending on the knowledge and the skill of the user the experiments can be analysed in different levels of difficulty to be able to take into consideration the varying prerequisites and qualifications of the end-user.

4 AKNOWLEDGMENTS

This work was supported by the CINCH-II-project as a part of the European Atomic Energy Community's 7th Frame-work Programme (EURATOM FP7 2007-2011) under grant agreement No. 605173.

5 REFERENCES

- [1] Nuclear Energy Agency, NUCLEAR EDUCATION AND TRAINING Cause for Concern? A Summary Report, Paris, 2000. ICRP, 2007. The 2007 Recommendations of the International Commission on Radiological Protection. ICRP Publication 103. Ann. ICRP 37(2-4).
- [2] John, J., Lehto, J., Koivula, T., Omtvedt, J.-P., J. Radioanal. Nucl. Chem. 2015, 1, 459-466.
- [3] Eckert, B., Altherr, S., Vetter, M., Jodl, H.-J., Eur J. Phys. 2007, 28, 127 González, A.J., 2011.
- [4] Schulz, W., Fournier, C., Vahlbruch, J.-W., Walther, C., Radiochimica Acta, in print.
- [5] Strahlenschutzverordnung vom 20. Juli 2001 (BGBl. I S. 1714; 2002 I S. 1459), zuletzt geändert durch Artikel 5 Absatz 7 des Gesetzes vom 24. Februar 2012 (BGBl. I S. 212).
- [6] Hopf, M., Physikdidaktik kompakt, Vol 2011, Auls Verlag in der Stark Verlagsgesellschaft, 2011, pp. 106-115.

Introduction and assessment of new heavy weight concrete shields using Monte Carlo simulation

Mahdi Saeedi-Moghadam^a, Mahdi Kazempour^c, Sedigheh Sina^d, Reza Jalli^a, Banafsheh Zeinali-Rafsanjani^{a,b}

^aMedical imaging research center, Shiraz University of medical sciences, Shiraz, Iran

^bNuclear medicine and molecular imaging research center, Shiraz university of medical sciences, Shiraz, Iran

^cDepartment of radiobiology, School of paramedical sciences, Shiraz university of medical sciences, Shiraz, Iran

^dNuclear Engineering Department, School of Mechanical Engineering, Shiraz University, Shiraz, Iran

Abstract. In constructing medical or industrial radiation facilities which use photon sources and require radiation shields, heavy-weight concretes are suitable materials. In this study the shielding properties of 21 Galena (PbS) concretes containing 7 borated minerals with three mixture patterns were investigated using MCNP4C Monte Carlo code and these heavy concretes with borated minerals are introduced as suitable materials for photon and neutron shielding. Two geometries of measurement (narrow and broad beam) were modelled in order to calculate the X and gamma radiation attenuation of the concretes. The X-ray energies of 40, 60, 90, and 120 kVp and gamma rays of 99m Tc, 131-I, 137-Cs, and 511keV annihilation photons were considered as radiation sources. The values of photon flux and the X-ray spectrum using mentioned concretes were compared with those of ordinary concrete. The results demonstrated that photon attenuations caused by heavy concretes which introduced in this study are more than ordinary concrete. Also it is revealed that the concrete containing Orthopinokiolite as the borated material made by the third mixing pattern has the best photon attenuation. According to the results, the shielding characteristics of concretes containing different borated minerals are similar in high photon energies, while in low energies the attenuation depends on the type of borated mineral used in the concretes.

KEYWORDS: *heavy weight concrete; shields; MCNP4C; simulation; radiation.*

1 INTRODUCTION

Heavy weight concretes have been widely used in radiation protection (density: 2900 to 6000 kg/m³) [1-16]. Different minerals have been proposed by different investigators, in constructing heavy concretes for radiation shielding purposes, i.e. Barite, Galena hematite–serpentine, ilmenite– limonite, basalt–magnetite[17], ilmenite, basalt, steel, magnetite, Ulexite, Datolite, and optical glass [1-16]. The aim of this study is Monte Carlo simulation of x, and gamma ray attenuation properties of multi-purpose high density borated concretes using MCNP4c code.

2 MATERIALS AND METHODS

Different minerals were proposed for construction of concretes applicable for neutron and photon shielding. Totally 21 concretes were constructed using different minerals according to Table 1.

Table 1: Mixing conditions for constructing concretes

	First pattern (Weight %)	Second pattern (Weight %)	Third pattern (Weight %)
Galena	56.3%	61.3%	66.3%
Borated minerals*	20%	15%	10%
Cement	17%	17%	17%
Water	5%	5%	5%
Micro silica	1.7%	1.7%	1.7%
Water to cement ratio	0.4%	0.4	0.4%

* Colemanite, Ulexite, Hydroboracite, Tourmaline, Datolite, Orthopinakiolite, and Priceite

1.1 MCNP4C Monte Carlo simulations

Table 2: The photon attenuations after concrete slabs with dimension of $0.1 \times 10 \times 10 \text{ cm}^3$ were obtained by MCNP4C code [18].

The attenuation of X-ray sources with kVp=40, 60, 90, and 120 Kv, and the gamma rays from TC-99m were studied in this study. IPEM 78 software[19] was used for obtaining photon spectra. For scoring the results, Tallies F4 and F5 were used.

3 RESULTS AND DISCUSSIONS

3.1 40kvp X-ray beam

Table 2, compares the photon attenuation properties ($\frac{I}{I_0}$) of the designed high density concretes (with 1mm thickness) for both narrow and broad beam geometries. Where I is the photon flux after 1mm concrete, and I_0 is the photon flux in the absence of the shields. According to the results, the designed concretes can be effectively used for radiation shielding of low energy photons. The high density concretes reduce the x-ray fluence from 0.34% to 2.11% of the fluence after the ordinary concrete.

Table 2: Relative transmission ($\frac{I}{I_0}$), for 1mm of different concretes.

	$\left(\frac{I}{I_0}\right)$ narrow beam geometry	$\left(\frac{I}{I_0}\right)$ Broad beam Geometry		$\left(\frac{I}{I_0}\right)$ narrow beam geometry	$\left(\frac{I}{I_0}\right)$ Broad beam Geometry
Hydroborasite_1	0.0775	0.0783	Datolite_2	0.0478	0.0645
Ulexite_1	0.0709	0.0743	Tourmaline_2	0.0454	0.0481
Colemanite_1	0.0684	0.0718	Orthopinakiolite_2	0.0405	0.0427
Priceite_1	0.0640	0.0673	Ulexite_3	0.0404	0.0431
Datolite_1	0.0612	0.0645	Hydroborasite_3	0.0430	0.0458
Hydroborasite_2	0.0585	0.0616	Colemanite_3	0.0395	0.0422
Tourmaline_1	0.0577	0.0608	Priceite_3	0.0378	0.0430
Ulexite_2	0.0540	0.0569	Datolite_3	0.0368	0.0374
Colemanite_2	0.0525	0.0553	Tourmaline_3	0.0354	0.0380
Orthopinakiolite_1	0.0500	0.0432	Orthopinakiolite_3	0.0326	0.0350
Priceite_2	0.0495	0.0523	Ordinary concrete	0.6019	0.6071

3.2 60 kvp X-ray beam

Table 3, compares the photon attenuation properties ($\frac{I}{I_0}$) for 60kvp x-rays. According to the results, the designed concretes can be effectively used for radiation shielding of low energy photons. The high density concretes reduce the x-ray fluence from 5.42% to 12.88% of the fluence after the ordinary concrete.

Table 3: Relative transmission ($\frac{I}{I_0}$), for 1mm of different concretes for 60kvp.

	$\left(\frac{I}{I_0}\right)$ narrow beam geometry	$\left(\frac{I}{I_0}\right)$ broad beam geometry		$\left(\frac{I}{I_0}\right)$ narrow beam geometry	$\left(\frac{I}{I_0}\right)$ broad beam geometry
Hydroborasite_1	0.0088	0.0095	Datolite_2	0.0032	0.0034
Ulexite_1	0.0074	0.0080	Tourmaline_2	0.0029	0.0031
Colemanite_1	0.0068	0.0074	Orthopinakiolite_2	0.0023	0.0024
Priceite_1	0.006	0.0065	Ulexite_3	0.0023	0.0024
Datolite_1	0.0054	0.0058	Hydroborasite_3	0.0026	0.0027
Hydroborasite_2	0.0049	0.0053	Colemanite_3	0.0022	0.0023
Tourmaline_1	0.0048	0.0051	Priceite_3	0.002	0.0021
Ulexite_2	0.0042	0.0044	Datolite_3	0.0019	0.0020
Colemanite_2	0.0039	0.0042	Tourmaline_3	0.0017	0.0018
Orthopinakiolite_1	0.0035	0.0038	Orthopinakiolite_3	0.0014	0.0015
Priceite_2	0.0035	0.0037	Ordinary concrete	0.4173	0.4224

3.3 90 kvp X-ray beam

Table 4, compares the photon attenuation properties ($\frac{I}{I_0}$) for 90kvp x-rays. The designed high density concretes reduce the x-ray fluence from 18.74% to 28.73% of the fluence after the ordinary concrete.

Table 4: Relative transmission ($\frac{I}{I_0}$), for 1mm of different concretes for 90kvp.

	$\left(\frac{I}{I_0}\right)$ narrow beam geometry	$\left(\frac{I}{I_0}\right)$ Broad beam Geometry		$\left(\frac{I}{I_0}\right)$ narrow beam geometry	$\left(\frac{I}{I_0}\right)$ Broad beam Geometry
Hydroborasite_1	0.221	0.230	Datolite_2		0.169
Ulexite_1	0.210	0.219	Tourmaline_2		0.164
Colemanite_1	0.206	0.214	Orthopinakiolite_2		0.154
Priceite_1	0.198	0.207	Ulexite_3		0.154
Datolite_1	0.194	0.202	Hydroborasite_3		0.160
Hydroborasite_2	0.189	0.197	Colemanite_3		0.152
Tourmaline_1	0.187	0.195	Priceite_3		0.149
Ulexite_2	0.181	0.189	Datolite_3		0.149
Colemanite_2	0.178	0.189	Tourmaline_3		0.144
Orthopinakiolite_1	0.173	0.181	Orthopinakiolite_3		0.137
Priceite_2	0.172	0.180	Ordinary concrete		0.731

3.4 120 kvp X-ray beam

The energy spectrum of the X-ray after the shield is shown in Figure 1.

Figure 1: Comparison of the energy spectrum after the high density concrete with 3rd mixing pattern concretes for 120kvp x-rays.

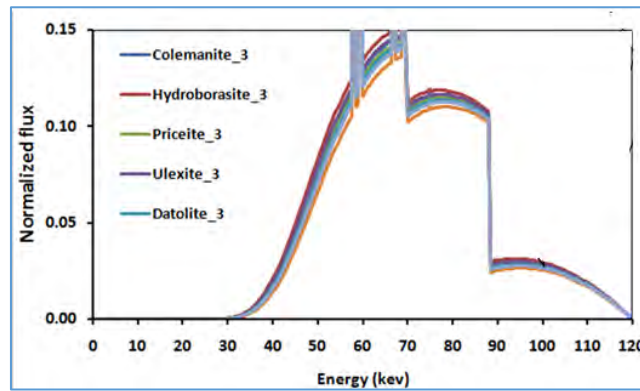


Table 5, compares the photon attenuation properties ($\frac{I}{I_0}$) for 120kvp x-rays. According to the results, the designed concretes can be effectively used for radiation shielding of low energy photons. The high density concretes reduce the x-ray fluence from 24.05 to 35.44% of the fluence after the ordinary concrete.

Table 5: Relative transmission ($\frac{I}{I_0}$), for 1mm of different concretes for 120kvp.

	$\left(\frac{I}{I_0}\right)$ narrow beam geometry	$\left(\frac{I}{I_0}\right)$ Broad beam Geometry		$\left(\frac{I_{oc}}{I_c}\right)$ narrow beam geometry	$\left(\frac{I_{oc}}{I_c}\right)$ broad beam geometry
Hydroborasite_1	0.29	0.30	Datolite_2	0.23	0.24
Ulexite_1	0.28	0.29	Tourmaline_2	0.22	0.23
Colemanite_1	0.27	0.28	Orthopinakiolite_2	0.21	0.22
Priceite_1	0.26	0.27	Ulexite_3	0.21	0.22
Datolite_1	0.26	0.27	Hydroborasite_3	0.22	0.23
Hydroborasite_2	0.25	0.26	Colemanite_3	0.21	0.22
Tourmaline_1	0.25	0.26	Priceite_3	0.20	0.21
Ulexite_2	0.24	0.25	Datolite_3	0.20	0.21
Colemanite_2	0.24	0.25	Tourmaline_3	0.20	0.21
Orthopinakiolite_1	0.23	0.24	Orthopinakiolite_3	0.19	0.20
Priceite_2	0.23	0.24	Ordinary concrete	0.79	0.80

3.5 Attenuation properties for ^{99m}Tc, ¹³¹I, ¹³⁷Cs, and annihilation photons

According to the results, the flux after ordinary concrete, for ^{99m}Tc gamma rays are more than the flux after the heavy concretes. For photons of I-131, Cs-137 with higher energies, no significant differences are observed between the flux after these concretes and the ordinary one. For these photons, the concretes constructed with the three mixing pattern show approximately equal attenuations, while for 140keV gamma rays of ^{99m}Tc the photon flux after the heavy concretes containing orthopinakiolite with the three mixing patterns are 55% to 62% of the flux after the ordinary concretes.

4 DISCUSSION AND CONCLUSION

According to the results, the concrete containing Orthopinokiolite, with the 3rd mixing pattern showed the best photon attenuation for lower energies. The photon reduction after Orthopinokiolite_3 is a significant reduction for 40, and kV_P X-ray which. The attenuation properties all other concretes are also more significant in lower energies. In low energy photons, the photon attenuation depends on the type of borated mineral used in the concretes. The proposed concretes can also be effectively used as neutron concretes for shielding radiotherapy rooms, and nuclear reactors.

5 REFERENCES

- [1] Bashter, II. Neutron relaxation lengths in light and heavy concrete shields. 1993.
- [2] Bashter, II. Radiation attenuation and nuclear properties of high density concrete made with steel aggregates. *Radiation effects and defects in solids*. 1997;140(3-4):351-64.
- [3] Bashter, II, Abdo AE-S, Abdel-Azim MS. Magnetite ores with steel or basalt for concrete radiation shielding. *Japanese journal of applied physics*. 1997;36(6R):3692.
- [4] Abdo AE-S, Kansouh WA, Megahid RM. Investigation of radiation attenuation properties for baryte concrete. *Japanese journal of applied physics*. 2002;41(12R):7512.
- [5] Akkurt I, Basyigit C, Kilincarslan S, Mavi B. The shielding of γ rays by concretes produced with barite. *Progress in Nuclear Energy*. 2005;46(1):1-11.
- [6] Akkurt I, Akyildirim H, Mavi B, Kilincarslan S, Basyigit C. Gamma-ray shielding properties of concrete including barite at different energies. *Progress in Nuclear Energy*. 2010;52(7):620-3.
- [7] Akkurt I, Akyildirim H, Mavi B, Kilincarslan S, Basyigit C. Radiation shielding of concrete containing zeolite. *Radiation Measurements*. 2010;45(7):827-30.
- [8] Akkurt I, Akyildirim H, Mavi B, Kilincarslan S, Basyigit C. Photon attenuation coefficients of concrete includes barite in different rate. *Annals of Nuclear Energy*. 2010;37(7):910-4.
- [9] Akkurt I, Basyigit C, Kilincarslan S, Mavi B, Akkurt A. Radiation shielding of concretes containing different aggregates. *Cement and Concrete Composites*. 2006;28(2):153-7.
- [10] Akkurt I, Basyigit C, Kilincarslan S, Beycioglu A. Prediction of photon attenuation coefficients of heavy concrete by fuzzy logic. *Journal of the Franklin Institute*. 2010;347(9):1589-97.
- [11] Demir F, Budak G, Sahin R, Karabulut A, Oltulu M, Un A. Determination of radiation attenuation coefficients of heavyweight-and normal-weight concretes containing colemanite and barite for 0.663 MeV γ -rays. *Annals of Nuclear Energy*. 2013;38(6):1274-8.
- [12] Maruyama T, Kumamoto Y, Kato Y, Hashizume T, Moriyuki Y. Attenuation of 4-32 MeV X-rays in Ordinary Concrete, Heavy Concrete, Iron and Lead. *Health physics*. 1971;20(3):277-84.
- [13] Mortazavi SMJ, Mosleh-Shirazi MA, Baradaran-Ghahfarokhi M, Siavashpour Z, Farshadi A, Ghafoori M, et al. Production of a datolite-based heavy concrete for shielding nuclear reactors and megavoltage radiotherapy rooms. *Iran J Radiat Res*. 2010;8(1):11-5.
- [14] Mortazavi SMJ, Mosleh-Shirazi MA, Maheri MR, Yousefnia H, Zolghadri S, Haji-pour A. Production of an economic high-density concrete for shielding megavoltage radiotherapy rooms and nuclear reactors. *Iran J Radiat Res*. 2007;5(3):143-6.
- [15] Mortazavi SMJ, Mosleh-Shirazi MA, Roshan-Shomal P, Raadpey N, Baradaran-Ghahfarokhi M. High-performance heavy concrete as a multi-purpose shield. *Radiation protection dosimetry*. 2010:ncq265.
- [16] Urabe I, Kobayashi K, Fujita Y, Tsujimoto T, Guangchuan J. Depth distribution of residual radioactivities in the concrete wall of an electron linac facility. *Health physics*. 1991;60(4):587-91.
- [17] Aghamiri SMR, Mortazavi SMJ, Razi Z, Mosleh-Shirazi MA, Baradaran-Ghahfarokhi M, Rahmani F, et al. Ulexite-galena intermediate-weight concrete as a novel design for overcoming space and weight limitations in the construction of efficient shields against neutrons and photons. *Radiation protection dosimetry*. 2013;154(3):375-80.

- [18] Bashter, II. Calculation of radiation attenuation coefficients for shielding concretes. *Annals of nuclear Energy*. 1997;24(17):1389-401.
- [19] Dem'yanova VS, Kalashnikov DV. Heavy Optical Glass in Concrete for Radiation Protection. *Glass and ceramics*. 2014;70(9-10):338-9.
- [20] Briesmeister JF. MCNP6-A general Monte Carlo N-particle transport code. Version 4C, LA-13709-M, Los Alamos National Laboratory. 2000.
- [21] Cranley K, Gilmore B J, Fogarty G W A, L D. Catalogue of diagnostic x-ray spectra and other data, IPEM Report No. 78; 1997.

Exposure Rate Assessment From Selected Cathode Ray Tube Devices

Ife-Adediran O. O.^{a*}, Arogunjo A. M.^{a,b}

^aFederal University of Technology Akure, PMB 704, Akure-Ilesha express way, Akure, Nigeria.

^bDepartment of Physics, University of Medical Sciences, Ondo, Nigeria.

Abstract. Cathode Ray Tube (CRT) Television (TV) receivers and Personal Computer (PC) monitors have become major elements in the modern work environment and everyday life as TV receivers serve a good number of useful applications in information dissemination while PC monitors serve as interface between users and computers. The concerns as to whether the use of these devices can affect human health have been due to observed effects such as eye changes or discomfort, adverse reproductive outcomes, skin disorders etc. This study is an assessment of the exposure rate in air due to radiation from these devices with sample measurements taken using a Geiger- Muller counter (Kindenoo blueGeiger PG-15). All the CRT devices show relatively high values of ambient dose rates in the range of $0.28 \pm 0.01 - 0.32 \pm 0.01$ $\mu\text{Sv/h}$ for TV receivers and $0.25 \pm 0.01 - 0.31 \pm 0.02$ $\mu\text{Sv/h}$ for PC monitors above their respective background measurement of 0.24 ± 0.01 $\mu\text{Sv/h}$ average. The study also revealed that all the CRT units showed a decreasing trend of exposure rates with distance with correlation coefficient as high as -0.97. The exposure rates are well below the Food and Drug Administration regulations in 21 C.F.R of 0.5 mR/h. The Annual Effective Dose (AED) results (i.e. 0.17 – 0.91) mSv/y are well below the limits of the *International Commission on Radiological Protection (ICRP)* 60 recommendations for detrimental effects and those to prevent non-stochastic effects in the ICRP 26 recommendation for the lens of the eye, foetus/embryo, skin and hands.

KEYWORDS: *cathode ray tube; television; dose rate; annual effective dose.*

1 INTRODUCTION

All matter is made up of atoms. Some atoms are naturally stable while others are unstable. Radioactivity is a natural phenomenon that occurs when an atom with an unstable nucleus spontaneously transforms, releasing energy in the form of ionizing radiation. The released radiation may take the form of particles (including electrons, neutrons, and alpha particles) or of electromagnetic gamma radiation or X-rays, all with different amounts of energy. Radiation can also be generated artificially by machines [1]. Ionizing radiation refers to radiation that has enough energy to remove an electron from a neutral atom or molecule, creating a free radical. Ionizing radiations are known for the DNA damage and cancer causing capabilities. Radiation from sources such as power lines, cell phones, and traffic radars are all classified as non-ionizing radiation because they are not capable of removing an electron from an atom [2]. Radiation may be emitted when charged particles deposit energy to a medium through direct coulomb interactions with orbital interactions with orbital electrons of the atoms in the medium [3] Different types of radiation have distinct damage potential described by their Linear Energy Transfer (LET). Alpha radiation has high- LET because it deposits a relatively large amount of energy in a small area before it stops. Beta, gamma and x-radiation are low-LET because they deposit energy in a more diffuse pattern [4].

Naturally occurring radioactive materials are common in the environment and in the human body. Ionizing radiation from outer space (cosmic radiation) bombards the earth constantly. The ionizing radiation from these and similar natural sources is called background radiation [5]. Average natural radiation background in the United States (U.S.) ranges between 0.526 mSv/y and 1.31 mSv/y [6]. Man-made sources of radiation (from commercial and industrial activities) account for approximately 0.2 μSv of the annual radiation exposure. X-rays and other diagnostic and therapeutic medical procedures account for approximately 1.2 mSv a year. Consumer products like tobacco and smoke detectors account for another 0.1 mSv of the exposure to radiation each year [7]. The Health Physics Society recommends that exposures below 0.1 Sv only be evaluated qualitatively as the risks are too small to be observed. Doses below 0.1 Sv are considered to be low [2].

Medical exposure remains by far the largest artificial source of exposure to ionizing radiation and continues to grow at a remarkable rate as it accounts for 98% of the contribution from all artificial sources and are now the second largest contributor to the population dose worldwide representing approximately 20% of the total [1]. In non-medical X-rays shielding, a protective tube housing is one that surrounds the X-ray tube itself, or the tube and other parts of the X-ray apparatus (for example, the transformer), and is so constructed that the leakage radiation at a distance of 1 m from the target cannot exceed 10 mSv in 1 hour when the tube is operated at any of its specified ratings [8]. However, there is no difference between the effects caused by natural or man-made radiation [9]. We live in a world where technology is rapidly evolving especially those related with the design of electronic equipment and gadgets. Since the last three decades, electromagnetic radiation (EMR) from power lines, home wiring, airport and military radar, substations, transformers, computers, cell phones and domestic appliances have been of great concern and the phenomena underlying this have been thoroughly studied over the past few decades. This is because they are suspected to be largely part of the cause of brain tumors, leukemia, miscarriages, chronic fatigue, headaches, cataracts, heart problems, stress, nausea, chest pain, forgetfulness, depression, aggressive behavior, sleep disturbance and other health and dermatological problems [10].

CRTs are the video display components of televisions and computer monitors [11]. A CRT consists of three basic parts: the electron gun (neck) assembly, the viewing surface (panel), and the glass envelope (funnel). The basic raw material in the CRT glass is silica (~50-60 wt. %) but other different metallic oxides such as barium oxide and lead oxide are required to be incorporated in CRT glass as shielding agents for harmful radiation [12]. The electron beam in the CRT is swept horizontally and vertically across the viewing face – the whole face normally being covered in about 1/70th of a second [13]. CRTs are usually housed in a plastic casing [14]. CRTs emit X-rays as a result of electron braking (bremsstrahlung) by the screen and walls of the tube and the amount of radiation increases proportionally to the accelerating voltage [15]. The bremsstrahlung energy spectrum is a continuum with photon energies that extend as high as the electron energy itself [4]. The box-shaped CRT computer monitors generally have quite high levels of radiation even at 30 cm compared to the modern low-radiation flat screens. Another item most likely to cause a health hazard in many offices is the computer monitor, or screen. For computer users, radiation from computers may be a substantial component of the total electromagnetic radiation which the body is exposed to; the magnetic portion of this electromagnetic radiation (which is probably more dangerous than the electric portion) can penetrate just about anything. The use of screen shields especially for computer monitors will not totally reduce the effect of the radiations from the screen because of the magnetic portion of the electromagnetic radiation [16]. EMFs from TVs may be one of the biggest hazards in our home because children often love to sit very close to the TV, exposing themselves to a steady flow of harmful EMFs for hours. TV sets with larger screens tend to emit stronger fields because they contain larger cathode-ray tubes with the components that produce EMFs. In general, the larger the TV screen, the stronger the EMFs that are produced and the further away you need to be, to get out of the range of the electromagnetic fields [17].

In one survey, the Bureau of Radiological Health (1981) of the United States Department for Health and Human Services, Food and Drug Administration, made measurements under controlled laboratory conditions of X-ray emissions from 125 Visual Display Units (VDUs). Out of the VDUs tested no detectable level of X-rays was found for 117 units, while eight units emitted levels around or above 0.5 mR/h at 5 cm from the screen surface [18]. Vijay (2012) also opined that the radiations of EMFs from CRT TV/PC set are harmful for the life of blood tissue; it was concluded in the study that CRT TV/PC screens are harmful for the blood tissue of human beings at some distances and heights of the CRT TV/PC screen from ground level [17]. Kokalari (2011) compared the exposure according to the type of the monitor (i.e. CRT versus LCD), for the same way of placement in the classroom (around the walls). In all the working places where measurements were taken, the values of the electric field (of low frequency) and the values of the power density (high frequency) for the classroom equipped with LCD type monitors, were smaller than those for the classroom equipped with CRT type monitors [19].

In this research, the ionizing radiation emission from different TVs and PCs of CRT was measured at different positions and distances. This study further probes into the behavior of these devices with respect to the emission of ionizing radiation from them as well as monitor the exposure of users and individuals to these radiations.

2 METHODOLOGY

A total of 450 sample measurements were made from CRT computers and television receivers of different manufacturers, models and sizes. The product types were selected randomly based on their availability and popularity. Background measurements were also recorded when the devices were not switched on. Measurements were taken at different distances from screen front and lateral sides in time blocks of 30minutes for a total of about 2 hours for each device. At each point, four to six measurements were taken to cater for the statistical fluctuations in radiation measurements. While taking the measurements, the devices were isolated from other devices with possible EMR emission. A Geiger-Muller counter (blueGeiger PG-15) from Kindenoo France was used for all measurements [20]. This device is capable of detecting Beta, Gamma and X- radiations with a dose rate measurement range of 0.05 μ Sv/h to 300 μ Sv/h and a maximum radiation dose measurement of 250 mSv in a maximum time of ten (10) years. This blue-tooth enabled, 1- 2AA battery powered device displays the results on a monochrome Liquid Crystal Display on the device. It can also be connected to an Android (TM) cell phone or interfaced with a computer for easy data logging. The sensor location for this device is well noted for proper exposure to the radiation to be measured.

The mean and standard error for repeated measurements was determined and recorded for each measurement position. Analysis of variance (ANOVA) with MINITAB 16.0 statistical software was also used to test the significance of difference between the sampling means of the measurements at various distances from emission screen. The null hypothesis was:

$$H_0^{(1)} - \text{All treatment (distance) means are equal}$$

A test of significant difference between means was also carried out within a 95% confidence level to determine if there was a statistically significant difference between the emissions at the screen front and lateral sides or if the difference could have arisen due to chance. The Linear correlation coefficient (r) was used to evaluate the degree of relationship between the dose rates and both the distances from emission screen and the corresponding area of emission The Annual Effective Dose (AED) for the mean values of background only and for background plus contribution to radiation from measured equipment, for the most relevant sets of measurements were obtained under the conditions shown in table 1 for **continuous** exposure, **occupational** exposure and exposure for the **general public**.

Table 1: Duration of exposure for occupational and general public exposures

S/N	CODITIONS	OCCUPATIONAL	GENERAL PUABLIC
1	Continuous exposure to background radiation	24 h/d, 365d/y	24 h/d, 365d/y
2	Exposure to background + PC monitor	24 h/d, 365.25 d/y for background radiation; 8 h/d, 300 d/y for PC monitors	24 h/d, 365 d/y for background radiation; 2 h/d, 300 d/y for PC monitors
3	Exposure to background + PC monitors + TV receivers	24 h/d, 365.25 d/y for background radiation, 8 h/d, 300 d/y for PC monitors ; 2 h/d, 365 d/y for TV receivers	24 h/d, 365.25 d/y for background radiation, 2 h/d, 300 d/y for PC monitors ; 4 h/d during a 365 d/y for TV receivers

3 RESULTS AND DISCUSSION

Mean values and Standard errors of Dose Rates (DRs) in ($\mu\text{Sv/h}$) at different distances (d) and Time Blocks (TB) were recorded and used for further analysis.

3.1 Distribution of Measurements

All the CRT devices show relatively high values of DR ($0.2848 \pm 0.0134 - 0.3232 \pm 0.0093$) $\mu\text{Sv/h}$ average for TV receivers and ($0.2484 \pm 0.0105 - 0.3112 \pm 0.0195$) $\mu\text{Sv/h}$ average for PC monitors above their respective BG measurements 0.2426 ± 0.0077 $\mu\text{Sv/h}$ average. The distribution of these measurements and the percentage of maximum DR above BG measurements are shown in figure 1 and 2 respectively. CRTs emit X-rays as a result of electron braking (bremsstrahlung) by the screen and walls of the tube and the amount of radiation increasing proportionally to the accelerating voltage [15]. This result is in contrast with the survey of the Bureau of Radiological Health (1981) of the United States Department with no detectable X-ray found for 117 units out of 125 [13].

Figure 1: The distribution of DR measurements for CRT units

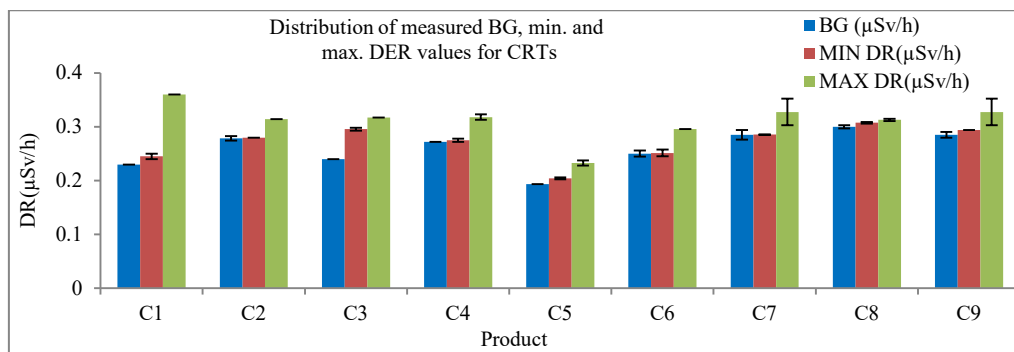
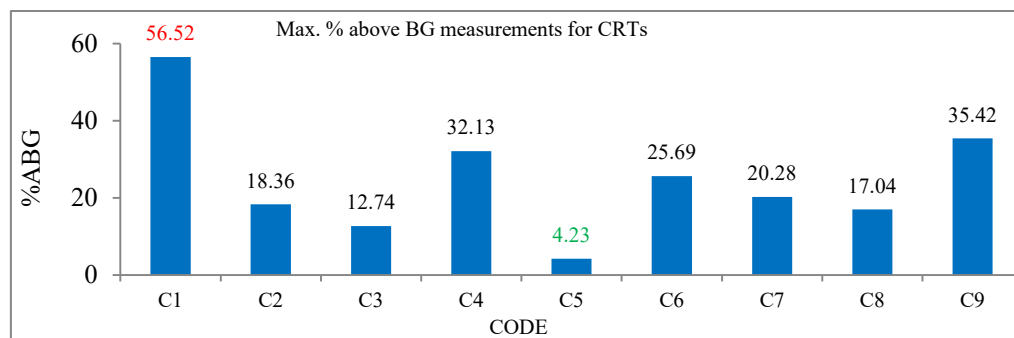


Figure 2: Percentage of maximum DR above Background measurements for CRTs

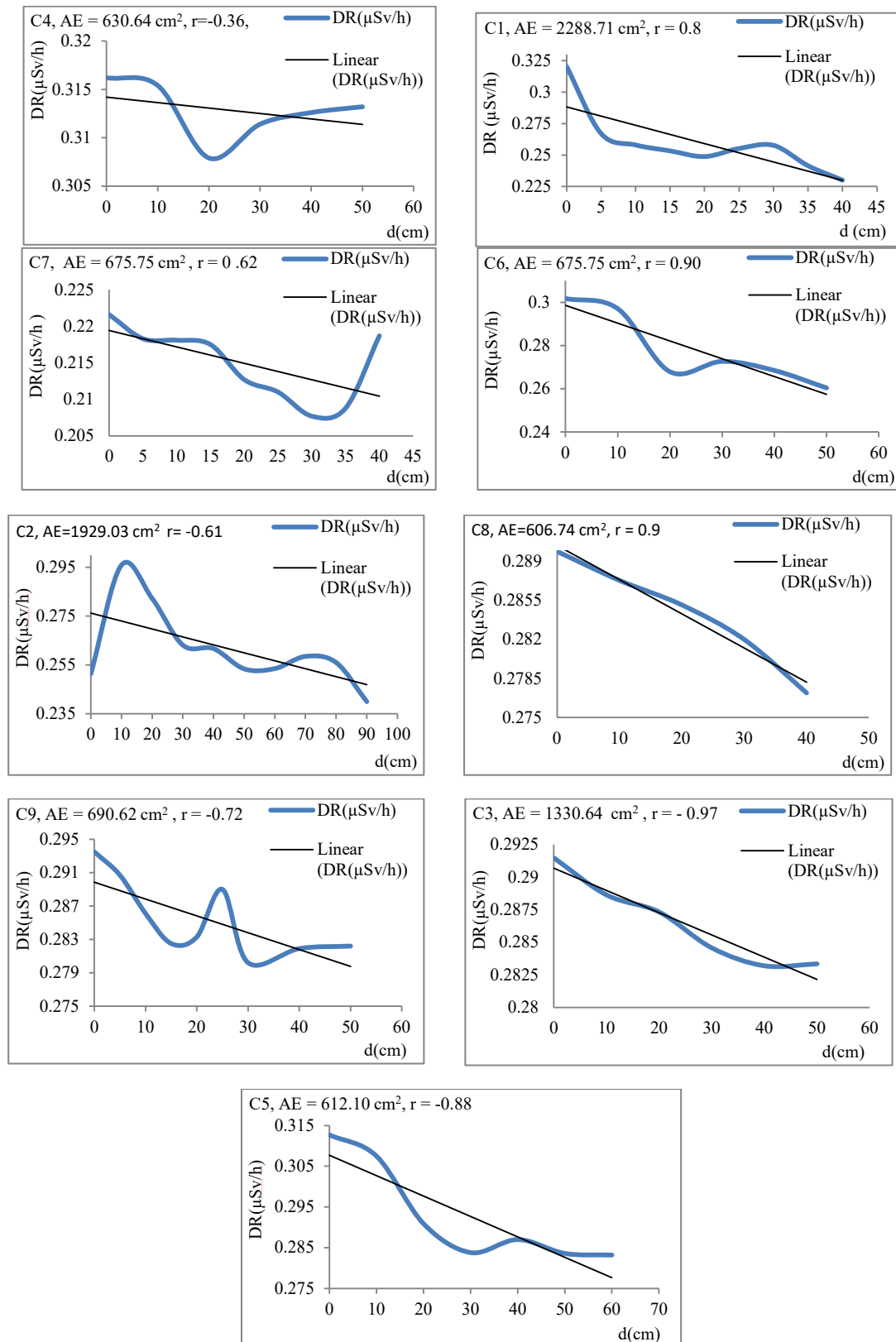


On the average, the exposure rate from the CRTs was 0.3091 ± 0.0113 $\mu\text{Sv/h}$ i.e. 24.85% above BG. This value is well below the Food and Drug Administrations 21 C.F.R. 1020.10 of 0.5 mR/h equivalent to 4.67 $\mu\text{Sv/h}$ at a distance of 5cm from any external surface [18].

3.2 Variation of Dose Rate with distance

All the CRT units showed a decreasing trend of exposure rates with distance as shown in figure 3 (a-i) with correlation coefficient as high as -0.97. The shapes of the curves also show that the X-rays produced are continuous (which is characteristic of bremsstrahlung) rather than having sharp spikes that denote characteristic discrete X-rays. This confirms that the X-rays produced are of low energy as discrete characteristic X-rays are expected to be produced in tubes with high voltages.

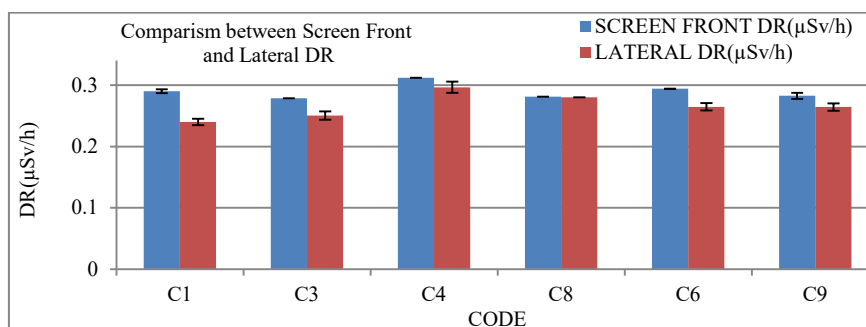
Figure 3 (a-i): DR against distance for CRT products



The cyclic (sinusoidal) variations observed reveal that the emissions do not travel in straight lines. This is likely to be as a result of the manner the electron beam is swept horizontally and vertically across the viewing face – the whole face normally being covered in about 1/70th of a second [13].

A further investigation of the results of Constantino *et. al.* (2000) that not only the screen, but also the lateral surfaces of CRTs emit low-level radiation, show that the lateral surfaces for CRTs have a generally lower exposure rate (0.2661 ± 0.0083) $\mu\text{Sv/h}$ than the screen surface (0.2898 ± 0.0050) $\mu\text{Sv/h}$. The statistical test for difference between means of DRs for screen front and lateral sides at the 95% confidence level showed that five (5) out of the six (6) CRTs (i.e. 83%) as shown in table 2 had statistically significant differences that are not due to chance. It can be said that the lateral surfaces for CRTs have generally lower exposure rate compared to the emission screens as shown in figure 4.

Figure 4: Comparison between screen front and lateral DR

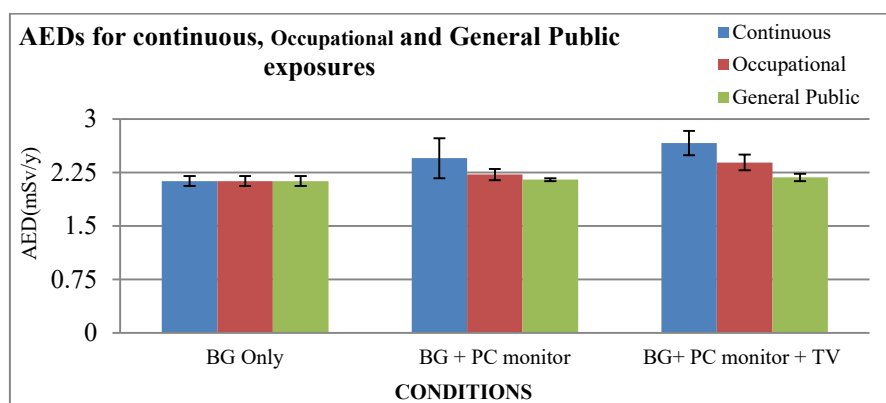


The (0.2661 ± 0.0083) $\mu\text{Sv/h}$ than the screen surface (0.2898 ± 0.0050) $\mu\text{Sv/h}$. For the CRT devices, there is no strong correlation between the DRs and AEs within and between different products.

Table 2: DRs (screen and Lateral measurements) for CRTs and LCDs

CODE	SCREEN FRONT DR ($\mu\text{Sv/h}$)	LATERAL DR ($\mu\text{Sv/h}$)	TEST RESULT FOR DIFFERENCE IN MEAN
C1	0.2900 ± 0.0032	0.2400 ± 0.0050	not due to chance
C3	0.2788 ± 0.0000	0.2506 ± 0.0067	not due to chance
C4	0.3121 ± 0.0000	0.3200 ± 0.0100	due to chance
C8	0.2811 ± 0.0000	0.2802 ± 0.0000	not due to chance
C6	0.2942 ± 0.0003	0.2646 ± 0.0006	not due to chance
C9	0.2827 ± 0.0049	0.2645 ± 0.0006	not due to chance

As can be seen from the figure 5.0 the excess effective dose from PC monitors amount to (0.05-0.60) mSv/y; i.e. (2.3 - 28.17) % above BG. Continuous exposure to both PC monitors and TV receivers results in an annual effective dose (17.37 – 32.86) % higher than that of BG alone. These results are comparable with that of Constantino *et. al.* (2000) with an excess annual absorbed dose from PC monitors only of 0.104 mSv/y; i.e. 11% above BG radiation and 28.8% for both PC monitors and TV receivers [15]. The AED results (2.13 – 2.83 mSv/y) obtained under various conditions due to exposure to these devices are well below the limits of ICRP 60 recommendations shown in table 4.8 for detrimental effects and those to prevent non-stochastic effects in the ICRP 26 recommendation for the lens of the eye, skin and hands; the AED values however exceed the ICRP 60 recommendation for Foetus/embryo.

Figure 5: AEDs for continuous, occupational and general public exposures

5 CONCLUSION

CRT PC monitors and TV receivers were found to have ionizing radiation emissions higher than the Background levels. Maximizing distance from the emission source is a control measure for the amount of ionizing radiation from PC monitors and TV receivers as the dose rates generally decreased with distance from emission screen. Larger Screen sizes do not necessarily result in increased ionizing radiation emission. They however result in more tissues/organs susceptible to biological effects of ionizing radiation. Since emission takes place through all the screen and lateral surfaces (Constantino *et. al.*, 2000). This study reveals that TV receivers and PC monitors constitute a part of artificial sources of ionizing radiation.

6 REFERENCES

- [1] UNSCEAR (2010). *Sources and Effects of Ionizing Radiation*. New York: United Nations Publication.
- [2] Alaska Department of Labor & Workforce Development Development. (2004). *Physical Agent Data Sheet (PADS)*. Labor Standards & Safety Division. Alaska: Occupational Safety and Health.
- [3] IAEA. (2005). *Radiology Oncology Physics: A Handbook for Teachers and Students*. (P. E.B., Ed.) Austria, Vienna: IAEA.
- [4] Herman Cember, T. E. (2009). *Introduction Health Physics*. United States: McGraw Hill Companies.
- [5] Alan Appleby, M. C. (1996). Factsheet. 1-3.
- [6] Sabol, J. and Weng, P. (1995). *Introduction to Radiation Protection Dosimetry*. Singapore: World Scientific Publishing Co. Ltd.
- [7] UNSCEAR (2000). *Sources, Effects and Risks of Ionizing Radiation: Report to the General Assembly, with annexes*. New York: United Nations.
- [8] Turner, J. E. (2007). *Atoms, Radiation, and Radiation Protection*. Weinheim, USA: Wiley-VCH.
- [9] CNSC (2012). Retrieved March 2015, from CNSC: nuclearsafety.gc.ca
- [10] Eck, W. V. (1985). Electromagnetic Radiation from Video Display Units: An Eavesdropping Risk? *North-Holland Computers & Security*, 269-286.
- [11] EPA. (2006). *Hazardous waste CRT rule*. Retrieved MARCH 2015, from www.epa.gov/osw
- [12] Lee C-H., C-T. Chang, K-S Fan, and T-C Chang. (2004). An overview of recycling and treatment of scrap computers. *Journal of Hazardous materials*, 93-100.
- [13] ILO (1994). *Visual Display Units: Radiation Protection Guidance*. Geneva, Switzerland: International Labour Office.
- [14] ICER. (2003). *New Approach To Cathode Ray Tube*. DTI.
- [15] Constantino Perez-Vega, Jose M. Zamanillo and Juan Saiz Ipina. (2000). Assessment of Ionizing Radiation from PC Computers and TV Receivers. *IEEE Transactions of Consumer Electronics*, 46(4), 1-48-1051.

- [16] Akinyemi M. L. and Usikalu. M. R (2010). Prudent Avoidance in Exposure to Extremely Low Frequency (ELF) Fields. *Scientific Research and Essays*, 5(16), 2295-2298.
- [17] Vijay Kumar, A. T. (2012). Study Of Harmful Effects Of Low Frequency Radiation Of Crt Tv/ Pc Screen On. *International Journal Of Current Research*, 4(5), 182-186.
- [18] Bureau of Radiological Health. (1981). *An evaluation of radiation emission from video display terminals*. Department of Health and Human Services, Rockville, Maryland.
- [19] Kokalari T. K. (2011). Evaluation of the Exposure to Electromagnetic Fields in Computer Labs of Schools. *Journal of Electromagnetic Analysis and Applications*, 248-253.
- [20] Al-Azmi, D. (2014) Gamma Dose Rate Measurements in Kuwait Using a Car-Borne GPS Integrated Dosimetric System. *World Journal of Nuclear Science and Technology*, 4, 163-169.

Case Study: Radiation Protection measures when designing an extension of a Nuclear Medicine Department

Youness Esserhir El Fassi^{a*}, Jean-Élie Fontaine^b, Mathieu Valla^b, Siham El Moghni^a, Youness Haddoudi^b, Paul Livolsi^b, Abdelmajid Choukri^a, Oum Keltoum Hakam^a

^aMaster in Nuclear Techniques & Radiation Protection, University of Ibn Tofail, Faculty of Sciences, Kenitra, Morocco

^bEuropean Master in Radiation Protection, University Joseph Fourier, Grenoble, France

Abstract. In the framework of a collaborative project between the Master program in Nuclear Techniques & Radiation Protection at the University of Ibn Tofail, Kenitra-Morocco and the European Master in Radiation Protection at the University Joseph Fourier, Grenoble-France, a group of five students from both masters have developed a remote collaboration case study on establishing a layout, zoning and shielding of a nuclear medicine department in addition to evaluating the radiation exposure of practitioners in different premises at this department. This case study was performed over three months of joint work, on an existing nuclear medicine service holding already a license for in vivo diagnosis for the use of ^{99m}Tc (62 GBq), ²⁰¹Tl (2,2 GBq) and ¹³¹I (629 MBq) and aimed to design an extension of this nuclear medicine department in order to implement three Iodine-131 therapy rooms and an acquisition of PET/CT unit which will use Fluorine-18 with a requested activity of (11 GBq) in a global surface of 300 m². We completed our study by proposing a radiological zoning of this new nuclear medicine department. Then we calculated the estimated doses to technicians and physicians that they could be exhibited in order to check whether they are within the prescribed annual dose limits. Thereafter, we have calculated the necessary shielding for the different locals to ensure that the basic protective measures in radiation protection are guaranteed throughout the nuclear medicine department.

KEYWORDS: *ease study; layout; zoning; shielding; dose measurements; nuclear medicine; PET/CT.*

1 INTRODUCTION

Nuclear medicine is a medical specialty that uses very small amounts of radioactive materials (radiopharmaceuticals) to diagnose and treat disease. Radioactive iodine (¹³¹I) can be used in medical therapies as a treatment as well as a diagnostic tool. For therapeutic purposes, it is mostly administered orally in NaI capsules form. The used activity of ¹³¹I is about 800 MBq for the treatment of hyperthyroidism, and approximately 4-6 GBq for thyroid cancers. These activities require hospitalization of the patient in particular equipped room and a specific careful attention should be given to the volatility of iodine-131 to prevent contamination of practitioners and patients. These activities require a comprehensive study of radiation protection issues and stringent measures to meet radiological safety.

Positron Emitted Tomography coupled to Computed Tomography (PET/CT) imaging technology provides both functional and anatomical information. It uses relatively high activities of radionuclides emitting radiation with an energy of 511 keV. This presents unprecedented radiation protection challenges in nuclear medicine and must be taken into account when constructing new facilities or extending existing ones. So, the establishment of a (PET/CT) implies more radiation protection measures. A radiation protection officer in a nuclear medicine service have to deal with all the problems resulting from all life cycle components of the used radioactive substance from receiving to waste disposal, passing by handling, injecting, measuring, imaging and storing.

In this work, we will develop a design for the extension of an existing nuclear medicine department including all locals necessary for diagnosis with PET/CT unit and for Iodine-131 therapy. In addition to the conception of the zoning areas, we will give an estimation of doses that could be received by all medicine service staff. We will also present necessary shielding measurements to keep exhibitions to radiations within the prescribed international standards.

*Presenting author, email: younesselfassi@hotmail.com

2 MATERIALS AND METHODES

The purpose of this work is to expand the activities of an existing nuclear medicine service providing in vivo diagnosis, to a new service made up by the acquisition of a new PET/CT GEMS mark and DISCOVERY ST4 type, combining with rooms for therapy activities. The existing nuclear medicine service had already an authorization for in vivo diagnostic. In addition to the use of medical radionuclides as Tc-99m (62 GBq), Tl-201 (2.2 Gbq), I-131 (629 MBq), a new radionuclide (Fluorine -18) will be used with a higher activity of 11GBq.

We have worked to establish a layout of nuclear medicine department which include PET/CT unit and the involvement of three iodine therapy rooms within a surface of 300 m².

The design has to take into account several issues including right placement of premises, air quality and infection control for a better radiation protection of patients and staff. We have proposed zoning areas including regulated and unregulated areas based on the dose calculated in locals. The shielding measurements were estimated at the PET/CT unit. Shielding was supposed mostly with barium concrete view its density compared to ordinary concrete. The calculations considered the estimated dose rate, the occupancy factor by workers and public in regulated and unregulated areas respectively.

The number of treatments at the department could achieve 1500 to 2000 patients per year including 1% of children, so it is imperative to estimate the dose received by technicians and physicians in order to check whether they are within the prescribed annual dose limits.

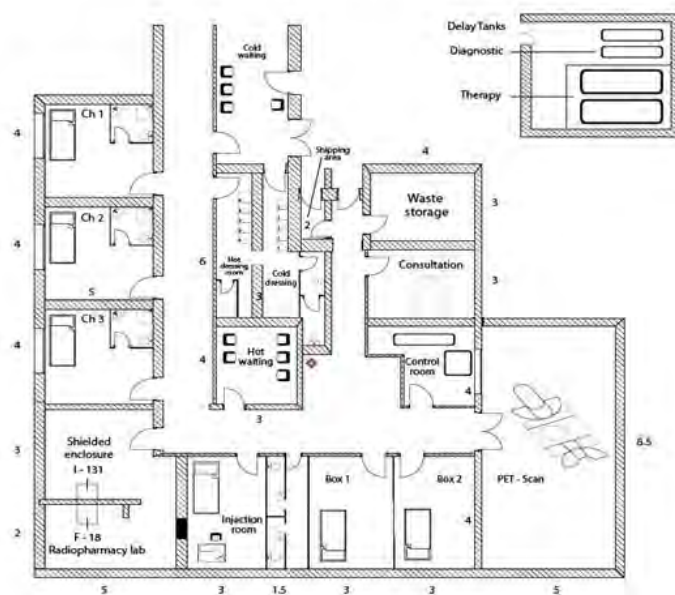
3 RESULTS AND DISCUSSION

The result of the case study includes the new design of the facility with the characteristics of premises and a proposal of zoning areas made through the effective dose rates applied in literature. Subsequently shielding measures have been calculated for PET/CT unit using two types of materials (ordinary concrete and barium concrete). At the end estimated dose rate for workers are presented in different procedures.

3.1 Design plan

The design plan is shown in figure 1 were we have proposed the conception of a nuclear medicine department which include PET/CT unit and 3 iodine-131 therapy rooms. The service combines between diagnosis and therapy in 300m² surface. The dimensions of locals are mentioned at the design plan in centimeter.

Figure 1: Proposed layout for nuclear medicine service including PET-CT unit and 3 Iodine therapy rooms.



The patient's path is proposed as following, the entrance for a diagnostic test performed from the cold waiting area where patient's accompanying can wait, the patient passes the cold dressing room then the hot dressing room. Once the patient is prepared for the diagnostic test he/she passed through the corridor to the injection room, then he/she rests at one of the two boxes. The patient empty his/her bladder at the toilet next the rest boxes. After 1 hour of rest the patient escorted to scanning room. 20 minutes later, the diagnosis has completed and it is followed by a consultation takes 20 minutes made by the physician to examine patient's healthcare. At the end the patient leaves the service by the exit door.

3.2 Design characteristics

The characteristics of the different locals proposed at nuclear medicine department are as following:

Cold waiting area requirements for a PET facility are relatively modest because of the pattern of workflow. The cold waiting area is for patients and any accompanying persons prior to administration of the radiopharmaceutical and so special shielding is not required. Access to the patient WC is provided in this area [1].

Laboratory of Radiopharmacy is an integral part of a nuclear medicine facility when on-site labelling and preparation takes place. It's adjacent to the injection rooms and it allows a practical route for waste disposal. The location has not created a new hazard to existing areas or personnel. It is also important that it is not immediately adjacent to areas where low level counting or imaging equipment is installed.

Radiopharmaceutical is divided into two distinct parts. On the one hand a high energy enclosure dedicated ^{18}F and the other a low-energy enclosure for the preparation of all other syringes. The link to the injection room is via an air locked pass through hatch. For security purposes, it's only being possible to lock the hatch from the radiopharmacy side [1, 2].

Injection room dimensions are 12 m^2 . A toilet dedicated for patient use is provided nearby, so that the patient does not have to walk through the department to empty his/her bladder prior to scanning. The equivalent dose rate at 1 meter from the patient is $54.5\ \mu\text{Sv} / \text{h}$. The room is classified controlled area.

Hot waiting Contains a separate area for trolley patients (1 - 2 trolleys) and accompanying staff will facilitate privacy and will help minimise exposure. The area is classified controlled area with an access restricted to nuclear medicine patients, accompanying persons and staff [2].

PET/CT room dimensions are 42.5 m^2 with an additional 15 m^2 for the control room/console area. Extra space provided within the scanning room reduces shielding requirements due to the decreased exposure at the boundaries. The control/console room provides direct access to the scanning room and is close to the dispensing and injection room.

The equivalent dose rate at 1 meter from the patient is $30.7\ \mu\text{Sv} / \text{h}$ after PET/CT imaging.

Consultation room received patients (injected or not) for an interview with a doctor [2]. The interview lasts approximately 20 minutes and 2 patients are seen per hour. The equivalent dose rate at 1 meter from the patients is $16\ \mu\text{Sv} / \text{h}$. The local is classified controlled area (green zone) with 1.3 meter radius as controlled area (yellow zone) around the patient.

Waste storage is dedicated to secure nuclear medicine department from radioactive waste. Access to this area should be strictly controlled and limited to designated personnel [1]. The local is classified controlled area (yellow).

3.3 Zoning

Locals in which are used Fluorine-18 and the adjacent areas to them are defined as controlled areas, supervised or uncontrolled depending on the activity and use of protection and containment measures implemented. For such example injection room, hot waiting area, PET/CT scanning room and waste storage are classified as controlled area (yellow) due to high activity of ¹⁸F. While the laboratory of radiopharmacy and consultation room, are classified controlled area (green) where the preparation of the radionuclide is performed in a shielded enclosure, however at the consultation room the classification returns to the radioactive decay of ¹⁸F.

The three iodine therapy rooms are classified controlled area (yellow) view the high activity administered to hospitalized patients and their occupation raging a period between 3 to 4 days.

All appropriate action is taken to prevent unauthorized access to areas where radioactive sources are used or stored.

Zoning was done according to the effective dose (E) received in 1 hour in the regulated areas referenced from IRSN publication [3].

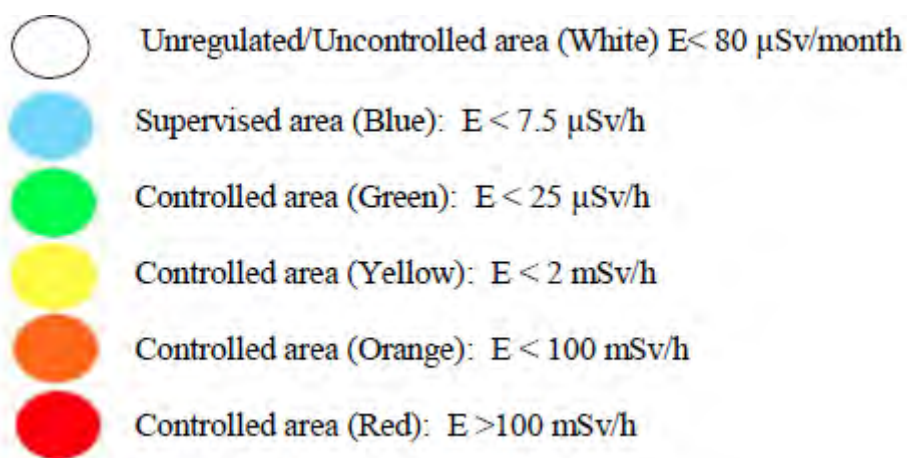
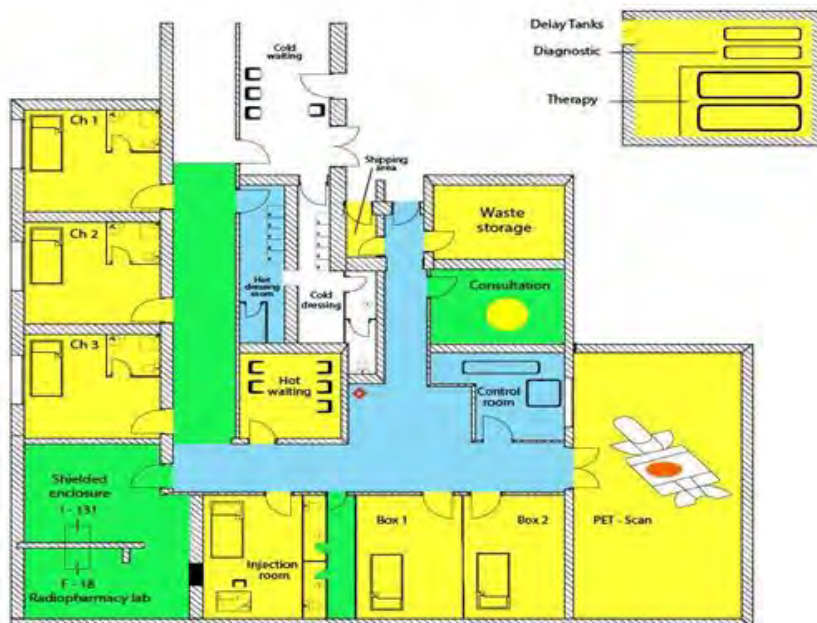


Figure 2: Proposed zoning for a diagnostic and therapeutic nuclear medicine service including PET-CT unit and 3 Iodine therapy rooms.



3.4 Shielding

The shielding PET/CT facilities present special challenges because of the high energy emissions involved in nuclear medicine services. The patient is the main source of radiation, and once the ($\approx 400\text{MBq}$) ^{18}F -FDG is injected, consideration has to be given to the journey of this patient through the facility. Thus the areas in which the patient spends time post-administration, particularly the injection room, waiting area and the scanning room, must be shielded [4,5].

We have used the linear attenuation shielding formula (1) to estimate shielding of premises [6].

$$I_B = I_A * e^{-\mu x} \quad (1)$$

Where, I_B : the shielded dose rate (mSv/h)

I_A : the initial dose rate (mSv/h).

μ : the linear attenuation coefficient (cm^{-1}).

x : the shield thickness (cm).

We have calculated the shielding at the whole PET/CT unit including shipping area, radiopharmaceutical laboratory, injection room, patient WC, hot waiting area, PET/CT imaging room, consultation room and waste storage.

The table1 presents the shielding measurement of injection room and rest boxes which radiation exposure to staff is similar in both spaces. Estimated distance at 2 meter from the patient.

Table 1: Shielding measurements of the injection room and rest boxes

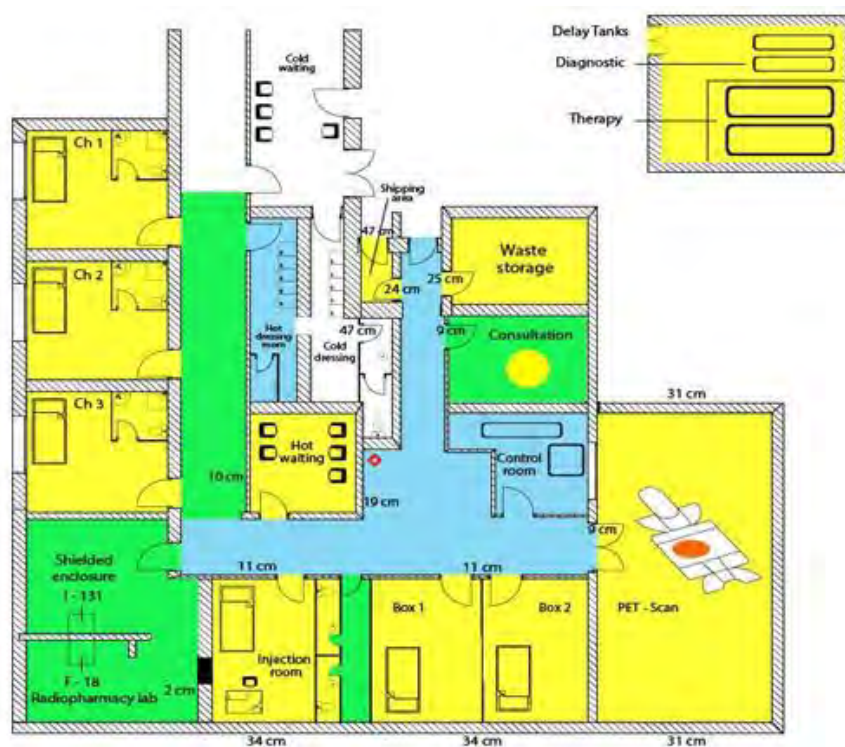
Injection room and rest boxes	Supervised area (corridor)	Controlled area (toilets)	Uncontrolled area
Ordinary concrete thickness (cm)	16.86	5.98	52.11
Barium concrete thickness (cm)	10.96	3.89	33.87

Thereafter, the table 2 shows the shielding measurement at PET/CT scanning room.

Table 2: Shielding measurements of PET/CT room

PET/CT room	Supervised area (corridor)	Uncontrolled area
Ordinary concrete thickness (cm)	12.65	47.24
Barium concrete thickness (cm)	8.22	30.70

However the figure 3 shows the remaining proposed shield of PET / CT unit using barite concrete material.

Figure 3: Proposed shielding for PET/CT unit in a nuclear medicine department

The design of the facility has minimized contact between staff and patient as far as possible without unduly compromising patient care, the shield play a critical role on the radiation protection of staff and the public.

The locals shielding differs from each other and this return to many factors, in terms of the radioactive source activity, patient residence time and workers occupancy factor.

3.5 Dose measurements

In this study we have estimated the radiation exposure of one technologist at chest level D (10 mm) and extremities level D (0.07mm) while performing ^{18}F -FDG injections, before imaging and after PET/CT scanning respectively. We have estimated also the dose rate received by physician at the consultation room. The calculation has experienced three distances from patients to show the radiation exposure that staff members could receive.

The estimated dose rate has measured 2 minutes after ($\approx 400\text{MBq}$) ^{18}F -FDG injection due to residence time of the technician at injection room (table 3).

Table 3: Estimated dose received by one technologist after (≈ 400 MBq) ^{18}F -FDG injection.

Distance from patient surface (m)	Chest level	Extremities level
	Dose/injection (μSv) 2 min of residence	Dose/injection (μSv) 2 min of residence
0.3	20	22.0
1	1.8	2.0

The estimated dose to chest of the technologist per injection at 1 meter were $1.8 \mu\text{Sv}$, however the average PET/CT whole body doses (in a well designed facility) are described by the ICRP is $2\text{--}4 \mu\text{Sv}/\text{patient}$ [8, 9].

We have estimated also the dose received by the technologist while positioning patient at PET/CT (table 4), the residence time was estimated in 5 minutes.

Table 4: Estimated dose received by one technologist while positioning patient for imaging.

Distance from patient surface (m)	Chest level	Extremities level
	Dose/positioning (μSv) 5 min of residence	Dose/positioning (μSv) 5 min of residence
0.3	34.0	37.3
1	3.1	3.4

The estimated dose to chest of the technologist per procedure was $3.1 \mu\text{Sv}$, however the positioning of patient for a PET/CT imaging was described by the ICRP in an average of $1\text{--}2 \mu\text{Sv}/\text{patient}$ [8, 9]. The dose received by the technologist in this procedure was higher than what is set by ICRP. In this case it's necessary to decrease the residence time of the technologist (5 minutes) in the aim to have a radiation exposure within the acceptance limits.

Then we have estimated the dose received in 1 minute after PET/CT imaging, considered as the residence time of a technologist after imaging at scanning room.

Table 5: Estimated dose received by one technologist after PET/CT imaging.

Distance from patient surface (m)	Chest level	Extremities level
	Dose/imaging (μSv) 1 min of residence	Dose/imaging (μSv) 1 min of residence
0.3	5.7	6.3
1	0.5	0.6

The estimated dose to chest of the technologist per PET/CT imaging was $0.5 \mu\text{Sv}$, however the dose to worker per typical ^{18}F -FDG Scan described by the ICRP is an average of $1\text{--}2 \mu\text{Sv}/\text{patient}$ [8, 9].

Thereafter we estimated the dose received by a physician during the consultation period for patients (table 6).

Table 6: Estimated dose received by one physician at consultation room.

Distance from patient surface (m)	Chest level	Extremities level
	Dose/consultation (μ Sv) 20 min of residence	Dose/consultation (μ Sv) 20 min of residence
0.3	89.1	97.8
1	8.0	8.8

We notice very well the importance of having a distance of one meter to patients (source) or more for an exhibition that does not exceed the acceptable limits.

In table 7 we have presented an estimation of the annual radiation exposure to a technologist and a physician in a PET/CT facility.

Table 7: Estimated annual radiation exposure to staff in a PET/CT facility

Radiation worker	Chest level	Extremities level
	Dose rate at 1 m from the patient (mSv/year)	Dose rate at 0.5 m from the patient (mSv/year)
Technologist	4.42	18.89
Physician	3.76	16.54

On an average of 7 patients are imaged in the PET/CT every day and divided into two technologists. The annual dose received to one technologist was 4.42 mSv, which is the total dose rate from the radiation exposure after (400 MBq) ^{18}F -FDG injections, during PET/CT imaging and after PET/CT imaging. In the other side on an average of 2 patients consulted per day and after 47 weeks of work, we have estimated the annual radiation exposure to one physician was 3.76 mSv. The estimated doses were in the acceptance limits wherein the typical annual whole body staff dose in PET/CT unit defined by the ICRP is <6 mSv [8].

4 CONCLUSION

In this case study we established a design plan for diagnostic and therapeutic purposes at an extended nuclear medicine department spread over a surface of 300 m². Thereafter, we performed the radiological zoning of this new nuclear medicine department and measured the shielding of the PET/CT unit in the aim to minimize the radiation exposure of the staff. The dose measurements for staff were all in the acceptance limits except the dose to chest of technologist while positioning the patient on the PET/CT. In this latest procedure, the staff members should take care to reducing their received dose by minimizing time or by maximizing distance and maximizing shielding in all instances involving radioactive sources.

The obtained results could be useful and could serve as a model for other nuclear medicine departments who envisage expanding their activities by combining between diagnosis and therapeutic purposes.

5 REFERENCES

- [1] The Design of Diagnostic Medical Facilities where Ionising Radiation is used. A Code of Practice issued by the Radiological Protection Institute of Ireland June 2009.
- [2] Institut de Radioprotection et de Sûreté Nucléaire (IRSN). Radioprotection : Secteur Médical Médecine nucléaire Diagnostic in vivo TEP-TDM ou TEP au fluor 18 et autres émetteurs de positons (FR 6).
- [3] Institut de Radioprotection et de Sûreté Nucléaire (IRSN). Radioprotection: Radionucléides F-18 (ED 4311).
- [4] G. S. Pant and S. Senthamizhchelvan 2006. Radiation Exposure to Staff in a PET/CT Facility. IJNM, 21(4): 100-103.
- [5] American Association of Physique Medical, Task Group 108: PET and PET/CT Shielding Requirements.
- [6] Ripan Biswasa, Hossain Sahadatha, Abdus Sattar Mollahb, Md. Fazlul Huqa, January 2016. Calculation of gamma-ray attenuation parameters for locally developed shielding material: Polyboron. Journal of Radiation Research and Applied Sciences Volume 9, Issue 1.
- [7] Taalab, Kh; and Mohsen, Z, December 2013. Radiation Exposure to Staff Using PET/CT Facility. Egyptian journal of nuclear medicine., Vol. 8, No. 2.
- [8] ICRP, 2007. The 2007 Recommendations of the International Commission on Radiological Protection. ICRP Publication 103.
- [9] International Atomic Energy Agency (IAEA), Staff and Public Doses L8 presentation.

Optimization of occupational exposure during first operations with ^{18}F in Cuba

Zayda Haydeé Amador Balbona *

Centre of Isotopes, Ave. Monumental y carretera La Rada, Km 3 $\frac{1}{2}$, San José de Las Lajas, Mayabeque, Cuba.

Abstract. The Republic of Cuba gets ready for the work with Positron Emission Tomography (PET) and the main radionuclide used for this is ^{18}F . It is required to import this radioactive material for the quality control of dose calibrators in hospitals that will have PET/CT. The occupational dose assessment is executed as a part of documentation for request the authorization to the Nuclear Regulatory Body with software Microshield version 5.0.3 and its maximum dose rate is determined in contact with the type A package and the value of the index of transport. Various handling postures and situations commonly encountered in laboratories are considered. Once received the solution with ^{18}F , is executed the radiological surveillance of the operations of preparation of the calibration solutions and the quality control of three dose calibrators properly. Additionally, for the controls of the effective doses are used electronic dosimeters, model Fisher Scientific EPD Mk2+ from United Kingdom. To optimize the occupational exposure among used measures are introduced the hot cell with 20 cm of Pb for the measurement of the initial activity of ^{18}F and the determination of the characteristics of the first safety barrier, the organization tasks among 4 workers, the employment of a peristaltic pump and of means of distancing of the source. The effective doses are less than 80 μSv and the minimal detection limit for TLD in Cuba (100 μSv per month). Staff received only the 10 percent of the estimated equivalent dose to hands. Preparation of the reference sources in solution and their weighing and dosage of pycnometers have the biggest contribution to workers exposures.

KEYWORDS: *Optimization; ALARA principle; occupational exposure; radiation safety; ^{18}F .*

1 INTRODUCTION

The future use of unsealed radioactive sources with positron emitters, mainly ^{18}F , in the Cuban Republic, requires that metrology activity has been guarantee for protection of patients. For this reason, dissolution of this radioisotope imported for calibration of dose calibrators in 2014. This service offered for the Metrology Department of the Centre of Isotopes (MD), has an accreditation taken into account [1] and the recognizing of the International Bureau of Weights and Measures (BIPM) [2] and the Mutual Recognizing Agreement (ILAC) [3].

As it knows, ^{18}F is a shorter-life radionuclide with half-life period of 109.77 minutes and decays mainly for positron emission (96.9%). The positron annihilates with an electron into two 511-keV antiparallel photons in opposed ways.

The purpose of this paper is achieved that occupational exposure during the operation for prepare reference dissolutions and calibration of dose calibrators in hospital are maintaining as low as reasonable achievable [4]. For this and beginning of projected values for exposure, are adopting measures that allow to reach this objective. Identified operations are those with higher contribution to exposure of workers.

*Presenting author, e-mail:zabalbona@centis.edu.cu

2 MATERIALS AND METHODS

It is execute the preparation of the reference dilutions for workers belong to MD [2-3] for calibration of three dose calibrators in a hospital in Cuba [5], which are related with a new computed tomography (CT) and positron emission tomography (PET) facility (PET/CT) in that place.

2.1 Dose Assessment from type A package with ^{18}F for CENTIS

As the selected supplier has not a type A package for ^{18}F , we need evaluate someone available for transport by air and terrestrial via to CENTIS in accordance to applicable requirements [6-7] and for request authorization to the Cuban Regulatory Body. The dimensions of this package are shown in Table 1. This has a plastic packaging, inside separators and a lead container. Their thicknesses are presented in Table 2. The height's container is 20.5 cm.

Table 1: Container's dimensions for ^{18}F .

External diameter (cm)	Height (cm)	Height of inside separator (cm)
28.8	39.7	7.8

Table 2: Thicknesses of the lead container for ^{18}F .

Lateral (cm)	Cover (cm)	Bottom (cm)
6.45	5.7	7.6

The dose assessment in contact with the external sides of package and a distance of 1 m from this is making with code Microshield Version 5.0.3 [8]. Taking into account its results are determined the maximum rate dose in contact and the transport index [6-7]. It is considering that source has 74 GBq for the day of transport in a volume of 2ml belongs to vial 10R.

2.2 Occupational exposure initial assessment for operations

The considered operations include the movement of radioactive material to the laboratory, preparation of the initial solution in a fumehood and dosage for preparation of samples that will send to the hospital. In the other hand, are taken for calculations the measurement in the dose calibrator, preparation of packages, control of transport index (TI) for the staff belongs to Radiation Protection Department (RPD), transport to the hospital and calibration of dose calibrators [8]. We assumed that all operations are making only for one person. Data for dose assessment are in Table 3.

Table 3: Data for dose assessment for operations with ^{18}F .

Activity GBq	Volume (ml)	Volume for dosage (ml)	Internal shielding for process (cm Pb)
5.22	2	0.3	3

2.2.1 Assessment of the effective dose.

Calculations are for the highest contribution to effective dose (E) of worker. We considered the radioactive decay of source. For load of dissolution and dosage in the fumehood a distance source- operator of 30 cm (average length of forearm) [10]), a shielding of 5 cm of lead and a point isotropic source, due to the distance source-operator is higher than 10 times the major dimension of the source. The employment of a peristaltic pump for the load and this operation delays only 1 minute.

During the measurement in the dose calibrator in CENTIS, the distance source-operator is 40cm (it is included a clip of 10 cm of long plus of the average length of forearm). The source is in a well in a depth of 30 cm and the effective dose is evaluated to the table level of height of 30 cm. Operation delay 3minutes.

For operations in the hospital, we contemplate the same aspects for calculation of E, but three times, due to the amount of dose calibrators.

2.2.2 Assessment of equivalent dose to hand.

In the same way we calculated the highest contributions to the equivalent dose to hand (Hp(0.07)). For this purpose, it assumed in the load of dilution in the fumehood, that the hand are 10 cm to the peristaltic pump, and a height of 20 cm respect to source (which volume is 2 ml). The vial is a 'penicillin' type with diameter of 2.3 cm and height 2.5 cm [10], inside of a lead container with thickness of 3 cm. It is considered a duration of 1 minute. For the dosage, the source is the same.

In the measurement in the dose calibrator in CENTIS, it is adopted a point source, since the distance source-operator is higher than 10 times of the highest dimension of the source and a duration of 3 minutes.

There are taking into account the same considerations for operations in the hospital, but repeat calculations three times.

2.3 Radiological surveillance

Environmental equivalent rate doses measured with the ALNOR RDS-120 universal survey meter, (Finland). This has an operation range about 0.05 $\mu\text{Sv/h}$ to 10 Sv/h and verified by Secondary Laboratory of the Center of Protection and Hygiene of Radiations (CPHR) [11], with maximum relative intrinsic error of 10 %. Russian chronometer also is used.

For measurement radioactive superficial contamination is used the monitor LB-122, (Berthold, Germany), calibrated also by CPHR with a factor of $2.271 \pm 2.045\text{E-}01$ [12].

Deep personal equivalent dose (Hp(10)) are controlled with electronic dosimeter Thermo Fisher Scientific EPD MK2+ (United Kingdom), calibrated by CPHR [13], with maximum relative intrinsic error in the range of the measurements of 6 %. Also are employed TLD offered by CPHR for Hp(10) and Hp(0.07), because this is the official dosimetry in Cuba.

In both cases Hp(10) are measured for gamma emitters with lower energy of 50 keV in the first case and 15 keV in the last, until 2 MeV.

Nevertheless, electronic dosimeters are very useful for workers when new practices introduced and allow us controlling the most risk operations.

3 RESULTS AND DISCUSSION

3.1 Dose Assessment from type A package with ^{18}F for CENTIS

The rate doses in contact with the type A package are show in the Table 4. As can be seen, category of this is II-yellow [6-7].

Table 4: Dose rate contact with package for the dissolution of ^{18}F .

Cover	Bottom	Lateral
E* (mSv/h)	E* (mSv/h)	E* (mSv/h)
0.76	3.2E-03	17.6E-03

From 1 m of the package is obtained 1 $\mu\text{Sv/h}$, and the TI is 0.1 [6-7].

3.2 Initial assessment of the occupational exposure belong to operations

Table 5 represents the estimated total values of E and Hp(0.07) for all operations with ^{18}F . The most significant is the high value of equivalent dose rate for hand. This conduces to analyze of operations and introduce of optimization measures.

Table 5: Estimated effective dose and equivalent dose to hands for the operations with ^{18}F .

Operations	Amount of operations	E (mSv)	Hp(0.07) (mSv)
Preparation of the reference dilutions	1	5.10E-01	7.53E+01
Calibration of dose calibrators	3	5.10E-01	7.54E+01
Total		1.02E+00	1.51E+02

3.3 Measures for the optimization of occupational exposure

To reduce occupational exposure “as low as reasonably achievable” we adopted the following measures:

- Distribution of the operations among four workers, taking into account their abilities.
- Use a hot cell with 20 cm of Pb for the measurement of the initial activity of ^{18}F and the determination of the characteristics of the first safety barrier.
- The employment of a peristaltic pump for transfer dissolution of ^{18}F and of means of distancing of the source.
- Waiting 2 hours for radioactive decay of ^{18}F , before beginning the operations of dosage to vials and syringe.

3.4 Radiological surveillance

A type a package received with category II-yellow and TI of 0.1 and rate dose in contact of the lead container of 8 $\mu\text{Sv/h}$ with 6.29 GBq, containing 2.2 ml of dissolution in a vial 10R.

The Table 6 are presents the results of radiological surveillance. We can appreciated the operation with highest contribution to occupational exposure belong to preparation of the reference dissolutions, dosage to 2 vials and 2 syringes with pycnometers and their weighing, due to the activity of the source yet presented (initially is 3.4 GBq).

Three packages are prepared for the hospital and their characteristics are:

- Package with a vial, category II-yellow and TI of 0.1.
- Package with a syringe, category II-yellow and TI of 0.2.
- Package with a sealed source of ^{137}Cs , category I-white.

Tables 7 y 8 shown registered values of Hp(10) with the electronic dosimeters and Hp(0.07) reported by CPHR [13].

The registered values of Hp(10) [15] allow confirm that the legal dosimetry consider those effective dose as null in Cuba, because are lower than 100 $\mu\text{Sv/h}$.

Table 6: Results from radiological surveillance of operations.

Number	Operations	Maximum environmental equivalent rate dose (mSv/h)	Duration (seg)	Workplace (point for measurement)
1	Transfer dissolution to CENTIS container.	133	6	Laboratory 1 (fumehood, on vial).
2	Moving away the case.	133	6	Laboratory 1. (On panel of pump (fumehood)).
3	Transfer to a vial for complete 3.5 ml.	0.11	17	Laboratory 1 (fumehood).
4	Load of 1.3 ml in a pycnometer.	9.9	65	Laboratory 2 (Balance, in worker's position, except in the two dosages).
5	Load of 2.2 ml in a second pycnometer.	15.2	110	Laboratory 2 (on the shielding in the table of the balance).
6	Weighing of the first pycnometer (twice).	1.3	60	Laboratory 2 (on the syringe).
7	Dosage 10 drops in a vial.	15	30	Laboratory 2 (on the shielding in the table of the balance).
8	Weighing of a pycnometer, after this dosage (twice).	1.18	120	Laboratory 3 (in worker's position with major permanency).
9	Dosage in a syringe of 17 drops.	1.27	30	Laboratory 3 (in worker's position with major permanency).
10	Weighing of pycnometers, after this dosage (twice).	0.11	120	
11	Weighing of a second pycnometer (twice).	1.84	120	
12	Dosage 15 drops in a second vial.	4.53	30	
13	Weighing of a pycnometer, after this dosage (twice).	1.62	120	
14	Dosage in a second syringe of 17 drops	1.54	30	
15	Weighing of a pycnometer, after this dosage (twice).	1.27	120	
16	Measurement of the first vial in a dose calibrator model Fidelli, calibrated with respect to standard.	0.094	60	
17	Measurement of the first syringe in a dose calibrator model Fidelli.	0.07	60	

18	Measurement of the first vial in a dose calibrator model CANPINTEC.	0.027	6	Laboratory 3 (in worker's position).
19	Measurement of the second vial in a dose calibrator model CANPINTEC.	0		
20	Measurement of the first syringe in a dose calibrator model CANPINTEC.	0.022	6	Laboratory 3 (in worker's position).
		0		
		0.033	6	
21	Measurement of the second syringe in a dose calibrator model CANPINTEC.	0		
		0.022	60	Laboratory 3 (in worker's position).
22	Preparation and characterization of the 3 packages.	< 0.500	180	Laboratory 2 (in contact with the packages).
23	Calibrations of the three dose calibrators in the hospital.	-	2 h	Hospital.
24	Preparation of 10 point sources. - Weighing of a pycnometer, (twice). - Dosage of 3 drops on paper of filter - Weighing of a pycnometer (twice).	0.15 1	2 h	Laboratory 2 (in worker's position, pycnometer and a drop on filter).
25	Preparation of 10 cylindrical sources in liquid scintillation vial with HiSafe and Ultimagol cocktail (5 of each one). - Weighing of a pycnometer, (twice). - Dosage of 3 drops in a vial. - Weighing of a pycnometer (twice).	0.56 7 0.25 2	2 h and 45 minute s	Laboratory 2 (in contact with the first vial with 3 drops of dissolution of ¹⁸ F).
26	Measurement of point sources in gamma spectrometer.	0.11 0	5 h	Laboratory 2.

The worker 1 receives 12 μ Sv until the measurement of the second syringe in the CANPINTEC. The calibration of the three dose calibrators in the hospital contribute with 3 μ Sv to the worker 2 and 4 μ Sv to the worker 4.

After the dosage of the first five point sources, they are leaven. For other five sources is used the second pycnometer. For the cylindrical sources, after the dosage of each vial they are behind lead shielding of 5 cm.

The preparation of the point and cylindrical sources imply 16 μ Sv to the exposure of worker 1.

The measurement of the point sources in the gamma spectrometer brings 4 μ Sv to worker 2 and 5 μ Sv to worker 4.

Table 7: Personal deep equivalent dose for staff measured with electronic dosimeters EPD MK2+.

Worker	Hp(10) (μ Sv)
1	28
2	25
3	75
4	13

In the Tables 7 and 8, we determinate the maximum values of the controlled dosimetric magnitudes and their relationship with those projected. With respect the projected values is obtained that 7.35% of E and 3.77% of Hp(0.07). This means there are shorter values than those were projected.

Table 8: Equivalent dose to hand registered with TLD by CPHR.

Worker	Hp(0.07) (mSv)
1	5.69
2	0.00
3	1.39
4	0.72

4 CONCLUSIONS

This paper shows the first experience of operations with unsealed source of ^{18}F in Cuba, which are reflected very good results with respect the occupational exposure. In the other hand, the type A package used for transportation by air has an acceptable low exposure.

There are introduced optimization measures taking into account the first dose assessment. These are the hot cell with 20 cm of Pb for the measurement of the initial activity of ^{18}F and the determination of the characteristics of the first safety barrier, the organization tasks among 4 workers, the employment of a peristaltic pump and of means of distancing of the source.

The exposures of related workers are 80 μSv for E. This value is lower than registered level for valor TLD in Cuba (100 μSv per month). The operations of preparation of references sources and the point sources (dosage and weighing) are the highest contribution to their exposure. The worker's experience, conditions for operations and the accomplishment of procedures allow not radiological occurrences are registered. This also allows that exposure levels are very lower than projected. The highest exposure worker receive a 7.35% of E and a 3.77% of Hp(0,07). For this reason, the traced purpose is fulfilling obtained for the first operations with ^{18}F in Cuba.

5 REFERENCES

- [1] National Office for Standardizations, General Requirements for the Competence of Testing and Calibration Laboratories, Cuban Standard, NC ISO/IEC 17025, Havana, Cuba (2006).
- [2] www.bipm.org, www.kcdb.bipm.org, International Recognizing of the International Office of Weights and Measures (BIPM) and Certificate of calibration of BIPM (2013).
- [3] www.onarc.cubaindustria.cu, Mutual International Cooperation Recognizing Agreement of Laboratories Accreditation (ILAC) (2013).
- [4] Department of Metrology of Radionuclides, Centre of Isotopes, DMR.PNO.009, Procedure for Calibration of Dose Calibrator, Revision 09, Havana (2014).
- [5] European Commission, Food and Agriculture Organization of the United Nations, International Atomic Energy Agency, International Labour Organization, OECD Nuclear Energy Agency, Pan American Health Organization, United Nations Environment Programme, World Health Organization, Radiation Protection and Safety of Radiation Sources: International Basic Safety Standards, General Safety Requirements, IAEA Safety Standards Series No. GSR Part 3, Vienna (2014).
- [6] Cuban Nuclear Regulatory Authority, Regulations for the Safe Transport of Radioactive Material, Resolution No. 121, Havana (2000).
- [7] International Atomic Energy Agency, International Atomic Energy Agency, Regulations for the Safe Transport of Radioactive Material, Specific Safety Requirements, N°

- SSR-6, Vienna (2013).
- [8] Afti Company, Grove Engineering, Microshield Version 5.0.3 (1998).
 - [9] National Office for Standardizations, Dose Calibrators: Protocol for the Use and Quality Assurance of the Measurements, Cuban Standard, NC 811, Havana, Cuba (2010).
 - [10] D. Delacroix, J. P. Guerre, Radionuclide and Radiation Protection Data Handbook, CEA/SACLAY, France, Radiation Protection Dosimetry, Vol. 76, Nuclear Technology Publishing (2002).
 - [11] Center of Protection and Hygiene of Radiations, Certificate of verification No. VER/13/105 (20/09/2013).
 - [12] Center of Protection and Hygiene of Radiations, Certificate of calibration CCS/1326 (06/12/2013).
 - [13] Center of Protection and Hygiene of Radiations, Certificate of calibration CPR/1422 for each electronic dosimeter (2014).
 - [14] Center of Protection and Hygiene of Radiations, Laboratory of External Dosimetric Magnitudes, Service TLD for Hp(0.07), Certificate No. BN-123-3-5-9-7-2014 (2014).
 - [15] Center of Protection and Hygiene of Radiations, Laboratory of External Dosimetric Magnitudes, Service TLD for Hp(10), Certificate No. BN-123-2-5-9-7-2014 (2014).

The Role of the Radiological Protection Team as a Stakeholder in the Design Phase of a Nuclear Facility: the Case of Brazilian Conversion Plant

Ana Cristina Lourenço^a, Wagner de Souza Pereira^{a,b}

^aIndustrias Nucleareas do Brasil, Resende, Rio de Janeiro, Brazil

^bUniversidade Veiga de Almeida, Tijuca, Rio de Janeiro, Brazil

Abstract. The project team management must identify the stakeholders that are actively involved in the project, determine their requirements, and then manage them to ensure the success of the project. Considering the nuclear facility and its important radiological safety requirements, it is easy to identify the Radiological Protection Team as the group of professionals with knowledge and expertise to exert influence over the project and its results. Radiological Protection (RP) practices and interventions are very well established during the operation of the nuclear facility but what about the design phase? Considering the Brazilian Conversion Plant project, many important issues were identified during technical meetings and brainstorming sessions of the project team and radiological protection team. Some main issues were addressed to RP as following: the ALARA principle for the occupational radiation exposures, the radiation sources, the radiation protection design features, and dose assessment. As result, the following activities were considered: designing radiological control and decontamination areas, locating equipment in order to ensure an easy access; optimizing the equipment design taking into account the principle of optimization, as well as indicating the transfer routes of equipment. The approach of both project and Radiological Protection teams was a very important interactive process and contributed to the decision making, as well as time and cost planning

Design Study of ELI-NP Beam Dumps: Radioprotection Issues and Monte-Carlo Simulations

Adolfo Esposito, Oscar Frasciello, Maurizio Pelliccioni

National Institute for Nuclear Physics - National Laboratories of Frascati INFN-LNF,
Frascati, Rome, Italy

Abstract. ELI-NP will be a new international research infrastructure facility for laser based Nuclear Physics to be built in Magurele, south west of Bucharest, Romania. The facility will provide a broad range of science covering new nuclear physics, astrophysics, fundamental high field physics as well as applications in nuclear materials, radioactive waste management, material science and life sciences. The ELI-NP project relies on a research facility equipped with, two laser system of 10PW each and a 720 MeV gamma beam system. The machine is an advanced source of gamma rays up to 20 MeV, based on Compton back-scattering. This paper describes the design study of both low energy 320 MeV and high energy 720 MeV (and suitable for a 840 MeV beam energy) beam dumps by means of Monte-Carlo simulations with FLUKA and MCNP codes. The discussion on what the best placement for the low energy dump could be is addressed. Our proposal was to install the low energy dump in the building basement, what resulted to be the best choice with respect to the planned placement at the machine level. Ambient dose equivalent and residual radioactivity results are exploited. The dumps' placement and layout are shown to be fully compliant with the dose constraints and environmental impact.

Preliminary Thermo-mechanical Design of the Main Dump for the High Energy Electron Beam Lines in ELI-NP

Adolfo Esposito^a, Lina Quintieri^b

^aNational Institute for Nuclear Physics-National Laboratories of Frascati, Frascati, Roma, Italy

^bENEA Centro Ricerche della Casaccia, Roma, Italy

Abstract. ELIONP will be a new international research infrastructure facility for laser-based Nuclear Physics to be built in Magurele, south west of Bucharest, Romania. The ELI-NP project consists of a research facility equipped with two laser systems of 10PW each and a 720 MeV gamma beam system. Particle dumps are commonly used in accelerators with the main goal to absorb completely the energy of the primary beam, limiting as much as possible the release of the ensuing secondary radiation produced inside the dumps itself. For this reason the high energy particle dumps are made of several materials, to shield and absorb either electromagnetic radiation (electrons, gammas, positrons) and hadronic ones, mainly constituted of photo-produced neutrons. Several configurations for the beam dump have been studied and analysed with multi-physics Finite Element codes (Ansys and Comsol), in order to individuate the best mechanical configuration (material disposal and geometrical dimension) and the most reliable heat transfer exchange system (with respect to temperature field and thermal gradients), in accordance with the radioprotection requirements, to keep the temperature in the dump at safe level also during the most severe hypothetical operating duty cycle. A short overview of the main design issues will be reported and the more promising investigated solutions will be presented and discussed.

Radioprotection Issues for the STAR Project

Adolfo Esposito, Oscar Frasciello, Fiorello Martire, Maurizio Pelliccioni

National Institute for Nuclear Physics - National Laboratories of Frascati INFN-LNF,
Frascati, Rome, Italy

Abstract. The STAR project (Southern european Thomson source for Applied Research), in commissioning phase at the Univ. of Calabria (Italy) is aimed at the construction of an advanced Thomson source of monochromatic tunable, ps-long, polarized X-ray beams, ranging from 20 to 140 keV. The X-rays will be devoted to experiments of matter science, cultural heritage, advanced radiological imaging with micro-tomography capabilities. The STAR source consists of an electron accelerator designed for electrons energies up to 350MeV. The paper describes the whole accelerator radiological protection concerns including shielding and environmental impact of accelerator operation. All calculations were performed by means of Monte-Carlo FLUKA code.

Cyclotron Production of Sc and V Radionuclides from Natural Titanium for Medical Applications

Ahmed Rufai Usman^a, Mayeen Uddin Khandaker^a, Hiromitsu Haba^b, Naohiko Otuka^c

^aDepartment of Physics, University of Malaya, Kuala Lumpur, Malaysia

^bNishina Center for Accelerator-Based Science, RIKEN, Wako, Saitama, Japan

^cNuclear Data Section, Division of Physical and Chemical Sciences, Department of Nuclear Sciences and Applications, International Atomic Energy Agency, A-1400 Vienna, Austria

Abstract. Cross-sections of $^{nat}\text{Ti}(d,x)^{48}\text{V}$, $^{43-48}\text{Sc}$ nuclear reactions were measured up to 24 MeV deuteron energy. High purity natural titanium foils were used as targets foils, arranged and activated in the popular stacked-foil method using AVF cyclotron at RIKEN, wako, Japan. The activated foils were then measured with a high resolution γ -ray spectrometry. The obtained experimental data were analyzed, compared with earlier published experimental literature and also with the evaluated theoretical data in the TENDL-2014 library. Reasonable agreement was found between present results and some previously reported data while a partial agreement is found with the evaluated theoretical data. The results are expected to enrich further the experimental database on this radionuclides of potential medical applications and help in understanding the discrepancies among the previous measurements.

KEYWORDS: titanium; cyclotron; 24-MeV deuteron; cross-sections; excitation functions; Sc; 48V.

Design Approval and Registration for Radiation Devices

BokHyoung Lee, SangEun Han, KiWon Jang, JongRae Kim, WooRan Kim, KyungWha Kim, Younjin Park

Korea Institute of Nuclear Safety, Daejeon, Republic of Korea

Abstract. Republic of Korea (South Korea) has been enforcing design approval and inspection requirements for radioisotopes incorporated devices and radiation generators (radiation devices), and more than 1,200 design certificate of radiation devices have been issued since 2003. Through those regulatory activities, we could confirm the safety of radiation devices made in the country or imported before supplying step. According to the Nuclear Safety Act, decree/regulations/notices related the act, radiation devices are divided with radioisotope incorporated devices and radiation generators. There are 5 types according to structural characteristics, such as complete protected, self-protected, cabinet, unattended & isolated, and portable. And radiation devices are classified according to characteristics of radiation using and objectives. In case a radiation device meets design requirements and shows sufficient safety performances, the design certificate is issued. Radiation devices are used whole around the world by many kinds of organizations including small users with insufficient radiation safety managements. And like other industrial products, a lot of radiation devices are imported and exported among countries. Considering those situations, ensuring radiation safety performance and quality in fabrication steps is very important to prevent incidents or accidents, such as radiation exposure. There are various forms of standards and requirements used by many regions or countries to ensure radiation safety from the stage of radiation device manufacture. If we have a system to ensure safety of radiation devices and some registries, which can be accepted by regulatory authorities, it will be very useful for upgrading radiation safety.

Preliminary Analysis of Radiation Characteristic for 250 MeV Proton Accelerator Driven Sub-critical System

Bin Li, Qi Yang, Bo Chang, Chao Liu, Liqin Hu

Institute of Nuclear Energy Safety Technology, Chinese Academy of Sciences, Hefei, Anhui, China

Abstract. Accelerator Driven subcritical System (ADS), a combination of accelerator, subcritical reactor core and spallation neutron target, has attracted many countries' attention due to its high transmutation ability and inherent safety. However, as an ADS facility, the couple of subcritical reactor with accelerator and spallation target brings problems for radiation protection. The introduction of accelerator makes the radiation outside the reactor of ADS, especially above the reactor cover, much more serious, due to particles leakage through beam duct and secondary radiation induced by beam losses. Therefore, to figure out the radiation characteristic at inside and outside of ADS sub-critical core could provide the guidelines for ADS shielding design. In this paper, the preliminary radiation characteristic for a 250 MeV proton accelerator driven sub-critical system based on present researches in ADS technology in China was assessed using Monte Carlo method code SuperMC, Geant4 and FLUKA. To improve calculation efficiency, a volume spallation neutron source was generated by Geant4 and used for subsequent neutronics analysis for many times. For simulation of proton beam losses, it was assumed that proton uniformly losses along the beam line, particles are emitted at a shallow angle of 0.05 degree in reference to beam transport direction and the maximum beam loss level is 1 W/m which is one of design limitations for accelerator. Preliminary results indicated that the spallation neutrons yield was about 2.6 per proton, whose average energy was about 8 MeV. At begin of cycle (BOC), the keff and ks of subcritical core was 0.97771 and 0.97917, respectively. The importance of fission neutrons was about 1.07. And there was no additional local shielding for non-replaceable stainless steel components inside reactor due to the fact that their irradiation damage during lifetime didn't exceed limitation and target window suffered serious irradiation damage and need to be replaced every year. For radiation above reactor cover, the leakage from beam duct which is inserted into core is the main contributor and the dose rate induced by the proton beam losses should not be neglected. The above results could be applied in guiding the shielding design for beam duct.

New CZT (H3D) Technology Employed at Cook Nuclear Plant Achieves Immediate Individual Isotopic Identification and Verifies Adequacy of Temporary Shielding

David Miller

Cook Nuclear Plant, Bredgman, Michigan, USA

Abstract. New CZT technology has been employed at the Cook Nuclear Plant to achieve immediate individual isotope identification of in-plant components and piping. Also, the capability of verifying the adequacy of temporary shielding installation on components and piping has been an important new ALARA tool for operating nuclear power plants. The H3D system includes spectrum analysis, GPS positioning and digital photo of area of interest. The H3D system have been found to be effective in controlling contamination, reducing worker dose and assessing LLRW shipment containers prior to transport. The prototype CZT system was used in pilot testing at Cook Nuclear Plant in 2013 by the Nuclear Engineering Department, University of Michigan. Design improvements were identified and incorporated into the commercial design. The H3D system was available to operating nuclear plants in January 2014. Over 30 nuclear plants participate in monthly CZT data analysis conference calls to share experience on new applications and lessons learned of the new technical capability of the H3D. The data analysis group is sponsored by the North American Technical Center, ISOE, located at the Cook Nuclear Plant. Each month, new discoveries are discussed within the data analysis group including low level detection of radiation, hot particle identification, documentation of streaming from temporary shielding packages and precise location of dose fields in plant components. Significant worker dose savings have been achieved by the rapid identification of dose fields using the 3D digital camera features and subsequent supplemental dose control measures. The H3D photos have also been used in pre-job worker ALARA briefs prior to the commencement of work activities. The pre-job briefs allow improved worker understanding of dose fields in the work area and worker practices to reduce their dose. The new ALARA tool has produced excitement within the operational health physics field due to the unique and innovative features of the H3D.

Radiation Protection for NORM Industries – Results of the European Joint Research Project ‘Metrology for Processing Materials with High Natural Radioactivity (MetroNORM)’

Franz Josef Maringer^a, Sylvie Pierre^b, Teresa Crespo Vazquez^c, Monika Mazanova^d, Pierino De Felice^e, Branko Vodenik^f, Mario Reis^g, Mikael Hult^h, Laszlo Szücsⁱ, Simon Jerome^j, Alexander Mairing^k, Roy Pöllänen^l, Andreas Baumgartner^m, Boris Bulanekⁿ, Boguslaw Michalik^o, Nathalie Michielsen^p, Julian Dean^j, Philippe Cassette^b, Franz Kabrt^a, Hannah Moser^a

^aFederal Office of Metrology and Surveying, Vienna, Austria, ^bCommissariat à l'énergie atomique et aux énergies alternatives, Paris, France, ^cCentro de Investigaciones Energéticas, Medioambientales y Tecnológicas, Madrid, Spain, ^dCesky Metrologický Institut Brno, Brno, Czech Republic, ^eAgenzia Nazionale per le Nuove Tecnologie, L'energia e lo Sviluppo Economico Sostenibile, Rome, Italy, ^fInstitut Jozef Stefan, Ljubljana, Slovenia, ^gInstituto Superior Tecnico, Lisbon, Portugal, ^hJoint Research Centre - European Commission, Geel, Belgium, ⁱMagyar Kereskedelmi Engedelyezési Hivatal, Budapest, Hungary, ^jNational Physical Laboratory, Teddington, UK, ^kNorwegian Radiation Protection Authority, Oslo, Norway, ^lSateilyturvakeskus, Helsinki, Finland, ^mUniversity of Natural Resources and Life Science Vienna, Vienna, Austria, ⁿStatni Ustav Radiacni Ochrany V.V.I., Praha, Czech Republic, ^oCentral Mining Institute, Katowice, Poland, ^pInstitut de Radioprotection et de Sûreté Nucléaire, Fontenay-aux-Roses, France

Abstract. Naturally occurring radionuclides are present in many natural resources. Industrial activities that exploit these resources may lead to enhanced potential for exposure to Naturally Occurring Radioactive Materials (NORM) in products, by-products, residues and wastes. Industries working with raw materials containing naturally occurring radioactive materials (NORM industries) produce large amounts of waste. Traceable, accurate, and standardised measurement methods and systems, in particular for in-situ applications, are needed to decide on the re-use of waste materials without increasing costs whilst avoiding contamination of the environment and radiation exposure of the public. A reliable measurement of natural radionuclides is required to ensure that the raw materials brought into the industrial process will not cause, as far as possible, increased radiation exposure due to enhanced activities of the final products and in the waste. This paper presents the results of the European joint research project ‘Metrology for processing materials with high natural radioactivity (MetroNORM, 2012-2016)’ carried out by 17 national metrology institutes, research institutes and industrial companies by developing measurement systems, methods and technique including in-situ systems which support innovative industrial processing of resources containing naturally occurring radioactive material, designing traceable measurement procedures for industrial NORM raw material, products, by-products, residues and waste, developing and establish traceable metrological reference materials and standard sources needed for calibration purposes for NORM measurement, improving decay data for selected natural radionuclides of the ²³⁸U, ²³⁵U decay chains, and to the rare earth element ¹³⁸La, focusing on decay chains description and gamma-ray intensities and half-life improvement, testing developed systems, standards and reference materials in industrial processing situations.

Effectiveness of the Shielding Mechanism in Rooms Housing X-ray Diagnostic Equipment - A Case Study of Mulago Hospital

Festo Kiragga, Rebecca Nakatudde, Akisophel Kisolo

Gulu University, North, Uganda

Abstract. The aim of the study was to determine the effectiveness of the shielding mechanism of rooms housing X-ray diagnostic equipment in Mulago hospital. This provided useful data needed to protect occupationally exposed workers, patients and the public from exposure to scattered radiation. The study was conducted in Mulago Hospital at the Uganda Cancer Institute, three selected centers at the Department of Radiology in new Mulago; Room 4 and CT room at the Second floor and the Casualty Center. Scattered radiation to the Operator's Console and to adjacent places was measured using thermoluminescent dosimeters (TLDs) for a month. Radiation leakages through the walls and doors to the members of the public were measured using a survey meter, scattered X-radiation received by radiation staff involved in the study were measured using TLD badges worn for a period of four weeks. The TLD badges were then read by the Harshaw TLD reader. The availability and effectiveness of the Lead aprons was also checked visually and suspicious ones exposed for verification. Scattered radiation in the imaging rooms varied between 1.20 mSv/month in the CT Room and 0.39 mSv/month from the Casualty Center. These results are much higher than the limits set by the Atomic Energy Council (AEC) for Uganda and International Atomic Energy Agency (IAEA) of 0.4 mSv/month for a medium sized room of 4 m×4 m. Average scattered radiation doses received by occupationally exposed workers were highest from Room 4 (plain radiography) of 6.0 mSv/yr and lowest in the Casualty center with 1.4 mSv/yr which are lower than the set maximum of 20 mSv/yr for occupationally exposed staff within the medical facility. Radiation leakages through selected doors were found to be 0.010 mSv/hr at the Uganda Cancer Institute and 0.012 mSv/hr from Room 4. The high levels of scattered radiation are attributed to the small size of imaging rooms & congestion due to the furniture and X-ray equipment which causes multiple scatter within the facility. The other causes were the technical state or condition of X-ray equipment, different examinations procedures and the human factors. The relatively high radiation doses received by some workers were attributed to differences in the number of patients handled in a given schedule and the poor radiation protection habits in some centers. These radiation doses are however within the recommended dose limits for the occupationally exposed workers. Since the study has indicated that the occupationally exposed workers were protected from the harmful effects due to the small doses received although the imaging rooms had a lot scattered radiation, care towards safety should therefore be undertaken during daily operation procedures, area classification and effective use of shielding gadgets to limit accidental exposures to radiation in all the rooms.

KIRDI'S Role in the Project "Promoting Safety, Self-reliance and Sustainability of Non-Destructive (NDT) Testing Facilities"

Humphrey Lumadede

Kenya Industrial Research and Development Institute (KIRDI), NAIROBI, Kenya

Abstract. As Kenya reaches for vision 2030, Nondestructive Testing Technology will required better quality and safety of operation, more reliable information on the current status, usability and an object's life expectation. Mechanical stresses are not visible to most of conventional NDT methods and they are usually the main and the first indicator of problems. The solution to this will be using the Indicator of Mechanical Stresses (IMS).The (IMS-Magneto-Anisotropic Indicator of mechanical stresses, searches for condition of deterioration to estimate the possible failure based on measuring concentration and the gradient of mechanical stress on Ferro-Magnetic parts. This early detection assures quality and safety is required of materials tested. Equipment used at Kenya Ports Authority (KPA) and in the Sugar factories are initially target for this investigation. The quality of stress release by Heat Treatment of vibration will be determined, quick check to identify high stress areas in welds will be done. Money will be saved on reliable inspection which sees the defect before it become a defect.

Requirements for Specific Safety Issues - Fire, Earthquake, and Flooding – at Large Particle Accelerator Facilities

Hee-Seock Lee^a, Arim Lee^a, Nam-suk Jung^a, Joohee Oh^a, Leila Mokhtari Oranj^b

^aPohang Accelerator Laboratory, Pohang University of Science and Technology (POSTECH), Pohang, Republic of Korea

^bDivision of Advanced Nuclear Engineering, Pohang University of Science and Technology (POSTECH), Pohang, Republic of Korea

Abstract. Radiation safety analysis is required fundamentally at an installation of a large particle accelerator facility and for getting its operation licence. The specific safety issues, fire, earthquake, and flooding are also reviewed in the process. However the safety issues are meaningful in the radiation safety analysis when those are related to radiation-induced hazards. At this paper, the hazard effects of fire, earthquake and flooding were studied in the view of type and beam power of particle accelerators. Regulations and policies at several countries and institutes are investigated. The degree of hazards and relative importance are discussed by considering residual activities and others. Finally basic idea to compensate related subjects in Korean nuclear safety regulation is suggested.

Modernisation of the Radiation Monitoring Systems at Research and Training Reactors in Hungary

János Petrányi^a, Dénes Elter^b, Imre Szalóki^c, Máté Solymosi^d, László Manga^e

^aGamma Co. Ltd., Budapest, Hungary

^bMTA Centre for Energy Research, Budapest, Hungary

^cInstitute of Nuclear Techniques, Budapest University of Technology and Economics, Budapest, Hungary

^dSomos Ltd., Budapest, Hungary

^eMVM Paks NPP Ltd., Paks, Hungary

Abstract. In the last few years a modernisation program of reactor radiation monitoring systems was started in Hungary. Two reactors were involved in this program, one of them is the Budapest Research Reactor, built in 1959, and at the present time it is operated by MTA Centre for Energy Research. The other reactor is the Training Reactor of BME NTI, which has been operated since 1971. This presentation will discuss the main steps of the modernization program of the radiation monitoring systems, new innovations, modern technical solutions and the planned developments. The area-, check point-, stack- and technology-monitoring and data central subsystems were affected by the modernisation. Beside the technical review, the operational experience of the working units OnREM (Online Radioactive Emission Monitoring) will be presented as well. This new monitoring system is fully developed and produced in Hungary. The side purpose of the applied technics was to enhance safety and security culture. The old monitoring systems were based on mainly scintillation type detectors and GM tubes. These first generation devices had only analogue signal outputs and external devices ensured power supply, outgoing signal processing and data evaluation. New solutions were implemented during the restoration such as intelligent probes and alpha, beta, gamma and neutron radiation measurements with the same detector system. In order to design the optimal solution, before the modernisations procedure a series of experiments were carried out in the Training Reactor of BME NTI. Based on the results, a specially designed scintillation detector was used to continuously measure isotope selective specific activity in the reactor primary circuit.

Environmental Radiation and Meteorological Monitoring Systems of a Greenfield Nuclear Power Plant

Juho Rissanen, Jussi Huutilainen

Fennovoima Oy, Helsinki, Finland

Abstract. Fennovoima is a Finnish energy company established in 2007. The target of the company is to construct new nuclear power in Finland and produce reasonably priced electricity for its shareholders. Fennovoima will build Hanhikivi-1, a greenfield nuclear power plant in Northern Finland. The reactor to be built is VVER-type AES-2006 pressurized water reactor with thermal power of 3200 MW. Fennovoima has submitted the Construction License Application to the Finnish Government in June 2015. The Construction License is scheduled to be granted in year 2017 after the Finnish Radiation and Nuclear Safety Authority (STUK) has given statement on the application. The commercial operation will begin in year 2024. In this presentation a short overview of the project will be given. In addition, tools for radiation protection and emergency preparedness of a nuclear power plant will be discussed. As a new company, Fennovoima has a great opportunity to build monitoring systems with the best available technology. Different aspects related to building of new systems, including environmental radiation monitoring network and meteorological monitoring will be covered. Moreover, the regulatory requirements given by STUK and how they are applied to the above mentioned monitoring systems of new nuclear power plant will be discussed.

Evaluation of Carbon -14 Released from Small Power Reactor

Kyo-Youn Kim, Ha-Young Kim, Jae Hoon Song

Korea Atomic Energy Research Institute, Daejeon, Republic of Korea

Abstract. Since Carbon-14 has a long half-life (5730 years) and high fluidity in the environment, it can be considered as one of the most important radionuclides. Carbon-14 is a radioactive isotope of carbon of considerable interest in nuclear power plants since it is present in most parts of the primary system of a nuclear reactor with a high production rate. In general, nuclear regulators request that 7.3Ci/yr should be used as an expected activity of Carbon-14 released from a nuclear power plant based on NUREG-0017 regardless of the power of the nuclear reactor. In addition, 10 CFR 50.36a requires that operating procedures be developed for the control of effluents and that the quantities of the principal radionuclides be reported. In fact, this approach to use the activity of Carbon-14 based on NUREG-0017 regardless of the power of nuclear reactor is inconsequential and too conservative. The quantity of Carbon-14 discharged can be estimated through sample measurements or by the use of a normalized C-14 source term, and scaling factors based on the power or estimated through use of the GALE code from NUREG-0017. This study shows that the Carbon-14 activity of a small reactor estimated by considering the scaling factors based on nuclear power is consistent when compared with the activity estimated by an activation calculation.

Development of a Methodology to Correlate Safety Classification of Components to the Maintenance Programme of a Facility

Muhammad Akbar

South African Nuclear Energy Corporation (NESCA), Pretoria, South Africa

Abstract. The purpose of safety classification of components is to identify those SSCs that are important to safety and that protect people and the environment from the harmful effects of ionizing radiation. The purpose of a maintenance programme for a nuclear facility is to provide the necessary measures that are required to detect and mitigate degradation of a functioning SSC, or to restore to an acceptable level the performance of safety functions of a failed SSC. A systematic approach is required to evaluate which maintenance tasks are to be performed, on which SSCs and at what intervals, in order to optimize availability and safety of the plant. Due to this, a methodology needs to be developed to correlate the safety classification of components to the maintenance programme of a facility, to ensure that the expected levels of safety performance are achieved. This paper presents the progress that has been made in terms of the development of such a methodology and the challenges it optimising such a system. The methodology focuses on how the safety classification of components impacts the SSC maintenance activities and frequencies, encompassing processes from the functional analysis to design modifications. The proposed methodology includes SSC performance monitoring and maintenance optimisation, which are key aspects in contributing towards a higher availability of SSCs performing safety functions, and therefore optimisation of protection of people and the environment against ionising radiation.

Applicability of Lessons Learned from the Fukushima Accident to Radioactive Material Users

Shawn Smith, Catherine Haney

US Nuclear Regulatory Commission, Rockville, MD, USA

Abstract. Shortly after the March 11, 2011, earthquake and tsunami that led to the accident at the Fukushima Dai-ichi nuclear power plant in Japan, the U.S. Nuclear Regulatory Commission (NRC) undertook actions to assess the accident and identify lessons learned for U.S. nuclear facilities. One of the actions was an assessment of the applicability of the lessons learned from the accident to non-operating reactors and non-reactor facilities. Very shortly after the accident, NRC staff performed limited assessments to ensure that no immediate safety concerns existed at these facilities and took safety measures where necessary, such as an independent verification of fuel facility licensees' abilities to prevent or mitigate the consequences of events that could challenge the safety or licensing bases of those facilities. With insights gained from NRC activities related to power reactors and from the results of inspections at fuel cycle facilities, NRC staff has more fully evaluated issues and possible actions related to other NRC-licensed materials, devices, and facilities. Based on the evaluation of lessons learned from the Fukushima accident, it was concluded that there is no need for regulatory action for radioactive material users in light of the accident. NRC is continuing additional assessment related to Fukushima lessons learned for NRC-regulated fuel facilities and a small subset of research and test reactors (RTRs). However, for radioactive material users, NRC has determined that further assessments are not needed based on Fukushima lessons learned and that the existing regulatory requirements and processes ensure adequate protection of public health and safety. Unsealed radioactive materials and sealed sources and devices used in industry, academia, and medicine are appropriately licensed and have sufficient engineering controls to protect the health and safety of workers and members of the public. Worker exposures are kept as low as is reasonably achievable and minimize the danger to life and property.

Local Shield Model around Beam Target Stations using Radiation Transport Code MCNPX

Tebogo Kupi^a, Johann van Rooyen^b, Raymond Njinga^a

^aNorth-West University, Mahikeng, South Africa

^bNESCA, Pretoria, South Africa

Abstract. A model of local shield around Horizontal Beam Target Stations (HBTS-1 and HBTS-2) was done using radiation transport code, MCNPX and compared to existing designs modelled with ANISN/HILO and ANISN/DOT in 1990. This was done to verify if MCNPX is suited for the local shields designs around radionuclide production beam target stations. Next, the local shield around HBTS-2 was modelled with MCNPX to find the optimal shield design, and to characterise the radiological performance. Results are as follows: The 1990 ANISN/HILO design of the local shield around HBTS-1 is reasonably close to optimal. The calculations proved that scaling down the HBTS-1 design to arrive at a design for HBTS-2 was necessary and that the existing HBTS-2 shield is closed to optimal. This study finally revealed that the present designs for the local shields around HBTS-1 and HBTS-2 are near-optimal, and that the Monte Carlo radiation transport code MCNPX is suited for particle-accelerator related shield design projects in the incident particle energy range under analysis, i.e. 66 MeV per nucleon.

Validation of Experimental Measurements of Activity for Radioisotopes in SAFARI-1 Reactor

Tholakele Ngeleka

NECSA, Pretoria, South Africa

Abstract. Ir-191 Test irradiations were conducted in SAFARI-1 for experimental purposes. The Target sample (Ir-191) was irradiated for a specific period in an isotope production rigs (IPRs) and the activity for irradiated sample (Ir-192) was measured. To ensure the correctness of the activity measuring method, the computational analyses using MCNP and FISPACT codes were also undertaken. SAFARI-1, the South African Fundamental Atomic Research Installation is operated by Nuclear Energy Corporation of South Africa (NECSA), a state owned nuclear facility. It is a multipurpose reactor and is also used for isotope production. The paper will presents the comparisons between the calculation results and experimental measurements.

Robotic HPGe Spectrometer for Radionuclide Analysis

Vladimir Gostilo, Alexander Sokolov

Baltic Scientific Instruments, Riga, Latvia

Abstract. Laboratory HPGe spectrometers with lead shield are the most widely used devices for precision radionuclide analysis in environmental objects (soil, water, air), medical and biological objects, radioactive materials and products. High energy resolution and registration efficiency of HPGe detectors, low level of instrument background provide low detection limits for radionuclides measurements in samples listed above. At that, the measurement time during the studies could be several hours and even days and larger quantity of the samples, their loading and reloading make the measurement process a real problem for the operator. The development results for robotic HPGe spectrometer for routine measurements at radionuclide analysis of radioactive materials are presented. The spectrometer has HPGe detector, which registration efficiency can be from 10 to 160%, multichannel analyzer, lead shield and robotic sampler based on industrial manipulator IRB120 by company ABB. Real metrological performance of spectrometer will depends on HPGe detector efficiency. For spectrometer with HPGe detector efficiency 30% performance is: detection limit for Cs¹³⁷ radionuclide specific activity, measurement time 1 hour is < 0.5 Bq/kg, absolute sensitivity to gamma flux for 30%*efficient detector is 4.5×10^{-3} pulse/quantum, instrumental background intensity for energy range 40 keV – 3 MeV is 5×10^{-4} , and Cs¹³⁷ radionuclide specific activity measurement error for measurement time 1 hour is $< 20\%$. The software of the spectrometer comprises the program SpectroLine for the calculation of the radionuclide activities as well as control program for the manipulator at sampling. The fully automated sample changer enables the user to measure up to 40 samples without having to interact with the Automated Spectrometer. This reliable robotic sample changer increases the productivity and reduces the possibility of health risks for the operator.

**The Proceedings of the 14th International Congress of the International Radiation
Protection Association
Volume 3 of 5**

Area 6: Radiation Detection and Dosimetry

A New Approach to Worker Internal Dosimetry and its Impact on Radiation Protection

Alan Birchall^{a*}, Vadim Vostrotin^b, Matthew Puncher^c, Alexander Efimov^b, Bruce Napier^d

^aAlan Birchall, Global Dosimetry Ltd., 1 Macdonald Close, Didcot, OX11 7BH. UK.

^bSouthern Urals Biophysics Institute (SUBI), Ozersk, Chelyabinsk, Russia.

^cPublic Health England (PHE), Chilton, Didcot, United Kingdom.

^dPacific Northwest National Laboratory, (PNNL), Richland, WA, United States.

Abstract. In order to quantify the risk of harmful effects following inhalation of plutonium aerosols, it is necessary to perform an epidemiological analysis, where both the health effects and the received internal dose can be quantified. An ideal cohort for such a study is located at the Mayak Production Association in Ozersk, Russia, where around 25,000 workers were potentially exposed to plutonium, and 8,000 of them provided urine samples on which an internal dose assessment could be based. This paper is concerned with the assessment of organ doses for these 8000 workers. The presentation gives a description of the biokinetic model and dosimetric assumptions made for the latest analysis (MWDS-2013), paying particular attention to where the methodology differs from that currently recommended by the ICRP. One major difference between this model and previous models is that it has been designed to deal with uncertainty in model parameters and measurement data explicitly. This has required a different type of model, referred to here as a hyper-model. Some of the advantages and disadvantages of dealing with hyper-models are discussed along with some of the problems encountered and solved during their practical implementation. The MWDS-2013 system can be regarded as 'state of the art' and the output will be used in the latest epidemiological study of the Mayak workforce. The results from this study are expected to further our understanding of plutonium biokinetics and the mechanisms of radiation induced cancers in humans and also quantify the associated risks more precisely. The results will lead to improvements in radiation risk protection standards and it is expected that some of the model developments will be incorporated into the forthcoming ICRP recommendations on occupational intakes of radionuclides.

KEYWORDS: *internal dosimetry; Mayak workers; uncertainty; realizations; Bayes; models.*

1 INTRODUCTION

As part of an ongoing study (Joint Coordinating Council on Radiation Effects Research (JCCRER) - Project 2.4), funded by the United States Department of Energy (USDOE), various protocols for assessing the internal doses of Mayak Production Association (PA) workers have been generated: DOSES-1995, DOSES-2000, DOSES-2005, and MWDS-2008. These doses have been used as inputs to epidemiological studies (JCCRER Project 2.1) to determine the risk of exposure to plutonium aerosols. The purpose of this paper is to present an overview of the latest Mayak Worker Dosimetry System MWDS-2013. A complete description of the MWDS-2013 system is presented elsewhere [1] with supplementary papers describing different aspects of the development and will be published together in a special journal edition.

One major difference between this model and previous models is that it has been designed to deal with uncertainty in model parameters and measurement data explicitly. This has required a different type of model, referred to here as a hyper-model. Some of the advantages and disadvantages of dealing with hyper-models are discussed along with some of the problems encountered and solved during their practical implementation. In this overview, attention will be directed to areas where the models and methodology differ from those currently recommended by ICRP for radiation protection, and the effect that this work has had on radiation protection in general. The focus of this paper is in internal dosimetry, and external doses to the Mayak workers are considered in separate paper.

* Presenting author, e-mail: globaldosimetry@gmail.com

The results from this study are expected to further our understanding of plutonium biokinetics and the mechanisms of radiation induced cancers in humans and also quantify the associated risks more precisely. The results will lead to improvements in radiation risk protection standards and it is expected that some of the model developments will be incorporated into the forthcoming ICRP recommendations on occupational intakes of radionuclides.

2 USE OF HYPER-MODELS

2.1 What is a hyper-model?

ICRP biokinetic models that are currently used for calculating internal doses in radiation [2,3,4] are compartmental models, where the rates of transfer of activity between compartments are described by fixed rate constants. Thus, a specific intake will give rise to a single dose. One of the main differences between the MWDS-2013 approach to calculating internal doses to Mayak workers and previous approaches is that in this approach it is required to take account explicitly of uncertainties in the biokinetic models. This is achieved by assigning not a single value, but a probability distribution to important rates within the model. This probability distribution represents the uncertainty of that parameter value for that worker, before any measurements are taken. It can be likened to a prior distribution used in Bayesian analysis. In order to differentiate this type of model from the standard model, the term hyper-model is used. A hyper-model is thus a model, where one or more parameter values are represented by a distribution. The term ‘hyper’ is consistent with the same term used in hierarchical Bayesian analyses, where hyper-priors are ones where a parameter of the prior is itself a distribution.

2.2 Computing with hyper-models

Running a hyper-model forwards is relatively straightforward. One can simply use a Monte Carlo approach, where for each run, a single parameter value is chosen at random from its distribution, and the end quantity is calculated. As this is repeated, a distribution of the end quantity is constructed. The output from a hyper-model with say a fixed intake is thus a distribution and not a single value. It is however important to note, that for non-linear models, such as the ones used in radiation protection, the mean of such a distribution is different than one would obtain if one chose a model where each of its parameter values were represented by the mean of the prior distributions. In other words, ignoring uncertainty on parameter values, as ICRP do, is likely to introduce a bias in the end result.

Running a hyper-model backwards (e.g. using it to estimate an intake from measurement data) is not so straightforward. The Monte Carlo approach described above fails because some models (model parameters) fit the data much better than others, and so should not be assigned the same weight. Instead of this, Bayesian methods, such as Markov Chain Monte Carlo Methods (MCMC) are commonly used [5]. There is however, a much simpler approach, the WeLMoS method [6] which uses a simple Monte Carlo approach and weights the intake according to the likelihood (goodness of fit to the data). Although both methods give the same results [6], there is a massive difference in the computational efficiency. In situations where the uncertainties tend to be large (e.g. internal dosimetry) the WeLMoS method is much faster. For a comparison of these approaches, see NCRP Report 164 [7]. For these reasons, it was decided to use the WeLMoS method [6] for all internal dose calculations in MWDS-2013.

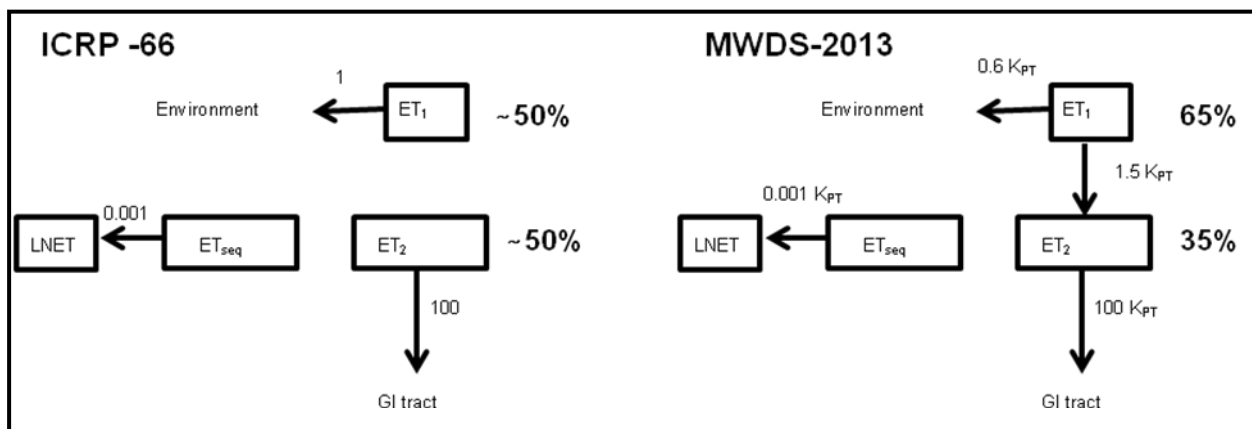
3 BOKINETIC MODELS

A full description [1] of all of the biokinetic models used in MWDS-2013 is outside the scope of this summary paper. In general, this paper will focus on where departures were made from current ICRP methodology.

3.1 Particle transport in the extra-thoracic region

Experiments carried out at PHE (formerly NRPB) indicate that unlike the representation in ICRP-66, activity deposited in the ET_1 region actually moves towards the ET_2 region [8]. The Project 2.4 team used the data from PHE to construct a new model of the extrathoracic region [9]. A comparison of both models is shown in Fig 1. Uncertainty in the MWDS-2013 hyper-model is achieved by having a random variable K_{PT} which is lognormally distributed with a median value of 1, and a geometric standard deviation of 1.73. The MWDS-2013 model for the extra-thoracic region has recently been accepted by ICRP [10] in its revision of biokinetic models for internal dosimetry, and will be used for calculating new dose coefficients for both workers and members of the public.

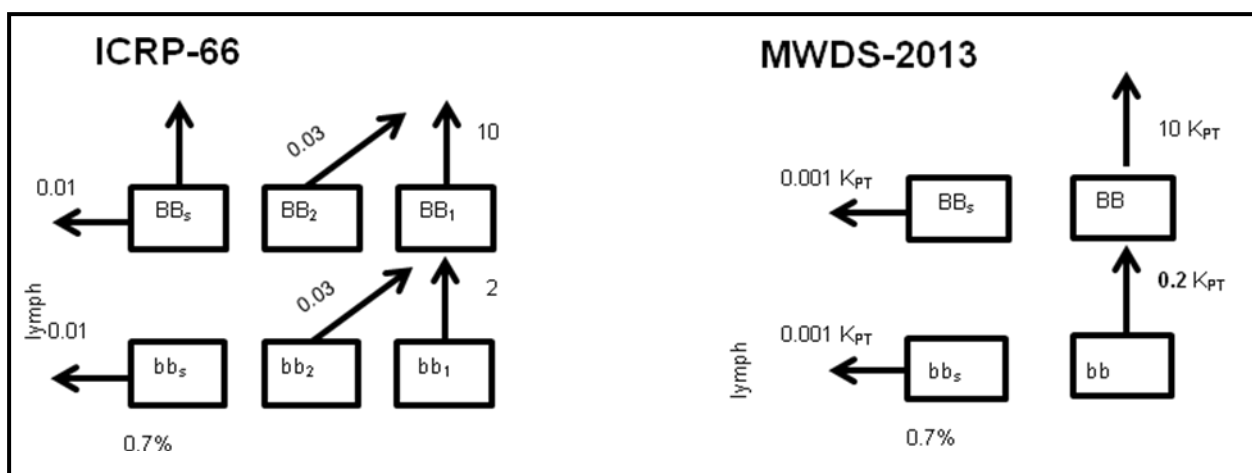
Figure 1: A comparison of the ICRP 66 model and the MWDS-2013 hyper-model of the extra-thoracic region of the lungs.



3.2 Particle transport in the upper airways

For the upper airways, the model recommended in ICRP Publication 130 [10] was chosen to be simpler and more accurate. Again, this was converted to a hyper-model by multiplying by the random variable K_{PT} . A comparison with the current ICRP Publication 66 model is shown in Fig 2.

Figure 2: A comparison of the ICRP 66 model and the MWDS-2013 hyper-model of the extra-thoracic region of the lungs.



3.3 Particle transport in the deep lung

For the deep lung, the model structure then being considered by ICRP, and later published in ICRP-130 [10] was adopted by MWDS-2013. This model was based on that developed by Gregoratto et al [11]. In order to make this into a hyper model, the default clearance parameters were replaced by lognormal distributions shown in Table 1.

Figure 3: The model structure adopted for MWDS-2013 was taken from the recently published ICRP-130 in preference to the currently used ICRP-66.

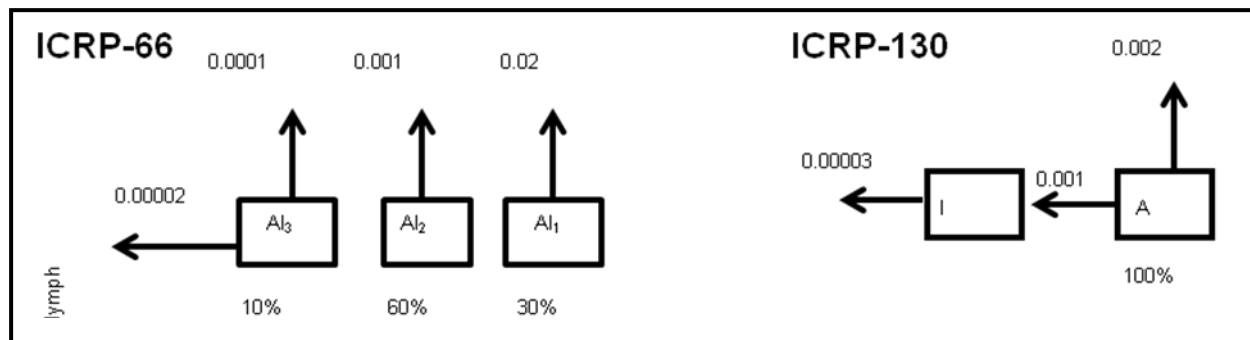


Table 1: Parameters of the lognormal distribution [11] used to represent particle transport rates in the deep lung, in the MWDS-2013 hyper-model of the deep lung.

Rate	Parameters of the lognormal distribution	
	Median (d ⁻¹)	GSD
A to bb	0.0013	3.2
A to I	0.001	4.5
I to lymph	0.0003	3

3.4 Binding to lung tissue

The Project 2.4 team spent a significant effort on re-analysing experimental data published on Beagle Dogs [12], and also commissioned further experimental measurements of the retention of plutonium nitrate in the upper airways of autopsy cases from the United States Transuranium and Uranium Registries (USTUR) [13,14]. It was concluded that this data could not be explained without the assumption of long term binding. The data from 20 autopsy cases carried out on Mayak workers who had been exposed to pure plutonium nitrate was used in a simultaneous Bayesian analysis [15] to quantify the bound fraction. The results showed that the posterior distribution of the bound fraction f_b could be adequately explained by a uniform probability distribution from 0 to 0.4%.

Although this is only a small fraction, it has a large affect on the dose. It has been shown [16] that a bound fraction of only 1% is enough to double the equivalent dose to the lungs. ICRP are currently considering this work, and it is highly likely that a bound fraction of 0.2% (the mean of the MWDS-2013 distribution) will be adopted as a default value for all actinides in the forthcoming ICRP Publication 130 Part 4.

3.5 Other biokinetic models

MWDS-2013 adopted the simpler ICRP-30 GIT Tract model [2] as opposed to the later Human Alimentary Tract Model [17], as the former was simpler to apply, and it probably wouldn't make much difference to calculated doses anyway (except perhaps dose to the GI tract itself). No uncertainties were considered in this model.

To describe the biokinetic behavior of plutonium following uptake to blood, MWDS-2013 used the Leggett systemic model [18]. A significant effort went into validating this model by comparing

estimates of intake based on both urine and autopsy data on Mayak workers [19]. Variability between workers, in the net amount of plutonium transferring to bone and liver, was modeled by restricting the total amount to (liver + bone) to be fixed at 0.9, while allowing the fraction between bone and liver to vary.

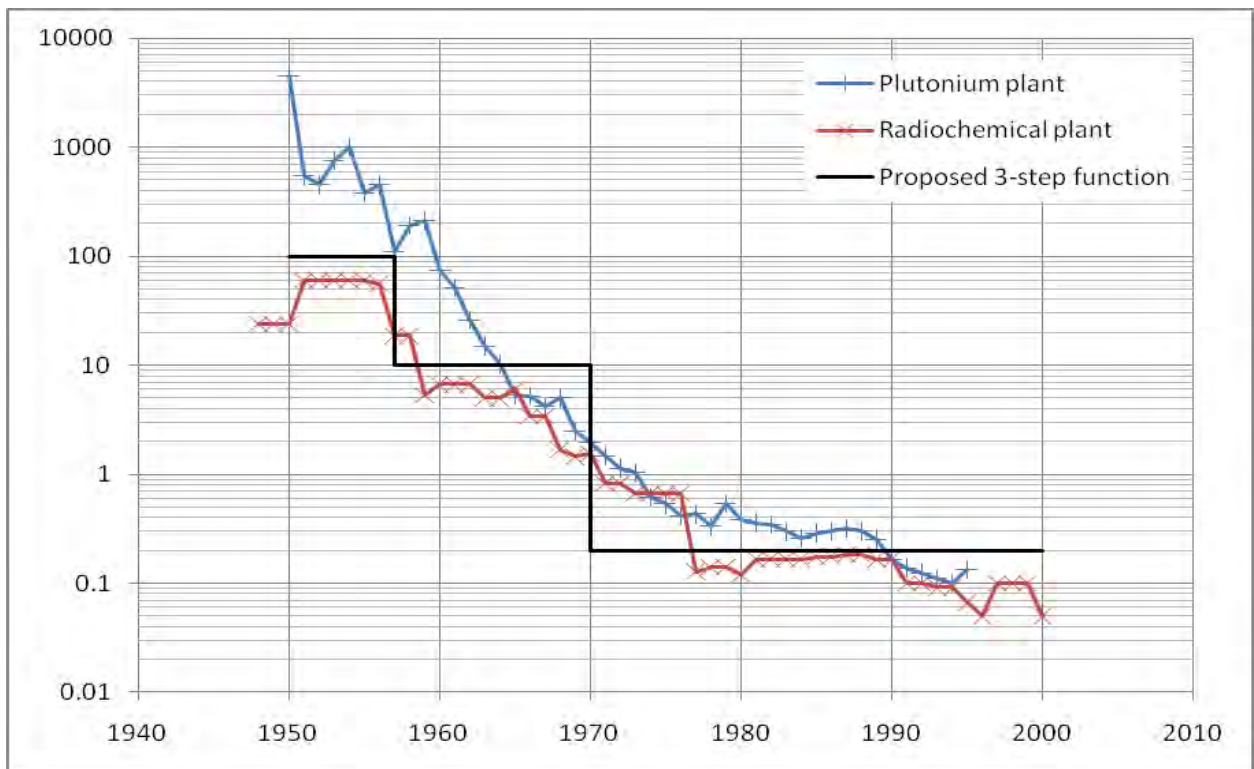
4 DOSIMETRY

MWDS-2013 used the currently recommended (in Europe and most of the world) ICRP dosimetric models. It is acknowledged that ICRP have recently spent a huge effort to update the Specific Effective Energies for all of the radionuclides, but this data was not (and still isn't) available. Use of the new SEE's is unlikely to make much difference to plutonium doses except perhaps for the skeleton. For the lungs, the dose to each of the three lung regions (BB, bb, AI) was calculated separately. Where a single lung dose was required, an average dose was calculated [20].

5 INTAKE REGIMES

An intake regime is a temporal pattern of intake (such as an acute or chronic intake) which is used to describe the intake rate as a function of time. Once this pattern is fixed (or assumed), it can be multiplied by a variable (Intake) to fit the actual intake to the measurement data. Data from plutonium air concentrations, sampled from many buildings and laboratories over the years at Mayak, have suggested that air concentrations were much higher in early years. A 3-step function, based on grouped monitoring data was used in MWDS-2013 to describe the intake regime (Fig 3).

Figure 4: A 3-step function (solid line), based on grouped air concentrations, is used to model the intake regime for workers. Uncertainties on the step function are taken into account.



The intake regime for a particular worker was calculated by combining this three-step function with the worker's own work history. Uncertainties in this step function were taken to be a factor of 10 for the first two steps and a factor of 2 for the third step. Because the intake is fit to urine data for each worker, the actual shape of the intake regime has little effect on organ doses.

6 MEASUREMENT UNCERTAINTY

A full treatment how uncertainty on the urine measurements of workers was estimated is outside the scope of this summary paper, and is dealt with in full elsewhere [1, 21]. The approach was to combine Type-A uncertainties (counting statistics, background counts, aliquot uncertainty, detector efficiency etc) which are approximated by normal distributions, and then approximate the resulting uncertainty by a lognormal distribution, the GSD of which is referred to as the scattering factor SF_A . Secondly, type B uncertainties (due to intra-subject variability, uncertainty in the sample duration, and the method used to normalise the data) are approximated by SF_B . The final uncertainty is thus represented by lognormal distribution with a scattering factor (GSD) given by:

$$\ln^2(SF) = \ln^2(SF_A) + \ln^2(SF_B) \quad (1)$$

If a measurement was made immediately after administration of DTPA, then the measurement value is reduced by a factor 62.3, and an appropriate increase in the associated uncertainty (SF) is made. Measurements recorded as below the decision threshold are treated as *Less than Limit of Detection* (<LOD) values with an associated uncertainty.

7 FITTING METHODOLOGY

So far, we have described the hyper-model used to relate intake to urinary excretion and organ dose, and the assumptions made about the intake regime for a particular worker. We have described how uncertainties are assigned to measurement data, which typically consists of 1 or more measurements of plutonium in a 24h urine sample. The fitting methodology is conducted as follows:

- Randomly choose a set of parameter values from the hyper-model (to create a model)
- Construct the complex intake regime for that worker
- Use the model to calculate the likelihood function of intake
- Weight this likelihood by the prior distribution on intake

The resulting distribution is proportional to the Bayesian posterior distribution of intake conditioned on the measurement data for that individual and the chosen set of parameter values. This intake distribution could be multiplied by a dose coefficient (which in turn depends on the chosen parameter values) to give the corresponding dose distribution to any organ. It should be noted here, that the output is not a single value of dose, but a distribution: the height of which depends on how well it fits the data, and the width is a measure of the uncertainty.

8 MULTIPLE HYPER-REALISATIONS

8.1 Calculating multiple hyper-realizations

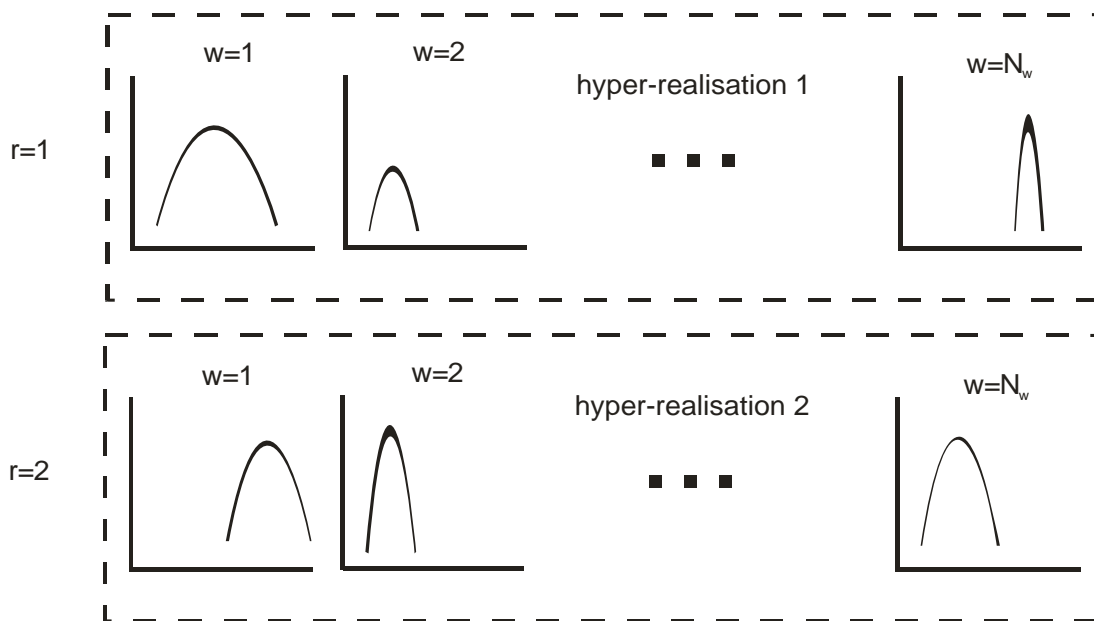
In order to extend this methodology to the entire cohort of workers, the process outlined in the previous section must be repeated for each worker. However, care must be taken when choosing these values. For parameters which are unknown, but assumed to be the same for each worker (termed *shared parameters*, e.g. absorption rates are assumed to be shared since they depend on the material inhaled), the same parameter values must be used for all the workers. Conversely, for *unshared parameters* (those assumed to be independent between workers, e.g. particle transport rates), different random parameter values are allowed to be chosen.

In this way, a distribution of X is constructed for each worker. X could be the intake or a particular organ dose in a particular year. This whole process is then repeated 1000 times, with different sets of random parameter values. Fig. 5 shows a schematic representation of the first two hyper-realizations.

8.2 Reducing the hyper-realizations to realisations

The multiple hyper-realizations contain all of the information that an epidemiologist would need on the uncertainties of organ doses for all workers, and all information concerning goodness of fit and shared and unshared uncertainty is preserved. Unfortunately, in order to make epidemiological calculations tractable, these hyper-realizations must be reduced to simpler realisations. A full discussion of how this can be achieved and the consequences of different approaches is given elsewhere [22]. For MWDS-2013, the process used to reduce hyper-realizations to realisation was to randomly sample once from each worker within the multiple hyper-realizations. This has the advantage over choosing the mean or mode of each distribution, since it does not lose information on the width (uncertainty) of these distributions. The output from MWDS-2013 internal dosimetry thus consists of 1000 realisations of organ doses, for each worker, in each calendar year.

Figure 5: A schematic representation of 2 hyper-realizations. w is the worker number for each of the N_w workers in the cohort, and r is the number of the hyper-realisation.



9 ACKNOWLEDGEMENTS

This work was conducted as part of the Joint Coordinating Committee for Radiation Effects Research Project 2.4, Mayak Worker Dosimetry. It was jointly funded by the U.S. Department of Energy (U.S. DOE) and the Federal Medical Biological Agency (FMBA) of the Russian Federation. We acknowledge the valuable support and assistance of Barrett Fountos, Program Manager, U.S. DOE's Office of Domestic and International Health Studies (AU-13) and of Sergey Romanov, Director of the Southern Urals Biophysics Institute.

10 REFERENCES

- [1] Birchall, A., Vostrotin, V., Puncher, et al., 2016. The Mayak worker dosimetry system (MWDS-2013) for internally deposited plutonium: An Overview. *Rad. Prot. Dosim* (in press).
- [2] ICRP, 1979. The 1979 Recommendations of the International Commission on Radiological Protection. Limits for Intakes of Radionuclides by Workers. ICRP Publication. ICRP Publication 30. *Ann. ICRP* 2 (3-4).
- [3] ICRP, 1994. The 1994 Recommendations of the International Commission on Radiological Protection. Human Respiratory Tract Model for Radiological Protection. ICRP Publication 66. *Ann. ICRP* 24 (1-3).

- [4] ICRP, 1994. The 1994 Recommendations of the International Commission on Radiological Protection. Dose Coefficients for Intakes of Radionuclides by Workers. ICRP Publication 68. Ann. ICRP 24 (4).
- [5] Gilks, W. R., Richardson, S. and Spiegelhalter, D. J. Introducing Markov Chain Monte Carlo. In Markov Chain Monte Carlo in Practice. Chapman and Hall, London (1996).
- [6] Puncher, M., Birchall, A. A Monte Carlo method for calculating Bayesian uncertainties in internal dosimetry. *Radiat Prot Dosim* 132: 1 - 12. (2008).
- [7] Bouville, A., et. al., 2010. NCRP Report 164. Uncertainties in Internal Radiation Dose Assessment. National Council on Radiation Protection and Measurements. ISBN: Uncertainties in internal radiation: dose assessment. p. cm. -- (NCRP report ; no. 164) Includes bibliographical references and index. ISBN 978-0-9823843-2-9 (alk. paper) 1. Radiation dosimetry. 2. Radiation--Dosage. I. National Council on Radiation Protection and Measurements. RA569.U15 2010.
- [8] Smith, J. R. H., Bailey, M. R., Etherington, G., et al., 2011. An experimental study of clearance of inhaled particles from the human nose. *Exp.Lung Res.* 37(2), pp.109–129.
- [9] Smith, J.R.H., Birchall, A., Etherington, G., et al., 2014. A revised model for the deposition and clearance of inhaled particles in human extra-thoracic airways. *Radiat Prot Dosimetry* 158 (2) pp.135-147.
- [10] ICRP, 2015. The 2015 Recommendations of the International Commission on Radiological Protection. Occupational Intakes of Radionuclides. ICRP Publication 130. Ann. ICRP 44 (2).
- [11] Gregoratto, D., Bailey, M. R., Marsh, J. W., 2010. Modelling particle retention in the alveolar–interstitial region of the human lungs. *Journal of Radiological Protection.* 30(3), pp. 491-512.
- [12] Puncher, M., Pellow, P. G. D., Hodgson, A., et al., 2016. The Mayak Worker Dosimetry System (MWDS-2013): A Bayesian Analysis to Quantify Pulmonary Binding of Plutonium in Lungs Using Historic Beagle Dog Data. *Radiation Protection Dosimetry* (in press).
- [13] Tolmachev, S. Y., Nielsen, C. E., Avtandilashvili, et al., 2016. The Mayak Worker Dosimetry System (MWDS 2013): Soluble plutonium retention in the lungs of an occupationally exposed USTUR case. *Radiation Protection Dosimetry.* In press.
- [14] Puncher, M., Birchall, A., Tolmachev, S. Y., 2016 The Mayak Worker Dosimetry System (MWDS 2013): A re-analysis of USTUR Case 0269 to determine whether plutonium binds to the lungs. *Radiation Protection Dosimetry* (in press).
- [15] Puncher, M., Birchall, A., Sokolova, A. B., et al., 2016. The Mayak Worker Dosimetry System (MWDS-2013): Plutonium binding in the lungs - an analysis of Mayak workers. *Radiation Protection Dosimetry* (in press).
- [16] Birchall, A., Puncher, M., Harrison, J., et al., 2010. Plutonium worker dosimetry. *Radiat Environ Biophys.* 49(2), pp. 203-212.
- [17] ICRP, 2006. The 2006 Recommendations of the International Commission on Radiological Protection. Human Alimentary Tract Model for Radiological Protection. ICRP Publication 100. Ann. ICRP 36 (1-2).
- [18] Leggett, R. W., Eckerman, K. F., Khokhryakov, V. F., et al., 2005. Mayak Worker Study: An Improved Biokinetic Model for Reconstructing Doses from Internally Deposited Plutonium. *Radiation Research.* 164(2), pp.111-122.
- [19] Birchall, A., Dorrian, M. D., Suslova, K. G., et al., 2016. The Mayak Worker Dosimetry System (MWDS-2013): A comparison of intakes based on urine versus autopsy data from Mayak workers using the Leggett systemic model for plutonium. *Radiation Protection Dosimetry* (in press).
- [20] Birchall, A., Marsh, J. W., 2016. The Mayak Worker Dosimetry System (MWDS-2013): How to weight the absorbed dose to different lung regions in the calculation of lung dose. *Radiation Protection Dosimetry* (in press).
- [21] Vostrotin, V., Birchall, A., Zhdanov, A., et al., 2016. The Mayak Worker Dosimetry System (MWDS-2013): Uncertainty in the measurement of Pu activity in a 24-hour urine sample of a typical Mayak PA worker. *Radiation Protection Dosimetry* (in press).
- [22] Birchall, A., and Puncher, M., 2016. The Mayak Worker Dosimetry System (MWDS-2013): How to reduce hyper-realizations to realisations. *Radiation Protection Dosimetry* (in press).

Approach to uncertainties in exposure, dose and risk estimates for uranium workers within the CURE project

Augusto Giussani^{a*}, Sophie Ancelet^b, Derek Bingham^c, Eric Blanchardon^b, Richard Bull^d, Estelle Davesne^b, James Grellier^{e#}, Olivier Laurent^b, Dominique Laurier^b, Matthew Puncher^f, Tony Riddell^f

^aBfS, German Federal Office for Radiation Protection, 85764 Oberschleißheim, Germany.

^bIRSN, Institute for Radiological Protection and Nuclear Safety, 92262 Fontenay-aux-Roses, France.

^cAWE, Aldermaston, Reading RG7 4PR, UK.

^dNuvia Ltd., Harwell Science and Innovation Campus, Didcot OX11 0RL, UK.

^eCREAL, Center for Research in Environmental Epidemiology, 08003 Barcelona, Spain.

^fPHE, Public Health England, CRCE, Chilton, Didcot OX11 0RQ, UK.

Abstract. The aim of the European concerted action CURE (Concerted Uranium Research in Europe) was to evaluate the feasibility of a large scale study of potential risks associated with uranium exposure in cohorts of miners, millers and other nuclear industry employees involved in the uranium cycle. CURE allowed the development of specific protocols for a future collaborative project integrating research in the fields of epidemiology, biology and dosimetry. An Uncertainty Working Group (UWG) was set up to deal explicitly with the issue of uncertainties. The UWG developed a matrix in order to standardize the collection of information between the different groups and thus characterize the different sources of uncertainty, ranking them in order of importance. Sensitivity studies were performed using sample data from uranium workers cohorts to evaluate the relative contribution of each source of uncertainty on dose estimates. Choice of pulmonary absorption type (when lung dose is the endpoint of interest) and handling of censored data (e.g. below detection limit) were identified as the primary sources of uncertainty. The final report delivered by the UWG proposed strategies for the development of methodologies for the propagation of uncertainties in dose estimates into estimates of risk, including the creation of a synthetic cohort as a tool for evaluating proposed methodologies.

KEYWORDS: *Uranium, miners, internal dose, uncertainty analysis.*

1 INTRODUCTION

Uranium occurs naturally in the environment as a mixture of three long-lived alpha-emitting isotopes: ²³⁴U (abundance by mole: 0.0054%, half-life: 2.455·10⁵ y), ²³⁵U (abundance by mole: 0.7204%, half-life: 7.04·10⁸ y) and ²³⁸U (abundance by mole: 99.2742%, half-life: 4.468·10⁹ y) [1, 2]. Uranium is a heavy metal, so it is potentially both radiologically and chemically toxic. The general population is routinely exposed to natural uranium through ingesting it in food and drinking water [3, 4]. Additionally, hundreds of thousands of workers involved in the nuclear fuel cycle are or have been occupationally exposed to uranium worldwide, due to its presence in various isotopic compositions at all stages of this cycle [5, 6].

In spite of that, the health impacts of chronic exposures to uranium are not well characterised. Most epidemiological studies have been limited by small study populations, inadequate control of confounders, lack of harmonization of methods for the estimation of radiation doses from uranium exposures [7].

To address these issues, several European groups joined together in the concerted action CURE (Concerted Uranium Research in Europe) [8, 9], funded by the DoReMi European Network of Excellence. CURE combined competencies in dosimetry, biology and epidemiology with a specific focus on occupational uranium exposures. Its aim was to evaluate the feasibility of a large scale study of potential risks associated with uranium exposure in cohorts of miners, millers and other nuclear

* Presenting author, e-mail: agiussani@bfs.de

Current address: University of Exeter Medical School, Exeter EX4, UK.

industry employees involved in the uranium cycle. The main result of the concerted action was an integrated research protocol, which serves as the basis for potential future large-scale collaborative research projects [8, 9].

During the course of CURE, a specific working group dealing with the issue of uncertainties was set up. Accounting for uncertainties in dosimetry and in dose-response models used in epidemiologic studies of uranium workers and miners/millers is indeed a demanding issue and a vast field of investigation. This is due to the complexity of dose assessment procedures, the various sources of uncertainty involved and to the advanced statistical methods that are needed to deal with such uncertainties.

The Uncertainty Working Group (UWG) put together members of all three main work packages of CURE: Epidemiology, Dosimetry and Biology. Its aim was to harmonize methods for evaluating uncertainties between the work packages, gain a better understanding of the magnitude of the different types of uncertainties, assess how uncertainties affect risk estimates, identify the limitations of existing approaches to the treatment of uncertainties and propose new solutions to address them in the future.

Since it was found that uncertainties related to the biological component of the CURE project could be best quantified and reduced by conducting pilot molecular epidemiology studies, the present short manuscript focuses on uncertainties related to dose estimation and epidemiological analyses. It briefly summarizes the activities and the main outcomes of the UWG on these specific issues.

2 ACCOUNTING FOR UNCERTAINTIES IN DOSE-RESPONSE MODELS

Risk estimates as obtained in epidemiology studies are usually expressed with confidence intervals that only reflect random fluctuations of the data. Uncertainty in exposure and dose estimates is recognized as a potentially important source of bias and increased uncertainty in the estimation of any radiation-induced risks [10, 11]. Research on the uncertainties related to the quantification of radiation doses due to internal exposure to radionuclides, has been recently a very active field [12-15]. The impact of specific sources of uncertainty, such as exposure measurement error, on the disease risk estimates is a relatively new but developing field in radiation epidemiology and several approaches are being developed and applied [16-21].

The analysis conducted by the UWG was limited by the short time and few resources available. It was mainly focussed on the identification and characterization of all the possible sources of uncertainties which may affect the processes of dose estimation and risk evaluation. Possible strategies for the elaboration of a rigorous method to propagate uncertainties from their sources to dose estimates and the integration of uncertainty into risk estimates, were also investigated.

2.1 The Uncertainty Matrix

Sources of uncertainties were listed and identified in the so-called Uncertainty Matrix. An excerpt from the matrix, showing a selection of sources of uncertainties within the dose assessment procedure and epidemiological analyses, is given in Table 1. The complete matrix is presented in Annex II to the final report of the UWG [22]. There the uncertainty sources are grouped according to the stage of the risk evaluation procedure they affect: dose assessment, "classical" epidemiology, molecular epidemiology and modelling.

This matrix was devised under the premise that once an uncertainty source has been identified it can potentially be reduced and/or quantified. The information given by the matrix is therefore as follows: definition of the uncertainty source, its potential effect(s) on risk analysis, whether the uncertainty due to this source is quantifiable and/or reducible, what measures could/should be taken in order to quantify and/or reduce the uncertainty and any potential pitfalls to be avoided. Three options were allowed as a response to the questions about whether a source is quantifiable or reducible: Yes, No and Conditional. Conditional means that the source can be quantified or reduced only if certain conditions

are met. For example: uncertainty on a sample measurement might be reduced if that sample is still available for further measurements; that means that this uncertainty source is conditionally reducible.

Table 1: Excerpt from the uncertainty matrix [22].

Source of uncertainty	Potential effects	Q? (a,b)	R? (a,b)	Measure(s) to quantify/reduce uncertainty (a)	Pitfalls to be avoided	Importance(c)
Bioassay below limit of detection or reporting limit	Over/under estimate doses and strength of association with disease risk	Y	C	Q: Sensitivity study/expert judgement. R: Access to measurements with more sensitive techniques.	Replacing all <DL with 0 or assuming all positive	H
Choice of pulmonary absorption Type	Large error on lung dose (bias/either direction)	Y	C	Q: Sensitivity study/expert judgement. If faecal and/or in-vivo data are available, judgements on the absorption type based on the monitoring data possible. R: Measurements/job exposure matrices, identification of U compounds at the workplace along the worker's career, when samples/data available	Using poor default values. Using specific type when compound is uncertain.	H
Normalization of bioassay into daily excretion	Over/under estimate doses and strength of association with disease risk	C	C	Q: Expert judgement. Conditional on information being available on the normalisation used for a technique. R: Access to creatinine, volume – not possible for old samples		M
Healthy worker effect	Decrease in incidence/mortality rates relative to general population.	Y	C	R: Considering unexposed workers from the cohorts as a reference population when quantifying dose response relationships		M
Insufficient follow-up time to observe mortality or incidence	Decrease in statistical precision of risk estimates.	Y	Y	Q: Conduct power calculations to estimate the amount of data needed R: Pool cohorts and extend their follow-up		L

^(a) **Q** = quantifiable - **R** = reducible

^(b) **Y** = yes - **C** = conditionally - **N** = no

^(c) **H** = high - **M** = moderate - **L** = Low

The last column of the matrix shows an assessment of the relative importance of that source of uncertainty. This assessment was derived using the knowledge and expertise of the UWG members and the results of sensitivity studies, or other research, conducted during the current, or previous, projects. The ranking of the uncertainty sources according to their importance is an indicator of the priorities for future research in this area.

It is acknowledged that this list is not exhaustive and that other sources of uncertainties could be further evaluated during future continuation of this work. It is also acknowledged that inclusion of improved radiobiological knowledge, like the identification of a possible marker of radiation-induced cancer and measurements of that marker in a larger epidemiological study, may also improve knowledge of low dose radiation effects and thus further reduce uncertainties in the analysis of epidemiological data using models of carcinogenesis or development of other diseases.

2.2 Case study in French workers to assess sensitivity of the dose estimates to the different uncertainty sources

In an analysis conducted at IRSN, data from a case-control study of French uranium workers were used to derive multiple dose estimates for some of these individuals using different assumptions with respect to the various sources of uncertainty. The analysis was performed using three cases:

- Case A, with all data below limit of detection (LOD) or reporting level (RL) (censored data)
- Case B, with only one uncensored data point, i.e. higher than LOD/RL.
- Case C, with several uncensored data points and several acute intakes.

The analysis covered following issues: how to deal with censored bioassay data, the modality of data fitting, choice of pulmonary absorption type, choice of acute or chronic exposure and, when unknown, assumptions about the duration of a chronic exposures.

Of all the biokinetic parameters, it is those related to the lung solubility of uranium compounds encountered in occupational settings that have the greatest impact on estimates of lung dose, as they govern the absorption from lung tissues to blood. This is particularly important because the majority of occupational exposures occur through inhalation and, as a result, lung dose is often a key endpoint in studies. However, the impact of this source of uncertainty on other endpoints, like doses to other organs and tissues, is much more limited. The modality for handling censored data and, to a lesser extent, the choice of the exposure regime, were identified as other primary sources of uncertainty for the scenarios considered.

2.3 Simulated case study for UK workers to assess how incorrect assumptions affect assessment of intake and dose

Additional information used in the ranking of the uncertainty sources was provided by a study conducted by Nuvia within the AIRDoseUK project (a "twin" project of CURE, also carried out within the framework of DoReMi WP5) [23]. This study evaluated the errors that are introduced in the assessment of intake and dose when interpreting bioassay measurements using incorrect assumptions. Artificial datasets, corresponding to three representative extreme cases for the Harwell site, were created. Analyses conducted using these artificial datasets confirmed that lung solubility assumptions were the most important source of reducible error when lung dose is the quantity of interest.

2.4 Further issues

Inadequate information on smoking was debated as a potentially significant source of uncertainty, but this premise is still to be tested. Uncertainties related to any improvements over time in the early diagnosis of diseases, and/or length of survival following diagnosis, were not considered to play a significant role, provided that birth cohort effects are properly taken into account in epidemiological models[24]. These and other sources are all indicated in the complete uncertainty matrix.

3 DISCUSSION: PRIORITIES FOR FUTURE RESEARCH

The uncertainty matrix, the results of the case studies and of other analyses (like those briefly summarized above) were used to identify following priority research needs in the field of health risk assessment pertaining to occupational exposures to uranium:

- (i) Characterization of best estimates and probability distributions of biokinetic and dosimetric model parameters and other parameters affecting the exposure scenario.
- (ii) The treatment of censored bioassay data (i.e. measurement below LOD or RL) for the assessment of doses to workers following a routine monitoring programme.
- (iii) The identification of suitable statistical methodologies to account for the uncertainty inherent in estimates of dose when estimating radiation-induced disease risk.

Deriving best estimates of parameter values is clearly essential, whether the primary dose deliverable is expressed in form of point estimates of dose or doses in the form of Bayesian (or other) probability distributions obtained from uncertainty analyses. Consequently, significant effort should be directed into deriving prior distributions for key parameters, particularly those representing “reducible” uncertainties as identified in the uncertainty matrix. Approaches similar to those developed as part of the EU funded projects Alpha-Risk and SOLO and under the US-funded JCCRER projects for Russian Mayak workers [25, 26] could be used to derive estimates of absorption parameters for uranium materials. Distributions (representing variability) derived for particle transport clearance rates and other physiological parameters for the Mayak workers could be used as a reasonable starting point for deriving distributions for parameters for the cohorts considered in CURE. Although it might be assumed that these distributions are likely to be material independent and similar across cohorts, scope exists to further refine these distributions using relevant uranium worker autopsy data, if available.

Regarding statistical methodologies to account for the uncertainty inherent in dose estimates when estimating disease risk, several options have been discussed and proposed in the UWG final report [22]. As shown during previous experience with the Alpha-risk project, propagating distributions reflecting uncertainties on dose estimates (derived by a theoretically correct Bayesian retrospective dosimetric framework) through to an epidemiological analysis can lead to a series of difficulties, notably numerical problems, when manipulating the data, due to different levels of apparent informativeness between and within cohorts.

A possible alternative approach could be to account for uncertainty on dose estimates through simple summary statistics: confidence or credible interval and standard deviation, for example. Even though they are less informative, these summary statistics could be more easily used than a probability distribution on dose to account for dose uncertainty when estimating disease risk from dose-response models.

Another alternative is represented by a so-called Bayesian structural approach based on a unique and coherent framework in which all the parameters of the measurement, exposure and disease models are estimated simultaneously allowing dose uncertainty to be propagated into risk parameter estimation. This approach is currently being applied to refine the risk estimates for lung cancer due to radon exposure in a uranium miners' cohort. and could be extended and specifically adapted to a study of uranium exposures of miners, millers and other nuclear workers.

Given the large number of subjects present in the cohorts identified by CURE (about 75000 miners, 6000 millers and 40000 nuclear fuel cycle workers), it is recommended to first test the proposed approaches in a series of feasibility studies conducted using smaller sets of representative subjects. The analyses could then be extended to all workers or miners/millers having similar individual characteristics or conditions of exposure and monitoring.

Alternatively, an *ad-hoc* synthetic cohort could be created by generating simulated dosimetric and health outcome data for a number of artificial subjects. The cohort could be constructed to have a particular risk and dose-response relationship, so that the methodologies for handling uncertainties in epidemiological analyses can be evaluated by their performance against results that are known. Other significant advantages of using a synthetic cohort are the evaluation and validation of methods currently used to investigate uncertainties in dosimetric data, and also the potential for sharing all data (dosimetric and epidemiological databases) between project members without the usual constraints of data protection and ethics. These studies would give important pointers to possible drawbacks and difficulties of implementing these methods in the full CURE cohorts, and help guide the development of new methods to deal with these issues.

4 CONCLUSION

The analysis conducted by CURE UWG has shown that the consideration of uncertainties in dose and risk estimation is a fast moving field of great interest. A considerable amount of information has been assembled on the potential sources of uncertainty in studies of workers with internal radiation exposures, the uncertainty matrix produced will be a useful reference for future work in this area. The UWG has proposed strategies for the development of future methodologies for the propagation of uncertainties in dose estimates into estimates of risk, including the creation of a synthetic cohort as a tool for evaluating proposed methodologies.

5 ACKNOWLEDGEMENTS

The CURE project was supported by the European Commission FP7 DoReMi Network of Excellence (grant number: 249689). PHE and Nuvia Ltd. received partial funding from the UK Nuclear Decommissioning Authority. IRSN received partial funding from AREVA.

This paper is dedicated to the memory of Matthew Puncher, who consistently contributed to the work presented here and unexpectedly passed away few days before the submission of this manuscript.

6 REFERENCES

- [1] Meija, J., Cople, T.B., Berglund, M. et al., 2016. Isotopic composition of the elements 2013 (IUPAC Technical Report). *Pure Appl. Chem.* 88, 293-306.
- [2] International Commission on Radiological Protection ICRP, 2008. Nuclear decay data for dosimetric calculations. ICRP Publication 107. *Ann. ICRP* 38(3).
- [3] Ansoborlo, E., Lebaron-Jacobs, L., Prat, O., 2015. Uranium in drinking water: A unique case of guideline value increases and discrepancies between chemical and radiochemical guidelines. *Environ. Int.* 77C, 1-4.
- [4] Agency for Toxic Substances and Disease Registry ATSDR, 2013. Toxicological profile for uranium. Atlanta, Georgia (USA). Retrieved 2016-04-26 from: <http://www.atsdr.cdc.gov/ToxProfiles/tp150.pdf>
- [5] United Nations Scientific Committee on the Effects of Atomic Radiation, 2010. UNSCEAR 2008 Report. Sources and effects of Ionizing Radiation. Annex B. Exposure of the public and workers from various sources of radiation. New York: United Nations.
- [6] Vaillant, L. 2014 Trends in occupational radiation exposure in nuclear fuel cycle facilities. An overview. Presentation at International Conference on Occupational Radiation Protection: Enhancing the Protection of Workers, Vienna, 1-5 December 2014. Retrieved 2016-04-26 from: <http://www-ns.iaea.org/tech-areas/communication-networks/orpnet/documents/cn223/10-schieber-vaillant-presentation.pdf>.
- [7] Zhivin, S., Laurier, D., Guseva Canu, I., 2014 Health effects of occupational exposure to uranium: do physicochemical properties matter? *Int. J. Radiat. Biol.* 11, 1-33.
- [8] Laurent O, et al. DoReMi - Low Dose Research towards Multidisciplinary Integration. Task5.8: Concerted Uranium Research in Europe (CURE). Final report. http://www.doremioe.net/pdf/doremi_TRA/D5_17_Report_Uranium_exposure.pdf (2015).
- [9] Laurent, O., Gomolka, M., Haylock, R. et al. 2016 Concerted Uranium Research in Europe (CURE): toward a collaborative project integrating dosimetry, epidemiology and radiobiology to study the effects of occupational uranium exposure. *J. Radiol. Prot.* (accepted for publication).
- [10] United Nations Scientific Committee on the Effects of Atomic Radiation, 2015. UNSCEAR 2012 Report to the General Assembly. Annex B. Uncertainties in risk estimates for radiation-induced cancer. New York, NY: United Nations.
- [11] Davesne, E., Casanova, P., Chojnacki, E., et al., 2010. Integration of uncertainties into internal contamination monitoring. *Health Phys.* 99,517-522.
- [12] Puncher, M., Birchall, A., Bull, R.K., 2013. A Bayesian analysis of uncertainties on lung doses resulting from occupational exposures to uranium. *Radiat. Prot. Dosim.* 156, 131-140.

- [13] Puncher, M. 2014. An assessment of the reliability of dose coefficients for intakes of radionuclides by members of the public. *J. Radio. Prot.* 34, 625-643.
- [14] Li, W.B., Klein, W., Blanchardon, E., et al., 2015. Parameter uncertainty analysis of a biokinetic model of caesium. *Radiat. Prot. Dosim.* 163, 37-57.
- [15] Spielmann, V., Li, W.B., Zankl, et al., 2016. Uncertainty quantification in internal dose calculations for seven selected radiopharmaceuticals. *J. Nucl. Med.* 57, 122-128.
- [16] Allodji, R.S., Thiébaud, A.C.M., Leureaud, K. et al. 2012. The performance of functional methods for correcting non-Gaussian measurement error within Poisson regression: corrected excess risk of lung cancer mortality in relation to radon exposure among French uranium miners. *Statistics in medicine* 31, 4428-4443.
- [17] Hoffmann, S., Rage, E., Laurier, D., et al., 2016. Accounting for Berkson and classical measurement error in radon exposure assessment using a Bayesian structural approach in the analysis of lung cancer mortality in the French cohort of uranium miners. *Radiat. Res.* (submitted).
- [18] Land, C.E., Kwon, D., Hoffman, F.O. et al., 2015. Accounting for shared and unshared dosimetric uncertainties in the dose response for ultrasound-detected thyroid nodules after exposure to radioactive fallout. *Radiat. Res.* 183, 159-173.
- [19] Simon, S.L., Hoffman, F.O., Hofer, E. 2015. The two-dimensional Monte Carlo: a new methodologic paradigm for dose reconstruction for epidemiological studies. *Radiat. Res.* 183, 27-41.
- [20] Stram, D.O., Preston, D.L., Sokolnikov, M., et al., 2015. Shared dosimetry error in epidemiological dose-response analyses. *PloS one* 10:e0119418.
- [21] Kwon, D., Hoffman, F.O., Moroz, B.E and Simon, S.L. 2016. Bayesian dose-response analysis for epidemiological studies with complex uncertainty in dose estimation. *Statistics in medicine* 35, 399-423.
- [22] Giussani, A., Ancelet, S., Atkinson, W., et al. 2014. Final Report of the Uncertainties Working Group (UWG). Available from the authors on demand.
- [23] http://www.doremi-noe.net/pdf/doremi_TRA/DoReMi_TRA_statement_V3.pdf
- [24] Muirhead, C. R., O'hagan, J. A., Hylock, R. G. et al. 2009. Mortality and cancer incidence following occupational radiation exposure: third analysis of the National Registry for Radiation Workers. *Br. J. Cancer* 100:206-212.
- [25] Puncher, M., Riddell, A. E., 2016. Bayesian analysis of plutonium exposures in Sellafield workers. *J. Radiol. Prot.* 36 1–19.
- [26] Radiation Protection Dosimetry Special Issue on the Mayak Worker Dosimetry System, in press [2016].

Joint Coordinating Committee on Radiation Effects Research Project 1.1: Techa River Population Dosimetry

Bruce A Napier^{a*}, Marina O Degteva^b, Evgenia I Tolstykh^b, Natalia B Shagina^b, Elena A Shishkina^b, Marina I Vorobiova^b, Nikolay G Bougrov^b, Lynn R Anspaugh^c

^aPacific Northwest National Laboratory, Richland, Washington 99352 USA

^bUrals Research Center for Radiation Medicine, Chelyabinsk, Russian Federation

^cLynn R. Anspaugh, Consulting, Henderson, Nevada 89044 USA

Abstract. Members of the Techa River Cohort (TRC) are being studied in an effort to test the hypothesis that exposure at low-to-moderate dose rates has the same effectiveness as exposure at high dose rates. The goal for the Techa River Dosimetry System (TRDS) is to provide the best possible assessment of individual external and internal doses for use in epidemiological studies of the TRC members and other persons who were exposed beginning in 1949 to releases of radioactive materials from the Mayak Production Association. A significant portion of these releases consisted of long-lived radionuclides, mainly ⁹⁰Sr. A large area in the same Urals region was also contaminated with long-lived radioactive materials in 1957 when the East Urals Radioactive Trace (EURT) was formed following an explosion of a high-level waste tank. Dose reconstruction in the TRDS is based on the use of a large number of measurements of long-lived radionuclides in people and in the environment and external exposure rate measurements in places where populations lived. The doses are supported strongly by 33,000 measurements made with a tooth-beta counter, 10,000 measurements of bones collected at autopsy, and 44,000 measurements made with a special whole body counter. The traditional approach of modeling all steps of the pathway of exposure is used as a backup only when other approaches were exhausted. The TRDS calculates doses from external exposures from living along the banks of the Techa River and in the region of the EURT and internal exposures from intakes acquired along the Techa River and in EURT villages. Individual residence-history data are used. The end point of dose accumulation is also determined individually. Medical X-ray exposure can be considered as a confounding source of radiation exposure for the TRC members and the TRDS calculates doses from X-ray procedures. The TRDS version created in 2000 was used initially to derive risk coefficients for the TRC members; an improved version (TRDS-2009) was later used. An update, providing individual uncertainty estimates, is scheduled for 2016. TRDS doses are being used in companion epidemiological studies. The TRDS methods have been referenced by the NCRP, supplemented by efforts of the European Commission, and are being incorporated by UNSCEAR.

KEYWORDS: *radiation effects; dose assessment; environmental assessment; Techa River.*

1 INTRODUCTION

The Chelyabinsk Oblast contained many of the former Soviet Union's major military production centers, including the largest plutonium production facility of the former Soviet Union in the closed city of Ozersk. Accidents, nuclear waste disposal, and day-to-day operation at the MPA reactor and radiochemical plant contaminated the Techa River. The period of highest releases was 1949-1956, with a peak of released activity in 1950-1951. In 1957, a nuclear waste storage facility exploded due to a chemical reaction - the Kyshtym accident. The radionuclide of primary dosimetric importance for atmospheric releases is ¹³¹I; Mokrov et al. [1] report that the total integrated release is about 37 PBq of ¹³¹I. Extensive information on the environmental situation and health status of the population exposed in the Techa river basin has been gathered at the Urals Research Center for Radiation Medicine (URCRM) over the past 50 years.

The combined dosimetric and epidemiologic study of the Techa River Cohort (TRC) is deemed important, as this cohort is one of a very few that can be studied to examine the question of whether there is a dose-rate-reduction factor in the induction of stochastic effects by radiation. This question

Presenting Author, email Bruce.Napier@pnnl.gov

represents a central issue in radiation protection of workers and the public. The overall scientific hypothesis to be tested by the combined dosimetric and epidemiologic study of the ETRC is 'Radiation dose delivered at low dose rates is equally as effective (in causing cancer and other stochastic effects) as the same dose delivered at high dose rates.

U.S. scientists work with Russian scientists and technical personnel at the Urals Research Center for Radiation Medicine (URCRM) on the project. These teams interact with other scientists from organizations such as the International Science and Technology Center (ISTC) and the European Union's Southern Urals Radiation Risk Research (SOUL) and Epidemiological Studies of Exposed Southern Urals Population (SOLO) projects.

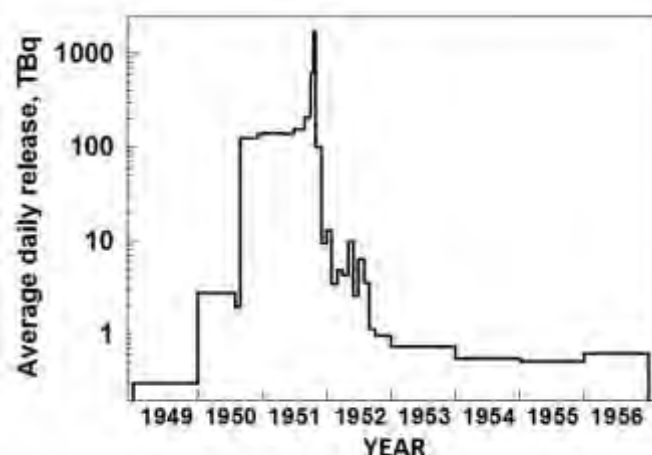
2 ENVIRONMENTAL RADIONUCLIDE RELEASES

The absence of reliable waste-management and waste-storage technologies during the first period of Mayak operation resulted in significant radioactive contamination of the Techa River. In the period 1949-1956, a total of 7.6×10^7 m³ of liquid waste with a total activity of 115 PBq was released into the Techa river system. A special project was established that included both experts from Mayak and the JCCRER [2] to evaluate the magnitude and timing of the releases. Scientists from Mayak were given full access to documents, workbooks, and files within the Mayak archives. Important documents regarding the early operation of Mayak were declassified and shared with project participants. These historical data on the Techa River contamination have been reviewed in English [3]. A complete re-evaluation of the source term was prepared by Degteva et al. [4].

The total estimated releases into the Techa River are shown in Figure 1. The total routine release was about 52 PBq; the total release from accidental overflows from the tank farms was about 63 PBq. There is significant uncertainty in the daily release values, but when integrated over the entire period, the overall uncertainty in the release is less than a factor of two.

The release was made up of a large number of radionuclides. Each waste stream had a different radionuclide composition, which also varied in time. The total release spectrum has been estimated for the purposes of dose reconstruction, based on the theoretical content of irradiated fuel stored for various effective decay periods [4].

Figure 1. Estimates of the dynamics of the total activity of radioactive releases from Facility B into the Techa River in 1949–1956 (adapted from Degteva et al. 2012)



3 CHARACTERISTICS OF THE DOSE RECONSTRUCTION SYSTEM

The foundation of the dose reconstruction for the Techa River Cohort is unique. Systematic measurements of radioactive contamination in and near the Techa River started in the summer of

1951. The contamination of the river water, bottom sediments, flood-plain soils, vegetation, fish, milk, and other foodstuffs, and external gamma-exposure rates were measured. In addition to medical examinations, individual data on the conditions of contact with the contaminated river (the distance of the house from the water's edge, the source of drinking water, fishing, etc.) were collected. Radiometric measurements of bioassay and autopsy samples were performed. All places and terms of residence inside the contaminated area were collected for the members of this registry for the purposes of individual-dose reconstruction. Also, extensive measurements of ^{90}Sr content in teeth were performed beginning in 1960 and in forehead bone beginning in 1976; whole-body counting for ^{90}Sr has been performed since 1974; at this time about 35% of the members of the Techa River Cohort have had at least one whole-body count.

A description of the general approaches and initial data sets used for the creation of the TRDS was provided by Degteva et al. [5,6]. The TRDS is designed as a modular database processor. That is, depending on the input data for an individual, various elements of several TRDS databases are combined to provide the dosimetric variables requested by the user. The input data include the following information for each member of the ETRC: identification code, year of birth, year of entry to the catchment area, year of migration from the catchment area, year of vital status determination, and residence history within the contaminated areas.

The basis of the past dose-reconstruction efforts for the Techa River Cohort has been summarized in several publications [5,6,7,8,9]. The absorbed doses due to external exposure were estimated on the basis of systematic measurements of gamma-exposure rate along the banks, supplemented with a detailed model of river transport of radionuclides and accumulation in soils, and the typical life-style patterns of the inhabitants of the riverside villages. This approach has given monthly and annual absorbed doses from external sources for different age groups in each village. Major recently completed activities included review of these data and provision of a more realistic assessment of external dose.

Reduction in uncertainty for internal dose due to ^{90}Sr is achieved by "splitting" the TRC into subcohorts with different dose-calculation protocols depending on the quality of individual-input data for estimation of dose. The three subcohorts of the ETRC are:

- Subcohort 1. Persons with individual body-burden measurements. The measurements are used for the evaluation of personal dose and its associated uncertainty.
- Subcohort 2. Unmeasured persons who had cohabitants (members of the same household) with individual measurements. It is assumed that those living in the same house would have had similar exposures, at least to sources of drinking water and food.
- Subcohort 3. Unmeasured persons for whom only residence-history data are available.

Another useful avenue of reducing uncertainty for integrated ^{90}Sr -body burdens has been further development of the strontium biokinetic model. The URCRM strontium biokinetic models now consider sex and age as variables [10, 11, 12].

The Techa River Cohort (TRC) consists of individuals who were born before 1950 and lived in any of the 41 villages situated along the Techa River from 1950 to 1960, plus about 5,000 persons who migrated to the villages after the period of high exposure but before 1960; the late entrants in the TRC have been restricted to those born before 1949 as for the original TRC. URCRM conducted extensive review of official documents (including taxation books, vital statistics and medical records) between the late 1960s and the 1980s to identify cohort members. As of October 2010, the TRC numbered 29,730 persons, about 58% of whom were women. Approximately 40% of the cohort was first exposed before age 20, 28% at ages 20–40, and 32% after age 40 years. The cohort is 80% Slav and 20% Tatar and Bashkir. The cohort is now relatively old; the youngest member is over 60 years old [13].

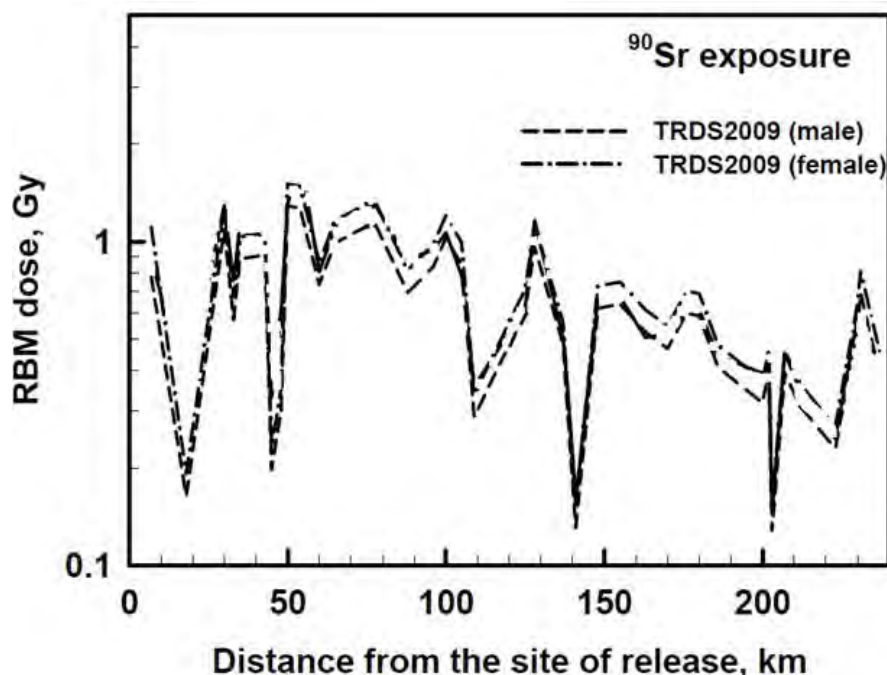
In addition, the URCRM Registry includes data on of 24,243 persons exposed in utero and/or the progeny of exposed parents, born in the catchment area after 1 January 1950 and identified as the “Techa River Offspring Cohort” (TROC). The TROC has the potential to provide direct data on radiogenic health effects in progeny from exposure of a general population to chronic low-dose-rate radiation [14].

Following the tank explosion in 1957, residents of the most highly contaminated villages were evacuated. About 1,100 of the evacuations took place within 7 – 14 days because of high levels of external exposure rate. Relocation of other settlements took place later, but was due to high levels of ^{90}Sr -contamination density (more than $2\text{--}4\text{ Ci km}^{-2}$ of ^{90}Sr); 2,280 persons were evacuated 250 days after the accident. Later (within 330 to 670 days after the accident) another 8,300 persons were removed from territories with contamination density $>2\text{ Ci km}^{-2}$ of ^{90}Sr [13]. In addition to the evacuated residents, about 8,000 additional people continued to live in the less-contaminated fringes of the EURT footprint.

In addition to exposure on the Techa River, the dosimetry system includes doses due to residence on the EURT area; 4,695 members of the TRC (16% of the entire cohort) were exposed on the EURT. Nevertheless, additions to individual red bone marrow doses for these persons were low: 5.5 mGy on average and 44 mGy at most [15].

Internal dose computation with use of the Techa River Dosimetry System TRDS-2009D gives estimates of doses for all cohort members who resided on the Techa River [14]. The initial estimates are based on village average-intake functions and external dose rates with consideration of an individual’s residence history, age, gender and the date of vital status or migration from the catchment area (the area of epidemiologic follow-up). Doses are highest to red bone marrow because the dominant radionuclide is ^{90}Sr . Significant variations from settlement to settlement are explained mainly by different sources of drinking-water (Techa River, wells or both sources). The levels have a tendency to decrease with distance from the release site (Figure 2), which is explained by reduction of ^{90}Sr concentration in the river water due to dilution. The highest doses are in the range of 2 Gy to red bone marrow. For individuals with whole-body counts, these generic village average doses are modified to account for the person’s actual measurements, and sometimes household-average internal exposure estimates for persons living in the same household.

Figure 2. Red Bone Marrow dose as a function of Techa River downriver distance



External dose estimates are made based on accumulation of gamma-emitting radionuclides in the bottom sediments and flooded soils, combined with assumptions on amounts of time spent near the river, outdoors in villages, and indoors [16]. External doses sharply decreased with distance from the release site because of sorption and decay of shorter-lived isotopes.

An additional potentially confounding factor is related to the fact that the Techa River cohort members have been provided medical monitoring at the URCRM for many decades, including extensive radiographic examinations. Six thousand four hundred and fourteen (6,414) members of the TRC (22% of the entire cohort) were exposed to x-rays for diagnostic purposes. Additions to individual doses in different organs of these persons were 30–35 mGy on average and 650–750 mGy at most. Therefore, this source of confounding exposure is also being addressed.

4 OBSERVATIONS

The JCCRER studies of the Mayak populations are valuable because radiation effects (cancer and non-cancer) are evident in these chronically-exposed groups. Radiation effects are commensurate with the Japanese LSS (Preston et al. 2007) and with the 15-Country Study (Cardis et al. 2007). Radiation effects appear to be linear with dose to <0.1 Gy. A significant result of most of the studies is that internal doses protracted over many years seem to be just as important as instantaneous external doses. Long-term chronic doses appear to have essentially the same effect as instantaneous acute doses; within the limits of the observations of these studies, the dose and dose rate effectiveness factor (DDREF) is approximately equal to 1, which has not been widely anticipated. Because the dose reconstructions for each cohort are still ongoing, these results may change in the future.

The studies do confirm that radiation is a weak carcinogen. The fraction of cancers in the Mayak and Techa River cohorts attributable to radiation is small.

Finally, events from the 1940s, 1950s, and 1960s still disrupt the lives of regional inhabitants. These populations deserve additional study and open communication about the results.

5 ACKNOWLEDGEMENTS

This work was conducted as part of the Joint Coordinating Committee for Radiation Effects Research Project 1.1, Techa River Dose Reconstruction. It was jointly funded by the U.S. Department of Energy (U.S. DOE) and the Federal Medical Biological Agency (FMBA) of the Russian Federation. We acknowledge the valuable support and assistance of Barrett Fountos, Program Manager, U.S. DOE's Office of Domestic and International Health Studies (AU-13) and of Alexander Akleyev, Director of the Urals Research Center for Radiation Medicine.

6 REFERENCES

- [1] Mokrov YG, Lyzhkov AV, Muzrukov VA, Pyatin NP, Rovny SI, Anspaugh LR, Napier BA. 2008. Reconstruction of Atmospheric Releases of ¹³¹I From Mayak Radiochemical Plant Stacks for the Period From 1948 To 1970, Part 2: Results of the Reconstruction of ¹³¹I Releases from the Stacks of the Reactor and Radiochemical Plants. JCCRER Project 1.4/CRDF Project RBO-20317 Report 11. Ozersk, Russia.
- [2] Anspaugh LR, Degteva MO, Vorobiova MI, Mokrov YuG, Napier BA. Dosimetry for members of the Extended Techa River Cohort. *Health Phys* 91: 393–394; 2006
- [3] Degteva MO, Vorobiova MI, Tolstykh EI, Shagina NB, Anspaugh LR, Napier BA. A review of data on releases of radioactive wastes from the Mayak Production Association into the Techa River in 1949–1956. Report on ISTC Project #2841; 2008 (available on http://biophys.urcrm.chel.su/publications/ISTC%202841_URCRM.pdf).
- [4] Degteva MO, Shagina NB, Vorobiova MI, Anspaugh LR, Napier BA. Re-Evaluation of Waterborne Releases of Radioactive Materials from the “Mayak” Production Association into the Techa River in 1949–1951. *Health Phys* 102: 25-30; 2012.

- [5] Degteva, M. O.; Vorobiova, M. I.; Kozheurov, V. P.; Tolstykh, E. I.; Anspaugh, L. R.; Napier, B. A. "Dose reconstruction system for the exposed population living along the Techa river," *Health Phys.* 78: 542-554; (2000)
- [6] Degteva, M. O.; Kozheurov, V. P.; Tolstykh, E. I.; Vorobiova, M. I.; Anspaugh, L. R.; Napier, B. A.; Kovtun, A. N. "The Techa river Dosimetry System: Methods for the reconstruction of internal dose," *Health Phys.* 79:; 24-35; (2000)
- [7] Degteva, M. O., Kozheurov, V. P.; Vorobiova, M. I. "General approach to dose reconstruction in the population exposed as a result of the release of radioactive wastes into the Techa river," *Sci. Total Environ.* 14:49–61 (1994).
- [8] Kozheurov, V. P., "SICH-9.1 A unique whole-body counting system for measuring Sr 90 via bremsstrahlung: The main results from a long-term investigation of the Techa river population," *Sci. Total Environ.* 14:37–48 (1994).
- [9] Kozheurov, V. P.; Degteva, M. "Dietary intake evaluation and dosimetric modelling for the Techa river residents based on in vivo measurements of strontium-90 in teeth and skeleton," *Sci. Total Environ.* 14:63–72 (1994).
- [10] Shagina NB, Tolstykh EI, Degteva MO, Anspaugh LR, Napier BA. Age and gender specific biokinetic model for strontium in humans. *J Radiol Prot* 35(1):87-127; 2015.
- [11] Shagina NB, Fell TP, Tolstykh EI, Harrison JD, Degteva MO. Strontium biokinetic model for the pregnant woman and fetus: application to Techa River studies. *J Radiol Prot* 35:659-676; 2015.
- [12] Shagina NB, Tolstykh TI, Fell TP, Smith TJ, Harrison JD, Degteva MO. Strontium biokinetic model for the lactating woman and transfer to breast milk: application to Techa River studies. *J Radiol Prot* 35:677-694; 2015.
- [13] Schonfeld SJ, Krestinina LY, Epifanova S, Degteva MO, Akleyev AV, Preston DL. Solid Cancer Mortality in the Techa River Cohort (1950–2007). *Radiat. Res.* 179, 183–189; 2013.
- [14] Kossenko MM, Ostroumova E, Granath F, Hall P. Studies on the Techa river offspring cohort: health effects. *Radiat Environ Biophys* 41: 49–52; 2002.
- [15] Shagina NB, Tolstykh EI, Degteva MO, Kozyreva OV, Anspaugh LR, Napier BA. 2012. Description of the Revisions to TRDS-2009 Code and Databases, Final Report for Milestone 5. JCCRER Project 1.1, Urals Research Center for Radiation Medicine, Chelyabinsk, Russia.
- [16] Degteva MO, Shagina NB, Tolstykh EI, Vorobiova MI, Anspaugh LR, Napier BA. 2009. Individual Dose Calculations with use of the Revised Techa River Dosimetry System TRDS-2009D. Final Report for Milestone 22. JCCRER Project 1.1, Urals Research Center for Radiation Medicine, Chelyabinsk, Russia.

Joint Coordinating Committee on Radiation Effects Research Project 2.4: Mayak Worker Dosimetry

Bruce Napier^{a*}, Alexander Efimov^b, Alan Birchall^c, Vadim Vostrotin^b, Matthew Puncher^d, Alexandra Sokolova^b, Klara Suslova^b, Scott Miller^e, Alexay Zhdanov^b, Evgeney Vasilenko^b

^aPacific Northwest National Laboratory, Richland, Washington 99352 USA.

^bSouthern Urals Biophysics Institute, Ozersk, Chelyabinsk, Russian Federation.

^cGlobal Dosimetry Ltd., 1 Macdonald Close, Didcot, OX11 7BH, UK.

^dPublic Health England (PHE), Chilton, Didcot, United Kingdom.

^eUniversity of Utah, Salt Lake City, Utah USA.

Abstract. A multi-year dose reconstruction effort is being conducted to produce representative dose estimates for workers at the Mayak Production Association, Ozersk, Russia, where plutonium production activities began in 1948. The goal for the Mayak Worker Dosimetry System (MWDS-2013) is to provide the best possible assessment of individual external and internal doses of Mayak workers who were exposed beginning in 1948 for use in epidemiological studies. The calculation methods and parameter distributions incorporated in the external irradiation components of MWDS-2013 are similar to those used in versions from 2005 and 2008 using historical film badge data; results are used to estimate annual radiation doses to organs of interest from gamma and neutron exposures and the uncertainties in the dose estimates. Medical X-ray exposure is considered a confounding source of radiation exposure for the Mayak workers, therefore the MWDS calculates doses from X-ray procedures. Calculations for the cohort of over 25,000 workers show that average external doses were quite high in the 1940s and early 1950s and fell to international norms by the 1970s. For internal dose, annual organ doses are estimated for Mayak workers exposed to plutonium aerosols. Dose estimates are derived from measurement data that consists mainly of activity of plutonium in urine samples. The system uses the latest biokinetic and dosimetric models, and unlike its predecessors, takes explicit account of uncertainties in both the measurement data and model parameters. About 8,000 workers have sufficient bioassay information to allow internal dose estimation. Internal doses for many organs significantly exceeded international norms for many years in the early period of Mayak operation. Both the external and internal dose methods separate shared from unshared uncertainties for the individual dose estimates. The dose estimates developed using the MWDS are being used in companion epidemiological studies. The MWDS methods have been supplemented by efforts of the European Commission and referenced by the International Commission on Radiological Protection.

KEYWORDS: radiation effects; external dosimetry; internal dosimetry; Mayak workers.

1 INTRODUCTION

From the onset of operations of the Mayak Production Association (Mayak PA), the key task of specialists at the Radiation Safety Department of Mayak and scientists of Southern Urals Biophysics Institute (SUBI) has always been to arrange individual dosimetry monitoring of the personnel. In the 1940s and 1950s it was only possible to measure external exposures. A corresponding program was introduced in June, 1948 and since then all workers have been monitored for individual external exposure.

The situation of monitoring internal exposures was more complicated. During the early years of the enterprise operation, primary attention was focused on the exposure to ⁹⁰Sr and ¹³⁷Cs. Assessments of body burdens of beta activity due to uranium fission, based on ¹³⁷Cs measurements in the period 1977–1995 showed, however that these activities were well below permissible levels. It took several years to realize that the major risk for personnel health originates from internally deposited plutonium. Although first attempts to assess plutonium body burdens were made in 1953, it was not until 1970 that it became possible to implement a set of techniques for measuring plutonium in biological

Presenting Author, email Bruce.Napier@pnnl.gov

material and to develop a human biokinetic model of plutonium transport and excretion. Assessments based on these methods revealed an excess of permissible levels in many cases.

The Mayak PA and SUBI archives contain information on external doses for about 100,000 persons including Mayak PA workers, personnel of contracting agencies, military personnel and those persons who were involved in the elimination of the consequences of the radiation accident at Mayak PA in 1957 and on internal doses for 8,694 Mayak PA workers. Current efforts focus on the Mayak Worker Cohort of 25,940 workers hired at any time from 1948 to 1982, of whom 25% are female.

2 EXTERNAL DOSIMETRY

Mayak worker radiation exposure was measured with photographic film dosimeters. The basic methods for compiling, standardizing, and analyzing the dosimetric records are described by Vasilenko et al. [1]. Archive records of measured external radiation annual dose were retrieved from Mayak record archives. A separate table of “daily” dose in the database was developed for each processed dosimeter during the period of 1948–1967 obtained from Mayak worker “Personal Logs” used historically in the recording of worker doses. The “daily dose” table contains 725,652 records for approximately 8,752 workers. These data have been analyzed to identify work locations and workers where comparatively higher doses to individual workers and to worker groups were recorded. The response of the respective Mayak PA personnel dosimeters to photon radiation has been measured using in-air and on-phantom exposures at the German National Research Center for Environment and Health (GSF) calibration facility; the extensive information obtained was used to mathematically model the dosimeter emulsion energy and angular response characteristics and, in combination with the exposure scenario, to calculate adjustments to the original registered dose. Radiation fields in Mayak facilities are a complex mixture of beta, photon, and neutron radiation. Thus, a worker’s dosimeter reading may not have been a reasonably accurate estimation of the radiation dose actually received in the workplace, particularly in the earliest days of operation when the dosimeters were of an early design and had significant variability in energy and angular response characteristics. Because it was not possible to produce a detailed, individualized description of the radiation environment for each worker, a limited number of exposure scenarios were developed to describe probable primary parameters of the radiation environment experienced by large groups of workers. For each of these scenarios, conversion factors were developed for application to the worker dosimeter readings. The conversion factors incorporated adjustments for dosimeter energy and angular response, the orientation of the worker relative to the radiation source, and the configuration (geometry) and energy of the radiation field. Exposure scenario conversion factors are applied to dosimeter results to improve the estimate of the dose actually received.

Supporting analyses were performed of other potential sources of significant occupational dose to Mayak workers such as neutron radiation, medical x-ray examinations, and airborne effluent, with the objective to assess the overall occupational dose to workers and to identify sources of uncertainty.

Work with the staff of the Mayak Production Association was halted in 2009. In order to provide a system within which uncertainty in the external doses could be estimated, a two-dimensional Monte Carlo external dosimetry computational system was developed. The first module in the external MWDS-2013 calculation accepts definitions of uncertain shared parameters and prepares a “static” output file of multiple realizations of each using a Latin Hypercube Sampling (LHS) method. Correlations may be applied to the shared parameters at the time of generation of the realizations. This file is used as input for all individuals in subsequent calculations.

The second module in the calculation accepts a list of desired cohort subjects defined in an input “cases” list and prepares a distribution of dose for each subject. This module calculates doses from four major routes of exposure:

- Direct gamma exposure
- Low-energy neutron exposure
- High-energy neutron exposure
- External exposures from medical procedures listed in the SUBI clinic records, if applicable for this individual.

The external dose module uses the existing database information as central values and applies variable “correction factors” to obtain the desired input distributions, obtained either from the static file of shared outer-dimension parameters created by Latin Hypercube calculation internally of unshared parameters. The module first prepares an “occupational history” for each individual for each year. A total of 60 years provides dates from 1/1/1948 through 12/31/2007. For medical x-ray exposures, data are aggregated by year for the period 1948 – 2007.

Output from the stochastic module is intended for use by the epidemiological team. Four files are generated, one for each exposure route. The files contain annual dose increments in units of mGy and are structured by individual, by year, by organ. As a result, the output files can become very large. To enable quick comprehension of the actual dose distributions, a summary generating module is available to use to determine univariate statistics on cumulative organ dose for selected (or all) individuals for whom dose estimates have been made.

Summary statistics on the external doses are provided in Table 1.

Table 1: Summary Statistics for Mayak Worker External Doses

Organ	Population Geometric Mean absorbed gamma organ dose (GSD 2 to 4), mGy									
	1948 - 1953	1954 - 1960	1961 - 1967	1968 - 1973	1974 - 1985	1986 - 1991	1992 - 2007			
Bone surface	192	62	21	8.5	5.2	4.1	2.1			
Liver	157	50	17	7	4.3	3.4	1.7			
Lung	164	52	18	7.3	4.4	3.5	1.8			
Organ	Population Geometric Mean absorbed neutron organ dose (GSD 3 to 10), mGy									
	1948 - 1953	1954 - 1960	1961 - 1967	1968 - 1973	1974 - 1985	1986 - 1991	1992 - 2007			
Bone surface	0.1	0.04	0.02	0.008	0.01	0.01	0.009			
Liver	0.1	0.04	0.03	0.01	0.02	0.01	0.01			
Lung	0.1	0.04	0.03	0.01	0.02	0.01	0.01			
Organ	Population Geometric Mean absorbed medical organ dose (GSD 2 to 4), mGy									
	1948-1959	1960-1969	1970-1999	2000-2007						
Bone surface	1.1	1.6	2.1	1.4						
Liver	0.3	0.4	0.5	0.8						
Lung	3.3	3.1	3.4	1.6						

3 INTERNAL DOSIMETRY

There are many differences between the model structures and methodology employed in this study compared with previous studies; the main difference is that this study take explicit account of uncertainties in model parameters. Previous studies use models which have a single value for all of the model parameters. In this study, probability distributions are specified for important parameters which reflect the uncertainty in that parameter value. To distinguish this type of model from the more usual type of model, they are referred to in this and the accompanying papers as hyper-models. The output of a hyper model is thus a distribution of a quantity rather than a single value.

The calculation of the output from a given hyper model (e.g., organ dose) is relatively straight forward to calculate. One simply chooses a random value for each parameter from its specified distribution and runs the model forward to obtain a unique dose. Repetition of this process will lead to the generation of a distribution of the required output. To use a hyper-model to fit values of a parameter to a given data set is more complicated, and requires use of Bayesian techniques. These techniques can be time consuming, and specific methods have been devised to decrease computation time. Within the Bayesian methodology, the initial distributions assigned to the parameters in the absence of data are referred to as prior distributions, and the resulting parameter distribution (taking into account the measurement data) are known as posterior distributions.

The input to the dose calculation consists of measurements of plutonium activity in urine samples donated by workers. In the Mayak cohort, there are also around 500 cases for which autopsy data as well as urine measurements were also available. The output for each worker consists of a series of organ doses delivered in each calendar year. For each organ, in a given year, the set of doses for every member of the cohort is referred to as a realization. In our case, since we use a hyper-model, the organ dose is not a single value, but a probability distribution of organ dose for that individual, and so to avoid confusion, this is referred to as a hyper-realization. In all, the output for MWDS-2013 consists of 1000 hyper-realizations (for each organ and for each calendar year).

If a parameter value is unknown, but the same for each worker, then it is referred to as shared. Conversely, if a parameter value is unknown, and different for each worker, it is referred to as unshared. Within each hyper-realization, shared parameters take on the same value, whereas unshared parameters are randomly chosen. The set of hyper-realizations thus preserves the information of shared and unshared parameters.

Thus, for each parameter, the following is specified:

- the prior probability distribution for that parameter
- whether it is 'shared' or 'unshared' between workers
- a representative/default value for the parameter

However, for the purposes of epidemiological analysis, in order to make risk calculations tractable, the hyper-realizations are currently reduced to representative realizations.

A complete description of the methods and models employed is provided in a companion paper from the IRPA symposium [2]. Summary statistics of the internal doses are provided in Table 2.

Table 2: Summary Statistics for Mayak Worker Internal Doses

Organ	Median, mGy	Mean, mGy	Maximum, mGy
Bone surface cells	108	707	46600
Liver	27	177	11300
Lung (weighted sum)	31	185	8980

4 JOB EXPOSURE MATRIX

The Project 2.4 team has been asked by the biostatisticians of the companion Project 2.2 epidemiological team to consider the possibility of developing a uniform and consistent system of internal dose estimation that would include both the monitored and unmonitored workers (i.e., the entire worker cohort). Such a system would include three sets of input data rather than the current two:

- A worker job matrix (an expanded version of the current worker history) and accompanying dose estimates;
- Urinalysis measurements; and
- Autopsy measurements.

The addition of the first data set would provide an individualized estimate of the internal dose estimate. The advantage of such a system is that it would allow not only the addition of annual dose estimates for unmonitored workers, but also consideration of all person-years since the start of employment rather than since time of first urinalysis.

The suggested approach is based on the facts that:

- a. exposure history is known for all workers in the cohort, but only approximately every third worker is provided with Pu dose estimates calculated by the results of individual bioassay;
- b. the interim calculation result for internal dose calculation in MWDS-2013 and MWDS-2016 is the value of inhalation intake, calculated for every year of a worker's exposure.

The suggested methodology includes the following steps:

Step 1. Several job categories are created by the approach to grouping work places and job titles, used in the grouping of the scenarios of external exposure. The expected number of these job categories is about 40.

Step 2. Conditions of exposure for each job categories can change with time, so an exposure scenario, assigned to job categories, should account for different conditions of exposure in certain periods of time.

Step 3. A list of workers is created for each job category. Some representatives from the list will be provided with individual bioassay results.

Step 4. Using the data on the value of annual inhalation intake for the monitored representatives of job categories, a distribution of the value of intake is plotted for certain periods of a job category existence. The statistical characteristics of the intake distributions are defined here as well.

Step 5. The distributions of intake for each year of a job category existence obtained at Step 4 are "assigned" to the years of employment of the unmonitored workers at the work places of a job category of interest. Doses are estimated.

Step 7. Validation of the approach by comparison of calculated and observed values of internal doses, assessment of potential bias and uncertainty.

Preliminary advantages of the suggested approach include harmonisation with the approach to dose calculation and their distribution, performed using the results of individual bioassay; and provision with initial data to form the exposure matrix according to work places and years of follow-up/monitoring.

Preliminary analyses show that there are monitored workers practically for each year of existence of each job category. The surrogate estimates of intake (and then of doses) for each year in a job category mostly will be based on 15% - 100% of the real data on Pu intake. This confirms the sufficiency of the initial data to implement the suggested approach to the JEM development and surrogate dose estimate. This work will be continued in the near future.

5 OBSERVATIONS

The Mayak Worker cohort has cumulative external organ doses comparable to the doses received by survivors at Hiroshima and Nagasaki.

External doses in the cohort are greater than nuclear sites in US, Canada, UK and 12 other countries involved in IARC 15 Country Study.

Internal doses from plutonium to lung, liver, and bone provide the largest available database for evaluation of alpha-particle exposure.

Analysis of the Mayak Worker Cohort has the potential to improve estimate of organ-specific radiation risk from protracted occupational exposure.

6 ACKNOWLEDGEMENTS

This work was conducted as part of the Joint Coordinating Committee for Radiation Effects Research Project 2.4, Mayak Worker Dosimetry. It was jointly funded by the U.S. Department of Energy (U.S. DOE) and the Federal Medical Biological Agency (FMBA) of the Russian Federation. We acknowledge the valuable support and assistance of Barrett Fountos, Program Manager, U.S. DOE's Office of Domestic and International Health Studies (AU-13) and of Sergey Romanov, Director of the Southern Urals Biophysics Institute.

7 REFERENCES

- [1] Vasilenko EK, Khokhryakov VF, Miller SC, Fix JJ, Eckerman K, Choe DO, Gorelov M, Khokhryakov VV, Knyasev V, Krahenbuhl MP, Scherpelz RI, Smetanin M, Suslova K, Vostrotin V. Mayak Worker Dosimetry Study: An Overview, *Health Physics* 93 (3), 190-206 (2007).
- [2] Birchall A, Vostrotin V, Puncher M, Efimov A, Napier B. A New Approach to Worker Internal Dosimetry and its Impact on Radiation Protection. *Proceedings of the 14th IRPA Congress, Cape Town, South Africa (2016).*

Waterfowl-specific Computational Models for use in Internal Dosimetry

Dawn Montgomery*, Jennifer Paloni, Nicole Martinez

Clemson University, Department of Environmental Engineering and Earth Sciences, Clemson, South Carolina, United States.

Abstract. This paper discusses the creation and use of computational dosimetric models for waterfowl with the purpose of determining Dose Conversion Factors (DCF) for ^{75}Se and ^{76}As using Monte Carlo techniques. The models utilize mallard (*Anas platyrhynchos*) specific organ densities, stylized representation of organs with the source organ defined as the liver and consideration of life stage, i.e., models are developed for both adult and duckling. Preliminary work in voxel and hybrid models are also discussed. Whole body DCFs from ^{75}Se for adult duck and duckling ($4.9 \times 10^{-4} \mu\text{Gy d}^{-1}$ per Bq kg^{-1} and $2.3 \times 10^{-4} \mu\text{Gy d}^{-1}$ per Bq kg^{-1} , respectively) were comparable to DCFs reported in ICRP 108 for duck and duck egg. The higher energy of the ^{76}As beta particles and photons compared with the electrons and photons associated with ^{75}Se resulted in consistently higher DCFs for ^{76}As in both the duck and duckling models for all organs with the greatest impact in the liver, as expected due to definition as the source organ. The DCFs for the adult duck were greater than those for the duckling for all but 3 cases (brain for both ^{76}As and ^{75}Se and gizzard for ^{76}As) due to the combination of a more compact geometry of the duckling and greater energy of the particles associated with ^{76}As . In general, the development of more comprehensive, yet practicable, dosimetric models of non-human biota allows for a greater ability to quantify potential dose-effect relationships and evaluate potential environmental radioecological impacts.

KEYWORDS: waterfowl; dose conversion factor; internal dosimetry; stylized model; Monte Carlo.

1 INTRODUCTION

1.1 Importance of investigating waterfowl

The current radiation protection system is evolving toward the holistic protection of man and his environment as opposed to protecting only man and assuming the environment to be protected as well [1-3]. There are different perspectives (e.g., anthropocentric, ecocentric, biocentric) concerning environmental radiation protection, yet the end objective of avoiding detrimental effects within the environment is the same. With this view, then, comes the need for more refined knowledge of dose-effect relationships and potential impacts to flora and fauna in radiation exposure scenarios. Of particular interest in this paper are waterfowl-specific dosimetric modeling techniques. Migratory waterfowl frequently inhabit wastewater ponds and other waterways near nuclear processing facilities and legacy sites and thus, are exposed to many radioactive contaminants. While the duck is the reference bird for the ICRP [2], there is little work dedicated to its internal dosimetry, particularly for non-homogeneous internal distribution of radioisotopes; presently, most dosimetry evaluations are relatively generic [2, 3]. There is some work concerning transfer factors [4], elimination rates [5] and general tissue activity concentrations [6-9] of waterfowl but, often the studies are for food chain analysis or general monitoring and documentation, not for dosimetric-specific analysis of the animal. Here we consider stylized models of an adult mallard duck (*Anas platyrhynchos*) and juvenile duckling with ^{75}Se and ^{76}As as representative isotopes of concern to determine Dose Conversion Factors (DCF) using Monte Carlo modeling techniques.

1.2 Selenium and Arsenic in the environment

Selenium is widespread trace element in the Earth's crust, exhibits both beneficial (i.e. is an essential nutrient) and toxic effects in biota with a narrow range between deficient and toxic levels and is taken up quickly in plants [10, 11]. Aquatic environments have been subjected to selenium contamination as a result of many anthropogenic activities, including mining and agricultural activities, posing health threats to biota in the area, particularly aquatic birds [11-14]. Arsenic, as is selenium, is also present in

* Presenting author, e-mail: damontg@clemson.edu

the environment at potentially toxic levels due to anthropogenic activities such as agricultural drainage and mining activities [15, 16]. Selenium-75, with a half-life of 120 days, decays via electron capture and is often used as tracer in various environmental applications or for medical diagnostics [17, 18]. Arsenic-76, a beta/gamma emitter with a 1.08 day half-life, has been reported to have been released from single pass production reactors at the Hanford Site into the Columbia River from 1944 to 1971 [19]. Both ^{75}Se and ^{76}As are byproducts of fission and the nature of their decays makes them relevant for internal dosimetric analysis. Additionally, these isotopes were specifically chosen to take advantage of the data that is available on distribution of these isotopes within duck tissues, largely uptake in the liver [15, 18].

1.3 Computational models

Accurate dosimetry is needed to establish appropriate dose-effect relationships, which in turn requires either direct measurement or rigorous modeling techniques for approximating dose. Although some supporting physical measurements can be made (e.g. bioassay), internal dosimetry necessitates some type of modeling approach [20]. The current recommendation (employed by both RESRAD-BIOTA and the ERICA tool) for determining dose to non-human biota is to consider ellipsoidal models with uniform radioisotope distribution representative of the organism of interest. These models are in turn used with radionuclide specific Monte Carlo physical transport models to determine whole body Dose Conversion Factors [2, 21]. The resultant DCF can be multiplied by the organism's activity concentration to obtain an absorbed dose rate; tabulated DCF values for certain reference organisms and isotopes are available (e.g. for Reference Animals and Plants in ICRP Publication 108 [2]). Other techniques used for dose assessments include use of mass ratios [22], more complex stylized phantoms considering internal organs as simple geometric shapes [23], voxel phantoms utilizing CT imagery to reconstruct organ geometry [24, 25] and most recently, hybrid phantoms which involve smoothing and refining the voxel phantoms [20]. While voxel and hybrid phantoms allow for a more anatomically accurate representation of the internal organs, they also come with a significant time cost for phantom creation which must be taken into account.

2 MATERIALS AND METHODS

2.1 Analysis of duck anatomy

An adult male mallard duck (*Anas platyrhynchos*) donated by a local hunter from the Colorado Front Range was dissected to aid in determining internal organ size, shape, location and specific tissue density for use in the creation of a stylized phantom. The external dimensions of the duck body, neck, head and bill were also used for the stylized phantom geometry. The internal location of each organ was noted and upon removal from the body cavity the size, shape and mass were documented. Each identified organ was weighed in air and in water (Mettler Toledo XS104 with density kit) for density (ρ) and volume (V) determination via:

$$\rho = \frac{A}{A-B}(\rho_0 - \rho_L) + \rho_L \quad (1)$$

$$V = \alpha \frac{A-B}{\rho_0 - \rho_L} \quad (2)$$

where A is the weight of the simple in air (g), B is the weight of the simple in water (g), ρ_0 is the density of water (1 g cm^{-3}), ρ_L is the density of air (0.0012 g cm^{-3}) and α is the balance correction factor (0.99985) which takes air buoyancy of the adjustment weight into account.

A deceased juvenile duckling, of less than one day in age and of unidentified breed, was donated by a farmer from Westminster, South Carolina. External measurements of the ducklings' body, neck, head and bill were taken for use in the duckling scale stylized model. A micro-CT (Bruker, SKYSCAN 1176) of the duckling specimen was performed at Godley-Snell Research Center, Clemson University for use in preliminary voxel and hybrid models.

2.2 Development of computational models

Stylized representations of the adult duck and duckling were created within the Monte Carlo N-particle 6 (MCNP6) transport code, version 1.0, to model radiation transport through the body with the liver being considered as the source of either ^{76}As or ^{75}Se [15, 18]. The resultant tabulated energy deposition was then used to determine the DCF for various internal organs and the whole body.

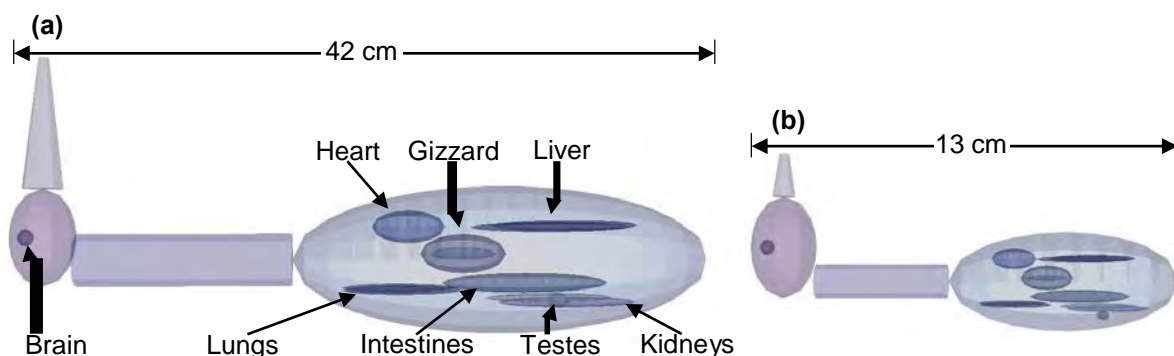
2.2.1 Stylized phantom creation

The stylized models of the duck and duckling consist of organs and body regions modeled as simple geometric shapes, mostly ellipsoids. The size, shape and location of organs were determined through knowledge of duck anatomy and dissection. The sizes of the duckling internal organs were estimated based on fractional comparison of the juvenile body and head dimensions and volumes to that of the adult duck. The brain dimensions were estimated at 1:2.29 of the adult and all other modeled internal organ dimensions were estimated at 1:3.26 of the adult. The shape description of the body regions and organs modeled as well as densities used for each tissue are listed in Table 1 and a 3D depiction of the duck and duckling stylized models are shown in Fig. 1.

Table 1: Description of the geometry and density of the stylized organs.

Organ	Description	Density (g cm^{-3})
Body	Ellipsoid	1.04
Heart	Ellipsoid	1.06
Gizzard	Ellipsoid	1.08
Gizzard Contents	Ellipsoid	2.66
Intestines	Ellipsoid	1.05
Liver	2 Ellipsoids	1.05
Lungs	2 Ellipsoids	0.89
Testes	2 Ellipsoids	1.03
Kidneys	2 Ellipsoids	1.06
Head	Ellipsoid	1.04
Brain	Sphere	1.10
Neck	Right Circular Cylinder	1.04
Bill	Right Truncated Cone	1.10

Figure 1: Stylized representations of the (a) adult duck and the (b) duckling. All organs identified on the adult duck model are present in the duckling model.



The density of the body, neck and head were assumed to be that of muscle determined from dissection. The density of the bill was estimated as that of cartilage reported in ICRU 44 [26] and the density of the gizzard contents was assumed to be the reported average of five types of rock [27]. All other densities were those determined for the organs during dissection. The elemental composition of all tissues in the models were based on human tissue for the same organ/tissue type [26]; preliminary work indicated that the elemental composition of most tissues is similar to that of human tissue, with the exception of bone, and thus, density is of greater importance for radiation transport at this stage of phantom development.

2.2.2 Source definition and determination of DCF

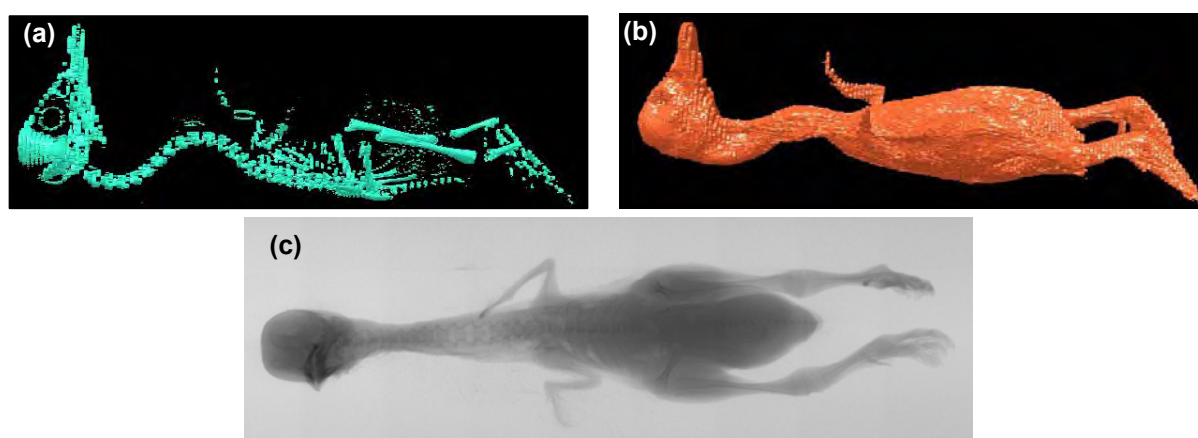
Within MCNP, the source organ was defined as the liver considering uniform distribution of either ^{76}As or ^{75}Se with disintegrations, simulating decay, being randomly distributed throughout the organ. Separate runs were conducted for each particle type, i.e. electrons/beta particles or photons, and each isotope considering only particles with a probability of occurrence of greater than 1%. Additionally, the average beta particle energies of ^{76}As were used over the beta spectrum to reduce significantly extended runtimes. The number of disintegrations was chosen to be 10^9 for ^{76}As photons, ^{75}Se photons and ^{75}Se electrons and 10^8 for ^{76}As beta particles in order to maintain reasonable run times while reducing variance. MCNP simulations were run on the Palmetto Cluster at Clemson University.

The tabulation of energies deposited per disintegration in each target organ (or group of organs) was made using the MCNP *f8 tally function which records the sum of all energies deposited in the tissue by the modeled particle type as well as secondary particles. The MCNP output for each target organ and the whole body was used to determine the corresponding DCFs by $K \cdot E$, where E is the energy deposited in a target per disintegration (MeV dis^{-1}) and K is a unit conversion with a numerical value of 0.013824 for a DCF in units of $\mu\text{Gy d}^{-1}$ per Bq kg^{-1} .

2.3 Preliminary development of voxel and hybrid models

The micro-CT of the duckling was imported into 3D-Doctor and preliminary reconstruction of the skeleton and the whole body was performed in automatic mode (Fig. 2). These preliminary models will be used as a starting point for future voxel and hybrid models for which the surfaces of the bones and internal organs must be contoured by hand for use in MCNP transport modeling.

Figure 2: Example 3D-Doctor automatic reconstructions of the (a) skeleton and (b) whole body from the (c) micro-CT image



3 RESULTS AND DISCUSSION

The higher energy of the ⁷⁶As beta particles and photons, compared with the electrons and photons associated with ⁷⁵Se, resulted in consistently higher DCFs for ⁷⁶As in both the duck and duckling models for all organs with the greatest impact in the liver, as expected due to definition as the source organ (Fig 3 (a) and (b)). The DCFs for the adult duck were greater than those for the duckling for all but 3 cases, brain for both ⁷⁶As and ⁷⁵Se and gizzard for ⁷⁶As (Fig 3 (c) and (d)). These differences are due to the combination of a more compact geometry of the duckling, the gizzard being the closest organ to the liver in general and the brain being significantly closer to the liver in the duckling than in the duck, and greater energy of the particles associated with ⁷⁶As.

Figure 3: Comparison of DCFs obtained using the stylized model for various organs with liver as the source organ. Specifically, (a) adult duck comparison of ⁷⁵Se and ⁷⁶As DCFs; (b) duckling comparison of ⁷⁵Se and ⁷⁶As DCFs; (c) comparison of duck and duckling DCFs for ⁷⁶As; and (d) comparison of duck and duckling DCFs for ⁷⁵Se.

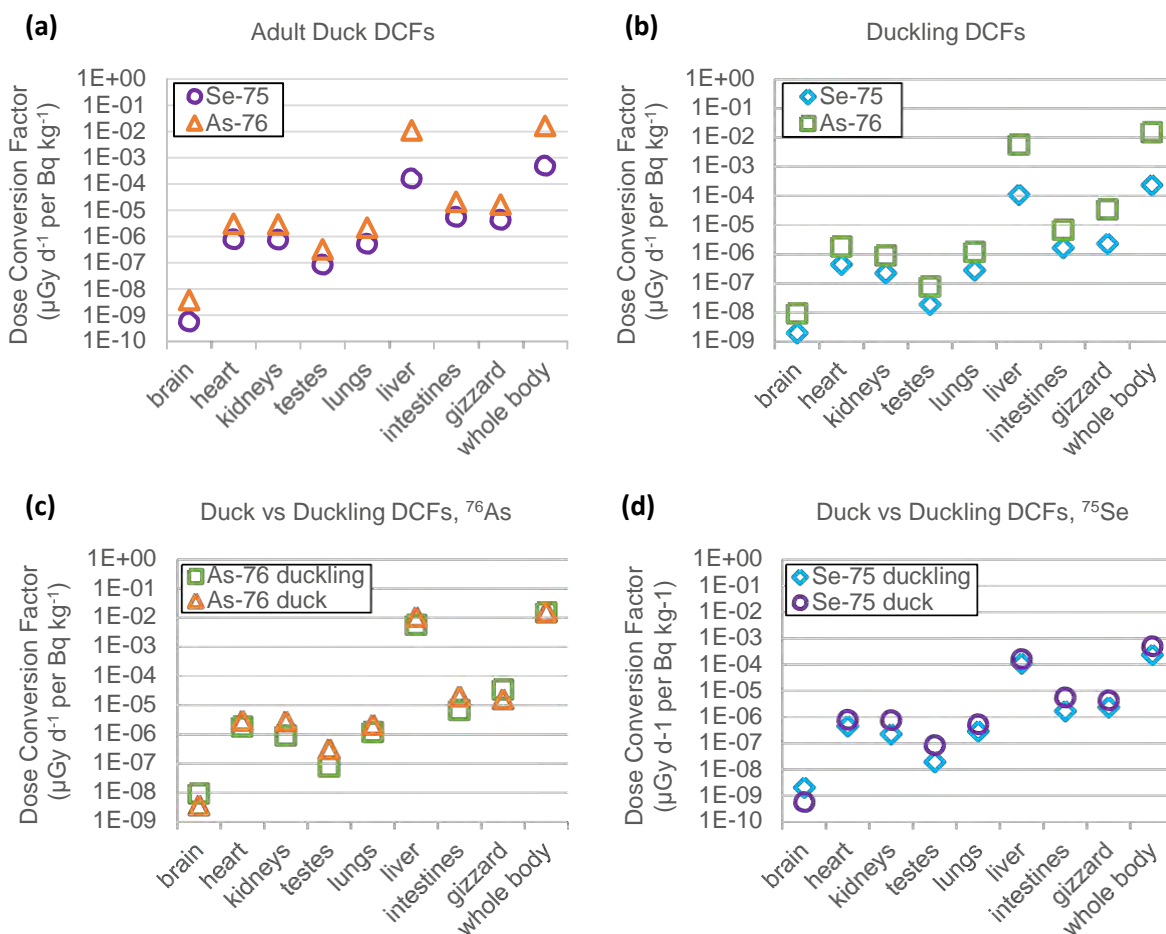


Table 2 lists the modeled whole body DCFs for an adult duck and duckling and ICRP 108 [2] reported values for an adult duck and duck egg reference organisms. The values are of similar magnitude even for the duck egg compared to modeled duckling, verifying that representation of the duck and duckling as stylized models produce reasonable results.

Table 2: Comparison of the whole body dose conversion factor for an adult duck and duckling obtained using the stylized model with the liver as the source organ to ICRP 108 [2] reported whole body dose conversion factor for an adult duck and for a duck egg for ^{75}Se .

Whole Body DCF for ^{75}Se ($\mu\text{Gy d}^{-1}$ per Bq kg^{-1})	ICRP 108	Stylized Model
Adult Duck	1.1×10^{-3}	4.9×10^{-4}
Duck Egg (ICRP)/Duckling (Model)	5.6×10^{-4}	2.3×10^{-4}

The relative errors associated with the whole body and the liver (source-target organ) tallies were 0.0001 or less for all particle types and isotopes. Relative error increases as the number of particles reaching the target organ decreases, i.e. for small organs or organs far from the source [20]. The relative error associated with each *f8 tally for the internal organs was typically < 0.01 for all photons and < 0.1 for ^{76}As beta particles and ^{75}Se electrons (intestines and gizzard). The relative error for the electrons associated with ^{75}Se was higher for organs that were not very close to the liver (heart, kidney, testes and lungs), but only greater than 0.5 for the testes of both the adult duck and duckling. However, the energy deposition was on the order of 10^{-11} MeV per disintegration for both cases making any dose and associated error negligible for this tissue. The error associated with energy deposition from ^{76}As beta particles to the brain of the duckling was also (slightly) greater than 0.5, but again the energy deposition was very low at 6.9×10^{-9} Mev dis^{-1} ; the brain received no deposition of energy from ^{76}As beta particles in the duck or ^{75}Se electrons in the duck or duckling due to the distance from the source.

4 CONCLUSION AND FUTURE WORK

Stylized, voxel and hybrid models have the advantage over simple ellipsoidal models of being able to discern the doses to individual organs, particularly when the source of internal exposure is not uniformly distributed over the whole body. The development of more comprehensive, yet practicable, dosimetric models allows for greater insight and quantification of potential dose-effect relationships of exposed populations of non-human biota for which current assessments are often minimal. Additionally, the models presented herein are easily modified to evaluate other radioisotopes of concern as well as account for spatial (i.e. varying uptake into multiple organs) and temporal heterogeneous internal distribution of radioisotopes when coupled with kinetic uptake evaluations, allowing determination of organ specific maximum absorbed dose rates and cumulative absorbed dose in future work. For example, varying uptake between the liver, kidney heart and lung for ^{75}Se , along with temporal changes and incorporation of voxel and hybrid phantoms, will be used to perform a more complete dosimetric analysis and to determine if any significant differences in organ doses result [18].

5 ACKNOWLEDGEMENTS

Funding for this project was provided by United States Nuclear Regulatory Commission Nuclear Education Grant #NRC-HQ-13-G-38-0002. We greatly thank the staff at Godley-Snell Research Center, especially Travis Pruitt, for their assistance and use of their Bruker micro-CT system.

6 REFERENCES

- [1] ICRP, 2007. The 2007 Recommendations of the International Commission on Radiological Protection. ICRP Publication 103. Ann. ICRP 37 (2–4).
- [2] ICRP, 2008. Environmental Protection: the Concept and Use of Reference Animals and Plants. ICRP Publication 108. Ann. ICRP 38 (4-6).
- [3] ICRP, 2009. Environmental Protection: Transfer Parameters for Reference Animals and Plants. ICRP Publication 114. Ann. ICRP 39 (6).
- [4] Thorne, M.C., 2003. Estimation of animal transfer factors for radioactive isotopes of iodine, technetium, selenium and uranium. *Journal of Environmental Radioactivity* 70, 3-20.
- [5] Halford, D.K., Markham, O.D., White, G.C., 1983. Biological elimination rates of radioisotopes by mallards contaminated at a liquid radioactive waste disposal area. *Health Physics* 45(3), 745–756.
- [6] Brisbin Jr., I.L., Kenamer, R.A., 2000. Long-Term Studies of Radionuclide Contamination of Migratory Waterfowl at the Savanna River Site: Implications for Habitat Management and Nuclear Waste Site Remediation. *Studies In Avian Biology* 21, 57–64.
- [7] Halford, D.K., Millard, J.B., Markham, O.D., 1981. Radionuclide concentrations in waterfowl using a liquid radioactive waste disposal area and to the potential radiation dose to man. *Health Physics* 40(2), 173–181.
- [8] Hanf, R.W., Dirkes, R.L., Duncan, J. P., 1992. Radioactive Contamination of Fish, Shellfish, and Waterfowl Exposed to Hanford Effluents: Annual Summaries, 1945-1972. Hanford Environmental Dose Reconstruction Project. PNWD-1986-HEDR. Battelle, Pacific Northwest Laboratories, Richland, Washington.
- [9] Markham, O.D., Halford, D.K., Rope, S.K., et al., 1988. Plutonium, Am, Cm and Sr in ducks maintained on radioactive leaching ponds in south eastern Idaho. *Health Physics* 55(3), 517-524.
- [10] Shamberger, R.J., 1981. Selenium in the Environment. *The Science of the Total Environment* 17, 59-74.
- [11] Spallholz, J.E., 2002. Selenium toxicity: cause and effects in aquatic birds. *Aquatic Toxicology* 57, 27-37.
- [12] Hamilton, S.J., 2004. Review of selenium toxicity in the aquatic food chain. *Science of the Total Environment* 326, 1-31.
- [13] Lemly, A.D., 2004. Aquatic selenium pollution is a global environmental safety issue. *Ecotoxicology and Environmental Safety* 59, 44-56.
- [14] Stanley Jr., T.R., Smith, G.J., Hoffman, D.J., et al., 1996. Effects of boron and selenium on mallard reproduction and duckling growth and survival. *Environmental Toxicology and Chemistry* 15(7) 1124-1132.
- [15] Pendleton, G.W., Whitworth, M.R., Olsen, G.H., 1995. Accumulation and loss of arsenic and boron, alone and in combination, in mallard ducks. *Environmental Toxicology and Chemistry*. 14(8), 1357-1364.
- [16] Hernandez, L.M., Gomara, B., Fernandez, M., et al., 1999. Accumulation of heavy metals and As in wetland birds in the area around Donana National Park affected by the Aznalcollar toxic spill. *The Science of the Total Environment* 242, 238-308.
- [17] Fernandez-Martinez. A., Charlet, L., 2009. Selenium environmental cycling and bioavailability: a structural chemist point of view. *Rev Environ Sci Biotechnol* 8, 81-110.
- [18] Wilson, D.S., Zhang, P., He, R., et al., 1997. Kinetics of selenium incorporation into tissues of female mallard ducks. *Toxicology* 122, 51-60.
- [19] Walters, W.H., Richmond, M.C., Gilmore, B.G., 1994. Reconstruction of Radionuclide Concentrations in the Columbia River from Handford, Washington to Portland, Oregon January 1950 – January 1971. Hanford Environmental Dose Reconstruction Project. PNWD-2225 HEDR. Battelle, Pacific Northwest Laboratories, Richland, Washington.
- [20] Martinez, N.E., Johnson, T.E., Pinder III, J.E., 2016. Application of computational models to estimate organ radiation dose in rainbow trout from uptake of molybdenum-99 with comparison to iodine-131. *Journal of Environmental Radioactivity* 151, 468-479.
- [21] Brown, J.E., Alfonso, B., Avila, R., et al., 2008. The ERICA Tool. *Journal of Environmental Radioactivity* 99, 1371-1383.

- [22] Gomez-Ros, J.M., Prohl, G., Ulanovsky, A., et al., 2008. Uncertainties of internal dose assessment for animals and plants due to non-homogeneously distributed radionuclides. *Journal of Environmental Radioactivity* 99, 1449-1455.
- [23] Martinez, N.E., Johnson, T.E., Pinder III, J.E., 2014. Influence of Lake Trophic Structure on Iodine-131 Accumulation and Subsequent Radiation Dose to Trout Thyroids. *Journal of Environmental Radioactivity* 131, 62-71.
- [24] Caffrey, E.A., Johansen, M.P., Higley, K.A., 2016. Voxel modeling of rabbits for use in dose rate calculations. *Journal of Environmental Radioactivity* 151, 480-486.
- [25] Martinez, N.E., Johnson, T.E., Capello, K., et al., 2014. Development and comparison of computational models for estimation of absorbed organ radiation dose in rainbow trout (*Oncorhynchus mykiss*) from uptake of iodine-131. *Journal of Environmental Radioactivity* 138, 50-59.
- [26] ICRU, 1989. Tissue Substitution in Radiation Dosimetry and Measurement. ICRU Report 44. Bethesda, MD
- [27] McConn, Jr., R.J., Gesh, C.J., Pagh, R.T., et al., 2011. Radiation Portal Monitor Project: Compendium of Material Composition Data for Radiation Transport Modeling. PNNL-15870 Rev. 1. Batelle, Pacific Northwest National Laboratory, Richland, Washington.

Project 1.2b: Techa River Population Cancer Morbidity and Mortality

Daniel O. Stram^a, Lyudmila Krestinina^b, Dale Preston^c, Alexander Akleyev^c

^aKeck School of Medicine, University of Southern California, Los Angeles, CA, USA

^bUrals Research Center for Radiation Medicine, Chelyabinsk, Russia

^cHirosoft Corporation, Eureka, CA

Abstract. Radioactive contamination of the Techa River resulted from activities of the Mayak Production Association (Mayak), which produced plutonium starting in 1948. Mayak is located in Ozersk, Russia. Total discharges into the Techa River between 1949 and 1956 amounted to 76 million m³ of radioactive waste with total activity of 1017 Bq (2.75 million curies). The highest doses were received by the residents of the Techa River villages. External exposure was due to the contamination of the river system components (water, river bottom, flood plain) and village locations with gamma-emitting radionuclides (137-Cs, 95-Zr, 95-Nb, 103-Ru, 106-Ru, and others). Internal exposure was due to intakes of radionuclides (mostly Sr-89, Sr-90, 137-Cs) with river water and locally produced foodstuffs. Over the years, dosimetric systems have been used to compute individual dose estimates for the exposed. The current system, called TRDS-2009, includes updates to the composition and temporal pattern of the releases, improved models for river transport, and increased individualization of individual doses, including use of individual measurements of 137-Cs and 90-Sr body burdens and more detailed data on residence locations. Further development of the TRDS (in 2016) will provide more detailed data on uncertainties in individual dose estimates using a multiple realization approach. Previous analyses of cancer mortality among the full Techa River cohort (TRC) members, and cancer incidence among Chelyabinsk subcohort of TRC, demonstrated significant dose effect for solid cancer and leukemia incidence and mortality. In current work we are extending the follow-up period to 60-years improving the quality and completeness of the mortality and incidence data, conducting analyses that provide quantitative estimates of radiation effects on cancer rates, and investigating influence of nonradiation factors in this unique subcohort of people chronically exposed and making this information available to the scientific community. In addition we are preparing the groundwork (statistical methods and software development) needed to incorporate dosimetric uncertainty into the calculations of the uncertainty in risk estimates, in preparation for the update of the Techa River Dosimetry System from TRDS-2009 to TRDS-2016.

1 INTRODUCTION

Most radiation protection guidelines are based on the assessment of radiation risk obtained from studies of populations exposed at high dose rates, including the atomic bomb survivors and cohorts of patients treated with radiotherapy for benign and malignant disease. In order to provide protection from radiation effects to populations exposed to chronic low-dose radiation, the protection guidelines relevant to low dose-rate exposures have historically been estimated by extrapolation from these high dose-rate studies. Studies of the health of populations exposed low dose rate exposures is needed in order to provide direct evidence for these health risks in order to reduce the uncertainties implicit in using high dose and dose-rate extrapolation in radiation protection.

Radioactive contamination of the Techa River resulted from activities of the Mayak Production Association (Mayak), which produced plutonium starting in 1948. Mayak is located in Ozersk, in the Southern Urals region of Russia. Total discharges into the Techa River between 1949 and 1956 amounted to 76 million m³ of radioactive waste with total activity of 10¹⁷ Bq (2.75 million curies). The highest doses were received by the residents of the Techa River villages. External exposure was due to the contamination of the river system components (water, river bottom, flood plain) and village locations with gamma-emitting radionuclides (137-Cs, 95-Zr, 95-Nb, 103-Ru, 106-Ru, and others). Internal exposure was due to intakes of radionuclides (mostly Sr-89, Sr-90, 137-Cs) with river water and locally produced foodstuffs. The Techa River Cohort (TRC) study provides a unique opportunity to quantify the long term effects of chronic, low-dose-rate exposure in a large unselected population.

2 MATERIALS AND METHODS

2.1 Cohort Definition

In 1967, the Urals Research Center for Radiation Medicine (URCRM) initiated a study of the long-term health effects of protracted low-dose-rate environmental exposure in this population [1]. The individuals studied in the TRC consists of approximately 30,000 persons who were born before 1950 and lived in any of the 41 villages situated along the Techa River between 1950-1960. About 60 percent of the cohort is women, the higher proportion of women reflects the deaths of adult males due to military service, accidents, or early deaths from disease. Cohort members identified with Tartar/Bashkir ethnicity make up about one-third of those exposed in Chelyabinsk Oblast (closer to the release sites) while virtually all of those exposed in Kurgan Oblast were identified as Slavs. Mortality follow-up is performed by regular systematic follow-up within the Chelyabinsk and Kurgan Oblasts, and within the Chelyabinsk Oblast for cancer incidence.

2.2 Follow-up for Mortality

Mortality follow-up for the Techa River Cohort members begins on the latest of January 1, 1950 or the date they came to live on the Techa riverside, whichever was later, and continues until the earliest of date of death, date of migration or other loss to follow-up, or December 31, 2006.

2.3 Follow-up for Cancer Incidence

Follow-up for solid cancer incidence is from 1956-2007 in the report from Davis et al [2]

2.4 Dosimetry

Dosimetry for the TRC makes use of large numbers of measurements of long-lived radionuclides in the human body and in the environment, as well as measurements of external exposure rates in places where the TRC members lived with pathway analysis used as a backup when other methods are exhausted. Development of dosimetry for the TRC has been an ongoing process and is still continuing. Here we focus on dose response analysis based upon the TRDS-2009 system. The TRDS-2009 estimates both external and internal dose histories for each participant. External exposures predominate for residences of villages located in the upper Techa region. External exposures peaked in 1951 and then declined. Individual exposure depends also on village distance along the river from the upstream contamination sources and of household distances from the shoreline as well as other individual and village factors. Internal exposures were through the consumption of Techa River water and cow milk which also depends on individual and village factors and is based on numerous data on tooth-beta counts and whole-body counts for the TRC members, detailed descriptions are provided by refs. [3,4]

2.5 Statistical Methods

Typically modeling of the cancer risks in the TRC in relation to dose utilizes excess relative risk modelling conducted using Poisson regression methods [Epicure, Hirosoft Corporation], applied to highly stratified person year and event count tables with stratification variables including detailed dose categories, gender, ethnicity, entry period, calendar time, age at entry, and time since first exposure. Dose (generally Gy) is lagged and time-varying as it accumulates over time. The excess relative risk models provide estimates of the increase in relative risk per unit dose with the baseline rate dependent upon such variables as attained age, sex, ethnicity, birth cohort, and allowing for modification of the ERR by factors including attained age, age at entry, gender and time since entry.

3 RESULTS

3.1 Dosimetry

Table 1 describes the distribution of individual dose estimates for the stomach and the red bone marrow (RBM). The dose to the RBM is principally the result of internal strontium exposure (beta particles). Stomach dose (and dose to most other organs) is dominated by external exposure. Dose for individuals are time dependent over the follow-up period, for both external and internal exposure, what is shown in Table 1 concern doses at the end of follow-up

Table 1: Cumulative dose distribution for cohort members based on TRDS 2006

	Median (Gy)	Mean (Gy)	90th %ile (Gy)	Maximum (Gy)
TRC Stomach dose	0.01	0.04	0.073	0.97
TRC RBM dose	0.24	0.41	1.05	9.0

3.2 Dose response

Here we summarize published results on dose response analysis from three papers [2,5,6] on solid cancer incidence and mortality and on leukemia incidence. In all cases the follow-up is over the period from 1950-2007 for mortality and 1953-2007 for cancer incidence.

3.3 Leukemia

Two-year lagged cumulative exposure to the RBM is treated as the exposure variable in the creation of the person years tables described above. Individual annual dose rates declined rapidly with time since initial exposure and distance from the release point with almost no additional dose accumulation by the end of follow-up. Over 90% of the cumulative RBM doses were attributed to radioactive strontium exposure.

At the end of the follow-up period there were 99 cases of leukemia identified including 27 CLLs and 25 CMLs. As there was no evidence of a dose response for CLL (ERR per 100 mGy = 0.01, $p > 0.5$). Most analyses focus on leukemia other than CLL. Figure 1 (from ref [5])

Figure 1: Estimate of risk of incidence of non-CLL Leukemia in the TRIC.

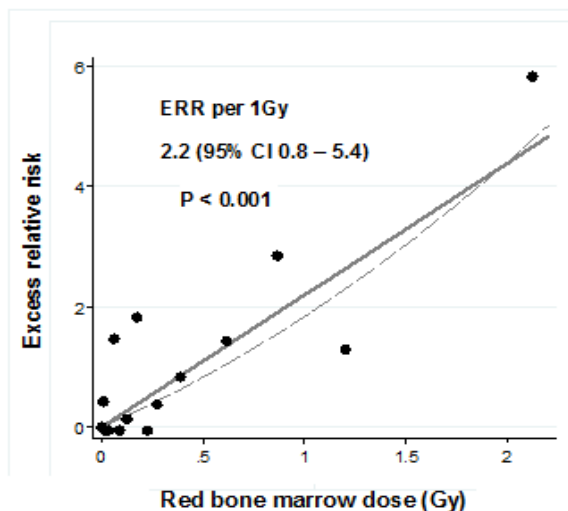
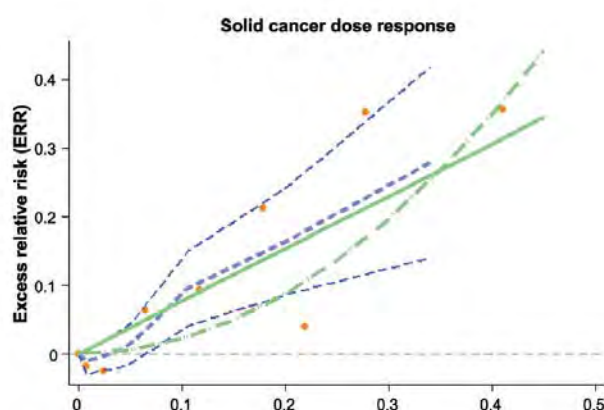


Figure 1 shows the overall dose response and both linear and linear-quadratic fits through the data. For these leukemias the change in the ERR per 100 mGy in a linear dose–response model was 0.22 (95% CI 0.08–0.54; $P < 0.001$). Under the linear dose response model it was estimated that half of the 72 non-CLL cases were associated with radiation exposure. Positive dose responses were seen for several subtypes or subgroupings of non-CLL leukemia including CMLs (ERR per 100 mGy 0.31, 95% CI 0.05-1.8) and acute/subacute leukemias as a group (8 AML, 1 ALL, and 32 other cases, ERR per 100mGy 0.18, 95% CI 0.04-0.59). The Krestinina et al [5] analysis examined numerous other aspects of the data including the linearity of the dose response, differences in the ERR by sex, ethnicity, age at diagnosis, age at exposure, and time since exposure. The estimated ERR was not found to be significantly dependent upon these variables.

3.4 Solid Cancer Incidence

There were a total of 1,933 solid tumors of all sites observed over the follow-up period. There was a statistically significant linear dose response for all solid cancers as a group which remained after adjusting for smoking in the baseline model ($p=0.02$). The estimated change in the ERR per 100 mGy was 0.07, 95% CI 0.013-0.15. Figure 2 (from Davis et al) depicts the solid cancer dose response in addition to linear, linear quadratic, and non-parametric fits to the data. Elevation in cancer risk in the dose range from 0-.5 Gy seems quite evident in the figure, although the shape at the low dose range is uncertain.

Figure 1: Solid cancer dose response, all are adjusted for smoking. Linear, linear-quadratic and nonparametric fits are shown.



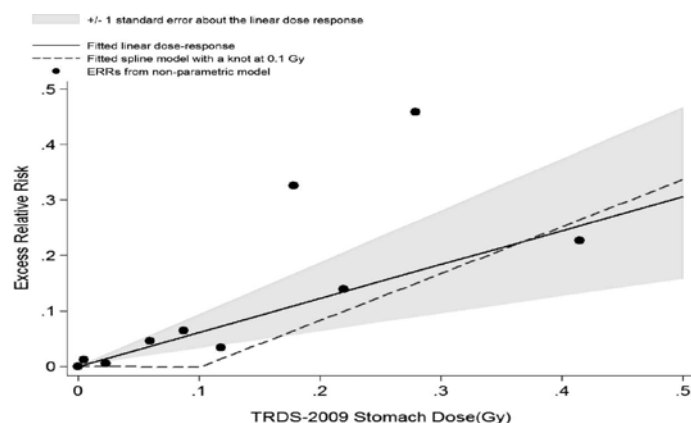
Further investigation showed no evidence that the radiation ERR varied significantly with sex, attained age, or reported ethnicity, or by age of exposure or time since exposure. In site specific analyses only esophageal and uterine cancer were found to display a significant dose response. The strongest ERR was seen for esophageal cancer with an ERR per 100 mGy of 0.46. Removing esophageal cancers still left a marginally significant response for the combination of all other cancers, suggesting that most solid tumors show some dose response.

3.5 Solid Cancer Mortality

There were a total of 2,303 deaths due to solid tumors of all sites reported by Schonfeld et al [6] over more than 50 years of follow-up (1950-2007). Among men, lung, stomach, and esophageal cancers were the most frequent causes of solid cancer death. For women, stomach, uterine, and breast cancers accounted for the largest numbers of solid cancer deaths.

Baseline models modeled the effects of birth cohort, ethnicity, time period and an age-dependent Oblast effect which reflected the prior observations that solid tumor rates are less in Kurgan Oblast than in Chelyabinsk; since doses are lower in Kurgan than Chelyabinsk failure to account for this difference would have led to an overestimation of effects.

Overall relative risk of solid tumor mortality by dose categories is depicted in Figure 3.

Figure 3: Solid cancer mortality based on TRDS-2009 stomach doses.

Shown are the fits of a linear model and a linear spline with a knot at 0.1 Gy as well as the observed mortality rates by dose categories after adjusting for the terms in the baseline described above. There is no evidence either for a linear-quadratic model compared to a linear model ($p > 0.5$) or for the threshold model at 0.1 Gy ($p = .46$). The overall linear trend produced an ERR/100 mGy of 0.061 (95% CI 0.004 - 0.127, $p = .03$). Based upon the linear model it was estimated that about 2 percent of deaths were associated with radiation exposure.

4 DISCUSSION

The Techa River Cohort is one of the few studies in which the long-term effects of chronic low-dose-rate radiation exposure can be evaluated in a large population. Each of the analyses of leukemia incidence, overall solid tumor incidence, and overall solid tumor mortality are significant in dose, and are well described by a linear dose response (ERR). Excess risk estimates per 100 mGy are not generally lower than those which would be expected based on other influential studies, even those where exposure is acute rather than protracted. However, other models e.g. purely quadratic, fit the data either as well or nearly as well as do the linear models, reflecting uncertainty in risk for the lowest dose categories.

There has been an evolution in the dosimetry systems used to estimate dose in this cohort. The TRDS 2009 doses used in the analyses described here includes information from many environmental measurements and individual assessments (including tooth and whole body counts). Nevertheless there remain uncertainties in the individual dose estimates which are not fully addressed in risk analyses.

A Monte Carlo dosimetry system expected later this year, TRDS-2016, will use the multiple realization approach [7-11] to describe uncertainties in dose; these will include shared uncertainties that affect either all or large groups of individual participant's doses simultaneously. We are presently developing software to incorporate the dosimetric uncertainty characterized by the multiple realizations into the uncertainty about the ERR risk estimates and other parameters. While we do not think that risk estimates will change simply because of uncertainty assessment, or that the significance of tests for non-zero dose response will be altered by incorporating dosimetric uncertainty[7], it is likely that confidence intervals for risk estimates will expand, although in a non-symmetrical way, with upper confidence bounds generally more affected than lower confidence bounds.

5 FUNDING

This work was conducted as part of the Joint Coordinating Committee for Radiation Effects Research (JCCRER) Project 1.2b under the auspices of the JCCRER Agreement of 1994 between the United States and the Russian Federation. It was jointly funded by the Russian Health Studies Program of the U.S. Department of Energy (DOE) and by the Federal Medical Biological Agency (FMBA) of the Russian Federation.

6 REFERENCES

- [1] Kossenko MM, Thomas TL, Akleyev AV, et al. The Techa River Cohort: study design and follow-up methods. *Radiat Res.* 2005; 164: 591-601.
- [2] Davis FG, Yu KL, Preston D, Epifanova S, et al. Solid Cancer Incidence in the Techa River Incidence Cohort: 1956-2007. *Radiat Res.* 2015; 184: 56-65.
- [3] Tolstykh EI, Degteva MO, Peremyslova LM, et al. Reconstruction of long-lived radionuclide intakes for Techa Riverside residents: strontium-90. *Health Phys.* 2011; 101: 28-47.
- [4] Tolstykh EI, Degteva MO, Vorobiova MI, et al. Reconstruction of long-lived radionuclide intakes for Techa Riverside residents. *Radiat Safety Prob.* 2006; 1: 68-79.
- [5] Krestinina LY, Davis FG, Schonfeld S, et al. Leukaemia incidence in the Techa River Cohort: 1953-2007. *Br J Cancer.* 2013; 109: 2886-2893.
- [6] Schonfeld SJ, Krestinina LY, Epifanova S, et al. Solid cancer mortality in the techa river cohort (1950-2007). *Radiat Res.* 2013; 179: 183-189.
- [7] Stram DO, Kopecky KJ. Power and Uncertainty Analysis of Epidemiological Studies of Radiation-related Disease Risk where Dose Estimates are Based Upon a Complex Dosimetry System; Some Observations. *Radiation Research.* 2003; 160: 408-417.
- [8] Land CE, Kwon D, Hoffman FO, et al. Accounting for Shared and Unshared Dosimetry Uncertainties in the Dose Response for Ultrasound-Detected Thyroid Nodules after Exposure to Radioactive Fallout. *Radiation Research.* 2015; 183: 159-173.
- [9] Simon SL, Hoffman FO, Hofer E. The two-dimensional Monte Carlo: a new methodologic paradigm for dose reconstruction for epidemiological studies. *Radiat Res.* 2015; 183: 27-41.
- [10] Kwon D, Hoffman FO, Moroz BE, et al. Bayesian dose-response analysis for epidemiological studies with complex uncertainty in dose estimation. *Stat Med.* 2016; 35: 399-423.
- [11] Stram DO, Preston DL, Sokolnikov M, et al. Shared dosimetry error in epidemiological dose-response analyses. *PLOS ONE.* 2015; 10: e0119418.

Assessment of equivalent dose of the lens of the eyes and the extremities to workers under nonhomogeneous exposure situation in nuclear and accelerator facilities by means of measurements using a phantom coupled with Monte Carlo simulation

Hiroshi Yoshitomi^{a*}, Masayuki Hagiwara^b, Munehiko Kowatari^a, Sho Nishino^a, Toshiya Sanami^b, Hiroshi Iwase^b

^aDepartment of Radiation Protection, Japan Atomic Energy Agency, 2-4 Shirakata, Tokai, Naka, Ibaraki 311-1195 Japan

^bRadiation Science Center, High Energy Accelerator Research Organization, 1-1 Oho, Tsukuba, Ibaraki 305-0801 Japan

Abstract. Proper assessment of the equivalent doses to the lens of the eye and extremities for radiation workers is important to ensure that the dose limits are not exceeded. Homogeneity of the radiation field greatly impacts on the assessment of eye lens and extremity doses. However, there has been no systematic approach to estimate (non-homogeneity in nuclear sector). The general aim of our project is to provide a comprehensive methodology to identify nonhomogeneous exposure situations. To fulfil this purpose, an index that represents the correlation between whole-body monitoring and eye lens or extremity monitoring was introduced for the screening of nonhomogeneous conditions. In this study, the followings which are essential for the next investigations to apply this method to the workplace field were carried out: (1) to establish the method to calculate the indices, (2) to verify the calculated indices by the measurements using phantom. The geometrical factors that should be taken into account for homogeneity in eye lens monitoring such as a distance and direction of face are also obtained in the calculations of (1).

KEYWORDS: *non-homogeneous exposure; equivalent dose; eye lens dose; extremity dose; dose assessment.*

1 INTRODUCTION

The equivalent doses to the lens of the eye and extremities for radiation workers should be assessed properly to ensure that the dose limits are not exceeded. Additionally, the emerging two issues has been demanding more appropriate evaluation of the equivalent doses of the lens of the eye and hands. One is the new occupational dose limit for the lens of the eye from the recent ICRP statement [1]: *i.e.* the dose limit for the lens of the eye for occupational exposure in planned situations was reduced from 150 mSv per annum to 20 mSv per annum averaged over 5 consecutive years and 50 mSv in any single year. The other is growing demand on the manipulation of highly activated materials in the maintenance works of an accelerator [2] and contaminated materials during the decommissioning works of nuclear facility, which increases the potential exposure risk to the extremities to a wider variety of radio-nuclides.

The equivalent doses to the lens of the eye and extremities from the whole-body monitoring can be commonly assessed from the view point of the cost and workload, if appropriate. On the other hand, this estimation might significantly underestimate the equivalent doses to the lens of the eye and extremities in nonhomogeneous exposure situations in some exposure cases [3]. An additional monitoring near the eye or extremities should be needed for the proper assessment. Therefore, homogeneity of exposure is one of key factors for adequate estimate of the equivalent doses to the lens of the eye and extremities [4, 5]. However, there has been no quantitative scheme to systematically estimate (non-) homogeneity of exposure.

Our project aims to provide a comprehensive and quantitative scheme to identify the nonhomogeneous exposure situations. This will help with proper implications of radiation protection measures even under nonhomogeneous exposure situation. Before starting radiation works, monitoring for radiation workers could be easily but reasonably planned, including whether or not an additional monitoring of the eye or extremities is required. For designing the scheme, the following issues have been investigated. (1)

* Presenting author, e-mail: yoshitomi.hiroshi@jaea.go.jp

Calculation platform for estimating the relationship between dose equivalent measured on the trunk and the lens of the eye and the extremity is being prepared. (2) Classification of nonhomogeneous exposure situation under typical radiation works at nuclear and accelerator facilities is being processed. (3) From reported radiation works, factors leading nonhomogeneous exposure are being drawn.

This work describes a proposal of introduction of quantitative index for nonhomogeneous exposure situation and an attempt of the screening of nonhomogeneous exposure situation based on a proposed “homogeneity index (HI)”. The proposed HI is defined by the ratio of eye lens or extremity dose to the dose measured on the trunk. This also represents the correlation between whole-body monitoring and lens of the eye or extremity monitoring. A set of the HIs obtained by Monte Carlo simulation incorporated with a mathematical phantom for some simplified exposure conditions is calculated. Verification of the HIs under both homogeneous and nonhomogeneous exposure situations is carried out by the benchmark measurements using a physical phantom. Calculations changing exposure conditions were also demonstrated, in order to identify the parameters that significantly impact on the HIs.

2 MATERIALS AND METHODS

2.1 Homogeneity index (HI)

To identify the nonhomogeneous exposure conditions quantitatively, the HIs defined as the ratio of the personal dose equivalent for the eye lens monitoring or the extremity monitoring to that for the whole-body monitoring are used:

$$HI_{\text{photon}}^{\text{eye}} = \frac{H_p(3)_{\text{head}}}{H_p(10)_{\text{trunk}}} \quad (1) \quad \text{for photon exposure to the eye lens,}$$

$$HI_{\text{electron}}^{\text{eye}} = \frac{H_p(3)_{\text{head}}}{H_p(3)_{\text{trunk}}} \quad (2) \quad \text{for electron exposure to the eye lens,}$$

$$HI^{\text{extremity}} = \frac{H_p(0.07)_{\text{extremity}}}{H_p(0.07)_{\text{trunk}}} \quad (3) \quad \text{for photon and electron exposure to the extremity}$$

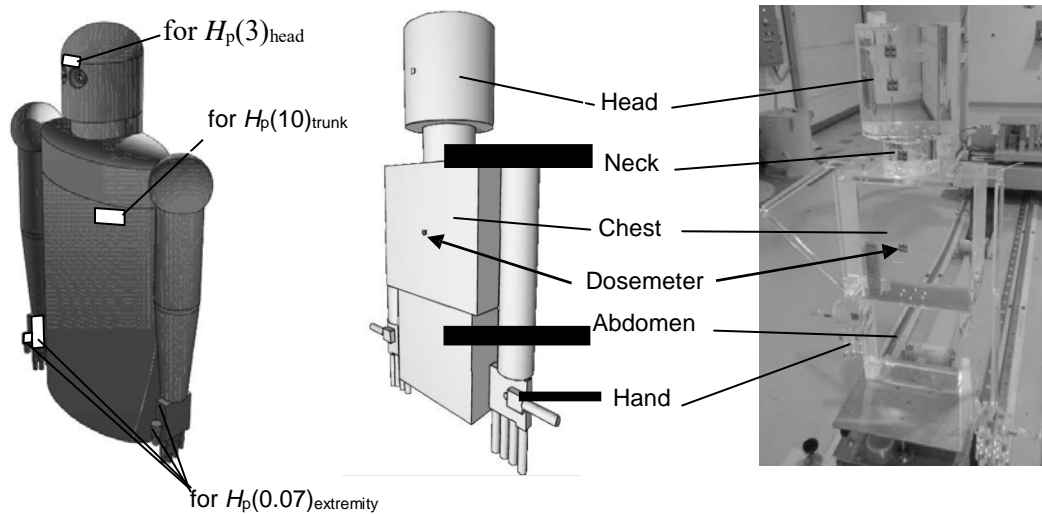
where, $H_p(d)$ is personal dose equivalent at a depth of d mm ($d = 0.07$ mm, 3 mm, or 10 mm) below a specified point indicated by a subscript on a mathematical phantom. The recommended depths d for the respective points in monitoring were chosen [6, 7]. $H_p(3)_{\text{trunk}}$ was used for electron exposure to the eye lens to identify the nonhomogeneous conditions regardless of the evaluation depth although it is not commonly evaluated using whole-body dosimeter. The required characteristics of the mathematical phantom for the purpose is to simulate absorption and scattered radiation by the human body and to change the posture easily. Hence, the geometry of the phantom was taken from the reference [8, 9] with some modification as follows: (1) Shoulder, upper arms, elbows, lower arms and hands were added to the phantom but legs were omitted. (2) Facial skeleton and ribs were only considered as bone ($\rho = 1.4$ g/cm³). (3) The medium of the phantom except for bones and eyes was chosen to be ICRU 4-element tissue ($\rho = 1.0$ g/cm³). Fig.1 shows the geometry of the phantom.

2.2 MC Simulations

Personal dose equivalents, $H_p(d)$, are directly calculated according to the definition [6] using Monte Carlo code PHITS 2.7.6 [10] with standard atomic data libraries to obtain the HIs. The mathematical phantom described in the previous section was set in a vacuum for parallel exposure or in a dry air for other exposure conditions. As illustrated in the Fig.1, the scoring volumes for the evaluation of $H_p(3)_{\text{head}}$ and $H_p(d)_{\text{trunk}}$ were located at 3 mm depth below the surface at the forehead (1.0 cm(L)×3.69 cm(W)×0.01 cm(D)) close to the eyes and at d mm depth below the left side of the chest (1.0 cm(L)×6.18 cm(W)×0.01 cm(D) for $d=3$ and 10 mm, 1.0 cm(L)×6.18 cm(W)×5 μm(D) for $d=0.07$ mm), respectively. The $H_p(0.07)_{\text{extremity}}$ was evaluated from the maximum values among the absorbed doses in four scoring volumes at 0.07 mm depth below the both palms (7.98 cm(L)×9.59 cm(W)×5 μm(D)) and both thumbs (1.0 cm(L)×1.0 cm(W)×5 μm(D)). These positions were corresponding to the

common monitoring positions with personal dosimeters. The obtained absorbed dose gives $H_p(d)$ as quality factor is recommended to be equal to 1 for both photons and electrons considered in this study.

Figure 1: Three dimensional view of the mathematical phantom (right) employed in this work for the calculations of the HIs and the physical phantom (centre: the modelling for calculations, left: the picture of the phantom) for the benchmark. The scoring regions to evaluate the $H_p(d)$ are also indicated.



The HI is used for the screening purpose to find the nonhomogeneous exposure conditions at the first step. Therefore, the exposure conditions to calculate HIs should be simplified as much as possible rather than simulate a specific radiation work. Some parameters that would characterise radiation works in the nuclear sector were categorised into three types: *i.e.* source-related, worker-related and source-to-worker-geometry-related parameters. The simplified exposure conditions are then constituted by the combination of these parameters. Some of the parameters used in this work are listed in Table 1.

Table 1: Some parameters considered for the calculation of the HI^{eye} in this work

Category of parameters		Range of the parameter	
Source-related	Type of radiation	Photon	Beta
	Energy (Nuclides)	^{241}Am , ^{137}Cs , ^{60}Co	$^{90}\text{Sr}/^{90}\text{Y}$, ^{106}Rh
	Source distribution	Parallel, Point, Planar(40 cm Φ)	
Worker-related	Direction of face	Down, Up	
Source-to-worker-geometry	Source position	Horizontal position: 40 ~ 110 cm in front of the body axis Height of the source: -20 cm ~ 60 cm above the eye level	

2.3 Benchmark

For the benchmark of the simulation results, the irradiations were performed using a simple water-filled physical phantom equipped with several dosimeters at the Facility of Radiation Standards (FRS) of Japan Atomic Energy Agency (JAEA). The physical phantom consists of 6 parts: *i.e.* head, neck, chest, abdomen and both hands. The position of the hands is able to change freely and the angle of the head is adjustable. Fig.1 also shows the geometry of the physical phantom and Table 2 summarises the specification of the phantom in detail. Small optically-stimulated luminescence dosimeters (OSLD) with $\text{Al}_2\text{O}_3:\text{C}$ as a sensitive material (nanoDotTM manufactured by Landauer, Inc.) were used to measure the dose at specified positions on the phantom. Except for the extremity measurements for beta-rays, the OSLDs were covered with PMMA slab filter with 2 mm thickness so that the total mass-

thickness over the sensitive region was around 300 mg/cm² [13]. OSL signals from the nanoDots™ were read using a microStar OSL reader (Landauer, Inc). Net OSL signals corrected for sensitivity were then directly used for comparison in this study.

As described in 2.2, the HIs were calculated from the absorbed dose on the ideal receptors made of soft tissue according to the definition of $H_p(d)$, which is different from the OSLD for the benchmark experiments. Therefore, four exposure conditions were chosen for the benchmark experiment so that they include both homogenous and nonhomogeneous exposure conditions and the responses of the OSLDs are identical to those of the ideal receptors from the view of the HI. To confirm this, another set of calculations using the mathematical phantom with the OSLDs was made. The OSLDs were precisely modelled according to the manufacturer data and placed on the surface of the mathematical phantom at the same positions as scoring regions for the simulations of the HI. Furthermore, the other set of calculations that fully simulates the experimental setup (see Fig.1) was made to ensure that response of the OSLD was calculated properly.

Table 2: The specification of the physical phantom used for benchmark

	Materials and shape	Dimension
Head	Water-filled cylinder with PMMA* walls	20 cm Φ ×20 cm(H) [11]
Neck	Water-filled cylinder with PMMA walls	12 cm Φ ×8 cm(H)
Chest	Water-filled slab with PMMA walls	30 cm(H)×30 cm(W)×15 cm(D) [12]
Abdomen	Water-filled slab with PMMA walls	25 cm(H)×25 cm(W)×12 cm(D)
Hand	Palm: PMMA cylinder Fingers: PMMA rod	Palm: 9 cm(H)×9.7 cm(W)×1.5 cm(D) Thumb: 1.9 cm Φ ×7 cm(L) Other fingers: 1.9 cm Φ ×10 cm(L)

* Polymethyl metaacrylate

3 RESULTS AND DISCUSSIONS

3.1 Framework of the method to identify nonhomogeneous exposure situations

The framework of the proposing methodology to identify nonhomogeneous exposure situations is described in the Fig.3. At the initial step, the HIs to quantify the (non-) homogeneity were calculated for simplified reference exposure conditions and then compared to the criteria level. Namely, an exposure condition for which the HI is greater than the criteria level could be nonhomogeneous and further investigation should be made in detail at the next step taking more specific information of the radiation work into account.

The criteria level was tentatively set to 1.5 in this paper. This value corresponds to the expanded uncertainty for assessed annual equivalent dose at or near the dose limit, 0.67 to 1.5 (factor 1.5), specified in the ISO 15382. From a view of the conservative estimation, lower criteria level was not considered. If the HI for a certain exposure situation is less than 1.5, the direct assessment from the whole-body monitoring with ideal dosimeter for that exposure situation will not underestimate the equivalent dose less than 0.67. It will be acceptable even though the dose level is near the dose limit and no correction have been made.

3.2 Benchmark

The results of the benchmark calculations and measurements for the HIs under four exposure conditions are summarised in Table 3. Good agreements within uncertainty between (a) and (b) shows that the OSLD can be used to measure the HI under these conditions. Good agreement within uncertainty between (c) and (d) indicates the successful modelling. Hence, the consistent values between (b) and (c) indicate the calculated HIs (shown as (a) in the Table 3) were verified by the experiments (shown as (d)). For the exposure conditions (1) to (3) and (5), these values were the same within uncertainties, but there found to be a gap for the exposure condition (4). This is because the

monitoring positions for head relative to those for the trunk were different between the mathematical phantom and the physical phantom. This effect is considered to be remarkable for the exposure of beta-rays with a short distance between the source and the phantom, which will increase the uncertainty of the HI.

Figure 2: The framework of the proposed method to identify nonhomogeneous exposure situations

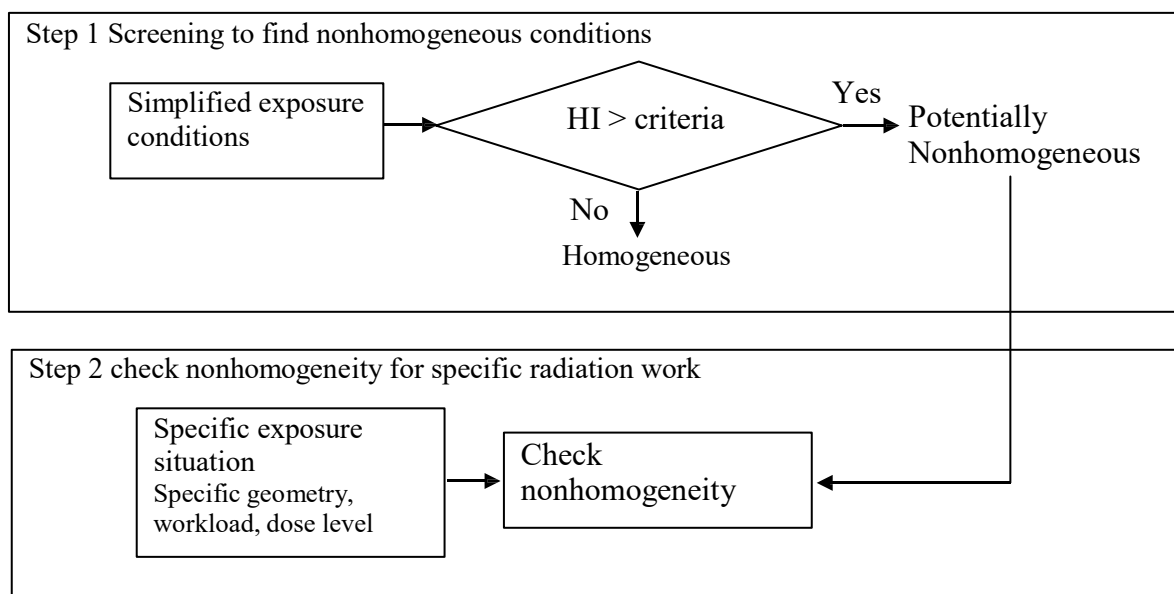


Table 3: Comparisons of the HIs obtained by simulation using (a) the mathematical phantom with ideal receptors, (b) the mathematical phantom with OSLD, (c) the physical phantom with OSLD and experiment using (d) the physical phantom with OSLD. (1), (2) and (5) belong to the homogeneous exposure condition while (3) and (4) belong to the nonhomogeneous exposure condition. Exposure conditions of (1) and (5) are the same but (5) is related to the extremity. The associated uncertainties are given for $k = 1$.

Exposure condition (source shape, nuclide and position*)	HI	Simulation		Experiment	
		Mathematical phantom (a) Ideal	(b) OSLD	Physical phantom (c) OSLD	(d) OSLD
(1) Parallel ^{60}Co	$\text{HI}^{\text{eye}}_{\text{photon}}$	1.02 ± 0.01	0.97 ± 0.01	0.97 ± 0.03	0.98 ± 0.01
(2) Point $^{90}\text{Sr}/^{90}\text{Y}$, 110 cm	$\text{HI}^{\text{eye}}_{\text{electron}}$	1.25 ± 0.04	1.28 ± 0.09	1.29 ± 0.04	1.29 ± 0.05
(3) Point ^{137}Cs , 40 cm	$\text{HI}^{\text{eye}}_{\text{photon}}$	2.37 ± 0.04	2.25 ± 0.07	2.20 ± 0.05	2.17 ± 0.16
(4) Point $^{90}\text{Sr}/^{90}\text{Y}$, 80 cm	$\text{HI}^{\text{eye}}_{\text{electron}}$	1.57 ± 0.02	1.54 ± 0.09	1.92 ± 0.02	1.89 ± 0.17
(5) Parallel ^{60}Co	$\text{HI}^{\text{extremity}}_{\text{photon}}$	1.02 ± 0.01	0.95 ± 0.05	0.97 ± 0.03	0.98 ± 0.03

* Values indicate the distances between the source and the longitudinal body axis of the phantom. The sources were placed at the same level of the eye.

3.3 Examples of the HIs

As for the equivalent dose to the extremities, the finger or palm dose monitoring has often been conducted in nuclear-related works in which hand is empirically considered to be highly exposed than trunk. Therefore, an attempt to calculate the HI for an obvious nonhomogeneous exposure situation for the hands in nuclear sector was firstly carried out. Manipulation of the point source as illustrated in Fig.3 has been considered to be the typical nonhomogeneous exposure situation for hands. The $\text{HI}^{\text{extremity}}$ for this exposure situation was calculated. The HIs for ^{137}Cs photons and $^{90}\text{Sr}/^{90}\text{Y}$ beta were determined to be 2.41 ± 0.04 and 3.52 ± 0.07 , respectively. If the criteria level is set to 1.5, it will be determined that both exposure situations are nonhomogeneous as expected.

Little study to investigate the nonhomogeneity exposure situations for the dose to the lens of the eye has been found. Hence, the HI^{eye} for ^{137}Cs point source above eye level and $^{90}\text{Sr}/^{90}\text{Y}$ point source at eye level were calculated as examples. The results are shown in Fig.4 (a) and (b), respectively, which implies that these exposure conditions were considered to be nonhomogeneous based on the criteria level of 1.5. Thirdly, the source positions where HIs are equal to 1.5 were determined both for ^{137}Cs and $^{90}\text{Sr}/^{90}\text{Y}$ point source from the various calculations (Fig.4 (c)). If a point source is closer to the body than it is on the boundary or above the boundary, the exposure is determined to be nonhomogeneous. These results demonstrate that handling point-like source within arm's reach above the eye level is considered to be the nonhomogeneous exposure situations in terms of eye lens.

Figure 3: The assuming typical geometry for handling the point source

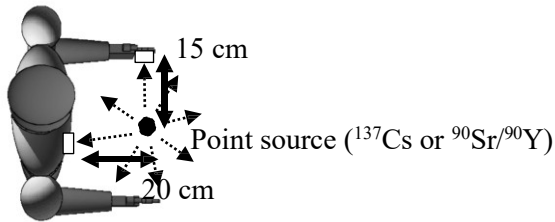
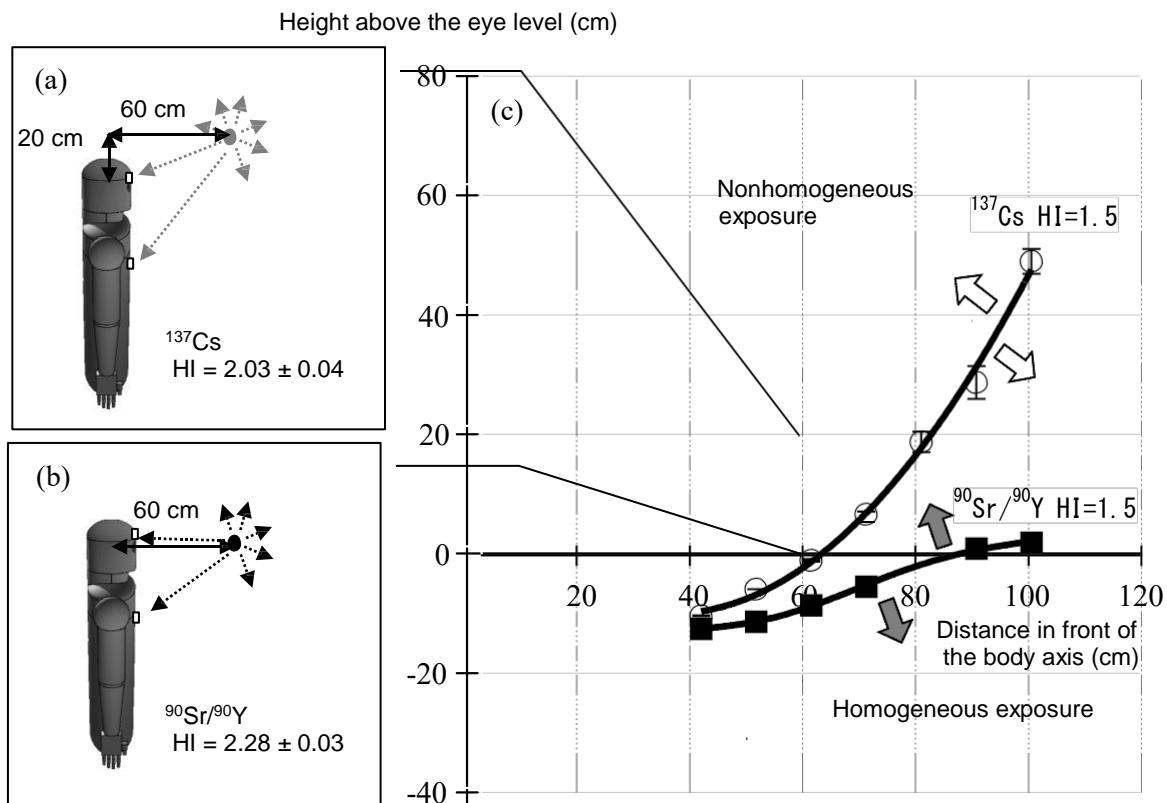


Figure 4: The HIs from (a) ^{137}Cs point source 20 cm above the eye level and (b) $^{90}\text{Sr}/^{90}\text{Y}$ point source at the eye level. The horizontal distance from the body axis is 60 cm for both case. (c) Boundary between nonhomogeneous exposure and homogeneous exposure conditions in the case that the criteria of 1.5 was selected. The longitudinal body axis of the phantom is aligned to the y-axis (the positive y-direction indicates the height above the eye level). The front face of the phantom looks into the positive x-direction.



3.4 Important parameters for the HIs

In the previous section, the HIs for the point source are demonstrated. The HIs should be calculated for the other simplified exposure conditions which is given by a combination of some parameters listed in Table 1. However, not all of the parameters significantly impact on the HI (Table 4). Source position is clearly impact parameters for the HI but some parameters such as wideness of the source and energy are less important for photons. For beta-rays the HI are found to be sensitive to most of the parameters.

Table 4: Influence of the parameters on the HI^{eye} . The reference condition for comparison is ^{137}Cs point source 60 cm away from the body axis at eye level for photon ($HI^{eye}_{photon} = 1.55 \pm 0.03$) and $^{90}Sr/^{90}Y$ point source 60 cm away from the body axis at eye level for beta ($HI^{eye}_{electron} = 2.28 \pm 0.03$).

	Source distribution	Energy	Direction of face	Source position
Photon HI^{eye}_{photon}	Planar (40 cm Φ) 60 cm at eye level ^{137}Cs	Point 60 cm at eye level ^{241}Am	Point, face down 60 cm at eye level ^{137}Cs	Point 100 cm at eye level ^{137}Cs
	1.44 \pm 0.04	1.33 \pm 0.01	1.78 \pm 0.02	1.15 \pm 0.02
Beta $HI^{eye}_{electron}$	Planar (40 cm Φ) 60 cm at eye level $^{90}Sr/^{90}Y$	Point 60 cm at eye level ^{106}Rh	Point, face down 60 cm at eye level $^{90}Sr/^{90}Y$	Point 100 cm at eye level $^{90}Sr/^{90}Y$
	1.22 \pm 0.03	1.91 \pm 0.02	2.84 \pm 0.10	1.43 \pm 0.03

4 SUMMARY

The proposed method would provide systematic methodology to identify the nonhomogeneous exposure situations in terms of eye lens and extremity doses. For the initial screening of nonhomogeneous exposure situations, the index, HI, to quantify the homogeneity of the exposure was introduced. The method to obtain HIs was established using Monte Carlo simulations coupled with the mathematical phantom. The calculated HIs reproduced the measured data regarding the homogeneity in the monitoring of eye lens and extremity. These results and a set of the obtained HIs for some simplified exposure conditions enable us to conduct further verification of this methodology, which is to apply this method to some of the exposure situations encountered in nuclear sector.

This study also reveals that handling source within arm's reach above the eye level may be potentially nonhomogeneous exposure situations in terms of eye lens and it would be possible to reduce parameters for the calculation of the HIs. It should be noted that further discussions regarding the criteria level for the HI will be needed.

5 ACKNOWLEDGEMENTS

The authors are grateful to Mr. M. Yoshizawa and Mr. T. Ohishi for helpful discussions. This work was supported by MHLW (Ministry of Health, Labour and Welfare, Japan) Hojokin Grant Number 150801-01.

6 REFERENCES

- [1] ICRP, 2012. ICRP statement on tissue reactions/early and late effects of radiation in normal tissues and organs-threshold doses for tissue reactions in a radiation protection context. ICRP Publication 118, Ann. ICRP 41(1/2).
- [2] Watanabe, H., Tanaka, S., Anazawa, Y., 1991. Radiation safety of Takasaki ion accelerators for advanced radiation application in JAERI. Jpn. J. Health Phys. 26, 395-404 (in Japanese).
- [3] Farah, J., Struelens, L., Dabin, J., et. al., 2013. A correlation study of eye lens dose and personal dose equivalent for interventional cardiologists. Radiat. Prot. Dosim. 157(4), 561-569.

- [4] IAEA, 2013. Implications for occupational radiation protection of the new dose limit for the lens of the eye. IAEA TECDOC No.1731.
- [5] ISO, 2015. Radiological protection – Procedures for monitoring the dose to the lens of the eye, the skin and the extremities. ISO 15382.
- [6] ICRU, 1992. Measurement of dose equivalents from external photon and electron radiations. ICRU Report 47.
- [7] ICRU, 1993. Quantities and units in radiation protection dosimetry. ICRU Report 51.
- [8] Behrens, R. and Dietze, G. 2011. Dose conversion coefficients for photon exposure of the human eye lens. *Phys. Med. Biol.* 56, 415-437.
- [9] ICRP, 2010. Conversion coefficients for radiological protection quantities for external radiation exposures. ICRP Publication 116, *Ann. ICRP* 40(2-5).
- [10] Sato, T., Niita, K., Matsuda, N., et. al., 2013. Particle and heavy ion transport code system PHITS, Version 2.5.2. *J. Nucl. Sci. Technol.* 50(9), 913-923.
- [11] Gualdrini, G., Mariotti, F., Wach, S., et. al., 2011. A new cylindrical phantom for eye lens dosimetry development. *Radiat. Meas.* 46, 1231-1234.
- [12] ISO, 1999. X and gamma reference radiation for calibrating dosimeters and doserate meters and for determining their response as a function of photon energy - Part 3: Calibration of area and personal dosimeters and the measurement of their response as a function of energy and angle of incidence. ISO 4037-3.
- [13] Yoshitomi, H., Ibrahimi, F., Eakins, J. et. al. A new eye dosimeter for Hp(3) measurements using OSL. to be submitted.

Implementation of Co-worker Models for the Reconstruction of Dose under an Occupational Radiation Exposure Compensation Program

James W. Neton*

U.S. National Institute for Occupational Safety and Health, Office of Compensation Analysis and Support, 1150 Tusculum Avenue, MS C-46, Cincinnati, Ohio 45226.

Abstract. Under the Energy Employees Occupational Illness Compensation Program Act (EEOICPA), the U.S. National Institute for Occupational Safety and Health (NIOSH) completes dose reconstructions for employees with cancer who are covered under the provisions of the Act. While the use of individual personnel monitoring is preferred in the completion of dose reconstructions, these data are often not available because either the worker was monitored and the data have been lost or the worker was potentially exposed and not monitored. In the absence of individual monitoring data, the implementing Federal regulation allows for the use of co-worker monitoring data to complete dose reconstructions. Co-workers are considered to be workers at the same site whose radiation monitoring measurements are considered to be representative or plausibly bounding of those received by one or more workers with no individual monitoring data. For dose reconstructions under EEOICPA, it is often difficult to locate a worker in a specific job at a specific location. Because of this, NIOSH has chosen to develop co-worker models that whenever possible cover a wide range of workers for a specific radionuclide at a specific time. To ensure that these models adequately represent the exposures of the unmonitored workers, NIOSH has defined a set of criteria that must be evaluated before personnel monitoring data can be used in a co-worker model. Among these criteria are: 1) the adequacy and completeness of the co-worker dataset; 2) the comparability of the monitoring program types; and, 3) the applicability of the data to the population being reconstructed, including the type of work activity and temporal similarity. The implementation of the above criteria to sites covered under EEOICPA are discussed.

KEYWORDS: *co-worker, dose reconstruction, exposure assessment.*

1 INTRODUCTION

Under the Energy Employees Occupational Illness Compensation Program Act (EEOICPA), NIOSH completes dose reconstructions for employees with cancer who are covered under the provisions of the Act. The methods used to complete these dose reconstructions are prescribed in Title 42 of the U.S. Code of Federal Regulations Part 82 [1]. While the use of individual personnel monitoring is preferred in the completion of dose reconstructions, these data are often not available because either the worker was monitored and the data have been lost or the worker was potentially exposed and not monitored. In the latter case, NIOSH has observed that, in accordance with the practices in effect at the time, only workers with the highest exposure potential were monitored or, in some cases, monitoring was conducted on representative members of the exposed population. In the absence of individual monitoring data, 42 C.F.R. Part 82 allows for the use other workers' data to complete dose reconstructions. Section 82.2 (b) states:

If individual monitoring data are not available or adequate, dose reconstructions may use monitoring results for groups of workers with comparable activities and relationships to the radiation environment.

The groups of workers specified in §82.2(b) are generically known as co-workers. Co-workers are considered to be workers at the same site whose radiation monitoring measurements are considered to be representative or plausibly bounding of those received by one or more workers with no individual monitoring data. Depending on the amount and specificity of the available worker and workplace data, the level of detail available for a coworker model can vary greatly. For dose reconstructions under EEOICPA, it is often difficult to position a worker in a specific job at a specific location.

*Presenting author, E-mail: jneton@cdc.gov

Because of this, NIOSH has chosen to develop coworker models that whenever possible cover a wide range of workers for a specific radionuclide at a specific time. This paper describes the process used by NIOSH to evaluate personnel monitoring data that is used in the reconstruction of doses for unmonitored workers who are covered under the EEOICPA.

2 EVALUATION CRITERIA

As indicated above, coworker datasets are established from monitored workers with comparable activities and relationships to the radiation environment. To accomplish this, one must carefully evaluate each coworker dataset to ensure that it is either representative of the distribution of exposures for the intended population or that it provides a plausible upper bound for those workers¹. Additional guidance on how to establish this is provided later in this paper. Prior to this, however, it is necessary to establish that the available internal or external monitoring measurements were technically capable of evaluating the monitored worker's exposure environment. If the techniques used to monitor exposed workers were inadequate, they clearly cannot be used to assess exposures for unmonitored workers. Criteria to consider when determining the technical adequacy of a dataset are provided below.

2.1 Data Adequacy

Coworker models are developed using individual bioassay² or personal dosimeter measurements. The measurement techniques employed must be evaluated to ensure that they are capable of quantitatively measuring the exposure of interest. When urine samples are used, this should include a review of the sample collection methods, any chemical processes employed, and the radiation counting equipment used. Among the items to be considered are: 1) representativeness of the bioassay sample collection method; 2) radiochemical recovery if chemical extraction techniques are used; 3) reduction in counting efficiency for alpha emitters due to self-absorption; and 4) reliability of the radiation counting equipment. If workers were exposed to a mixture of radionuclides (e.g., a combination of fission and activation products or actinides), and the samples were measured using a non-specific assay (beta, gamma, or alpha counting), the relative contribution of each radionuclide in the mixture must be evaluated.

When *in vivo* measurements are used, the overall measurement program must be carefully reviewed to ensure that the data accurately represent the quantity of the radionuclide in the organ of interest. This includes the adequacy of the phantoms used to calibrate the partial or whole body measurement geometries and a review of the methodology used to quantify a measurement's limit of detection. For the measurement of low energy photons (e.g., those below 100 keV) emitted from the lungs, the program's ability to correct for self-absorption due to varying chest wall thickness should be considered. Because certain radionuclides of interest do not emit photons that can be detected by an *in vivo* measurement, facilities sometimes infer the radionuclide of interest based on the measurement of one of its progeny. In this case, it is important to verify the validity of the assumptions that were made regarding the degree of radionuclide equilibrium between the progeny and its parent. Similarly, if ratios are employed to infer the amount of a contaminant (e.g., quantifying the amount of ²³⁹Pu based on a measurement of ²⁴¹Am in the lung), the ratio that is applied should be based on a well-established analysis of exposure conditions within the facility. For external exposure monitoring, it is important to consider the ability of the monitoring devices (e.g., film badges or thermoluminescent dosimeters) to detect the energies and types (beta, gamma, or neutron) of radiation that were present in the workplace. For those situations in which there is a measurement bias, corrections to the measured readings must be established prior to use in a coworker model. In addition, a review of the adequacy of the calibration methods employed and the extent that fading is a factor should be addressed.

¹ Under 42 CFR 83.13(c)(1), radiation doses are considered to be estimated with sufficient accuracy if NIOSH has established that it has access to sufficient information to estimate the maximum radiation dose, for every type of cancer for which radiation doses are reconstructed, that could have been incurred in plausible circumstances.

² While urinalysis is the bioassay method most often used for developing coworker models, *in vivo* measurements (e.g., lung or whole body counts) are sometimes used. If lapel breathing zone air samples are available, these may also be used, provided they have been determined to meet the data adequacy and completeness criteria outlined in this document.

The quality of the available data also needs to be considered. This would include a review of the appropriate collection and analysis of blank samples. When paired measurements are available, the precision between measurements should be examined. If widely different results from the same aliquot are observed, the effect this might have on the usefulness of the data should be considered. At facilities where chelation therapy may have been used (e.g., the administration of DTPA), the data should be reviewed to ensure that samples taken from personnel who were administered chelating agents are removed from the data set.

Finally, the amount of dose that could have been received, but not detected by a routine monitoring program, must be evaluated to determine if the magnitude of this “missed” dose is within the plausible bounds of exposures received by the workers. In certain cases, where the monitoring frequency was low (e.g. one measurement per year) and the limit of detection of the measurement is high, the coworker model might predict exposures that are well above any credible scenarios for that facility.

2.2 Data Completeness

Once the measurement techniques have been found to be technically acceptable, the amount of available monitoring data must be evaluated to determine if there are sufficient measurements to ensure that the data are either bounding or representative of the exposure potential for each job/exposure category at the facility. This analysis should look, not only at the total amount of data that are available, but also consider any temporal trends in data availability. A useful technique to establish this is to conduct a gap analysis. That is, the available monitoring data should be reviewed against the number and types of workers that were involved in radiological activities over time at the facility. As part of this analysis, the number of monitoring samples for each identifiable job category should be compared to the total number of workers who were potentially exposed in that job category. For the purposes of this effort a job category need not be an individual job title. Instead, a job category could consist of several job titles if there is reason to believe that exposures in those job categories would be similar.

If the number of potentially exposed workers in each category is unknown, a useful starting point is to look at the distribution of samples among the various categories of workers represented in the claimant population at that site. Table 1 provides an example of this for the categories of workers who were monitored for ²³⁹Pu at the Nevada Test Site. In this particular analysis, the radiation safety staff was monitored to a larger extent than workers directly involved in site activities. Thus, a coworker model based on these data would not necessarily reflect the exposure conditions of the unmonitored production/process workers. If, in fact, it can be established that the categories of workers were potentially exposed, yet inadequately monitored, it could preclude the development of a sufficiently accurate coworker model, unless it can be established that the exposures to another, adequately monitored category of workers reliably bounds the initial category’s exposures.

Table 1: Number of Pu-239 Samples (Percent of Samples) by Time Period and Job Category at the Nevada Test Site

	All Job-Specific Workers	Rad Safety Staff	Laborers	Welders and Wiremen	Miners	Security
Total Number of Samples	290	206	2	0	8	74
1963–1967	30 (10.34%)	28 (13.59%)	2 (100.00%)	-	0 (0.00%)	0 (0.00%)
1968–1970	34 (11.72%)	31 (15.05%)	0 (0.00%)	-	2 (25.00%)	1 (1.35%)
1971–1980	79 (27.24%)	76 (36.89%)	0 (0.00%)	-	3 (37.50%)	0 (0.00%)
1981–1992	147 (50.69%)	71 (34.47%)	0 (0.00%)	-	3 (37.50%)	73 (98.65%)

Any identified gaps (i.e., periods of time where a small percentage of the workers were monitored) in the monitoring data should be reviewed to determine if there is a reasonable basis for the lack of monitoring data. For example, there may have been a temporary stoppage in the work at a facility due to the initiation of maintenance operations or facility upgrades. If the monitoring gap is found to exist during long periods of potentially elevated exposure, it may not be possible to develop representative coworker models during this time period.

The number and types of discreetly identified activities will vary widely among covered facilities. At Atomic Weapons Employer (AWE) facilities that worked with uranium metal, there may only be one activity, while large Department of Energy (DOE) facilities will likely have multiple operations. One area that needs to be considered at each facility is the difference in exposure potential between maintenance and trades workers versus those involved in routine process operations.

Facilities with the potential for internal and/or external exposure to a large percentage of the workforce would require many more samples than one in which the potential for exposure was limited to just a few workers. In addition, the variability of the exposure potential should be considered. It has been observed, for example, that some national laboratories conducted work under many different experimental configurations, resulting in a wide variety of exposure potentials. In this case, it might not be possible to generate a single coworker model that adequately captures all categories of unmonitored worker doses.

Although there is no hard and fast rule for the minimum number of data points required to represent a given time interval, approximately fifteen values has been cited as a reasonable number for performing statistical tests on censored datasets [2]. Because our dose reconstruction program estimates parameters from the data, a default minimum of 30 person measurements is recommended per each discrete time interval and/or stratum being evaluated (e.g., 30 measurements per year if a coworker model is being developed based on annual samples or measurements). The minimum number of samples should, of course, be considered in light of the number of workers potentially exposed to the airborne source-term. For example, the number of samples necessary to be representative of the exposures at a uranium foundry, where airborne activity is generally widespread, will be greater than the number required of a small glove box operation where six workers were involved in the manipulation of plutonium parts. In the latter situation, it may be that samples for three out of six workers could be used to bound exposures for the three who were not monitored. Where the distribution of the data has large geometric means and/or standard deviations, the number of samples required will also be greater.

Finally, if electronic records or summary databases are used to develop the coworker model, these should be reviewed against a representative sampling of original data where possible to verify that they contain a complete and unbiased listing of all the data collected by the site. Documents to be considered in this review will vary depending on availability, but examples include hard copy lab records, summary health and safety reports, and NOCTS claimant file data. If hard copy records are being used, the legibility of the information should be carefully examined. For hard copy records that are manually entered by NIOSH, a quality control program to optimize the accuracy of data transcription should be established. If electronic records cannot be audited or are not an accurate representation of the monitoring records, they should not be used.

3 REVIEW AND ANALYSIS OF MONITORING PROGRAM DATA

Finalized coworker datasets reside in an electronic database, usually in the form of a spreadsheet or relational database. The original data that goes into the final coworker model is provided electronically to NIOSH in the form of various historical databases or in hardcopy format. In the process of converting the original data (electronic or hardcopy) into a single final coworker dataset, a log of the various manipulations that were required to produce the data in final form should be maintained, so that the final process is reproducible. This includes such practices as: 1) the deletion of any suspect outliers; 2) the removal of urine samples for workers on chelation therapy; and, 3) the conversion to units consistent with programmatic needs. Each version of any manipulated dataset should be maintained for future reference. The following sections provide guidance on evaluating the applicability of the finalized coworker's dataset to the unmonitored workforce.

3.1 Applicability of Monitoring Data to Unmonitored Workers

Prior to applying a site's worker monitoring data to estimate the exposures of unmonitored workers, the type of personnel monitoring program employed at the covered facility must be established. In general, three types of monitoring programs have been employed at sites covered under EEOICPA. These programs, listed in hierarchical order of preference for use in coworker modeling are: 1) routine, representative sampling of the workers; 2) routine measurement of workers with the highest exposure potential; and 3) the collection of samples after the identification of an incident. Because they are not representative of the overall distribution of exposures, programs that rely on measurement of the highest exposed workers or are incident-based require more careful consideration.

For routine monitoring programs, a review of the program should be conducted to determine the basis for the selection of program participants. It must be established who was monitored and why they were monitored. This can most easily be established through a review of the site's radiological control program documentation. In this evaluation there must be a demonstration that the monitored population consisted of: 1) a representative sample of the exposed population, or; 2) the workers with the highest exposure potential. In these cases, the assignment of a coworker dose from the distribution of measured values would either be representative of the worker's exposure in the first case or claimant favorable in the second case. Even though the program documentation might indicate that routine sampling was conducted, it is important to verify that the site's procedures were followed by a review of the samples that were actually collected.

A variation of the routine monitoring program is one in which workers are intermittently monitored on an as-needed basis (i.e. only when the potential for exposure existed). This would occur, for instance, in a short-duration project that created an internal and/or external exposure potential. Based on the specifications in project work plans or radiological work permits, certain classes of workers would be monitored at the end of the project to document that the exposure controls that were put in place were adequate. In these situations, it may be possible to use the monitoring data collected during the project close-out to place a plausible upper limit on the exposures of the unmonitored workers.

In some situations, sites have relied on incident-based sampling to monitor worker exposure. Because there are temporal gaps in the monitoring data, it is more difficult to demonstrate that this type of sampling can be used to develop representative or plausibly bounding coworker models. Prior to the use of incident-based sampling in a coworker model, the effectiveness of workplace controls must be demonstrated through the review of routine air monitoring samples and/or periodic contamination surveys. If one can demonstrate that the effectiveness of workplace administrative and/or engineering controls was adequate to prevent exposures, except during upset conditions, it may be possible to use incident-based sampling in a coworker model. When possible, this review should also include interviews with workers to verify that the written program requirements were consistently followed.

It has been observed at a number of sites that different classes of workers during the same time period may have had monitoring programs that were conducted for different purposes. For example, construction and building trade workers, who worked intermittently in radiological areas, may have been monitored only when an incident was thought to have occurred, while those employees involved in routine process operations would have been routinely monitored on a frequency commensurate with their exposure potential. In this case, it would not be appropriate to combine the monitoring data for these two groups of workers into a single coworker model that assumes a chronic exposure pattern. Rather, the default in this case should be to consider separate coworker models.

3.2 Analysis and Application to the Unmonitored Population

If after review of the monitoring program data, it is established that: 1) there is sufficient data to construct a representative coworker model, and; 2) the data can reasonably be represented by a statistical distribution (e.g., a log-normal or a Weibull distribution), the fitted distribution can be used to represent the exposures observed in the overall monitored population. For workers that are considered to have worked in environments with a potential for elevated exposure, the 95th percentile of the distribution should be used as an upper bound of their exposure during the modeled time period. Although it could be argued that the job categories that fall under this criterion should be listed, any attempt to do so might be artificially restrictive. This decision is most accurately made using the information available at an individual site, the claimant interview and other documents that might be in the worker's records. For workers who were less likely to be highly exposed and/or were intermittently exposed in the workplace, the full distribution (i.e., the geometric mean and its associated standard distribution if a lognormal fit is used) should be used as representative of their potential for exposure during the modeled period.

When multiple bioassay samples are present during a monitoring period for a given individual, it is appropriate to average the values so that a single statistic can be computed for that individual. The use of a single value for each monitored person in a given monitoring interval is appropriate because the desired coworker model represents a distribution of individual worker excretion results, as opposed to a distribution of all samples collected. The use of an average value for each worker is called the One-Person-One-Statistic (OPOS) method. Rather than compute a simple average of the measured values, each individual bioassay result should be weighted by the fraction of the year it represents (i.e., a time-weighted OPOS).

In the Time-weighted OPOS method, the statistic computed is defined as the maximum possible weighted mean of the face values for all the censored and uncensored excretion results for one person in a year, where the results are weighted by the numbers of days that the person was assumed to have excreted the measured value. The formula for the statistic computed using the Time-weighted OPOS method is the following:

$$\text{Time-weighted OPOS} = \frac{\sum_{j=1}^{m+1} y_j d_j}{\sum_{j=1}^{m+1} d_j}$$

where:

- m = the number of days when the person had excretion results in the year,
- y_j = the average daily excretion results (can be either uncensored or censored),
- d_j = the number of days that the person was exposed at result y_j .

The average daily excretion result y_j is computed as the arithmetic mean of all the excretion results that a person had in one day:

$$y_j = \frac{1}{n_j} \sum_{i=1}^{n_j} x_i, \text{ for } 1 \leq j \leq m$$

where:

n_j = the number of all excretion results for a person in a day.

The average daily excretion result y_{m+1} that is used in the formula for the Time-weighted OPOS, represents the first excretion result from the following year, if that result is available, or the last excretion result from the current year, if there are no samples in the following year; so, y_{m+1} is defined as follows:

$$y_{m+1} = \begin{cases} y_p, & \text{if the individual had a sample in the following year} \\ y_m, & \text{if the individual had no sample in the following year} \end{cases}$$

where:

y_p = first average daily excretion result in the following year.

The d_{m+1} value that is used in the formula for the Time-weighted OPOS, represents the number of days from the last day when an excretion occurs during the current year until the end of the current year.

3.3 Time Interval of the Modeled Data

The amount of data that are available directly influences the time intervals used in the coworker model. As stated in section 2.2, a minimum number of 30 samples per monitored interval is recommended. Based on a review of the currently available datasets, a modeled interval of one year strikes a good compromise between the availability of data and the need to ensure that the samples are contemporaneous with ongoing operations. In certain situations, there are sufficient data to develop quarterly models, but this is the exception rather than the norm. If, because of data limitations, it is necessary to consider time intervals beyond one year in the coworker model, any changes in site practices or operations should be evaluated to ensure that the data can be validly combined. In general, grouped time intervals should not exceed a 3 year period, unless there is stringent justification for doing so.

4 EVALUATION OF STRATIFICATION

The distribution of a potentially more highly exposed population should be evaluated as a separate standalone distribution in situations where: 1) accurate job categories and/or descriptions can be obtained for all workers making up the general coworker dataset; 2) there is reason to believe that one of the job categories is more highly exposed; and, 3) there were unmonitored workers in this job category. If it can be demonstrated, however, that there were no unmonitored workers with the potential for exposure in this more highly exposed population, then stratification would not be necessary.

Once a dataset has been stratified based on job category, a statistical analysis should be conducted to determine if the two datasets should be modeled separately. This analysis consists of a two-tiered evaluation where the stratified distributions are first compared on a year-by-year basis (or other selected monitoring interval) to determine if any of the individual distributions are significantly different. If a significant difference is observed in any of the modeled time intervals, then a test of practical significance is employed. This test compares the slopes of the chronic intake models over the time periods where a statistically significant difference in the modeled distributions was observed [3].

5 SUMMARY AND CONCLUSIONS

While the use of individual personnel monitoring is preferred in the completion of dose reconstructions under the EEOICPA, these data are often not available because either the worker was monitored and the data have been lost or the worker was potentially exposed and not monitored. To complete dose reconstructions for workers with incomplete monitoring data, NIOSH relies on co-worker models that are either representative or plausibly bounding of the exposures for these workers. The development of co-worker models requires careful evaluation of the quality and quantity of the available data. Included in the evaluation are reviews of: 1) the data adequacy and completeness; and 2) the representativeness of the data to the unmonitored population. To account for the variability in sampling inherent in bioassay monitoring programs, a time-weighted average of an individual's monitoring results over the time period modeled should be used. Once an acceptable co-worker data set is identified, the 95 percentile of the modeled distribution can be used to represent exposures for workers with a potential for elevated exposure, while the 50th percentile can be applied to workers with less potential for exposure. The distribution of a potentially more highly exposed population should be evaluated as a separate standalone distribution in situations where: 1) accurate job categories and/or descriptions can be obtained for all workers making up the general coworker dataset; 2) there is reason to believe that one of the job categories is more highly exposed; and, 3) there were unmonitored workers in this job category.

6 ACKNOWLEDGEMENTS AND DISCLAIMER

The author wishes to acknowledge the contributions of Tim Taulbee, Dave Allen, and Daniel Stancescu of NIOSH and Tom LaBone and Nancy Chalmers of the ORAU Team for their contributions to the development of the co-worker model concepts described in this paper.

The findings and conclusions in this paper are those of the author and do not necessarily represent the views of the National Institute for Occupational Safety and Health

7 REFERENCES

- [1] U.S. Department of Health and Human Services. Methods for radiation dose reconstruction under the Energy Employees Occupational Illness Compensation Program Act of 2000, final rule. Washington, DC: U.S. Government Printing Office; 42 CFR Part 82; 2002.
- [2] Singh, A., N. Armbya, and A. K. Singh, 2013, *ProUCL Version 5.0.00 Technical Guide*, EPA/600/R-07/041, U.S. Environmental Protection Agency, Office of Research and Development, Washington, D.C., September.
- [3] ORAU 2014. *Analysis of Stratified Coworker Datasets*, ORAU-RPRT-0053, Rev. 02, Oak Ridge Associated Universities Team, Cincinnati, Ohio. October 2, 2014.

Experience with Wound Dosimetry in Uranium Mining and Processing

John Takala, Kari Toews

Cameco Corporation, 1131 Avenue W South, Saskatoon SK, Canada

Abstract. Wounds represent a potential intake route to workers and while significant wound intakes in the uranium mining and processing industry are relatively infrequent, they can occur. NCRP Report No. 156 has provided a comprehensive set of models to evaluate potential intakes and the inclusion of these models in commercially available software packages has facilitated the assessment of potential cases. This paper will review recent experience with wound dosimetry from uranium ore and natural uranium.

KEYWORDS: *wound dosimetry; uranium processing; uranium mining.*

1 INTRODUCTION

Dosimetry programs must assess all potential exposure pathways and in the uranium mining and processing industries it is typical to assess doses from external radiation and inhaled radioactivity. Wounds represent another potential intake route to workers and while significant wound intakes in the uranium mining and processing industry are relatively infrequent, they can occur. NCRP Report No. 156 [1] has provided a comprehensive set of models to evaluate potential intakes from wounds and the inclusion of these models in commercially available software packages has facilitated the assessment of potential cases. In recent years Cameco Corporation has had two incidents, one with uranium ore and another with natural uranium (UF₄), which resulted in the need to calculate doses to workers from wounds caused by contaminated equipment. While the medical treatment of the workers remained the top priority, steps were taken to assess the potential dosimetric implications of the incidents. In both cases follow-up urine bioassay samples were collected for several months to ascertain the doses. The results of the dose assessments were included in workers official dosimetry records.

2 WOUND CASE #1

2.1 Incident Description

On November 14, 2012 a worker at Cameco's Eagle Point mine, an underground uranium mine located in northern Saskatchewan Canada, was injured when he was struck by a piece of heavy mobile equipment underground. During the incident the worker was dragged by the equipment and suffered significant injury to his foot and lower leg, resulting in an intake of uranium ore via the wound. The worker had the majority of the skin in the injured part of the leg removed and there were deep wounds to the underlying tissue. The worker was located close to a pile of uranium ore when the incident occurred and the wounded tissue was exposed to broken ore as he was dragged by the equipment.

The injured worker was treated with first aid and stabilized at the scene. He was evacuated to the surface and met by site ERT personnel and transported to the medical clinic for further treatment by the nurse. He was later transported to a hospital in Saskatoon, Saskatchewan by air ambulance. The extent of the worker's injury was a broken lower leg and ankle on the left leg and a crushed ankle and foot on the right leg. While the worker lost two toes on his right foot, he was eventually able to return to work. The investigation identified a single root cause related to this incident, inadequate guidance regarding expectation for communications when performing underground activities in heavy equipment work areas.

2.2 Dosimetric Analysis

The intake and dose estimate for this incident was determined through fitting of the uranium in urine bioassay data to the NCRP Report 156 wound models with the computer software packages IMBA Professional Plus [2] and AIDE [3].

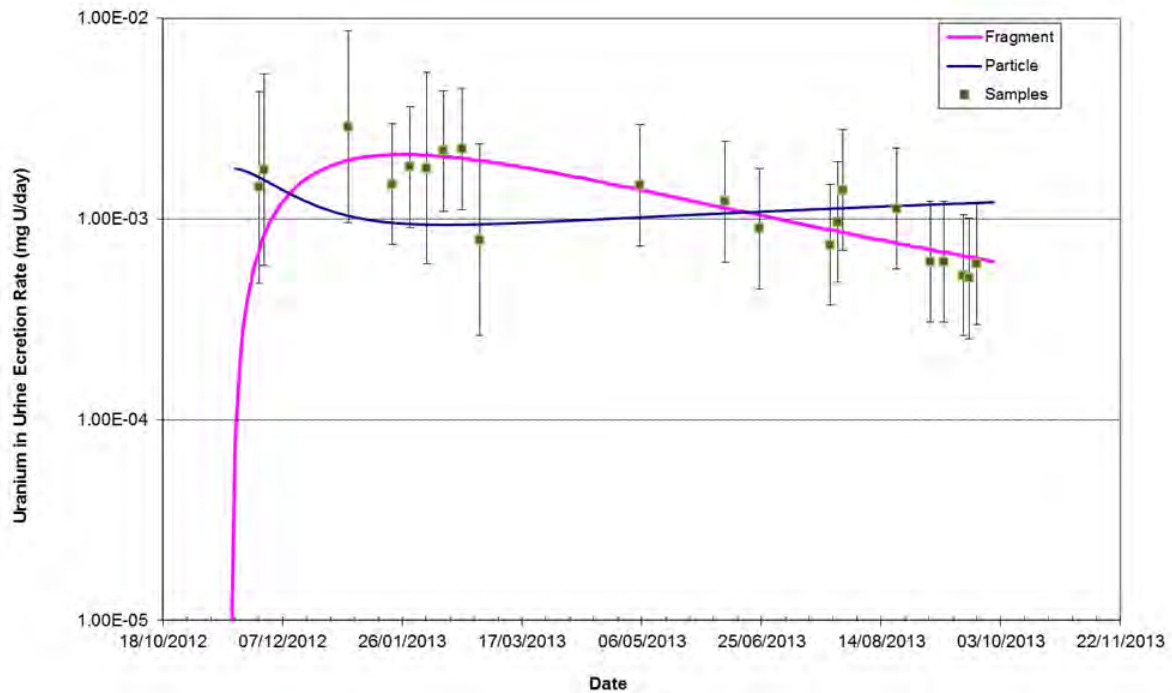
The material entering the wound was uranium ore, meaning it contained uranium isotopes in natural abundance and all of the radionuclides in the uranium decay series. The decay products of uranium-238 are generally present in secular equilibrium and this assumption was used in the dose calculations. The process for determining the amount of each radionuclide present was to calculate the total uranium intake from the uranium in urine results and assume the rest of the decay series had the same activity as uranium-238.

Based on the definitions of intake and retention models from NCRP Report No. 156, the material entering the wound was most likely either a particle or a fragment. This material was low-grade uranium ore and not soluble, so not likely to be well described by the various chemical classes used in the NCRP models. The material that the worker was exposed to was a mixture of ground ore of varying sizes from slurry-like to rock fragments, but not colloid-like, which is the other NCRP model type. Because the most appropriate model was unknown at the time dose modelling was initiated, both the fragment and particle models were initially considered.

It is worth noting again that this wound was very deep and the most likely location of any remaining material was deep inside the tissues and distributed over the foot and lower leg of the worker. In addition, the wound was thoroughly flushed several times and as noted earlier, there was little intact skin remaining at the injury location. Given the nature of this injury and the depth and distribution of any residual material, there was no basis for assessing skin dose for this case.

The worker provided urine bioassay samples from November 27, 2012 until September 23, 2013, with a total of 21 (approximately) 24-hour total-void samples. The delay between the incident and the collection of first urine sample was due to the fact the initial focus was on the treatment of the physical injuries. As will be described further below, the duration of sampling was required in order to distinguish between the two intake models (i.e. particle versus fragment model) for this incident. All samples were analysed for uranium in urine content at Cameco's Port Hope Conversion Facility laboratory. This lab is used to analyze samples for Cameco's Port Hope Conversion Facility and Blind River Refinery operations as part of their Internal Dosimetry Service License and has a detection limit of 0.2 µg uranium/litre. In addition, an attempt was made to measure the thorium-230 content in the urine samples, however, given the amount of uranium present, the expected concentration of thorium-230 in the urine was below the detection limits. While this was expected from the implied level of potential intakes from the observed uranium (and the assumption of secular equilibrium) and was not useful in narrowing the model selection, it did provide some limited confirmation of the estimated intake from the models.

The software package IMBA Professional Plus was used to model the uranium intake using both the particle and fragment wound models. Figure 1 presents a visual comparison of the of the expected excretion curves for each model to the actual bioassay data. The expected excretion amounts for each model are similar, however the actual shape of the curves differ; the particle model decreases initially then increases over time while the fragment model peaks and then slowly decreases over time. Because the values are similar, it is only after a number of months when the curves begin to diverge that it was possible to distinguish between the two. Visually, the bioassay samples appear to follow the fragment curve reasonably consistently over the entire period, while the particle model shows a trend of underestimating the uranium in urine during the first half of the period and overestimating the results in the last half.

Figure 1: Comparison of Expected Excretion Curves to Bioassay Samples

IMBA can perform curve fitting to data using both least squares and maximum likelihood fitting methods. For each a probability of chi-squared parameter (p) is calculated as a measure of goodness of fit. The statistical significance of the fit is 1.0 for the fragment model and 0.92 for the particle model. It is important to point out that up until August, 2013 both models had essentially identical significance values for their fit to the data. As samples from August and September were entered the significance values of the fits began to diverge along with the predicted trends, with the fragment fit improving slightly to $p=1$ and the particle fit consistently decreasing in significance as more samples were collected. That trend, in combination with the visual trend of the fragment model more closely following the actual urine results, supports the conclusion that this wound intake is best estimated using a fragment model.

Based on the fragment model the estimated uranium intake from the uranium in urine bioassay data was 81.6 mg of U-Nat. This equates to an activity of 2055.6 Bq for U-Nat or 1007.4 Bq for U-238, which would be the activity for the rest of the radionuclides in the uranium-238 decay series.

Once the appropriate model was determined for the intake, the dose from the remaining radionuclides in the uranium-238 decay series could be calculated. IMBA was used to model the thorium-230 dose. However, IMBA does not have biokinetic models for all of the remaining decay products in the series, nor is it able to model the short-lived decay products of radium-226 in full equilibrium. The software AIDE was used to model the dose from the remainder of the decay series from radium-226 and the subsequent decay products. Each of the radionuclides was assumed to have an activity of 1007.4 Bq and the radionuclide-specific biokinetic models were used. Table 1 presents the dose associated with each of the radionuclides and the software used for each calculation.

Table 1: Results of Dose Modelling

Radionuclide	Estimated Intake (Bq)	Dose (mSv)	Software
Natural Uranium	2055.6	0.18	IMBA
Thorium 230	1007.4	15.6	IMBA
Radium 226 – Polonium 210*	1007.4*	0.31	AIDE
Total Effective Dose		16.1	

*This includes Ra-226, Rn-222, Po-218, Pb-214, Bi-214, Po-214, Pb-210, Bi-210 and Po-210

From this analysis, it was concluded that the total effective dose to the worker as a result of this intake was 16.1 mSv and the intake was best estimated by a fragment wound model. The dose from this incident was below the regulatory annual dose limit (i.e., 50 mSv/y) and the worker's total dose, from both routine work duties and this wound intake, was 18.7 mSv and is also below the implied five-year limit of 20 mSv/y.

3 WOUND CASE #2

3.1 Incident Description

On February 10, 2011, a UF₆ operator was performing routine work which involved changing a drum dryer blade in the UF₆ production building. The blade stuck and while the employee was trying to pull the blade out, his hand slipped along the blade's edge, causing a laceration to the left index finger at the inside base of and perpendicular to the left index finger. The employee was wearing PVC gauntlet chemical gloves at the time of the incident. The worker stated that a visible amount of UF₄ was present on the drum dryer blades.

The worker sought immediate first aid, which involved rinsing of the wound and the application of a bandage. He was then transported to the local hospital. The wound was rinsed and re-bandaged and then after a period of time a physician sutured and bandaged the wound. On March 9, 2011 the worker had follow-up surgery to address some nerve damage sustained from the injury.

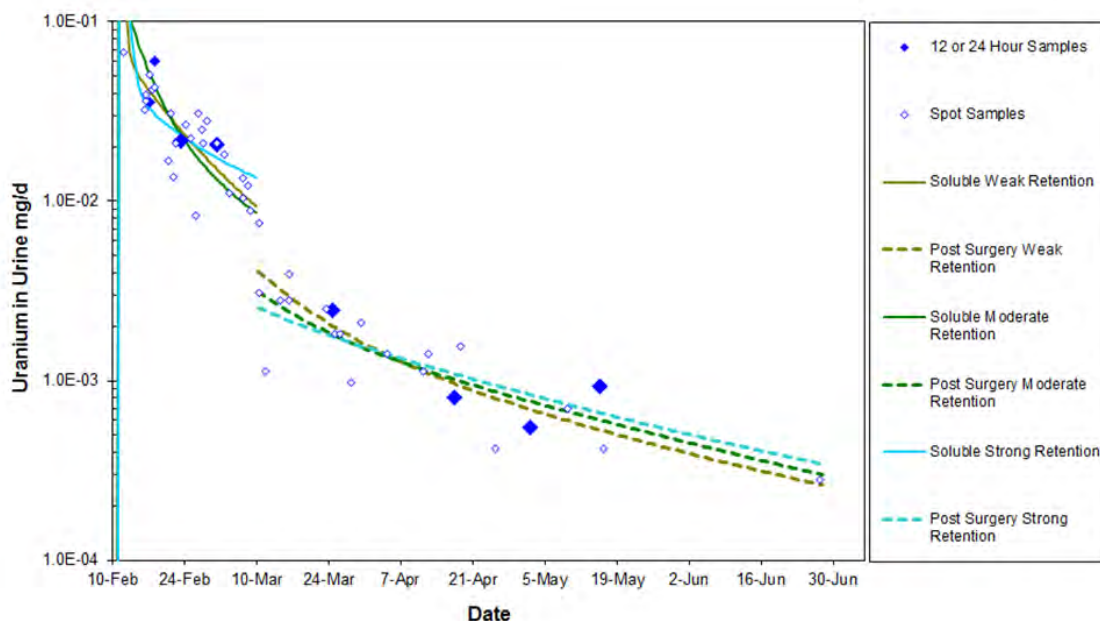
3.2 Dosimetric Analysis

The dose calculation for the skin from uranium in a wound is an unusual and challenging dosimetric problem. The overall approach was to estimate uranium intake and retention as determined by fitting the uranium in urine bioassay data to the NCRP Report 156 wound model with software package IMBA. Additional modelling of the uranium in wound was done with the assistance of Health Canada with the program AIDE. Data from monitoring of the uranium in the wound with Cameco's lung counter and related physical phantoms was also used to validate the modelling results. Finally, the dosimetric calculations had to account for the physical situation and ongoing medical developments (e.g. size of wound, impact of surgery), which complicated the analysis.

Prior to discussing the dosimetric calculations it is worthwhile to briefly review the main physical points of the wound itself. The worker's left index finger was lacerated by a sharp drum dryer blade that had UF₄ on it. The cut to the finger was estimated by the worker to be about "one inch across". Subsequent measurements of scar tissue confirmed this estimate with a measured length of 2 to 2.5 cm; the length of the cut was conservatively set at 2 cm for the purposes of dosimetry. The cut was relatively deep and went to the bone or very close to it and severed a nerve, which was the primary motivation for the follow-up surgery. Ultrasound measurements of the finger showed the depth of the cut, as measured by the skin to bone distance, to be 1.1 cm; for the purposes of dosimetry the depth of the cut was conservatively set at 1.0 cm.

Figure 2 shows observed uranium in urine data and the various urinary excretions curves using some of the NCRP wound models. There are several important points to Figure 2. First it is apparent there is a discontinuity in the urine data around March 9. There was reconstructive surgery performed on this date and the wound was cleaned out, which led to an immediate and significant decrease in the concentration of uranium in urine, which indicates that uranium was physically removed from the wound site. While this was a positive development, it did complicate the dosimetric analysis. Because of this, theoretical excretion curves were determined for the pre and post-surgery data separately. The observed urine data was taken while the worker was placed on work restrictions that minimized the likelihood of any exposures to uranium compounds. Upon returning to work at the end of June, after a plant shutdown, the worker submitted a urine sample and indicated a strong desire to return to normal work duties. As further bioassay data was unlikely to significantly improve the understanding of the nature of the intake, he was allowed to return work. Subsequent urine samples indicate that he had minor intakes from inhalation of soluble uranium compounds, which masked the signal from the uranium from the wound; note that dose from these intakes have been handled as part of Port Hope Conversion Facility's routine internal dosimetry program.

Figure 2: Uranium in Urine Excretion – Observed and Predicted from Wound Dosimetry Models.



From Figure 2 it is apparent that three of the models, that is, soluble weak retention, soluble moderate retention, and soluble strong retention, provide a reasonable fit to the excretion data. As the form of the uranium was a UF_4 powder, it is not surprising that fragment, particle, and colloid models do not fit the observed urine excretion pattern. In addition, UF_4 nominally has a medium solubility in simulated lung fluid studies, so it is not surprising that the “soluble avid retention” is also a poor fit to the data.

Table 2 provides a summary of the calculated initial intake into the wound from the three models that show a reasonable fit to the observed urine data. In addition, the table shows the effective dose for each of the models without accounting for the decrease in uranium in the wound post-surgery. This was done due to the limitations of IMBA in calculating the effective dose from a wound and provides an overestimate of the effective dose. This analysis shows that the effective dose from the wound is very small and of little concern.

Table 2: Estimated Wound Intakes from Urine Data

Model Name	Calculated Intake (mg U-Nat)	Effective Dose (mSv)
Soluble Weak Retention	3.03	0.16
Soluble Moderate Retention	2.34	0.13
Soluble Strong Retention	2.94	0.16

There is little statistical difference in the fits of the three models, as calculated by IMBA, with all having a probability of Chi-squared parameter at 1.0 (actually $p=0.999$ for soluble strong retention). To determine which of the NCRP wound models should be used, the predictions of the amount of uranium in the wound from the program AIDE were compared to measurements taken of the wound on February 17 and February 21 with Cameco's lung counter.

The efficiency of the lung counter for this particular situation was determined with a physical phantom of a hand provided by Health Canada [4]. Specifically, the efficiencies of the lung counter were determined with a line source of natural uranium and using 5 and 10 mm tissue equivalent overlays to assess the impact of varying depths of the contamination in the wound. Note that the calibration was done for four low energy peaks present in natural uranium (i.e., 16 keV, 63keV, 92 keV, and 186 keV) to give a range of predictions shown in Table 3.

Table 3: Predicted and Observed Uranium in Wound on February 19

Predicted Soluble Weak Retention	Predicted Soluble Moderate Retention	Predicted Soluble Strong Retention	Observed Range of U-Nat Present in Wound
0.06 mg U-Nat	0.23 mg U-Nat	1.27 mg U-Nat	0.21 to 0.57 mg U-Nat

The results of Table 3 show that predictions of the soluble moderate retention model fell within the range of the observed amount of uranium in the wound. The other two models were well outside the observed range of U-Nat that was measured and were therefore rejected. As a further indication of the inadequacy of the soluble strong retention model, another detailed measurement of the wound was taken on May 20 and no activity in the wound was detected. The soluble strong model predicted that there should have been activity in excess of the decision level, but none was detected. This further strengthened the conclusion that the soluble moderate retention model was the most compatible with the observed data.

The monitoring of the contamination in the wound with the lung counter provided some additional insights into the amount of uranium in the wound and its profile. Determining the profile of the contamination with depth in the wound is important because the dose to the skin depends upon how much uranium was deposited in the sensitive skin layer, which is 1 to 3 mm deep [5] with a nominal thickness of 1.25 mm [6]. The cut was 10 mm deep and if all the uranium was deposited deep in the cut the skin dose would be essentially zero. Because the efficiency of shielding with depth is a function of energy, the different low energy x-ray and gamma peaks can offer insights into how the uranium was deposited. Using a hand phantom made with parts supplied by Health Canada, the different efficiencies for four low energy peaks from a line source of natural uranium at varying depths (i.e. 0 mm, 5 mm, and 10 mm) and a uniform distribution of activity from the surface to 10 mm depth were determined.

The contamination profiles that yielded the most consistent results for all energy peaks were a line source located 5 mm below the surface of the skin and an even distribution of contamination in the cut (i.e., from 0 to 10 mm). In addition to Cameco's monitoring, Health Canada did detailed Monte Carlo modelling to see if it was possible to provide greater clarity in the distribution of uranium in the wound by looking at relative ratios of low energy peak heights. While there were some fits that suggested no contamination may be present to a depth 2 mm, the work also could not exclude the

possibility of uranium contamination being present with an even distribution along the cut to a depth of 10 mm [4]. Thus, for the purposes of the skin dose calculation the contamination was assumed to be evenly distributed throughout the entire plane of the cut.

The amount of the uranium in the wound at the time of the measurements with the lung counter was estimated to be 0.37 mg (U-Nat). This was quite close, but somewhat higher than the predicted amount of 0.23 mg (U-Nat) by the soluble moderate retention of the NCRP wound model based upon urinalysis data. It was reassuring that these two independent approaches yielded consistent results. It was difficult to determine which approach was more reliable, as there are considerable uncertainties with both (e.g. use of default wound solubility parameters, efficiencies based on assumed depth profiles of contamination). Given these uncertainties, it was decided to scale the initial intake so that the predicted amount of uranium in the wound on February 19 was the average results of the two approaches (i.e. 0.30 mg U-Nat). This increased the initial intake by a factor of 1.3 (i.e. 0.30/0.23), which also increased the final dose. This was viewed as a reasonably conservative approach to the dose calculation.

The Canadian Nuclear Safety Commission (CNSC) Radiation Protection Regulations [8] require that the committed equivalent dose be calculated for skin over an area of 1 cm². In this case because the contamination was natural uranium, the dose was completely dominated by alpha particles due to their energy, the use of the radiation weighting factor, and the short range of alpha particles in tissue means all the energy will be absorbed at the wound site.

To calculate the skin dose it was necessary to model the amount of uranium present in the wound as a function of time. The sensitive layer of the skin has a depth of 1 to 3 mm [5] with a nominal depth of 1.25 mm for reference man [6]. Because the wound and contamination extended beyond the layer of sensitive skin tissue, the calculated dose was independent of the exact depth of this layer. The reason for this is as the depth of the sensitive layer is increased the volume increases, which would lower the dose, but because the contamination extends past the skin layer, the amount of uranium also increases proportionally.

The dose was calculated with the following formula.

$$Dose\ rate = \bar{E}_{\alpha} \times 20 \div tissue\ mass \times \#of\ decays\ per\ second$$

The average alpha energy was taken from ICRP Publication 107 [7] and the tissue mass based upon a tissue depth of 1.25 mm and tissue density of 1.1 g/cm³ [5]. Because the uranium was assumed to be uniformly spread over the plane of the cut (2 cm x 1 cm), the amount of uranium in the present was scaled to that present in the sensitive volume (i.e., a factor of 0.0625=1/2 x 0.125/1.0). The detailed results are in Table 4.

Table 4: Dose Conversion Factor U-Nat Radionuclides

Nuclide	Average Energy (MeV)	Bq/mg U-Nat	Tissue Mass (kg)	Equivalent Dose Rate per mg U-Nat (mSv/s)
U-238	4.187	1.23E+01	1.36E-04	7.59E-05
U-234	4.76	1.23E+01	1.36E-04	8.63E-05
U-235	4.393	5.76E-01	1.36E-04	3.72E-06
Total mSv/s				1.66E-04

To calculate the equivalent dose to the skin the amount of uranium in the wound was modelled as a function of time. This is not possible with IMBA, but is an option with the software AIDE, hence it was to calculate the wound activity per unit intake for the soluble moderate retention model as a function of time. The dose was calculated by the following formula.

$$Dose = \sum_{i=0}^t Initial\ Intake \times Activity\ per\ unit\ take_i \times time_i \times 1.66 \times 10^{-4} mSv/s \quad (1)$$

where: time was in seconds.

For the period before the surgery (March 11) the dose calculation is straightforward. As noted previously, the initial intake into the wound was estimated to be 2.34 mg and then conservatively increased by a factor of 1.3 (i.e. 0.30/0.23) to agree with the average estimate of the amount of the uranium in the wound from the urine bioassay modelling and lung counter measurement on February 19. The equivalent dose for the period from February 10 to March 11 is estimated to be 132 mSv.

After the surgery on March 11, it is feasible that the committed equivalent dose to the skin was zero because all the uranium was removed in this zone. The surgery included removing the damaged tissue around original cut including some excess skin tissue. Deeper muscle tissue around the cut would not have been removed to the same degree and likely retained the uranium. This situation would explain the large drop in uranium in urine and hence the modelled uranium intake post-surgery; the intake from the post-surgery urine results was modelled to be only 37% of the intake from the pre-surgery urine results (i.e. 0.87 mg versus 2.34 mg). Nonetheless, the committed equivalent dose was calculated by conservatively assuming there was no preferential removal of uranium in the skin layer. This was done by scaling the modelled post-surgery intake from the uranium in urine data by the same factor of 1.3. On this basis the committed equivalent dose was calculated to be 178 mSv, which means that an additional equivalent dose of 46 mSv could be delivered to the skin over nearly 50 years post-surgery (i.e. to 2061). These results are summarized in Table 5.

Table 5: Summary of Equivalent Dose Calculation

Time Period	Equivalent Dose (mSv)
Incident to surgery (Feb 11 to Mar 11)	132
March 11 to 50 years post incident	46

From this analysis it can be concluded that the committed equivalent dose to the skin was well below the regulatory dose limit of 500 mSv [8]. The committed equivalent dose was probably less than 178 mSv, as it is likely most, if not all, of the uranium in the skin was removed during the surgery on March 11. This would have limited the committed equivalent dose to 132 mSv. However, to be conservative the value of 178 mSv was used for the reported committed equivalent dose to the skin. This calculated dose should only be viewed as one that meets specific regulatory requirements. As noted earlier, the committed effective dose to the worker is estimated to be 0.2 mSv, which is much less than the regulatory annual dose limit of 50 mSv.

4 CONCLUSION

Injuries caused by uranium-contaminated equipment need to be assessed for dosimetric implications. Experience to date suggests that only significant injuries have a reasonable potential to cause significant doses. The effective dose from natural uranium was found to be small, but the Canadian regulatory requirements for the skin dose calculations could result in a more significant committed equivalent dose. With regard to uranium ore, the main driver of the dose is Th-230 and substantive doses are possible even if the Th-230 is not detected in the urine. In both cases the urine samples were collected for several months, which enabled there to be a reasonable level of confidence in the modelled results. Finally, it was important to keep the workers informed of the results to ensure their ongoing cooperation in the follow-up work.

5 ACKNOWLEDGEMENTS

Cameco would like to thank Health Canada for its assistance and the use of a hand phantom.

6 REFERENCES

- [1] NCRP, 2006. Development of a Biokinetic Model for Radionuclide-Contaminated Wounds and Procedures for their Assessment, Dosimetry and Treatment. NCRP Report No. 156. National Council on Radiation Protection and Measurements.
- [2] IMBA Professional Plus version 4.1.3.1 2009. Health Protection Agency. Birchall, A., James, A., Jarvis, N., Davis, K., Puncher, M., Smith, F., Peach, A.
- [3] AIDE Version 6.1 2009. Bertelli, L.
- [4] Health Canada 2011. Kramer, G., personal communication.
- [5] ICRP, 1992. The Biological Basis for Dose Limitation in the Skin. ICRP Publication 59. Ann. ICRP 22 (2).
- [6] ICRP, 1975. Report on the Task Group on Reference Man. ICRP Publication 26.
- [7] ICRP, 2008. Nuclear Decay Data for Dosimetric Calculations. ICRP Publication 107. Ann. ICRP 38 (3).
- [8] Canadian Nuclear Safety Commission 2000. Radiation Protection Regulations SOR/2000-203.

Response of $^{10}\text{B}+\text{ZnS}(\text{Ag})$ as neutron detector in Radiation Portal Monitors

Karen A. Guzmán-García^{a*}, H.R. Vega-Carrillo^b, Eduardo Gallego^a, Alfredo Lorente^a, Juan A. González^c

^aETSI Industriales, Universidad Politécnica de Madrid, José Gutiérrez Abascal, 2, 28006 Madrid, Spain.

^bUnidad Académica de Estudios Nucleares, Universidad Autónoma de Zacatecas, Ciprés 10, Fracc. La Peñuela, 98000, Zacatecas, Mexico.

^cETSI Caminos, Canales y Puertos, Universidad Politécnica de Madrid, Profesor Aranguren 3, 28040 Madrid, Spain.

Abstract. Radiation Portal Monitors installed in border areas to detect illicit traffic of radioactive and nuclear materials, have the capability of detecting both gamma rays and neutrons. Neutron detection is important for homeland security to detect Special Nuclear Materials. Usually, neutron detectors based on ^3He pressurized tubes have been deployed, but this is being affected by the scarcity in ^3He supplies; so alternatives to ^3He for thermal neutron detection are under investigation. The aim of this work is to study the suitability of multi-layered $^{10}\text{B}+\text{ZnS}(\text{Ag})$ neutron detectors, as an innovative replacement to ^3He detectors. Using the MCNPX code, the response of these detectors was calculated from the number of $^{10}\text{B}(\text{n},\alpha)^7\text{Li}$ reactions induced for different geometries and varying the thickness of the intermediate layers of PMMA used as light guide. Results for a ^{252}Cf neutron source at 200 cm distance in free air and in air with ground show that the closer the detector is to the ground, and the higher thickness of PMMA, the greater is the detector efficiency. We conclude that $^{10}\text{B}+\text{ZnS}(\text{Ag})$ detectors could be considered as an alternative to the ^3He detectors.

KEYWORDS: *neutron detectors; special nuclear materials SNM; radiation portal monitors RPMs; ^3He neutron detectors.*

1 INTRODUCTION

Radiation Portal Monitors systems (RPM) usually consist on a set of neutron and gamma-ray detectors, normally installed in border areas, with the purpose to intercept illicit traffic of nuclear or radioactive materials. Neutron detectors are used for Special Nuclear Material (SNM) detection, like ^{239}Pu , with ^3He proportional counters being widely used [1, 2]. However, since 2009, the ^3He shortage has encouraged searching for alternative neutron detectors [3].

The aim of this work was to study the features of $^{10}\text{B}+\text{ZnS}(\text{Ag})$ scintillation detectors to detect neutrons in RPMs. These detectors have a $\text{ZnS}(\text{Ag})$ scintillator mixed with enriched ^{10}B . The neutron response of different $^{10}\text{B}+\text{ZnS}(\text{Ag})$ detectors, with different arrays, were calculated by Monte Carlo methods using the MCNPX code [4]. The neutron response was assessed from the number of $^{10}\text{B}(\text{n},\alpha)^7\text{Li}$ reactions induced, by 29 monoenergetic sources and by a ^{252}Cf neutron source at 200 cm distance.

2 MATERIALS AND METHODS

2.1 Description of the N-15 neutron detector of $^{10}\text{B}+\text{ZnS}(\text{Ag})$

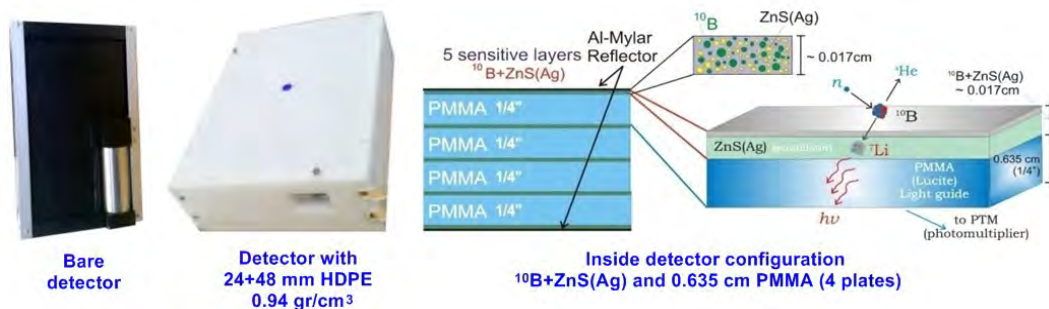
The N-15 detection system was manufactured by BridgePort Instruments, LLC [5]. This detector uses a mixture of $\text{ZnS}(\text{Ag})$ with highly enriched ^{10}B as neutron detector and several intermediate screens on polymethyl methacrylate (PMMA or Lucite) acting as guide of light pulses to a photomultiplier tube (PTM). The PTM has an embedded high voltage supply and multichannel analyser eMorpho® digital electronics. The external size of the bare N-15 detector is 23 x 36 x 4 cm³.

* Presenting author, e-mail: ingkarenguzman@gmail.com

The detector's sensitive area is composed of five transparent ~ 0.017 cm-thick layers of a mixture of ZnS(Ag) and ^{10}B enriched boron. These layers are arranged in four PMMA plates sizing $23 \times 36 \times 0.635$ cm³. The PMMA function is twofold, as light guide and as neutron moderator. All the set is surrounded by $\sim 8\mu\text{m}$ thick aluminium Mylar as light reflector.

The detector is covered by an outer moderator made of high density polyethylene (0.94 g cm⁻³), HDPE; the moderator thickness is 48 mm in the back and lateral faces, 36 mm in the top and bottom, and 24 mm-thick in the front ($24+48$ mm). Figure 1 shows the overall geometry of inside, bare and moderated detector.

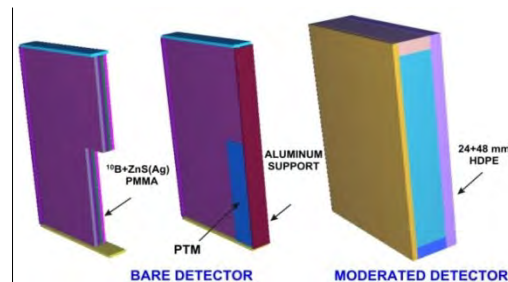
Figure 1: N-15 detector; bare and moderated detector.



2.2 Monte Carlo calculations

Using the MCNPX code [4], a model of the N-15 detector was built including all details such as: the sensitive layers ~ 0.017 cm, the four plates of PMMA 0.635 cm-thickness, the PMT as a cylinder of $5.7\text{Ø} \times 19.4$ cm and the moderator $24+48$ mm HDPE. Here, the PMT was modelled as an empty cylinder of glass (Figure 2).

Figure 2: N-15 geometry (MCNPX Model)

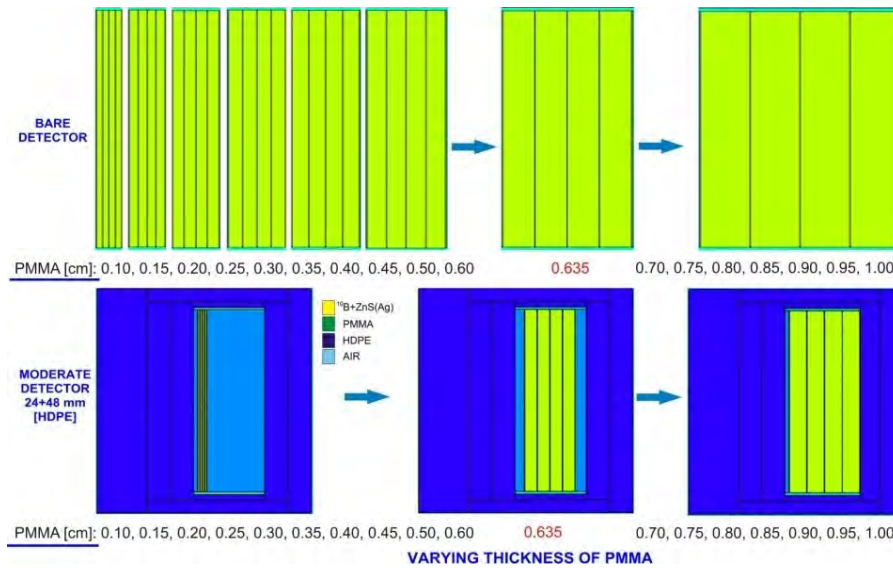


In a previous work, the detector response was calculated for 29 simulated monoenergetic neutron sources with energies ranging from 10^{-9} to 20 MeV [6], for the bare detector (without moderator) and with the HDPE moderator. The response was estimated using tally f4 [7] where the number of $^{10}\text{B}(n,\alpha)^7\text{Li}$ reactions were calculated, using the target 107 for the reaction [8].

2.2.1 Response evaluation varying PMMA thickness

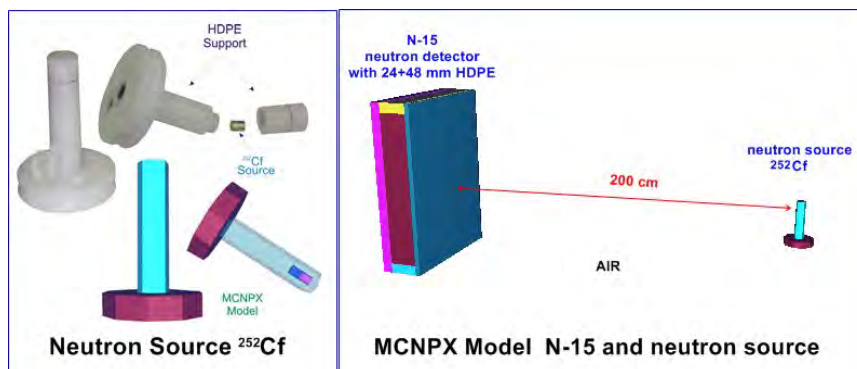
Using MCNPX different models were made, varying the thickness of the inner PMMA layers [0.1, 0.15, 0.20, 0.25, 0.30, 0.35, 0.40, 0.45, 0.50, 0.55, 0.60, **0.635**, 0.70, 0.75, 0.80, 0.85, 0.90, 0.95, 1.00 cm-thickness] (Figure 3); these thicknesses will be compared to 0.635 cm-thick PMMA from the actual detector thickness.

Figure 3: N-15 geometry (MCNPX Model); varying the PMMA-thickness, bare and moderated detector.



Here the response was estimated in counts per second per nanogram of ^{252}Cf [cps-ng ^{252}Cf] when the detector was located at 200 cm from a ^{252}Cf neutron source. In this case, the neutron source was modelled from the existing neutron source in the Laboratorio de Medidas Neutrónicas, Universidad Politécnica de Madrid, LMN-UPM, as show in Figure 4.

Figure 4: ^{252}Cf neutron source from LMN-UPM and MCNPX model.

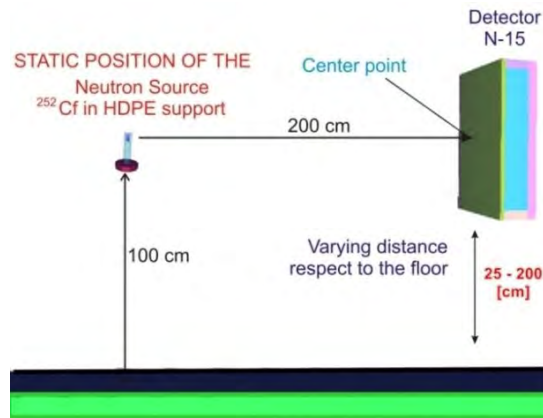


The response was also calculated using 29 monoenergetic neutron sources, for the bare detector and with 24+48 mm HDPE, both for the actual detector with 0.635 cm PMMA layers and for an increased PMMA thickness of 0.800 cm.

2.2.2 Response evaluation varying the distance with respect to the ground

Models were made with the N-15 detector positioned 200 cm from the ^{252}Cf source and the response was calculated varying the distance between the detector's centre and the floor at 25, 50, 75, 100, 125, 150, 175 and 200 cm as it is shown in Figure 5. Here, the ^{252}Cf source was fixed at 100 cm above the floor. This response was in the aim to study the room-return effect [9] above ground.

Figure 5: N-15 (MCNP Model); varying N-15 distances respect to the ground.

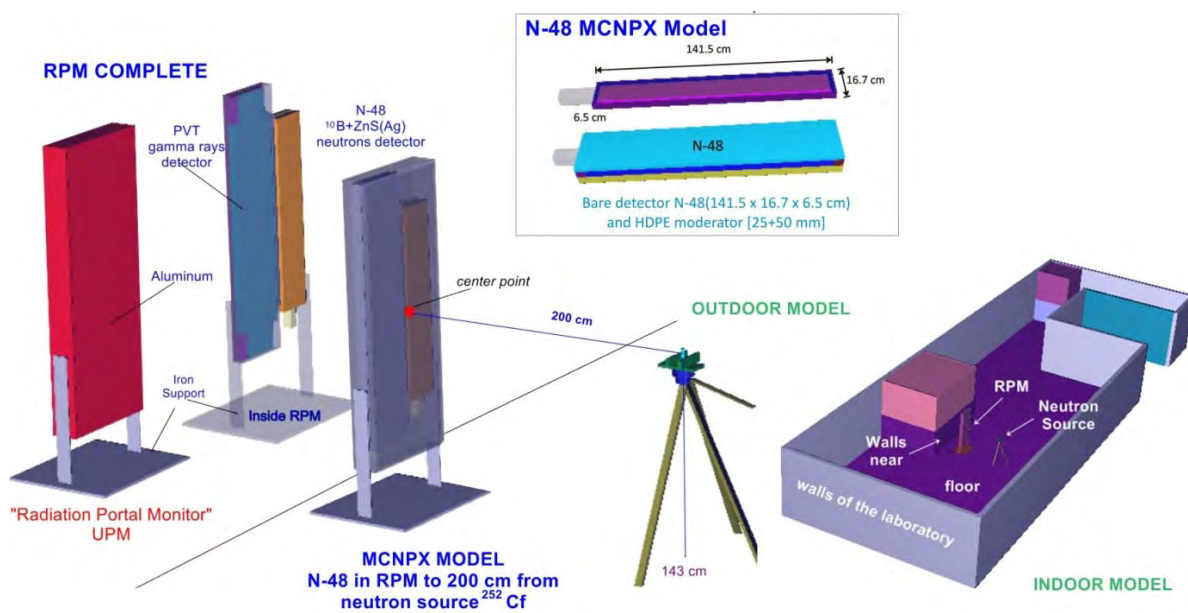


2.2.3 MCNPX model of a large detector model N-48 in a RPM

The N-48 detector has an external size of 141.5 x 16.7 x 6.35 cm³ [10]. Using MCNPX code, a model was built including all the detector details: the sensitive area, composed of five transparent ~0.017 cm-thick layers of a mixture of ZnS(Ag) and 95% ¹⁰B enriched boron –the Ag was not included in the model–; like in the N-15 detector, these layers are arranged in four plates of PMMA with 1.19 g/cm³ density, sizing 120 x 15.2 x 0.635 cm³; the photomultiplier tube, modelled as an empty cylinder and the aluminium supports.

In this case the detector is installed in a RPM together with a gamma detector of PVT, in similar conditions to its normal operation at customs. Two conditions are simulated: outdoors with only air and ground and inside of a laboratory with walls around. The response was estimated in cps-ng of ²⁵²Cf of a neutron source of ²⁵²Cf located at 200 cm distance. Figure 6 shows the overall geometry according to the MCNPX model.

Figure 6: Radiation Portal Monitor with neutron detector ¹⁰B+ZnS(Ag) type N-48. MCNPX models of the outdoors and indoors conditions simulated.



In all Monte Carlo calculations, the number of histories was large enough to obtain uncertainties less than 5%. For the MCNPX calculations, cross-sections were taken from the ENDF/B-VI library, where the $S(\alpha, \beta)$ treatment was included to take into account the thermalized neutron interactions [7].

3 RESULTS

3.1.1 Performance of detector (N-15) with varying PMMA thickness

Figure 7 shows the response of both cases of PMMA-thickness: the actual thickness of PMMA N-15 detector, 0.635 cm, and a greater thickness of 0.800 cm, for 29 monoenergetic neutrons sources; bare and moderated detector (HDPE 24+48).

The bare detector clearly points the difference between both cases, showing that the 0.800 cm thick-PMMA detector has a similar response but with a greater efficiency with respect to the actual 0.635 cm-thick detector. In the moderated detector, the response is less sensitive to the change in PMMA thickness, due to the moderation effect of the HDPE case; however, it still shows that the 0.800 cm-thick has a higher response than the actual 0.635 cm-thick detector.

Figure 7: Calculated N-15 detector response as a function of neutron energy, for PMMA-thickness 0.635 cm (actual detector) and 0.800 cm (comparison model)

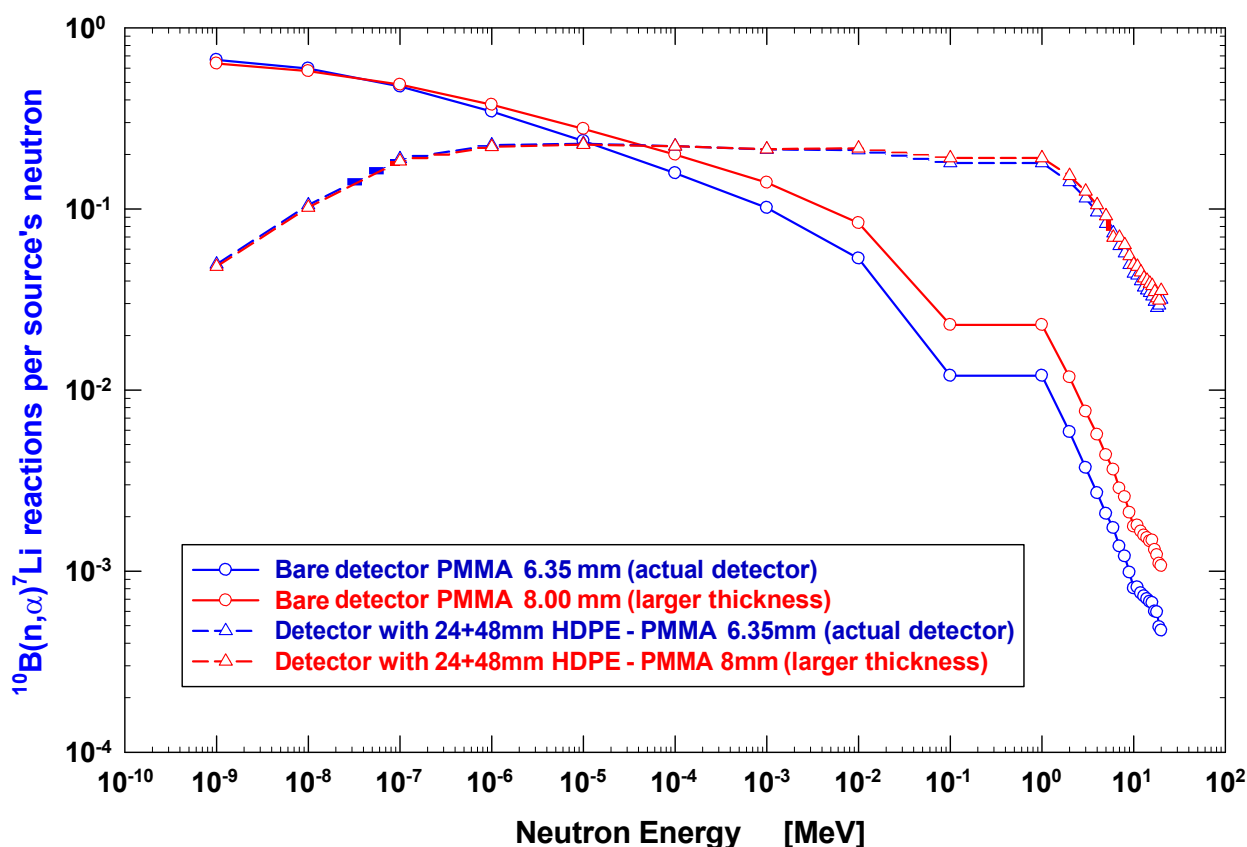
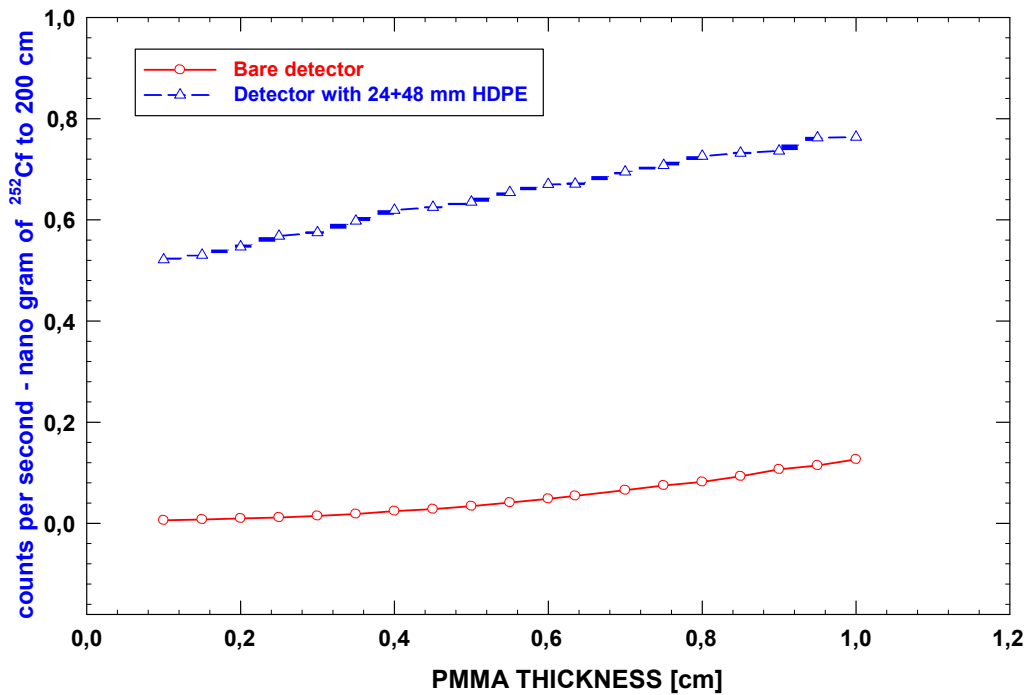


Table 1 below shows the calculated count rates per ng of ^{252}Cf at 200 in air. The calculated values were scaled up to neutron source strength, where 1 ng of ^{252}Cf produces 2340 n/s [11]. Table 1 includes percent difference in response with respect to the actual detector, showing that an increase of the PMMA plates thickness up to 1 cm can increase the efficiency of detection up to ~134% for bare detector and up to about ~13% in the case of the moderated detector with 24+48 mm HDPE, Figure 5.

Table 1: Calculated count rates per ng of ²⁵²Cf and difference in percent respect the actual detector (0.635 cm thickness PMMA)

PMMA thickness [cm]	Bare detector MCNPX cps-ng ²⁵² Cf	~ % respect to the 0.635 cm PMMA	Detector with HDPE MCNPX cps-ng ²⁵² Cf	~ % respect to the 0.635 cm PMMA
0.10	0,0056 ± 0.0011	-89,57	0,521± 0.020	-22,31
0.15	0,0073 ± 0.0013	-86,51	0,530 ± 0.020	-20,95
0.20	0,0094 ± 0.0016	-82,67	0,546 ± 0.022	-18,50
0.25	0,0112 ± 0.0018	-79,23	0,567 ± 0.022	-15,35
0.30	0,0143 ± 0.0022	-73,38	0,575 ± 0.023	-14,29
0.35	0,0183 ± 0.0024	-66,33	0,597 ± 0.024	-10,89
0.40	0,0239 ± 0.0031	-55,60	0,619 ± 0.024	-7,70
0.45	0,0276 ± 0.0033	-48,67	0,625 ± 0.024	-6,82
0.50	0,0336 ± 0.0037	-37,50	0,635 ± 0.025	-5,30
0.55	0,0407 ± 0.0042	-24,56	0,654 ± 0.026	-2,46
0.60	0,0478 ± 0.0047	-10,83	0,670 ± 0.026	-0,091
0.635	0,0538 ± 0.0050	-	0,671 ± 0.026	-
0.70	0,0653 ± 0.0057	21,288	0,695 ± 0.027	3,60
0.75	0,0745 ± 0.0061	38,42	0,708 ± 0.028	5,52
0.80	0,0816 ± 0.0063	51,57	0,726 ± 0.028	8,23
0.85	0,0925 ± 0.0068	71,76	0,732 ± 0.028	9,15
0.90	0,1063 ± 0.0075	97,42	0,736 ± 0.028	9,77
0.95	0,1139 ± 0.0078	111,45	0,762 ± 0.028	13,66
1.00	0,1260 ± 0.0084	134,08	0,764 ± 0.029	13,89

Figure 8: Calculated N-15 detector response with varying PMMA-thickness; bare and moderated detector



3.1.2 Detector performance (N-15) varying the position with respect to the ground

Table 2 shows the calculated detectors response, in cps per ng of ^{252}Cf , in free air conditions with the centre of the detector located at varying distances from the floor. Uncertainties of these results are only those from the Monte Carlo calculations.

Table 2: Calculated count rates per ng of ^{252}Cf , varying the position of detector above ground at 200 cm from the ^{252}Cf source.

Distance above ground (cm)	Detector N-15
200	0.57 ± 0.04
175	0.66 ± 0.04
150	0.70 ± 0.04
125	0.81 ± 0.05
100	0.85 ± 0.05
75	0.86 ± 0.05
50	0.83 ± 0.05
25	0.78 ± 0.04

The detector efficiency varies depending on the position with respect to the floor. The detector receives the largest count rate when its centre is located at 75 cm above floor, probably due the amount of scattered neutrons from the floor.

3.1.3 Performance of a large detector (N-48) in a RPM

Table 3 shows the calculated response of a large detector (N-48 type), in a complete RPM as in Figure 6, in cps per ng of ^{252}Cf , for representative indoors and outdoors conditions with the centre of the detector located at 200 cm from the neutron source of ^{252}Cf . Again, the calculated values were scaled up to the neutron source strength, where 1 ng of ^{252}Cf produces 2340 n/s [11].

Table 3: Calculated count rates per ng of ^{252}Cf for the large N-48 detector in the RPM.

MCNPX calculated count rates at 200 cm from the ^{252}Cf source [cps-ng ^{252}Cf]		
Detector type	Indoors	Outdoors
N-48	2.14 ± 0.06	1.57 ± 0.04

As it can be observed, the detector efficiency is highly variable depending on the environment conditions, with a count rate approximately higher in up to 38% indoors, due to neutron scattering by the walls that contributes to the increased count rate in that point.

4 CONCLUSIONS

One first conclusion from the simulations presented here is that a cost-effective way to improve efficiency of multi-layered $^{10}\text{B}+\text{ZnS}(\text{Ag})$ neutron detectors, is to increase the thickness of the intermediate PMMA layers: its increase from 0.635 cm to 1.000 cm, can amplify up to 13% the detection efficiency of the moderated detector, while the cost increase would be not relevant.

Another conclusion is that for this kind of detectors, the position with respect to the ground is an important feature, due to the detector response to scattered neutrons [9]. Therefore, the use of these detectors in actual RPM should be characterized in situ according to their position above ground.

Finally, it appears that $^{10}\text{B}+\text{ZnS}(\text{Ag})$ detectors are an interesting alternative to replace ^3He detectors in RPMs. By improving their geometry and by increasing the amount of ^{10}B it would be feasible to increase the detector efficiency, aiming to reach the target of 2.5 cps/ng ^{252}Cf , considered as a goal to use this type of detectors as an alternative in RPMs [12] that could satisfy the ANSI standard requirement[13].

5 ACKNOWLEDGEMENTS

The first author, K.A. Guzman, thanks the PhD grant received from CONACyT and COZCyT, Mexico.

6 REFERENCES

- [1] Kouzes RT, JH Ely, LE Erikson, et al, 2010. Neutron detection alternatives to for ^3He homeland security. *Nuclear Instruments and Methods in Physics Research A*, 623, pp. 1035-1045.
- [2] Cooper RG, 2004. SNS Detector Plans *Nuclear Instruments and Methods. Physics Research A* 529: 394– 398.
- [3] Kouzes RT. 2009. The ^3He Supply Problem. Technical Report PNNL-18388, Pacific Northwest National Laboratory, Richland, WA.
- [4] Pelowitz DB. 2008. MCNPX User's Manual Version 2.6.0. Report LA-Cp-071463. Los Alamos National Laboratory. USA.
- [5] BridgePort Instruments, LLC. 2013. *Neutron Detector System R2D-nDet, Device-Specific data Sheet*. R2D-nDet-15 ds 1095, 03. <<http://www.bridgeportinstruments.com/>>
- [6] Guzmán-García, K.A., Vega-Carrillo, H.R., Gallego E., et al, 2016. Study of a $^{10}\text{B}+\text{ZnS}(\text{Ag})$ neutron detector as an alternative to ^3He -based detectors in Homeland Security. *Applied Radiation and Isotopes* (in press). DOI: 10.1016/j.apradiso.2016.03.015.
- [7] Vega-Carrillo H.R., Guzmán-García K.A., Gallego E. et al, 2014. Passive neutron area monitor with pairs of TLDs as neutron detector. *Radiation Measurements* 69, 30-34. DOI:10.1016/j.radmeas.2014.08.006.
- [8] Vega-Carrillo H.R., Barquero R., Mercado G.A., 2014. Passive neutron area monitor with CR39. *International Journal of Radiation Research* 11, 149-153.
- [9] Vega-Carrillo H.R., Manzanares E., Iñiguez M., et al, 2007. Study of room-return neutrons. *Radiation Measurements* 42, 413-419. DOI: 10.1016/j.radmeas.2007.01.036.
- [10] BridgePort Instruments, LLC. 2011. *Neutron Detector System, Device-Specific data Sheet*. R2D-nDet-48.<<http://www.bridgeportinstruments.com/>>
- [11] Vega-Carrillo HR. 1988. Medición del espectro de neutrones y rayos gamma de una fuente de Californio-252 en un medio de tejido equivalente. *Revista Mexicana de Física* 34, 25-29.
- [12] Woodring M.L., Ely J.H., Kouzes R.T., et al, 2010. Boron-lined multitube neutron proportional counters test. Report PNNL-19726. Pacific Northwest National Laboratory, USA.
- [13] ANSI N42.35. 2006. American National Standards Institute, IEEE, New York, NY. Baker.

Wrist, finger, and crystalline dosimetry study with radiopharmacists and nursing technicians for various applications and tests, using various radiopharmaceuticals, for adjustment of a percentage factor between difference values obtained at the extremities to optimize the dosimetry in nuclear medicine services.

Maria Inês Calil Cury Guimarães^a, Sato, Karen A. K.^a, Leandro F. Souza^a, Leia R. Santo^a, Elaine C. Santo^a, Ivani B. Melo^a, Heber S. Videira^b, Julia A. Gonzalez^a, Carlos A. Buchpiguel^a, Josefina da Silva Santos^a, Adélia Sahyun^c

^a Centro de Medicina Nuclear – InRadHC- FM Universidade de São Paulo – Brazil.

^b Cyclopet – Brazil.

^c Empresa Átomo – Brazil.

Abstract. The doses received by nuclear medicine workers, radiopharmacists and nursing technicians, in their extremities is a well-known concern. The ring-shaped dosimeter is usually not well accepted by most workers, who claim to have trouble adapting. This study gets the dosimetry of the extremities and of crystallines of workers who inject or label. Those data was used in finding a correlation factor that fits a ratio of the difference between the values obtained at the extremities. Four workers with TLD, ring, and wrist dosimeters, goggles without lenses with dosimeters in their temples participated. Radionuclides used: ^{99m}Tc, ⁶⁷Ga, ¹⁸F, ¹³¹I and ¹¹¹In. They were performed for ^{99m}Tc: 20 elutions (504,384 MBq); 49 lables (258,075 MBq) and 199 fractionation (143,346.51 MBq). 14 fractionations for ¹⁸F (3,885.74 MBq), 4 procedures with ¹³¹I (266.4 MBq), 3 fractioning of ⁶⁷Ga (886.89 MBq) and 1 for ¹¹¹In (185 MBq). The ring dosimeter presented a dose of 11 mSv, while the pulse dosimeter registered 7.78 mSv on the right and 5.40 mSv on the left, for radiopharmaceutical. The goggles used indicated a dose of 0.43 mSv on the left side and on the right side 0.52 mSv. The nursing team showed: nurse A: 1.13 mSv in the ring, and 0.23 on the wrist. Nurse B: 1.11 mSv in ring and 0.90 mSv in wrist dosimeters, nurse C: 0.73 mSv in ring and 0.56 mSv in wrist. The goggles were worn only by nurse B and it indicated 0.19 mSv. The differences between the doses received by workers wrists and rings were from 20% to 30%. The dose to the crystalline is in accordance with the recommended limits. Finding a factor of reliability between wrist and finger dosimetry will facilitate the optimization of this dosimetry and help workers and the services.

KEYWORDS: *dosimetry; extremity; crystalline; radiopharmaceuticals; optimization.*

1 INTRODUCTION

For workers in nuclear medicine, especially the radiopharmaceutical and nursing technicians who apply the medication to the patients, the final doses they receive is a concern. Although the annual equivalent dose limit for these workers extremities is high (500 mSv / year), the doses have to be controlled and linked to good practices¹.

Currently in Brazil there are 11 certified laboratories for the provision of external individual monitoring service and not all of them provide ring dosimetry. This type of dosimeter is also not well accepted by the majority of workers, who claim to feel much difficulty in using both ring and glove. Moreover, they also show concern about throwing the ring dosimeter away when disposing the gloves in the contaminated waste.

As an alternative to this situation, there is wrist dosimetry which is also located in the ends of the worker. Nevertheless, many radioprotection organizations claim this assessment of equivalent dose received by the worker at the ends is not sufficient to evaluate the dose in the final ends. It is said that there is a potential difference between these kinds of measurements^{2,3}.

In order to improve the quality of dosimetry performed in nuclear medicine services, this work focuses in the dosimetry of the extremities, fingers and wrists, and eye crystalline of workers. Those workers are responsible for injecting in patients (nursing technicians) and withdraw, mark, and distributing radiopharmaceuticals (pharmaceutics), and find a correlation factor which set a percentage difference between the values obtained in these ends. With these data we can choose between the use of ring

dosimetry or the possibility of continuing the pulse dosimetry, therefore known the percentual of this difference can optimize dosimetry and thus improve the quality of measurements.

2 METHODS

They are being studied four workers who directly handle radioactive material and are using each at the ends: a dosimeter type ring and a wrist, with the exception of radiopharmaceutical that uses a dosimeter on each wrist and a ring. The dosimeters are TL (thermoluminescent), and have been adapted for use in finger. Individuals Occupationally Exposed (IOE's), also use the dosimeter chest TL in addition to the ends dosimeters. It was also placed in a safety goggle that protects against biological material a dosimeter in each rod to measure the radiation that can reach the worker's crystalline. Each team has one goggle, but only a worker uses it in each team. Radionuclides used in the period were: ^{99m}Tc , ^{67}Ga , ^{18}F , ^{131}I e ^{111}In .

3 RESULTS

The radiopharmacist recorded for the period with respect to ^{99m}Tc radioisotope, a total of 20 elutions (13,632 or 504,384 MBq mCi); 49 marks (258,075 GBq or 6,975 mCi) and 199 fractioning (143,346.51 MBq). Were performed 14 fractioning for radioisotope ^{18}F (3774.74 105.02 MBq or mCi); 4 procedures with ^{131}I (266.4 MBq or 7.2 mCi), 3 fractioning of ^{67}Ga radioisotope (886.89 MBq or 23.97 mCi) and 1 to ^{111}In (or 185 MBq 5 mCi). The ring type dosimeter used by the worker registered a dose of 11 mSv, while the right wrist showed dose of 7.78 mSv and the left and 5.40 mSv. The radiopharmaceutical is right-handed. The goggles presented dose of 0.43 mSv left and right side 0.52 mSv. The recorded time work carried out by professional was between 30 seconds of removing the material and 1 minute in the elutions.

The nursing staff⁶, for the same amount of activity, except for the marking and the elutions, showed the following results:

- Nurse A: 1.13 mSv in the ring and 0.23 on the wrist;
- Nurse B: 1.11 mSv and 0.90 mSv ring pulse;
- Nurse C: 0.73 mSv and 0.56 mSv in the ring on the wrist.

The goggles were used only by nurse B and it was registered 0.19 mSv on the right and BG on the left. The distance between the position of the eyes of the IOE and the radioactive material to be applied to the patient's arm, has approximately between 30 and 40 cm. The application duration is approximately 1 minute.

Table 1: Presentation of doses obtained to wrist, ring and crystalline measures for a month for Individuals Occupationally Exposed (IOE's) in Nuclear Medicine service.

IOE	RIGHT WRIST (mSv)	LEFT WRIST (mSv)	RING (mSv)	ROD GOGGLES RIGHT (mSv)	ROD GOGGLES LEFT (mSv)
RADIOPHARMA/	7.78	5.40	11	0.52	0.43
NURSE: A	0.23		1.13		
NURSE: B	0.90		1.11	0.19	BG
NURSE: C	0.56		0.73		

The difference between the doses received by workers at the wrists and rings was between 20% and 30%, which already shows a good standard for use of pulse dosimetry using this factor correction if future doses are present within these limits adopted in the country. The dosimetry of the crystalline stayed with low levels and considerably below the dose limit which is 20 mSv per year^{4,5}.

4 DISCUSSION

The data also show that the workers have a good technical efficiency, since their doses are lower than the standards established by current standards in the country and the recommendations made by global radioprotection organizations.

5 CONCLUSION

Finding a factor of reliability between wrist and finger dosimetry can facilitate the optimization of this dosimetry and help workers and services that find it difficult to adopt this methodology to have greater control over their exposure.

6 ACKNOWLEDGMENT

Special Thanks to Rodrigo Calil Cury Guimarães and Olavo de Mendonça Guimarães for help in data review.

7 REFERENCES

- [1] IAEA- Safety Standards Series Assessment of Occupational Exposure Due to External Sources of Radiation Jointly Sponsored By The International Atomic Energy Agency And The International Labour Office Safety Guide No. RS-G-1.3 (1999).
- [2] International Commission on Radiological Protection. ICRP Publication 103. Recommendations of the ICRP. Annals of the ICRP, vol. 37/2-4. Elsevier; 2008.
- [3] International Commission on Radiological Protection. Recommendations of the International Commission on radiological Protection. ICRP Publication 60 (Oxford Pergamon) (1990).
- [4] Norma CNEN-NN 3.05 - Requisitos de Segurança e Proteção Radiológica para Serviços de Medicina Nuclear (Resolução CNEN 159/13). Dezembro de 2013.
- [5] Norma CNEN-NN 3.01 – Diretrizes Básicas de Proteção Radiológica. Resolução 164/14. Março de 2014.
- [6] Teófilo Moltó Caracena, João G. M. Gonçalves, Paolo Peerani, Eduardo Vendrell. *Virtual Reality Based Accurate Radioactive Source Representation And Dosimetry For Training Applications*: European Commission - Joint Research Centre, Ispra, Italy.

Direct Surface Contamination Measurement of Low Energy Beta and Electron Capture Isotopes

Michael Iwatschenko-Borho*, Reinhard Loew

Thermo Fisher Scientific Messtechnik GmbH, Frauenaauracher Str. 96, 91056 Erlangen, Germany

Abstract. Most surface contamination survey meters have a very low sensitivity for electron capture (EC) and low energy (LE) beta emitters. This work proposes the direct measurement of such surface contamination by a dual scintillation probe in a new measuring mode as a fast and straightforward alternative to laboratory analysis via liquid scintillation techniques. This new mode can be alternatively selected and complements the normal usage of a dual probe for beta / alpha discrimination. Compared to most conventional beta/gamma friskers an order of magnitude enhancement of detection sensitivity can be achieved. Additionally it is shown, that this new operation mode provides an improved detection limit and even more significant improvement of the signal to noise ratio for further isotopes such as C-14 (or S-35) under difficult (elevated and/or variable) gamma background conditions.

1 INTRODUCTION

A number of neutron activation products, that are relevant during operation or decommissioning of a nuclear power plant, are sometimes referred to as "hard-to-detect isotopes" due to the lack of energetic radioactive emission.

Table 1: Characteristics of some activation products [1]

Half-life (a)	5730	0,24	0,08	0,85	2,7	100
Beta max (keV)	156	168				66
X-ray (keV)			5	5,5	6	
Emission probability			22 %	25 %	28 %	
Gamma (keV)			320	835		
Emission probability			9,8 %	100 %		

Some of those isotopes need to be considered as well in hospitals (S-35, Cr-51) or for leakage testing of X- ray fluorescence, - diffraction and -scattering devices (Fe-55) and gas chromatography instruments (Ni-63). The screening levels for clearance is typically rather high for these isotopes (100 Bq/cm²) with the exception of Mn-54 where a level of 0,1 Bq/cm² [2] has recently been proposed.

For direct contamination measurement of those activation products it is known that flow type gas filled detectors containing Argon can be used. Alternatively thin inorganic scintillators, such as CsI(Tl) or NaI(Tl), preferentially with Beryllium entrance window, can be applied for EC-nuclide detection. Unfortunately these detectors are quite fragile and expensive.

This work is investigating the possibility to use the less cumbersome and less expensive large area detectors based on ZnS(Ag) coated organic scintillators (Fig. 1). These detectors are well known and

* Presenting author, e-mail: michael.iwatschenko@thermofisher.com

established for the measurement of higher energy beta and alpha general purpose surface contamination monitoring. The ZnS(Ag) layer provides a high light output compared to the plastic scintillator, so any ionizing particles that are stopped in the layer will provide a brighter signal than particles stopped in the plastic. This fact is used to discriminate alpha particles from high energy beta particles and has been used for simultaneous alpha/beta measurement for decades.

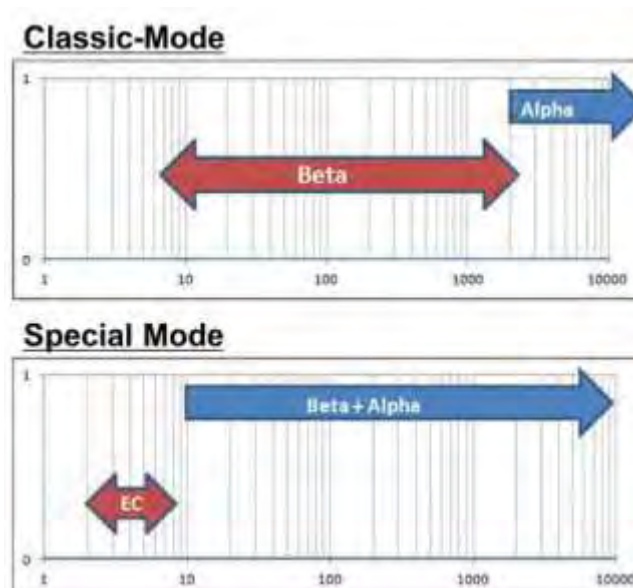
Figure 1: RadEye SX connected to 100 cm² dual probe DP6



2 IMPLEMENTATION OF THE NEW MEASUREMENT CONCEPT

The popular dual scintillation probe DP6AD (or DP6BD) has been in production for more than 2 decades: Its protective grille has a transmission of 80 % and the mylar entrance window of 1,2 mg/cm² provides good transmission for the X-rays of the EC nuclides and decent transmission for low energy betas. Using specially selected low noise DP6 probes, indicated by a “+” suffix and suitable and proprietary electronic circuitry and algorithms, the principle of signal enhancement for short range particles, stopped in the ZnS(Ag) layer, can be applied to EC/ LE-beta isotopes too. For that purpose a new measuring mode “Special Mode” (Fig. 2) has been implemented in the general purpose survey meter RadEye SX which complements the normal usage of the dual probe for beta/alpha discrimination.

Figure 2: Schematic description of the energy ranges (keV) for 2 alternative operation modes



The narrow pulse height window for the EC and low energy beta radiation rejects most of the normal background events in the plastic scintillator caused by gamma radiation and secondary cosmic radiation, since those events mostly deposit much more energy in the plastic scintillator. Thus a win-win situation arises in respect to the detection of Fe-55 or Ni-63 by the increased signal amplification and the reduction of the gamma and muon background count rate due to the upper threshold of the energy window.

3 DUAL VERSUS BETA DETECTOR

Comparison measurements were performed in 3 mm distance with 10 cm x 15 cm² large area sources overlapping the detector area of 6,7 x 15 cm². The same photomultiplier, entrance window, window grid and detector housing was used for both sets of measurements in order to exclude any individual variance between the instruments that was unrelated to the scintillator and operation mode.

Table 2: Comparison of Background and Efficiency for Dual and Beta Detector

Gamma Background or Nuclide	Measured Unit	Dual Probe DP6AD+		Beta Probe BP19	Dual ("EC") vs. Beta Probe Signal/Noise Ratio Improvement @ 1 μSv/h
		Channel "EC" (3-10 keV)	Channel "BETA" (> 20 keV)	Gross Channel	
@ 0,1 μSv/h	cps	4	5	7	
@ 1 μSv/h	cps	20	100	90	
Fe-55	cps/(Bq/cm ²)	2,7	0,00	0,30	4050%
Ni-63	cps/(s ⁻¹ /cm ²)	4,0	0,1	3,0	600%
C-14	cps/(Bq/cm ²)	10	4	11	409%
Co-60	cps/(Bq/cm ²)	5	16	23	98%
Sr/Y-90	cps/(Bq/cm ²)	1	34	37	12%

It can be seen from table 2 that the ZnS(Ag) layer provides good detection of the low energy X-rays of Fe-55 and helps to amplify the scintillation signal of the low energy beta radiation of Ni-63. Furthermore, the narrow energy window of the EC-channel reduces the gamma back-ground count rate in the elevated Cs-137 field and thus provides a significantly improved signal to noise ratio up to C-14 compared to the beta detector. Please note that in table 2 the response for Ni-63 is related to the surface emission rate of the source (2 Pi efficiency).

Calculation of the minimum detectable count rate R_n can be performed according to [3]:

$$R_n = (k_{1-\alpha} + k_{1-\beta}) \sqrt{R_0 \left(\frac{1}{t_0} + \frac{1}{t_b} \right)}$$

where R_0 is the background count rate (cps), t_b is the measurement time (s) and t_0 is the background count time (s). The parameters $k_{1-\alpha}$ and $k_{1-\beta}$ are set to 1,645 for 5% false alarm rate and 95% detection probability. For $t_0 = 30$ s and $t_b = 10$ s (as an example) the minimum detectable count rate of 2,4 cps at 0,1 μSv/h corresponds to 0,9 Bq/cm² for Fe-55 in the case of the "EC" channel of the dual probe versus 3,2 cps and 4,55 Bq/cm² for the beta scintillator.

4 DISCUSSION OF FURTHER ADVANTAGES

In order to visualize the superior performance depicted by the numeric information displayed with the dual detector in the new “Special Mode”, screen shots are displayed in Fig 3 to 5.

4.1 Impact of Background Radiation for Dual and Beta Probe

Figure 3: Displayed counts rates for background and Fe-55



In Fig 3, it can be seen that the EC-channel reading for the Fe-55 contamination is 147 times higher than the low background reading and still 23 times larger than the reading at 1 µSv/h background. For the beta (BP19) detector the corresponding numbers are just 8,8 times 0,68 times. In other words, the confidence of the user in the significance of an elevated reading in the EC-channel to be indeed related to a contamination rather than being caused by a slight variation of the background is greatly enhanced.

4.2 Impact of Beta Energy on the Count Rate Display

The dual channel concept of the “Special Mode” provides additional insight into the prevailing energy of measured beta radiation. I.e. even in the absence of EC-nuclides valuable additional information regarding the energy distribution of beta contamination can be gained during routine surveys (Fig 4). As it is possible to set 2 different alarm levels for the EC and the BETA-channel.

Figure 4: Dual channel display for different mean beta energies



4.3 Quick Discrimination between Electron Capture and Low Energy Beta Nuclides

While the count rates for both electron capture isotopes (Fe-55) and very low energy beta emitters (Ni-63) are concentrated in the EC-channel, an easy and instantaneous discrimination can be made by slightly increasing the distance of the detector to the contaminated surface (Fig 5).

Figure 5: Dual display for Fe-55 and Ni-63 in different distance to the 150 cm² source



5 SET-UP, CALIBRATION AND INTERCOMPARISON

The consistent set-up of the instrument and detector combination, e.g. after exchange of a damaged mylar window or a damaged photomultiplier requires a few extra steps compared to the set-up and calibration in the classic beta/alpha operation mode.

If the probe is to be used in the classic beta/alpha dual mode as well, the “normal” set-up procedure should be done first. A high energy beta source (typically Sr/Y-90) is used to determine the beta sensitivity and spill-over into the alpha channel, and an alpha source (e.g. Am-241) is required for determination of the alpha sensitivity and the alpha into beta spill-over. By verification of the alpha sensitivity to be within the allowed tolerances, the thickness of the mylar window is verified and a related mistake in the repair process can be ruled out. If this step has been passed successfully, a sensitivity measurement using Ni-63 in the new EC/BETA mode is not mandatory and the verification of the X-ray response (e.g. using Fe-55) is sufficient. However, if no alpha sensitivity measurement can be performed, a measurement using a low energy beta emitter (preferably Ni-63) should be performed to verify the thickness of the mylar entrance window and exclude any significant dust deposition. The setting of the best operating voltage in the EC/BETA mode is accomplished by taking a Fe-55 and background plateau curve and selecting the voltage with the best signal to noise ratio, whereas a minimum Fe-55 sensitivity must be achieved and a maximum background count rate must not be exceeded. A stringent test for a possible light leak needs to be performed in the EC/BETA-mode. If no Fe-55 large area source is available, the set-up can be performed using a Ni-63 source as well.

Since conventional large area sources for EC and low energy beta emitters may have significant variations in the homogeneity and self-absorption in the source, the diagnosis of the detector performance using different check source specimen at different locations can be problematic. It is therefore recommended to use a large area test adapter made of natural lutetium-oxide ceramics (Fig. 6), which provides perfect reproducibility of the particle emission rates and energy distribution. Details of the general advantages of using such a “transfer” standard based on primordial natural Lu-176 can be found in reference [4].

Figure 6: Large area lutetium oxide test-adapter: 100 cm² of high density Lu₂O₃ ceramic tiles are mounted to an aluminium backing



6 CONCLUSION

The direct and sensitive surface contamination measurement of low energy beta and electron capture nuclides can be achieved by leveraging the high light-output of the ZnS(Ag) layer of high-performance large area dual phosphor detectors even in elevated gamma dose rate fields. This enables both cost reduction and time saving when performing contamination surveys of hard to detect radionuclides.

7 ACKNOWLEDGEMENTS

This work was triggered and stimulated by a request from Andy Glover, Heysham 2 Power Station, EDF Energy, UK.

8 REFERENCES

- [1] Nuclides 2000: An Electronic Chart of Nuclides, 1.00, JRC, 1999.
- [2] ANSI/HPS N13.12-2013 Surface and Volume Radioactivity Standards for Clearance, 2013.
- [3] IEC 60325:2002, Radiation protection instrumentation - Alpha, beta and alpha/beta (beta energy >60 keV) contamination meters and monitors.
- [4] Iwatschenko-Borho, M. (2008), Test Adapters Based on Natural Lutetium – a Discussion of Benefits versus Conventional Check Sources, proceedings of IRPA 12 Buenos Aires.

The Facility of Radiation Standards in Japan Atomic Energy Agency, present status and its research works on dosimetry

Munehiko Kowatari*, Hiroshi Yoshitomi, Sho Nishino, Yoshihiko Tanimura, Tetsuya Ohishi, Michio Yoshizawa

Division of Radiation Protection, Japan Atomic Energy Agency, 2-4 Shirakata, Tokai, Naka, 319-1195 IBARAKI, Japan.

Abstract. The Facility of Radiation Standards (FRS) in the Japan Atomic Energy Agency (JAEA) offers various kinds of radiation calibration fields for calibration and testing for over three decades. The FRS-JAEA offers reliable X-ray, gamma-ray, beta-ray and neutron calibration fields with a vast range of variety. The quality and a set of neutron calibration fields are particularly mentioned. Neutron calibration fields with energies ranging between 0.025 eV and 19 MeV enable users to check the whole items for performance test required for neutron dosimeter. Two different sets of beta-ray calibration fields were established and served for regular calibration of dosimeters mainly used in nuclear industries. Recent research accomplishments on gamma-ray calibration fields can extend the upper limit of the energy up to 6 MeV. In addition to them, a simulated workplace neutron calibration field has been newly established for calibration of neutron dosimeters used inside the nuclear reactors.

KEYWORDS: radiation standards; SSDL; mono-energetic neutron; gamma-ray; beta-ray.

1 INTRODUCTION

Any radiation workplace and every radiation worker must be monitored in an appropriate manner, using radiation protection instruments. These radiation protection devices also should be well-calibrated so that they can provide reliable information on exposures to workers and public. Since the proper implementation of radiation monitoring to workplace, radiation workers and environments is required to secure, safe and sustainable operation of nuclear facility, calibration of radiation protection devices are to be properly made at well-defined radiation calibration fields.

For more than three decades, neutron, X, gamma-ray and beta-ray calibration fields have been served for radiation protection purposes at the Facility of Radiation Standards (FRS) in Japan Atomic Energy Agency (JAEA). After the installation of the 4 MV Van-de-Graaff accelerator in 2000, mono-energetic neutron calibration fields and the 6-7 MeV high energy gamma-ray calibration field were established. As a comprehensive secondary standard dosimetry laboratory (SSDL), the FRS has been making contributions to provide reliable and various radiation calibration fields for radiation protection purposes not only in Japan but also in Asian region.

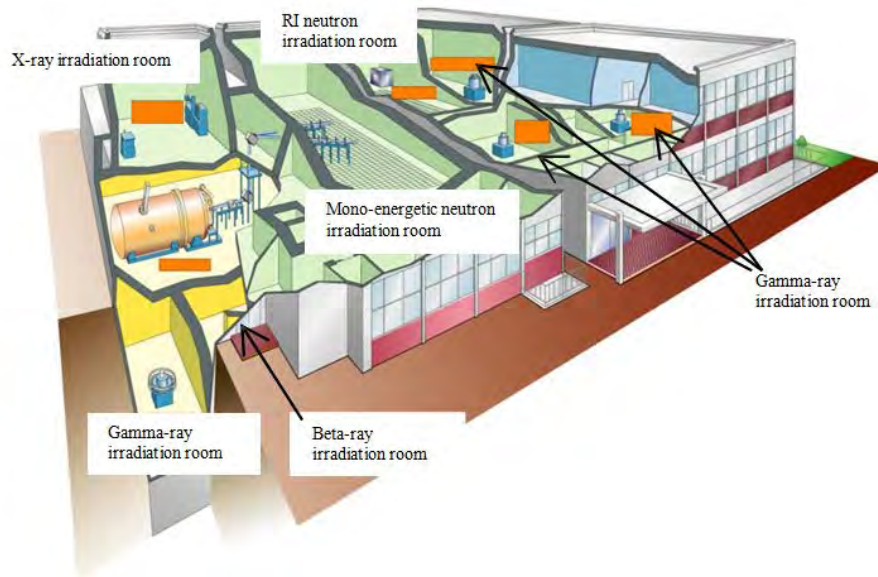
2 OVERVIEW OF NEUTRON, X AND GAMMA RAY AND BETA RAY CALIBRATION FIELD AT THE FRS

The FRS-JAEA has been originally built in 1980 and is remarkably contributing to regular calibrations of radiation protection instruments which are used not only inside JAEA but also other institutes, hospitals and nuclear power plants in Japan. The FRS-JAEA is a three-story reinforced concrete building, with one basement floors, which has a floor area of 4153 m² in total. Various kinds of sealed neutron, gamma-ray and beta-ray sources, the 4MV Van-de-Graaff accelerator, four gamma-ray irradiators, two X-ray generators are equipped inside radiation controlled areas, in order to establish various kinds of radiation calibration fields.

* Presenting author, e-mail: kowatari.munehiko@jaea.go.jp

At the FRS-JAEA, a huge amount of dosimeters are calibrated for their annual calibrations, namely, 30,000 pieces of personal dosimeters, 2,600 survey-meter type dosimeters and 700 sets of installed type dosimeters in total. On 11th March 2011, the FRS-JAEA also had seriously damaged from the great-east Japan earthquake and been deeply contaminated due to the consequence the Fukushima nuclear accident. However, one month after the accident, the FRS-JAEA resumed its operation and offered calibration service, even under contaminated circumstance [1].

Figure 1: Overview of the facility of radiation standards in Japan Atomic Energy Agency (FRS)



2.1 Neutron Calibration field

The FRS has been established and providing the ISO8529-1[2] specified radio-isotope (RI) neutron calibration fields, ten different energies of mono-energetic neutron calibration fields ranging from 8 keV to 19 MeV. The thermal neutron calibration field (0.025 eV) produced by ^{252}Cf sealed RI source coupled with the graphite pile with a dimension of $150^w \times 164^d \times 150^h \text{ cm}^3$ was also established and operating[2]. The series of well-defined neutron calibration fields with a very wide range of neutron energies allows the FRS to provide comprehensive test environments so that manufacturers can check the whole energies to be tested for responses of their dosimeters at one laboratory.

There are four sealed RI neutron source available in the neutron-scatter suppressing irradiation room at the FRS. Two X3 type encapsulated $^{241}\text{Am-Be}$ sources with nominal activities of 37 GBq and Two X1 type sealed ^{252}Cf sources with 2 GBq and 199.8 MBq, respectively are installed at the FRS. The neutron emission rates are determined by the primary standard laboratory. Anisotropy factors for sources with their protection cases were experimentally determined using a high precision long counter in accordance with recommendations of ISO 8529-1[2]. When dosimeters are calibrated, bare $^{241}\text{Am-Be}$, bare ^{252}Cf and/or D_2O moderated ^{252}Cf source is positioned at the centre of a $12.5 \times 12.5 \times 11.7 \text{ m}^3$ irradiation room using the aluminium source stand on the zinc plated iron grating floor.

Table 1: Characteristics of mono-energetic neutron calibration field at the FRS-JAEA

Energy	Nuclear reaction	$\Phi_{Max}(\text{cm}^{-2} \text{ s}^{-1})$	$H^*(10)_{Max}(\mu\text{Sv h}^{-1})$	Uncertainty (k=2)
8 keV	$^{45}\text{Sc}(p,n)^{45}\text{Ti}$	70	2.4	14%
27 keV	$^{45}\text{Sc}(p,n)^{45}\text{Ti}$	110	8.5	12%
144 keV ^(a)	$^7\text{Li}(p,n)^7\text{Be}$	3,000	1400	7%
250 keV	$^7\text{Li}(p,n)^7\text{Be}$	2,000	1400	7%
565 keV ^(a)	$^7\text{Li}(p,n)^7\text{Be}$	6,000	7,000	5%
1.2 MeV	$^3\text{H}(p,n)^3\text{He}$	1,000	1,500	7%
2.5 MeV	$^3\text{H}(p,n)^3\text{He}$	2,000	3,000	6%
5.0 MeV ^(a)	$^2\text{H}(d,n)^3\text{He}$	7,000	10,000	7%
14.8 MeV ^(a)	$^3\text{H}(d,n)^4\text{He}$	3,000	6,000	12%
19 MeV	$^3\text{H}(d,n)^4\text{He}$	180	380	25%

^(a) they are traceable to the primary standards in AIST, Japan

Using the 4 MV Van-de-Graff accelerator, mono-energetic neutron calibration fields produced by the nuclear reactions with ten different energies are also available at the FRS [3-6]. The characteristics of the fields are shown in Table 1. Basic quantities of each field was well-determined using a newly developed neutron monitoring system coupled with the precision long counter [3-6] and precise acceleration voltage control system for ensuring the nuclear resonance reaction of $^{45}\text{Sc}(p,n)^{45}\text{Ti}$ [4]. Irradiation room is also designed so that scattered neutrons by floor, walls and the ceiling could be reduced at a point of test. The irradiation room has $11.5 \times 16.5 \times 12.5 \text{ m}^3$, and at its mid-height has an aluminium-grating floor to reduce scattered components from floor, wall and ceiling. Mono-energetic neutron fields with energies with 144 keV, 565 keV, 5.0 and 14.8 MeV are also traceable to those established in the primary metrological laboratory in Japan, the National Institute of Advanced Industrial Science and Technology (AIST), by measuring neutron fluence at the point of test using the transfer detector with spherical polyethylene moderator.

With regard to the thermal neutron calibration field, a point of test was set at the distance of 40 cm from the surface of the graphite pile and thermal neutron fluence rate was determined by gold foil activation method [3]. Neutrons with energy above 1 eV might affect the calibration factor of neutron dosimeters. Calibration factors of neutron dosimeters to net thermal neutron are also evaluated by subtracting readings obtained under the condition that dosimeters are covered with Cd case from those obtained by uncovered condition.

2.2 X and gamma-ray calibration field

Two X-ray irradiators and four gamma-ray irradiators with ^{137}Cs and ^{60}Co radioactive sources have been installed and operated for generating the wide energy range of X and gamma ray calibration fields, with energy ranges between 16.5 keV (for the ISO X ray narrow series) and 1.25 MeV (for ^{60}Co gamma-ray). In addition to irradiators, the 6-7-MeV high energy gamma-ray calibration field produced by the accelerator can broaden the gamma-ray energy range up to 6-7 MeV.

Table 2: Characteristics of ISO-narrow series X-ray calibration field at the FRS-JAEA [8]

Tube voltage (kV)	First half-value layer (mm) ^(a)		Effective energy (keV)		Typical air kerma rate per tube current (mGy h ⁻¹ mA ⁻¹) at 1 m
	ISO	JAEA	ISO	JAEA	
20	0.32	0.376	15.0	15.8	11.1
25	0.66	0.709	19.2	19.7	8.9
30	1.15	1.28	23.3	24.2	5.4
40	0.084	0.0755	31.7	30.5	8.9
60	0.24	0.221	46.2	44.8	10.5
80	0.58	0.600	63.9	64.7	4.5
100	1.11	1.18	82.5	84.7	2.1
120	1.71	1.83	100	103	2.1
150	2.36	2.52	118	122	14.9
200	3.99	4.25	166	174	6.6
250	5.19	5.52	208	223	6.5
300	6.12	6.46	253	271	6.7

^(a) Material of half-value layer (HVL) between 20 and 30 kV is aluminium and material of HVL above 30kV is copper.

Using two X-ray generators installed at the FRS-JAEA, X-ray calibration fields are served for radiation protection purposes. X-ray calibration fields have been established at the FRS-JAEA, according to recommendation of the ISO4037-1 [7] and also recommended by the Japanese Industrial Standards (JIS) [9,10]. Table 2 shows a comparison of basic quantities of the ISO-narrow series at the FRS-JAEA. From a series of measurement of spectra and reference air kerma rate for each tube voltage condition, ISO-narrow series X-ray calibration fields at the FRS-JAEA have almost the same basic characteristics as specified in the ISO [7]. As for the X-ray calibration fields recommended in JIS, the Quality Index (QI) which is derived from dividing the effective X-ray energy by the X-ray tube voltage is introduced for specifying the characteristics of the X-ray beam. The half-value layer, the homogeneity coefficient, the effective X-ray energy and the QI were also determined for each kind of X-rays [9, 10].

Table 3 summarizes the specifications of gamma-ray calibration fields at the FRS-JAEA. There are four gamma-ray irradiators available in each irradiation room. One of the irradiator is a panoramic gamma-ray irradiator so that users can irradiate through a full 360 degree for periodical checking of personal dosimeters. The collimated gamma-ray irradiators and the calibration tables are installed in other three irradiation rooms. Irradiators and calibration tables can be operated by remote control outside of the room. Each irradiator has thick lead storage and four sealed radiation sources (¹³⁷Cs and/or ⁶⁰Co) with different activities are stored inside each irradiator. In addition to irradiators, collimated gamma-ray calibration fields around 1 µGy h⁻¹ by sources that can be handled with tongs were also established. Reference air kerma rates were determined by the reference ionization chamber (Exradin type A5, A6 and A8) calibrated by the AIST.

After the tragic Fukushima nuclear disaster, accommodation of demand on calibration of survey meters used for the decontamination work was a pressing issue. In addition to the increase of calibration of surface contamination density survey meters, calibration of dosimeters used in the regions whose dose rate is below 1 µSv h⁻¹ is also increasing. The FRS-JAEA has been making significant contributions to accommodate the demand for decontamination and remediation works in Fukushima area, by establishing a reliable ¹³⁷Cs gamma-ray calibration field so that survey meters could be calibrated in such a low dose rate.

Table 3: Specifications of gamma-ray calibration fields at the FRS-JAEA

Type of RI	Type of Gamma-ray field	Gamma-ray energy (keV)	Range of air kerma rate ^(a) (nominal)
¹³⁷ Cs	Uncollimated	662	2 μ Gy h ⁻¹ - 3.5 mGy h ⁻¹
	Collimated		1 μ Gy h ⁻¹ - 40 mGy h ⁻¹
⁶⁰ Co	Uncollimated	1250	2 μ Gy h ⁻¹ - 35 μ Gy h ⁻¹
	Collimated		1 μ Gy h ⁻¹ - 1.0 Gy h ⁻¹

^(a) As of 1st April 2016

2.3 Beta-ray calibration field

Two different kinds of beta-ray calibration fields are set up and served for regular calibrations at the FRS-JAEA. Table 4 shows the comparison of beta-ray calibration fields produced by two different irradiation systems. The Beta-Secondary Standard 2 (BSS2) has been installed so that calibration fulfilling the requirement of ISO 6980 [11] can be implemented. The BSS2 is composed of three beta-ray sealed sources, ¹⁴⁷Pm, ⁸⁵Kr and ⁹⁰Sr-⁹⁰Y, beam-flattening filters, the source stand, and the control unit. The nominal activities of sources are 3.7 GBq for ¹⁴⁷Pm, 3.7 GBq for ⁸⁵Kr and 460 MBq for ⁹⁰Sr-⁹⁰Y, respectively. Reference 70 μ m tissue equivalent absorbed dose rate for each source are well determined by the German metrological laboratory, Physikalisch Technische Bundesanstalt (PTB). The BSS2 is now served for regular calibrations of personal dosimeters.

Another beta-ray irradiation system is also available at the FRS-JAEA. The JAEA Beta irradiation System (JBS) is composed of alignment apparatus, precise scale and sealed beta-ray sources, ¹⁴⁷Pm, ²⁰⁴Tl and ⁹⁰Sr-⁹⁰Y fabricated by the former Amersham Corporation. 70 μ m tissue equivalent absorbed dose rate at a point of test for each source was measured using the extrapolation chamber manufactured by PTW-Freiburg (model 23392). Prior to the determination of the tissue equivalent absorbed dose rate for JBS, reference 70 μ m tissue equivalent absorbed dose rates were measured in the BSS2 and measured results were in quite good agreement with reference values [12]. Comparing with the BSS2, sources for JBS have a larger active area of 4.2 cm in diameter and a thinner source cover. The JBS is categorized as an ISO 6980 series 2 sources and is mainly used for performance test and periodically testing of dosimeters.

Table 4: Comparison of ⁹⁰Sr-⁹⁰Y beta-ray calibration fields produced by BSS2 and JBS [12]

System	Nominal activity (MBq)	Diameter and thickness of active area	Range of Calibration distance (cm)	Range of 70 μ m tissue equivalent absorbed dose rate (mGy h ⁻¹) ^(a)
BSS2	460	0.6 cm ^o ; 0.4 cm ^t	11 - 50	20 – 400
JBS	740	4.2 cm ^o ; 0.2 cm ^t	20 – 100	5 - 200

^(a) As of April 2016

3 RECENT RESEARCH ACTIVITIES REGARDING CALIBRATION FIELD AT THE FRS

3.1 Graphite-moderated neutron calibration field using ^{241}Am -Be sources

A simulated workplace neutron field using two ^{241}Am -Be sources and the graphite pile was newly developed, in order to accommodate the demand on more proper calibration of neutron dosimeters used inside nuclear power plants. Taking advantage of calibration factors of dosimeters obtained in the simulated workplace neutron fields would allow to monitor neutron ambient dose equivalent rates for proper evaluation of exposures of workers due to neutrons leaking from heavily shielded walls and doors inside reactors.

Using the same graphite pile ($150^w \times 164^d \times 150^h \text{ cm}^3$) as used for thermal neutron field, a simulated workplace neutron field was established by setting two ^{241}Am -Be sources with activities of 37 GBq inside the pile. A point of test was set 75 cm from the surface of the pile at the mid height of the pile. To reduce unexpected thermal neutron components, thermal neutron shielding sheet is set on the surface of the pile. Two different neutron fields can produce at a point of test by changing the position of sources inside the pile. Comparing with source position A, one of the ^{241}Am -Be sources is set deeper inside the pile at source position B. This leads to increase neutron components with energies below 100 keV.

Table 5: Comparison of basic quantities of graphite-moderated neutron calibration fields [13]

Source position	Fluence averaged energy (MeV) ^(a)	Typical fluence rate ($\text{cm}^{-2} \text{ s}^{-1}$) ^(a)	Typical ambient dose equivalent rate ($\mu\text{Sv h}^{-1}$) ^(a)
A	0.84	87.7	0.84
B	0.60	51.2	0.60

^(a) Measured results in August 2013

Table 5 summarizes obtained basic quantities of the graphite-moderated neutron calibration fields for each source position. The neutron spectra obtained at a point of test were expected prior to the measurement by Monte Carlo calculations using MCNP-5 and a series of spectrometry using the Bonner Multi-sphere Spectrometer (BMS) at a point of test was performed to determine basic quantities of the field [13]. Measured ambient dose equivalent rates for both source positions were all in good agreement with those calculated within 4% [13].

3.2 The 6-7-MeV high energy gamma ray calibration field (the R-F field)

At the FRS in JAEA, the 6-7-MeV high energy gamma-ray calibration field specified as a R-F field in ISO4037-1 [7] has been established and operating for regular calibration of personal dosimeters for radiation protection [14,15]. Using another beamline with the same accelerator as used for mono-energetic neutron calibration fields, protons with an energy of 2.7 MeV bombard a thick CaF_2 target and 6-7-MeV high-energy gamma rays are produced by the nuclear reaction of $^{19}\text{F}(p, \alpha\gamma)^{16}\text{O}$. The point of test was set 100 cm from the surface of the target chamber. Introducing a PMMA-made build-up plate with a dimension of $30 \times 30 \times 2.5 \text{ cm}^3$, air kerma rates at the point of test was experimentally determined by direct measurement using an ionization chamber coupled with a conventional thin build-up cap for ^{137}Cs and ^{60}Co gamma ray fields. In the table 6, dosimetric quantities of the R-F field are summarized and consistent with those obtained in PTB [16], and specified in ISO4037-1[7].

Table 6: Characteristics of the R-F field at the FRS-JAEA

Incident proton energy (MeV)	2.7
Mean gamma-ray energy (MeV)	
Φ	4.17 ± 0.01
K_{air}	6.31 ± 0.01
$H^*(10)$	6.28 ± 0.01
$H_p(10)$	6.15 ± 0.01
Typical air kerma rate unit beam current ($\mu\text{Gy h}^{-1} \mu\text{A}^{-1}$) at 1 m	91.2 ± 4.3
Typical range of personal dose equivalent rate, $H_p(10)$ ($\mu\text{Sv h}^{-1}$)	20 - 4000
Ratio of neutron contribution to total dose equivalent (%)	< 0.5

Inter-comparison of reference air kerma rate of the R-F field in PTB was performed. Using the reference ionization chamber used for determining the reference air kerma rate at the FRS-JAEA, air kerma rates in the R-F field in PTB under the free-in-air condition and the condition that the build-up plate was introduced were measured and compared with reference values by PTB. Results were in good agreement with each other.

3.3 Inter-comparison between the FRS and the Secondary Standard Dosimetry Laboratory (SSDL) in Asian region

With regard to collaborative research work on dosimetry, a series of experiments on measurement of radiation fields and calibrations of personal dosimeters has been intensively conducted between Korea Atomic Energy Research Institute (KAERI) and the FRS-JAEA for inter-comparison [17]. The aim of the inter-comparison is to ensure that reliable calibration service has been provided and to broaden knowledge on the radiation calibration fields and the calibration technique. Reference physical quantities of radiation standard field that both institute determined independently were compared. Air kerma rates in the ISO narrow series X-ray calibration fields was measured each institute and were in quite good agreement with each other. Measured dose equivalent per fluence ($h^*(10)$ and $h(10)$) for the D2O-Cf neutron calibration fields indicate that both institutes established reliable fields, taking into account the differences in structure of the D2O moderator assemblies [18]. Results from intensive studies on calibrations of personal dosimeters also showed that almost identical calibration factors could be obtained in RI neutron and beta-ray calibration fields in each institute. Another inter-comparison in the ^{137}Cs gamma-ray standard field between the Thailand Institute of Nuclear Technology (TINT) and the FRS-JAEA has started. As a preliminary phase of the inter-comparison, passive type dosimeters (OSL dosimeter) that both institutes use for personal monitoring are irradiated with certain personal dose equivalents like 1 mSv in $H_p(10)$ in the ^{137}Cs gamma-ray calibration field. Both institutes report the readings from OSLDs that are irradiated at each institute and results of reading were satisfactory, taking into the accompanying uncertainties of irradiated doses.

4 SUMMARY

The present status on the X-ray, gamma-ray, beta-ray and neutron calibration fields at the FRS-JAEA is given in the paper. The FRS-JAEA has been making contribution to radiation protection sectors by offering the reliable calibration fields for more than three decades. By establishing the 6-7-MeV high energy gamma-ray calibration field using the accelerator, the upper limit of the energy of calibration field was extended up to 6 MeV. In addition to the ISO specified mono-energetic and RI source neutron calibration fields, the graphite-moderated neutron calibration fields has been established for regular calibration of neutron survey meters used inside nuclear reactors. In the beta dosimetry region, the BSS2 that fully satisfies the requirement of the ISO 6980-1 is served for regular calibration of dosimeters and another irradiation system called the JBS is also used for performance tests and periodical checks for dosimeters.

Annual numbers of dosimeters calibrated at the FRS-JAEA are more than 30,000 pieces for personal dosimeters, 2,600 survey-meter type dosimeters and 700 sets of installed type dosimeters, respectively. It should also be pointed out that a large amount of survey meters used for decontamination and remediation works in affected Fukushima areas are being calibrated at the FRS-JAEA.

One of the missions of the FRS-JAEA is to play a role as a leading SSDL in Asian region. Some of preliminary studies collaborating with SSDL in other Asian countries got started for a couple of years. All the calibration fields at the FRS-JAEA are open to the business and research domains in Asian-Pacific region. Sharing the knowledge on the radiation calibration field and calibration techniques is always welcoming and rewarding us.

5 ACKNOWLEDGEMENTS

Authors deeply appreciate Dr. Yasuhiro YAMAGUCHI who offered continuing support and constant encouragement. Authors also would like to thank Mr. Katsuya KAWASAKI, Mr. Yosuke TATEBE, Mr. Shigeru SHIMIZU and Mr. Katsutoshi FUJII for their continuous dedications to the FRS-JAEA. Finally, authors also respectfully offer our condolences to Mr. Yoichi KAJIMOTO, who had been largely committed to the management of the FRS-JAEA for about decade.

6 REFERENCES

- [1] Yoshitomi, H., Tatebe, Y., et al., 2014. Practice for reducing contamination of controlled area under the influence of Fukushima nuclear accident. *Progress in Nuclear Science and Technology*, 4 pp. 81-84. doi: 10.15669/pnst.4.81.
- [2] Uchita, Y., Saegusa, J., Kajimoto, Y., et al., 2005. Characteristics of Thermal Neutron Calibration Fields Using a Graphite Pile. JAERI-Tech 2005-012. [in Japanese]
- [3] Tanimura, Y., Yoshizawa, M., Saegusa, J., et al., 2004. Construction of 144, 565 keV and 5.0 MeV monoenergetic neutron calibration fields at JAERI. *Radiat. Prot Dosimetry*, 110(1-4) pp.85-89 doi:10.1093/rpd/nch197.
- [4] Tanimura, Y., Saegusa, J., Shikaze, Y., et al., 2007. Construction of monoenergetic neutron calibration fields using $^{45}\text{Sc}(p, n)^{45}\text{Ti}$ reaction at JAEA. *Radiat. Prot Dosimetry*, 126(1-4) pp. 8-12. doi:10.1093/rpd/ncm004.
- [5] Tanimura, Y., Tsutsumi, M., and Yoshizawa, M., 2014. Determination of neutron fluence in 1.2 and 2.5 MeV mono-energetic neutron calibration fields at FRS / JAEA. *Progress in Nuclear Science and Technology*, 4 pp. 392-395. doi: 10.15669/pnst.4.392.
- [6] Tanimura, Y., Fujii, K., et al., 2014. Neutron fluence monitoring system in mono-energetic neutron fields at FRS / JAEA. *Progress in Nuclear Science and Technology*, 4 pp. 388-391. doi: 10.15669/pnst.4.388.
- [7] ISO, 1996. X and gamma reference radiation for calibrating dosimeters and dose rate meters and for determining their response as a function of photon energy. Radiation characteristics and protection methods. International Standard ISO 4037-1.
- [8] Shimizu, S., Sawahata, T., Kajimoto, Y., et al., 2011. Establishment of Medium-Hard X-ray Reference Fields for Performance Tests of Radiation Measuring Instruments Based on International Standard. JAEA-Tech 2011-008. [in Japanese].
- [9] Shimizu, S., Sawahata, T., Kajimoto, Y., et al., 2010. Establishment of Medium-Hard X-ray Reference Fields for Performance Tests of Radiation Measuring Instruments Based on National Standard. JAEA-Tech 2010-009. [in Japanese].
- [10] Shimizu, S., Fujii, K., Kawasaki, T., et al., 2010. Establishment of Soft X-ray Reference Fields for Performance Tests of Radiation Measuring Instruments Based on National Standard. JAEA-Tech 2010-005. [in Japanese].
- [11] International Organization for Standardization. 2006. Nuclear energy-Reference beta-particle radiation-Part 1: Methods of production. ISO 6980-1.
- [12] Yoshitomi, H., Kowatari, M., Suzuki, T., 2014. Characteristics of Beta Reference Radiation Fields at the Facility of Radiation Standards (FRS), JAEA for their Practical Applications in Beta Dosimetry. *Proceeding of AOCR-4. YS3*.

- [13] Nishino, S., Tanimura, Y., Ebata, Y. and Yoshizawa, M., 2016. Development of the Graphite-Moderated Neutron Calibration Fields using ^{241}Am -Be sources in JAEA-FRS. 2015, Proceeding of ISORD-8, to be published.
- [14] Kowatari, M., Tanimura, Y., and Tsutsumi, M., 2014. Measurement of air kerma rates for 6-7 high-energy gamma-ray field by ionisation chamber and build-up plate. *Radiat. Prot. Dosimetry* 162(4) pp. 446-458. doi:10.1093/rpd/nct366.
- [15] Kowatari, M. and Tanimura, Y., 2015. Establishment of 6-7 MeV high-energy gamma ray calibration fields produced using the 4MV van de graaf accelerator at the facility of radiation standards (FRS), Japan Atomic Energy Agency, *Radiat. Prot. Dosimetry* 168(3) pp. 300-313. doi:10.1093/rpd/ncv347.
- [16] Behrens, R. and Rottger, S., 2008. Characterisation of three high-energy photon and fast neutron reference fields. *Radiat. Prot. Dosimetry*. 132(3), 283-296.
- [17] Yoshitomi, H., Tanimura, Y., Tatebe, Y., 2014. Series Studies on Inter-comparison of Radiation Calibration Fields and Calibration Techniques between KAERI and JAEA. Proceeding of AOCR-4. PP2(2).
- [18] Kowatari, M., Fujii, K., et al. 2008. An Inter-Comparison of the Neutron Calibration Fields by D_2O Moderated ^{252}Cf Sources at JAEA and KAERI. *J. Nucl. Sci. Technol.*, suppl. 5. pp. 217-220.

Evaluation of radiation detectors for a possible integration into the automated survey system TIM in the Large Hadron Collider (LHC)

Markus Widorski^{a*}, Frédéric Aberle^b, Cristina Adorisio^a, Daniel Perrin^a

^aCERN, 1211 Geneva 23, Switzerland.

^bHEPIA, HES-SO, 1202 Geneva, Switzerland.

Abstract. The Large Hadron Collider (LHC) is the most recent accelerator constructed at CERN, the European Organization for Nuclear Research. The LHC accelerates and collides proton beams but also heavier ions. It is installed in a 27 km circumference tunnel, about 100 m underground. The operation of high-energy accelerators unavoidably leads to the activation of the accelerator components and tunnel infrastructure. The evaluation of the radiological conditions of the underground beam areas has to be done after beam stop before workers can enter the accelerator tunnel. Thus, whenever the accelerator switches from Beam Mode to Access Mode, the CERN Radiation Protection (RP) group is in charge to give clearance for any access requested. The clearance is based on the radiological risk assessment, which requires results from dose rate measurements. These are performed by about 180 fix installed radiation monitors and by technicians performing detailed measurements either in situ, when accompanying the worker or prior to the access of the workers. The radiological measurements relying on human intervention involve the exposure of personnel and is time consuming. This study aimed to replace part of this task by an automatic device (RP-TIM) and this solution should be of benefit for machine operation (reduced down time) and for the RP personnel (reducing individual dose and exposure to any risk linked to the machine tunnel, i.e. oxygen deficiency, cryogenic, fire).

The detector installed on the TIM is required to measure ambient dose equivalent rates in a gamma field reliably in short time intervals over a large dynamic range. As the detector is continuously moved alongside the accelerator, the device has to be capable to work in scanning mode with a high read out rate and with no time lag in the response to changing radiation levels. The device has to be robust and insensitive to mechanical shocks or temperature variations. Scintillation detectors deliver a good statistical output, can be relatively robust but need to be adapted to measure ambient dose equivalent rates over a large dynamic range. We have performed radiometric and dynamic tests on three different scintillation detectors, evaluating and comparing them against the requirements. While the radiometric results fit the needs, the dynamic response behaviour has turned out to be more difficult to achieve.

KEYWORDS: *TIM; LHC; dynamic measurements; ambient dose equivalent rate measurement; ATOMTEX BDKG-24; THERMO SCIENTIFIC FH40 FHZ672.*

1 INTRODUCTION

At CERN, the European Organization for Nuclear Research, physicists and engineers are probing the fundamental structure of the universe. They use the world's largest and most complex scientific instruments to study the basic constituents of matter – the fundamental particles. Founded in 1954, the CERN laboratory sits astride the Franco-Swiss border near Geneva. It was one of Europe's first joint ventures and now has 21 member states.

The Large Hadron Collider (LHC) is the most recent accelerator constructed at CERN. The LHC accelerates and collides proton beams, but also heavier ions. It is installed in a 27 km circumference tunnel, about 100 m underground.

The TIM (Train Inspection Monorail) train was developed at CERN to allow remote inspections in the LHC tunnel outside beam operation periods. The train travels battery powered on mono-rail installed at the tunnel ceiling at speed of up to 5 m/s. Before an intervention can take place in the accelerator tunnel, Radiation Protection (RP) needs to give clearance. The clearance is based on a radiological risk assessment which includes results from radiation and radioactivity measurements. Measurements relying on human intervention lead to radiation exposure of RP personnel and are time consuming. Replacing part of the measurement task by an automatic device should benefit the machine operation because of reduced down time and the RP personnel through the reduction of individual doses and

* Corresponding author, e-mail: markus.widorski@cern.ch

reducing the risk of travel-related or ODH accidents. Automation will allow more frequent and reproducible survey measurements without accessing the tunnel. This measurement data is useful for the forecast of the evolution of residual dose rate levels.

2 REQUIREMENTS

To map the dose rates in the LHC tunnel in a reasonable time, the TIM train should pass an LHC sector of 3.4 km length in less than 45 minutes. Accounting for slowdowns due to obstacles and doors, a maximum target speed of 1.5 m/s was chosen. For a spatial resolution of 50 cm, the resulting minimum readout frequency for a detector would be 3 Hz. Most commercial devices are limited to a readout frequency of 1 Hz. Consequently, the maximum speed was relaxed to 0.5 m/s in the long straight sections and to 1.5 m resolution in the arc sections. The internal data treatment is required to be sufficiently fast and with an appropriate filtering to reduce the cross-influence between measurement points.

It is challenging to identify commercially available devices, which can measure ambient dose equivalent rate over a large dynamic range, with a fast response and a high readout frequency. Further important factors to be met are weight and size, readout and remote power switching capabilities. The detectors should cover a common energy range and have a good isotropic response in at least one plane. The required large dynamic range comes from potential dose rate ranges, which are expected in the different LHC sectors throughout its life time. While the largest levels are to be found in the focusing and collimator regions, the arc sectors may only show levels in the order of the natural background.

Table 1 summarises the most important identified detector requirements.

Table 1: Identified detector requirements

Parameter	Requirement
Measured quantity	H*(10)
Energy range	60 keV – 1.3 MeV
Angular response	Isotropic response in one plane
Sensitivity	Min. 20 cps for 0.1 μ Sv/h (^{137}Cs)
Dynamic range	0.1 μ Sv/h – 100 mSv/h
Readout frequency (f)	min. 1 Hz
Response time	1/f to reach 0.9 x final value
Weight	< 5 kg for the probe
Power	Battery operation and automatic startup on powering

3 DEVICE SELECTION

Three devices were selected to test against the defined requirements.

The SAPHYMO PCMx detector was initially developed and adapted for the TIM train. The rather bulky device provides a readout rate of 4 Hz and covers a large dynamic range. This detector is no longer commercially available at reasonable cost; however, for comparison reasons the detector was included in this study. In order to equip further TIM trains with detectors, two commercial devices were identified which could potentially comply with the requirements derived in the previous paragraph.

One instrument consists of two detectors to cover the full dynamic range. The Thermo Scientific FH40 and FHZ672 each provide each data readout capabilities. According to the measured level, an algorithm would need to be implemented in order to choose the output of the corresponding detector. In this study, the performance of each detector was tested separately; no algorithm had been chosen

and tested at this stage. The BDKG-24 detector offered the radiometric properties according to the manufacturer's specifications with a single detector. A number of other detectors had been considered but excluded due to non-compliance with the requirements according to their technical specifications.

The PCMx and BDKG-24 probes are based on organic scintillators of very different size, achieving a high dynamic range by switching between counting and current mode. The combined device consists of an organic scintillator for the low dose rate range (FHZ762) and a proportional counter for the high dose rate range (FH40). The selected detectors are shown in Figure 1.

Figure 1: Detectors studied for their suitability to be implemented on the TIM train. Left: ATOMTEX BDKG-24, Centre: Thermo Scientific FH40 & FHZ762, Right: Saphymo PCM-X



4 MEASUREMENTS

Two sets of measurements were performed to qualify the performances of the different detectors.

The radiometric properties such as energy dependence, angular dependence and dynamic range, were measured in the CERN Calibration Facility using the standard reference radiation fields for ^{241}Am , ^{137}Cs and ^{60}Co . Figure 2 shows the irradiator used in the calibration facility.

The dynamic properties, readout frequency and response time, were determined using a 6 m linear rail system and a moving radioactive source. A ^{137}Cs source of sufficient activity was mounted on the rail and moved with speeds of up to 3 m/s alongside the different detectors, generating a time varying radiation field. Figure 2 shows the linear rail system.

Figure 2: CERN Calibration Facility with irradiator (left) and linear rail test bench (right).



5 RESULTS

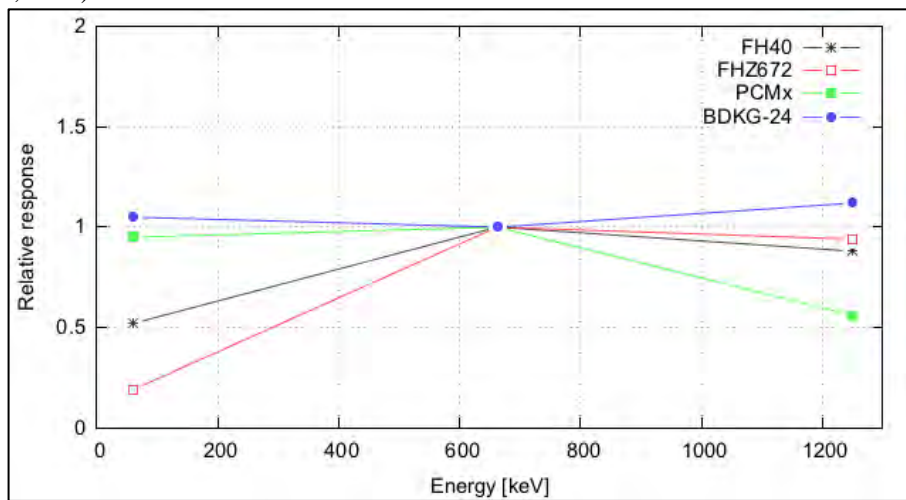
5.1 Radiometric properties

The angular dependence was determined for all detectors in vertical and horizontal orientation for three different source energies. In the most suitable orientation – around the central axis of the cylindrical detectors, the deviation over 360 degrees was less than <10% compared to the reference direction for all detectors. The angular dependency is not shown here.

The energy dependence was determined for lateral radiation incidence for three different energies. Figure 3 shows the results for the four different detectors.

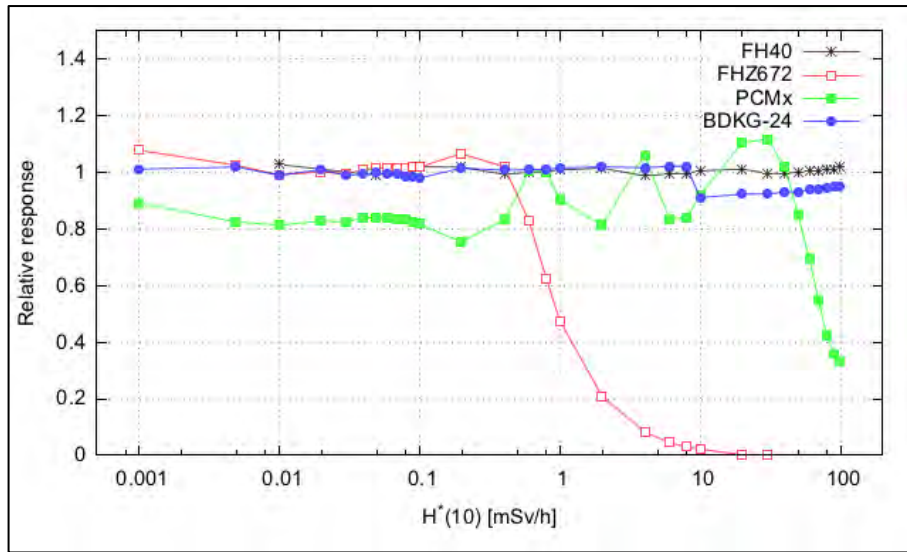
The BDKG-24 showed the most linear response. The deviation compared to the reference energy of ^{137}Cs is only of a few percent for ^{241}Am and ^{60}Co . Both detectors, FH40 and FHZ672, show a deviation at lower energy. For the FHZ672 one would need to adapt spectrum weighting factors as the radiation incidence is different compared to the manufacturers specification. The PCMx shows an underestimation for higher energies as no energy compensation is done.

Figure 3: Energy dependence for lateral incidence at three different gamma energies (^{241}Am , ^{137}Cs , ^{60}Co)



For the dynamic range, the PCMx shows a strong non-linearity and does not reach the full range. The BDKG-24 covers the full range and shows an excellent linearity, with a small stop for very high dose rates. The combined FH40 and FHZ672 detectors would cover the full dynamic range. It is clear that both detectors need to be combined to meet this requirement. At lower dose rate, the FH40 will provide only reliable results at very long integration times due to the low sensitivity of the proportional counter. Figure 4 shows the relative response over the dynamic range between $1 \mu\text{Sv/h}$ and 100mSv/h .

Figure 4: Linearity over the dynamic range from 1 $\mu\text{Sv/h}$ to 100 mSv/h ambient dose equivalent rate (^{137}Cs).

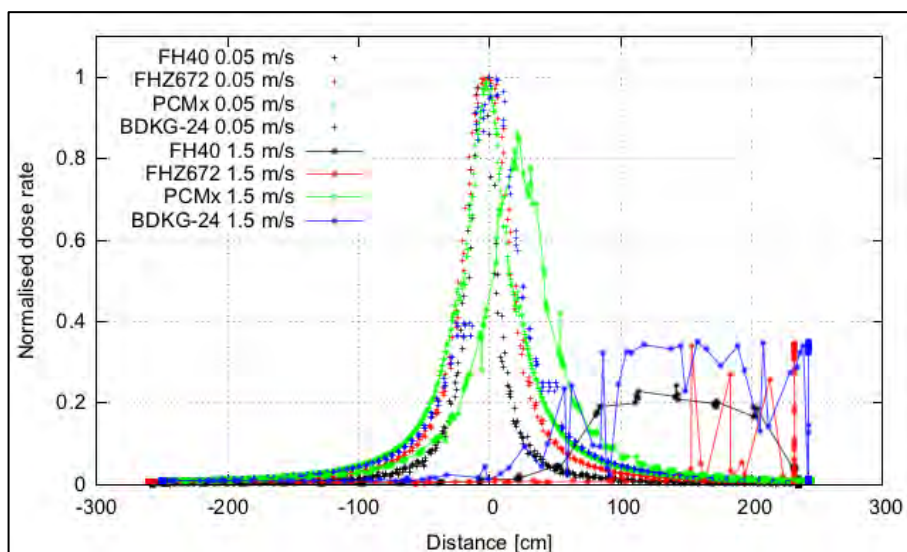


5.2 Dynamic properties

The dynamic properties were determined at different speed of a radioactive source passing by the detectors. A reference dose rate profile was measured at a very low speed of 0.05 m/s, with dose rates ranging between about one $\mu\text{Sv/h}$ up to a few hundred $\mu\text{Sv/h}$. Dose rate profiles then measured at increased speed from 0.5 m/s up to 3 m/s were compared with the reference profile. The profiles were compared how well they could reproduce the reference profile. Both for the maximum measured value and the position shift of the peak value in the profiles were determined.

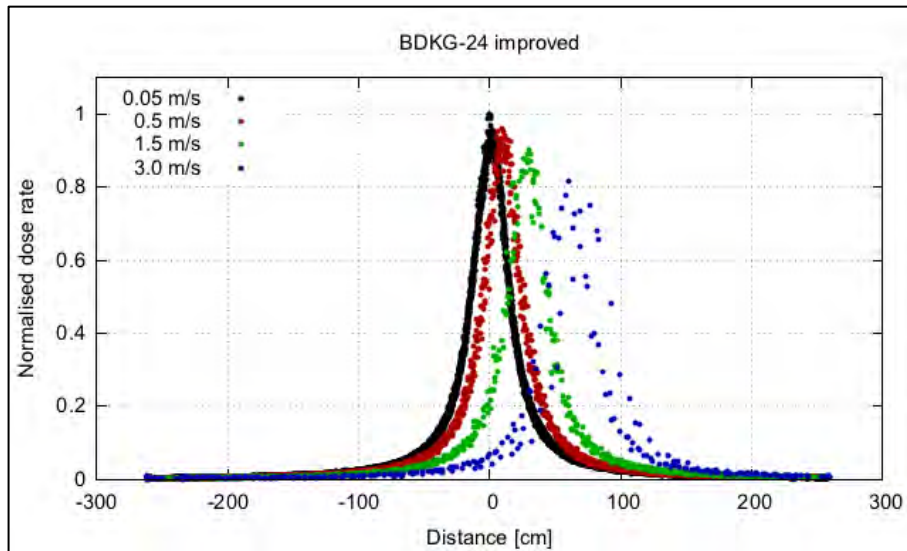
Figure 5 shows the normalised reference profiles and the profiles at 1.5 m/s for all devices, acquired over multiple source passages. With exception of the PCMx, which offers a readout rate at 4 Hz and was designed for that purpose, none of the devices was capable to reproduce the reference profile at the required speed.

Figure 5: Dose rate profiles measured at reference (0.05 m/s) and operational speeds (0.5-1.5 m/s) by the different detector types.



After the first tests, the BDKG-24 detector, which offered very good radiometric properties, was modified by the manufacturer to increase the readout rate to 10 Hz and to shorten the response time. The dynamic properties of the modified BDKG-24 detector are shown in Figure 6. The changes in the maximum value and peak can be described by a simple linear model in the range between 0 and 3 m/s. The maximum value is reduced by 8% per m/s and the peak is shifted by a lag of 20 cm per m/s. It must be noted that these dynamic properties measurements were performed at a maximum dose rate of about 600 $\mu\text{Sv/h}$ lacking stronger radioactive sources. Hence, no conclusion can be drawn for fast rate changes to higher levels or in higher ranges.

Figure 6: Dose rates profiles measured with an improved version of the BDKG-24 detector at different speeds up to 3 m/s.



6 CONCLUSION

We could identify and test a detector with promising properties to satisfy the requirements for the use on the TIM. The BDKG-24 detector offers a large dynamic range, a low angular and energy dependence and a low weight and small size. The improved version shows satisfactory dynamic properties in terms of readout frequency and response time within the tested range. The BDKG-24 will be now integrated into four TIM trains in the LHC tunnel for further testing and to allow precise and accurate remote ambient dose equivalent rate measurements.

7 ACKNOWLEDGEMENTS

We kindly acknowledge the support from Thermo Scientific, Erlangen, Germany and the provision of detector for testing purposes from ATOMTEX, Belarus. We further acknowledge Eike Hohmann for the provision of the linear test bench system from Paul-Scherrer-Institut, Villigen, Switzerland.

Investigations into Radiation Dose Distribution in a Computed Tomography Fluoroscopy Room: Monte Carlo Studies

Prince Kwabena Gyekye^{a#}, Frank Becker^{b*}, Geoffrey Emi-Reynolds^a

^aRadiation Protection Institute, Ghana Atomic Energy Commission, P. O. Box LG80, Legon Accra, Ghana.

^bInstitute for Nuclear Waste Disposal, Karlsruhe Institute of Technology, Karlsruhe, Germany.

Abstract. The radiation dose distribution in a computed tomography fluoroscopy (CTF) room has been investigated using Monte Carlo N-Particle eXtended (MCNPX). The aim of the study was to identify zones in the room with reduced radiation doses in order to indicate preferred positions for staff during CTF procedures. Dose distribution in the CTF room with and without phantom on the couch, with and without scatter radiation from the surroundings (walls, roof and floor) were simulated through energy deposition mesh tally at a height of 138.3 cm from the floor of the room. Radiation dose contours were drawn from the obtained mesh tallies using GNUPlot. Without phantom on the couch the radiation dose levels in the CTF room were low as compared with the scenario employing a phantom. The radiation dose levels in the room were also low when the amount of scatter radiation from the surroundings was deactivated. The sides of the CTF gantry parallel to the patient couch were identified to be the zones with the lowest dose levels in the room for all the scenarios considered.

KEYWORDS: *Monte Carlo; staff dose; scatter radiation; computed tomography; fluoroscopy.*

1 INTRODUCTION

Medical interventional procedures have improved due to the introduction of Computed Tomography Fluoroscopy (CTF) [1] in medical radiology. The influence of patient breathing and motion on image formation during radiology has reduced due to the intrinsic functionality of the CTF [2]. The efficient application of CTF for interventional procedures requires the presence of a medical staff in the room. For this reason, the medical staff is exposed to scatter radiation from the patient, CTF gantry, patient table [3, 4], and walls of the room [2].

Radiation exposure to staff have been observed to be high as reported in other studies [5-7] and due to the high current application of CTF, doses are high compared with conventional fluoroscopy [2]. The medical staff is expected to protect themselves with lead aprons, goggles, thyroid shield, and gloves where applicable and necessary to minimise the radiation exposure.

This paper presents Monte Carlo investigations into radiation dose reduction techniques to the medical staff when in the CTF room. The dose distributions in the room are investigated with different phantoms (voxel phantom and Perspex) including the influence of CTF room surroundings. Recommendations of possible advantageous standing positions for medical staff are given.

2 MATERIALS AND METHOD

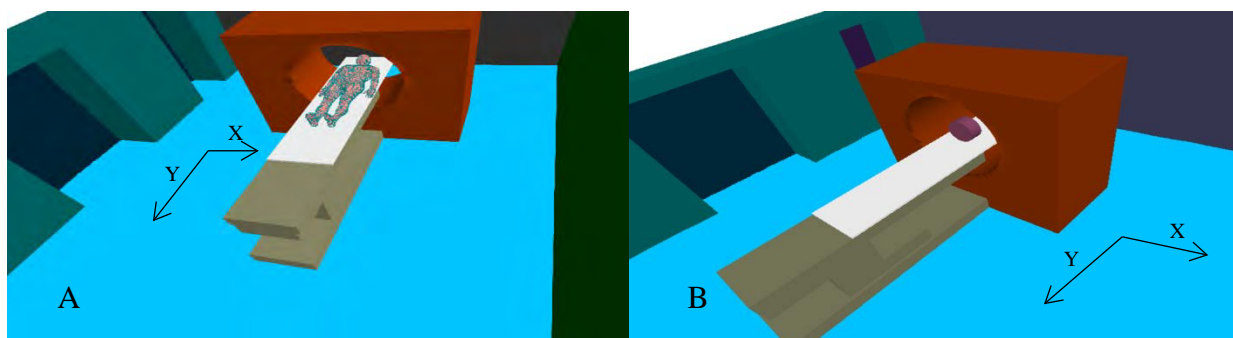
2.1 Modelling

A CTF X-ray tube (represented by 36 point sources at 10° intervals), bowtie-filter, and collimator for a Toshiba Aquilion One 640 slice Computed Tomography (CT) scanner at Korle-Bu Teaching Hospital, Accra [8] were modelled using methods reported by Figueira *et al* [9] and Gu *et al* [10]. An ionisation chamber was also modelled using specifications as given by Gu *et al* [10]. The CTF gantry block, patient table, protective equipment and CTF room were modelled using SimpleGeo [11]. Computational supine mesh phantom of height 175.6 cm according to Cassola *et al* [12], Perspex phantom of height and diameter of 15 cm and 32 cm, respectively, were employed.

* Presenting author, e-mail: frank.becker@kit.edu # Corresponding author, e-mail: pgyekye@yahoo.com

All the individual models were spatially put together on one platform using VOXEL2MCNP [13] as shown in Fig. 1. The models on the VOXEL2MCNP platform were exported to MCNPX input files for simulation.

Figure 1: Scenario with voxel phantom (A) and Perspex (B) on the patient couch



2.2 Spectrum Generation

The photon energy spectrum was generated using SpekCalc [14]. The following specifications of 120 kVp, a tungsten anode angle of 12 degrees, and a 2.5 mm thick aluminium filter were chosen for SpekCalc to generate the necessary spectrum for diagnosis. The mean energy of the spectrum amounted to 54.45 keV. The MCNPX [15] radiation transport code with mesh (PEDEP) tally results for photon was used for the simulations. One billion five hundred million (1.5×10^9) number of particles were tracked in order to have a good compromise between relative error and reasonable computational time.

2.3 Verification of Computed Tomography Fluoroscopy

The modelled computed tomography fluoroscopy machine was verified by measuring computed tomography dose index (CTDI) value at 120 kVp, 100 mA, collimation of 40 mm, tube rotation time of 1 s (full 360 degree tube rotation) from the Toshiba Aquilion One 640 slice CT scanner using a Perspex body phantom (32 cm diameter) and a CT Dose Profiler probe connected to a Barracuda X-ray multimeter, running the Ocean software on a computer [16]. The conversion factor to change the PEDEP: p mesh tally results from $\text{MeV}/\text{cm}^3/\text{particle}$ to $\text{mGy}/100\text{mA}$ in a specified medium of density was calculated using the ratio of measured CTDI_{100} in air per 100mA to simulated CTDI_{100} in air per particle [9,10].

2.4 Scatter Radiation Distribution in the Room

The investigation of the scattered radiation in the CTF room was done by modeling the CTF machine in the room with no object (voxel or Perspex phantom) on the couch. The same model was used again but with voxel and Perspex phantom on the couch alternatively. The energy deposition per unit volume for photon particles in the CTF room in each of the scenario was tabulated. To investigate the effect of the CTF room walls on the scatter radiation in the room, the energy deposition per unit volume for a photon particle in the room was found using the model of the CTF machine with a voxel phantom on the couch in a room with no surroundings (walls, roof and floor). The results of the energy deposition per unit volume at 138.3 cm from the floor in the room for all the scenarios considered were tabulated and converted to $\text{mGy}/100\text{mAs}$ using the verified conversion factor. Dose contours were eventually drawn using GNUPlot 5.0 [17].

3 RESULTS AND DISCUSSIONS

The measured $CTDI_{100}$ in air was 27.01 mGy/100mA and the simulated energy in ionisation chamber in air was 5.97×10^{-8} MeV/g/particle. The calculated conversion factor was 4.52×10^8 mGy.g.particle/100mA/MeV. Using the conversion factor, the simulated $CTDI_{100}$ was 5.96 mGy/100mAs compared with the measured weighted $CTDI_{100}$ 5.94 mGy/100mAs at 120 kVp. The measured and simulated $CTDI_{100}$ is comparable since the percentage deviation is 0.36 %. The relative error associated with the simulation of energy deposition per unit volume in air in the room varied from 0.009 to 0.515, depending on the proximity of the volume of air to the source of radiation.

The radiation dose distribution in air in the CTF room when there is nothing on the patient couch is illustrated in Fig. 2. The radiation dose distribution in air in the CTF room when a Perspex phantom is placed on the patient couch to give scattering effect is shown in Fig. 3. The radiation dose distribution in air in the CTF room when a voxel phantom is placed on the couch to give scattering effect is illustrated in Fig. 4. The radiation dose distribution in air in the CTF room when a voxel phantom is placed on the patient couch in a room with no surroundings is shown in Fig. 5. The Fig. 2 - 5 show room length and breadth on a linear scale representing x and y axis while the dose distribution (mGy/100mAs) was obtained on a log scale representing the z-axis. The z-axis was plotted on a log scale to clearly show the radiation distribution pattern for the low doses in the room. All the figures show a high dose in the magnitude of about 1×10^{11} mGy/100mAs on the log scale (representing actual value of 1.58 MGy/100mAs). This high dose represents the modelled point source of radiation. The lowest dose of Fig. 2, 3, 4, and 5 are in the magnitude of about 1, 10, 100, and 10 mGy/100mAs on the log scale respectively (representing actual value of 0.78, 1.88, 18.40, and 2.89 mGy/100mAs, respectively).

Comparing the lowest doses of Fig. 2, 3 and 4, it can be seen that an object on the patient couch contributes more scatter radiation in the room. The lowest dose in air in the room with Perspex on the couch is about 2.4 times that with no phantom on the couch. Also, the lowest dose in air in the room with voxel phantom on the couch is about 23.5 times that with no phantom on the couch. The size of the voxel phantom is bigger than that of the Perspex phantom and hence the lowest dose distribution by voxel phantom is more than that of Perspex phantom by a factor of 9.8. Additionally, the material composition of both phantoms is not the same and hence would interact with radiation differently. The surroundings (walls, roof and floor) of the CTF room contribute more scatter radiation in the room as illustrated by comparing the lowest dose in air of Fig. 4 and 5 by a factor of 6.4. This suggests that scatter radiation distribution in the room is influenced by its surroundings and hence the room size matters.

The scatter radiation patterns in the room for all the scenarios are not the same. From all the Figures, it can be seen that the highest dose distribution in air is at the source of the radiation (yellow colour) whilst the lowest dose in air (indicated by the darkest colour) is at the sides of the CTF gantry parallel to the patient couch. This is because there is shielding of the radiation by the CTF gantry. By this observation, occupancy in the room is recommended to be on the sides of the CTF gantry if possible for reduced radiation exposure. Alternatively, engineering techniques at the manufacturers' level should be explored to enable the staff stand at this position during the procedure.

Figure 2: Dose distribution in air in the CTF room with no object on the patient couch

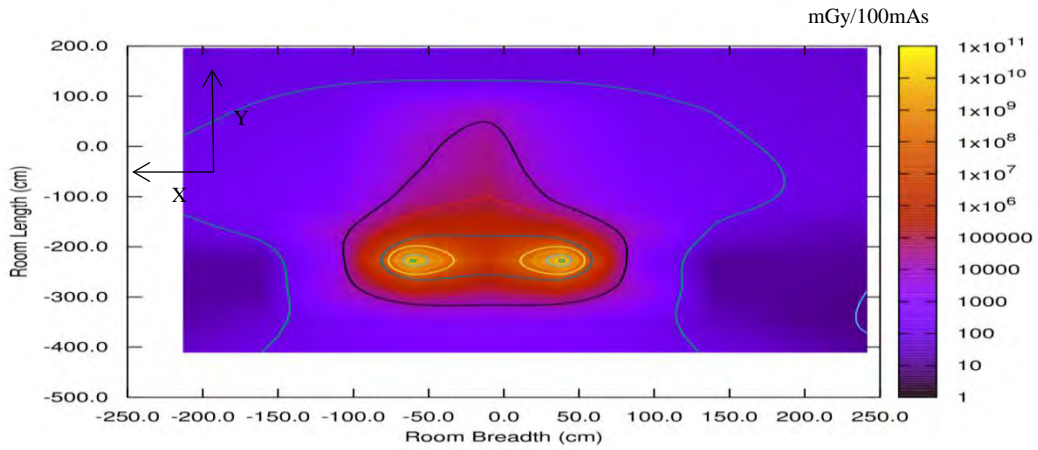


Figure 3: Dose distribution in air in the CTF room with a CTDI Perspex phantom on the patient couch

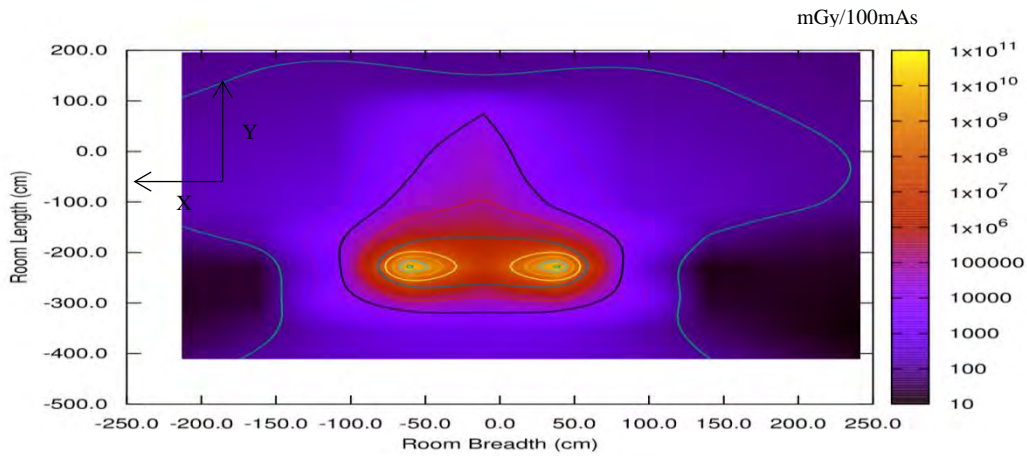


Figure 4: Dose distribution in air in the CTF room with a voxel phantom on the patient couch

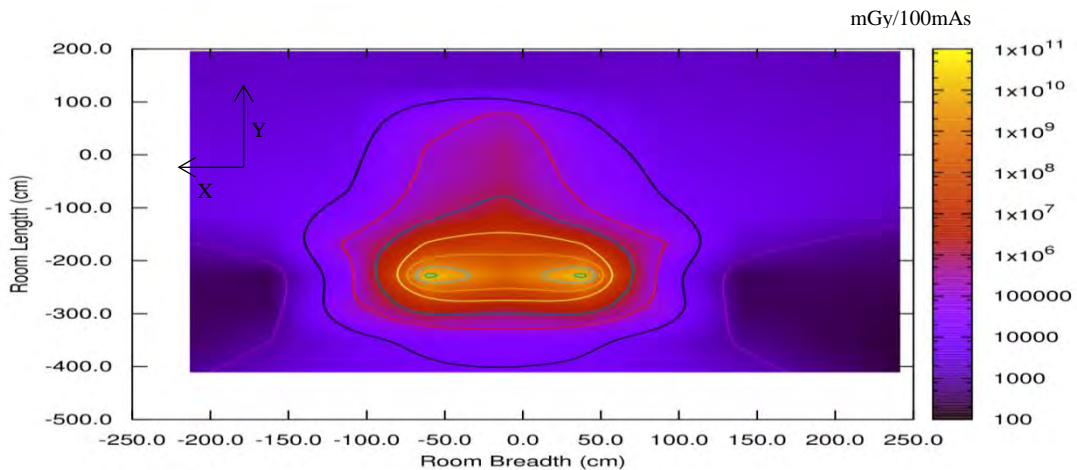
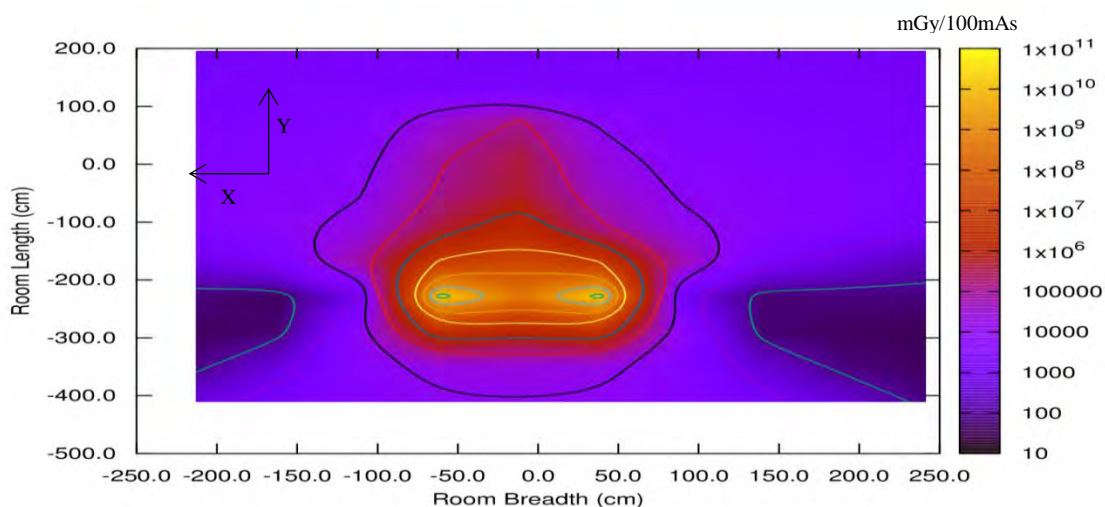


Figure 5: Dose distribution in air in the CTF room with a voxel phantom on the patient couch in boundless surroundings



4 CONCLUSION

The scatter radiation pattern and dose distribution in the CTF room has been investigated. The presence of a phantom on the patient couch has been found to increase the lowest dose in air in the room by a factor of 23.5 and 9.8 for voxel and Perspex phantom, respectively. The CTF room surrounding (wall, floor and roof) has also been found to increase the lowest dose in air in the room by a factor of 6.4. The dose distribution patterns in the room were not the same for the scenario with no phantom on couch, scenario with phantom (Perspex and voxel) on couch, and scenario with no surrounding.

The staff in the CTF room is recommended to stand on the sides of the CTF gantry if possible for reduced radiation exposure. Engineering techniques at the CTF manufacturers' level are also recommended to be explored to make standing on the sides of the CTF gantry by the staff possible.

5 ACKNOWLEDGEMENT

This work was supported by the International Atomic Energy Agency [GHA11026] in collaboration with the Institute for Nuclear Waste Disposal at Karlsruhe Institute of Technology, Germany.

6 REFERENCES

- [1] Carlson, S. K., Bender, C. E., Classic, K. L., et al., 2001. Benefits and safety of CT fluoroscopy in interventional radiologic procedures. *Radiology*. 219: 515-520.
- [2] Tack, D., Kalra, M. K. and Gevenois, P. A., 2012. (eds) Radiation Dose from Multi-detector CT, *Medical Radiology Diagnostic Imaging*. Book Chapter: Buls, B., Vandenbroucke, F. and De Mey, J. Dose reduction in CT fluoroscopy. DOI: 10.1007/174_2011_453, Springer-Verlag Berlin Heidelberg.
- [3] Kato, R., Katada, K., Anno, H., et al., 1996. Interventional radiology of the abdomen and pelvis with real-time CT fluoroscopy. *Radiology*. 201: 478.
- [4] Seibel, R. M., Sehnert, C., Plassmann, et al., 1997. Interventional procedures with real time CT. *Radiology*. 205: 383.
- [5] Nawfel, R. D., Judy, P. F., Silverman, S. G., et al., 2000. Patient and personnel exposure during CT fluoroscopy-guided interventional procedures. *Radiology*. 216: 180-184.
- [6] Silverman, S. G., Tuncali, K., Adams, D. F., et al., 1999. CT Fluoroscopy-guided abdominal interventions: Techniques, Results and Radiation Exposure. *Radiology*. 212: 673-681.

- [7] Stoeckelhuber, B. M., Leibecke, T., Schulz, E., et al., 2005. Radiation Dose to the Radiologist's Hand During Continuous CT Fluoroscopy-Guided Interventions. *Cardiovasc Intervent Radiol.* 28:589–594.
- [8] Korle-Bu Teaching Hospital. Radiology Department. MRI/CT Scan Centre. Accra. Ghana. Retrieved 2016-4-26 from: <http://www.kbth.gov.gh/16/radiology-department.html>.
- [9] Figueira, C., Becker, F., Blunck, C., et al., 2013. Medical staff extremity dosimetry in CT fluoroscopy: an anthropomorphic hand voxel phantom study. *Phys. Med. Biol.* 58: 5433-5448.
- [10] GU, J., Bednarz, B., Caracappa, P. F., et al., 2009. The development, validation and application of a multi-detector CT (MDCT) scanner model for assessing organ doses to the pregnant patient and the fetus using Monte Carlo simulations. *Phys. Med. Biol.* 54: 2699-2717.
- [11] Theis, C., Buchegger, K. H., Brugger, M., et al., 2006. Interactive three-dimensional visualization and creation of geometries for Monte Carlo calculations. *Nuclear Instruments and Methods in Physics Research Section A* 562(2): 827–829.
- [12] Cassola, V. F., de Melo Lima, V. J., Kramer, R. et al., 2010. FASH and MASH: female and male adult human phantoms based on polygon mesh surfaces: I. Development of the anatomy. *Phys. Med. Biol.* 55: 133-162.
- [13] Pölz, S., Laubersheimer, S., Eberhardt, J. S., et al., 2013. Voxel2MCNP: a framework for modeling, simulation and evaluation of radiation transport scenarios for Monte Carlo codes. *Phys. Med. Biol.* 58: 5381-5400.
- [14] Poludniowski, G., Landry, G., DeBlois, F., et al., 2009. SpekCalc: a program to calculate photon spectra from tungsten anode x-ray tubes. *Phys. Med. Biol.* 54: N433-N438.
- [15] Pelowitz, D. B. (2008). MCNPX USER'S MANUAL. Version 2.6.0, Los Alamos National Laboratory Report LA-CP-07-1473.
- [16] RTI Electronics AB. Sweden. Retrieved 2016-4-26 from: <http://rtigroup.com/products/product-detail/ocean-2014>.
- [17] GNUPlot 5.0. Retrieved 2016-4-26 from: <http://www.gnuplot.info/>.

PIMAL: A GUI-Driven Software Package To Conduct Radiation Dose Assessments Using Realistic Phantom Postures

Shaheen Dewji^{a,*}, Mauritius Hiller^a, Nolan Hertel^{a,b,**}, Sami Sherbini^c, Mohammad Saba^c

^aOak Ridge National Laboratory, Center for Radiation Protection Knowledge, Oak Ridge, TN, USA

^bGeorgia Institute of Technology, Nuclear and Radiological Engineering Program, Atlanta, GA, USA

^cUnited States Nuclear Regulatory Commission, Rockville, MD, USA

Abstract. Although receptors may be in a variety of postures when they are exposed to radiation fields, dose coefficients and dose reconstructions have largely been carried out with the computational phantoms in positions with arms straight and attached to the torso and legs straight and joined together. Since 2007, the U.S Nuclear Regulatory Commission funded Oak Ridge National Laboratory to address this issue by developing a phantom capable of articulating limbs through a software platform entitled “Phantom wIth Moving Arms and Legs” (PIMAL). Using a graphical user interface (GUI), PIMAL generates a stylized phantom model for use in the Monte Carlo N-Particle (MCNP) code simulation to determine organ equivalent doses. The latest version PIMAL 4.0 has recently been launched as part of the United States Nuclear Regulatory Commission’s Radiological Protection Computer Code Analysis and Maintenance Program (RAMP). The capabilities, functionality, and recent updates of the PIMAL software will be discussed. Validation of the PIMAL phantom model, as well as case studies contrasting vertical and customized (articulated) human body geometry will be presented.

KEYWORDS: *anthropomorphic phantoms; Monte Carlo simulation; MCNP; dose reconstruction; International Commission on Radiological Protection (ICRP).*

Notice: This manuscript has been authored by UT-Battelle, LLC, under Contract No. DE-AC0500OR22725 with the U.S. Department of Energy. The United States Government retains and the publisher, by accepting the article for publication, acknowledges that the United States Government retains a non-exclusive, paid-up, irrevocable, world-wide license to publish or reproduce the published form of this manuscript, or allow others to do so, for the United States Government purposes. The Department of Energy will provide public access to these results of federally sponsored research in accordance with the DOE Public Access Plan (<http://energy.gov/downloads/doe-public-access-plan>).

1 INTRODUCTION

Historically, phantoms for radiation protection applications were and largely continue to be developed in an upright standing position [1][2][3]. While upright phantoms are sufficient for standard reference positions and irradiation geometries, the estimation of doses for receptors in non-standard configurations requires customizable phantoms to accurately reproduce the body position vis-à-vis exposure to the radiation source. For realistic scenarios, a phantom with limbs in positions corresponding to the receptor’s actual posture is therefore preferred.

Since its initial development in 2007, ORNL has recently updated, expanded, and released¹ the software package, “Phantom wIth Moving Arms and Legs” (PIMAL) [4][5]. Using a graphical user interface (GUI), PIMAL enables the user to adjust the limbs of the phantom in articulated positions to better customize the position of the phantom for estimation of radiation doses. By using the GUI to adjust the limbs, PIMAL creates an file in the format of a Monte Carlo N-Particle (MCNP) transport code [6] input with a geometry corresponding to the phantom whose limbs are in the same configuration as the one modeled in the GUI [4][5].

* Corresponding author, e-mail: dewjisa@ornl.gov

** Presenting author, e-mail: nolan.hertel@me.gatech.edu

¹ PIMAL is available through the United States Nuclear Regulatory Commissions’ (NRC) Radiological Protection Computer Code Analysis and Maintenance Program (RAMP) website. Upon registration approval, PIMAL should be free of charge for most entities / users. Registration for PIMAL is available on the following website: <https://www.usnrc-ramp.com/content/registration-pimal-code>. PIMAL is currently available only for Windows systems.

Figure 1: PIMAL phantom (a) Upright 3D visualization; (b) Articulated 3D visualization; (c) Vised in seated configuration with multiple phantoms².

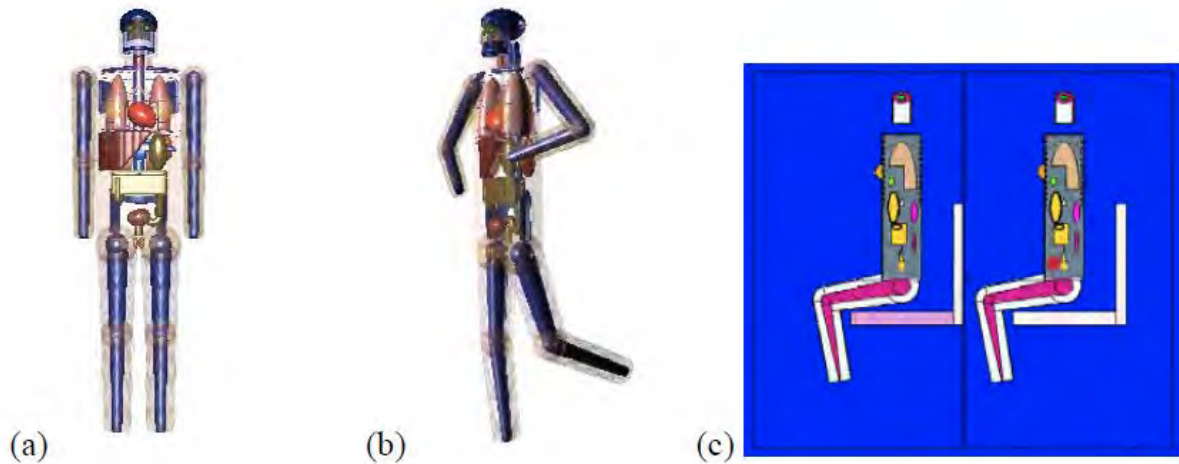


Figure 2 shows a screenshot of the PIMAL GUI. The left section of the screen visualizes a rendered image of the phantom, while the right section houses a series of tabs that permit the user to customize PIMAL, including sliders that allow the user to set the angles of the joints (“Sliders” tab). Alternatively, the angles of the joint can also be entered in text boxes (“Text” tab).

Figure 2: PIMAL GUI interface.

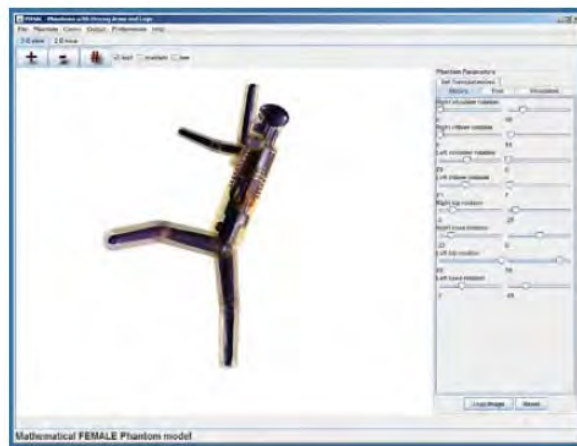


Figure 2 shows the “Simulation” tab in the right plane that allows various parameters to be set for the simulation. This allows the novice MCNP user to insert various source configurations to the input file, and permits experienced MCNP users to manually modify the generated input file with custom preferences.

² Note that PIMAL 4.0 can only create the output for a single articulated phantom. Advanced MCNP users may combine two PIMAL output files to customize and create their own array of articulated phantoms. See [10][11] for examples.

Following MCNP source settings can be made via the GUI (Figure 3):

- **MODE card:** Neutron or neutron and photon source particle
- **ERG (energy) card:**
 - Monoenergetic source with user defined source particle energy (MeV)
 - ^{60}Co , ^{131}I , ^{134}Cs radionuclide source
 - X-ray sources between 80 and 120 kVp
 - AmBe or PuBe neutron source.

Several external source irradiation geometries can be set, including:

- Point source (centered at X, Y, Z coordinates)
- ICRP Publication 116 [7] specified geometries
 - AP (anterior-posterior),
 - PA (posterior-anterior),
 - LLAT (left lateral),
 - RLAT (right lateral)
 and
 - ISO (isotropic).

Internal source organ volume sources can be set within organs of the body, including many of the ICRP 103 [8] organs employed in the computation of effective dose.

- Brain
- Thyroid
- Heart Wall/Content,
- Stomach Wall/Content
- Liver
- Left/Right/Both Lungs
- Left/Right Kidney
- Pancreas

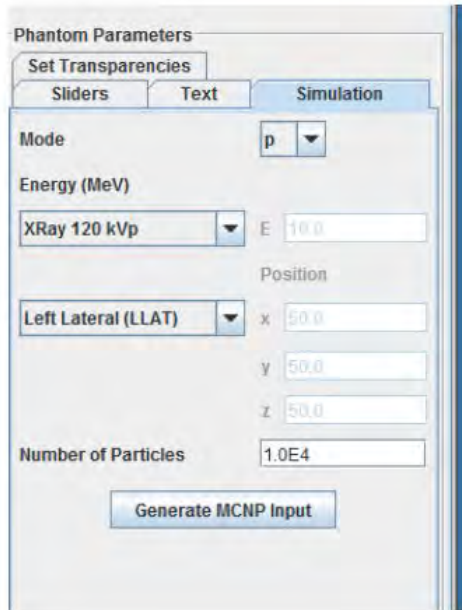
Once parameters have been set within the GUI, an MCNP input deck is generated. This file can either be edited/run outside of PIMAL via the MCNP command prompt or run natively within PIMAL (which calls upon MCNP to run). If run within PIMAL, an organ dose table is displayed within PIMAL upon completion of the MCNP run (Figure 4).

1.2 PIMAL in peer-reviewed literature

Applications of PIMAL in peer-reviewed literature include a study on a glovebox worker comparing an upright phantom with a worker in a realistic posture, using PIMAL to create the phantom [9]. This study shows organ dose differences between the upright vertical and the realistic phantom setup of approximately 20- 50 %.

Another study investigates the Estimated External Doses to Members of the Public from Patients with ^{131}I Treatment [10][11]. Various configuration like a release patient sitting in a bus next to a member of the public (Figure 1c) a patient sitting in the bed wall to wall with a member of the public or a patient lying in a nursing home with a caregiver next to the bed are studied. For distances of the patient and the member of the public under 1 m, differences in the whole body dose between an upright phantom and the phantom in a realistic configuration of more than a factor of 10 are possible.

Figure 3: Simulation parameters in PIMAL. **Figure 4:** Organ dose output table in PIMAL.



Organs	Photon Dose Tally: 216	Relative Error (1 sigma) Tally: 216
liver	1.1923E-17	0.0690
bone marrow	4.1495E-17	0.0558
colon	7.6621E-18	0.0230
lungs	6.8379E-18	0.0142
stomach	3.4212E-18	0.0600
primary bladder	3.3118E-18	0.0372
pancreas	6.0469E-17	0.0234
liver	1.2728E-17	0.0145
esophagus	4.3682E-18	0.0643
thyroid	3.1268E-17	0.0394
skin	2.5151E-17	0.0020
bone surface	2.8916E-17	0.0070
adrenals	6.8135E-18	0.0665
brain	2.1963E-17	0.0127
extrathoracic airways	1.6579E-17	0.0298
small intestine	5.7630E-18	0.0253
kidneys	1.6708E-17	0.0288
muscle	1.1500E-17	0.0041
pancreas	2.7678E-18	0.0728
spleen	9.3348E-18	0.1265
thyroid	4.4414E-18	0.0713
prostate	7.6569E-18	0.1806
eyes	3.1013E-17	0.0421

2 METHODOLOGY

In the calculation of gender averaged effective dose, ICRP Publication 103 defines effective dose as [8]:

$$E = \sum_T w_T \left[\frac{H_T^M + H_T^F}{2} \right] \quad (1)$$

where

H_T^M is the equivalent dose to organ, T, of the male phantom

H_T^F is the equivalent dose to organ, T, of the female phantom, and

w_T is the tissue weighting factor

The equivalent dose (H_T) to the organ or tissue, T, is given as [8]:

$$H_T = \sum_R w_R * D_{T,R} \quad (2)$$

where

w_R is the radiation weighting factor, and

$D_{T,R}$ is the absorbed dose in tissue, T, by radiation type, R.

The inability to reproduce a phantom in a realistic articulated position can potentially misrepresent organ doses (and hence effective dose) compared to that of the standard upright phantom. As a result, a case study was developed for the adult male PIMAL phantom to compare the organ doses for the phantom upright (Figure 5) compared to in a 90 degree bent over position (Figure 6). The phantom was irradiated by a monoenergetic AP source, 200 cm wide x 200 cm height plane at 100 cm distance from PIMAL center, consistent with ICRP Publication 116 standard irradiation geometries. For both the upright and bent phantoms, AP simulations were conducted with monoenergetic photon sources at 0.05 MeV, 0.1 MeV, 0.5 MeV, 1.0 MeV and 5.0 MeV.

Figure 5: The adult male PIMAL stylized phantom in upright position with AP source (side view).

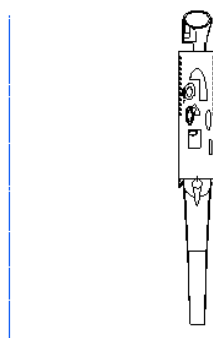
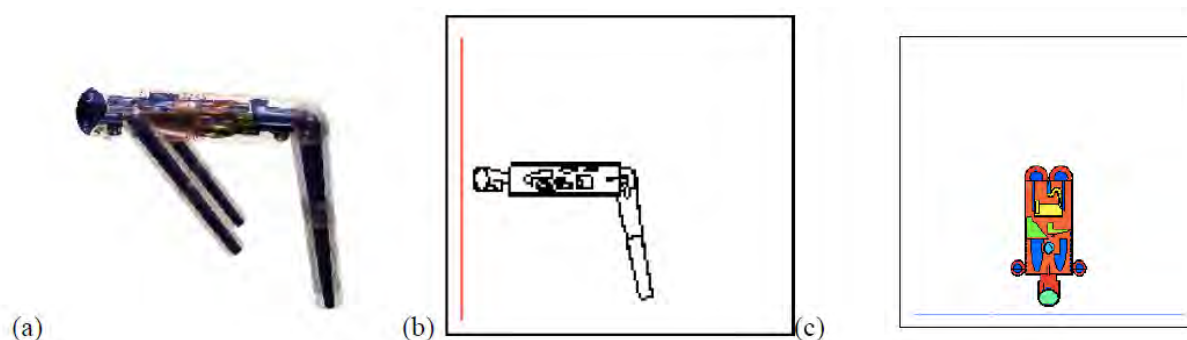


Figure 6: The adult male PIMAL stylized phantom bent in fully bent articulated (90 degree) position: (A) PIMAL phantom software visualization; (B) PIMAL shown in VisEd with AP source (side view); (c) PIMAL shown in VisEd with AP source (aerial view).



Organ doses were estimated in the exposed individual using the kerma approximation. The kerma approximation was implemented in the Monte Carlo simulations using the volume-averaged track-length fluence estimator along with the kerma factors from the MCNP6 nuclear data tables. Electrons were not tracked in these simulations, but bremsstrahlung photons were generated and tracked.

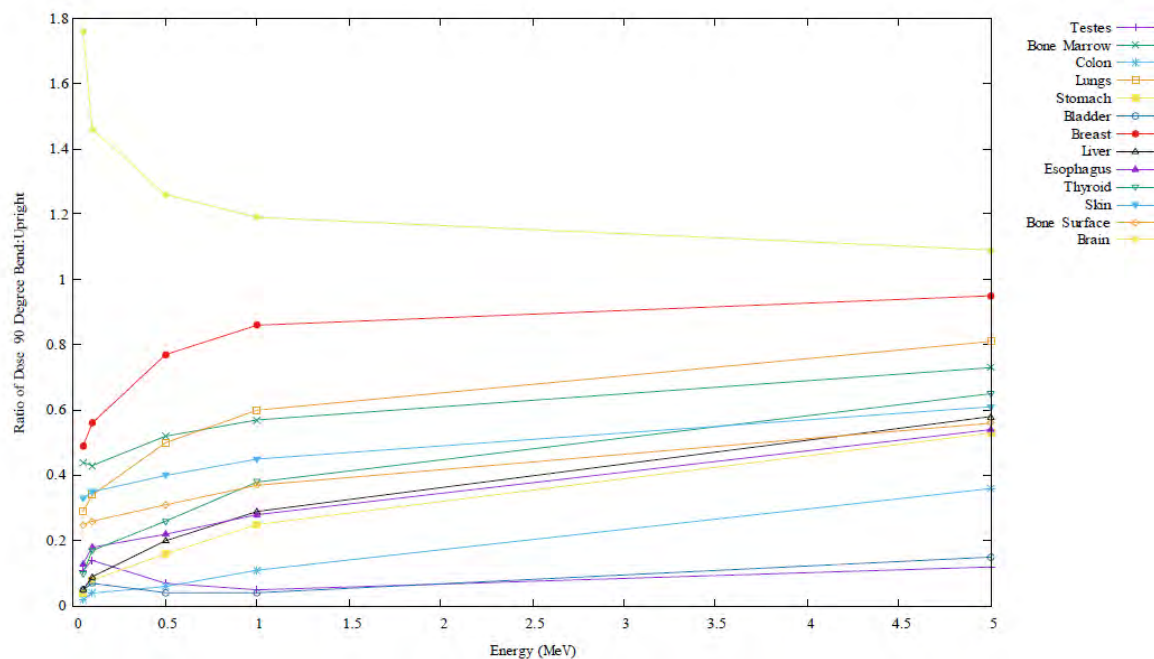
3 RESULTS AND CONCLUSIONS

The ratios of the organ doses of the male PIMAL in the bent to the upright position with an AP irradiation source are given in Figure 7. The organs constituting the ICRP Publication 103 [8] remainder organs have been removed from Figure 7. These PIMAL results do not adopt the ICRP Publication 116 skeletal fluence-to-dose response functions [7] (but can be added manually by the user in the MCNP input deck). Simulations were run with 1×10^9 source particles, resulting in errors $< 2.7\%$ in the adrenal glands.

As expected, the brain exhibited the highest variance when in the bent position, compared to the upright position, given the location of the AP source, as a function of energy. In cases where tissue or organ doses are estimated to be higher in the articulated position compared to the upright position, the dose to the tissue or organ is underestimated using the upright phantom, resulting in inaccurate organ doses as a function of phantom geometry. The brain is underestimated (by using upright) vis-à-vis bent AP by as much as 76% at 0.05 MeV and 9% at 5.0 MeV, hence underestimating equivalent dose and contribution to effective dose.

In cases where the tissue or organ doses are estimated to be lower in the articulated position compared to the upright position – the upright position overestimates the organ dose, which results in calculated higher effective doses than actually received in a given exposure scenario. The testes and bladder exhibited the highest variation as underestimation of dose when bent over, followed by the colon, stomach, esophagus, bone surface, skin, bone marrow, lungs and breast. Remainder organs disregarded. Testes and urinary bladder are over estimated (by using upright) vis-à-vis bent AP by as much as 88% and 96%, respectively, hence overestimating the equivalent dose and contribution to effective dose. Overall, adequate consideration is not given to organ position relative to the irradiation field if the receptor is exposed while in a non-upright position.

Figure 7: Ratio of organ doses of articulated PIMAL (90 degree bend) to upright PIMAL with AP source at energies ranging from 0.05 MeV to 5 MeV.



4 ACKNOWLEDGEMENTS

This work was funded by the United States Nuclear Regulatory Commission under contract number NRC-HQ-60-11-D-0024 with Oak Ridge National Laboratory.

5 REFERENCES

- [1] E.Y. Han, W.E. Bolch, K.F. Eckerman. Revisions to the ORNL series of adult and paediatric computational phantoms for use with the MIRD schema. *Health Phys.* 90, 337–356 (2006).
- [2] International Commission on Radiological Protection. ICRP Publication 110: Adult Reference Computational Phantoms. 39 (2009).
- [3] X.G. Xu, An exponential growth of computational phantom research in radiation protection, imaging, and radiotherapy: a review of the fifty-year history *Physics in Medicine and Biology*, 2014, 59, R233-R302H.
- [4] Akkurt, K.F. Eckerman, 2007. Development of PIMAL: Mathematical Phantom with Moving Arms and Legs. ORNL/TM-2007/14.
- [5] M. Bellamy, H. Akkurt, D. Wiarda, S. A. Dewji, M. Hiller, G. Kora, K. Eckerman, K. Griffin, M. Saba, S. Sherbini, PIMAL: Phantom with Moving Arms and Legs. NUREG/XXXX, 2016. (*In review*)
- [6] D. B. Pelowitz, “MCNP6 User’s Manual Version 1.0,” Vol. LA-CP-13-00634, Rev. 0, 2013.

- [7] International Commission on Radiological Protection. ICRP Publication 116: Conversion Coefficients for Radiological Protection Quantities for External Radiation Exposures. 40 (2010).
- [8] International Commission on Radiological Protection. ICRP Publication 103: The 2007 Recommendations of the International Commission on Radiological Protection. 37 (2007). [9] H. Akkurt, K.B. Bekar, K.F. Eckerman. Assessment of Organ Doses for a Glovebox Worker Using Realistic Postures with PIMAL and VOXMAT. *ORNL/TM-2007/14*.
- [10] S.A. Dewji, M.B. Bellamy, N.E. Hertel, R.W. Leggett, S. Sherbini, M. Saba, K.F. Eckerman. Estimated dose rates to members of the public from external exposure to patients with ¹³¹I thyroid treatment. *Med Phys* 42, 1851 - 1857, 2015.
- [11] S.A. Dewji, M. B. Bellamy, N.E. Hertel, R.W. Leggett, S. Sherbini, M. Saba, K.F. Eckerman. Assessment of the Point-Source Method for Estimating Dose Rates to Members of the Public from Exposure to Patients with ¹³¹I Thyroid Treatment. *Health Phys*, 109, 233 - 241, 2015.

Comprehensive Study on the Response of Neutron Dosimeters in Various Simulated Workplace Neutron Calibration Fields

Sho Nishino^a, Katsuya Hoshi^b, Norio Tsujimura^b, Munehiko Kowatari^a,
Tadayoshi Yoshida^b

^aDepartment of Radiation Protection, Nuclear Science Research Institute, Japan Atomic Energy Agency, 2-4 Shirakata, Tokai, Ibaraki 319-1195, Japan

^bDepartment of Radiation Protection, Nuclear Fuel Cycle Engineering Laboratories, Japan Atomic Energy Agency, 4-33 Muramatsu, Tokai, Ibaraki 319-1112, Japan

Abstract. In order to investigate how neutron dosimeters respond in the continuous neutron fields in workplaces, we performed performance test of four widely-used neutron survey meters at various simulated workplace neutron calibration fields established in two calibration facilities (the FRS and the ICF) in JAEA. As a result, we found that neutron survey meters represented good performance at the fields which have spectral components in the energy range above 1 MeV. On the other hand, survey meters significantly over or underestimated neutron dose equivalent at the fields which have spectral components only in the energy range below 1 MeV.

KEYWORDS: *simulated workplace neutron calibration fields; neutron survey meter.*

1 INTRODUCTION

Reliable measurement of neutron dose still has difficulties in workplaces. Neutron dosimeters, which are used for radiation protection purposes, are generally calibrated in the field produced by ²⁵²Cf and ²⁴¹Am-Be RI neutron sources, as recommended by International Organization for Standardization (ISO) [1]. However, neutron spectra observed in actual workplaces are, in most case, significantly different from those by RI neutron sources. Therefore, dosimeters often over- or under-estimate neutron dose equivalent in workplaces due to their imperfect energy responses. In the EVIDOS project [2], the responses of commercially available area monitors and personal dosimeters were systematically evaluated in various workplaces and calibration fields. As a result, the response of area monitors distributed between 0.5 and 1.5 in term of ambient dose equivalent, $H^*(10)$, however, personal dosimeters significantly over- or under-estimated neutron dose equivalent especially in the fields with soft spectra. Saegusa et al. mentioned the importance of the fields-specific calibration of neutron dosimeters, by evaluating relationship between predicted readings of dosimeters and actual dose equivalent using calculated energy responses of dosimeters and neutron spectra data of various workplaces [3].

For the fields-specific calibration of neutron dosimeters, a lot of simulated workplace neutron calibration fields have been developed at the calibration facilities in the world. In Japan Atomic Energy Agency (JAEA), several different types of simulated workplace neutron calibration fields have been established and operating at the Facility of Radiation Standards (FRS) and the Instrument Calibration Facility (ICF). These fields show different neutron spectra whose fluence-averaged energies range from several tens of keV to a few MeV. However, it is not systematically understood how the responses vary when the same neutron dosimeter is calibrated at different types of simulated workplace neutron fields.

In this paper, we show $H^*(10)$ responses of some neutron survey meters obtained in various simulated workplace neutron calibration fields in the FRS and the ICF, collating with characteristics of neutron fields, and give fundamental policy for calibrations of neutron survey meters used in workplaces with continuous neutron spectra.

Correspondent e-mail: nishino.sho@jaea.go.jp

2 NEUTRON CALIBRATION FIELDS ESTABLISHED AT THE FRS AND THE ICF

In the FRS and the ICF, two calibration facilities in JAEA, four kinds of simulated workplace neutron calibration fields have been constructed, in addition to reference neutron calibration fields using ^{252}Cf and $^{241}\text{Am-Be}$ sources, and thermal neutron calibration field authorized in ISO 8529 series [1]. Calibration fields used in the study are summarized in Table 1. The characteristic of simulated workplace fields are briefly described below;

Graphite-moderated $^{241}\text{Am-Be}$ fields (FRS): Moderated neutron calibration fields using two $^{241}\text{Am-Be}$ sources and a graphite moderator (150 cm(W) × 164 cm(D) × 150 cm(H)) [4]. The sheet containing gadolinium with a thickness of 1 mm is put on the surface of graphite moderator in order to decrease an amount of thermal neutrons. Two fields with different neutron spectra are available by changing positions of neutron sources. The spectra are similar to those in workplaces of nuclear fuel processing facilities.

D₂O-moderated ^{252}Cf field (FRS): Moderated neutron calibration field using ^{252}Cf sources and a spherical D₂O moderator (30 cm in radius) [5]. The field is authorized in ISO8529-1 [1]. D₂O sphere is covered by a cadmium shell with a thickness of 1 mm, in order to decrease an amount of thermal neutrons. The spectrum is similar to those in workplaces of nuclear reactors.

PMMA/steel-moderated ^{252}Cf field (ICF): Moderated neutron calibration fields using ^{252}Cf source and PMMA and/or steel moderators [6]. Twelve fields with different neutron spectra are available by changing combination and dimension of moderators. The fields simulate spectra given in workplace of MOX fuel facilities.

D₂O-moderated $^{241}\text{Am-Li}$ field (ICF): Moderated neutron calibration fields using two $^{241}\text{Am-Li}$ sources and a cylindrical D₂O moderator (27 cm(φ) × 30 cm(H)) with/without PMMA (15 mm in thick). The neutron energy distribution is limited only in the energy range below 1 MeV, because $^{241}\text{Am-Li}$ source hardly emits neutrons with energy higher than 1 MeV. The fields simulate spectra in workplace near a shipping cask of spent nuclear fuel.

Table 1: Fluence-averaged energies and reference ambient dose equivalent rates of neutron calibration fields established in the FRS and the ICF.

	Calibration Field ^{*1}	Number of Fields	Fluence-averaged Energy [MeV]	Reference H [†] (10) rate ^{*2} [μSv h ⁻¹]
FRS	^{252}Cf (fast)	1	2.13	< 1430
	$^{241}\text{Am-Be}$ (fast)	1	4.16	< 110
	D ₂ O- ^{252}Cf (moderated)	1	0.55	< 4.6
	graphite-moderated $^{241}\text{Am-Be}$ (moderated)	2	0.86/0.60	49.3/21.4
	graphite-moderated ^{252}Cf (thermal)	1	2.5×10^{-8}	9.6
ICF	^{252}Cf (fast)	1	2.0	1630
	$^{241}\text{Am-Be}$ (fast)	1	4.16	< 76
	$^{241}\text{Am-Li}$ (fast)	1	0.41	8.4
	PMMA/steel-moderated ^{252}Cf (moderated)	12	0.44~1.7	203~1450
	D ₂ O- $^{241}\text{Am-Li}$ (moderated)	2	0.058/0.041	1.3/0.8

*1 fast: fast neutron field, moderated: simulated workplace neutron field, thermal: thermal neutron field.

*2 Reference H[†](10) rates are values in Jun 2015.

Neutron spectra and Reference dose equivalent rates

The simulated workplace neutron calibration fields at the FRS and the ICF have been established independently in different periods. However, simulated workplace neutron calibration fields are basically established in accordance with the recommendation of ISO12789 series [7],[8] that provide the guideline for producing and characterizing simulated workplace neutron fields.

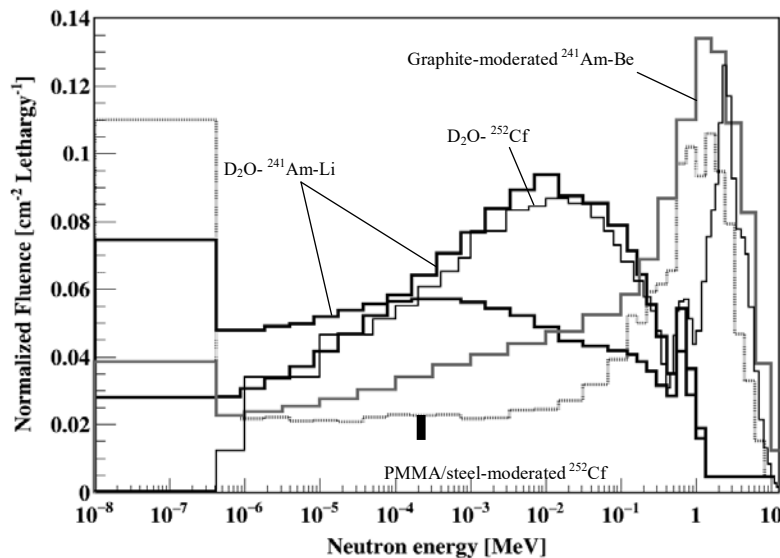
The neutron energy spectra at the point of test are evaluated experimentally using the Bonner Multi-sphere Spectrometer (BMS). The BMS used in the FRS consists of a spherical BF_3 -filled proportional counter (5.1 cm in diameter, 0.26 atm) and polyethylene moderators with 8 different thicknesses of 1, 2, 3, 4, 6, 8, 10 and 14 cm, respectively. The BMS used in the ICF, meanwhile, consists of a spherical ^3He -filled proportional counter (5.1 cm in diameter, 5 atm) and polyethylene moderators with 8 different thicknesses of 1.5, 2.3, 3, 4, 5, 7, 9 and 11.5 cm, respectively. The response functions of BMSs were independently evaluated. The thermal neutron fluence was measured separately by the cadmium difference method if needed. The spectra were unfolded using SANDII code [9] in conjunction with initial guess spectra calculated by the Monte-Carlo simulation code MCNP [10]. With regards to D_2O -moderated ^{252}Cf and D_2O -moderated $^{241}\text{Am-Li}$ fields, the spectra of direct neutrons are evaluated by the shadow-shield method. On the other hand, as for graphite-moderated $^{241}\text{Am-Be}$ and PMMA/steel-moderated ^{252}Cf fields, angle-integrated energy spectra containing room-scattered neutrons are evaluated. Some representative spectra are shown in Figure 1.

Reference ambient dose equivalent $H^*(10)$ rate was determined from neutron energy spectra measured using the BMS, as below,

$$H^*(10) = \sum_E \Phi(E) \cdot h^*(10; E)$$

where $\Phi(E)$ is neutron fluence, $h^*(10; E)$ is conversion coefficients from neutron fluence to dose equivalent, taken from ICRP Publication 74 [11].

Figure 1: The representative energy spectra of simulated workplace neutron calibration fields at the FRS and the ICF [4]-[6]. The spectra are normalized so that a total fluence equals to 1.



3 EXPERIMENT AND RESULTS

We carried out the performance tests of four different neutron survey meters in the neutron calibration fields at the FRS and the ICF, in order to understand the relationship between the response of neutron survey meters and the energy spectra of neutron fields. The survey meters to be tested, Studsvik 2202D, ALOKA TPS-451C, Fuji elec. NSN1 and Fuji elec. NSN3, are widely used in nuclear facilities in Japan. The appearance and characteristics of those are shown in and Figure 2 and Table 2. It should be pointed out that the principles of neutron detection are different between the former three and the latter one. The former is moderated-neutron detecting type using BF_3 or ^3He detector with polyethylene moderator. And the latter, that is NSN3, is a recoil proton-detecting type using mixed gas ($\text{CH}_4 + \text{N}_2$), moreover the effective area for low energy neutrons is compensated by $^{14}\text{N}(n, p)^{14}\text{C}$ reactions. NSN3 is much lighter (~ 2 kg) than others because it does not require moderators.

The quantity to be evaluated in the test is $H^*(10)$ response (hereafter $R_{H^*(10)}$), which is defined as a reading of survey meter divided by the reference ambient dose equivalent $H^*(10)$ rate of the fields. Note that $R_{H^*(10)} (> 1)$ and $R_{H^*(10)} (< 1)$ mean over and underestimation of neutron dose, respectively. Moreover, $R_{H^*(10)}$ given at each calibration fields is normalized by the $R_{H^*(10)}$ given at ^{252}Cf fast neutron calibration field, to make comparison easy.

Figure 2: The appearance of neutron survey meters to be tested.

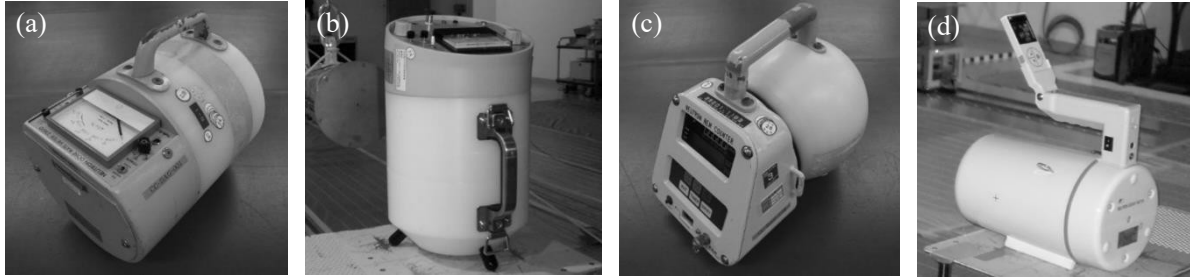
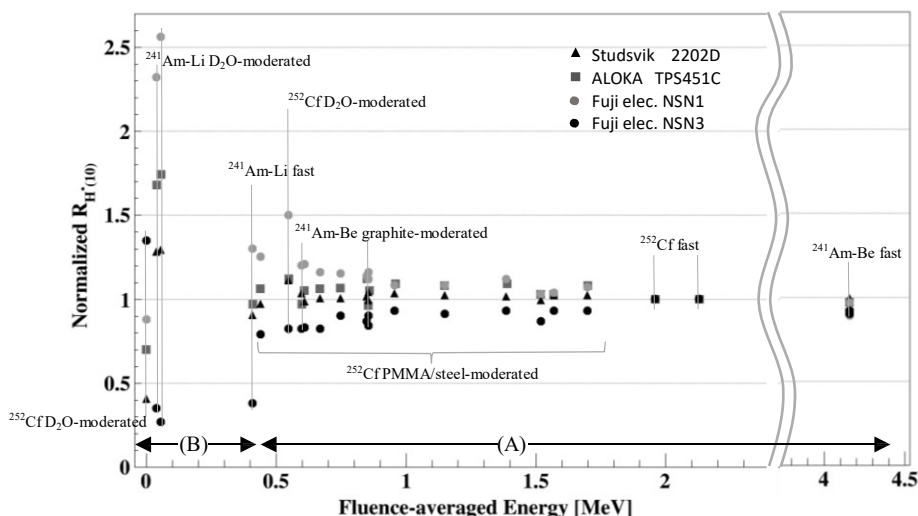


Table 2: The characteristics of neutron survey meters to be tested.

Instruments	Characteristics	Type of detection
(a) Studsvik 2202D	shape: cylindrical , weight: 10.5 kg detector: BF_3 , 2.5 cm ϕ \times 12.6 cm moderator: 21.5 cm ϕ \times 23 cm	moderated neutron: $^{10}\text{B}(\text{n}, \alpha)^7\text{Li}$
(b) ALOKA TPS451C	shape: cylindrical , weight: 9 kg detector: ^3He , 2.5 cm ϕ \times 15.5 cm moderator: 21 cm ϕ \times 23 cm	moderated neutron: $^3\text{He}(\text{n}, \text{p})^3\text{H}$
(c) Fuji elec. NSN1	shape: spherical , weight: 7 kg detector: ^3He , 5.2 cm ϕ moderator: 21 cm ϕ	moderated neutron: $^3\text{He}(\text{n}, \text{p})^3\text{H}$
(d) Fuji elec. NSN3	shape: cylindrical , weight: 2 kg detector: mixed gas (CH_4+N_2) size: 16.4 cm ϕ \times 29.0 cm	recoil proton: $^1\text{H}(\text{n}, \text{n})^1\text{H}$ moderated neutron: $^{14}\text{N}(\text{n}, \text{p})^{14}\text{C}$

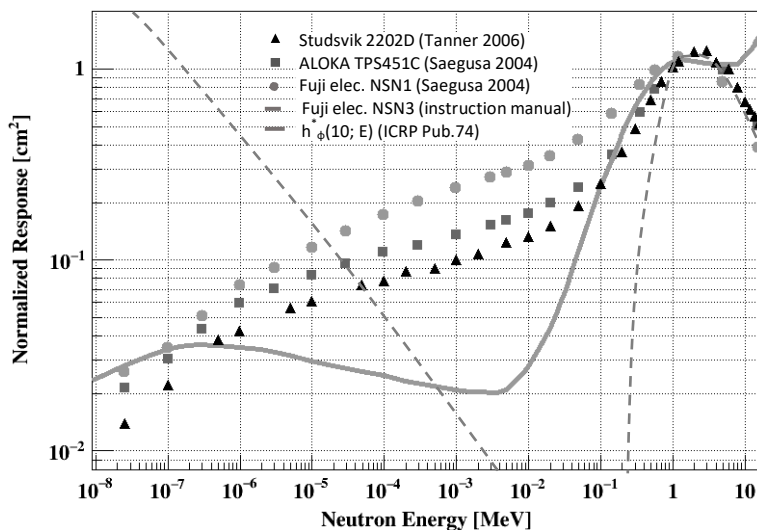
The $R_{H^*(10)}$ values of survey meters given at each calibration field are shown in Figure 3 as a function of fluence-averaged energies of the calibration fields. The uncertainties of $R_{H^*(10)}$ derived from statistical uncertainties in measurements are less than about 3%, though they are not shown in the figure for simplification. The trend of $R_{H^*(10)}$ distribution significantly changes at around the fluence-averaged energy of 0.4 MeV. In the fields whose averaged energies are greater than 0.4 MeV, ^{252}Cf , $^{241}\text{Am-Be}$, $\text{D}_2\text{O-}^{252}\text{Cf}$, graphite-moderated $^{241}\text{Am-Be}$ and PMMA/steel-moderated ^{252}Cf fields (shown in the Figure 3 as (A)), $R_{H^*(10)}$ of all survey meters distribute within 1.0 ± 0.3 , except $R_{H^*(10)} = 1.5$ of NSN1 given at the $\text{D}_2\text{O-}^{252}\text{Cf}$ field. Moreover, $R_{H^*(10)}$ values weakly correlated with fluence-averaged energy of fields. The correlation is represented as $R_{H^*(10)} = a(E_\phi - E_{\phi, \text{cf}}) + 1$, where E_ϕ is fluence-averaged energy and a is a proportional constant. If the correction factor is provided, a dispersion of $R_{H^*(10)}$ is settled within 1.0 ± 0.1 . On the other hand, the fields whose averaged energies are less than about 0.4 MeV, $^{241}\text{Am-Li}$, $\text{D}_2\text{O-}^{241}\text{Am-Li}$ and thermal neutron fields (shown in the Figure 3 as (B)), $R_{H^*(10)}$ were significantly dispersed especially at $\text{D}_2\text{O-}^{241}\text{Am-Li}$ fields. $R_{H^*(10)}$ reached up to 2.5 (NSN1) and down to 0.3 (NSN3). Furthermore, $R_{H^*(10)}$ shows significantly different trends depending on type of detection; moderated neutron-detecting type shows most overestimated value at $\text{D}_2\text{O-}^{241}\text{Am-Li}$ fields, however, recoil proton-detecting type shows most underestimated value at the same fields.

Figure 3: The relationship between $R_{H^*(10)}$ values of survey meters and fluence-averaged energies of the calibration fields.



Between (A) and (B) -fields shown in the figure 3, calibration fields categorized in the (B) have no neutron components with energy range above 1 MeV. On the other hand, calibration fields designated as (A) have neutron components with energies above 1 MeV in the spectra. This was a rather important feature than the fluence-average energy of the fields. Neutron survey meters is designed whose response function could reproduce fluence-to-ambient dose equivalent conversion coefficient $h^*_\phi(10; E)$ in the whole energy region. In Figure 4, the energy responses of neutron survey meters (taken from [12]-[14]) are shown together with $h^*_\phi(10; E)$ taken from ICRP Publication 74 [11]. The each response function is normalized by that for ^{252}Cf source. In the energy range above 1 MeV, $h^*_\phi(10; E)$ is much higher than those in other energy ranges. Therefore, in most survey meters, the response function is optimized in the energy range of 1 MeV to a few MeV, so as to give an accurate dose in this range. On the other hand, the response of survey meters in the energy range below 1 MeV doesn't match $h^*_\phi(10; E)$ so much. The $R_{H^*(10)}$ distribution given in this work would be then explained as follows: If the fields has spectral components in the energy range above 1 MeV, the contribution of this range would be dominant to expected total dose. At the same time, response in below 1 MeV hardly affect to total dose. On the other hand, if the fields has spectral components only in below 1 MeV, response that is so far from the ideal $h^*_\phi(10; E)$ is to be directly reflected in expected total dose. The response function of NSN3 in energy range below 100 keV is quite contrary to others. This is the reason why $R_{H^*(10)}$ for NSN3 showed quite different tendency.

Figure 4: The energy response of neutron survey meters. A Fluence-to-dose equivalent conversion coefficient $h^*_\phi(10; E)$ is overwritten in the figure.



4 CONCLUSION

In this work, we experimentally revealed the responses of neutron survey meters in the continuous neutron fields, using simulated workplace neutron fields in the FRS and the ICF. As a result, we found that neutron survey meters significantly over or underestimate neutron dose equivalent at the fields whose neutron energy distribution is limited in the energy range below 1 MeV. Therefore, we must be careful for radiation protection at, for example, workplaces near transfer casks for nuclear fuel (or debris), or workplaces of Boron Neutron Capture Therapy (BNCT) using accelerators, in which neutrons with energy below 1 MeV are dominant.

For more exact measurements of neutron dose equivalent at workplaces, a fundamental policy for calibration of neutron survey meters are suggested as below. For the survey meters used in the workplaces which have spectral components in the energy range above 1 MeV, the calibration using ^{252}Cf or $^{241}\text{Am-Be}$ source recommended in ISO 8529 series is appropriate. However, for the survey meters used in the workplaces which have spectral components only in the energy range below 1 MeV, the field-specific calibration using simulated workplace calibration fields is strongly required.

5 REFERENCES

- [1] International Organization for Standardization 2001 Reference Neutron Radiations—Part I: Characteristic and Methods of Production, International Standard, 8529-1(Geneva, Switzerland: ISO).
- [2] Schuhmacher, H. et al., “Evaluation of Individual Dosimetry in Mixed Neutron and Photon Radiation Fields (EVIDOS), Final report (Summary)”, 2005.
- [3] Saegusa, J., Tanimura, Y., Yoshizawa, M., “Relation between Neutron Dosimeter Readings and Calibration Fields for Various Workplace spectra”, 2004, Proceedings of IRPA-11.
- [4] Nishino, S., Tanimura, Y., Ebata, Y. and Yoshizawa, M., “Development of the Graphite-Moderated Neutron Calibration Fields using $^{241}\text{Am-Be}$ sources in JAEA-FRS”, 2016, Proceedings of ISORD-8, to be published.
- [5] Tsujimura, N., Yoshida, T. and Takada, C., “Development of Moderated Neutron Calibration Fields Simulating Workplaces of MOX Fuel Facilities”, Japanese Journal of Health Physics Vol. 40 (2005) No. 4 P 354-359.
- [6] Kowatari, M., Fujii, K., Takahashi, M. et al., “Evaluation of the characteristics of the neutron reference field using D₂O-moderated ^{252}Cf source”, (2007), Radiat. Prot. Dosim. 1-7
- [7] International Organization for Standardization 2008 Reference Neutron Radiations—Simulated Workplace Neutron Calibration Fields: I. Characteristic and Methods of Production, International Standard, 12789-1(Geneva, Switzerland: ISO).
- [8] International Organization for Standardization 2008 Reference Neutron Radiations—Simulated Workplace Neutron Calibration Fields: II. Calibration Fundamentals related to the Basic Quantities, International Standard, 12789-2(Geneva, Switzerland: ISO).
- [9] W. N. McElroy., S. Berg., T. Crockett., R. G. Hawkins. : “A Computer-Automated Iterative Method for Neutron Flux Spectra Determination by Foil Activation”, AFWL-TR-67-41 (1967).
- [10] Briesmeister, J. E. (ed.): “MCNP- A General Monte Carlo Code N-Particle Transport Code Version 4B”, LA-12625-M (1997).
- [11] International Commission on Radiological Protection (ICRP). Conversion coefficients for use in radiological protection against external radiation. ICRP Publication 74. Annals of the ICRP, 27(4), (1996).
- [12] Saegusa, J., Yoshizawa, M., Tanimura, Y. et al., “Evaluation of energy response for neutron dose-equivalent meters made in Japan”, Necl. Instrum. Meth., A516(1): 193-202, (2004).
- [13] Tanner, R. J. et al, “Practical implimecation of neutron survey instrument performance”, 2006, Health Protection Agency Report, HPA-RPD-016.
- [14] Instruction manual of Portable Neutron Survey Meter NSN3, Fuji Electric Co. Ltd.

Estimation of basic characteristics about scintillation type survey meter using multi pixel photon counter

Toshioh Fujibuchi

Department of Health Sciences, Faculty of Medical Sciences, Kyushu University, Fukuoka, Japan

Abstract. Survey meters are portable radiation detection and measurement instruments used to check personnel, equipment and facilities for radioactive contamination, or to measure external or ambient ionizing radiation fields to evaluate the direct exposure hazard. Detectors based on scintillation are known as scintillation detectors and belong to the class of solid state detectors. Scintillating phosphors include solid organic materials such as anthracene, stilbene and plastic scintillators as well as thallium activated inorganic phosphors such as NaI(Tl) or CsI(Tl). A photomultiplier tube (PMT) is optically coupled to the scintillator to convert the light pulse into an electric pulse. Recently, some survey meters use photodiodes in place of PMTs. The photodiode calls multi pixel photon counter (MPPC). In this study, the basic characteristics of the three kinds of survey meter using MPPC were estimated. We used C12137 (Hamamatsu Photonics K. K., Japan), T-GMK2-S(TAC Inc., Japan), and iMetry(Seed Technology Ltd.,China) as scintillation survey meter using with MPPC. Both CsI(Tl) is used as a scintillator. TCS-172(Hitachi aloka Co. Ltd., Japan) which was NaI(Tl) scintillation survey meter using with PMT, was used to compare with MPPC survey meters. We used three radioisotope point sources (Cobalt-60, Cesium-137, and Barium-137). Dose rate characteristics, direction characteristics, energy characteristics were estimated. The linearity of the dose rate were confirmed from 0.1 $\mu\text{Sv/h}$ to 100 $\mu\text{Sv/h}$ with TCS-172B and C12137, from 0.3 $\mu\text{Sv/h}$ to 100 $\mu\text{Sv/h}$ with T-GMK2-S and from 0.1 $\mu\text{Sv/h}$ to 20 $\mu\text{Sv/h}$ with iMetry.

KEYWORDS: *survey meter; multi pixel photon counter.*

1 INTRODUCTION

Survey meters are portable radiation detection and measurement instruments used to check personnel, equipment and facilities for radioactive contamination, or to measure external or ambient ionizing radiation fields to evaluate the direct exposure hazard. The hand-held survey meter is probably the most familiar radiation measuring device to society owing to its wide and highly visible use. The most commonly used hand-held survey meters are ionization type, Geiger-Muller (GM) type and scintillation detector type. The choice of detector depends on the type of radiation going to measure, energy, and quantity to be measured. The above-mentioned type survey meters are available in portable meters with capable of measuring radiation count rate in $\mu\text{Sv/hr}$.

Detectors based on scintillation (light emission) are known as scintillation detectors and belong to the class of solid state detectors. Certain organic and inorganic crystals contain activator atoms, emit scintillations upon absorption of radiation and are referred to as phosphors. High atomic number phosphors are mostly used for the measurement of gamma rays, while plastic scintillators are mostly used with beta particles. Scintillating phosphors include solid organic materials such as anthracene, stilbene and plastic scintillators as well as thallium activated inorganic phosphors such as NaI(Tl) or CsI(Tl). A photomultiplier tube (PMT) is optically coupled to the scintillator to convert the light pulse into an electric pulse.

Recently, Multi-Pixel Photon Counter (MPPC) as the photodetector which using semiconductor has been developed 2). MPPC is an aggregate of avalanche photodiode which did each pixel size small up to tens micrometer. MPPC can be used by low voltage, and it does not undergo influence in a magnetic field, therefore MPPC is expected to apply in the wide range of areas 3,4). It's used for PET-MRI at the medical field 5). The survey meter for using MPPC was used is sold from several manufactures.

In this study, basic characteristics of three kind of survey meter for which using MPPC were estimated. The utility on the radiation management was considered by comparing with the scintillation system survey meter of the conventional PMT type.

2 MATERIALS AND METHODS

2.1 Detectors

We used C12137 (Hamamatsu Photonics K. K., Japan), T-GMK2-S(TAC Inc., Japan), and iMetry(Seed Technology Ltd.,China) as scintillation survey meter using with MPPC. Both CsI(Tl) is used as a scintillator. TCS-172(Hitachi aloka Co. Ltd., Japan) which was NaI(Tl) scintillation survey meter using with PMT, was used to compare with MPPC survey meters.

Table 1: Specifications of survey meters.

Product name	Scintillator crystal	Volume of scintillator [cm ³]	Photon detector	MCA
TCS-172B (ALOKA)	NaI(Tl)	12.87 ($\phi 2.54 \times 2.54$)	Photomultiplier	No
C12137 (Hamamatsu Photonics)	CsI(Tl)	4.5 ($2 \times 1.5 \times 1.5$)	MPPC	Yes
iMetry (Seed studio)	CsI(Tl)	2 ($2 \times 1 \times 1$)	MPPC	Yes
T-GMK2-S (TAC)	CsI(Tl)	0.5 ($2 \times 0.5 \times 0.5$)	MPPC	Yes

Figure 1: Photographs of detectors. Left upper: iMetry, Right upper:c12137 and Right middle: T-GMK2-S.



2.2 Radiation source

We used three radioisotope point sources (Cobalt-60 with 1173 keV and 133 keV, Cesium-137 with 662 keV, and Barium-133 with 81 keV, 303keV and 356 keV).

2.3 Dose rate characteristics

We estimated dose rate characteristics using Cesium-137 radiation source with detector to source distance change from 5cm to 60 cm.

2.4 Direction characteristics

We estimated direction characteristics for horizontal axis and vertical axis using Cesium-137 radiation source. The geometry of estimations are shown in Fig.2.

3 RESULTS

3.1 Dose rate characteristics

The linearity of the dose rate were confirmed from 0.1 $\mu\text{Sv/h}$ to 100 $\mu\text{Sv/h}$ with TCS-172B and C12137, from 0.3 $\mu\text{Sv/h}$ to 100 $\mu\text{Sv/h}$ with T-GMK2-S and from 0.1 $\mu\text{Sv/h}$ to 20 $\mu\text{Sv/h}$ with iMetry.

3.2 Direction characteristics

All survey meters of the energy characteristic sensitivities were less than $\pm 20\%$ with the theoretical value. Scintillation survey meter using MPPC could measure gamma-ray energy spectrum. Scintillation survey meter using MPPC can be useful in radiation management.

4 CONCLUSION

Scintillation survey meter using MPPC were shown good responses. These survey meters can be useful in radiation management.

Figure 2: The geometry of direction characteristics estimation.

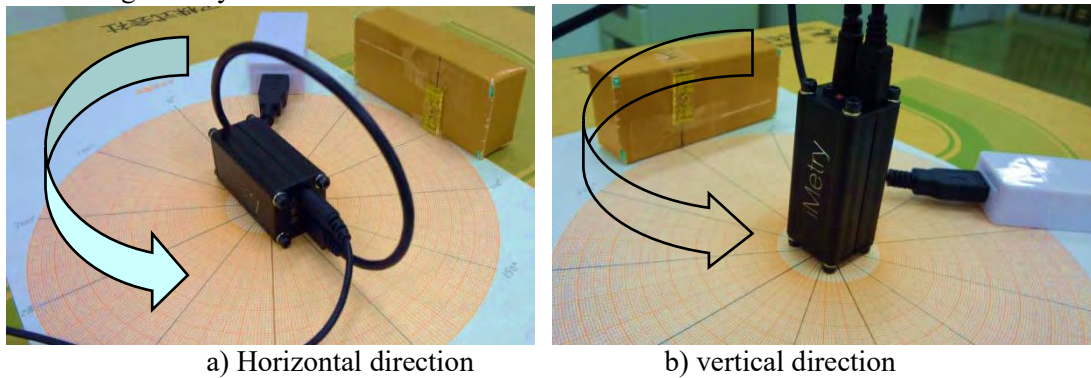


Figure 3: Count rate and dose rate characteristics of MPPC survey meters.

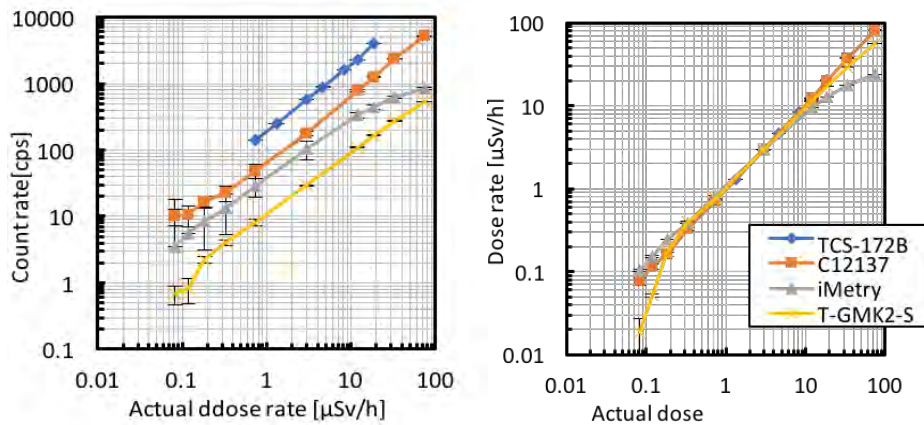
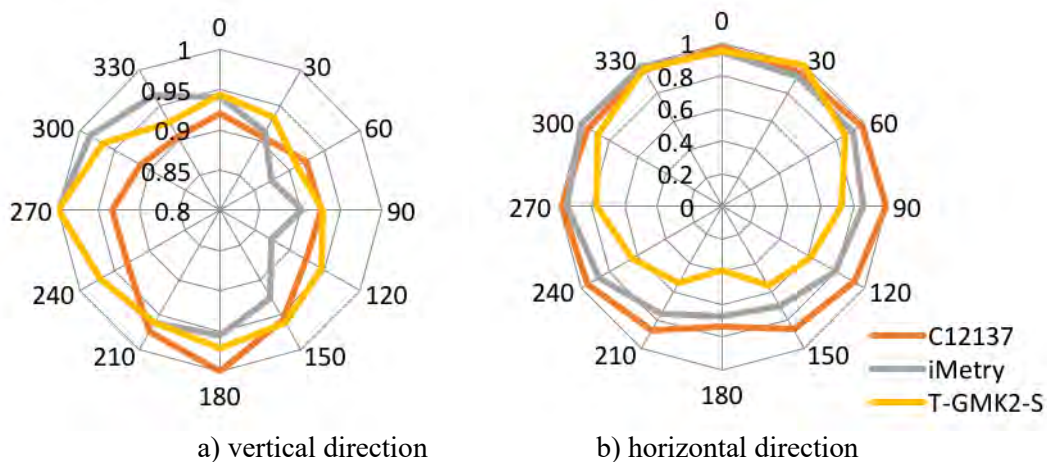


Figure 4: Direction characteristics of MPPC survey meters.



5 REFERENCES

- [1] Nishizawa K, Maekoshi H. Thyroidal ¹²⁵I monitoring system using an NaI (TI) survey meter. *Health Phys.* 1990 Feb;58(2):165-9.
- [2] Buzhan P, Dolgoshein B, Filatov L, Ilyin A, Kantzerov V, Kaplin V, Karakash A, Kayumov F, Klemin S, Popova E, Smirnov S. Silicon photomultiplier and its possible applications *Nuclear Instruments and Methods in Physics Research A* 504 (2003) 48–52.
- [3] Kolb A, Lorenz E, Judenhofer MS, Renker D, Lankes K, Pichler BJ. Evaluation of Geiger-mode APDs for PET block detector designs. *Phys Med Biol.* 2010 Apr 7;55(7):1815-32.
- [4] Bieniosek MF, Olcott PD, Levin CS. Readout strategy of an electro-optical coupled PET detector for time-of-flight PET/MRI. *Phys Med Biol.* 2013 Oct 21;58(20):7227-38.
- [5] Huizenga J, Seifert S, Schreuder F, Dam HTv, Dendooven P, Löhner H, Vinke R, Schaart DRA. Fast preamplifier concept for SiPM based time-of-flight PET detectors. *Nucl Instrum Methods.* 2012; A695:379–84.

Comparison of dose rate measurements of commercially available hand-held gamma detectors with radiation protection dose meter

Theo Köble*, Hermann Friedrich

Fraunhofer-INT, D-53879 Euskirchen, Germany

Abstract. The control of rooms and areas where nuclear or radioactive material is stored or used is often performed with the use of commercially available hand-held gamma detectors using their dose or dose rate measurement capability. These devices are also often used by policemen or firemen. Reliable dose rate values are of great importance for the personal safety of the user in case of an elevated radiation field or generally for a first estimation of the threat generated by the radiation source. Therefore dose rate measurements were performed at Fraunhofer INT with the available hand-held gamma detectors under identical conditions. Seven hand-held gamma detectors of different type and size were investigated. The results of the dose rate measurements were compared among each other. For an assessment of the quality of the dose-rate measurements with hand-held gamma detectors a comparison with a calibrated dose rate measuring device for radiation protection FH 40 was made. It was seen that each hand-held gamma detector gave reproducible results for the gamma dose rate. However, the measured mean of the dose rate measurements with each hand-held device differed considerably, at a maximum by a factor of 3. Normally the measurement values were in the same order of magnitude. Except one all devices were not calibrated for radioprotection purposes. Taking into account that in Germany even for devices intended for radioprotection purposes only a precision of the dose rate of +/- 30 % is required the measurement results with hand-held devices can be regarded as reasonable good. Dose rate measurements with hand-held gamma detectors should be handled with care but in general the values obtained are good enough for personal safety and a first threat estimation although in general first responders would be required to carry a special radiation protection dosimeter in addition.

KEYWORDS: *hand-held gamma detector; dose rate; comparison.*

1 INTRODUCTION

The control of rooms and areas where nuclear or radioactive material is stored or used is often performed with the use of commercially available hand-held gamma detectors using their dose or dose rate measurement capability. These devices are also often used by policemen or firemen. Reliable dose rate values are of great importance for the personal safety of the user in case of an elevated radiation field or generally for a first estimation of the threat generated by the radiation source.

Therefore dose rate measurements were performed at Fraunhofer INT with the available hand-held gamma detectors under identical conditions. Seven hand-held gamma detectors of different type and size were investigated. The results of the dose rate measurements were compared among each other. For an assessment of the quality of the dose-rate measurements with hand-held gamma detectors a comparison with a calibrated dose rate measuring device for radiation protection FH 40 was made.

2 HAND-HELD GAMMA DETECTORS

Tab. 1 shows the basic characteristics like detector type and crystal size of the hand-held gamma detectors which were tested. We included devices which are primarily intended to measure dose and dose rate as well as devices which are intended for identification of nuclides. Detectors with different types and sizes of scintillators and low resolution semiconductors as well as proportional counters which are in common use were selected for testing. The FH 40 radiation protection dose rate meter was used as reference instrument.

*Presenting author, e-mail: theo.koeble@int.fraunhofer.de

Table 1: Basic characteristics of the hand-held gamma detectors

Detector Name	Manufacturer	Detector Type	Crystal Size [mm]
FH 40	Thermo	Proportional Counter	-
InSpector 1000	Canberra	LaBr ₃ (Ce)	38 (Ø) x 38 (Length)
RadEye PRD	Thermo	NaI(Tl)	18 (Ø) x 31 (Length)
IdentiFINDER	FLIR	NaI(Tl)	36 (Ø) x 51 (Length)
Interceptor	Thermo	CZT	7 x 7 x 3.5
Raider	FLIR	CZT	Eight Crystals: each has size of 1 cm ³
STORA-TU	Ecotest	Proportional Counter	-
TERRA	Ecotest	Proportional Counter	-

According to the manufacturer's data sheet information the used gamma detectors were designed for the following purposes. The FH 40 is a digital survey meter designed for radiation protection measurements. It is a stand-alone unit with an internal proportional detector [1]. The InSpector 1000 is a hand-held LaBr₃(Ce) spectrometer with a built in GM detector (high dose rate) for use primarily in first responder, customs, homeland security, and health-physics applications [2]. The RadEye PRD is a NaI(Tl)-detector designed for detection and localization of radiation sources and for dose rate measurements conducted by security forces, steel and recycling industry or first responders [1]. The IdentiFINDER is a hand-held digital gamma spectroscopy and dose rate system with an integral NaI(Tl) scintillation detector and a GM detector. It is suited for homeland security, industrial, medical, nuclear power generation and nuclear fuel cycle applications. The main features are nuclide identification, spectrum analysis, dose and dose rate calculation, and source finding [3]. The Interceptor is a Spectroscopic Personal Radiation Detector (SPRD) with a large volume CZT detector. It is an instrument for personal safety, screening for nuclear materials, for localization of sources and is capable of categorizing and identifying of radionuclides [1]. The Raider is a hand-held high resolution semiconductor CZT radiation detector and identification unit designed for rapid identification and verification of radioactive materials [3]. The STORA-TU detector is a hand-held proportional counter designed for measurement of gamma and X-ray radiation equivalent dose rate [4]. The TERRA hand-held detector has a built-in gamma, beta sensitive Geiger-Muller counter for the measurement of gamma and X-ray radiation equivalent dose and equivalent dose rate [4].

3 MEASUREMENT SETUP

The measurements were carried out with calibrated test sources. The sources were positioned in a distance of 10 cm from the reference point of the detector as indicated by the manufacturer. For each measurement the device was restarted and the reading of the display was recorded 60 sec after the restart to take care of the integration time which some of the detectors use. For each device and source five measurements were performed and mean and variance calculated. Fig. 1 shows the devices and the principle set-up. The sources used for the measurements are listed in Tab. 2.

Figure 1: Measurement setup with hand-held gamma detectors**Table 2:** Used Sources

Source name	Isotope	Activity [kBq]
Cs1	^{137}Cs	249.8
Cs2	^{137}Cs	42.0
Co1	^{60}Co	206.1
Co2	^{60}Co	2.0
Ba1	^{133}Ba	76.7
Eu1	^{152}Eu	5.2
	^{154}Eu	3.3
	^{155}Eu	2.0
U1	^{238}U	460.0

4 RESULTS

As an example the results for all detectors under test with the ^{137}Cs source No. 1 are shown in Fig. 2. The reference dose rate obtained with the FH 40 is drawn as a solid line. The reference dose rate obtained with the FH 40 is drawn as a solid line. Taking into account the error bars the measured values of all detectors agree with the +/- 30 % range around the FH 40 reference value indicated by the dashed lines. It should be noted that the +/- 30 % for the reference instrument has to be regarded as a possible systematic deviation, not as a statistical one.

Figure 2: Results for the source Cs1

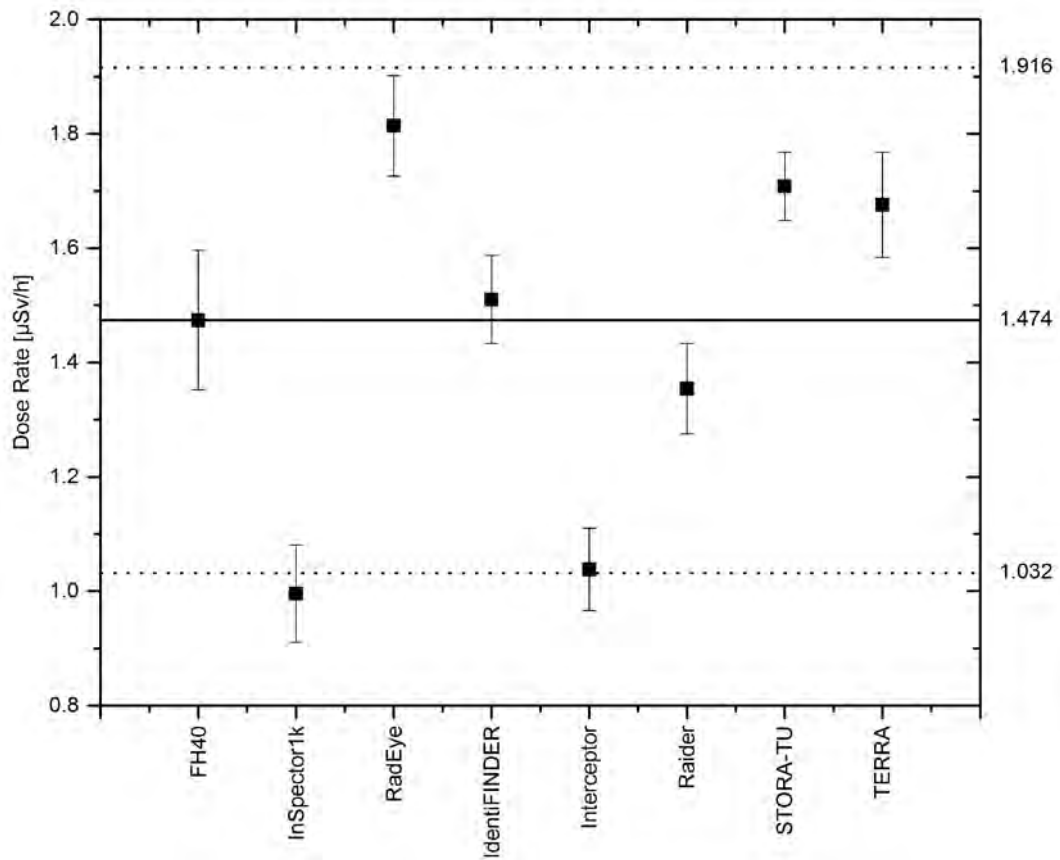
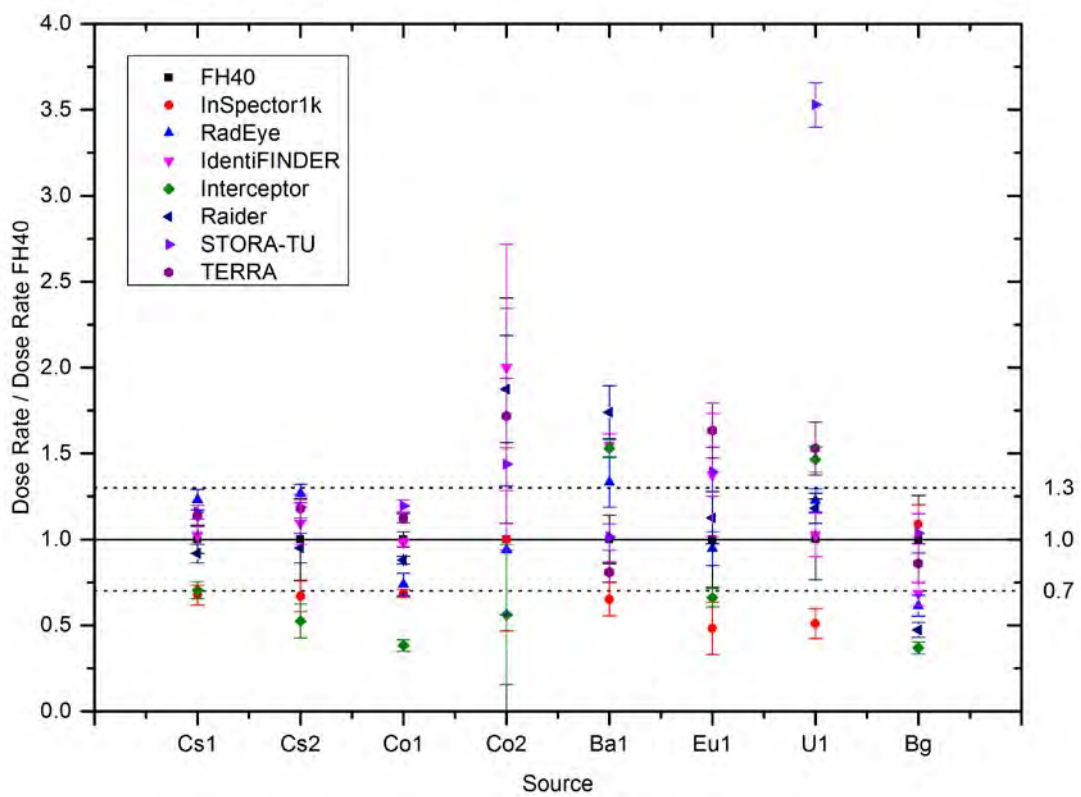


Figure 3: Dose rate results for different detection systems depending on used sources



In Fig. 3 the measurement results of all detectors and all sources are shown together with measurements of the ambient background. All measurement results were normalized to the FH 40 reference measurements after subtracting the background. In general the variations of the measurements of a single device for each source are small although the confidence intervals for different detectors for the same source in general do not overlap well. The confidence interval in general also does not overlap well with the confidence interval of the reference instrument FH 40. If the possible deviation of +/- 30 % from the true value of the dose rate allowed for radioprotection instruments in German legislation is also taken into account most of the measurement results for the detectors are acceptable. Exceptions are for the Interceptor and Inspector1k results which are tending to be systematically low and one not understood large outlier for the STORA-TU for Uranium.

5 DISCUSSION

It was seen that each hand-held gamma detector gave reproducible results for the gamma dose rate. However, the measured mean of the dose rate measurements with each hand-held device differed considerably, at a maximum by a factor of 3. Normally the measurement values were in the same order of magnitude. Except one all devices were not calibrated for radioprotection purposes. Taking into account that in Germany even for devices intended for radioprotection purposes only a precision of the dose rate of +/- 30 % is required the measurement results with hand-held devices can be regarded as reasonable good. This compares well to results Pebida et. al. [5] found in their tests of radiation detectors used in homeland security applications where hand-held radiation detectors were directly compared to calibrated air-kerma rates according to the ANSI N42.34 standard which requires also +/- 30 % for ^{137}Cs .

6 CONCLUSION

Seven hand-held gamma detectors with different detector types not primarily intended for dose rate measurements for radiation protection purposes were tested with common sealed radioactive sources and compared to the dose rate determined by the dose rate meter FH40. For the hand-held devices tested the indicated dose rate values can be regarded as reasonable. However, dose rate measurements with hand-held gamma detectors should be handled with care. Although in principle the values obtained are good enough for personal safety and a first threat estimation in general first responders would be required to carry a special radiation protection dosimeter in addition.

7 REFERENCES

- [1] <https://www.thermofisher.com/de/en/home/industrial/radiation-detection-measurement.html>
- [2] <http://www.canberra.com/products/default.asp>
- [3] <http://www.flir.de/threatdetection/content/?id=63317>
- [4] <http://ecotest.ua/products/>
- [5] Pibida, L., Minniti, R., O'Brien, M., Unterweger, M., 2005. Test of Radiation Detectors used in Homeland Security Applications. Health Physics 88/5, 84-90.

Estimation of detective efficiency of CdZnTe semiconductor detector and NaI(Tl) scintillation detector

Takatoshi Toyoda^{a*}, Toshioh Fujibuchi^b

^aDepartment of Health Sciences, Graduate School of Medical Sciences, Kyushu University, 3-1-1 Maidashi Higashi-ku Fukuoka, Japan

^bDepartment of Health Sciences, Faculty of Medical Sciences, Kyushu University, 3-1-1 Maidashi Higashi-ku Fukuoka, Japan

Abstract. In this study, Using cadmium zinc telluride (CdZnTe) semiconductor detector and thallium-doped sodium iodide (NaI(Tl)) scintillation detector, detective efficiency of two detectors were calculated experimentally. Then using Monte Carlo Code PHITS, detective efficiency of two detectors was calculated. CdZnTe detector was GR-1 made by Kromek Group plc., NaI(Tl) scintillation detector was made by EMF Japan Co.. We used three radioisotope point sources (⁶⁰Co, ¹³⁷Cs and ¹³³Ba), detective efficiency for each photo peak of two detectors were calculated experimentally. In Monte Carlo simulation, shapes of radioisotope point source and detecting elements were constructed. The number of electrons which generated in detector elements counted using [t-deposit] section, and energy spectrum of electron was calculated. Comparison of measurement and calculation was good agreement in GR-1, however Comparison in EMF211 did not match, because scintillation light must be considered.

KEYWORDS: *detective efficiency=measurement=Monte Carlo simulation; PHITS.*

1 INTRODUCTION

Compact medical cyclotron is used to obtain positron-emitting radionuclides, such as ¹⁸F. While operating cyclotron, neutron is produced secondarily. The neutron cause activation of vicinity the target and inside vault room. The thermal neutron fluences can be measured by using gold foil activated method. In this method, detective efficiency of detector is one of the most important factor to calculate activity of gold foils correctly [1]. However, estimating detective efficiency manually is difficult.

Calculating detective efficiency using Monte Carlo simulation is a method to estimate detective efficiency automatically. In Monte Carlo simulation, the number of electron deposited at detector can be calculated. Detective efficiency calculated using MCNPX code showed good agreement with the calculation data [2, 3].

In this study, we used cadmium zinc telluride (CdZnTe) semiconductor detector and thallium-doped sodium iodide (NaI(Tl)) scintillation detector, detective efficiency of two detectors were calculated experimentally. Furthermore, we used Monte Carlo code PHITS [4], detective efficiencies of two detectors were calculated.

2 MATERIAL AND METHOD

We used EMF211 (EMF Japan Co., Ltd., Japan) as NaI(Tl) scintillation detector and: GR-1 (Kromek Group plc, United Kingdom) as CdZnTe semiconductor detector. The shape of NaI(Tl) crystal was cylinder, and its size was 7.62 cm (in diameter) × 7.62 cm (in height). The shape of CdZnTe crystal was cube, and its size was 1 × 1 × 1 cm³. Both detector have Multi Channel Analyzer. EMF211 have 2048 channels, and GR-1 have 4096 channels. Radioisotope point source and its activity at measurement day were below: ¹³³Ba 73.3 kBq (half-life: 10.51 years), ¹³⁷Cs 7.27 kBq (half-life: 30.1 years), and ⁶⁰Co 39.6 kBq (half-life: 5.271 years) [5].

Particle and Heavy Ion Transport Code System (PHITS) version 2.80 (Japan Atomic Energy Agency, Japan) was used as Monte Carlo simulation code.

* Presenting author, e-mail: rikigakuga@gmail.com

2.1 Measurement of detective efficiency using radioisotope point source

Gamma-ray energy spectrum emitted from each radioisotope point source were measured using NaI(Tl) scintillation detector and CdZnTe semiconductor detector. In measurement of CdZnTe semiconductor detector, lead shield was used to reduce back ground radiation. Measurement time was 600 seconds. Distance between detector and radioisotope point source was changed 0 cm and 5 cm. Measurement system are shown in Fig.1 and Fig. 2.

After measurement, net counts at each photo peak was calculated. Photo peak energies were 81 keV and 356 keV of ^{133}Ba , 662 keV of ^{137}Cs , 1172 keV and 1333 keV of ^{60}Co . Detective efficiency at each energy was calculated based on equation (1),

$$\varepsilon = \frac{C_{net}}{A \times R \times 0.5 \times t} \quad (1)$$

where, ε (non-unit) was detective efficiency, C_{net} (counts) was net counts of photo peak, R (%) was γ -ray emitting rate each radioisotope energy. A (Bq) was radioactivity of radioisotope point source, 0.5 was solid angle from radioisotope point source to detector, t (seconds) was measurement time [6].

Figure 1: Measurement alignment of EMF211



Figure 2: Measurement alignment of GR-1



2.2 Calculating efficiency using PHITS

Detector element and shape of radioisotope point source was constructed on PHITS. X-ray image of detector element was used as a reference. X-ray images of two detectors are shown Fig. 3 and Fig. 4.

Figure 3: X-ray image of EMF211

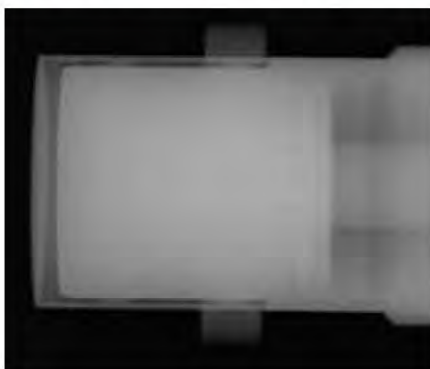


Figure 4: X-ray image of GR-1



[t-deposit] section was used to calculate the number of electrons which were deposited in detector crystal, and its energy spectrum. Calculated energy spectrum was compared with the measurement data. Cutoff energies of photon and electron were set 1.0 keV respectively. Energy resolution of electron counted in the detector was adjusted “dresol” parameter in [t-deposit] section. This parameter set to fit the photo peak at each energy. Calculation was carried out to satisfy enough relative error: less than 1.0%. Fig. 5 and Fig. 6 are shown the structure of two detector element constructed on PHITS.

Figure 5: Detector element of EMF211 on constructed PHITS

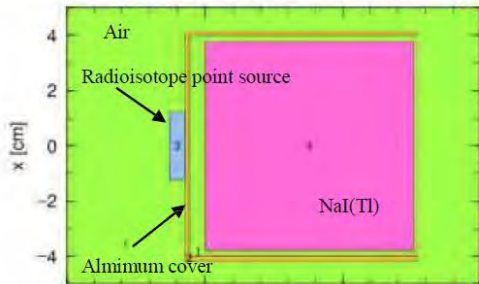
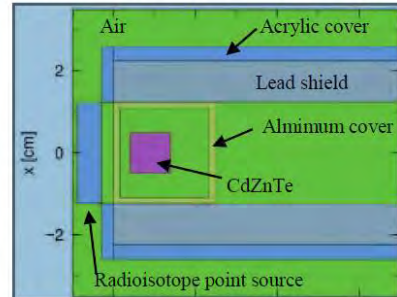


Figure 6: Detector element of GR-1 constructed on PHITS



3 RESULTS

3.1 Measurement of detective efficiency

Results of detective efficiency are shown Fig. 7 and Fig. 8. Detective efficiency of GR-1 became smaller as energy increased. However detective efficiency of EMF211 at 356 keV was almost the same as that of EMF211 at 662 keV.

Figure 7: Measured detective efficiency of EMF211

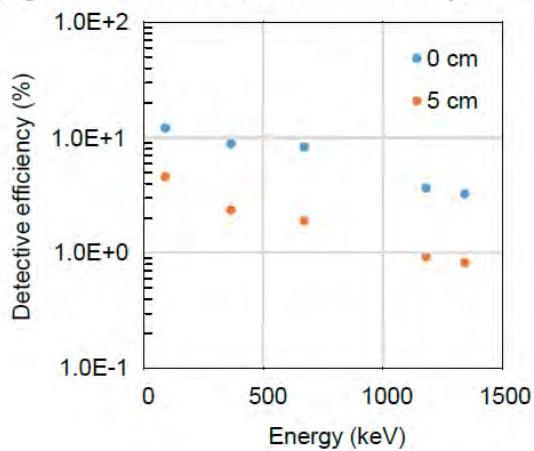
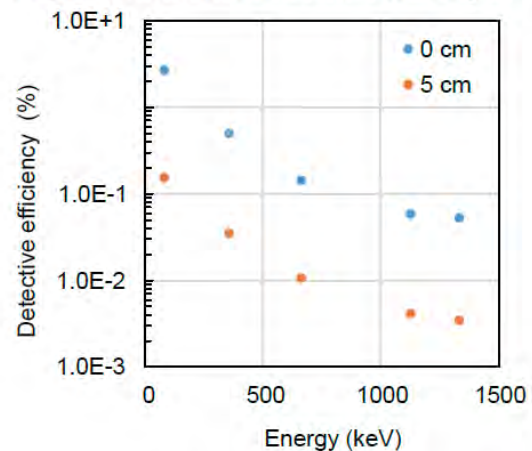


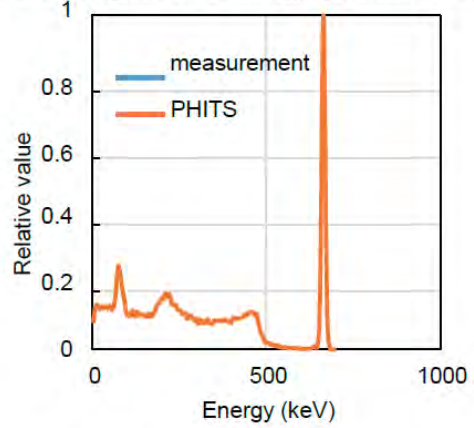
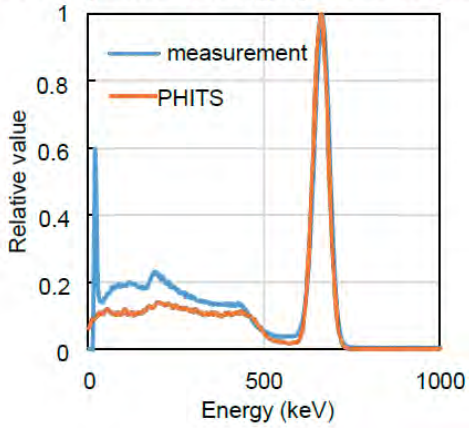
Figure 8: Measured detective efficiency of GR-1



3.2 Comparison of energy spectrum between measurement and calculation

Comparison of energy spectrum of ¹³⁷Cs between measurement and calculation are shown Fig. 9 and Fig. 10. Each results was normalized in count at 622 keV. Around the photo peak, measurement result and calculation result showed good agreement.

Figure 9: Comparison of energy spectrum of EMF211 **Figure 10:** Comparison of energy spectrum of GR-1



3.3 Calculation of detective efficiency

Calculation results of GR-1 and EMF211 are shown in Fig. 11 and Fig. 12. Both results showed lower as energy increased.

Figure 11: Calculated detective efficiency of EMF211

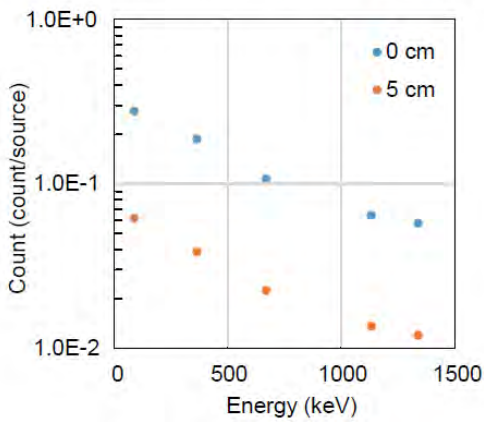
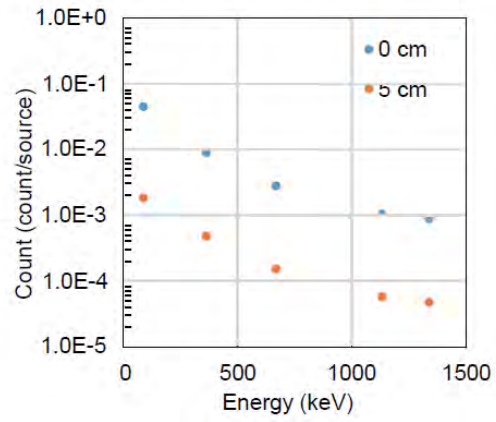


Figure 12: Calculated detective efficiency of GR-1



3.4 Comparison between measurement and calculation of detective efficiency

Comparison between measurement and calculation of detective efficiency are shown in Fig.13, Fig.14, Fig.15, and Fig.16. Comparison of GR-1 showed good agreement, but that of GR-1 did not correspond with the results at 662 keV.

Figure 13: Comparison calculation and measurement of EMF211 at 0 cm

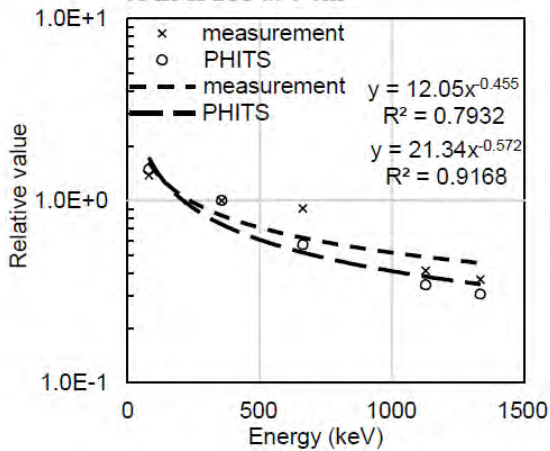


Figure 14: Comparison calculation and measurement of EMF211 at 5 cm

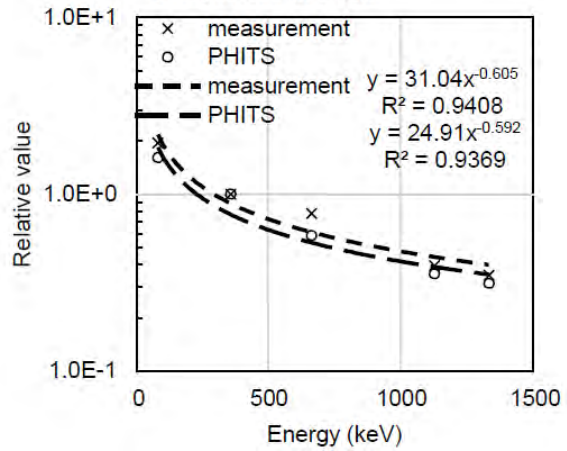
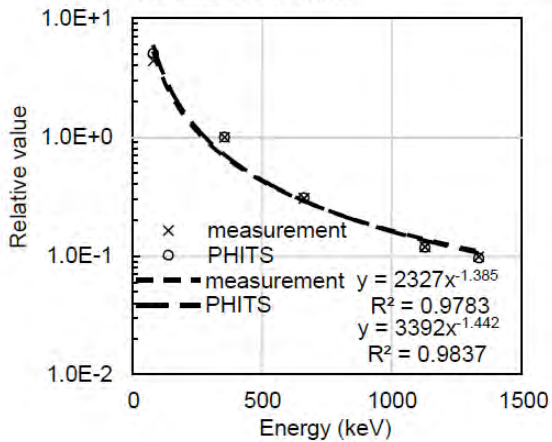
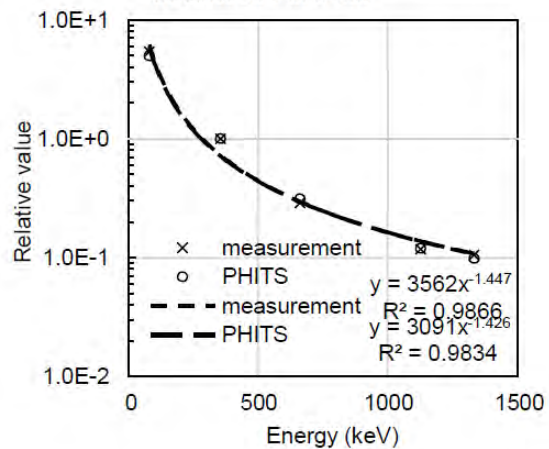


Figure 15: Comparison calculation and measurement of EMF211 at 0 cm**Figure 16:** Comparison calculation and measurement of EMF211 at 5 cm

4 DISCUSSION

In comparison measurement and calculation results, results of GR-1 showed good agreement between measurement and calculation. Maximum difference of GR-1 at 0 cm was 7%, and that at 5 cm was 15%. However, the results of EMF211 did not show good agreement between measurement and calculation. The maximum difference of EMF211 at 0 cm was 48%, and that at 5 cm was 32%. The difference between measurement and calculation of EMF211 was large, because scintillation light was not considered in calculation. Accuracy of calculation increase when scintillation light take into account [7].

In the measurement, activity of ^{137}Cs was lower than other radioisotope point sources. In measurement of detective efficiency, enough intensity of radioisotope point source was needed to get good counting statistic, otherwise wrong detective efficiency may be calculated. Therefore, using radioisotope point source which have more higher activity should be used. Moreover, energy spectrum of ^{60}Co and ^{133}Ba have an effect of sum peak. Detective efficiency measured by EMF211 was affected by this effect, so effect of sum peak should be compensated, or detective efficiency was measured using another radioisotope point source which was not affected sum peak effect [2, 8].

5 CONCLUSION

Calculation of detective efficiency matched measurement detective efficiency, so detective efficiency of CdZnTe semiconductor detector can be calculated using Monte Carlo simulation. However, comparison of detective efficiency did not match between measurement and calculation, especially NaI(Tl) scintillation detector. Scintillation light must take into account to increase accuracy of calculation.

6 REFERENCES

- [1] Kobayashi, K., Yamamoto, Y., Kimura, I., et al., 1988. Measurement of Neutron Flux Spectrum by Multi-Foil Activation Method at the Central Graphite Cavity of UTR-KINKI. Annual Report of Kinki University Atomic Energy Research Institute. Vol. 25, 21-34.
- [2] Salgado, C. M., Brandão, L. E. B., Schirru, R. et al., 2012. Validation of a NaI(Tl) detector's model developed with MCNP-X code. Progress in Nuclear Energy 59, 19-25.
- [3] Akkurta, I., Tekin, H. O., Mesbahi, A., 2015. Calculation of Detection Efficiency for the Gamma Detector using MCNPX. Special issue of the International Conference of Computational and Experimental Science and Engineering 128, 332-334.
- [4] Sato, T., Niita, K., Matsuda, N., et al., 2013. Particle and Heavy Ion Transport Code System PHITS, Version 2.52, J. Nucl. Sci. Technol, 913-923.

- [5] Japan Radioisotope Association, 2011. Radioisotope pocket data, book. 11th edn. Japan.
- [6] Gordon, G., Hemingway, J. D., 2002. Practical gamma-ray spectrometry, The nikkon kougyou shinnbun, Ltd. Japan
- [7] Hirayama, H., 2004. Physics Phenomena Generally not Considered in Calculation -In the Case of X-ray and Gamma-ray detector-. KEK Preprint. High Energy Accelerator Research Organization.
- [8] Akkurt, I., Gunoglu, K., Arda, S. S., 2014. Detection Efficiency of NaI(Tl) Detector in 511–1332 keV Energy Range. Science and Technology of Nuclear Installations. 1-5.

A study of Energy-Compensating Metal Filter of Semiconductor Detector for Personal Dosimetry in X-ray Diagnosis

Kento Terasaki^{a*}, Toshioh Fujibuchi^b, Hiroo Murazaki^c, Taku Kuramoto^c,
Yoshiyuki Umezu^c, Yang Ishigaki^{d,e}, Yoshinori Matsumoto^f

^aDepartment of Health Sciences, Graduate School of Medical Sciences, Kyushu University, 3-1-1 Maidashi, Higashi-ku, Fukuoka-shi, Fukuoka 812-8582, Japan.

^bDepartment of Health Sciences, Faculty of Medical Sciences, Kyushu University, 3-1-1 Maidashi, Higashi-ku, Fukuoka-shi, Fukuoka 812-8582, Japan.

^cDivision of Radiology, Department of Medical Technology, Kyushu University Hospital, 3-1-1 Maidashi, Higashi-ku, Fukuoka-shi, Fukuoka 812-8582, Japan.

^dGraduate School of Information Systems, The University of Electro-Communications, 1-5-1 Chofugaoka, Chofu-shi, Tokyo 182-8585, Japan.

^eYaguchi Electric Corporation, Kaemon 301, Kanomata, Ishinomaki-shi, Miyagi 986-1111, Japan.

^fDepartment of Applied Physics and Physico-Informatics, Keio University, 3-14-1 Hiyoshi, Kouhoku-ku, Yokohama-shi, Kanagawa 223-8522, Japan.

Abstract. For radiation workers, radiation dose management is important. Especially medical staff working in fluoroscopy-guided procedures such as interventional radiology can be exposed to high dose. Low-cost dosimeter named Pocket Geiger has developed for ordinary people to own a radiation detector following Fukushima Daiichi Nuclear Power Plant accidents. The dosimeter combines a PIN photodiode detector and a smartphone. In our study, in order to utilize the Type 1 of the Pocket Geiger series in medical X-ray examination, optimal metal filters for energy compensation were examined using a Monte Carlo calculation code PHITS. And an appropriate threshold level to eliminate the background noise was considered. As a metal filter, aluminum, copper, brass, and tin were used. Tube voltages were set from 50 to 110 kV. The variance of the absorbed dose ratio of silicon to air was $\pm 7\%$ from 70 to 110 kV of the tube voltage with an aluminum filter, with 23 keV for the cutoff energy in the calculation. The aluminum filter was found to be the appropriate metal filter for energy compensation of the Pocket Geiger. Moreover, the relative response ratio of some commercial active personal dosimeters to DDX6-WL was measured. To examine an appropriate threshold level for the Pocket Geiger Type 1, the threshold of 5%, 4%, and 3% were set. As a result, 5% was found to be an appropriate threshold level. The Pocket Geiger with suitable energy compensation can be useful tool for dose monitoring of medical staff during fluoroscopy-guided procedures.

KEYWORDS: *semiconductor detector; personal monitoring; energy compensation filter; threshold setting; Monte Carlo calculation; interventional radiology.*

1 INTRODUCTION

With the increasing use of X-ray fluoroscopic examinations, management of radiation dose has become increasingly important for medical staff during fluoroscopy-guided procedures such as interventional radiology (IVR). The tube voltage commonly used in IVR ranges from 60 to 120 kV. With increasingly complex procedures and fluoroscopy time, the staff is often exposed to high dose rates during procedures.

To reduce exposure doses, medical staffs wear protective aprons and use a personal dosimeter, such as a Glass Badge, to monitor exposure doses. The Glass Badge is the most popular dosimeter for personal monitoring in clinical practice. However, it cannot measure exposure doses in real time. Individual

* Presenting author, e-mail: kento.terasaki@gmail.com

monitoring in real time is helpful for knowing exposure doses at first sight during IVR. A system to measure and display the exposure dose in real time has been developed and sold [1]. However, this system is very expensive. We previously produced a wireless dose monitoring system using an inexpensive semiconductor detector and evaluated the basic characteristics for pulse radiation in diagnostic X-rays [2]. However, there were some issues with this method, such as the system could not accurately measure doses in high-dose-rate areas and the improvement of sensitivity of the detector in the energy range of diagnostic X-rays was required.

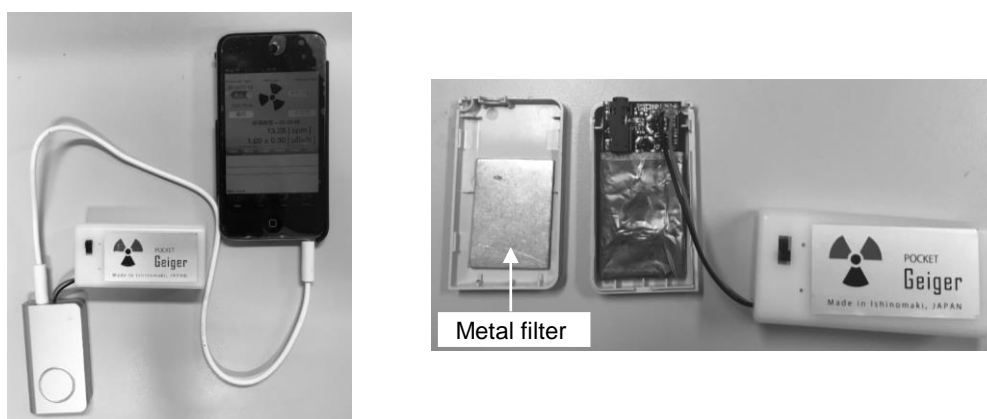
In this study, to utilize a semiconductor detector (Pocket Geiger) in medical X-ray examination, a suitable metal filter and the threshold level were examined for the energy compensation by a Monte Carlo calculation and measurement.

2 MATERIALS AND METHODS

2.1 Pocket Geiger

After the Fukushima Daiichi Nuclear Power Plant accident in 2011, an inexpensive and open-sourced mobile radiation detector named Pocket Geiger (POKEGA; Radiation-Watch JAPAN, Miyagi, Japan) was developed for public use by volunteer scientists and engineers [3–5]. The POKEGA is a semiconductor detector, not a Geiger-Müller counter, which was developed for gamma-ray measurement. To reduce costs, a combination of a PIN Si photodiode detector connected to a smartphone was adopted. Moreover, various types of POKEGA were developed with modifications, such as to the smartphone OS or to the sensor. In this study, we used the POKEGA Type 1 (Fig. 1).

Figure 1: Pocket Geiger Type 1



2.2 Energy dependence

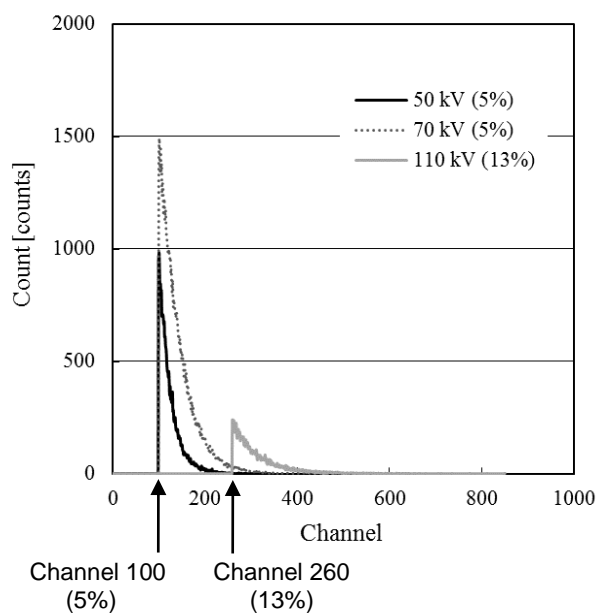
Chen et al. examined the energy response of the PIN Si photodiode and filter compensation in the measurement and Monte Carlo calculation using the EGS4 code. Moreover, they also studied the effect of the threshold level and the dimension of the active volume of the photodiode. The measurement was performed in the X-ray field with effective energies ranging from 46 to 202 keV and by using Cs-137 and Co-60 gamma-ray sources [6].

In this study, the optimal metal filter for energy compensation and threshold setting were investigated in the measurement and a Monte Carlo calculation using the PHITS code (ver. 2.80) was performed [7]. The sensor was composed of silicon and sandwiched by front and back metal filters. The source of radiation exposure was scattered X-rays from the ICRU slab phantom with a tube voltage setting of 50 to 110 kV. The spectra of scattered X-rays were calculated using a free software program [8]. To examine the optimal metal filter for energy compensation of the POKEGA in diagnostic X-rays, we simulated the response of the detector with four metal filters of aluminum, copper, brass, and tin.

Moreover, to eliminate the background noise caused by thermal excitation within the detector, threshold or cutoff energy values were set.

For determining the cutoff energy values, the relationship between the energy and the threshold level was examined in the following way. First, the pulse height distribution was obtained using the multichannel analyzer in the POKEGA. Fig. 2 shows the pulse height distribution for each tube voltage. Here, the tube voltage was regarded to be equivalent to the maximum energy, and the corresponding relationship between the maximum energy and the channel for each tube voltage was examined.

Figure 2: Measured pulse height distribution for each tube voltage.



The energy dependence with the previous optimal metal filter was compared with some commercial active personal dosimeters (APDs). These dosimeters were located on a worker-phantom to take into account backscatter from a human body, and the scattered X-rays from a patient-phantom were measured simultaneously. The following dosimeters were selected for this study: (1) EPD-G (Thermo Fisher Scientific K.K., Kanagawa, Japan), (2) PDM-107 (Hitachi Aloka Medical, Ltd., Tokyo, Japan), (3) PDM-122B-SHC (Hitachi Aloka Medical, Ltd., Tokyo, Japan), (4) PDM-127-SZ (Hitachi Aloka Medical, Ltd., Tokyo, Japan), (5) DDX6-WL (Radcal Co., California, USA), and (6) POKEGA Type 1.

The fluoroscopic conditions in the energy dependence experiment were 50–110 kV and 1.2 mA. The dosimeters was irradiated until DDX6-WL reached 10 μ Gy. We examined the relative response ratio of 1 cm personal dose equivalent $H_p(10)$ measured by the APD to air kerma measured by DDX6-WL. Moreover, to examine an appropriate threshold level for the POKEGA Type 1, the threshold of 5%, 4%, and 3% were set. And an appropriate threshold level was determined as the relative response ratio approached 1.

3 RESULTS AND DISCUSSION

Fig. 3 shows the relationship between the photon energy and the channel. The cutoff energy value corresponding to a threshold of 5% (Channel 100) was 23 keV and that corresponding to a threshold of 13% (Channel 260) was 41 keV.

Fig. 4 shows the result of the energy dependence in the calculation when the cutoff energy value was set to 23 keV with each metal filter. The vertical axis shows the absorbed dose ratio of silicon to air.

The nearly equal responses were found between copper and brass filters because the brass consisted of 70% of copper and 30% of zinc. As shown in this figure, the ratio was the most constant when using an aluminum filter. The variance of this ratio was $\pm 7\%$ from 35.2 to 41.2 keV when 23 keV was set as the cutoff energy value. The sensitivity decreased in the low-energy region when using copper, brass, and tin filters. Because these metal filters are composed of high-atomic-number materials, high absorption was observed in the low-energy region.

Fig. 5 shows the relative response ratio of some commercial active personal dosimeters (APDs) to DDX6-WL. As shown in the figure, the response ratio of POKEGA Type 1 to DDX6-WL approached 1 when the threshold level of 5% was set. Therefore, 5% was found to be an appropriate threshold level for the POKEGA Type 1. An appropriate setting of the threshold level is important since the response of the detector changes significantly.

Figure 3: Relationship between the photon energy and the channel.

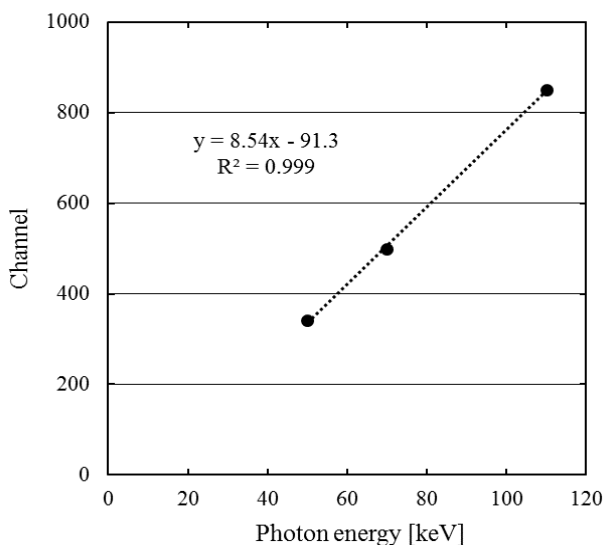


Figure 4: Energy dependence in the calculation. (Cutoff energy = 23 keV)

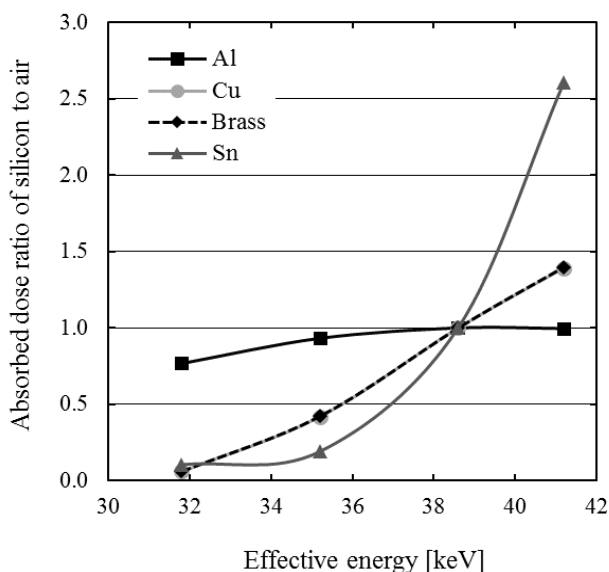


Figure 5(a): Relative response ratio (Threshold = 5%)

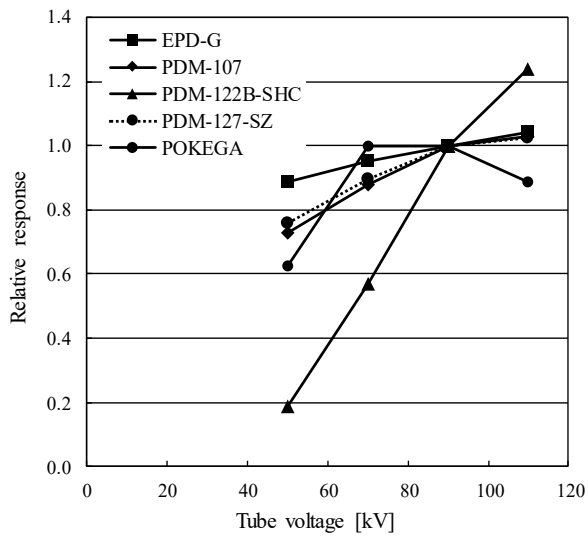


Figure 5(b): Relative response ratio (Threshold = 4%)

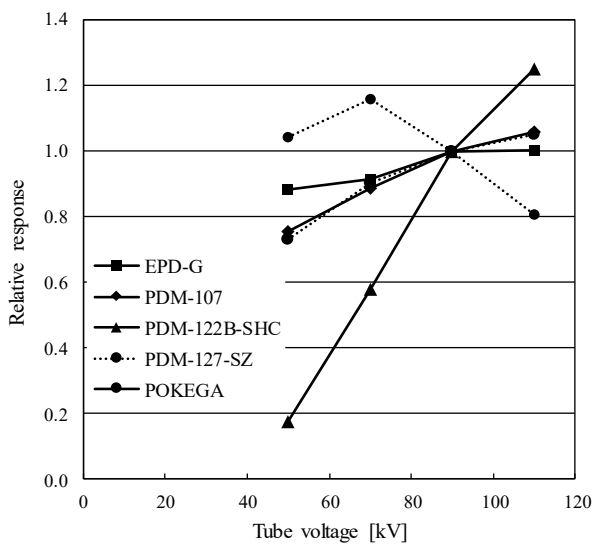
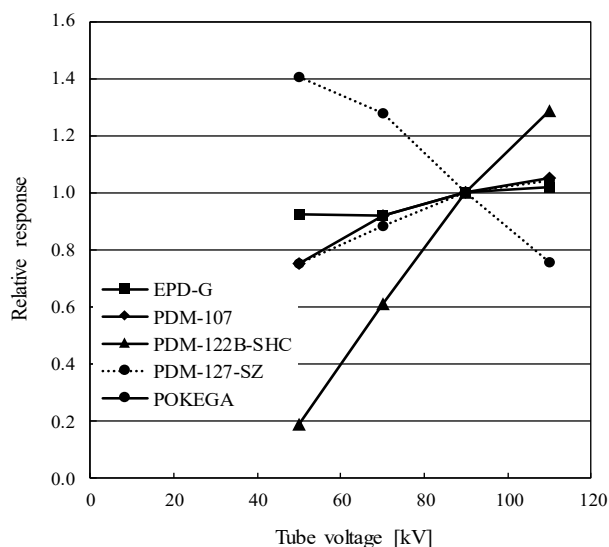


Figure 5(c): Relative response ratio (Threshold = 3%)

4 CONCLUSION

In this study, the optimal metal filter and the threshold level to improve the energy dependence of the POKEGA Type 1 were determined. The POKEGA may become a useful tool for dose monitoring of the medical staff in clinical practice.

5 REFERENCES

- [1] <http://www.raysafe.com/Products/Staff/RaySafe%20i2>
- [2] Fujibuchi, T., Murazaki, H., Kuramoto, T., et al., 2015. Evaluation of an Experimental Production Wireless Dose Monitoring System for Radiation Exposure Management of Medical Staff [in Japanese]. *Jpn. J. Radiol. Technol.* pp. 691–696.
- [3] <http://www.radiation-watch.org>
- [4] Ishigaki, Y., Matsumoto, Y., Ichimiya, R., et al., 2012. Ultra-low-cost Radiation Monitoring System Utilizing Smartphone-connected Sensors Developed with Internet Community. *Proc. of IEEE Sensors Conference 2012*, 652–655.
- [5] Ishigaki, Y., Matsumoto, Y., Ichimiya, R., et al., 2013. Development of Mobile Radiation Monitoring System Utilizing Smartphone and Its Field Tests in Fukushima. *IEEE SENSORS JOURNAL*. pp. 3520–3526.
- [6] Chen, C.R. and Jiang, S.H., 1993. Energy Response and Filter Compensation of PIN Si Photodiode for Personal Dosimetry Application. *IEEE Trans. Nucl. Sci.* pp. 857–862.
- [7] Sato, T., Niita, K., Matsuda, N., et al., 2013. Particle and Heavy Ion Transport Code System PHITS, Version 2.52. *J. Nucl. Sci. Technol.* pp. 913–923.
- [8] <http://www.fujita-hu.ac.jp/~hid-kato/>

Determination of fission radionuclides activities in a real fission gamma-ray field

Žlebčík P.^{a,b*}, Malá H.^a, Huml O.^b

^aNational Radiation Protection Institute (SÚRO), Prague, Czech Republic

^bDepartment of Nuclear Reactors, Czech Technical University, Prague, Czech Republic

Abstract. The goal of the presented work was to identify short-lived fission products (half-lives from hours to days) and determine their activities in a real complex gamma-ray radiation field that can be encountered in case of nuclear power plant accidents. For the measurements, a semiconductor HPGe detector with a relative efficiency of 35% was used. Gamma-ray fields with various levels of dose rates were created by an irradiated fuel elements in a reactor core at the VR-1 reactor. In some cases difficulties can be experienced with measurements, detection and evaluation of radioisotopes because of the large number of gamma-ray energy lines. Detected gamma lines depend on the measurement start time and decreases rapidly with time after the irradiation. Energy lines of selected fission radionuclides that were not detected at the beginning can be found in the later acquired spectrum, which relates to the decrease of the Compton continuum in time. For automatic acquiring and evaluation of spectra in different time after an irradiation REXX language script was created. In the first step, MCNP burnup calculations consist of isotopic compositions and activities of the fuel elements were calculated. In the second step, MCNP model of the HPGe detector was created. After that, detector efficiency calibrations of the fuel elements were simulated by the MCNP and used for estimation of selected fission products activities from spectra.

KEYWORDS: *HPGe detector; fission products; gamma-ray spectra; Monte Carlo calibration; MCNP.*

1 INTRODUCTION

Detection systems with semiconductor HPGe detectors are commonly used for a broad range of applications. In this work, the use of the HPGe detector in real fission gamma-ray fields is described. To provide the fields, fuel elements were irradiated in the core of the VR-1 reactor situated at the Czech Technical University in Prague. For determination of selected fission products activities (I-131, Te-132, I-135 and Xe-135) two approaches were chosen. First, with use of burnup calculations in the MCNP, activities of selected fission products in the fuel elements after the irradiation were calculated. Secondly, the MCNP detailed model of the HPGe detector and fuel elements have been prepared. The Pulse High Distribution (PHD) and a point efficiency curve of the HPGe detector were simulated by the MCNP [1] and compared with experimental measurements in order to validate the model of the HPGe detector. After successful comparison for more precisely estimation of radionuclides activities in the fuel elements, efficiency curves were created for them by the MCNP. In this kind of measurements, materials of the fuel elements cause the extreme absorption especially of low-energy photons. For these purposes, the Monte Carlo technique is very useful to determine influence of the geometry and material on the detector efficiency.

2 METHODOLOGY

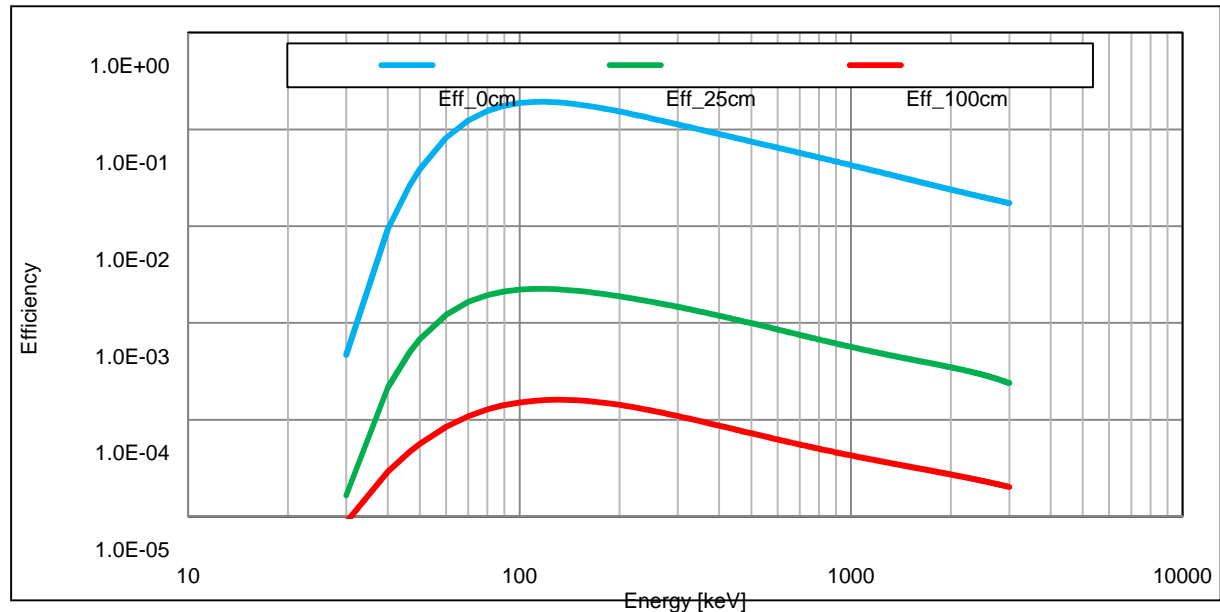
2.1 Detector and sources

A conventional coaxial HPGe detector [2] and LYNX digital signal analyser has been used for experimental measurements. The main specifications of the detector are as follows: the crystal diameter is 61 mm, the length is 56.5 mm, the crystal to window front distance is 6 mm, relative efficiency is 35 %, FWHM at 1.33 MeV is 1.8 keV, FWHM at 122 keV is 0.875 keV, and the peak/Compton ratio is 60:1. Number of channels was set to 8192 and the energy range between

* Presenting author, e-mail: pavel.zlebcik@suro.cz

30 keV - 3000 keV. The experimental efficiency calibrations of the HPGe detector were performed by measuring standard point sources prepared by the Czech Metrological Institute for 3 geometries: on the endcap of the detector (Eff_0 cm), at the 25 cm distance from the front of the detector (Eff_25 cm) and at the 100 cm distance from the front of the detector (Eff_100 cm), see the Fig.1.

Figure 1: Experimentally determined point source efficiency curves of the HPGe detector



2.2 Experimental measurements

The HPGe detector was used for measurements in real gamma-ray fields generated by the fuel elements irradiated at the VR-1 reactor. For the irradiation two types of fuel elements were chosen – pellet UO_2 enriched to 4.3 % U-235 and EK-10 fuel pin enriched to 10 % U-235. The pellet diameter in the form of UO_2 is 7.61 mm with central hole diameter of 0.75 mm and 12.72 mm height. The EK-10 fuel pin in the form of UO_2 dispersed in magnesium has a diameter and height of 7 mm and 160 mm, respectively. Cladding material is aluminum. For the irradiation dry vertical channel C6 in the reactor was chosen (Fig. 2). After the irradiation the fuel elements were transported to the reference measurement position. The distance of the HPGe detector to the fuel element was set to 100 cm. Time between pulling out the fuel elements from the reactor core to placing to the reference position was approximately 10 minutes. Gamma-ray spectra of the UO_2 pellet and EK-10 fuel pin in various times after the irradiation were acquired and analyzed by the GENIE™2000 software. For automatic acquisition and evaluation of spectra script in REXX language was created.

2.3 Monte Carlo simulations

MCNP model of the VR-1 reactor was used for burnup calculation of the fuel elements generating complex gamma-ray fields. The parameterized model of the VR-1 reactor in the MCNP was generated by APOBAB system [3] developed at the Czech Technical University in Prague, Department of Nuclear Reactors. Simulation of the depletion process in the MCNP uses internal CINDER90 module [4]. Parameters of the irradiation were set up by the BURN card describing time of irradiation, reactor power level and other depletion parameters. The EK-10 fuel pin and UO_2 pellet in a polyethylene box were prepared and implemented to the model of the VR-1 reactor, see the Fig. 2. For the above described fuel elements activities of the selected fission radionuclides after the irradiation were calculated.

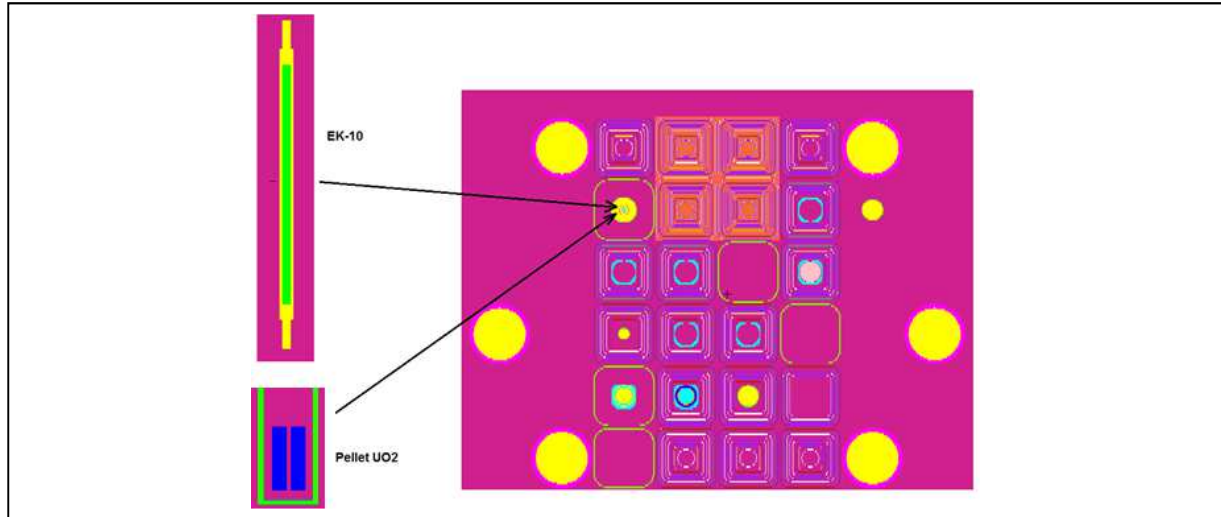
MCNP models of the HPGe detector and the fuel elements were prepared. For estimation of selected fission products activities efficiency calibration curves of the HPGe detector for both types of the fuel elements and point source (at the 100 cm distance from the front of the detector) were simulated by the

MCNP. To get the shape of the Gaussian photopeaks, GEB (Gaussian Energy Broadening) card was used in simulations. The experimental value of the FWHM, was fitted with formula (1):

$$FWHM = a + b\sqrt{E + cE^2} \quad (1)$$

where a, b, c are input parameters for MCNP and E is the photon energy in MeV.

Figure 2: MCNP models of the VR-1 reactor core, EK-10 fuel pin and UO₂ fuel pellet [4]



3 RESULTS

The created MCNP model of the HPGe detector was validated by comparison of experimentally determined and simulated efficiency curves. For illustration, comparison of efficiency curves for point source on the endcap of the detector is shown in Fig. 3. In addition measured and calculated spectra of radionuclides used for calibrations were compared. Simulated and measured spectrum of Co-60 is shown in Fig. 4. Experimentally determined efficiency curves and measured spectra are in good agreement with the simulations carried out in the MCNP. The difference between experimental and simulated efficiencies was not greater than 6 %. With use of burnup calculations, activities in the fuel elements after the irradiation were calculated. Results are shown in Fig. 5 and Fig. 6

Figure 3: Experimental and simulated efficiency curves for point source on the endcap of the HPGe

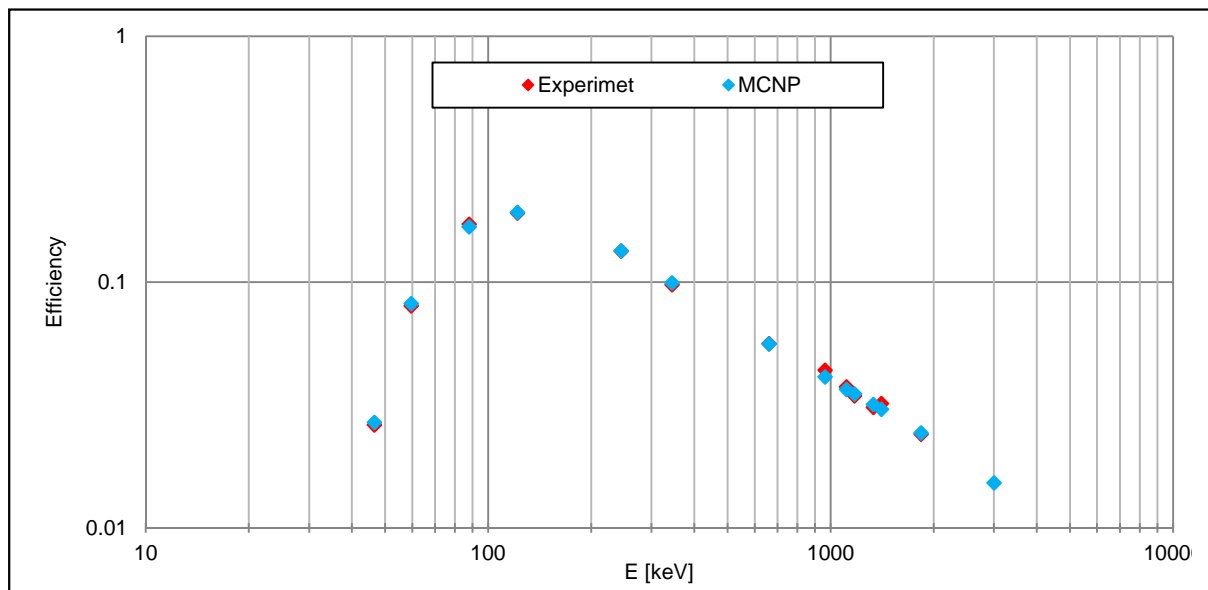


Figure 4: Experimental and simulated spectrum of Co-60 point source on the endcap of the HPGe

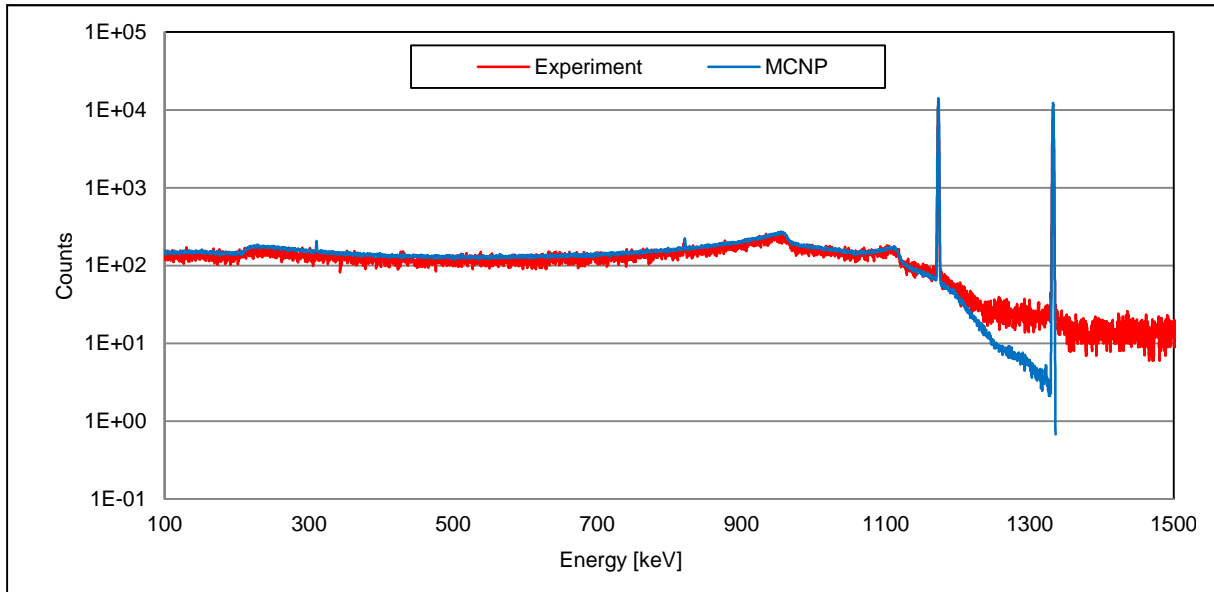


Figure 5: MCNP estimation of all fission products activities in the EK-10 fuel pin and UO₂ pellet for variety irradiation conditions

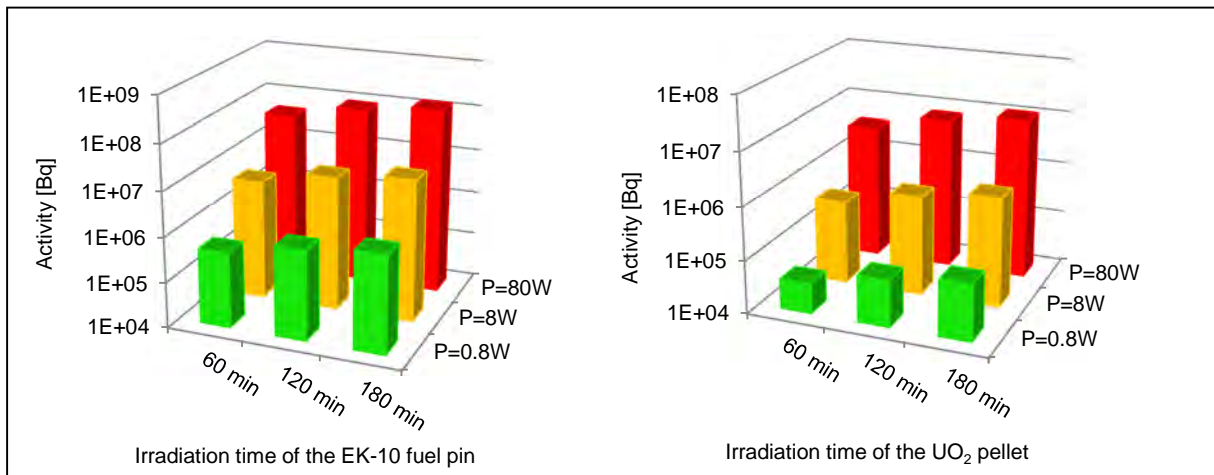
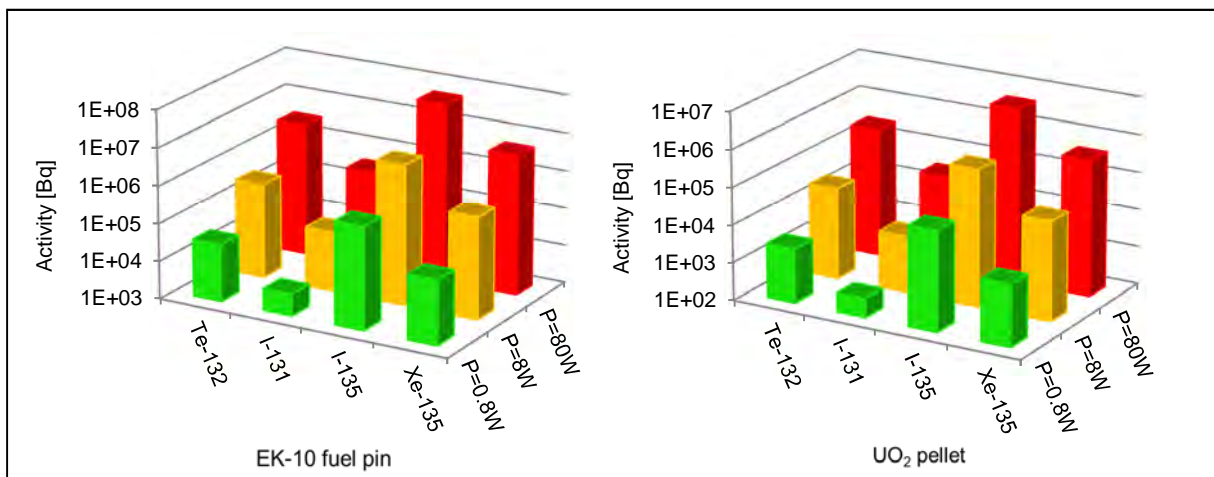


Figure 6: MCNP estimation of selected fission products activities in the EK-10 fuel pin and UO₂ pellet after the 120 min. irradiation for various powers



The fuel elements for 120 min at the power of 8 Watts were irradiated. The EK-10 fuel pin was removed from the reactor core on 4th February 2015 at 12:20. Spectra of the EK-10 were acquired for 3600 s by REXX sequence after 85 min (Spectrum 1), 218 min (Spectrum 2) and 345 min (Spectrum 3), see the Fig. 7. The UO₂ fuel pellet was removed from the reactor core on 5th February 2015 at 12:18. Spectra of the UO₂ were acquired after 55 min (Spectrum 1), 176 min (Spectrum 2) and 298 min (Spectrum 3), see the Fig. 8. The number of peaks detected in spectra by spectrometry analysis is listed in Table 2.

Efficiency curves of the HPGe detector for both types of the fuel elements and point source (at the 100 cm distance from the front of the HPGe) calculated by the MCNP were used for the activities estimation (Fig. 9). The activities of selected fission products calculated from the acquired spectra were compared with the MCNP burnup calculation, as can be seen in the Tab. 3 and 4. The activities in the column A were determined by using the simulated point source efficiency without self-absorption correction while the activities in the column B were estimated by using the simulated efficiency of the fuel elements with self-absorption and geometry correction. In addition the activities of the short-lived I-135 and Xe-135 determined by spectroscopy analysis had to be corrected for decay of I-135 and growth of Xe-135 by K_1 factor. The activities of I-135 and Xe-135 were divided by 0.65 and 2.89 respectively.

Figure 7: Spectra of the EK-10 fuel pin acquired in various times after the irradiation

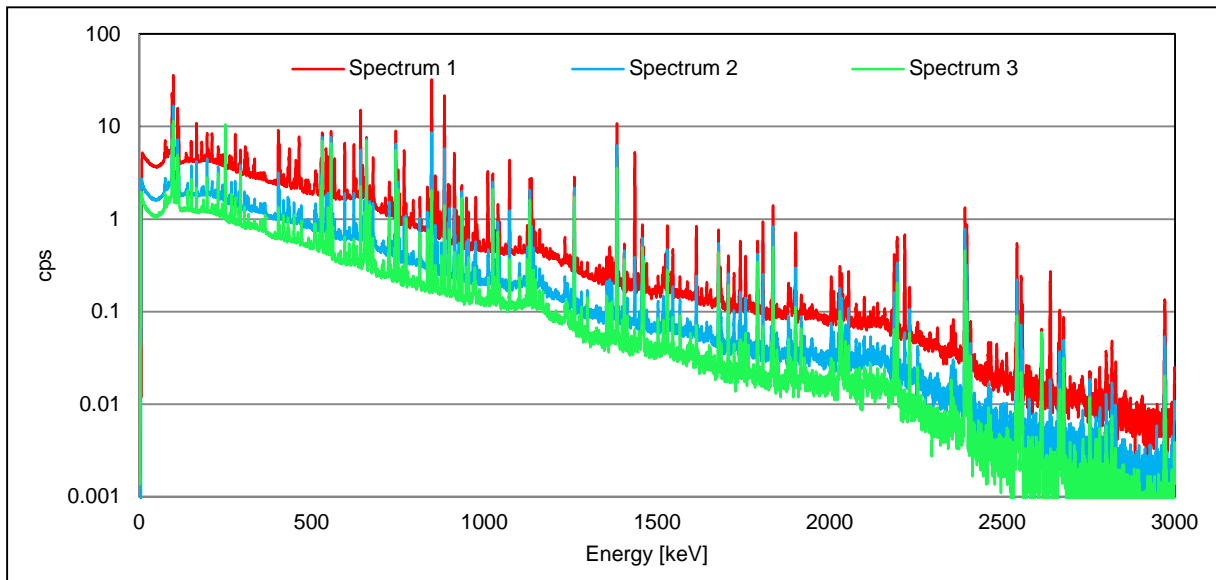


Figure 8: Spectra of the UO₂ pellet acquired in various times after the irradiation

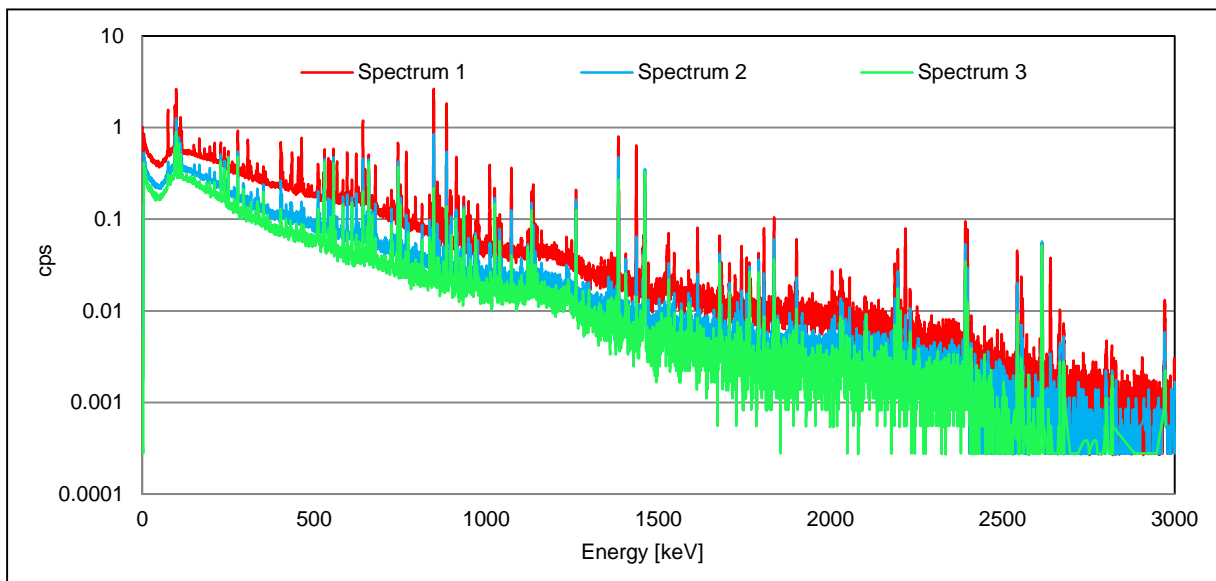


Table 2: The number of detected peaks in acquired spectra

Fuel element	Spectrum	Number of peaks
EK-10 fuel pin	Spectrum 1	356
	Spectrum 2	316
	Spectrum 3	279
UO ₂ pellet	Spectrum 1	249
	Spectrum 2	182
	Spectrum 3	177

Figure 9: MCNP efficiency curves of sources at the 100 cm distance from the front of the HPGe

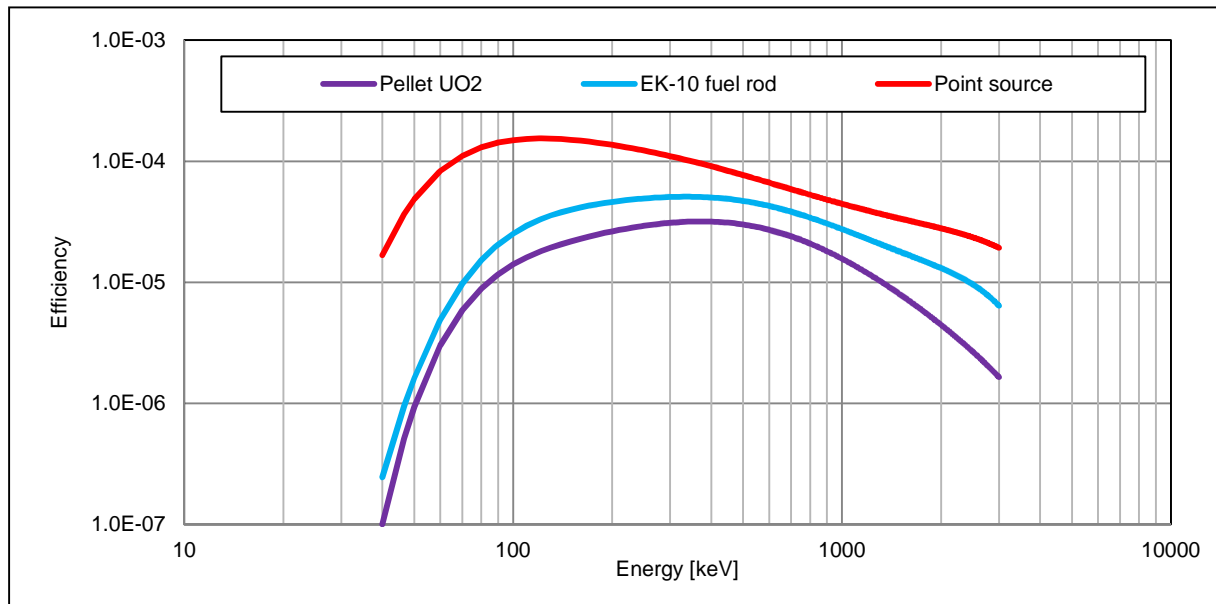


Table 3: Estimated activities of the selected fission products in the EK-10 fuel pin

Nuclide	Energy [keV]	Intensity [%]	K ₁	A Activity [Bq]		B Activity [Bq]		C Activity [Bq]
I-131	364.5	81.2	-	2.04E4		3.47E4		
I-131	637.0	7.30	-	4.21E4	2.08E4	5.23E4	3.51E4	3.74E4
Te-132	228.2	88.2	-	6.82E4	6.82E4	1.69E5	1.69E5	3.19E5
I-135	546.6	7.20		1.55E6		2.04E6		
I-135	836.8	6.70		1.59E6		1.84E6		
I-135	1038.8	8.00		1.82E6		2.08E6		
I-135	1131.5	22.7	0.65	1.63E6	2.29E6	1.84E6	2.88E6	5.19E6
I-135	1260.4	28.9		1.62E6		1.83E6		
I-135	1457.6	8.70		1.78E6		1.99E6		
I-135	1678.0	9.60		1.59E6		1.75E6		
I-135	1791.2	7.80		1.61E6		1.77E6		
Xe-135	249.8	90.0	2.89	3.55E6	1.23E5	8.20E5	2.74E5	5.07E5
Xe-135	608.2	2.90		7.33E6		1.05E6		

Table 4: Estimated activities of the selected fission products in the UO₂ fuel pellet

Nuclide	Energy [keV]	Intensity [%]	K ₁	A		B		C
				Activity [Bq]	Activity [Bq]	Activity [Bq]	Activity [Bq]	
I-131	364.5	81.2	-	8.92E2	8.92E2	1.91E3	1.91E3	3.12E3
I-131	637.0	7.30	-	-	-	-	-	-
Te-132	228.2	88.2	-	7.79E3	7.79E3	1.85E4	2.11E4	2.67E4
I-135	546.6	7.20	-	1.05E5	-	1.5E5	-	-
I-135	836.8	6.70	-	7.28E4	-	8.41E4	-	-
I-135	1038.8	8.00	-	1.39E5	-	1.56E5	-	-
I-135	1131.5	22.7	0.65	1.01E5	1.19E5	1.13E5	1.68E5	4.33E5
I-135	1260.4	28.9		9.90E4	-	1.11E5		
I-135	1457.6	8.70		9.91E4	-	1.13E5		
I-135	1678.0	9.60		8.51E4	-	9.86E4		
I-135	1791.2	7.80	-	1.03E5	-	1.20E5	-	-
Xe-135	249.8	90.0	2.89	1.11E4	3.84E3	3.84E4	1.33E4	4.22E4
Xe-135	608.2	2.90		-	-	-		

4 CONCLUSION

Several gamma-ray spectra of the irradiated fuel elements were acquired and evaluated at the 100 cm distance from the fuel elements. The spectra of the HPGe detector changed significantly in time. Therefore, energy lines of selected fission radionuclides that were not detected well in the beginning can be found in the later acquired spectrum due to, the decrease of the Compton continuum in time – typically in this case I-131 (364.8 keV). The activities of selected fission products (I-131, Te-132, I-135 and Xe-135) in the fuel elements were determined by several ways as can be seen in Tab. 2 and 3. First, for a rough estimation of the activities (column A), simulated efficiency calibration curves for point source at the 100 cm distance from the front of the detector were used. Secondly, for more precisely estimation of the activities, models of the fuels and the HPGe detector were created. Efficiency curves for the both type of the fuels were calculated and used for estimation of the activities (column B). Activities calculated by the MCNP burnup calculation (column C) are in good agreement with the activities determined from the acquired spectra (especially column B). The ratios of the activities are shown in Tab. 5. Activities estimated from the spectra are in all cases lower than calculated by the MCNP burnup calculation.

Table 5: Ratios of the estimated activities

Nuclide	EK-10 fuel pin		UO ₂ pellet	
	A/C	B/C	A/C	B/C
I-131	0.5	1	0.3	0.7
Te-132	0.2	0.5	0.3	0.8
I-135	0.4	0.6	0.3	0.4
Xe-135	0.2	0.5	0.1	0.3

5 ACKNOWLEDGEMENTS

The experiments were carried out using the MONTE-1 device supported by the Ministry of the Interior of the Czech Republic within the security research program VG20132015119. The work was supported by the Ministry of the Interior of the Czech Republic MV-25972-53/OBVV-2010 for the year 2016.

6 REFERENCES

- [1] X-5 Monte Carlo Team: MCNP - A General Monte Carlo N-Particle Transport Code, Version 5, Volume II: User's Guide, 2003
- [2] Canberra Industries, Inc.: Germanium Detectors User's Manual, 2013
- [3] Bílý, T. - Frýbort, J. - Heraltová, L. - Huml, O. - Svoboda, O. - et al.: Citlivostní analýza MCNP modelu školního reaktoru VR-1 Vrabec, Technická zpráva, Prague: Faculty of Nuclear Sciences and Physical Engineering, 2008. 1. 49 s.
- [4] HUML, O - ŽLEBČÍK, P. - SKLENKA, L. - RATAJ, J. – ŠTEFÁNIK, M.: Monte Carlo Simulation of Radionuclide Inventory of Irradiated Nuclear Fuel for Generation of Complex Fission Gamma Ray Fields, in Nuclear Science Symposium and Medical Imaging Conference, San Diego, USA, 2015

Radiation-induced Color Bleaching of Methyl Red in Polyvinyl Alcohol (PVA) Film Dosimeter

Awad Alzahrany^{a,b}, Ahmed Basfar^{a,b}, Khalid Rabaeh^{a,c}

^aAtomic Energy Research Institute, King Abdulaziz City for Science and Technology, (KACST), RIYADH, Saudi Arabia

^bAtomic Energy Sector, King Abdullah City for Atomic & Renewable Energy (KACARE), RIYADH, Saudi Arabia

^cMedical Imaging Department, Faculty of Allied Health Sciences, Hashemite University, Zarga, Jordan

Abstract. Radio-chromic film based on polyvinyl alcohol (PVA) containing different concentrations of methyl red (MR) dye for 0.25 and 0.5 mM has been introduced as high dose dosimeter. The dosimeters were irradiated with gamma ray from ⁶⁰Co source at doses from 5 to 60 kGy. UV/VIS spectrophotometry was used to investigate the optical density of unirradiated and irradiated films in terms of absorbance at 424 nm. The dose sensitivity of MR-PVA film dosimeter increases gradually with increases of concentrations of MR dye. The effects of irradiation temperature, relative humidity, dose rate and the stability of the response of the films after irradiation were investigated and found that these films could be used as routine dosimeter in industrial radiation processing. The useful dose range of developed MR-PVA film dosimeters is in the range of 5-60 kGy.

Characterization of HPGe Detectors using Computed Tomography

Angelica Hedman^{a,b}, Jalil Bahar Gogani^a, Micael Granström^a, Lennart Johansson^b, Jonas Andersson^b, Henrik Ramebäck^{a,c}

^aSwedish Defence Research Agency, Umeå, Sweden

^bUmeå University, Umeå, Sweden

^cChalmers University of Technology, Göteborg, Sweden

Abstract. Computed Tomography (CT) high-resolution imaging have been used to investigate differences in detector parameters when cooling a small n-type HPGe detector and a medium sized p-type HPGe detector to operating temperatures. The findings were compared to calculated linear temperature expansions of different parameters inside the detector and detector dimension data made available by the manufacturer. Parameters investigated were e.g. the air gap between crystal and end cap. The air gap increased by (0.38 ± 0.07) mm for the n-type detector and by (0.40 ± 0.15) mm for the p-type detector when the detectors were cooled compared to at room temperature. Monte Carlo calculations indicate that these differences have a significant impact on the efficiency in close geometries (< 5 cm). In the energy range of 40-700 keV with a source placed directly on endcap, the change in detector efficiency with temperature is 1.9-2.9% for the n-type detector and 0.3-2.1% for the p-type detector. The measured air gap thickness when cooling the detector was 1.1 mm thicker than manufacturer data for the n-type detector and 0.2 mm thicker for the p-type detector. In the energy range of 40-700 keV and with a source on endcap, this result in a change in detector efficiency of 5.2-7.1 % for the n-type detector and 0.2-1.0 % for the p-type detector, i.e. the detector efficiency is overestimated using data available by the manufacturer.

Optimized Detector for in Situ Low Energy Gamma Spectrometry in Close Geometries

Angelica Hedman^{a,b}, Göran Ågren^a, Lennart Johansson^b, Jalil Bahar Gogani^a,
Henrik Ramebäck^{a,c}

^aSwedish Defence Research Agency, Umeå, Sweden

^bUmeå University, Umeå, Sweden

^cChalmers University of Technology, Göteborg, Sweden

Abstract. In situ gamma spectrometry is a fast, important and reliable method for measurements of radionuclide contaminated surfaces. The aim of this work was to find the best possible detector for contamination measurements of low energy gamma radiation in close geometries. Simulations have been made using MCNP (Monte Carlo N-Particle code) where different detector parameters e.g. window material and crystal size, have been varied to find the best combination from a sensitivity point-of-view for close measurements of a contaminated surface with a background spectra of natural radionuclides. The detection limit and the minimum detectable activity (MDA) was calculated. The detection limit increases with larger crystal diameter and thickness while the MDA decreases with larger diameter and thinner crystal.

Delineation of Radiation Dose Pattern in Radiation Workers and Dose Optimization Using Dose Reduction Methodologies

Ajai Kumar Shukla, Dhiraj Kumar Tewari

Department of Nuclear Medicine, Sanjay Gandhi Postgraduate Institute of Medical Sciences, Lucknow, Uttar Pradesh, India

Abstract. Medical exposures contribute to about eighty per cent of the total population exposures and hence pose a major challenge to not only optimize them but also make the justified from radiation safety viewpoint. The present study was undertaken to analyse and delineate the radiation dose pattern in radiation workers of this institute engaged in handling of radiation sources and radiation generating machines including CT and fluoroscopic X-rays located in various departments. The data was analysed five year block wise starting from year 2005 to 2013. In the initial block of 2005-2009, the institute had 234 radiation workers in various departments whereas this figure registered a significant increase gradually over the years and became 288 in 2013. The cumulative radiation dose was observed to be 421.80 mSv with an average dose of 1.80 mSv. In order to further optimize these doses the radiation workers were asked to undergo rigorous, comprehensive and continuous training related to safety aspects and dose reduction methods were deployed in diagnostic as well as therapeutic uses resulting into extremely positive results from radiation safety view point. The cumulative dose had reduced to 115.95 mSv in the block year 2009-13 even though the number of radiation workers increased from 234 to 288 and work load also substantially enhanced. Further analysis revealed that in the block year 2005-09 a large fraction of radiation workers i.e. 213 (93.16%) fell in the dose range of 0-5 mSv with an average dose of 3.04 mSv whereas only 2(0.85%) radiation workers were observed to have fallen in the dose range of 20mSv and above with an average of 23.05 mSv. This trend continued even in the block year 2009-13 except for the fact that the number of radiation workers falling in the dose range of 5-10 mSv increased to 184 (63.88%). Continuous and comprehensive training on safety aspects, implementation of adequate quality assurance procedures, safety culture and appropriate use of dose reduction methodologies resulted into drastic reduction of both cumulative and average doses to radiation workers of the institute.

Establishment of a National Dose Register in South Africa

Alan Muller, Nthabiseng Mohlala

National Nuclear Regulator, Cape Town, South Africa

Abstract. The IAEA Safety Standards require Regulatory Bodies to make provisions for establishing, maintaining and retrieving records of occupational exposure. Several countries, have established a central register for occupational exposures. In South Africa, the nuclear industry and radiation sources applications are regulated by two Regulatory Bodies. Several Dosimetry Service Providers and reporting systems exist, with no central registry for the management of all occupational exposures. The Regulatory Bodies proposed the use of the IAEA Regulatory Authority Information System (RAIS), software developed by the IAEA to assist Member States in managing regulatory control programmes. RAIS is a web application which is installed on an SQL Server. The necessary technical support from the IAEA was obtained for the establishment of a National Dose Register (NDR) in South Africa at one of the Regulatory Bodies. A NDR Steering Committee was formed consisting of some of the major Dosimetry Service and Data Providers covering all nuclear and radiation technologies to oversee the identified activities to be implemented in designing and operationalizing the NDR. The establishment of the NDR was progressed in accordance with approved Project Plans with assistance from IAEA Experts. A phased approach was followed in the execution of the project, and an IAEA Expert Mission was associated with each phase. Some of the main activities included a feasibility study to determine the scope of the work to be performed, a review of the designs of existing stakeholder databases, an analysis and proposed mechanisms of data exchange and formats between Data Providers and the NDR, drafting of the legal and regulatory basis, continuous customizing of the template and NDR solution, training to Data Providers, Pilot Studies to import occupational exposure records, access control as well as the upload of historical data. It has been demonstrated that a NDR can be established in a country with more than one regulatory entity, and which is accessible to various Dosimetry Service and Data Providers. The IAEA RAIS has been shown as a viable tool to efficiently establish and maintain an integrated system of occupational dose records which assists in increased confidence in the record keeping of occupational exposures.

Public In Vivo Thyroid Monitoring for Dose Estimation after Accidental Intake of I-131. Experiences from Scandinavia

Asser Nyander Poulsen^a, Henrik Roed^a, Lilián del Risco Norrlið^b, Mats Isaksson^c, Bjorn Lind^d, Óskar Halldórson Holm^e, Jussi Huikari^f

^aStatens Institut for Strålebeskyttelse (SIS), Copenhagen, Denmark

^bStrålsäkerhetsmyndigheten (SSM), Stockholm, Sweden

^cThe Salgrenska Academy, Univ of Gothenburg, Göteborg, Sweden

^dNorwegian Radiation Protection Authority (NRPA), Østerøs, Norway

^eIcelandic Radiation Safety Authority (GR), Reykjavik, Iceland

^fFinnish Radiation Safety Authority (STUK), Helsinki, Finland

Abstract. Release from nuclear accidents includes short-lived I-131, which is a major contributor to dose received by exposed individuals. Due to the biological role of iodine, I-131 accumulates in the thyroid gland on the front of the neck - a fact that allows rapid screening for I-131 intake with handheld instruments (triage). Selected individuals may subsequently be appointed to a calibrated measurement, and estimation of dose. Public monitoring can help delimit and substantiate health risk and may alleviate fear. A calibrated measurement will typically take place at a laboratory or clinical setting with instruments calibrated against a neck-like phantom with a certified I-131 or long-lived “mock-iodine” source in place of the thyroid. The thyroid gland is the organ mostly affected by I-131 and dose estimation may be based on single organ dose only. However, for the sake of standardization and substantiation of risk, I-131 intake and organ dose-distribution can be estimated using ICRP biokinetic models and dose-coefficients. The outcome of a coordinated Scandinavian proficiency test conducted in 2012-13 (NKS THYROID, 5 countries, 30 locations, 96 detectors and gamma cameras) is presented along with conclusions from a stakeholder meeting held afterwards. Identified future tasks include evaluation of the following: organization of national internal dosimetry expertise; regional capacity and setup/response time; national standardization of procedures and instrumentation; instrument detection limits and compatibility with Ba-133+Cs-137 “mock iodine”; practicability of I-131 calibrations; strategies for registration, record-keeping, health-risk communication; key uncertainties affecting measurement and dose-estimate; development of a report template and validated data analysis tool; implementation of relevant standards (ISO-28218, ISO-11929, IDEAS 2013, JCGM 100:2008 “GUM”).

Comparison of Radiation Dose Assessment Methodology used for the Public Living in the Area Contaminated with Radioactive Materials

A Ra Go, Min Jun Kim, Kwang Pyo Kim

Kyung Hee University, Yongin-Si, Gyeonggi-Do, Republic of Korea

Abstract. After Fukushima Daiichi NPP accident, Japanese government has continued to remediate the large contaminated area. Japanese authority used measured air dose rate to estimate radiation dose. However the radiation doses might be overestimated using the method. Therefore, it is necessary to accurately estimate radiation doses received by residents of evacuation directive lift area. The objective of this study was to select the proper dose assessment methodology by comparing various dose assessment methodologies. In this study, three dose assessment methodologies were considered; Japan Atomic Energy Agency (JAEA) methodology, Jacob methodology, and RESRAD. To compare the methodologies, dose assessment was conducted for indoor worker who lived in evacuation directive lifted area. In addition, radiation dose was estimated over time to predict radiation dose to the general public by the daily life. For the evaluation of radiation dose, information of radioactive material concentrations in soil was collected by National Regulation Authority Japan survey data between 2013 and 2014. As a result of comparing the three dose assessment methodologies, annual effective dose ranged from 0.22 to 4.95 mSv/y by JAEA model (mean of 1.43 mSv/y), from 0.09 to 0.31 mSv/y by Jacob model (mean of 0.91 mSv/y), and from 0.07 to 2.89 mSv/y by RESRAD (mean of 0.77 mSv/y). JAEA model results were two times higher than Jacob and RESRAD model results. Jacob model results were 14% higher than RESRAD results. JAEA model was assessed conservatively than the other models. JAEA model estimate radiation dose to the public based on measured air dose rate rather than radionuclide concentrations (Cs-134, Cs-137) in soil. Comparing the predictive dose values by Jacob model and RESRAD, the difference in radiation doses increased with calendar time. It can be explained that Jacob model considered vertical migration of radioactive materials in soil using attenuation function. Comparing different dose assessment models, radiation doses varied depending on model. The results of this study can be used to select the proper dose assessment methodology for the public living in the area contaminated with radioactive materials. *This study is supported by Grant 20141510101630 from the Energy Technology Development Project of Korea

Argentinian Intercomparison Exercise on Internal Dosimetry: ^{131}I Thyroid Monitoring

Ana Rojo, Nancy Puerta, Sebastian Gossio, Ines Gomez Parada

National Regulatory Authority, Buenos Aires, Argentina

Abstract. The Internal Dosimetry Laboratory (LDI) of the Nuclear Regulatory Authority (ARN) has the task of promoting national exercises with the aim of verifying the technical capabilities on internal dosimetry of Technical Support Officers (TSO) in Argentina. With that object in 2014, a national intercomparison exercise was organized, including direct measurements of activity organ burdens and the interpretation of them in terms of intake and effective dose. The national TSOs were called to participate. The LDI provided a neck phantom with a $^{133\text{m}}\text{Ba}$ standard, a specific protocol to perform the measurements and a description of a simulated exposure scenario for estimating the intake and the effective dose. The participants included two TSOs from Argentinian nuclear power plants, two from atomic centers, one from nuclear medicine center and one from ARN. This paper presents the analysis of the results reported by these six TSOs. The analysis of participant performance included the study of the reported detection limit, activity trueness and repeatability based on ISO 28218 and it was complemented with a study of the reported activity and uncertainty applying E_n -score method. The dose assessment results were analyzed according to IDEAS Guidelines criteria. It could be confirmed that 100 % of the laboratories fulfilled the trueness and precision criteria and 67 % of the reported activity and uncertainty were satisfactory. Five out of six participants completed the dose assessment. Four out of six reported intake and $E(50)$ with a relative bias less than 10 %.

Performance Comparison of OSLD ($\text{Al}_2\text{O}_3:\text{C}$) and TLD ($\text{LiF}:\text{Mg,Cu,P}$) in Accreditation Proficiency Testing

Alexander Romanyukha, Mathew Grypp, Anthony Williams

Naval Dosimetry Center, Bethesda, Maryland, USA

Abstract. The U.S. Navy uses a dosimetric system, which employs the $\text{LiF}:\text{Mg,Cu,P}$ thermoluminescence dosimeters (TLDs), developed and produced by Thermo Fisher Scientific. The dosimeter consists of four $\text{LiF}:\text{Mg,Cu,P}$ chips, mounted on an aluminum card and placed in a plastic holder. The holder contains a unique filter for each chip, which make possible to determine shallow, deep, and neutron dose equivalents. The TLD-based dosimetric system is nationally accredited and is used by the Navy for dose of record. Every two years, the Naval Dosimetry Center (NDC) performs proficiency testing to maintain its national accreditation. Since 2007, the U.S. Navy has started testing InLight Basic - OSLN Optically Stimulate Luminescence dosimeters (OSLD) manufactured by Landauer. A OSLD slide has four $\text{Al}_2\text{O}_3:\text{C}$ discs inserted in a case. The case contains a unique filter for each disc, e.g. copper, aluminum, ABS, and polyamide film. The case and slide assembly go into a clamshell holder. Similar to the TLDs, OSLDs are able to determine shallow, deep, and neutron dose equivalents. In 2011 and 2013 NDC performed proficiency testing for both systems. Here we present a comparison of the performance of TLD ($\text{LiF}:\text{Mg,Cu,P}$) and OSLDs ($\text{Al}_2\text{O}_3:\text{C}$) in five categories of proficiency testing in 2011 and 2013. Irradiation of the dosimeters for proficiency testing was conducted under controlled conditions and includes irradiation with photons, neutrons, beta particles and selected mixtures of these radiations. All irradiations were performed at the Pacific Northwest National Lab (PNNL). The delivered doses were not reported to the NDC. The official comparison of delivered and reported doses was conducted by PNNL in terms of dose bias and its standard deviation for each category of accreditation. In total, the NDC reported to the PNNL doses for 162 dosimeters of each type (TLD and OSLD). Both NDC tested dosimetric systems have passed the established limits. The comparison of OSLD and TLD system performance in each category will be discussed.

Test of Ring, Eye Lens and Whole Body Dosimeters for the Dose Quantity Hp(3) to be used in Interventional Radiology

Agnieszka Szumska, Renata Kopeć, Maciej Budzanowski

Institute of Nuclear Physics PAN, Krakow, Poland

Abstract. In its statement on tissue reactions approved on 21st April 2011, the International Commission on Radiological Protection (ICRP) reviewed its recommendation concerning the equivalent dose limit for the eye lens and reduced the dose limits for occupationally exposed persons to 20 mSv in a year, averaged over defined periods of 5 years, with no single year exceeding 50 mSv. This limit was approved and written down in the new EURATOM directive 2013/59 and in the IAEA BSS of July 2014. For that reason, the necessity to monitor the eye lens may become more important than it was before. However, specially dedicated dosimeters for the dose quantity Hp(3) are using very rarely. Commonly use are only whole body personal dosimeters for the personal dose equivalent quantities Hp(10) worn on the trunk and ring dosimeters worn on finger to measure the quantity Hp(0.07). First of them are calibrated on a slab phantom and second one on rod phantom while a cylindrical phantom much better represents the head and is recommended to calibrate the eye lens dosimeters. Therefore, in this work firstly it was investigated whether dosimeters from routine use calibrated on a slab and rod phantom can be used as an eye lens dosimeter, worn close to the eyes - on the thyroid collar and could deliver correct results. Secondly it was also investigated what is the difference between dose readouts if we calibrated this dosimeters on a standard phantoms and on a cylindrical phantom dedicated to eye lens dose assessment.

From Filter Swipe Test to Bioavailability: A Rapid Experimental Approach to Assess Actinide Behaviour Following Internal Contamination

Anne Van der Meeren^a, Agnès Moureau^a, Sylvie Coudert^a, Pierre Laroche^b, Jaime Angulo^a, Nina Griffiths^a

^aCEA, Bruyeres le Chatel, France

^bAREVA NC, Paris, France

Abstract. Following exposure to radioactive elements, distribution from the contamination site to the tissues results from the transfer across biological barriers. This depends primarily on the physicochemical properties of the contaminant. In the case of accidental or intentional dispersion of radionuclides a first approach is to characterize the contaminants. Filter swipe tests are commonly used to adsorb radioactive materials of the surrounding environment prior to different analyses. The present work describes the uptake of different actinide elements and forms onto filters “swipe test” followed by solvent dissolution of the filter. The resulting solution was then incorporated into agarose gels in culture wells in order to evaluate the transfer of the radionuclide from the static gel phase into a biological medium representative of plasma or interstitial fluid (dynamic fluid phase). Transfer of radionuclide from static to fluid phase reflects contaminant bioavailability. Actinide recovery was determined by liquid scintillation counting, alpha spectrophotometry or external counting using a germanium detector. The first test was to determine the best solvent in order to maximize actinide recovery. Plutonium (Pu) recovery was some 15 % and Americium (Am) 10 % using filters soluble in dimethyl formamide. When included in the agarose gel the transfer of Pu or Am from this resulting filter-solvent-agarose mixture was similar to that using actinide in solvent but without the filter after 2h incubation. In addition Am transfer was greater than Pu in agreement with the known solubility of each element. Addition of DTPA to the external medium led to enhanced transfer of both actinides. The results indicate that actinides “recovered” from swipe test filters behave in a similar way to the control form and as expected considering individual solubility properties. These data indicate that it is possible to gain an insight not only on the physical properties but also on the biological behavior of the radiocontaminant associated with a “filter swipe test”. This test is simple, rapid and inexpensive and could be potential resource for the nuclear industry in conjunction with other measurements. This approach could provide an insight for possible decorporation therapy and may be of particular importance given the different compositions of actinides or other radioelements during decommissioning procedures. Financial support from Areva NC is gratefully acknowledged.

Microphotonics Approaches to Nuclear Forensics Analysis

Bobby Bhatt, Hudson Angeyo, Alix Dehayem-Massop

University of Nairobi, Nairobi, Kenya

Abstract. Nuclear terrorism has been identified as one of the most serious security threats facing the world today. Nuclear security aims at the prevention and detection of and response to the theft, sabotage, unauthorized access, illegal transfer or malicious acts involving nuclear material. As a response to combat illicit trafficking of nuclear and radiological material (NRM), a relatively new discipline, Nuclear Forensics (NF) emerged. NF is an important tool for analysis and establishing the relationship between NRM and their attribution to monitor nuclear security. Traditional nuclear forensic science makes use of analytical techniques (Gamma spectroscopy, alpha spectrometry, mass spectrometry, profilometry and electron microscopy), which were developed for applications related to the nuclear fuel cycle. Unfortunately, most of these techniques used in the nuclear forensics analysis are destructive, invasive, time-consuming and destroy the integrity of the sample. Photonics overcomes these limitations to a great extent. Laser-ablation, inductively coupled-plasma mass spectrometry (LA-ICPMS), optical microscopy, tunable diode laser absorption spectroscopy (TD-LAS), light detection and ranging (LIDAR) and ultra-violet visible near infra-red (UV-Vis-NIR) spectrophotometry are among the few photonic techniques which are already in use in NF analysis. However, these techniques are faced with challenges with regard to analyzing NRM for quantitative information in limited size non-destructively, non-invasively and rapidly. The critical challenge in NF at the moment is the lack of direct, rapid and non-invasive analytical techniques for detection, microanalysis and imaging of NRM. This necessitates the development of techniques for rapid analysis (qualitative and quantitative) of NRM. Microphotonics, which deals with directing light on a microscopic scale has the requisite ability to perform NF microanalysis non-invasively, non-destructively and with high sensitivity. We are employing machine learning (ML) based microphonic techniques namely laser induced breakdown spectroscopy (LIBS) and laser Raman spectromicroscopy (LRS) for NF analysis. LIBS is a spectroscopic technique, in which the radiation emitted by the micro plasma on focusing a powerful laser beam onto the sample is used to fingerprint the element associated with the spectral peaks. LRS uniquely identifies and images samples based on molecular vibrations following little or no sample preparation. Although these techniques have a huge potential to identify and quantify at standoff distance the elemental, molecular, microstructural and isotopic composition of trace NRM their practical utility is limited by the complexity of the samples and (multivariate) data interpretation. We overcome these limitations by combining the techniques with ML techniques to help reduce the data dimensionality and extract subtle NF signatures from the spectra and images in aid of nuclear security. We report here the progress made in using the outlined microphonic approaches for NF analysis and attribution in support of nuclear security and safeguards.

Determination of Scattering Factors Associated to the *In Vivo* Monitoring of Iodine-131 in the Thyroid

Bernardo Dantas^a, Fabiana Lima^b, Ana Letícia Dantas^a, Eder Lucena^a, Rodrigo Gontijo^c, Carlaine Carvalho^d, Clovis Hazin^{b,d}

^aInstituto de Radioproteção e Dosimetria, Rio de Janeiro, RJ, Brazil

^bCentro Regional de Ciências Nucleares, Recife, PE, Brazil

^cUniversidade Federal de Minas Gerais, Belo Horizonte, MG, Brazil

^dUniversidade Federal de Pernambuco, Recife, PE, Brazil

Abstract. The internal dose due to intake of radionuclides by humans can be estimated by *in vivo* direct measurements in the human body and *in vitro* analysis of biological indicators. *In vivo* techniques consist on the identification and quantification of radionuclides present in the whole body and in specific organs and tissues. Activities measured in organs should present uncertainties within pre-set limits in monitoring programs for occupationally exposed individuals. This study aims to evaluate the sources of uncertainty associated with the results of *in vivo* monitoring of iodine 131 in the thyroid. The reference values adopted in this study are based on the criteria suggested by the General Guide for Estimating Effective Doses from Monitoring Data (Project IDEAS/European Community) for high-energy photons (>100 keV). Besides the parameters presented by the IDEAS Guide, it has also been evaluated the fluctuation of the counting due to phantom repositioning, which represents the reproducibility of the counting geometry. Measurements were performed at the *In Vivo* Monitoring Laboratory of Institute of Radiation Protection and Dosimetry (IRD) and at the Internal Dosimetry Laboratory of Regional Center of Nuclear Sciences (CRCN-NE), branches of the Brazilian Nuclear Energy Commission (CNEN). In both institutions, the experiment was performed using a NaI(Tl)3"x3" scintillation detector and a neck-thyroid phantom developed in IRD. Scattering factors were calculated and compared in different counting geometries. The results show that the technique present reproducibility equivalent to the values suggested in the IDEAS Guide and measurement uncertainties comparable to international quality standards for this type of *in vivo* monitoring.

μ -TPC: A New Recoil Nuclei Telescope for Low Energy Neutron Fields characterization

**Benjamin Tampon^a, Daniel Santos^b, Olivier Guillaudin^b, Jean-François Muraz^b,
Lena Lebreton^a, Thibaut Vinchon^a, Nadine Sauzet^b**

^aIRSN/PRP-HOM/SDE/LMDN, Saint Paul Lez Durance, France

^bCNRS/IN2P3/LPSC, Grenoble, France

Abstract. To measure both energy and fluence of neutron fields, with energy ranging from 8 keV to 1 MeV, a new recoil nuclei telescope is under development at IRSN, in collaboration with the LPSC (CNRS/IN2P3/Grenoble). The measurement strategy requires the track reconstruction of recoiling nuclei down to a few keV, which can be achieved with a low pressure gaseous detector using a micro-pattern gaseous detector. A mixture of gas is used as an n-p converter to detect neutrons within the detection volume. Then, electrons produced by the ionisation of the gas by the proton recoil, are collected by the pixelised anode (2D projection). A self-triggered electronic able to perform the anode readout at a 50 MHz frequency gives the third dimension of the track. The scattering angle is deduced from this track using algorithms. The proton energy is determined taking into account the ionisation quenching factor. The system will be shortly presented with the associated methods used to determine the energy and fluence. This article will emphasize the proton energy calibration procedure and the quenching factor measurements. The ion source COMIMAC, dedicated to the measurements of these factors will be shown. This source, developed by LPSC, is able to produce protons and electrons with an accurate energy ranging from 1 keV to 50 keV.

A Passive Neutron Dosimeter for Measurement in Mixed Neutron-Photon Fields

Sören Mattsson, Maria Christiansson, Christian Bernhardsson

Medical Radiation Physics Malmö, Department of Translational Medicine, Lund University, Malmö, Sweden

Abstract. Despite great efforts to develop environmental and personal passive dosimeters for neutron radiation, there is to date no equipment that can be considered as a solution to the problem. Dosimeters that are available today have shortcomings in their properties, and the combination of different dosimeter types that would be needed often turns 1) so expensive that the cost will be a barrier to their use, and 2) their use is so complex that only a few experts in radiation protection can fully use the methodology. The aim of the present project is to develop a simple, effective and inexpensive neutron dosimeter for determination of ambient dose equivalent and personal dose equivalent from neutrons in mixed photon/neutron fields. This project combines the highly sensitive salt (NaCl)-OSL dosimeter for photon radiation with a neutron converter in the form of thin gadolinium foils enclosing the salt. This dosimeter registers neutron- as well as photon dose contributions. Using an identical salt dosimeter without gadolinium cover determines the photon contribution. With this twin dosimeter, both photon and neutron dose contributions can be estimated. This report describes the design and optimization of the construction as well as tests and a preliminary calibration of the dosimeter for estimation of neutron dose equivalent in mixed neutron and photon beams from a ^{252}Cf -source. Currently, the lowest dose equivalent possible to quantify is around 1 mSv for neutrons and 0.1 mSv for the photon component. The current study shows the potential of the developed neutron dosimeter and encourages to continued studies within the area.

The Russian Human Radiobiological Tissue Repository: A Unique Resource for Studies of Plutonium-Exposed Workers

Christopher Loffredo^a, David Goerlitz^a, Svetlana Sokolova^b, Leonidas Leondaridis^a, Mariya Zakharova^b, Valentina Revina^b, Evgeniya Kirillova^b

^aGeorgetown University, Washington, DC, USA

^bSouthern Urals Biophysics Institute, Ozersk, Chelyabinsk Oblast, Russia

Abstract. The Russian Radiobiological Human Tissue Repository (RHTR) at the Southern Urals Biophysics Institute in Ozersk, Russia, was established to maintain and expand a collection of biological samples that are critical to supporting the overall mission of deepening the understanding of the long term health consequences of chronic, low dose radiation exposures. RHTR facilitates a wide range of basic and molecular epidemiology studies designed to assess the relationship between radiation exposure and multiple health outcomes and cellular responses. Two main groups of subjects have been enrolled from 1951 to the present time: exposed workers at the Mayak facilities, and residents of Ozyorsk who were never occupationally exposed to ionizing radiation (controls). Tissues and biospecimens are collected with signed, informed consent of participants, and all specimens are annotated with demographic, occupational, dosimetry, and medical information including pathology data. Protocols for specimen collection, processing, storage, and quality control at RHTR are continually updated and brought into compliance with international best practices guidelines. To date, surgical and/or biopsy tissues have been collected and stored from over 800 individuals, and autopsy tissues and whole organs are available from nearly 1,000 individuals. A second major capacity of the RHTR is the collection and storage of blood samples, consisting of suspensions of leukocytes, lymphocytes, immortalized B-cells, erythrocytes, plasma, serum, and blood DNA from workers and controls. Familial blood DNA is available from parent-offspring triads where at least one of the parents was an exposed worker. Additional collections in the RHTR include oral epithelial cells, saliva, induced sputum, and bone marrow from selected individuals. The biological materials and their annotated data are available to and have been shared with interested scientists worldwide, via the RHTR web site, which enables the sharing of information with the scientific community and application processes. Examples will be described to illustrate the role of RHTR in facilitating state-of-the-art radiobiological research, using this unprecedented and unique resource.

Radiation Protection Dosimetry (2017), Vol. 173, No. 1-3, pp. 10–15

doi:10.1093/rpd/ncw303

Characterization and Measurement of Dosimetry X-ray Beam on Kenya

Collins Omondi, David Otwoma

Kenya Bureau of Standards, Nairobi, Kenya

Abstract. The need for the specification of X-Ray beam quality arises from the fact that several parameters required for the determination of absorbed dose, depend on the X-Ray source energy. The aim of the presentation is to analyze the performance of X-Ray source (Dosimetry) by indirectly specifying the radiation beam quality through measurements of half value layer (HVL), tube potential and air-kerma. This involve determination of qualitative and quantitative of X-Ray beam, physical characteristic, energy deposition and calibration of photon. The quantity air kerma is used for calibrating the reference photon radiation fields and Ionization chamber as reference instrument. The charge collected by the ionization chamber is measured with an electrometer, and corrections are applied to account for the effects of air temperature, air pressure, ionic recombination and other influence parameters. The measurements are carried out in Secondary Standard Dosimetry Laboratory (SSDL) that have X-ray beams. Different HVL beams measurements results are obtained by introducing different added filtration. The HVL increases with increasing filter thickness as the beam become increasingly harder because it contains a greater proportion of higher-energy photons.

International Standards on Radioactivity Measurement for Radiological Protection: Status and Perspectives

Dominique Calmet^a, Roselyne Ameen^b, Aude Bombard^c, Stephane Brun^a, Francois Byrde^d, Jing Chen^e, Jean-Marie Duda^a, Maurizio Forte^f, Marc Fournier^g, Ales Fronka^h, Thomas Haugⁱ, Margarita Herranz^j, Amir Husain^k, Simon Jerome^l, Martin Jiranek^m, Steven Judge^l, Sang Bog Kimⁿ, Pieter Kwakman^o, Jeanne Loyen^g, Montse LLaurado^p, Rolf Michel^q, David Porterfield^r, Andry Ratsirahonana^a, Anthony Richards^s, Katerina Rovenska^h, Tetsuya Sanada^t, Christoph Schuler^u, Laurence Thomas^v, Shinji Tokonami^w, Andrey Tsapalov^x, Takahiro Yamada^y

^aCommissariat à l'énergie atomique et aux énergies alternatives, 92265 Fontenay aux Roses Cedex, France, ^bALGADE, 1 Avenue du Brugeaud - BP 46 - 87250 Bessines sur Gartempe, France, ^cTrisKem International, Campus de Ker Lann, Parc de Lormandière, Rue Maryse Bastié, 35170 Bruz, France, ^dGruppe Radioaktivität, Eidgenössisches Departement für Verteidigung, Bundesamt für Bevölkerungsschutz, 3700 Spiez, Switzerland, ^eRadiation Protection Bureau, Health Canada, 775 Brookfield Road, Ottawa, Ontario, K1A 1C1, Canada, ^fARPA Lombardia, Centro Regionale di Radioprotezione, Via Juvara 22, 20129 Milano, Italy, ^gAutorité de sûreté nucléaire, 15 rue Louis Lejeune, 92541 Montrouge Cedex, France, ^hNational Radiation Protection Institute, Bartoškova 28, Praha 4 140 00, Czech Republic, ⁱEberhard Karls-University of Tuebingen, Isotope lab & radiation protection, Auf der Morgenstelle 24, 72076 Tübingen, Germany, ^jDepartment of Nuclear Engineering and Fluid Mechanics, alda Urquijo s/n, 48013 Bilbao, Spain, ^kKinectrics Inc. 800 Kipling Avenue, Unit 2 Toronto, Ontario, M8Z 5G5, Canada, ^lThe National Physical Laboratory, Queens Road, Teddington, Middlesex TW11 0LW, United Kingdom, ^mFaculty of Civil Engineering, Czech Technical University, Thákurova 7, 166 29 Praha 6, Czech Republic, ⁿEnvironmental Technologies Branch, Chalk River Laboratories, Station 51A, Chalk River, Ontario, K0J 1J0, Canada, ^oRIVM, Laboratory for Radiation Research, PO Box 1, 3720 BA Bilthoven, The Netherlands, ^pDepartamento Química Analytica, Laboratori de Radiologia Ambiental, Facultat de Química- Universitat de Barcelona, Martí i Franques, 1-11, 08028 Barcelona, Spain, ^qStrahlenschutz und Radioökologie Wilh.-Henze-Weg 14; D-31303 Burgdorf, Germany, ^rLos Alamos National Laboratory, PO Box 1663, MS G740, Los Alamos, NM 87545, USA, ^sBSI, 389 Chiswick High Road, London W4 4AL, UK, ^tHokkaido University of Science, Department of Radiological Technology, Faculty of Health Sciences, Sapporo, Japan, ^uPaul Scherrer Institut, CH-5232 Villigen PSI, Switzerland, ^vAFNOR, 11 rue Francis de Pressensé, 93571 La Plaine Saint-Denis cedex, France, ^wDepartment of Radiation Physics, Institute of Radiation Emergency Medicine, Hirosaki University, Hirosaki City, Aomori 036-8564, Japan, ^xLaboratory of Radiation Safety in Building, Research Institute of Building Physics, Russia, Academy of Architecture and Building Science, Moscow, Russia, ^yJapan Radioisotope Association, 28-45, Honkomagome 2 ,Bunkyo-ku, Tokyo1138941, Japan

Abstract. Radiological protection is a matter of concern for members of the public and thus national authorities are more likely to trust the quality of radioactivity data provided by accredited laboratories using common standards. Normative approach based on international standards aims to ensure the accuracy or validity of the test result through calibrations and measurements traceable to the International System of Units. This approach guarantees that radioactivity test results on the same types of samples are comparable over time and

space as well as between different testing laboratories. Today, testing laboratories involved in radioactivity measurement have a set of more than 150 international standards to help them perform their task. Most of them are published by the International Standardization Organization (ISO) and the International Electrotechnical Commission. This paper reviews the most essential ISO standards that give guidance to testing laboratories at the different stages from sampling planning to the transmission of the test report to their customers, summarizes recent activities and achievements and present the perspective on new standard development of the ISO Working Groups dealing with radioactivity measurement in connection of radiological protection.

KEYWORDS: *international standard; radioactivity test method; environmental and food monitoring; radioprotection.*

RadiationProtectionDosimetry(2017),Vol.173,No.1-3,pp.55–62

doi:10.1093/rpd/ncw342

A Method for Response Time Measurement of Ionization Chamber Type Survey Meter

Dehong Li^a, Bin Guo^a, Jianwei Wang^a, Di Wu^{a,b}, Xingdong Li^a

^aNational Institute of Metrology, Beijing, China

^bUniversity of South China, Hengyang, Hunan, China

Abstract. Ion current chambers have responses that are proportional to absorbed energy and hence are widely used in measurement of dose. The ions generated in the chamber are collected through external circuit. The measuring process of the survey meter can be seen as a charging process of the capacitor through the load resistance. The response time depends on the load resistance and the capacitance of the chamber and its associated circuitry. In general, the response time of ionization chamber dosimeter changes from a few seconds to tens of seconds, which leads the displayed value of instrument significantly different from the actual dose rate during measuring a short pulse of radiation. The actual dose rate can be obtained by using the measured value and response time. The different radiations for the same dose rates but different exposure times were measured and corrected by using the response time given by the instructions of the Model 451B ionization chamber survey meter. It was found that the correction values were increased with the increase of the exposure time, so the conclusion that the response time is longer than 8s which is given by the instructions could be gotten. To obtain a more accurate response time of the survey, an experience formula based on the circuit theory and the response time was established, and verified with experiment data. According to this method, the response time of the first range of model 451P ionization chamber survey meter which is (0-5) uSv/h is about 13.2s that is longer than 8s. And the response time of the model 451P is about 7.3s, but not the 5 s mentioned in the instructions. Therefore, the response time of the instrument which is used for correcting the actual dose rate should be obtained at first when dose rate of a short pulse radiation is measured using an ionization chamber type survey meter. It should be noted that the response time is different for the different ranges, because the survey meter has several ranges accomplished by varying the value of resistance.

The Primary Standard for Air Kerma at the NIM for the Gamma Radiation of ^{137}Cs

Dehong Li^a, Peiwai Wang^a, Jianwei Huang^a, Bin Guo^a, Di Wu^{a,b}

^aNational Institute of Metrology, Beijing, China

^bUniversity of South China, Hengyang, China

Abstract. At the National Institute of Metrology (NIM) a cylindrical cavity ionization chamber was designed and constructed as primary standard to measure air kerma for ^{137}Cs γ rays. This instrument was used mainly for radiation protection calibration purposes. Ground protection structural and the collector of the chamber were optimized through theoretical calculations of the electric field distribution. The applied correction factors for air density, recombination losses, humidity, stem scattering, wall effect (wall attenuation wall scattering mean origin of electrons) axial non-uniformity and radial non-uniformity are described. The physical constants, correction factors, results of measurements and estimated uncertainties for the determination of the ionization current are summarized. Monte Carlo simulation studies were also made, using EGSnrc. A direct comparison of the standards for air kerma of the NIM and of the Bureau International des Poids et Mesures (BIPM) was carried out in September 2014 in the ^{137}Cs radiation beam at the BIPM. The comparison result, evaluated as a ratio of the NIM and the BIPM standards for air kerma, is 0.9967 with a combined standard uncertainty of 0.0021. An indirect comparison using one transfer chamber belonging to the NIM was also made. A similar result was obtained when evaluating the comparison using the calibration coefficients of a transfer chamber. The results are analyzed and presented in terms of degrees of equivalence for entry in the BIPM key comparison database. These studies intend to characterize the radiation field and ionization chamber by simulation and experiment and to obtain correction factors for the cylindrical cavity ionization chamber. Further work is needed to obtain more accurate correction factors.

Dosimetry for Radiological Protection at the New Research Facility, ELI-NP

Elena Iliescu, Sorin Bercea, Iani Mitu, Aurelia Celarel, Constantin Cenusă

“Horia Hulubei” National Institute for R&D in Physics and Nuclear Engineering (IFIN-HH), Magurele, Romania

Abstract. ELI will be the only European and International Center for high-level research on ultra-high intensity laser, laser-matter interaction and brevity will go beyond the current state-of-art by several order of magnitude. The third pillar of this project, ELI-NP, is going to be finalized in Magurele (near Bucharest, Romania) and will focus on laser-based nuclear physics. The radiation beams and fields that will be produced in the ELI-NP are strongly different from all the applications of dosimetry developed in Romania until now. In the ELI-NP White Book, the main types of radiation are given and their characteristics (of these beams/fields). In order to identify the adequate technical solutions for the dosimetric and radiometric instruments for radioprotection in different areas of the ELI-NP facility, different calculations (based on simulations) were performed. These estimations of the source-terms were necessary to establish the main technical and metrological characteristics of the different classes of instrumentation to be used for the dosimetry for radioprotection. These instruments must cover the main four of dosimetry for ELI-NP: i. personnel dosimetry, ii. area dosimetry (monitoring), iii. environment dosimetry (monitoring). The devices dedicated to the above first three items must fulfill the regular requirements regarding the radiological protection of the personnel and environment and will serve to obtain the licenses by the Romanian Nuclear Authority (CNCAN). In the Radiation Protection Dosimetry, according the regulations and the practice, the following kinds of measurements are needed: 1. area measurements: fixed instruments (monitors), mobile instruments (monitors), portable instruments; 2. personnel dosimetry: portable dosimetric systems/instruments : dosimetric films, TLD, personnel electronic (dose rate meters). The aim of this paper is to present which are the specific requirements for the dosimeters to be used at ELI-NP and the solutions established at this moment for the individual monitoring.

Determination of a Urine Reference Level for an Individual Monitoring Programme for Uranium

Frik Beeslaar

NESCA, Pretoria, South Africa

Abstract. Introduction: Individual monitoring for exposure to uranium can be complicated, especially for a multi physiochemical environment where parameters such as enrichment, solubility and AMAD vary significantly. Bioassay monitoring based on urine analyses is used to monitor an individual's intake of uranium. Urinary reference levels are used as a trigger for further investigation following a positive urine result. The reference level, based on a predetermined committed effective dose (CED) will vary with changes in the physiochemical characteristics of the uranium and the exposure scenario. Objectives and Methodology: The aim of the study is to determine a single reference level for uranium in urine. This level should be at a level that is low enough to ensure doses above 1 mSv is not overlooked, but also high enough in order to prevent unnecessary investigations. The aim is to quantify the sensitivity of the CED calculation for changing parameters. Simulated bioassay measurements are generated in order to evaluate the effect of changing input parameters. Results: Acute intake results in an overestimation between 5% to 40% in comparison with chronic. An error in the route of intake can lead to a 20 times under- or overestimation of the CED. The CED is significantly less dependent on AMAD. The over/under estimation is ~ 4%. The total activity decreases for low enrichments where after it increases as the enrichment increases per unit ^{235}U measured in urine. Changes in absorption type can lead to an underestimation or over estimation of several orders in the CED. Conclusion: Chronic intake was found to be the most realistic exposure scenario, however acute intake was assumed. Inhalation was found to be the most probable route of intake. AMAD does not need to be considered and the ICRP default value of $5\ \mu\text{m}$ can be used. A default enrichment of 30% is assumed for all exposures, implying a maximum underestimation of 2% at 10% enrichment and maximum overestimation of 17% at 50% enrichment. Based on the prevailing exposure scenario a default of Type M was decided. The sensitivity of the various input parameters has been quantified and a decision was made on the most adequate assumptions. A reference level of $40\ \text{ng}\ ^{235}\text{U/l}$ was determined, representing a dose of approximately 0.5 mSv.

Data Recording Regarding the Dose Assessment due to X-ray Generator Sources and the ^{241}Am Calibration Curve Usefulness

Felicia Mihai, Ana Stochioiu, Catalina Tuca

Horia Hulubei National Institute for Physics and Nuclear Engineering, IFIN-HH, Magurele, Romania

Abstract. The dosimeter survey services assures radiation monitoring for persons which are occupational exposed at different sources that emitting beta, gamma and x rays radiation. The occupational exposed workers from the medical or industry areas use x-ray generators applying different voltages, current intensity and metallic filters in order to obtain clear images considering the investigation reason. The individual dosimeters are more or less influenced by type of radiation sources, more exactly by the energy of the source. Halide film dosimeter is influenced considerable by radiation energy or by the applied voltage on the x-ray generator. This feature can be an advantage or disadvantage depending on the interest of application. In this work are presented the influence of the applied voltage on the halide film dosimeter response in order to obtain the dose assessment for occupational exposures with good accuracy. In this way, two or three halide film dosimeters were exposed to the x-ray generator at the following voltages: 40 kV, 80 kV, 130 kV maintaining the same current intensity and using an Al filter of 3.0 mm. The conventional true dose values were 0.50 ± 0.023 mSv and 1.00 ± 0.022 mSv. On the other hand, halide film dosimeter were exposed to the ^{241}Am standard source on the $0.10 \div 10.00$ mSv dose range in order to establish the correction between doses given by x-ray generator and those calculate with the ^{241}Am calibration curve. The greatest differences were obtained in case of 40 kV at the dose of 1.00 ± 0.022 mSv and 130 kV with 0.50 ± 0.023 mSv dose, almost $|0.17|$ mSv and $|0.10|$ mSv respectively. Otherwise, the differences were under $|0.08|$ mSv. But the ratios between optical densities recorded on the halide film under plastic and metallic filters of the dosimeter badge show exactly which was the voltage applied during the investigation procedure. The optical density ratios of the plastic/Pb filters were $7.11 \div 7.44$ for 40 kV, $6.5 \div 5.5$ for 80 kV and $4.6 \div 3.5$ kV for 130 kV.

Integrated Operational Dosimetry System at CERN

Gérald Dumont, Fernando Baltasar Dos Santos Pedrosa, Pierre Carbonez, Doris Forkel-Wirth, Pierre Ninin, Eloy Reguero Fuentes, Stefan Roesler, Joachim Vollaire

CERN, CH-1211 Geneve 23, Switzerland

Abstract. CERN upgraded its operational dosimetry system in March 2013 to be prepared for the first Long Shut-down (LS1) of CERN's facilities. The new system allows the immediate and automatic checking and recording of the dosimetry data before and after interventions in Radiation Areas. A total of 66 operational dosimeter readers were installed near each access point. The readers are connected to a central server allowing direct data transmission and recording via a dedicated database. To facilitate the analysis of the data in context of CERN's approach to ALARA ("As Low As Reasonably Achievable"), this new system is interfaced to the Intervention Management Planning and Coordination Tool (IMPACT). IMPACT is a web-based tool widely used in all CERN's accelerators and their associated technical infrastructures for work planning, i.e. coordination and approval of interventions (work permit principle). It constitutes a centralized repository for the intervention information on all facilities (accelerators, experiments, etc.). For Radiation Areas, the IMPACT tool also integrates processes related to the application of the ALARA principle, including the Work and Dose Planning and the radiological work permit ("Dossier d'intervention au milieu radioactif", DIMR). The coupling of the operational dosimetry database with the IMPACT repository allows a direct and almost immediate comparison of the actual dose with the estimations, in addition to enabling the configuration of alarm levels in the dosimeter in function of the intervention to be performed. This integration was paramount in maintaining, and even improving, the follow-up of activities ensured by the Radiation Protection Group during LS1 in 2013-2014. During this period, 2,837 different users intervened in Radiation Areas to perform 4,598 activities identified in IMPACT resulting in 128,368 entries in the operational dosimetry database.

KEYWORDS: *ALARA; CERN; DMC; LDM; dosimetry; DOSISERV; IMPACT; RP.*

RadiationProtectionDosimetry(2017),Vol.173,No.1-3,pp.233–239

doi:10.1093/rpd/ncw327

Biodosimetry of in Vitro Human Lymphocytes exposed to ^{60}Co γ -rays and DNA Incorporated ^{123}I

Hein Fourie^a, Jacobus Slabbert^b, Richard Newman^a, Philip Beukes^b, Neil Rossouw^b

^aStellenbosch University, Stellenbosch, Western Cape, South Africa

^biThemba LABS, Somerset West, Western Cape, South Africa

Abstract. Biodosimetry is a measurement of a biological response and is used as a surrogate for radiation dose measurements. The cytokinesis-block micronucleus assay is one of the biodosimetry assays recommended by the IAEA and ICRU to be used in response to radiation emergencies. For example, it was one of the dosimetry methods employed shortly after the Fukushima Daiichi nuclear disaster in 2011 and also in long-term studies of health risks following the radiation exposure. ^{123}I is a short-lived isotope commonly utilized in Nuclear Medicine, along with ^{125}I and ^{131}I . Apart from its administration in diagnostic medicine, it also poses an uptake risk during the production and dispensing of the radionuclide. The iodine isotopes emit Auger electrons during their radioactive decay. Auger electrons have been shown to cause significant damage to cellular DNA, similar to that of high linear energy transfer (LET) particles such as neutrons, protons and alpha particles, if absorbed into the nucleus of the cell. We wish to make use of the Geant4 Monte Carlo toolkit, an open-source code used for high-energy particle simulations at CERN, to estimate the absorbed dose in lymphocytes due to the radioactive decay of ^{123}I since direct dose measurements are not possible. Ultimately, we aim to produce micronuclei dose-response curves for human lymphocytes exposed to ^{60}Co γ -rays and DNA incorporated ^{123}I . The ^{60}Co γ -ray induced micronuclei showed a linear-quadratic dose response, characteristic of low-LET photon exposures. An inter-donor variation in the responses was observed, a well-known phenomenon due to the inherent radiosensitivity unique to each person. Making use of the microdosimetry calculations, the Auger electron exposures showed a linear response to the amount of incorporated ^{123}I . This is characteristic of high-LET particle exposures. A reduction in the inter-donor variation of the responses was observed, also characteristic of exposures by high-LET particles. The microdosimetry results using Geant4 differed slightly when compared to similar calculations by other Monte Carlo codes. Regardless, dose-response curves were obtained for isolated human lymphocytes exposed to ^{60}Co γ -rays and Auger electrons from DNA incorporated ^{123}I . These curves may be used in prospective and retrospective biodosimetry studies.

Development of Radiation Portal Monitoring System based on Energy Weighted Algorithm for Gamma Spectroscopy

Hyuncheol Lee^a, Wook-Geun Shin^a, Han Rim Lee^b, Chang-Il Choi^c, Chang-Su Park^c, Hong-Suk Kim^c, Chul Hee Min^a

^aYonsei University, Wonju, Republic of Korea

^bHanyang University, Seoul, Republic of Korea

^cKorea Institute of Nuclear Safety, Daejeon, Republic of Korea

Abstract. Polyvinyl toluene (PVT) plastic scintillator has been employed for a radiation portal monitoring (RPM) system installed in an airport or port to prevent illicit trafficking of special nuclear material. But due to the poor energy resolution of the plastic scintillator detector, RPM system is suffer from the false alarms with the naturally occurring radioactive material (NORM). The purpose of this study is to demonstrate the new algorithm distinguishing the illicit radioactive materials from NORM based on the energy-weighted count with the plastic scintillation detectors of the low energy resolution. The proof-of-principle RPM system of $5 \times 100 \times 5$ cm³ plastic scintillator was developed. The signal generated in the PVT with the incident gammas was processed with the pre-amplifier and amplifier, and then the energy spectra was analysed with LabVIEW program. The spectra were re-calculated with the energy-weighted algorithm to remarkably increase the Compton edge and to determine the original energy of the incident gammas. Our results show that the optimal parameter for the in-house developed RPM system is 1.0 kV of high voltage, 100 pF of input capacitance, 0.5 μ sec of shaping time and 160 gains for amplifier. The energy spectra of ¹³³Ba, ¹³⁷Cs and ⁶⁰Co (> 80 μ Ci) were measured with detection distance of 1 m for 2 min, and the energy weighted spectra showed Compton edge peak on 0.204, 0.485 and 1.065 MeV, respectively, while the theoretical Compton edge was 0.207, 0.477 and 1.041 MeV, respectively. For those isotopes, the maximum difference was assessed as 2%. The current study successfully demonstrated with the development of the proof-of-principle RPM system that the radioisotope could be accurately distinguished with the plastic scintillation detector by employing the energy weighted algorithm notably increasing the Compton edge.

Results of the EURADOS Intercomparisons IC2014 on Whole Body Dosimeters for Photons

Hannes Stadtmann^a, Tom Grimbergen^b, Andrew McWhan^c, Ana Maria Romero^e, Markus Figel^d, Christian Gärtner^a

^aSeibersdorf Labor GmbH, Seibersdorf, Austria

^bNuclear Research and Consultancy Group (NRG), Individual Monitoring, Arnhem, The Netherlands

^cCavendish Nuclear Limited, Berkeley, UK

^dHelmholtz Zentrum München, München, Germany

^eCentro de Investigaciones Energéticas, Medioambientales y Tecnológicas (CIEMAT), Madrid, Spain

Abstract. EURADOS, the European Radiation Dosimetry Group, has now been performing international intercomparisons for whole body dosimeters for individual monitoring services (IMS) for more than 17 years. Since 2008, these whole body intercomparisons have been performed on a regular basis every two years. In the most recent whole body dosimeter intercomparison, IC2014, there was total of 96 participating monitoring services from 35 countries with 112 dosimetry systems. The irradiation plan consisted of nine irradiation setups with five different photon radiation qualities (S-Cs, S-Co, RQR 7, W-80, and W-150) and two different angles of radiation incidence (0° and 60°). Selected aspects of dose linearity, energy and angular response were tested and analysed for all participating dosimetry systems. This paper describes the individual results for the personal dose equivalent quantities Hp(10) and, if supplied, for Hp(0.07) for all participating systems and compares these with the “trumpet curve” performance criteria set out in ISO 14146. In addition, the new data is compared with the results of the previous intercomparisons.

Improving Potential in a Retrospective Dosimetry using Common Plastics by Extracting Inorganic Materials

Insu Chang, Jang-Lyul Kim, Jungil Lee, Tae-Hyoung Kim, Seung-Kyu Lee, Bong-Hwan Kim

Korea Atomic Energy Research Institute, Dajeon, Republic of Korea

Abstract. Optically stimulated luminescence (OSL) has been applied in a variety of radiation dosimetry fields, such as personal dosimetry, environmental radiation monitoring, dating, and retrospective radiation dosimetry from radiation accident. In retrospective radiation dosimetry, recently, many researches have been carried out for dose reconstruction using personal electronic devices such as mobile phones, IC card. Possibilities of new retrospective materials are continually investigated. Plastics is one of investigated retrospective materials. It is cheap and widely used in human life. Basically, plastics consist of organic or inorganic compounds. In some plastics, inorganic fillers (SiO₂, alumina etc.) are added to make unique properties for their applications. These inorganic fillers have suitable OSL properties for retrospective dosimetry. However, inorganic fillers are mixed with other compounds, it makes lower OSL sensitivity and weak heat resistance. This study investigated that how to improve the potential use in a retrospective dosimetry using common plastics. We have applied chemical extracting method to extract inorganic materials from common plastics. It improves the potential of use of common plastics in retrospective accident dosimetry. Therefore, we suggest that the extracting inorganic materials could be a method for improving retrospective dosimetric properties of common plastics material.

Performance of Eye Lens Dosemeters in use in Europe

Isabelle Clairand^a, Merce Ginjaume^b, Filip Vanhavere^c, Eleftheria Carinou^d, Josiane Daures^e, Marc Denoziere^e, Edilaine Honorio da Silva^c, Maria Roig^b, Sara Principi^b, Laurent Van Rycheghem^a

^aInstitute for Radiological Protection and Nuclear Safety (IRSN), Fontenay aux Roses, France

^bUniversitat Politcnica de Catalunya (UPC), Barcelona, Spain

^cBelgian Nuclear Research Centre (SCK-CEN), Mol, Belgium

^dGreek Atomic Energy Commission (GAEC), Athens, Greece

^eCEA-LIST Laboratoire National Henri Becquerel (CEA-LNHB), Gif-sur-Yvette, France

Abstract. Due to recent epidemiological evidences of radiation induced opacities and cataracts to the eye lens, ICRP has recommended an equivalent dose limit of 20 mSv in a year for the lens of the eye, averaged over defined periods of 5 years, with no single year exceeding 50 mSv. Medical staff, in particular, those involved in interventional radiology and cardiology can be exposed to doses close to the new limit and will thus require monitoring of the lens of the eye. Within this framework, the European Radiation Dosimetry Group (EURADOS) has organized in 2014 an intercomparison exercise for eye lens dosemeters. A total of 20 European Individual Monitoring Services from 15 different countries participated. All participants used thermoluminescent detectors with various types of filters and holders. Nine provided the Eye-DTM system and the rest provided different systems of various designs. The irradiations were carried out with 10 photon fields chosen to cover the energy and angle ranges encountered in medical workplaces. Participants were asked to report the doses in terms of H_p(3) using their routine protocol. The analysis of the results has been based on ISO 14146 standard. Results are globally satisfactory since 17 participants provided 90% of their response within the standard required limits. For a minority of participants some discrepancies compared to reference doses were observed for the irradiations setups characterized by large angles and/or low energies.

Contemporary Radiation Protection Trends – Do we need a New Yype of Digital Personal Dosemeters to be used in Medicine, Homeland Security, Environmental Protection and Emergencies?

Ivica Prlic^a, Marija Suric Mihic^a, Mladen Hajdinjak^b, Tomislav Mestrovic^a, Zdravko Cerovac^c

^aInstitute for Medical research and Occupational Health, Zagreb, Croatia

^bHaj_Kom Ltd, Zagreb, Croatia

^cALARA Instruments Ltd, Zagreb, Croatia

Abstract. Legal personal dosimetry is based on the use of passive dosimeters such as film, thermoluminescent (TLD) or optically simulated (OSL) dosimeters. Modern technology, special use for security purposes, emergencies and extensive use of radiation imaging in medicine and industry imposes use of upgraded dosimetric devices which could provide additional information on radiation exposure such as information on exposure dose rates, data on the exposure occurrence, duration of the exposure, etc. Majority of available active electronic personal dosimeters (AEPD), due to a type of detector used, are not suitable for measurements in pseudo-pulsed or pulsed radiation fields used in interventional radiology (IR) and cardiology (IC) or border cargo inspections. An AEPD type ALARA OD, based on GM tube, was used to measure the levels and structure of the occupational exposure of workers that are predominantly exposed to scattered X-ray radiation of the continuous and pulsed radiation fields. The 3D H*(10) isodose patterns were constructed. Second set of measurements was performed at border crossings during the regular customs x-ray and LINAC cargo screening procedures. A time varying dose pattern was investigated.

Rare-earth Doped Silica Fibres for Dosimetry Applications in Medicine

Ivan Veronese^a, Mauro Fasoli^b, Norberto Chiodini^b, Eleonora Mones^c, Cristina De Mattia^a, Eduardo D'Ippolito^a, Marie Claire Cantone^a, Anna Vedda^b

^aUniversità degli Studi di Milano, Dipartimento di Fisica, Milano, Italy

^bUniversità degli Studi di Milano Bicocca, Dipartimento di Scienza dei Materiali, Milano, Italy

^cMedical Physics Department, Azienda Ospedaliera Maggiore della Carità, Novara, Italy

Abstract. Scintillating optical fibre sensors have shown promising results for ionizing radiation monitoring and therefore can be useful for dosimetry applications in the medical field. In fact, they may enable a remote, punctual and real-time dose assessment. This work aims to review the recent progresses in the development and characterization of rare-earth doped silica fibres. The radioluminescent and dosimetric properties of Ce, Eu and Yb-doped fibres are described in terms of sensitivity, reproducibility, and linearity of their responses. Moreover, the advantages and challenges in the use of these fibres for radiation therapy dosimetry are shown. For such application, an effective approach to deal with the stem effect contribution, that is a spurious luminescent signal originated in the passive fibre as a consequence of the exposition to ionizing radiations (e.g. Cerenkov light and intrinsic fluorescence) must be considered. The stem effect mainly occurs in the UV-VIS, therefore, the opportunity to use a dopant like Yb, emitting in the near infrared region, suitable for an optical discrimination of the dosimetric signal, is presented and discussed.

DosiKit, Innovative Solution for On-site External Radiation Biodosimetry

Julie Bensimon^a, Caroline Bettencourt^a, Sandrine Altmeyer^b, Arnaud Tupinier^b, Nicolas Ugolin^b, Sylvie Chevillard^b

^aAcubens, Antony, France

^bCEA, Fontenay-aux-Roses, France

Abstract. The efficient management of a nuclear accident or attack requires the identification of irradiated individuals, and the estimation of absorbed dose to optimize medical care. Numerous approaches have been developed to quantify the radiation dose absorbed by an individual. However, none of these methods can be used directly on site after an accident since they require both a dedicated laboratory and specialized staff. Furthermore, they do not provide information about the localization of irradiation and results can only be available D+1 or D+2 after receipt of biological samples. To develop appropriate emergency management tools, we invented a new operational, portable and noninvasive radiation biodosimetry device, allowing the measurement of external irradiation, either global or localized, directly on the field of a radiological accident. This device -concretely two portable suitcases, one containing individual kits and the other containing all the equipment necessary for the analysis- allows the classification of irradiated individuals into three groups (<0.5 Gy, 0.5-3 Gy, >3 Gy). Results are provided in less than 45 minutes, and analysis can be performed up to 10h hours after irradiation by non-specialists after a simple training. Our technology relies on the quantification of radiation-induced or -modified proteins proportionally to the radiation dose received, taking into account individual radiosensitivity. The diagnosis is obtained after biological material sampling (blood drop from the fingertip, hair bulbs sampled over different parts of the body) followed by protein extraction and analysis. The proteins quantification allows the assessment of radiation dose absorbed by the individual and of the time of exposure as well. Results obtained from the blood indicate the whole body average dose, whereas results obtained from hair bulbs allow the detection and quantification of partial body irradiation, thus giving a map of body irradiation. This technology is protected by two patents.

Analysis of Photon Energy Distribution at the Working Places in Nuclear Power Plants Using In-situ CZT Detectors

Jeongin Kim, Seokon Kang, Meeseon Jeong

Radiation Health Institute, Korea Hydro & Nuclear Power, Seoul, Republic of Korea

Abstract. Radiation field information in nuclear power plants should be provided for optimal job planning and radiation dose management for workers. Photon energy distribution information can be used to design proper shielding for high dose jobs or to reconstruct specific organ doses of workers. So it is important to monitor the radiation source terms to analyze the radiation field. Generally, portable scintillation spectrometers or high purity germanium detectors with in-situ object counting system can be used to measure the radioactivity directly for the assessment of photon energy field characteristics in the working places. However, both devices cannot be easily applied to the detection of source terms in reactor coolant systems(RCS) because of the low energy resolution and the inconvenience with liquid nitrogen cooling respectively. Radiation detectors using CdZnTe(CZT) can overcome these weak points. A CZT has much higher resolution than NaI and not need additional cooling devices. The CZT detectors have been applied to radiation protection tools at several nuclear power plants and the reports show good results. CZT detection systems, however, still need in-situ calibration process for proper measurement conditions before application. In this study, three different sizes of CZT element were used for various dose rates at major working places during refuelling outage periods of nuclear power plants. For the proper calibration, 3D geometrical modelling of main RCS pipe-lines with a Monte-Carlo radiation transport code was carried out. Results showed that the mean photon energy was lower than standard energy for personal dosimeter calibration. Also, the time fluctuation of major radio-nuclides such as Co-60 and Co-58 was well agree with extracted coolant measurements. From the results, CZT detection system shows the possibility of application to radiation source term analysis in reactor coolant systems and used to obtain the proper information of major radiation source to workers for establishing pre-job dose planning.

Monte Carlo Approach to Accidental Dose Reconstruction Based on the EPR Measurements of Absorbed Dose to Human Teeth

Jeongin Kim, Hoon Choi, Byoungil Lee

Radiation Health Institute, Korea Hydro & Nuclear Power, Seoul, Republic of Korea

Abstract. EPR(electron paramagnetic resonance) is well known accidental dose estimation technology using a part of human body or personal belongings like teeth, nails and mobile phones. However, the absorbed dose to teeth measured by EPR devices cannot always represent the whole body dose to the victim. In most cases, the EPR dose estimation results can be referred to the reconstruction of accidental exposure situation. So it is important to estimate the relation between absorbed dose to teeth and equivalent doses to critical organs or whole body dose for various situations. In this study, a voxelized mathematical human phantom with Monte Carlo radiation transport code and a real physical phantom were used to estimate the dose relation between the teeth and the whole body for some simple irradiation geometries and medical radiation treatment conditions. The teeth inside the mathematical phantom were additionally modelled and personal TLDs(thermo luminescence dosimeter) on chest and TL chips inside the real phantom were located. Results showed that there was not much difference between teeth dose and whole body dose in most whole body irradiation geometries except some extreme cases and enough possibility for rapid whole body accidental dose assessment for wide gamma irradiation conditions. However, the dose response relation by the EPR systems for teeth dose estimation should be established for various irradiation conditions for accurate dose assessment due to the tissue attenuation of incident low energy photons and localized irradiations.

Development of two new single-exposure, multi-detector neutron spectrometers for radiation protection applications in workplace monitoring

J.M. Gómez-Ros^{a,b}, R. Bedogni^b, D. Bortot^c, C. Domingo^d, A. Esposito^b, M.V. Introini^c, M. Lorenzoli^c, G. Mazzitelli^b, M. Moraleda^a, A. Pola^c, D. Sacco^{b,e}

^aCIEMAT, Av. Complutense 40, 28040 Madrid, Spain

^bIFNF – LNF Laboratori Nazionali di Frascati, via E. Fermi n. 40, 00044 Frascati, Italy

^cPolitecnico di Milano - Dipartimento di Energia, Via Ponzio 34/3, 20133 Milano, Italy

^dUAB, Physics Department, 08193 Bellaterra, Spain

^eINAIL-DIT, Via di Fontana Candida 1, 00040 Monteporzio Catone, Italy

Abstract. The measurement of neutron spectra is an essential issue for the accurate determination of radiation protection quantities whose dependence on fluence varies nearly two orders of magnitude depending on neutron energy, according to the variation in the quality factor Q values with neutron energy. This communication describes the main features and applications of two new instruments (Gómez-Ros et al. 2017), based on multiple active thermal neutron detectors located within a single moderator, that permit to unfold the neutron spectrum (from thermal to hundreds of MeV) and to determine the corresponding integral quantities (total fluence, ambient dose equivalent) with only one exposure. This makes them especially advantageous for neutron field characterization and workplace monitoring in neutron-producing facilities. One of the devices has spherical geometry and nearly isotropic response, the other one has cylindrical symmetry and it is only sensitive to incident neutron from a given direction. In both cases, the used active detectors have been specifically developed looking for the criteria of miniaturization, high sensitivity, linear response and good photon rejection. The response matrix, calculated with MCNPX, has been validated by experimental irradiations in neutron reference fields with a global uncertainty of 3%. The measurements performed in realistic neutron fields (around radionuclide sources, medical LINACs, research accelerators) have permitted to determine the neutron spectra and the integral quantities mentioned above, in particular $H^*(10)$. These real-time online spectrometers have been developed in the framework of a collaboration between five European laboratories and can be available for replication and distribution to other institutions under collaboration agreement.

RadiationProtectionDosimetry(2017),Vol.173,No.1-3,pp.104–110
doi:10.1093/rpd/ncw349

The Influence of the Dose Calculation Resolution of VMAT Plans on the Calculated Dose for Eye Lens and Optic Apparatus

Jong Min Park^a, So-Yeon Park^a, Jung-in Kim^a, Hong-Gyun Wu^b, Jin Ho Kim^a

^aDepartment of Radiation Oncology, Seoul National University Hospital, Seoul, Republic of Korea

^bDepartment of Radiation Oncology, Seoul National University College of Medicine, Seoul, Republic of Korea

Abstract. The effect of dose calculation grid size on the accuracy of calculated doses in the treatment planning system (TPS) for each eye lens and optic apparatus was investigated. A total of 20 patients who received volumetric modulated arc therapy (VMAT) for head and neck (H&N) cancer located at nasal cavity were selected retrospectively for this study. All patients were treated with VMAT technique and the treatment plans were generated with the Eclipse system using 6 MV photon beams. For dose calculation, the sizes of calculation grids were varied from 1 mm to 5 mm at intervals of 1 mm. After that, dose calculations with various calculation resolution were performed maintaining same number of monitor units (MUs). The planning risk volume (PRV) for each eye lens, each optic nerve and optic chiasm were defined with a 2 mm margin from each structure. The calculated maximum dose delivered to left and right eye lens increased from $14.9 \text{ Gy} \pm 19.1 \text{ Gy}$ to $16.6 \text{ Gy} \pm 17.8 \text{ Gy}$ and from $7.5 \text{ Gy} \pm 3.1 \text{ Gy}$ to $9.8 \text{ Gy} \pm 3.9 \text{ Gy}$, respectively, as increasing the size of dose calculation grid from 1 mm to 5 mm. Those values for PRV of each lens also increased from $17.1 \text{ Gy} \pm 19.6 \text{ Gy}$ to $19.9 \text{ Gy} \pm 18.1 \text{ Gy}$ and $9.7 \text{ Gy} \pm 3.8 \text{ Gy}$ to $13.2 \text{ Gy} \pm 4.8 \text{ Gy}$, respectively. For left and right optic nerves, the calculated maximum delivered doses increased from $47.5 \text{ Gy} \pm 15.1 \text{ Gy}$ to $48.6 \text{ Gy} \pm 15.0 \text{ Gy}$ and from $47.7 \text{ Gy} \pm 11.8 \text{ Gy}$ to $48.9 \text{ Gy} \pm 11.5 \text{ Gy}$, respectively. Those values for PRV of each optic nerve increased from $51.7 \text{ Gy} \pm 13.3 \text{ Gy}$ to $52.0 \text{ Gy} \pm 13.9 \text{ Gy}$ and from $51.8 \text{ Gy} \pm 10.0 \text{ Gy}$ to $52.4 \text{ Gy} \pm 10.9 \text{ Gy}$, respectively. In the case of optic chiasm and its PRV, those values increased from $44.0 \text{ Gy} \pm 12.6 \text{ Gy}$ to $45.0 \text{ Gy} \pm 12.8 \text{ Gy}$ and from $49.6 \text{ Gy} \pm 11.4 \text{ Gy}$ to $49.7 \text{ Gy} \pm 12.0 \text{ Gy}$, respectively. For eye lens, differences in the maximum dose delivered to left and right eye lens were 11.6% and 31.4%, respectively, as increasing the size of dose calculation grid from 1 mm to 5 mm. To evaluate exact delivered dose to eye lenses as well as optic apparatus, of which volumes are small, the size of dose calculation grid should be small when calculating dose distributions with patient CT images.

Dosimetry Aspects for the Development of an Irradiator for Cross-linking of Cables using ^{60}Co Gamma Rays

Jain Reji George, B K Pathak

Board of Radiation & Isotope Technology Department of Atomic Energy, Navi Mumbai, Maharashtra, India

Abstract. Cross-linking provides significant commercial benefits to wire and cable insulation. Ionizing energy is an efficient means of cross-linking the polymers to improve many cable properties including insulation. In this process chemical bonds are formed between layers of polymer molecule to produce three-dimensional insoluble network. The present methods of cross-linking are thermal/chemical/e-beam from accelerators. E-beam cross-linking is the latest and improves properties like fire resistance, flame properties, abrasion resistance, stress crack resistance etc. However there is a limitation of e-beam penetration in large diameter cables (>0.030 m dia.) restricting its application. Therefore the feasibility of processing multi core cables of large diameters with gamma rays was explored. The insulation jacketing of multi core cables are made of PVC or PE. The dosimetric aspects were studied for a cable irradiator- design which has been made in such a way that the cable will move through a pipe housed in Gamma Irradiation Cells (GICs) each of which have ^{60}Co source pencils (BRIT made BC-188) of 7.4PBq arranged around the pipe in a suitable diameter (PCD). The pipe can accommodate cables of diameters up to 0.072m. The cells have effective irradiation lengths (~1m) and lead shielding of adequate thickness. The objective of the study was to evaluate the dose profile in cables when irradiated in a gamma irradiation cell and to optimize the PCD of source pencil arrangement to get the appropriate Dose Uniformity Ratio with the specified target dose of 100kGy & to arrive at no. of irradiation cells required for a suitable through-put. Based on the results of the study a gamma irradiator with multiple number of irradiation cells is under development in BRIT, a unit of the Department of Atomic Energy, India.

Development and Applications of Super Monte Carlo Simulation Program for Advanced Nuclear Energy Systems

Jing Song, Liqin Hu, Pengcheng Long, Tao He, Lijuan Hao, Mengyun Cheng, Huaqing Zheng, Shengpeng Yu, Guangyao Sun, Tongqiang Dang, Qi Yang, Bin Wu, Chaobin Chen, Ling Fang, Yican Wu, FDS Team

Key Laboratory of Neutronics and Radiation Safety, Institute of Nuclear Energy Safety Technology, CAS, Hefei, China, China

Abstract. The Monte Carlo (MC) methods have been broadly adopted in design and analysis of advanced nuclear energy systems. However, there are still great challenges in the current MC methods including the calculation modelling of complex geometries, simulation of deep penetration problem in radiation shielding, slow convergence of complex calculation, lack of experimental validation for new physical features, etc. SuperMC is a general purpose, intelligent and multi-functional program for the design and safety analysis of nuclear systems. It is designed to perform the comprehensive neutronics calculation, taking the radiation transport as the core and including the depletion, radiation source term/dose/biohazard, material activation and transmutation, etc. It supports the multi-physics coupling calculation including thermo-hydraulics, structural mechanics, biology, chemistry, etc. The main technical features are hybrid MC-deterministic methods and the adoption of advanced information technologies. The main usability features are automatic modelling of geometry and physics, visualization and virtual simulation and cloud computing services. The latest version of SuperMC can accomplish the transport calculation of n , γ and can be applied for criticality and shielding design of reactors, medical physics analysis, etc. SuperMC has been verified by ~ 2000 benchmark cases. The ICSBEP and the SINBAD were used to verify the correctness. The fusion reactors (International Thermonuclear Experimental Reactor ITER reference models, FDS-II, etc.), fast reactors (IAEA-BN600, IAEA-ADS, etc.), PWR (BEAVRS, HM, TCA, etc.) and cases from the IRPhEP were employed for validating the comprehensive capability for reactor applications. The benchmarking results have been compared with MCNP, demonstrating higher accuracy and calculation efficiency of SuperMC, and also significant enhancement of work efficiency due to its functions of automatic modelling and visualized analysis. As the supplementary of validation experiments of MC software for advanced nuclear energy systems applications, experiments of Dual Functional Lithium Lead (DFLL) blanket, variance of reactivity coefficient were conducted. SuperMC has been applied in the nuclear design and analysis of ITER and the China Lead-based Reactor (CLEAR).

Study of Eye Lens Dose at the Nuclear Industries in Sweden

Lisa Bäckström^a, Karin Andgren^b

^aVattenfall, Gothenburg, Sweden

^bVattenfall, Solna, Sweden

Abstract. The nuclear industries in Sweden have performed a joint study regarding equivalent dose to the lens of the eye. Vattenfall engineering organised the activities and among the participating sites were nuclear power plants, a nuclear fuel factory and waste workplaces. The project was a result of requirements from the Swedish Radiation Safety Authority, and the outcome of the project has been reported to the authority. The study was divided into four parts: Calculations of equivalent dose to the lens of the eye: The sites identified situations/professions where the whole body dosimeter was not good enough for estimation of the eye lens dose. Critical situations are when the whole body dosimeter is shielded and/or when beta particles with energies above 700 keV are present. Eye lens doses were estimated using MicroShield (for photon radiation) and MCNP5 (for beta radiation). Testing of headband dosimeter measuring Hp(3): Reference irradiations for a TLD headband dosimeter from Public Health England, PHE was performed at PTB in Germany. The purpose of the testing was to study the fulfilment of performance requirement for personal dosimeters set up by the Swedish Authority. Measurements of equivalent dose to the lens of the eye: 140 workers used the headband dosimeter from PHE during their work at radiological controlled area. The doses registered by the headband dosimeters were compared to the doses registered by the whole body dosimeters. Shielding factors for protective eye eyewear: Shielding factors for eight different protective eyewear were studied.

Direct Ion Storage Dosimetry Roadmap

Kip Benett^a, Michael Lantz^a, Matti Vuotilla^b, Jani Rakkola^a

^aMirion Technologies (DSD), Irvine, CA, USA

^bMirion Technologies (HPD), Turku, Finland

Abstract. Introduction: The Direct Ion Storage (DIS) technology for personal passive Dosimetry has been in use for more than 20 years. The DIS-1 dosimeter is in high use throughout Europe and the Instadose dosimeter is currently being used by over 100,000 people world-wide. However, how and why did Mirion see the need to create a new electronic dosimeter for the market? This paper will analyse the technology roadmap of the DIS dosimeter family and compare/contrast it with the standard types of Dosimetry on the market today (i.e. Film, TLD, OSL, RPL) and will include some test data. Roadmap Review Summary: DIS technology: the main emphasis of all DIS dosimeters is to allow the hospital/power plant/industrial site to have immediate access to dose data that they would otherwise have to wait because of shipping back to a processor or loading into a large reader. DIS-1: Badges can be read throughout facility using readers connected to network. Administrator in Dosimetry office can review all results. Military DIS: Badges can be read remotely using battery operated hand-held reader. Reader data downloaded into computer and analysed back in Dosimetry office. Instadose 1: Badge read on-line using secure program via a USB contained on the dosimeter and USB port on a standard computer. Service based model where a Dosimetry service analyses all readings and reports exceptions to the end user/administrator. Instadose 2: Similar to instadose 1, but transmits its dose information via blue tooth and smart phones, iPads, BLE adaptable computers, or a stand alone Wifi compatible "reader". Service based model where a Dosimetry service analyses all readings and reports exceptions to the end user/administrator. Readings are performed via a manual pushbutton on the dosimeter or using an electronic calendar.

Implementation of a New BeOSL Dosimetry Platform Utilizing Lean Manufacturing Tools

Kip Bennett^a, Mike Lantz^a, Joel White^a, Gordon Sturm^a, Reiner Esser^b, Timo Wiedenmann^c, Jay Thomas^d

^aMirion Technologies (DSD), Irvine, CA, USA

^bDosimetries GmbH, Munich, Germany

^cCreados GmbH, Munich, Germany

^dNext Level Partners, Naples, FL, USA

Abstract. Introduction: Late in 2014 Mirion Technologies made a decision to implement a new BeOSL Dosimetry platform from Dosimetries GmbH. In order to perform an implementation of such magnitude in a short amount of time lean manufacturing processing events/tools including kaizen, 3P, standard work, and cell building were performed. In early 2015 Mirion completed the implementation of the BeOSL Dosimetry platform, passed NVLAP accreditation, and started badging over 70,000 wearers with the new dosimeter. Methods: Implementation of the BeOSL platform was performed using lean techniques: Kaizen – Japanese term for “change for the better”, 3P – Production Preparation Process detailing steps and poke yokes (error proofing) into the process, cCreation of Standard Work playbook – based on demand and capacity of the equipment this playbook is used to determine staffing levels and machinery needed to meet the demand. Results: Using the lean tools Mirion was successful in launching its BeOSL Dosimetry system for a July 1, 2015 wear date. There are over 70,000 active wearers of the dosimeter. Utilizing the lean tools kept all groups (technical, operations, IT, sales) on task for a successful completion of the project. There were roadblocks along the way, but without utilizing lean manufacturing it would have been much worse.

Monte Carlo calibration of the whole body counting detection system for *In Vivo* measurement of people internally contaminated with ^{90}Sr

Karin Fantínová^{a,b}, Pavel Fojtík^a, Irena Malátová^a

^aSÚRO, Bartoškova 28, Prague 140 00, Czech Republic

^bCzech Technical University in Prague, Břehová 9, Prague, 114 19, Czech Republic

Abstract. This paper is focused on calibrations of an HPGe whole body counting (WBC) detection system for measurement of pure beta emitters through the produced bremsstrahlung radiation. Calibrations were performed with the use of UPh-02T block whole body phantom and Lawrence Livermore National Laboratory (LLNL) realistic torso phantom. Neither of these physical phantoms is appropriate for such calibrations; therefore, specific ^{90}Sr sources which can account for recent as well as previous contaminations have been manufactured to be used with the UPh-02T phantom. Calibrations with the LLNL torso phantom were carried out using Monte Carlo (MC) technique. Different scenarios of the ^{90}Sr distribution in the human tissues were considered for the spectrometer calibrations – very recent contamination, when ^{90}Sr is distributed in soft tissue, previous contamination, when the radionuclide is distributed mostly in bone, and their combinations. This work is dealing mainly with ^{90}Sr , which can be considered as a main potential source of internal contamination caused by pure beta emitters, and marginally also with other pure- or practically pure-beta emitters such as ^{32}P and ^{89}Sr .

KEYWORDS: $^{90}\text{Sr}/^{90}\text{Y}$ bremsstrahlung; internal contamination; *In Vivo* measurement; HPGe whole body counter; Monte Carlo calibration; MCNP6.

RadiationProtectionDosimetry(2017),Vol.173,No.1-3,pp.111–117

doi:10.1093/rpd/ncw324

Backscatter Response of Different Personal Dosimeter Detectors for Water Slab and Cylindrical Calibration Phantoms

Kristine Marie Romallosa^a, Hiroshi Yoshitomi^b

^aPhilippine Nuclear Research Institute, Quezon City, The Philippines

^bJapan Atomic Energy Agency, Tokai, Japan

Abstract. Calibration of dose rate meters are in terms of the ambient dose equivalent $H^*(d)$ measured in-air while calibration of personal dosimeters are in terms of the personal dose equivalent $H_p(d)$ measured at the surface of a phantom that simulates the backscatter and attenuation effects of the human body. However, backscatter from the tissue tends to be higher at low energies. That is, for low energy photons and depending on the body part exposed, the actual dose deposited to the tissue is higher than the dose of the incident radiation. In addition, for the same incident dose, the dose deposited to the human torso is also higher than the other body parts. Although the dose equivalent quantities were based on the ICRU tissue, it is not practical to use it in the routine calibration of personal dosimeters. ISO phantoms such as the water slab, water pillar and PMMA rod phantoms are typically used but by doing so, a different backscatter response is obtained. Common calibration procedures however do not apply correction factors when using the ISO phantoms primarily because the acceptable uncertainty in the assessment of occupational personal doses is in the order of +30%. However, this still could affect the accuracy of calibrations particularly for low energy photons. This study investigates the backscatter response of various personal dosimeters on two types of water phantoms and how it is affected by incident photon energy. Personal dosimeters are made of various types of detectors which in turn have different response characteristics. During calibration, a portion of the dosimeter response will be from the backscattered photon. However, the backscattered photon at the phantom surface will have a different energy spectrum from that of the incident photons. Depending on the energy dependence and detector size it is expected that different dosimeters will have a different response even if the same calibration phantom is used. Hence correction factors maybe necessary for a more accurate calibration of personal dosimeters.

Dosimetric Uncertainty Analysis of the Optically Stimulated Luminescence Dosimeter System in the Philippines

Kristine Marie Romallosa, Marianna Lourdes Grande, Estrella Caseria

Philippine Nuclear Research Institute, Quezon City, The Philippines

Abstract. When the occupationally exposed workers wear personal dosimeters, several factors affect the accuracy of the measured dose received in the workplace. Unlike in a laboratory where all the measurements conditions are known, factors such as radiation beam orientation, beam uniformity, and overall dosimeter performance will introduce uncertainties in the evaluated personnel dose. In this paper, uncertainty analysis of the reported the personal dose equivalent, $H_p(10)$, of the optically stimulated luminescence dosimeter system used by the Philippine Nuclear Research Institute in monitoring the occupationally exposed personnel in the country is investigated. Influence factors such dosimeter reading, fading, energy dependence, nonlinear and angular dependence and its effect in the reported dose are calculated. The result is then compared with the acceptable combined expanded uncertainty based on the ICRP recommendation for individual monitoring. This is essential in ensuring that the dosimeter system used is within the acceptable limits and hence suitable for use in the protection of occupationally exposed workers.

Development of the Electronic Personal Dosimeter Based on Scintillator for a Mobile Phone Application

Kyeongjin Park^a, Daehee Lee^a, Hyunjun Yoo^a, Eunjoong Lee^a, Hyunduk Kim^a, Hojong Chang^a, Gyuseong Cho^a, Alexander Solodov^b

^aKorea Advanced Institute of Science and Technology, Daejeon, Republic of Korea

^bKhalifa University, Abu Dhabi, United Arab Emirates

Abstract. After the Fukushima nuclear power plant accident, concern of the radiation exposure has been dramatically increased. Thus, demand for Electronic Personal Dosimeter (EPD) is constantly on the rise and there is an expectation of increase in usage of EPD in the future. The existing EPD is specialized to radiation experts also, it costs few thousands USD and it is not efficient to carry due to the large size. Reliability of the measurement is low for radiations except the radiation from Cs-137 which is standard source. Therefore, high reliable EPD and easily accessible device for the public is needed. The purpose of this study is development of the scintillator based EPD which is portable, high sensitive and able to connect to the mobile phone for the general people. Module of the EPD sensor is consisted of scintillator, photodiode and signal processing circuit. To minimize the price, we used CsI(Tl) scintillator, PIN diode and signal processing ASIC in this research. The proposed EPD sensor is spectral dependency. Thus, it can detect not only Cs-137 but also wide energy range of the radiation for various fields including industry and medical fields. The developed EPD was using lower amount of output channel than current EPD by low bit ADC for decrease of power consumption. Obtained spectrum by low bit ADC was converted from spectrum to dose by using the self-developed dose conversion algorithm for monitoring system. The sensor module was made of CsI(Tl) size of $3 \times 3 \times 3 \text{ mm}^3$ and PIN diode size of $3 \times 3 \text{ mm}^2$ and the spectrum was obtained by check source. It was determined that proposed sensor was able to separate the radiation energy from 122 keV to 1.33 MeV. The energy resolution of Cs-137 (662 keV) was 12 %. In addition, error range of dose assessment, which was acquired by 6 bit ADC, was satisfied to IEC standard 61526. From this result, it was confirmed that proposed sensor can provide efficient battery usage and memory management. Currently, assembly of the sensor module is completed and ASIC chip is on the test. In this conference, we will present status of the module development, contents of the research and results of the experiment.

Salty Nuts and Snacks for Retrospective Dosimetry

Maria Christiansson, Christian Bernhardsson, Therese Geber-Bergstrand, Sören Mattsson, Christopher Rääf

Medical Radiation Physics, ITM, Lund University, Malmö, Sweden

Abstract. In retrospective dosimetry for emergency dose assessments the method of using optically stimulated luminescence (OSL) in common crystalline materials accessible in the public surroundings has proven to be very useful. Furthermore, laboratory studies have shown that salt for alimentary use (NaCl) has a high sensitivity to ionizing radiation when read-out with OSL. However, to use ordinary salt for retrospective individual dosimetry requires salt that has been kept close to the exposed individual. For this reason the OSL response of different kinds of salty snacks have been investigated since they are more likely to be found close to man, e.g. in handbags, backpacks or pockets. Snacks, such as nuts and potato chips, are normally stored in aluminum or cardboard packages to preserve the crisp and taste. Especially one of the investigated packages provides very good conditions for storing the induced OSL signal after exposure to ionizing radiation. By using different kinds of snacks and then exposing either the salt alone or the salt mixed with parts of the snack to ionizing radiation, the dosimetric properties of commonly available salty snacks have been investigated. The OSL-response for the salt was investigated using a TL/OSL reader (TL/OSL-DA-15; Technical University of Denmark, Risø Campus, Roskilde, Denmark) equipped with a 20 MBq (2009-04-09) $^{90}\text{Sr}/^{90}\text{Y}$ source. Irradiations were performed using a ^{60}Co source at a distance of 5.5 m. The internal $^{90}\text{Sr}/^{90}\text{Y}$ source was used to give calibration doses. A common household salt brand previously being found to be highly sensitive to radiation was also used as a reference. This study shows that some of the snack packages available in the Swedish supermarkets may well sustain a radiation induced OSL-signal in the salt without significant loss due to optical fading. Furthermore, salt scraped off from almonds and from cashew nuts showed the highest sensitivity of the investigated snacks, with a minimum detectable dose (MDD) as low as 1 mGy.

Dosimetric Evaluation of a Radiological Accident involving a Gammagraphy Industrial Source of ^{192}Ir (44 Ci)-Multidisciplinary Approach

Marina Di Giorgio^a, Analía Radl^a, Adrian Discacciatti^a, Diana Dubner^a, Sebastian Gossio^a, Francois Trompier^b, Ezequiel Soppe^a, Adriana Coppola^c, Mayra Deminge^a, Julieta Rearte^a, Ana Molinari^a, Ignacio Menchaca^a, Fabio Lopez^a, Gaston Castro^c, Mariana Egan^c, Mercedes Portas^c

^aNuclear Regulatory Authority, Buenos Aires, Argentina

^bInstitut de radioprotection et de sûreté nucléaire (IRSN), Fontenay Aux Roses, France,

^cHospital de Quemados GCBA, Buenos Aires, Argentina

Abstract. A radiological accident with a ^{192}Ir source (44 Ci; 1.63 TBq) occurred in a Thermoelectric Power Station located in Río Turbio (Santa Cruz) on August 27th, 2015, due to an industrial radiography operation carried out by two operators (workers A and B). On September 8th, 2015 the Argentinean Nuclear Regulatory Authority (ARN) was reported on this matter. According to the operators' statements, two gammagraphy shots were performed. At the time of the removal for the first shot, the source got stuck. In order to achieve the projection they proceeded with the total removal of the source, but it was actually retreated back to the equipment. As operators believed that the source was outside the shielding, they waited until the exposure time finished and made the source store operation. As the source was already inside its shielding, it was thence removed therefrom. Worker A entered the irradiation enclosure and performed the plate change and guide tube positioning for the second shot. Such operation was conducted with the source outside its shielding, being the moment of maximum exposure of worker A. Objective: Describe a multidisciplinary approach performed for the evaluation of the whole and/or partial body absorbed dose by both operators through clinical dosimetry (including kinetics of depletion of lymphocytes, neutrophils and platelets), biological dosimetry (dicentric assay), physical and computational dosimetry (conventional-MicroShield-MCNP/3Dosim) and EPR on fingernails. The radiographer (worker A) was derived to the Burns' hospital for diagnosis and treatment of the localized lesion: dry epithelitis on his left hand index finger, which evolved into moist epithelitis. A favourable response was observed with early local recovery after treatment. Estimation of eye lens dose was conducted and future risk of developing cancer was assessed. The expression of the adhesion molecules as well as changes in the subpopulation of Regulatory T lymphocytes and the level of C-reactive protein were determined to characterize the inflammatory response. The event was classified level 3 according INES scale. Conclusion: Multidisciplinary dose estimation allowed to guide the medical treatment and to support radiation protection decisions within the regulatory frame.

In Light Optically Stimulated Luminescence Dosimetry for Occupational Workers in the Philippines

Marianna Grande^a, Kristine Romallosa^a, Estrella Caseria^a, Ahmad Bazlie^b

^aPhilippine Nuclear Research Institute, Quezon City, Manila, The Philippines

^bMalaysian Nuclear Agency, Bangi, Selangor, Malaysia

Abstract. In the Philippines, the Radiation Protection Services Section (RPSS) under the Philippine Nuclear Research Institute (PNRI) currently offers dosimetry services to occupationally- exposed workers. Since the late quarter of 2012, the PNRI-RPSS had started offering the OSL Dosimetry Service in order to replace the previous Film Badge Dosimetry Service which served about ten thousand (10,000) workers. Currently, the OSL Dosimetry Service monitors about five thousand (5,000) workers. In this study, photon deep dose validation was performed through a comparison method. A sample of pre-exposed PNRI OSL dosimeters were sent to the Secondary Standards Dosimetry Laboratory of the Malaysian Nuclear Agency (SSDL-MNA) which was read with the laboratory's manual reader, and a set of pre- exposed MNA OSL Dosimeters were sent to PNRI which was read with the two (2) PNRI OSL manual readers. The output of each reader was plotted in an accuracy graph and it was found out that all photon deep dose values were within +10% of the delivered doses.

Particle Size Distributions of Radioactive Aerosols in the Atmosphere

Miroslav Hýža, Petr Rulík, Helena Malá, Vera Beckova

National Radiation Protection Institute (SÚRO), Prague, Czech Republic

Abstract. The radiological importance of radioactive aerosol particles depends not only on the kind of radionuclide and its chemical form but also on the aerodynamic properties of the particles, mainly on their size. This work presents size distributions of a radioactive aerosol in the boundary layer of atmosphere. The samples were taken continuously in 2015/2016 at SÚRO laboratory in Prague. In the past, size distributions were analyzed in the Czech Republic during radiation events (Chernobyl 1986; Fukushima 2011) or at industrial facilities such as uranium mines. The aim of this study was to establish reference "background" aerosol size distribution associated with natural radionuclides ^7Be , ^{210}Pb and artificial ^{137}Cs based on a longer time series, which would take into account natural variations. Size distributions of ^{222}Rn and ^{220}Rn decay products and their potential use for coagulation studies of an associated aerosol are also discussed. In several samples, ^{210}Po was also determined, which allows estimating its residence time. The samples were taken using three six-stage high-volume cascade impactors with cut-offs between 0.39–10.2 μm (flow rate 34 m^3/h) and a nine-stage cascade impactor with cut-offs between 0.16–18 μm (flow 7 L/min). The radionuclide activity was determined using the HPGe gamma spectrometry and radiochemical separation followed by alpha spectrometry analysis in the case of ^{210}Po . Resuspended ^{137}Cs distribution was compared to distributions obtained during the Chernobyl and Fukushima NPP monitoring and natural ^{226}Ra distribution was compared to distributions measured in the mines.

Optical Stimulated luminescence from Citrine for High-Doses Dosimetry

Maria Ines Teixeira^{a,b}, Linda V.E. Caldas^a

^aInstituto de Pesquisas Energéticas e Nucleares, IPEN – CNEN/SP, Sao Paulo - Sao Paulo, Brazil

^bCentro Universitário SENAC - Tiradentes/SP, Sao Paulo - Sao Paulo, Brazil

Abstract. In the sterilization of medical and pharmaceutical products, food and flower preservation, and treatment of electrical cables and al-treatments of different materials is used the irradiation process by high-doses because it presents advantages varies. Several Brazilian stone samples were already studied at IPEN for use in radiation dosimetry, using the techniques of thermoluminescence (TL), optical absorption (AO) and optically stimulated luminescence (OSL). Different kinds of glasses and sand from Brazilian beaches were studied at IPEN and showed favorable characteristics for their use for high-dose dosimetry. The possibility of using semi-precious stones from Brazilian as topaz, amethyst and jasper, and jade samples from different parts of the world, have been studied and tested at IPEN, using the technique of thermoluminescence. The objective of this work was to study citrine samples for application in high-dose dosimetry, using the OSL technique. The thermal treatment for reutilization of the materials was 300°C during 1h in an unsealed oven. The samples were irradiated using a Gamma Cell-220 system of ⁶⁰Co (dose rate of 1.47 kGy/h), with doses from 50 Gy up to 300 kGy. The reproducibility of the OSL response presented a maximum variation coefficient of 5.7%. The lower detection limit was obtained as 350 mGy for the citrine pellets. The results show that the OSL detectors based on citrine may be useful for high-dose dosimetry in industrial processes and in the sterilization process of materials in hospitals.

Performance Data of a new Active Personal Dosimeter in Respect to Gamma, Beta and Pulsed X-ray Radiation

Michael Iwatschenko-Borho^a, Alan Laing^b, Ling Luo^c, Cassidy McKee^c, Greg Nelson^c, Ralf Pijahn^a, Norbert Trost^a

^aThermo Fisher Scientific Messtechnik GmbH, Erlangen, Germany

^bThermo Fisher Scientific RMSI, Ferndown, UK

^cThermo Fisher Scientific RMSI, Oakwood, OH, USA

Abstract. Like its predecessor, the Thermo Scientific EPD Mk2+, the Thermo Scientific EPD TruDose is a personal dosimeter that uses a PIN diode to quickly and accurately measure the personal dose and dose rate of ionizing radiation. The EPD TruDose maintains the compact, rugged design of the Mk2+ while incorporating several durability and performance improvements. It also offers significant incremental enhancements that are highly important for the operational performance, such as integrated wireless communication modules, vibration alarm, durability in harsh environments and radically improved clarity of the user interface. This paper will briefly go through a few of these features, but focus on the radiation measurement performance and dosimetry related improvements of the instrument which allow the usage in a even wider range of work place fields, including any pulsed medical X-ray fields. The instrument features a new fast scan mode, which drastically increases the frequency at which detector counts are read and analyzed for dead time correction and over-range detection. This allows the EPD TruDose to closely follow the intensity modulations of modern medical X-ray devices. The instrument can thus provide the correct integrated dose and dose rate, and will alert the user if a peak dose rate exceeding the instrument's measuring range is detected. Dose-rate calculations in the EPD TruDose are done by a new Advanced Digital Filter, which has a much faster response to rapidly changing radiation levels than the Mk2+, providing a shorter response to sudden changes of the radiation field. Thus, provided a proper dose rate alarm has been set, the new EPD TruDose can contribute to a personal dose reduction by providing the wearer with an instantaneous audible, visual and/or vibration alarm, so that he can react accordingly.

Calibration of Conventional Survey Meters for Soft X-ray Below 5 keV

Masahiro Kato^a, Tadahiro Kurosawa^a, Toshihiko Hino^b, Yoshinori Inagaki^b

^aNational Institute of Advanced Industrial Science and Technology, Tsukuba, Japan

^bHamamatsu Photonics K.K., Iwata, Japan

Abstract. Soft x-rays with the photon energy below 5 keV have been widely used in the research and development fields such as the elemental analysis, materials evaluation, basic process of radiation physics and chemistry, and so on. Generally, soft x-rays with several keV are used in synchrotron radiation facilities, or built in an equipment. In these cases, the several keV x-rays hardly make a problem about the radiation protection because operators are shielded perfectly from the radiations. In these years, the several keV x-rays produced from small x-ray generators have been utilized for removing the static electricity and measurement about the aerosol. Since soft x-rays with the energies have only weak penetrating power, they may be handled without shielding if they are under atmospheric pressure. However, it is important to measure the dose rate around the actual work space or in the vicinity of the x-ray source. The soft x-rays with several keV have been mainly measured in the term of particle fluence (in the unit of m^{-2}) or power (in watt), but the measurement standard in the term of dose equivalent (in Sv) has not been available. In this study we have measured the dose equivalent for soft x-ray with the photon energy below 5 keV produced from an electrostatic remover (L12536, Hamamatsu Photonics K.K.) using an extrapolation chamber (C112-A, Applied Engineering inc.), which is used as the primary standard for beta dosimetry in National Metrology Institute of Japan. The uncertainty of the dose equivalent measurement was 2.9 % with the coverage factor $k=2$. Besides, two conventional survey meters have been calibrated against the extrapolation chamber. In this calibration measurement, the uniformity of the soft x-ray field is measured using a small volume ionization chamber (23344, PTW). The mass attenuation coefficient has been estimated using a spectra of the x-ray measured using a CdTe detector (XR-100T-CdTe, SEIKO EG&G CO.,LTD.). The uncertainty of the calibration constant of the survey meter was 4.2 % ($k=2$).

Retrospective Review of Dosimeter Film Processing

Mirela Kirr, Christopher Passmore

Landauer, Glenwood, Illinois, USA

Abstract. Dose monitoring records and accuracy in dose measurement are continuously tested during the dose reconstruction or epidemiological studies. While reconstructing data for dosimeters analyzed in modern times is achieved with relative ease, performing analytical measurements for dosimeters dating as far back as to 1954, has proven to be more challenging. Film dosimeters from 1954 to 2002 reside deep in the salt mines outside in Hutchinson, Kansas and were recently retrieved for reanalysis in support of the Million Worker Study (Boice, 2012) that is being conducted in the United States of America. The purpose of the study is to provide scientifically evidence of effects radiation risk when exposures are received gradually over time (Bouville et al. 2015). Since most of the film dosimeters were analyzed in the early days of Dosimetry, way before 1983, when the performance testing standards were introduced in the United States, the desire was to verify the accuracy of the reading and the dose calculation that was reported initially. A sample of participants was selected and their associated film dosimeters were retrieved from archive (Underground Vaults & Storage, Salt Mine). The dosimeters were reanalyzed using current Macbeth TD 931 reader, and compared to the results of the past to determine the accuracy of the process. In this study the accuracy of the measurement data and dose calculation was within 10%. Being able to retrieve historical records and film dosimeters to provide validation of recorded doses is a true testament to the foresight of Dosimetry Pioneers to institute quality throughout the analytical process and preserving these records well before regulations required their preservation.

Design of Long Counter Having Flat Response from Few keV up to 150 MeV

Mohamed Mazunga^{a,b}, Taosheng Li^b, Yanan Li^b, Jieqiong Jiang^b, Yican Wu^b

^aUniversity of Science and Technology of China, Hefei, Anhui, China

^bInstitute of Nuclear Energy Technology, CAS · FDS Team, Hefei, Anhui, China

Abstract. We have designed an extended range neutron long counter on the basis of work optimized using Super Monte Carlo (SuperMC 2.3.2 Professional Edition) code. The problem of the existing traditional long counters is that their response function falls rapidly above 5 MeV. We proposed a new designed by adding two layers of converter material inside the polyethylene moderator. The relatively low density chromium and high density lead metals converted a single high energy neutron to two lower energy neutrons by the (n, 2n) spallation reaction. This slow down the incident high energy neutron to a region where the moderating cylinder and ³He counter responded well. The response function at lower neutron energies were improved by inserting small polyethylene cylinder in front of ³He counter, together with thermal neutron absorber materials and small air holes drilled in polyethylene moderator. In this design we achieved to extent the flat response function of the long counter from few keV up to 150 MeV. The total fluctuation of response curve is less than $\pm 9\%$ over the entire energy range. The angular response of the designed long counter was calculated at various neutron energies, it confirmed that the long counter is less affected by scattered neutron. The designed long counter is suitable to be used as standard neutron monitor for measurement of neutron fluence at high-energy neutron source.

Measurement of Occupational Doses of Ionising Radiation to the Whole body of Diagnosis Radiologists

Maryam Pourkaveh

Hamadan University of Medical Sciences, Hamadan, Iran

Abstract. Background and purpose: To present the results of occupational radiation doses investigated through a diagnosis radiologists at Hospitals of Mazandaran Medical Science Universities in north of Iran at 2015. This research was carried out to determine measurement of occupational doses of ionising radiation to the whole body of diagnosis radiologists. Materials and Methods: This study was done in order to determine personnel operation in the units of hospitals radiologist related to University of Mazandaran Medical Science in 2015. Five group were issued with a series of TLD dosimeters to wear during their routine position work. These dosimeters were worn at defined positions on the whole body and the absorbed dose to each position was measured. It was concluded that the use of dosimeters attached to the inside arms of protective whole body is the optimum solution for surface body dosimetry. Data collection tools are made of a researcher check list that was used after obtaining suitable letter and validity indexes. Results: The measured natural radiation background was 0.08 mSv, and the measurement range for annual absorbed dose was 0.28 mSv to 5.98 mSv. The largest to the smallest radiation exposure was observed in the following worker groups respectively: technologists, physicists, radiologists, nurses and officer staff. Comparison of these three scores in technical, protective and technological operation fields showed a meaningful difference ($p < 0.05$). Conclusion: The overall quality of personnel operations were nearly desirable and in need of continuous education, supervision and evaluation. Also, a representative sample of occupational exposures personnel was surveyed in an effort to determine levels of radiation exposure in diagnosis radiologists at Hospitals of Mazandaran Medical Science Universities in north of Iran. This study found that annual exposure levels ranged from 0.28- 7.98 mSv. Technologists were in the upper in this radiation exposure within five groups. Also, This study found before technologists, physicist upper in this radiation exposure. Furthermore, this study showed, the maximum dose is radiology staff and data for the application of the principles of radiation protection this section is important.

KEYWORDS: *occupational doses; ionising radiation; diagnosis radiologists; whole body; hospital personnel.*

Calculation of 2D Dose Distribution in an Inhomogeneous Phantom using Artificial Neural Network with Best Training Method

Mahdi Saeedi-Moghadam^a, Banafsheh Zeinali-Rafsanjani^{a,b}, Kamal Hadad^c, Sepideh Sefidbakht^a

^aMedical Imaging Research Center, Shiraz University of Medical Sciences, Shiraz, Iran

^bNuclear Medicine and Molecular Imaging Research Center, Shiraz University of Medical Sciences, Shiraz, Iran

^cNuclear Engineering Department, School of Mechanical Engineering, Shiraz University, Shiraz, Iran

Abstract. Treatment planning systems were developed in order to facilitate treatment planning in radiotherapy. Beam dose distribution data is one of the requirements of these systems, but it is very time consuming to measure or calculate these data. Artificial neural network (ANN) can be one of the fast calculation methods which help to reduce the time of dose calculation but it needs to train well, in order to have more accurate calculations. In this study ANN was trained by the data which was calculated by MCNP5. The objective of this study is finding the best method of training the ANN using MCNP5 modelling. A simulated linear accelerator beam was used in this study. An inhomogeneous phantom was modelled using MCNP5. The phantom was a water phantom with a 1-cm-thick cork layer in the depth of 5 cm. To verify the model the experimental measurements and calculations of PDD in inhomogeneous phantom compared with together. Multilayer-perceptron network with back-propagation learning algorithm was used in order to design the neural network. ANN was trained by the model calculations. Different kinds of training methods were tested to find the best method for training the model. In order to check the accuracy of ANN the results of PDD and beam profiles in the field of $15 \times 15 \text{ cm}^2$ were predicted by ANN with different training methods and compared with the MCNP5 calculations. A good agreement was seen between the result of MCNP5 and experimental measurements. Trainbfg training method had the least error in inhomogeneous region for PDD calculations, around 0.6% and max error of 0.86%. Trainbfg training method was also the most suitable method for beam profile calculations. The percentage differences in summit and tail regions for this training method were 4.50 and 1.10 respectively. This study revealed that the best training method is Trainbfg and this method can perform accurately in both PDD and beam profile calculations. The test results of the ANN in the field size of $15 \times 15 \text{ cm}^2$ were shown that the ANN model is completely accurate in 2D dose calculations, so that this model can accurately use for dosimetric calculations and its other advantage is decreasing the time of calculations to the reasonable level for clinical use.

Photoneutron Secondary Cancer Risk Estimation by a Novel Position-Sensitive Detection Method

Mehdi Sohrabi, Amir Hakimi

Department of Energy Engineering and Physics, Amirkabir University of Technology, Tehran, Iran

Abstract. Photoneutron (PN) secondary cancer risk (PN-SCR) estimation of patients undergoing radiotherapy is highly important when high-energy X-ray beams of medical accelerators are applied. For accurate estimation of the PN-SCR, a position-sensitive method is required since the PN dose varies from point to point in any location in and out of the treatment beam. The methods applied so far in the literature for PN-SCR estimation mostly provide PN dose at single points such as at the isocentre or at similar points. In this paper a position-sensitive method is introduced for the first time based on using mega-size polycarbonate (MSPC) detectors which make one capable to determine the PN-SCR estimation at any point on any organ desired in and out of the beam. The method also provides dose profile and isodose distribution for different single X-ray doses and field sizes in a Siemens ONCOR Linac. The MSPC detectors with an area of $50 \times 50 \text{ cm}^2$ are processed in mega size electrochemical etching chambers making the PN-induced recoil track images observable by the unaided eyes. The PN dosimetry method introduced is high position-sensitive with a high spatial resolution and highly insensitive to high energy X-ray doses in addition to a number of other advantages. The method provides superior characteristics for PN-SCR estimation studies and other similar applications.

A New Method for Effective Dose Calculation based on the Ambient Dose Height Distribution

Niroojiny Sangarapillai^{a,b}, Mario Liebmann^{a,b}, Bjoern Poppe^a, Heiner von Boetticher^b

^aCarl von Ossietzky University, Oldenburg, Germany

^bKlinikum Links der Weser, Bremen, Germany

Abstract. The effective dose is a widely used quantity to assess the ionizing radiation related risk and can be of value for comparing the relative doses from different exposures. In radiation protection practice, it is usually estimated based on measurements of the depth personal dose equivalent which “is taken as an assessment of the effective dose under the assumption of a uniform whole body exposure” (ICRP 103, par. 144). Radiology is the area of occupational exposure in which most of the radiation exposed personnel is employed and where this assumption generally is not fulfilled, because only a part of the body is protected by the protective clothing. To solve the difficulties with the highly heterogeneous exposure of the medical personnel during radiologic interventions for monitoring measurements different techniques to assess the effective dose using one or two dosimeters were suggested. With this work an offline method is presented which allows the effective dose calculation through measurement of a height distribution of ambient dose. Therefore, this method can be used for analyzation and optimization of working places in a faster and more accurate way than through analyzation of monthly readout dosimeters. Using voxelized anthropomorphic phantoms a height distribution of gender specific conversion factors and correction factors from ambient dose to effective dose is developed, enabling a direct conversion of a measured or even manufacturer given ambient dose distribution to effective dose. This model already includes different radiation protection clothing and the effects of beam hardening of the radiation field through different thicknesses of protection clothing. Additional radiation protection equipment such as permanent ceiling or patient couch mounted protection shields is included in the ambient dose distribution - measured at the personnel position. For a first application of this new method, effective dose for the examiner at interventional computed tomography examinations was calculated for two different clinical scanners with different gantry angulations and a male and female examiner phantom wearing radiation protection vests of three different Pb equivalent thicknesses and a thyroid protector. Expanding to this example of usage for radiology, this method is universally applicable.

Development of a New Optical Reading Technique for Dosimetric Gels based on the Analysis of the Scattering Light

Olivier Bleuse^{a,b}, Régine Gschwind^a, Yannick Bailly^b

^aUniversity of Bourgogne Franche Comte - laboratory Chrono Environnement - IRMA team, Montbéliard, France

^bUniversity of Bourgogne Franche Comte - laboratory FEMTO ST - MIE team, Belfort, France

Abstract. Chemical dosimetry, is a promising metrology technic for ionizing radiations. By their constitution, dosimetric gels represent real tridimensional detectors that can be adapted for all volumes, where radiation responses and metrological characteristics are dependent of reagent concentrations of the gel. They are mainly composed of water (like the human body), which gives to gels, a very good water/tissue equivalence. Used as such a detector, dosimetric gels are of interest in a lot of areas, especially in the medical domain. Firstly, this presentation will summarize the theoretical approach about dosimetric gels and their reading technics. We focus on polymer gels: their chemical aspects and the creation of microdomains. Their characteristics of microdomains were studied and are function of the absorbed dose (size, number). Secondly, we will introduce our new optical reading method, based on the Lorenz – Mie theory to determine the correlation between microdomains and the absorbed dose. Different optical parameters were studied: the scattering angle, the wavelength of the source, the polarization ratio and the refractive index of gels. Consequently, dosimetric gels can be read with a high spatial accuracy (less than 10 μm) and with a great sensitivity (less than 0,25 Gy) depending of gel's reagents concentrations. The influence of these parameters will expose and demonstrate in clinical conditions for the quality control in radiation therapy. Our innovative approach could become the reference reading technic for polymer gels because of its low cost and high accuracy in comparison with MRI and others readings strategies. To conclude, we will illustrate different applications of this method as a radiation detector. One clinical example will be shown in the case of a radiotherapy treatment quality control.

Performance Assessment of the Criticality Dosimetry System at The Belgian Nuclear Research Centre SCK•CEN

Olivier Van Hoey^a, Filip Vanhavere^a, Marcel Reginatto^b

^aThe Belgian Nuclear Research Centre SCK-CEN, Mol, Belgium

^bPhysikalisch-Technische Bundesanstalt PTB, Braunschweig, Germany

Abstract. In places where fissile materials are being handled, human error or failure of the safeguards system could lead to a criticality accident. Although such accidents almost stopped occurring as a result of the high level of today's safety technology, the risk of a criticality accident can never be absolutely eliminated. Criticality dosimetry systems must be able to measure neutron doses in the range between 0.25 and 10 Gy with dose rates up to 10^5 Gy/s. Since the sensitivity of neutron detectors usually depends strongly on the neutron energy, the system must be able to reconstruct the energy spectrum or at least estimate the average energy. According to IAEA recommendations, the system must allow a quick separation of exposed and non-exposed persons immediately after the accident. Within 48 hours the dose must be reconstructed with an uncertainty of less than 50% and less than 25% four days later. The criticality dosimetry system at the Belgian Nuclear Research Centre SCK•CEN is accredited according to ISO17025 by the Belgian accreditation body BELAC and monitors about 4000 nuclear workers. The system is based on four activation detectors: gold with and without cadmium shielding, indium and sulphur. Indium allows quick separation of exposed and non-exposed persons using a gamma survey meter. The ^{198}Au and $^{115\text{m}}\text{In}$ activities of respectively the two gold detectors and the indium detector are determined with gamma spectrometry using a germanium detector, the ^{32}P activity of the sulphur detector with liquid scintillation beta counting. The four activities are then inserted in a self-developed program calculating the neutron energy spectrum – and thus any dose quantity of interest – based on an iterative algorithm starting with a user defined spectrum. Participation in an international intercomparison at the SILENE reactor (CEA Valduc), yearly tests at the BR1 reactor (SCK•CEN) and theoretical performance studies using reference criticality spectra have shown compliance of the SCK•CEN criticality dosimetry system with the IAEA recommendations. Comparison of the current iterative algorithm and a new Bayesian algorithm showed good agreement. Further, an MCNP model of the criticality dosimeter has been developed to investigate the effect of the human body, the detector holder and the neutron impact angle.

PROCORAD's International Proficiency Testing for Radio-Bioassays

Robert Fottorino^a, Bernadette Peleau^b, Christian Hurtgen^a

^aPROCORAD, Fontenay Aux Roses, France

^bAREVA, Beaumont Hague, France

Abstract. In France, some specific Medical Biology Laboratories (MBL) are in charge of the monitoring of nuclear workers. These MBL, specialized in radiotoxicological tests, must be accredited according to ISO 15189 and have ministerial certification. The accreditation of radiobioassay analyses requires notably Proficiency Testing (PT) between laboratories and, in the field of radiotoxicology, one of the most important PT providers is PROCORAD, a non-profit making association – law of 1901 - that works for the promotion of quality control of radiotoxicological analysis since 1995. Its specifications are to provide real biological samples spiked with various radionuclides and to send them around the world to environmental or medical laboratories, involved in radiotoxicological analysis. Ten comparison exercises are annually organized: Tritium, Actinides (except Uranium), Uranium, Carbone 14, Sulphur 35, Strontium 90, Gamma – X emitters, Surprise test and Polonium in urine and Actinides in fecal ashes. The results obtained by all the laboratories are both statistically and anonymously exploited, thanks to a homemade software entitled Procostat which is in conformity with the requirements of the standard ISO 13528. This conformity is the first step of an accreditation of PROCORAD according to the standard 17043. Procorad PT's program answers to a definite demand from laboratories in charge of radiotoxicological analysis. For some years, more than 70 participants from all over the world have signed up to participate in these comparison exercises. Apart from an assessment of the different laboratories performance, the comparison exercises organized by PROCORAD enable the laboratories to evaluate the techniques implemented in terms of accuracy, reproducibility and specificity.

Assessment of Dose Calibrators Performance in Nuclear Medicine Department in Sudan

Suhaib Alameen

College of Medical Radiologic Science, Khartoum, Sudan

Abstract. Nuclear medicine uses many different radioactive isotopes for radiation diagnostics and therapy. The amount of radioactivity has to be determined exactly before it is applied to patients. The dose calibrators have to measure the radioactivity of gamma and beta with the different energies precisely for high quality imaging and for applying and the right amount of radiation to treat disease. This study was carried out to assess the performance of dose calibrators with work in nuclear medicine departments in Khartoum state. two department were included in this study , Radiation and Isotopes Centre of Khartoum (RICK) and Nilein Medical Diagnostic Centre (NMDC), four Quality Control were carried out using two standard radionuclides “ ^{137}CS and ^{57}CO ” which were accuracy , constancy , linearity and geometry. All results that obtained from this study has been compared with the international standard ($\pm 5\%$) and the results showed that the dose calibrators has good performance and there is no need for any correction tables or factors or maintenance.

A Simple, Reliable and Inexpensive Microscopy-Based Method for Radiation Biodosimetry

Sudhir Chandna, Shwetajali Nimker, Kanupriya Sharma, Vijaypal Singh

Institute of Nuclear Medicine and Allied Sciences, Delhi, India

Abstract. A major systemic effect of whole-body or partial body irradiation includes suppressive effect on haematopoiesis observed at relatively lower doses around 1Gy-2Gy whereas effects on gastrointestinal (GI) and nervous system appear at relatively higher doses in that order. Blood cells may get depleted after radiation exposure depending on the extent of dose received. Current methods for peripheral blood based radiation biodosimetry include assessment of lymphocytopenia as well as radiation-induced chromosome aberrations in circulating blood lymphocytes. In this study, we used a new and simple method for assessing response of immature red blood cells containing high RNA content in mice after total body irradiation at doses ranging from 25cGy-10Gy irradiation. We devised a simple microscopy technique involving whole blood smears processed suitably and stained with propidium iodide (PI) to distinguish reminiscent RNA-containing young erythrocytes from mature red blood cells. The technique proved to be far simpler and user-friendly as compared to other microscopy-based methods including acridine orange and methylene blue staining, even though we performed validation with these latter methods. Using this new procedure, mouse polychromatic erythrocytes (PCEs) were found to be partially depleted within 24h-48h at doses 2Gy onwards, 3Gy-10Gy causing depletion of PCEs below 0.5% by 48h post-irradiation. Similar results were obtained with conventional microscopy techniques using acridine orange and methylene blue for reticulocyte analysis of mice following total body irradiation. With a dose-dependent delay, recovery of these immature red blood cells to normal levels could be observed by PI staining within 2-4 weeks following irradiation at 3Gy-7.5Gy. Animals irradiated at 10Gy suffered irreversible depletion in PCEs by 48h that failed to recover. Also, Kaplan Meier analysis of animal population survival was in good agreement with the response of this new assay. The propidium iodide based microscopy technique proved to be reliable, inexpensive and easy for quantitation of reticulocytes/PCEs. Its major strength lies in its ability to unequivocally detect young erythrocytes and to assess the radiation-induced suppression of erythropoiesis in a user-friendly manner

Secondary Neutron Dose Assessment from Proton Therapy Using Passive Scattering at The National Cancer Centre (NCC)

Sang Eun Han^{a,c}, Se Byeong Lee^b, Gyuseong Cho^c, Kyeongjin Park^c

^aKorea Institute of Nuclear Safety, Daejeon, Republic of Korea

^bNational Cancer Center, Goyang, Republic of Korea

^cKorea Advanced Institute of Science and Technology, Daejeon, Republic of Korea

Abstract. Proton therapy is one of the advanced option for cancer treatment nowadays. But secondary neutrons during treatment is not a few and being a potential risk to human health. The purpose of the study is to assess secondary neutron dose in the treatment space during proton therapy at NCC. Passive scattering beam mode was considered because it is the most neutron generating condition. MCNP (ver. 6) Monte Carlo simulation was conducted based on the precise modelling with CAD drawings and architectural information of NCC. Five proton beam settings from 190MeV to 230 MeV were selected from the conventional treatment plan. Through the simulation, three dimensional neutron flux and dose profile over the treatment room was acquired with dense detector arrays, and neutron doses were acquired on the basis of ICRP74 ambient dose equivalent conversion factors. As a result, we could figure out three things. First, neutron is dominant risk in secondary radiation field and photon contribution was less than 2% except for target position. Second, predominant neutron energy bands were near 500 keV, 2 MeV and 50 MeV from the neutron energy spectrum analysis, and these high energy neutrons mainly contributed to total neutron dose equivalent. Finally, Continuous secondary neutron dose profiles were acquired and values were varied from 3.90 ± 0.03 mSv at end of the field to 0.33 ± 0.01 mSv at 100cm lateral distance per one Gray (Gy) proton beam absorbed dose in target. Also, Measurement with He-3 neutron detector were done in the treatment room to support the simulation and result was lower than simulation up to 13%.

Traceable Measurements for Radiation Protection Industry in South Africa

Sibusiso Jozela

National Metrology Institute of South Africa, Pretoria, South Africa

Abstract. The recommendations regarding dosimetric quantities and units in radiation protection dosimetry are set forth by the International Commission on Radiation Units and Measurements (ICRU). The recommendations on the practical application of these quantities in radiation protection are established by the International Commission on Radiological Protection (ICRP). The Radiation Protection and Safety of Radiation Sources: International Basic Safety Standards (BSS) requires that monitoring and measurements be conducted on the quantities necessary for the verification of compliance with the safety standards. The BSS also requires that equipment used for this purpose be properly maintained, tested and calibrated, at appropriate intervals, against standards that are traceable to national or international reference standards. In South Africa, according to the Hazardous Substances Act, 1973 (Act No. 15 of 1973), the regulatory body requires the authority holders to ensure that their monitoring equipment is calibrated by the approved body. An approved body should maintain reference radiation fields that are traceable to a national standards body. This traceability chain provides quality assurance of the equipment used in industry where the lives of users (radiation workers) and patients are at risk. Through the measurement units and measurement standards act No. 18, of 2006, the National Metrology Institute of South Africa (NMISA) was mandated to provide South African industry and environmental, health and safety sectors with fit-for-purpose measurements and measurement standards. This is achieved by keeping and maintaining the national measurement standards and units to an acceptable international standard; and by disseminating traceability to the South African industry. The latest developments and services provided by the radiation dosimetry laboratory of NMISA in ensuring a high quality of life and good radiation safety practice through accurate measurements are presented.

Development of the Performance Testing Procedure for the New Proposed Portable Gamma Irradiation System

Seung Kyu Lee, Hyungjoon Yu, Insu Chang, Hyungtaek Kim, Jungil Lee, Jang-Lyul Kim, Bong-Hwan Kim

Korea Atomic Energy Research Institute, Daejeon, Republic of Korea

Abstract. Radiation monitors are widely used to measure dose levels in nuclear facilities. These monitors must be calibrated by using reference radiation fields. However, it is difficult and inconvenient to remove the fixed radiation monitors or gamma zone monitors for checking their calibration and to reinstall them. The calibration of these monitors needs portable gamma-ray sources. The use of portable gamma-ray sources is limited by the available distance from the monitors and the intensities/dose rates of the sources. In the present study, a 2169 MBq (reference date: 2015.11.25) ^{137}Cs gamma-ray source, housed in a lead container with a narrow collimation to provide a cone beam, was used. Several attenuators (different thickness of metal filters, such as aluminium, copper, and tin filters) were made to obtain varying dose rates. The reduced dose rates were measured by using ionization chamber (PTW LS01). Monte Carlo N-Particle extended (MCNPX) simulations were also performed for all the attenuators. Excellent agreement was found between the experimentally measured dose rates and the respective simulated values. In a further study, testing procedures and a protocol for new proposed techniques by using different attenuators will be developed for the future use, and this method of simulation and experimental verification of dose rates is planned to be carried out for several gamma monitoring systems.

Development of the Probabilistic Internal Dosimetry Code

Siwan Noh^a, Jai-Ki Lee^a, Jong-Il Lee^b, Jang-Lyul Kim^b

^aHanyang University, Seoul, Republic of Korea

^bKorea Atomic Energy Research Institute, Daejeon, Republic of Korea

Abstract. In internal dose assessments, many biokinetic models and parameters are used and necessarily, each model and parameter have uncertainties. These uncertainties are propagated through internal dose assessment, which results in significant uncertainties in the estimated dose. In addition, uncertainties also occur in the intake activity estimation from multiple bioassay measurement data. Nevertheless, the point estimation which does not consider uncertainties are widely used in internal dose assessment because of simplicity. However, the interval estimation (i.e. probabilistic assessment) is required for accidental internal exposure or sensitivity analysis. Internal dosimetry from bioassay data is divided into two parts: intake estimation using measured activity and intake retention function, and dose estimation using internal dose coefficients. Probabilistic estimation for the intake retention fractions and the internal dose coefficients can be implemented using Monte Carlo analysis that propagates uncertainties in biokinetic models. Bayesian estimation is used to estimate interval of intake activity from bioassay data. From these two methods, comprehensive probabilistic internal dose assessment can be performed. In this study, we developed the probabilistic internal dose assessment code using MATLAB language. In this code, users can select which factors and parameters are considered as having uncertainties or not and use default uncertainty data in NCRP publication 164 or input user-defined data based on GUI. Then, the code calculates the probabilistic distribution for intake retention and excretion fractions using the Monte Carlo method. Next, the code repeats the Bayesian estimation with sampled fractions from the distribution to obtain a set of intake activity distributions and combine them into one distribution. Finally, the code calculates the probabilistic distribution for internal dose coefficient using Monte Carlo method and combine it with the intake activity distribution. Also, this code provides a sensitivity test function to identify which factors are important or not to reduce the uncertainty of internal dose. We expect that this code can be used usefully for accidental internal exposure situations and academic purposes.

Effect of Radon Progeny on Real Time Alpha-CAM Monitoring in Uranium Facility

TaeHyung Kim, JunBok Lee, Jong Il Lee, Bong Hwan Kim

Korea Atomic Energy Research Institute, Daejeon, Republic of Korea

Abstract. Alpha-CAM technology has been developed and has evolved over a period several decades in response to the need for an instrument that is continuously sampling workplace air. The real-time Alpha-CAM has advantage of continuous sampling, monitoring and alarm capability when detection of a significant accumulation of specific radionuclides of concern occurs. When using the real-time Alpha-CAM measurement, it is most important to remove extraneous counts due to radon and radon progeny(radon progeny) alpha emissions will increase sensitivity and reduce the false alarms. The sensitivity of the Alpha-CAM methods is highly dependent on the accuracy of the background compensation method. The background issue for using Alpha-CAM monitoring is that typically radon and its progeny (radon progeny) are often found in elevated concentrations in indoor environments. In this Study, to evaluate the radon compensation performance of actually used Alpha-CAM in uranium treatment facility in KAERI(Korea Atomic Energy Research Institute), we installed additional radon detector(RAD7) near by the Alpha-CAM(i-CAM), and compared the radon concentration from RAD7 with the gross alpha concentration, compensated radon, from I-CAM. i-CAM radon compensation method was very well worked removal the radon progeny more than 100 times compared with radon concentration from RAD7. But the trend of I-CAM measurement result was similar to radon progeny behavior. It seems to not completely removal the radon progeny. In uranium facility, It is possible to occur the malfunction by radon progeny because uranium has very low DAC(Derived Air Concentration). Thus, in order to set the alarm level or DAC when using real time Alpha-CAM, there is a need to reflect the characteristics of the facilities by radon progeny effect.

PoCAMon – All in one Personal Online Continuous Air Monitor, Gamma Dose Meter and Gas warner

Thomas Streil

SARAD GmbH, Dresden, Saxony, Germany

Abstract. The PoCAMon combines a very compact design with a high flow rate and long battery life. Its size and weight are still acceptable for carrying by one person. The unit measures long-lived aerosols as well as short-lived Radon/Thoron daughters by alpha spectroscopy and beta counting. The radioactive aerosols and particles are collected on the surface of a high resolution membrane filter. The alpha and beta decays on the filter are measured by a high-end semiconductor radiation detector (400 mm²). This allows a perfect separation of the different decay products. The increased pump rate (more than 3 l/ min) is suitable for lower detection limits. The low noise rotary van pump is processor controlled and guarantees a constant flow rate over the whole measuring time. A sensor measures permanently the pressure drop on the filter in order to recognize an exhausted or perforated filter instantly. With the 3.8 Ah NiMH battery pack the PoCAMon achieves an operation time of more than 30 hours. The quality control is a main issue of any radiation measurement. Therefore the PoCAMon records a complete alpha spectrum for each measured value. This allows the monitoring of the device's perfect operation in each moment of the measurement. Optional can be integrated a 10 cm³ LaBr Scintillator coupled with a Silicon Photo Multiplier as high sensitive Gamma Dose meter including nuclide Identification by an Energy resolution of 4 %. There are options for additional sensors for carbon monoxide and combustible gases as needed in underground mines to warn the staff and switch off the device in case of dangerous explosive concentrations. All measured data are stored in a 2GB memory card and can be accessed with a PC or laptop via a USB interface. Data transmission and device control can also be done via wireless ZigBee network or via a server for stationary operation with network access. A barometric pressure sensor and a GPS receiver are further optional features of the device.

Implementation of ICRP 116 Dose Conversion Coefficients for Reconstructing Organ Dose in a Radiation Compensation Program

Timothy Taulbee^a, Keith McCartney^b, Richard Traub^b, Matthew Smith^b, and James Neton^a

^aCenters for Disease Control and Prevention (CDC), National Institute for Occupational Safety and Health (NIOSH), 1150 Tusculum Ave, Mail Stop C-45, Cincinnati, Ohio, 45226 USA

^bDade Moeller and Associates, 1835 Terminal Drive, Richland, Washington, 99354 USA.

Abstract. Under the U.S. Energy Employee's Occupational Illness Compensation Program Act (EEOICPA) of 2000, the National Institute for Occupational Safety and Health (NIOSH) is responsible for reconstructing worker radiation doses that are subsequently used to determine the probability that a worker's exposure caused a specified cancer. Since 2000, NIOSH has used dose conversion coefficients published by the International Commission on Radiation Protection in report 74 (ICRP 74) to determine organ dose from external sources of radiation. In 2010, the ICRP issued publication 116 that used more realistic models than ICRP 74, included separate values for both males and females, and provided conversion coefficients for 14 additional organs. NIOSH has developed a Monte Carlo method to sample the energy/organ specific distribution of the ICRP 116 conversion coefficients to determine the uncertainty in the organ dose. In addition, the development of irradiation geometry factors (IGFs) was required to convert a dosimeter dose measured at various wear positions (center chest, pocket, and collar) on the front of the body to values that are compatible with ICRP 116 organ dose conversion coefficients. Using Monte Carlo methods, IGFs were developed for both neutrons and photon exposures to male and female workers for rotational (ROT) and isotropic (ISO) exposure geometries. The IGFs range from 1.2 to 2.1 for photons in the rotational geometry (ROT) depending on gender, dosimeter location and photon energy. The final component considered in worker dose reconstruction is the measured dose and its associated uncertainty. Each of the components and their uncertainty distributions are combined using Monte Carlo methods to compute the mean organ dose and the combined total uncertainty used in the probability of causation calculation.

KEYWORDS: *dose reconstruction; probability of causation; organ dose; ICRP 116; Monte Carlo modelling; MCNP; exposure geometry.*

RadiationProtectionDosimetry(2017),Vol.173,No.1-3,pp.131–137

doi:10.1093/rpd/ncw305

Tracking System for Radiation Works Using Passive RFID Technology to Enhance Radiation Protection

Yunjong Lee^a, Jin Kyu Kim^a, Jinwoo Lee^a, Young-Hwan Ryu^{b,e}, Ho-Sung Kim^{c,e},
Kyung-Rae Dong^{d,e}, Eun-Jin Choi^f

^aKorea Atomic Energy Research Institute, Jeongup, Jeollabuk-do, Republic of Korea

^bDepartment of Radiology, Seoul Medical Center, Seoul, Republic of Korea

^cDepartment of Nuclear Medicine, Asan Medical Center, Seoul, Republic of Korea

^dDepartment of Radiological Technology, Gwangju Health College University, Gwangju, Republic of Korea

^eDepartment of Nuclear Engineering, Chosun University, Gwangju, Republic of Korea

^fDepartment of Public Health and Medicine, Dongshin university, Naju, Jeonnam, Republic of Korea

Abstract. An advanced Radio Frequency Identification (RFID) system capable of tracking and monitoring a wide range of materials and components has been developed. This paper describes the design of an RFID Radiation works Tracking System. It is designed to track a moving person in a wide area, such as laboratories or nuclear power plants, using the RFID technology. Radiation workers need to be moved from office to Radiation zone and vice versa every day. For radiation safety officers, obtaining a safe action for their workers is a critical issue. At times, many radiation workers are tirelessly employed without realizing that they've been contaminated. Contaminated areas are increasing because of those situations. Radiation officers had difficulty finding the cause and solving the problems. Radiation officers can easily recognize the person who accesses the area and the place which are contaminated by using a tracking system and can prevent them from additional pollution. The proposed system has hardware and software components. The hardware architecture consists of an RFID passive tag, an RFID tag reader, a web server and a database server. The database server is located in the office of the radiation safety officer. The tag readers are distributed around the laboratory. The tags are programmed with Radiation work's profiles and are worn by the Radiation works. Communication between the tag reader and the server is done via LANs. These experiments showed that the RFID tags were effective and stable enough to be used for successfully tracking and monitoring radiation workers. The worker safety system developed in this research utilized the passive RFID tracking technology whose advantages are its efficient tracking capabilities, low cost, and easy maintenance.

Capability Study of Multi-function Dose Rate Meter Based on Hemisphere CdZnTe Detector

Ying Wang, Wenjun Xiong, Zhiping Luo, Jizeng Ma, Ling Chen

China Institute of Atomic Energy, Beijing, China

Abstract. The common dose rate meter mainly detects γ ray with energy above 50keV. The hemisphere CdZnTe detector has good detective efficiency and energy resolution for low energy X ray and γ ray. The capability of multi-function dose rate meter based on hemisphere CdZnTe detector was discussed from aspects including detectable energy range, energy resolution, environmental applicability and angle response. Except angle response, other aspects show that multi-function dose rate meter based on CdZnTe detector has more advantages than common dose rate meter (such as the ionization chamber, etc.) in area monitoring. The hemisphere CdZnTe not only can measure ambient dose equivalent rate but also can identify nuclides. In order to improve the angle response, the solution by using two hemisphere CdZnTe detectors to share anode was given in this paper.

Combination of Automated Chromatographic Separation and Off-line Cherenkov Counting in Determination of Low Level Activity of Sr-90

Željko Grahek, Ivana Coha

Rudjer Boskovic Institute, Zagreb, Croatia

Abstract. Radiostrontium as a high yield fission product with long physical (28.75 years) and biological half-life (~12 years), is one of the most hazardous radiocontaminants in the environment. Therefore, almost all environmental radioactivity monitoring programs include its quantitative determination. Due to its radiochemical properties standard procedure for its determination is complicated and time consuming. (ima ga u rečenici prije) In recent years fully automated approach for monitoring pure beta emitters has been developed. However, there is a lack of prompt and reliable methods for determination of low-level activities in environmental samples. In our laboratory semi-automated procedure for determination of $^{89,90}\text{Sr}$ in liquid waste was established. Procedure includes separation of strontium from matrix on Super Lig 620 column followed by off line on column detection via Cherenkov counting on commercially available instrument. The goal is further development of mentioned method for monitoring environmental occurrence of ^{90}Sr and determination of low level activity of ^{90}Sr by Cherenkov detection. Nowadays, Cherenkov counting can be successfully used for quantitative determination of ^{90}Sr in wide range of activities by using modern commercial LSC. In addition, several years ago first commercially available TDCR (triple-to-double coincidence ratio) instrument was released by Hidex Company. It uses TDCR technique, which is an absolute counting method for obtaining counting efficiency without external or internal standard sources. However, in open literature only few papers were published about using TDCR for quantitative determination of ^{90}Sr by Cherenkov counting. Therefore, in this paper semi-automated procedure for determination of low level activity of ^{90}Sr which includes separation of strontium from matrix on chromatographic column followed by off line on column detection via Cherenkov counting will be presented. As quantitative determination requires accurate and precise determination of the detection efficiency it will be shown how Cherenkov counting efficiency (double and triple to double) for strontium isotopes depends on type of media, volume, color, etc., and how detection limit can be improved by optimization of these parameters.